PIERS 2011 Suzhou

Progress In Electromagnetics Research Symposium

Abstracts

September 12–16, 2011
Suzhou, CHINA

www.emacademy.org
www.piers.org

PIERS 2011 Suzhou Abstracts

Published by

The Electromagnetics Academy
777 Concord Avenue, Suite 207
Cambridge, MA 02138

www.emacademy.org
www.piers.org

ISSN: 1559-9450
ISBN: 978-1-934142-17-2

Progress In Electromagnetics Research Symposium

September 12–16, 2011

Suzhou, CHINA

PIERS 2011 SUZHOU ORGANIZATION

PIERS Founding Chair

J. A. Kong, MIT, USA

PIERS Chair

L. Tsang, University of Washington, USA

PIERS 2011 Suzhou General Chair

C. D. Gong, Soochow University, China

PIERS 2011 Suzhou Organization Committee Chair

L. Gao, Soochow University, China

PIERS 2011 Suzhou International Advisory Committee

S. Barmada
L. C. Botten
J. Brady
C. H. Chan
D.-C. Chang
W. C. Chew
C.-K. Chou
H. T. Chuah
S.-T. Chun
N. Engheta
A. K. Fung
Z.-H. Gu
L. Gurel
T. M. Habashy
M. Hallikainen
Y. Hara
H.-C. Huang
A. Ishimaru
E. Jakeman
K. Kobayashi
A. Komiyama
L.-W. Li
I. V. Lindell
S. G. Liu
K. M. Luk
S. Mano
G. D. McNeal
K. K. Mei
Y. Miyazaki
P. Pampaloni
A. C. Priou
K. D. Senne
R. T.-I. Shin
E. C. Slob
M. Tateiba
P. M. van den Berg
D. Watts
T. Yamasaki
K. Yasumoto
W.-X. Zhang

PIERS 2011 Suzhou Technical Program Committee

S. J. Anderson
A. Baghai-Wadji
G. Berginc
W.-M. Boerner
H. Braunisch
Y. J. Cai
C. T. Chan
H.-W. Chang
H. S. Chen
H. Y. Chen
K.-S. Chen
T. J. Cui
V. L. Druskin
Y. Du
A. Z. Elsherbeni
H. T. Ewe
Y. J. Feng
H. Fernandes
L. Gao
J. C. Goswami
S. L. He
W. Hong
B. Hou
K. Iwatsuki
Y.-Q. Jin
R. Kubacki
Y. Lai
M. K. Li
Q. H. Liu
S. Lucyszyn
J. T. Lue
A. Massa
E. L. Miller
M. Moghaddam
Z.-P. Nie
Y. Okuno
D. Omeragic
M. Oristaglio
K. Ouchi
J. P. Pribetich
R. Ramer
L.-X. Ran
C. M. Rappaport
A. K. Sarychev
C. Seo
X.-Q. Sheng
Y. V. Shestopalov
J.-C. Shi
A. Sihvola
R. Talhi
S. Tjuatja
M. S. Tong
D. P. Tsai
J. Vrba
C.-F. Wang
H. G. Wang
B.-I. Wu
C.-J. Wu
M. Y. Xia
G. Q. Xie
T.-S. Yeo
W.-Y. Yin
M. Zaslavsky
X. M. Zhang
H.-X. Zheng
J. Zhou

PIERS 2011 Suzhou Organizing Committee

Y. J. Cai	H. Chen	H. S. Chen	L. S. Chen
J. T. Huangfu	S. Lee	Z.-Y. Li	H. J. Luo
J. Q. Luo	L. Mo	T. Pan	M. R. Shen
Y. L. Song	Q. H. Wang	J. H. Wu	P.-L. Xie
S. Xu	J. J. Yu	S. Q. Zhu	

PIERS 2011 SUZHOU SESSION ORGANIZERS

D. Ahn	Y. Avishai	Y. J. Cai	D.-C. Chang
H.-W. Chang	H. Y. Chen	N.-K. Chen	C.-J. Cheng
H.-T. Chuah	Y. M. Deng	J.-W. Dong	Y. Du
H. T. Ewe	Q. Fu	L. Gao	E. Gescheidtová
J. G. Guan	S. L. He	J. S. Hou	J. F. Hu
J.-H. Jou	K. Kobayashi	V. C. Koo	Y. Lai
Y.-C. Lan	R. A. Lewis	J. H. Li	W. X. Li
L. Liu	Y. L. Lu	A. Massa	Y. Okuno
K. Ouchi	H. Qin	C.-W. Qiu	A. G. Radwan
K. N. Rozanov	Y. Shao	Y. V. Shestopalov	J.-C. Shi
L.-H. Shi	R. Touzi	D. P. Tsai	H. P. Wang
J. L. Wei	C.-J. Wu	G. Q. Xie	Y.-Z. Xie
T. Yamasaki	P. Yang	S. W. Yang	T.-J. Yang
X. Yang	W. H. Yu	Y. T. Yu	F. L. Zhang
J. J. Zhang	J. Zhou	L. Zhou	

PIERS 2011 SUZHOU EXHIBITOR

- ☐ EM SOFTWARE & SYSTEMS — CHINA

PIERS 2011 SUZHOU SPONSORS

- ☐ Soochow University
- ☐ Zhejiang University
- ☐ The Electromagnetics Academy at Zhejiang University
- ☐ Centre for Optical and Electromagnetic Research of Zhejiang University
- ☐ The Electromagnetics Academy
- ☐ Suzhou Association for Science and Technology

PIERS 2011 SESSIONS

Session 1A1
Passive Optical Waveguide Theory and Numerical Modelling

Method of Connected Local Fields for Large Scale Modeling of Passive Waveguide Devices

Hung-Wen Chang and Sin-Yuan Mu
Department of Photonics, National Sun Yat-Sen University, Taiwan

Abstract— We present the method for connected local fields (CLF) for large scale modeling of passive waveguide devices. CLF is a novel method for obtaining numerical solutions of the 2-D Helmholtz equation. This recently published result [1] is derived from a local field expansion (LFE) of a local field defined for the square region surrounded by all eight neighboring points as depicted in Figure 1. The main equation called LFE-9 is a compact nine-point, frequency dependent, FD-like formulation given below:

$$u_c = \frac{1}{4}\frac{J_4\left(\sqrt{2}V\right)\cdot\left(u_r+u_u+u_l+u_d\right)+J_4\left(V\right)\cdot\left(u_{ne}+u_{nw}+u_{se}+u_{sw}\right)}{J_0\left(V\right)\cdot J_4\left(\sqrt{2}V\right)+J_0\left(\sqrt{2}V\right)\cdot J_4\left(V\right)}, \quad \text{(LFE-9)}$$

where the normalized frequency $V = k\Delta$ is the product of wavenumber the spacing between grid point. These coefficients possess superior numerical dispersion properties in both temporal and spatial domains.

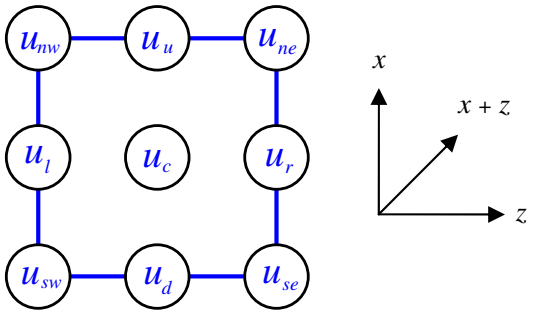

Figure 1: Compact 9-point stencil consisting of u_c and all adjacent points.

REFERENCES

1. Chang, H.-W. and S.-Y. Mu, "Semi-analytical solutions of Helmholtz equation by the method of connected local fields," *Progress In Electromagnetics Research*, Vol. 109, 399–424, 2010.

Error and Dispersion Analysis of LFE-9 Formulae in the Theory of Connected Local Fields

Hung-Wen Chang and Sin-Yuan Mu
Department of Photonics, National Sun Yat-Sen University, Taiwan

Abstract— We present a rigorous error and dispersion analysis of local field expansion (LFE) formulation in the theory of connected local fields. LFE-9 is a compact nine-point, frequency-depedent coefficients for obtaining numerical solutions of two-dimensional Helmholtz equation in a homogeneous medium [1]. We study and derive the order of local truncation errors for both the traditional FD and the novel LFE-9 stencils. The order for LFE-9 is given in term of the Bessel function of the first kind of order eight. The argument of this Bessel function is inversely proportional to normalized frequency. Our results show that the full nine-point stencil formulae is approaching theoretical limit given by the Nyquist-Shannon sampling theorem.

REFERENCES

1. Chang, H.-W. and S.-Y. Mu, "Semi-analytical solutions of Helmholtz equation by the method of connected local fields," *Progress In Electromagnetics Research*, Vol. 109, 399–424, 2010.

Interference Effect of Fiber Bragg Gratings Using Coupled Mode Method

Nai-Hsiang Sun[1], **Chia-Ming Hu**[1], **Ping-Hung Lin**[1], **and Shih-Chiang Lin**[2]

[1]Department of Electrical Engineering, I-Shou University, Kaohsiung, Taiwan
[2]Department of Communication Engineering, I-Shou University, Kaohsiung, Taiwan

Abstract— In this paper, we analyze the fiber Bragg gratings with two input signals. The coupled mode theory is used to calculate the interference effect of this structure. The formulas of transmission and reflection efficiencies are presented in this paper. In our setup, two optical input powers are launched into both ends of the fiber Bragg grating. The expressions of both inputs can be expressed as A_0 and $B_o e^{j\theta}$. Since the two inputs have a different phase of θ, the interference effect forms in the fiber Bragg gratings, and the output powers vary with respect to the phase. The FBG becomes phase dependent because changing the phase of one or both of the incident light waves produces significant changes in the reflected and transmitted light of the FBG. We can design the parameter of the Fiber Bragg gratings so that the fields of the two input signals cancel in one end, while they enforce each other in the other end. Such a phase-controlled FBG can be applied to high speed interconnects, modulation, routing, and switching.

Analysis of Grating-assisted Contra-directional Couplers

Nai-Hsiang Sun, Chia-Ming Hu, and Shou-Feng Tsai
Department of Electrical Engineering, I-Shou University, Kaohsiung, Taiwan

Abstract— A grating-assisted directional coupler (GADC) consisting of two nonsynchronous waveguides and a grating region is in reality a single, composite waveguide. Since two nonidentical waveguides in close proximity are not synchronous, a periodic grating structure can lead to power transfer between the waveguides. These couplers are important elements for many optical applications. In this paper, we analyze a grating-assisted contra-directional coupler (GACC) which consists of similar structures to a GADC: Two nonidentical waveguides and a grating. For codirectional coupling, the group velocities of the two coupled modes are parallel. On the other hand, the group velocities are antiparallel for contradirectional coupling. For a GACC, the power is excited in one waveguide at the input end. Different from GADCs, the power transfers to the other waveguide with different propagation direction for GACCs. In this paper, the Floquet-Bloch Theory is applied to analyze the GACC structure.

Improving the Pseudospectral Optical Waveguide Mode Solver Using the Penalty Skill

Po-Jui Chiang[1], **Nai-Hsiang Sun**[2], **and Chia-Ming Hu**[2]

[1]Department of Electronic Engineering, National Kaohsiung University of Applied Sciences
Kaohsiung, Taiwan
[2]Department of Communication Engineering, I-Shou University, Taiwan

Abstract— A penalty method for imposing boundary conditions at material interfaces is considered in the recently developed multidomain pseudospectral optical waveguide mode solver. Working as a flexible perturbation at the boundary, the method is demonstrated to offer better numerical convergency and stability. The solver is applied to the optical fiber for the assessment of its numerical performance, to the classical benchmark rib waveguide for comparing with existing high-accuracy results, and to the fused fiber structure for demonstrating its robustness in calculating the effective indices.

Surface Integral Equation Method for Surface Plasmon Mode in Optical Fibers

Jung-Sheng Chiang[1], **Ming-Jeng Huang**[1], **Wen-Ying Hong**[1], **Nai-Hsiang Sun**[1], **and Shih-Chiang Lin**[2]

[1]Department of Electrical Engineering, I-Shou University, Kaohsiung, Taiwan
[2]Department of Communication Engineering, I-Shou University, Kaohsiung, Taiwan

Abstract— We report a new numerical approach, base on the surface integral equations formulations, to model the metal-clad optical fiber for analysis of surface plasmon modes. The surface plasmon modes are essentially the electromagnetic waves that are propagating at optical frequencies on an interface between a metal and dielectric. The metal-clad optical fibers supporting surface plasmon modes have the property of being highly localized with fields that decay away from the surfaces. The surface integral equation method, base on the surface integral equations formulations, considers that the metal-clad optical fiber is consisted of two homogeneous media: one is silica in the core and the other is the metal. Employing the Green's functions in these two mediums, only the fields on the interface (or boundary) between the metal and silica is needed to be considered. Surface integral equation method is proposed to calculate the surface plasmon modes of the metal-clad optical fibers. The modes of a metal-clad fiber having cladding of negative dielectric constant can be classified in two families according to the value of n_{eff} with respect to n_{co}. For $n_{eff} < n_{co}$, it can obtain modes very similar to the ordinary guided modes of dielectric fibers, with an oscillatory behavior within the core. The first family of modes is called oscillating guided modes. For $n_{eff} > n_{co}$, we obtain other kinds of modes that are strongly localized at the interface. The second family of modes is said surface plasmon modes The variations of the effective index with fiber core radius are presented for surface plasmon and oscillating guided modes.

Gaussian Wave Propagation in Alternating Positive and Negative Coupling Waveguide Arrays

Keivan Mahmoud Aghdami and Fatemeh Mokhtari
Physics Department, Payame Noor University, Tehran 19395-4697, Iran

Abstract— The study of linear and nonlinear phenomena in coupled waveguide arrays as an evidence of discrete indexed optical medium has attracted a lot of attention over the past decade and is investigated in one and two dimensions [1]. The coupling in waveguide lattices is due to light electric field leakage and is mathematically defined as a specific overlap integral between the linear modes of adjacent waveguides. So far the sign of coupling parameter has been considered positive in most of the works in this area, where the portion of electric field penetrate to first adjacent neighbours are in phase with itself. More recently, negative coupling has also been proposed [2], which is physically equivalent to an additional phase shift of π caused by the coupling.

In this article, propagation of a Gaussian beam in arrays of waveguides with alternating positive and negative coupling, in the absence and in presence of nonlinear phenomenon is studied numerically and compared to homogenous positive coupling case [3]. Here, Gaussian beam evolution is simulated when propagate along waveguides and its route is investigated by several initial phase difference of waveguides which is caused by input beam tilt angle.

Behaviour of light is described by one-dimensional discrete nonlinear Schrodinger equation with alternating positive and negative coupling (AC) for array of N waveguides as [2].

$$i\frac{dE_n}{dz} + \beta E_n + (-1)^n \kappa (E_{n-1} - E_{n+1}) + \gamma |E_n|^2 E_n = 0 \tag{1}$$

where the field amplitude in nth waveguide is E_n, β is propagation constant at individual waveguide and $(-1)^n\kappa$ is alternative coupling coefficient between $n-1$ and nth guide. z is the propagation coordinate and the fourth term illustrates nonlinear Kerr phenomenon in which γ is proportional to the Kerr nonlinear coefficient. As so defined, the coupling coefficient switches between positive and negative signs periodically across the waveguide arrays. Runge-Kutta method is used in order to solve coupled Equation (1) and to simulate light propagation.

Light propagation through 6 cm long, 41 AC-coupled guide is simulated in Figs. 1(a) and (b) in lack of nonlinear effect ($\gamma = 0$) for initial phase difference $\varphi = 0$ and $\varphi = \pi/2$ respectively, correspond to the tilt angle $t = 0$ and $t = 1.1°$. Its major differences to DC coupling [3] are obvious especially for $\varphi = \pi/2$ which energy had been selftrapped in a sideling route.

A periodic change in outgoing intensity distribution is seen by a continuous change in tilt angle (Fig. 2(a)). Energy flows along two transversally symmetric channels when exposure is vertical and this frequently happens in $\varphi = m\pi$ ($m = 0, 1, 2, \ldots$), while intensity tends to concentrate at centre in $\varphi = m\pi/2$. Difference is significant in comparison to the analogous plot for DC coupling in Fig. 2(b) [3].

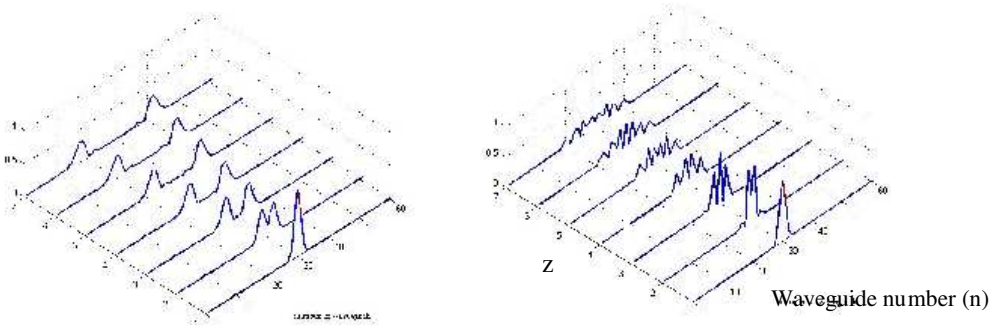

(a) (b)

Figure 1: Evolution of a Gaussian beam in an AC coupling waveguides in $\varphi = 0$ (a) and $\varphi = \pi/2$ (b) initial phase difference.

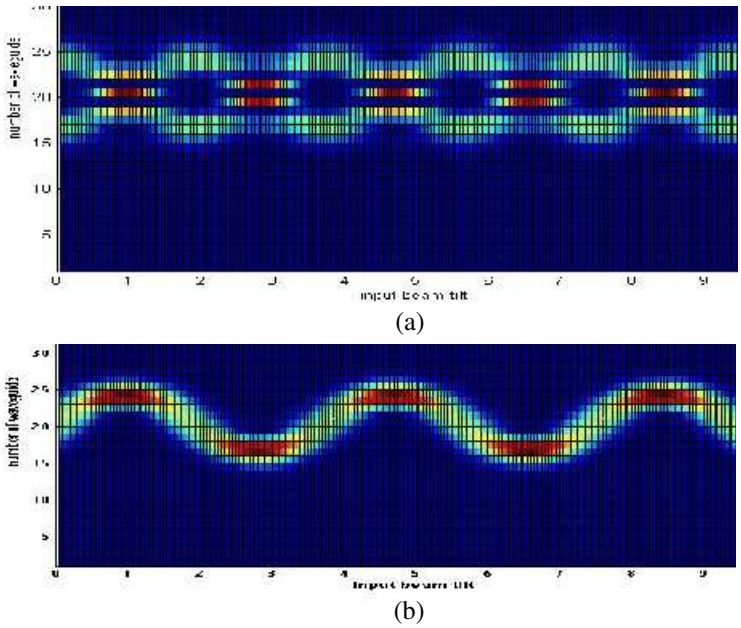

Figure 2: Outgoing energy distribution vs. Input beam tilt angle for AC (a) and DC (b) coupling.

Our results indicates light propagation is influences slightly by non-linear phenomena (γ) while we observed a considerable effect in DC case specially for $\varphi = m\pi$.

REFERENCES

1. Lederer. F., G. I. Stegeman, D. N. Christodoulides, G. M. Assanto, and Y. Silberberg, "Discrete solitons in optics," *Phys. Rep.*, Vol. 463, 1–126, 2008.
2. Nikolaos, K. E., P. Zhang, Z. Chen, D. N. Christodoulides, C. E. Ruter, and D. Kip, "Wave propagation in waveguide arrays with alternating positive and negative couplings," *Phy. Rev. A*, Vol. 81, 053817, 2010.
3. Mahmoud, A. K., A. Gharaati, and F. Mokhtari, "Control of self-focusing and self-defocusing in the waveguides array," *Jap. J. Appl. Phys.*, to be printed, 2011.

Surface and Non-surface Gap Solitons at the Junction of Two Periodic Lattices with Phase Mismatch

K. Mahmoud Aghdami and S. Alidust
Physics Department, Payame Noor University, Tehran 19395-4697, Iran

Abstract— Interface between different physical media, age of materials like crystals and some others stats that system has a defect can support a special class of localized waves known as surface waves. Nonlinear response of materials makes possible dynamic control of surface localization. These modes are identified as surface solitons. In this paper we search surface and nonsurface gap solitons exist at interface between two similar photorefractive crystals with periodic refractive indexes that one has a phase difference respect to another in the interference. In the case of defocusing media this system is described by the nonlinear Schrodinger equation for dimensionless amplitude of the light field q:

$$i\frac{\partial q}{\partial z} = -\frac{1}{2}\frac{\partial^2 q}{\partial x^2} - q|q|^2 - pR(x) \tag{1}$$

$R(x)$ is refractive index profile and given by $R_{left}(x) = \mathrm{Cos}^2(\Omega x)$ at $x \leq 0$, and $R_{right}(x) = \mathrm{Cos}^2(\Omega x + \phi)$ at $x > 0$, where Ω is the modulation frequency, ϕ is phase difference between two lattices and p is lattice depth. To understand the basic properties of surface gap solitons, it is needful to consider the Floquet-Bloch spectrum of the linear infinite lattice and to found band gap structure. For the nonlinear response solitons appear as defect modes inside the gaps. We search for stationary solutions in the form of $q(x) = w(x)\exp(ibz)$, b is real propagation

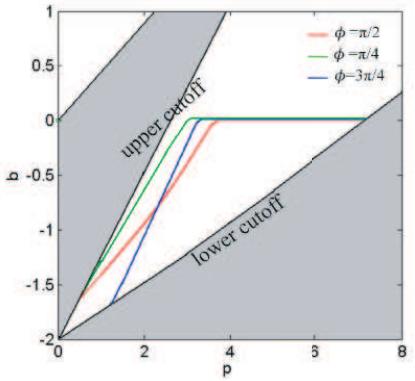

Figure 1: Existence region of solitons $\Omega = 2$.

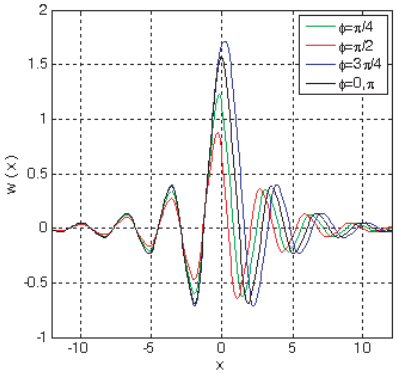

Figure 2: Fundamental modes $p = 3$, $b = -0.8$, $\Omega = 2$.

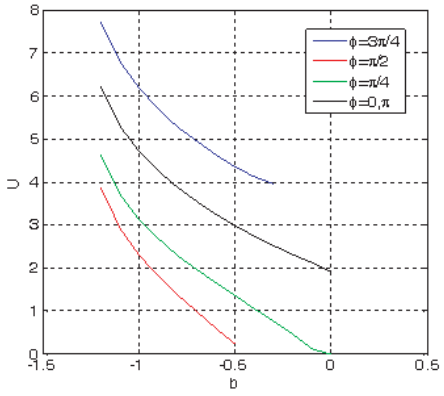

Figure 3: Energy flow $p = 3$, $\Omega = 2$.

constant. When $\phi \neq 0$, π surface solitons appear at interface that is bounded in region as shown in Figure 1. Fundamental modes for different value of ϕ are shown in Figure 2. For nonsurface solitons localized in lattice, because of nonlinearity.

Energy flow is calculated as $U = \int_{-\infty}^{\infty} |q|^2 dx$ that Equation (1) admits to be conserved and monilitically increases when the absolute value of propagation constant increases (Figure 3).

We also deal with localization of energy at right and left of interface and found energy distribution for $\phi \neq 0$, π is different at right and left.

REFERENCES

1. Ye, F., Y. V. Kartashov, V. A. Vysloukh, and L. Torner, *Optics Letters*, Vol. 33, 1288, 2008.

Session 1A2
Electromagnetic Theory and Design on the Optical Dispersive Materials, Invisible Cloak and Photonic Crystals

Novel Characteristics of Reducing Wide-band Crosstalk for Guiding Microwave in Corrugated Metal Strip Lines with Subwavelength Periodic Hairpin Slits

Jin Jei Wu[1], **Tzong-Jer Yang**[1], **Her-Lih Chiueh**[2], **Linfang Shen**[3], **Weilien Ou Yang**[1], **and Chih-Hsiang Wen**[1]

[1]Department of Electrical Engineering, Chung Hua University, Hsinchu 30012, Taiwan
[2]Department of Electronic Engineering, Lunghwa University of Science and Technology Kueishan, Tayouan 333, Taiwan
[3]Department of Information Science and Electronic Engineering Electromagnetic Academy, Zhejiang University, Hangzhou 310058, China

Abstract— A new type of microstrip line on which the spoof surface plasmon polaritons (SPPs) can propagate in microwave band is developed and a scheme for reducing the wide-band crosstalk between transmission lines is proposed. The microstrip line structure is designed by introducing periodic subwavelength hairpin structure on the edge of conventional microstrip lines. Numerical methods are used to analyze the dispersion relation and guiding bandwidth in microwave regime. Besides, we experimentally verify that such periodically structured microstrip lines support spoof SPPs in the frequency range between 200 MHz and 8 GHz. Compared with the quasi-TEM mode in conventional microstrip line, the spoof SPPs mode can be highly localized on the surface of the structured microstrip lines, and so the crosstalk between different structured microstrip lines is very weak.

A New Practicable GLLH EM Invisible Cloak without Exceeding Light Speed Wave

Jianhua Li[1, 2], **Ganquan Xie**[1, 2], **Lee Xie**[1], **Feng Xie**[1], **and Hao Zhou**[2]

[1]GL Geophysical Laboratory, USA
[2]Hunan GL, Supercomputational Science Center, China

Abstract— By GL no scattering inversion, we discovered a novel practicable GLLH invisible cloak without exceed light speed violation. It has refractive index $N > 1$ and can be fabricated by conventional optical materials. In our paper ArXiv 1050.3999v1, we proposed a GLLH electromagnetic (EM) invisible cloak with novel front branching and without exceed light speed violation [1]. Next, we published it in PIERS 2010 and international conferences. Before May 1, 2011, one year passed after our paper ArXiv 1050.3999 published in ArXiv, no other paper published to study cloak without exceeding light speed. By searching keyword "without exceed light speed" in the Google, four web pages are presented which are only records of our GLLH invisible cloak. In May 1, 2011, Janos Perczel1 and Ulf Leonhardt published their paper ArXir 1105.0164v1 titled "Invisibility Cloaking without superluminal propagation." [2]. Our paper [1] and Ulf paper [2] have common research goal and object that for solving fundamental "exceeding light speed problem" in the invisible cloak. In this paper, GL no scattering inversion is presented. No scattering electromagnetic wave propagation through the GLLH cloak media and novel wave front branching are presented. Our GLLH cloak in [1] and Ulf cloak in [2] is different. The difference between our GLLH cloak in [1] and Ulf cloak in [2] are presented. The copyright and patent and all right are reserved by GL Geophysical Laboratory.

REFERENCES

1. Xie, G., J. Li, L. Xie, and F. Xie, "GLLH EM invisible cloak with novel front branching and without exceed light speed violation," arXiv:1005.3999v1 [physics.optics], May 2010, http://arxiv.org/abs/1005.3999v1.
2. Perczel, J. and U. Leonhardt, "Invisibility cloaking without superluminal propagation," arXiv:1105.0164v1 [physics.optics], May 2011, http://arxiv.org/abs/1105.0164.

Analysis of Multiple Filtering Properties in a Superconductor-dielectric Superlattice at Terahertz Frequency

Wei-Hsiao Lin[1], **Chien-Jang Wu**[2], **Tzong-Jer Yang**[3], **and Shoou-Jinn Chang**[1]

[1]Institute of Microelectronics and Department of Electrical Engineering
Center for Micro/Nano Science and Technology, and Advance Optoelectronic Technology Center
National Cheng Kung University, Tainan 701, Taiwan, R.O.C.
[2]Institute of Electro-Optical Science and Technology, National Taiwan Normal University
Taipei 116, Taiwan, R.O.C.
[3]Department of Electrical Engineering, Chung Hua University, Hsinchu 300, Taiwan, R.O.C.

Abstract— In general, a photonic-crystal multichanneled transmission filter (MTF) with resonant transmission peaks within the photonic band gap (PBG) can be achieved by using the photonic quantum well (PQW) as a defect. In this paper, without using any defect in a superconductor-dielectric photonic crystal (SDPC), it is possible to achieve an MTF in a high-temperature SDPC in the terahertz (THz) frequency. We calculate the THz spectroscopic properties, such as the transmittance, reflectance, and absorptance, in a one-dimensional high-temperature SDPC. Interestingly, we find that there exists the discrete comb-like transmission spectrum, leading to a possible design of an SDPC MTF at THz. Instead of within PBG, these comb-like transmission peaks locate within the photonic passband, which can be further explained by the band structure calculated by the Bloch-Floquet theorem. The emergency of these peaks is found to be crucially controlled by the thickness of the superconductor layer. The number of peaks is closely related the number of periods, that is, there will be N-1 peaks if the number of periods is N. The number of resonant peaks is further explained by the evanescent resonant coupling mechanism. The results suggest that an SDPC can be used as a frequency-selective filter or dense wavelength-divided multiplexer of in the THz superconductor electronics.

The Momentum of Photon May Explain the Measurement's Paradox in the Subatomic World

Antonio Puccini
Department of Neurophysiology, Order of Malta, Naples, Italy

Abstract— As we know particles of the subatomic world, that is quantum objects (QOs), do not have defined properties until we observe them making a Measurement (M). Before the M the QO is *delocalized*, it is potentially detectable in one of the points of its *wave volume*. We can just presume approximately their structure and behaviour, but we have not certitude. According to Quantum Mechanics before the M it is not possible to tell if it is a particle or a wave.

In order to make a M of a QO, we need to illuminate it, however, as we learn from Quantum Mechanics, we change, against our will, the subatomic system we are trying to measure. As Feynman reminds us, to observe electrons, we need a light because the light rebounding on electrons make them visible, but the light affects electron behaviour. When light is sent on an electron, it makes the electron vibrate thus behaving in a different manner. Therefore, the photons (Ps) are indispensable to carry out a M.

As we know also the P has a its own *momentum (p)*, according to the formula: $p = h/\lambda$, where h is Planck's constant and λ is the wavelength of the considered P. In the case of a medium visible P its p is: $p = 6.625 \cdot 10^{-27}\,[\mathrm{erg} \cdot \mathrm{s}]/5 \cdot 10^{-5}[\mathrm{cm}]$, that is:

$$p = 1.325 \cdot 10^{-22}[\mathrm{g} \cdot \mathrm{cm/s}] \tag{1}$$

Our calculations show that a P of the optic band hits an electron with a *momentum*, a *dynamic-mass,* bigger than the mass of the electron itself. This may explain why the M induces the well-known changes on the observed QO and may contribute to solve the enigma of the *M's Paradox.*

A Ground-plane Cloak Made of Subwavelength Elliptical Rod Arrays

Hanhong Gao[1], **Baile Zhang**[3], **and George Barbastathis**[2, 3]

[1]Department of Electrical Engineering and Computer Science
Massachusetts Institute of Technology, Cambridge, USA
[2]Department of Mechanical Engineering, Massachusetts Institute of Technology, Cambridge, USA
[3]Singapore-MIT Alliance for Research and Technology (SMART) Centre, Singapore

Abstract— After the original ideas proposed by Ulf Leonhardt and John Pendry, invisibility cloak has attracted a lot of research attention. Cloaks operating at microwave and optical regimes have been designed and experimentally verified, with implementations such as metamaterials, layered structures and so on. Macroscopic cloaks for visible light have also been realized with natural materials as simple as calcite. A ground plane cloak is able to hide objects on a flat ground plane under a "carpet" as if they do not exist. Through a transformation between the "physical space" and "virtual space", light illuminating the cloak is reflected in the same way as being reflected by a perfect mirror. Quasiconformal mapping was firstly applied to facilitate metamaterial fabrication of optical cloaks. However, though the anisotropy has been minimized, it still leads to a lateral shift at the output which makes the cloak detectable. Also, the size of the cloaking region is limited in the order of one wavelength.

We propose a ground-plane cloak made of subwavelength elliptical rod arrays, which conquers the two key difficulties in the realization of cloak materials — inhomogeneity and anisotropy. This cloak is located on a perfect electric conductor (PEC) ground plane, operated in two-dimensional (2D) plane perpendicular to the the ground plane under TM illumination (electric field lying in the 2D plane). An infinite cloaking region is created by squeezing the space, making the ground plane interface away from the its original location. In this way, the squeezed medium is homogeneous, but it has to be anisotropic in order to let the ground plane appear at its original position. The anisotropic medium is realized by subwavelength elliptical rod arrays, which exhibit different effective refractive indices under illumination from different directions. This subwavelength nanostructure consists of square unit cells with elliptical silicon rods immersed in air, which is easy to fabricate. The size of the unit cell is about 1/8 of the free space wavelength. Outside the cloak, the index-matched isotropic homogeneous medium is realized by subwavelength circular rod arrays. Therefore, this cloak is of infinite size and is easier to implement with nanofabrication technique. Lateral shift is eliminated since elliptical rod arrays are used to achieve the anisotropic medium. By proper tuning of the size of the unit cell, this cloak design works in both microwave and optical regime.

ACKNOWLEDGMENT

This works is supported by Singapore's National Research Foundation through the Singapore-MIT Alliance for Research and Technology (SMART) Centre and Air Force Office of Scientific Research MURI program on Nanomembranes under contract No. FA9550-08-1-0379.

Measurement of Conductivity for Thin Metal Films at Various Frequencies by Microwave Microstrip Method

Jih-Hsin Liu[1], **Hsin-Yuan Miao**[1], **Bin-Wei Huang**[1], **and Wen-Hsiang Wang**[2]

[1]Department of Electrical Engineering, Tunghai University, Taichung, Taiwan
[2]Department of Physics, National Tsing Hua University, Hsin Chu, Taiwan

Abstract— The frequency dependence of conductivity of metal films with thickness less than skin depth was measured by a microwave microstrip method under T-junction structure. The T-junction microstrip is superior to ring and strip-line resonators for yielding much accurate results with a simple fabrication process. The analysis of the transmission coefficient S_{21} spectra and revised equations of anomalous skin effect for the microstrip made of different metallic films reveals that the surface resistance behaves like nearly a one-half power law dependence on the frequency which is in congruence with the results derived from free electron model subjecting to electron phonon interaction for a simple metal.

ACKNOWLEDGMENT

This work was supported by the National Science Council of the Republic of China under the contract NSC 99-2218-E-029-001-.

Homogeneous Beam Squeezer with Low Reflectance

Hongyi Xu[1], **Baile Zhang**[2, 3], **George Barbastathis**[2, 3], **and Handong Sun**[1]

[1]Division of Physics and Applied Physics, School of Physical and Mathematical Sciences
Nanyang Technological University, 21 Nanyang Link, Singapore 637371, Singapore
[2]Singapore-MIT Alliance for Research and Technology, (SMART) Center
Singapore 117543, Singapore
[3]Department of Mechanical Engineering, Massachusetts Institute of Technology
Cambridge, Massachusetts 02139, USA

Abstract— A main challenge in photonics is how to compress the bulky volume of photonic devices in order to bridge them with electronic devices. The representative case of this is how to squeeze an electromagnetic beam while keeping its beam profile unaltered. One of traditional methods is to make a gradient decrease of the radius of a waveguide, and thus have it gradually couple to one with a smaller radius. However, the significant drawback of this method is that a flat slope, i.e., a large decreasing length (at least 5 times longer than the wavelength) will be required in order to well preserve the beam profile and reduce electromagnetic reflection. As a result, the characteristic length of the squeezer will be several times larger than that of the wavelength, making it impossible for the large integration of photonic circuit. To solve the problem, a beam squeezer has been designed based on transformation optics method. The idea of the transformation optics method takes the advantage of the invariant nature of the Maxwell Equation. It is able change the special profile of electromagnetic wave by applying the transformation on the material's permittivity and permeability appearing in the form of tensor. With this method the new squeezer has demonstrated the advantage in the preservation of beam profile, with its volume 90% smaller than traditional none-transformed squeezers. Besides, it is able to reduce reflectance in the squeezing process and thus increase the conversion efficiency. Moreover, different from the common inhomogeneous transformation, a new transformation method is employed to have the waveguide homogeneously compressed and thus greatly reduce the difficulty in fabrication.

Electro-optic Phase Modulator Based on Guide Mode Resonance of Grating Waveguide Structure

Wen-Kai Kuo, Shin-Chung Chu, and Chih-Hao Chang
Institute of Electro-optical and Material Science, Nation Formosa University
64 Wenhua Rd., Huwei, Yunlin, Taiwan 63208, Taiwan, R.O.C.

Abstract— The guide mode resonance (GMR) effect in a grating waveguide structure can be excited by the phase-matching condition between the incident wave and the leaky guide-mode supported by structure [1]. The GMR effect of waveguide grating structure can be applied to construct a class of optical filters with a narrow resonance wavelength [2]. An electro-optics phase modulator based on guide mode resonance (GMR) of a grating waveguide structure is presented in this paper. The grating structure on the device is fabricated through UV cured nano-imprinting technique and a titanium oxide (TiO_2) layer is deposited on the grating structure. Then, polymer-dispersed liquid crystal (PDLC) is poured on TiO_2 surface of GMR to form the phase modulator. The completed structure is as shown in Fig. 1. The measurement system to obtain the phase properties of the GMR electro-optic phase modulator is shown in Fig. 2 This system is adopted from the electro-optic heterodyne interferometer originally proposed by Chen [3]. In the experiment, the incident angle was fixed at the bias point, the apply voltage is an AC voltage and the peak-to-peak voltage was increased from 0 V to 20 V in steps of 2 V. The experimental result is shown in Fig. 3. The modulator can achieve a phase modulation index of 26.75°/V.

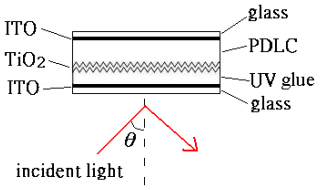

Figure 1.

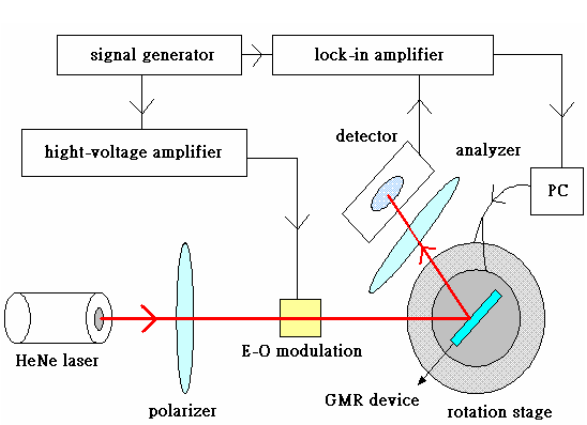

Figure 2.

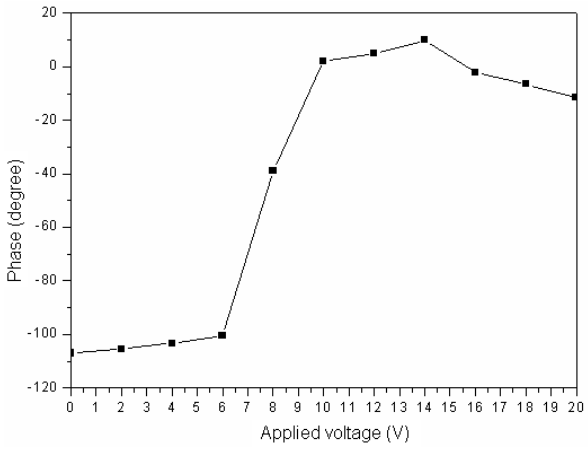

Figure 3.

REFERENCES

1. Sharon, A., D. Rosenblatt, and A. A. Friesem, "Resonant grating-waveguide structures for visible and near-infrared radiation," *J. Opt. Soc. Am. A*, Vol. 14, 2985–2993, 1997.
2. Liu, Z. S., S. Tibuleac, D. Shin, P. P. Young, and R. Magnusson, "High efficiency guided-mode resonance filter," *Opt. Lett.*, Vol. 23, 1556–1558, 1998.
3. Chen, K. H., C. C. Hsu, and D. C. Su, "Measurement of wavelength shift by using surface plasmon resonance heterodyne interferometry," *Opt. Comm.*, Vol. 209, 167–172, 2002.

High Birefringence and Low Loss of Photonic Crystal Fibers with Modified Elliptical Air-holes in Fiber Cladding

Yuan-Fong Chau[1] and You Zhe Ho[2]

[1]Department of Electronic Engineering, Ching Yun University, Jung-Li 320, Taiwan, R.O.C.
[2]National Taiwan University, Taiwan, R.O.C.

Abstract— Birefringence and confinement loss of four patterns of index-guiding photonic crystal fibers (PCFs) are investigated and compared by the numerical finite element method. The proposed case 3 structure is composed of a modified elliptical air-holes cladding and a core of solid silica surrounded with two reduced air-holes near the core area. The maximal mode birefringence and lowest confinement loss of case 3 structure at the excitation wavelength of $\lambda = 1550\,\text{nm}$ can be achieved to the order 10-2 on mode birefringence magnitude and less than 10–5 dB/km on the confinement loss, respectively. This result can be prospects of sensor and other optical device applications.

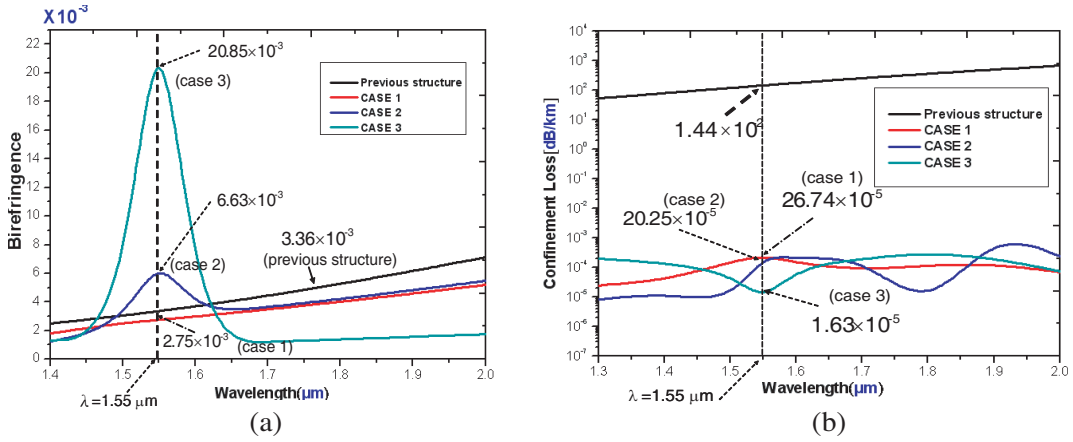

Figure 1: (a) Birefringence as function of wavelengths for the four cases of PCFs with the parameters $\Lambda_x = \Lambda_y = 1.00\,\mu\text{m}$, $r = 0.4\,\mu\text{m}$ for previous circular air-hole case, $\Lambda_x = 1.9\,\mu\text{m}$, $\Lambda_y = 2.2\,\mu\text{m}$, $a = 0.45\,\mu\text{m}$, $b = 0.542\,\mu\text{m}$, elliptical ratio $\eta(a/b) = 0.83$ for cases 1–3, and ring number $N = 5$. (b) Confinement loss as a function of wavelength for proposed four cases of PCFs, with the same parameters used in Fig. 4, and the number of rings is $N = 5$.

REFERENCES

1. Knight, J. C., T. A. Birks, P. St. J. Russell, and D. M. Atkin, "All-silica single-mode optical fiber with photonic crystal cladding," *Opt. Lett.*, Vol. 21, 1547–1549, 1996.
2. Russell, P. St. J., "Photonic crystal fibers," *J. Lightwave Technol.*, Vol. 24, 4729–4749, 2006.
3. Couny, F., F. Benabid, and P. S. Light, "Large-pitch kagome-structured hollow-core photonic crystal fiber," *Opt. Lett.*, Vol. 31, 3574–3576, 2006.
4. Argyros, A. and J. Pla, "Hollow-core polymer fibres with a kagome lattice: potential for transmission in the infrared," *Opt. Express*, Vol. 15, 7713–7719, 2007.
5. Noda, J., K. Okamoto, and Y. Sasaki, "Polarization-maintaining fibers and their applications," *J. Lightwave Technol.*, Vol. 4, 1071–1089, 1986.

A Study on the Properties of Optical Absorption of Buckpaper

J. L. Ciou, H. Y. Miao, and J. H. Liu
Department of Electrical Engineering, Tunghai University
181 Taichung Harbor Road, Section 3, Taichung 40704, Taiwan, R.O.C.

Abstract— Based on the remarkable properties and the extraordinary performance in theory, carbon nanotube (CNT) has been attracted numerous of attention and research interest since it has been found from 1991. The theme of this study is trying to make CNTs as the practical material.And, make a great breakthrough for real application of CNTs.

First, the unique dispersion and filtration process were introduced to form a bulk material (with the idea of bottom up), so called buckypaper (BP), from few grams of CNTs. That causes the superior nature of CNTs could expand and homogenize from a nano scale to macro scale. Then, in order to figure out the properties of BP, several measurement were conducted. For example, SEM, EDX, X-Ray, Hall Effect and so on. Besides, with the process of doping and coating to make BP be modified was the other topic in this study. Finally, stocking with modified BP as the sensor for light detector is the main innovative contributions of this study.

In the preliminary measurements the results show that (1) no matter SWCNTs-BP or MWCNTs-BP, under the low temperature of I-V test, all behave as a negative temperature coefficient of material and with a singularity temperature of resistivity around 150 K. (2) The four points test, in the room temperature shows that the resistivity of BP fall into the range of $10^{-4}\,\Omega\cdot$m, it's in the semimetal rank. It is strong support from (1) and (2) to know that BP is a semiconductor and with excellent conductivity property. In addition, BP also could be re-modified its electrical characteristic by means of micro-coating with metal or metal oxides.

The photoconductivity and photo voltage test radiated by different wavelengths of visible light were conducted in this study with the samples of stacking BP which include before and after modified. The results show that (1) there was no obvious reactions be observed on the samples of pristine BP stacking. (2) The reactions of those samples stacking with modified BP, especially coating with Ti or Zn, go up quite substantially. For example with the conduction of applied bias current of 0.1 mA, the stacking of Ti-SWCNTs-BP and Zn-MWCNTs-BP could get the photo voltage of 20 μV under the stimulating of 23 mW, 940 nm IR, 0.4 mV under the stimulating of 48 mW, 470 nm blue light and 28 μV under the stimulating of 23 mW, 405 nm UV. And, a maximum photo voltage of 6 μV could be observed under the stimulating of blue light with no any of applied bias current.

It overcomes the CNTs application bottleneck with BP material in this study, and re-modified its electrical characteristic by means of micro-coating with metal or metal oxides. It presumed that schottky barrier and dember effect play important role in the whole stacking sample, and could transfer the vibration effect under IR stimulating to the photoelectric effect under blue light stimulating. This shows a powerful evidence of CNTs as a prospect candidate for applications on photoelectric devices.

Enhanced Free Exciton Emission in Crystalline Ultrathin ZnO Films Grown on Si-nanowires by Atomic Layer Deposition

Yuan-Ming Chang[1], **Jiann Shieh**[2], **Pei-Yuan Chu**[1], **Hsin-Yi Lee**[3, 4], **Chih-Ming Lin**[5], **and Jenh-Yih Juang**[1]

[1]Department of Electrophysics, National Chiao Tung University, Hsinchu 300, Taiwan
[2]Department of Materials Science and Engineering
National United University, Miaoli 360, Taiwan
[3]National Synchrotron Radiation Research Center, Hsinchu 300, Taiwan
[4]Department of Materials Science and Engineering
National Chiao Tung University, Hsinchu 300, Taiwan
[5]Department of Applied Science
National Hsinchu University of Education, Hsinchu 300, Taiwan

Abstract— Room-temperature ultraviolet (UV) luminescence was investigated for the atomic layer deposited ZnO films, which were grown on silicon nanowires (Si-NWs) fabricated by self-masking dry etching in hydrogen-containing plasma. For films deposited at 200°C, an intensive UV emission corresponding to free-exciton recombination (~ 3.31 eV) was observed with a nearly complete suppression of the defect-associated broad visible range emission peak. On the other hand, for ZnO films grown at 25°C, albeit the appearance of the abovementioned defect-associated broad visible emission, the UV emission peak was observed to shift by ~ 60 meV to near the direct band edge (3.37 eV) recombination emission. The high resolution transmission electron microscopy (HRTEM) examinations showed that, indeed, the microstructure of the obtained ZnO films for the former case was of continuous crystalline nature, while that for the latter displayed a microstructure consisting of ZnO nanocrystals with a mean diameter of 4 nm embedded in a largely amorphous matrix. The blue shift of the UV emission peak in the latter films, thus, might have been due to the effects of quantum confinement on the free-exciton recombination. Additionally, the results also demonstrate order of magnitude enhancement in emission efficiency for the ZnO/Si-NWs structure, as compared to that of ZnO directly deposited on Si-substrate under the same conditions.

Session 1A3
Synthetic Aperture Radar: Algorithms and Applications

Comparison for Cultivated Laver Detection in Shallow Water Using Two ALOS PALSAR Full-pol Data

Jung-Hwan Song[1], **Chan-Su-Yang**[1], **and Sudhir Kumar Chaturvedi**[1, 2]

[1]Korea Ocean Satellite Center, Korea Ocean Research & Development Institute
ANSAN, Republic of Korea
[2]Indian Institute of Technology Madras, Chennai, India

Abstract— Cultivated laver nets are used in shallow oceanic regions in order to provide the important seafood's and is very much useful for industries to extractseafood from the ocean which contains the huge amount mineral resources. The motion of laver is normallyinfluencedby the different environmental conditions likewind, ocean waves and currents, intertidal effects. This abstract presents the concept for detection of the laver net with the help of radar remote sensing satellite like synthetic aperture radar imagery for the purpose to facilitate coastal farm in the shallow water zone near to the coast of Yellow sea, Korea, which have a very high intertidal variation. Two ALOS-PALSAR full polarizations SAR data were acquired over the area in the different dates and approximately same UTC. The back-scattered energy measured by the sensor was different due to variation of movements of the nets under the oceanic condition. In one case image net was not able to distinguish and so the comparison and detection was cumbersome, the reason for this might be the merged back-scattered signals of waters and net, and the net was under the water, in second case, the signature differs from the background as may in this case the net laver net conditions was high and not fully underwater to provide the high backscatter signals. The decomposition & polarimetry entropy distributions are applied to distinguish the back-scattered signals for the detection. In future, high resolution C and X band sensor data may be applied to check the performance estimation like for example, the floating structure gives the high back-scattered signal in C band fully polarization mode than the ocean surface.

Design of Satellite-based Oil Spill Monitoring System

Chan-Su-Yang[1], **Jung-Hwan Song**[1], **and Sudhir Kumar Chaturvedi**[1, 2]

[1]Korea Ocean Satellite Center, Korea Ocean Research & Development Institute
ANSAN, Republic of Korea
[2]Indian Institute of Technology Madras, Chennai, India

Abstract— An important cause of marine pollution is oil spilling over the sea surface. Normally the oil spills are constantly presents in the main ship traffic area & routes, close to offshore structures where the oils are extracted from the deep oceans, this spilling is in the continuous way due to unwanted loading effects onto the offshore structure by means of ocean waves but the amount of spills may be small.SAR is the most applicable sensor for operational oil spill detection & monitoring over the large oceanic area as it covers the wide area and operates at all weather, day & night. The spilling of oil causes the bad effect onto the environment like ocean pollutionetc.This abstract describes basic concept design for oil spilled integrated system with help of satellite data like SAR as well as optical sensors.Since wavy conditions causes to dampen the oil surface which have lower mass density as compares to the huge saline ocean waters and therefore, they appears on the top of the oceanic surface. The oil spilled area is normally darker in the SAR and optical images than the surrounding background oceanic area.the main concept here is to merge the back-scattered signals and sea-surface radiation from sea-surface to and to carry out the performance for both the case with corresponding damping ratio obtained through the oil- water molecular interaction which forms two layered geometry and corresponding geometry are known to be the layered geometry, this layered geometry may consists of wavy currents, oceanic surface becomes smoothen, if we consider as small fetch for our consideration for the oil spilling research, the scattered fields are generated due to the continuous interaction of water and oil molecules in the ocean and which may provide the dark spot signatures into SAR imageries. Once the generation of scattered and radiation field are over, so one need to estimate the surface roughness for to detect and identify the oil-spilled surface automatically. Microwave data can be obtained through the various sensors in the different modes and polarization for the purpose to estimation of roughness.

Dependency of Microwave Backscattering from Ocean Surface on Ocean Winds Using Airborne Dual-frequency Polarimetric Synthetic Aperture Radar

Akitsugu Nadai, **Toshihiko Umehara**, **Takeshi Matsuoka**, **Makoto Satake**, **Tatsuharu Kobayashi**, **Jyunpei Uemoto**, **and Seiho Uratsuka**
National Institute of Information and Communications Technology, Japan

Abstract— The environment of the coastal ocean depends strongly to the ocean wind field, which has small-scale variation due to the coastal topography. Therefore, the ocean surface wind field with high spatial resolution is important to consider the environment of coastal area. The winds are described as a vector with two parameters (wind speed and direction, or east-west and north-south components of wind). Synthetic aperture radar (SAR) has enough spatial resolution to measure such small scale variation of wind filed. Some methods are proposed to measure the ocean wind vector using single channel spaceborne SAR. To estimate the wind vector using the normalized radar cross section (NRCS) in single polarization of single frequency, some external data is indispensable. The coarse spatial resolution of the external data leads measurement error in estimated ocean winds. In this paper, the dependency of backscattering from ocean surface on ocean winds is analyzed in the parallel polarizations of the X- and L-bands using the results of multiple (three or more) observations in same area in a short time by with different azimuth using an airborne dual-frequency polarimetric SAR.

The dependency of NRCS of ocean surface on wind direction is analyzed with a geophysical model function. For the X-band HH polarization, the asymmetric dependency on wind direction, that is the difference of NRCS between the up- and down-wind conditions, is much larger than that of the X-band VV polarization, though the symmetric dependencies are almost same. This peculiarity of the asymmetric dependency of NRCS in the X-band suggests the possibility of measurement of ocean surface wind only using the X-band polarimetric SAR data. The polarimetric rate of X-band also changes with the wind direction. On the other hand, the dependency of the NRCS in the L-band parallel polarizations is almost same. The dependency of NRCS on wind direction shows difference with the wind speed.

These results of this study suggest the possibility of the ocean surface wind measurement with high spatial resolution using X-band polarimetric SAR.

Ship Detection by Synthetic Aperture Radar with Ground-based Maritime Radar with AIS

Eun-Sung Won and Kazuo Ouchi
Department of Computer Science, School of Electrical and Computer Engineering
National Defense Academy, 1-10-20 Hashirimizu, Yokosuka, Kanagawa 239-8686, Japan

Abstract— Ship detection by synthetic aperture radar (SAR) is expected to take an important role in monitoring and controlling maritime traffic, fishing activity and illegally operating ships; and several commercial ship detection and identification systems are in operation. One of the main requirements in the current and future systems is to improve the detection accuracy for small ships.

The purpose of this study is to examine the ability of extracting and identifying ships by ALOS-PALSAR (Advanced Land Obssering Satellite - Phased Array L-band SAR) with a ground-based maritime radar with AIS (Auto Identification System). Visual observation with video camera and optical data by AVNIR-2 (Advanced Visible and Near Infrared Radiometer-type 2) on board of ALOS were used as supplemental data. The PALSAR data were in FBS 34.3 (Fine Beam Single at 34.3° off-nadir angle) mode acquired on the 18th of December 2008 over the test site in Tokyo Bay, Japan.

In this study, we used the algorithms based on image amplitude, MLCC (Multi-Look Cross-Correlation) [1] and a variance filter first proposed by Arii [2]. The total of 37 ships were confirmed by AVNIR-2, AIS, and visual observation using video camera, which is considered as the "true" number of ships. The number of detected ships was 23, 23 and 32 by the amplitude-based method, MLCC, and variance filter respectively, and the corresponding mean peak to background noise ratio (PBNR) was 1.38 dB, 1.48 dB, and 4.50 dB respectively. Thus, our result showed that the variance filter performed best, followed by MLCC and amplitude-based methods.

REFERENCES

1. Ouchi, K., S. Tamaki, H. Yaguchi, and M. Iehara, "Ship detection based on coherence images derived from cross-correlation of multilook SAR images," *IEEE Trans. Geosci. Remote Sens. Lett.*, Vol. 1, No. 3, 184–187, 2004.
2. Arii, M., "An analysis of scattering from a floating object on the sea using three-component scattering model for polarimetric radar," *Asia Pacific-Radio Science (AP-RASC) 2010*, Toyama, Japan, Sept. 2010.

Preliminary Design for Integration of SAR and AIS for Ship Identification

Sudhir Kumar Chaturvedi[1, 2], **Chan-Su-Yang**[1], **Jung-Hwan Song**[1], **and P. Shanmugam**[2]

[1]Korea Ocean Satellite Center, Korea Ocean Research & Development Institute
ANSAN, Republic of Korea
[2]Indian Institute of Technology Madras, Chennai, India

Abstract— This abstract describes the preliminary design concept for an integration system of SAR and AIS data. SAR sensors are used to acquire image data over large coverage area either through the space borne or airborne platforms in UTC. AIS reports should also obtained on the same date as of the SAR acquisition for the purpose to perform integration test. Once both data reports are obtained, one need to match the timings of AIS data acquisition over the SAR image acquisition time with consideration of local time & boundary to extract the closest time signal from AIS report in order to know the AIS based ship positions, but still one cannot be able to distinguish which ships have the AIS transponder after projection of AIS based position onto the SAR image acquisition boundary. As far as integration is concerned, the ship dead-reckoning concept is most important forecasted position which provides the AIS based ship position at the time of SAR image acquisition and also provides the hints for azimuth shift which occurred in SAR image for the case of moving ships which moves in the direction perpendicular to the direction of flight path. Unknown ship's DR estimation is to be carried out based on the initial positions, speed and course over ground, which has already been shorted out from AIS reports, during the step of time matching. This DR based ship's position will be the candidate element for searching the SAR based ship targets for the purpose of identification & matching within the certain boundary around DR. The searching method is performed by means of estimation of minimum distance from ship's DR to SAR based ship position, and once it determines, so the candidate element will look for matching like ship size match of DR based ship's dimension wrt SAR based ship's edge, there may be some error during the matching with SAR based ship edges with actual ship's hull design as per the longitudinal and transverse axis size information obtained from the AIS reports due to blurring effect in SAR based ship signatures, once the conditions are satisfied, candidate element will move & shift over the SAR based ship signature target with the minimum displacement and it is known to be the azimuth shift compensation and this overall methodology are known to be integration of AIS report data over the SAR image acquisition boundary with assessment of time matching. The expected result may provide the good accuracy of the SAR and AIS contact position along with dimension and classification of ships over SAR image. There may be possibilities of matching speed and course from candidate element with SAR based ship signature, but still the challenges are presents in front of us that to estimation of speed and course by means of SAR data, if it may be possible so the expected final result may be more accurate as due to extra matching effects and the results may be used for the near real time performance for ship identification with help of integrated system design based on SAR and AIS data reports.

On the SAR Image Classification by Rotation of the Covarience Matrix in the Four-component Scattering Power Decomposition

Mitsunobu Sugimoto and Kazuo Ouchi
Department of Computer Science, School of Electrical and Computer Engineering
National Defense Academy, 1-10-20 Hashirimizu, Yokosuka, Kanagawa 239-8686, Japan

Abstract— As more and more synthetic aperture radar (SAR) systems utilize polarimetric information recently, polarimetric SAR (POLSAR) theory has grown rapidly. While traditional SAR systems handle only mono-polarimetric information, data acquired through POLSAR systems contain several polarimetric information, that is HH HV VH and VV (the first letter represents transmitted signal and the second letter represents received signal).

Using the four-component scattering power decomposition, one can decompose these data into four power categories: surface scattering power, double-bounce scattering power, volume scattering power, and helix scattering power. The four-component scattering power decomposition is a powerful tool to analyse acquired data through POLSAR systems. However, some limitations still exist in this method. Volume scattering comes from both forested areas and urban areas. From our commonsense point of view, these two types of areas have quite different characteristics against each other. Therefore, these two areas should be separated.

A modification is applied to the four-component scattering power decomposition based on the covarience matrix. By appropriately rotating the covarience matrix, we were able to distinguish forested areas from urban areas. We also analysed the effect of the size of the processing window (i.e., ensemble average) during the process above. As expected, if the size is too small, the result is too noisy and do not reflect the ground data very well. On the other hand, if the size is too large, the output becomes rougher. The appropriate window size varies depending on the situation. Thus, we should take this into consideration when using this method.

Our result shows that the rotation of the covarience matrix in the four-component scattering power decomposition contributes to better understanding and interpretation of POLSAR data.

Ocean Waveheight Estimation Using Polarization Ratio of Synthetic Aperture Radar Data

Mitsunobu Sugimoto[1], **Nobuaki Shiroto**[2], **and Kazuo Ouchi**[1]

[1]Department of Computer Science, National Defense Academy, Japan
[2]Department of Civil and Environmental Engineering, National Defense Academy, Japan

Abstract— Ocean wave research by SAR has been conducted since 1970s. Although early studies have established practical methods to measure ocean wave spectra and the direction of waves from SAR images, it is still not easy to measure the waveheight, for SAR images include nonlinear modulation effects such as velocity bunching, hydrodynamic modulation and cutoff of wave spectra in azimuth direction. Several techniques have been developed for retrieving wave spectra from SAR image spectra. However, the previous methods require spectral inverse analysis which is very complex and applicable only under limited conditions.

A new technique for estimating wave height of range-traveling ocean waves by using polarization ratio of synthetic aperture radar (SAR) data is presented. Unlike the previous methods based on sacattering models such as composite surface model, the proposed method does not require any scattering models that strongly affect the estimation accuracy. Polarization ratio of the backscattered power from the ocean surface at vertical to that at horizontal polarization (VV/HH) is closely correlated to the local incidence angle which reflects local water surface slope. First, linear relationship between incidence angle and polarization ratio was derived from the trend of the entire target area. Then, the pixels on the polarization ratio image correspond to the steepest slope points were selected with reference to the HH backscatterd power image. The mean steepest slope of ocean surface was estimated from the selected pixels and the linear relation between incidence angle and polarization ratio. Finally, assuming sinusoidal waves, mean wave height was estimated from the steepest slope and mean wave length estimated from the HH image. This method was applied to each divided 3×3 km subareas and spatial distribution of wave height was estimated.

Evaluation of Typhoon-damaged Forests by PolSAR and InSAR Images

Haipeng Wang[1] **and Kazuo Ouchi**[2]

[1]Key Laboratory of Wave Scattering and Remote Sensing Information (MoE)
Fudan University, Shanghai 200433, China
[2]Department of Information Science, National Defense Academy
1-10-20, Hashirimizu, Yokosuka 239-8686, Japan

Abstract— In this study, the forests destroyed by typhoons are extracted and the damage levels are quantitatively estimated the by using high-resolution polarimetric synthetic aperture radar (PolSAR) and interferometric SAR (InSAR) data. The study area is located in Tomakomai, Hokkaido, Japan. The typhoon "Songda" (Japanese typhoon number 18) attacked the area in September 8th, 2004 and caused heavy damage over 50% in many stands. The forests map showing damaged stands from ground survey is available for comparison.

Radar cross section (RCS) approach and polarimetric decomposition analysis were employed to extract typhoon damaged area by using L-band Pi-SAR data, and the accuracies of 64.1% and 77.7% were obtained for RCS and decomposition data respectively. The experimental results do not appear in very good agreement with those observed from ground. There could be two reasons for this discrepancy. The first is that the ground-observation is subjective and does not specify damage areas within each stand, so that the ground-observation map shows "average damage" of each stand. The second is that fallen trees were still there when Pi-SAR observation was made. Half-fallen trees can be regarded as equivalent to standing trees by Pi-SAR, and they were categorized as fallen trees by ground-observation.

To improve the accuracy of the extraction, InSAR technique was considered in this study because of its ability to retrieve target height information. For the typhoon-damaged forests, the damaged level is highly related to tree height change. Even the fallen trees were not cleared, the change of their heights could be detected by single-pass InSAR, and therefore, the damage level can then be evaluated by comparing surface height difference computed from two single-pass interferograms before and after the typhoon.

ACKNOWLEDGMENT

This work was partially supported by the National Science Foundation of China under Grants 60971091 and 40901201, and in part by the Grants-in-Aid Scientific Research (C:22560436) of the Japan Society for the Promotion of Science.

Detection and Evaluation of Building Damages in Earthquake from VHR Optical and SAR Images Using Multiple Mutual Information Techniques

Tian-Lin Wang and Ya-Qiu Jin
Key Laboratory of Wave Scattering and Remote Sensing Information (MoE)
Fudan University, Shanghai 200433, China

Abstract— High-resolution and all-day all-weather synthetic aperture radar (SAR) technology is one of most important advances in satellite-borne remote sensing. SAR remote sensing, including PolSAR (polarimetric SAR) and InSAR (interfermetric SAR), has been applied to the change detection of terrain surfaces, urban and suburb study, and natural hazards monitoring etc. Its all day and all weather observation with canopy penetration can provide critical information, especially when conventional satellite-borne or air-borne optical photographing becomes not feasible under bad weather situation.

However, SAR image over certain areas in pre-event is not always available. How to automatically detect and evaluate the terrain surface change in all data fusions during the event and post-event is of great importance.

In this paper, a new approach to use both VHR (very high resolution) optical image of pre-event and a SAR image of post-event is presented for change detection and evaluation of building damages in earthquake. Based on information of optical image of pre-event, SAR images of buildings, damaged or no-damaged, are first numerically simulated by our MPA (mapping and projection approach), and are then, using the mutual information, employed for similarity analysis with real image post-event. Three models of building damage, i.e., collapsed, subsided and deformed, are proposed. Multiple mutual information (MI), including normalized MI (NMI), gradient MI (GMI) and regional MI (RMI), are applied and compared for MI detection of building damages. Based on the maximum, mean value and height deviation in NMI, GMI and RMI, the building damages can be detected and evaluated for three damage models.

As example, the optical images of Ikonos and Geo-Eye of pre-event and post-event, respectively, and SAR images of Cosmo-Skymed and Radarsat-2 of post-event during Haiti earthquake 2010 are applied in this MI experiment. Fig. 1 shows a result as follows.

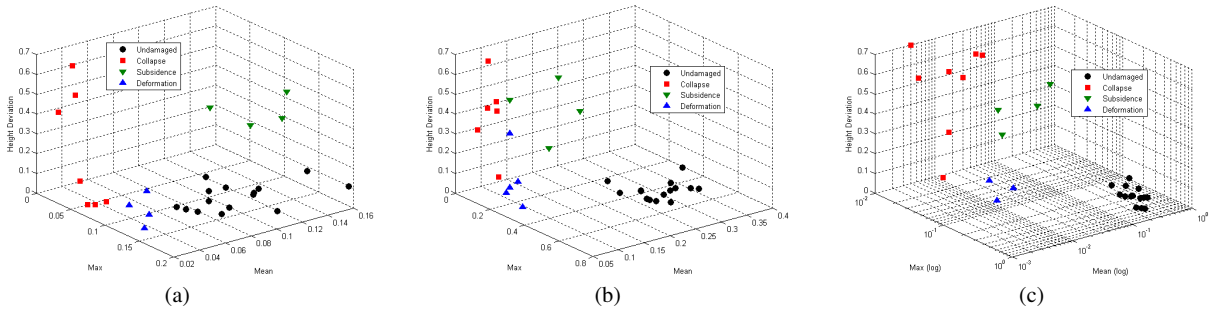

Figure 1: Detection and evaluation of building damages in Haiti earthquake.

Session 1A4a
AC Transport, Impedance Spectra, Magnetoimpedance

Magneto-impedance of [$Co_{40}Fe_{40}B_{20}$/Cu] Multilayer Films

S. U. Jen[1], **T. Y. Chou**[1], **and C. K. Lo**[2]

[1]Institute of Physics, Academia Sinica, Taipei 11529, Taiwan, R.O.C.
[2]Physics Department, National Taiwan Normal University, Taipei 11677, Taiwan, R.O.C.

Abstract— $[Co_{40}Fe_{40}B_{20}(20\text{-}z)/Cu(z)]_5$ multilayer films, with $z = 0 - 6$ nm, were deposited on glass substrates by the magnetron sputtering method at room temperature. During the film-deposition period, a dc magnetic field, $h = 40$ Oe, was applied to introduce an easy axis for each film sample. Cross-section transmission electron microscope (X-TEM) photos showed that there are sharp interfaces between neighboring layers. Ferromagnetic resonance (FMR), magneto-impedance (MI), electrical resistivity (ρ), and magnetic hysteresis loops (MHL) of these films were studied. From MHL and ρ measurements, we obtain saturation magnetization $4\pi M_s = 12.51 - 15.5$ KG, the anisotropy field $H_k = 0.022 - 0.031$ KG, and $\rho = 168 - 236$ μΩ-cm. From FMR, we can determine the uniform Kittel-mode-resonance frequency $f_{FMRK} = 1407 - 1963$ MHz. In the $h||L$ case, L is length of the film, MI spectra show the uniform Killel-mode-resonance (UKR) at $f_0 = 2081$ MHz and the non-uniform Walker-mode-resonance (NWR) at f_n, where $n = 1, 2, 3$, and 4. In the $h||w$ case, where w is width of the film, MI spectra show UKR at $F_0 = 2431$ MHz and NWR at F_n. We find f_0 and F_0 are shifted from f_{FMRK}, respectively, and within errors $f_n = F_n$. The in-plane spin waves are responsible for those relative shifts.

The Phenomenon of Positive Magnetoimpedance in $La_{0.75}Sr_{0.25}MnO_3$ PLD Film

Yifei Wang, **Hua Liu**, **and Jifan Hu**
School of Physics, State Key Laboratory for Crystal Materials
Shandong University, Jinan 250100, China

Abstract— In the present work, $La_{0.75}Sr_{0.25}MnO_3$ polycrystalline film was grown on Si (1 0 0) substrate by pulsed laser deposition. Negative magnetoimpedance $\Delta Z/Z_0 = -2.64\%$ was obtained under a low field of 500 Oe for the film with an 800°C annealing. For the film with a liquid nitrogen treatment after an 800°C annealing, a positive magnetoimpedance occurs at 10 MHz. The peak value of $\Delta Z/Z_0$ is 48.1% under 200 Oe. We suggested that the negative magnetoimpedance for the film with 800°C annealing is connected with a decrease of permeability induced by DC low fields, whereas the positive magnetoimpedance for the film with liquid-nitrogen treatment was connected with an increase of permeability with field, due to the existence of transverse anisotropy developed in the film during the liquid-nitrogen treatment process. With Machado-Rezende model on magnetic domain motion, we calculated the field dependence of transverse susceptibility χ. When a transverse anisotropy field H_A exists, the transverse susceptibility χ should have a peak at a field $H = H_A$.

Magnetoimpedance in Perovskite $La_{0.7}Sr_{0.3}MnO_3$ Ceramics

Hua Liu, **Qingfang Huang**, **and Jifan Hu**
State Key Laboratory for Crystal Materials, School of Physics
Shandong University, Jinan 250100, China

Abstract— The $La_{0.7}Sr_{0.3}MnO_3$ manganite prepared by sintering method exhibits a giant magnetoimpedance. Its AC magnetoresistance $\Delta R/R_0$ could reach -9.53%, magnetoimpedance $\Delta Z/Z$ is 3.05% at 200 kHz under a low field of 1.8 kOe at room temperature, which is more sensitive than its dc colossal magnetoresistance. With an increase of ac frequency, there is a maximum of the GMI effects. To investigate the intrinsic origin of the GMI effect, electrodynamics theory was used to simulate the frequency dependence of magnetoimpedance effect. The influences of frequency, permeability and sample thickness upon the effect of giant magnetoimpedance were investigated.

Investigation of the Electrical Properties of BCN-codoped TiO_2 Thin Film Using Impedance Spectroscopy

Ling Zhang, Yongfang Zhang, Liangguo Yan, and Fang He
School of Resources and Environment, University of Jinan, Jinan 250022, China

Abstract— Titanium dioxide has attracted much attention in the past decades. When it was doped by some elements, such as C, N, P, S and B, the conductibility will be obviously changed. In this work, the BCN-doped TiO_2 by nanostructured films was fabricated by co-deposit method. The structure was studied by X-ray diffraction measurement. The microstructure was observed by FE-SEM and XPS. The investigation of ac impedance spectra for BCN-doped TiO_2 thin film was performed. The grain resistance, resistance of grain boundary, and the capacitance in the film were determined from impedance technique.

Impedance Spectroscopy Study on the Bulk of TiO_2

Ling Zhang, Yongfang Zhang, Liangguo Yan, and Fang He
School of Resources and Environment, University of Jinan, Jinan 250022, China

Abstract— Titanium dioxide has attracted much attention in the past decades. It was extensively used in environmental interest in dye-sensitized solar cells and gas-sensing devices. Impedance spectroscopy is a very useful and important technique due to the possibility of using this method for discriminating between grain boundary capacitance (C_{gb}) and grain boundary resistance (R_{gb}) contributions. In our work, the bulk of the TiO_2 was prepared by sol-gel method. The structure was studied by X-ray diffraction measurement. The microstructure was observed by FE-SEM and thermal analysis (TG/DTA). The impedance Spectroscopy was investigated.

Giant Magnetoimpedance in Nanocrystalline Fe-Zr-B-Cu Ribbon

Ling Zhang, Yongfang Zhang, Liangguo Yan, and Fang He
School of Resources and Environment, University of Jinan, Jinan 250022, China

Abstract— The Fe-Zr-B-Cu ribbon was prepared by melt-spun technique. The ribbons were annealed at different temperature. The structure of Fe-Zr-B-Cu ribbon was studied by X-ray diffraction measurement. The α-Fe nanocrystals occur. The magnetoimpedance was observed in nanocrystalline Fe-Zr-B-Cu ribbons.

Session 1A4b
Modeling, Processing, and Inversion of EM Geophysics and Their Applications

New Scattered Potential Finite-difference Method with Anisotropic Background to Simulate Multi-component Induction Logs

Junsheng Hou, **Michael Bittar**, **Dagang Wu**, **Luis Sanmartin**, **and Baris Guner**
Halliburton Energy Services, Inc., 3000 N Sam Houston Parkway E, Houston, TX 77302, USA

Abstract— Multi-component induction (MCI), or triaxial induction logging, is the latest and most practical development of traditional induction. Compared to traditional induction, MCI logging is able to provide both horizontal and vertical formation resistivity (or their inverse, conductivity), formation dip, and strike angle in a wide range of borehole-formation environments besides traditional induction logs. The latest MCI applications showed that all additional information is highly necessary for accurate and reliable evaluation of low-resistivity, thin-bed laminated reservoirs. In general, one-dimensional (1-D) and/or three-dimensional (3-D) inversions of MCI data are required for determining the formation properties outlined above. Moreover, the MCI logs in both oil-based mud (OBM) and water-based mud borehole environments usually include significant borehole effects. Hence, the MCI measurements must be corrected for the borehole effects before they are processed for the 1-D inversion and further data interpretations.

It is easy to see that 3-D forward simulation of MCI logging measurements plays an important role in developing MCI data correction methods, understanding logging tool physics, and 3-D data inversion. Although some 3-D numerical simulation algorithms of MCI logging measurements have been studied in recent years (e.g., Wang et al. 2001, Newman et al. 2002, Davydycheva et al. 2003, Gao et al. 2004, and Hou et al. 2009), fast and accurate simulation of MCI logs in complicated 3-D borehole-formation environments is still an open topic in the electromagnetic (EM) logging domain.

The authors (2009) previously developed an effective, scattered-potentials, (SP) finite-difference (FD) algorithm for simulation of general borehole EM fields, but its accuracy and computational speed still have room for improvement. As an extension of our previous work, we have improved the previous SPFD algorithm for the numerical simulation and analysis of MCI logs in deviated/vertical wells surrounded by anisotropic formations. We implemented a transversely isotropic (TI)/anisotropic conductive medium as the simulation background in the scheme. This new SPFD algorithm is able to easily handle arbitrary formation strike, tool eccentricity, and its azimuthal angle by some coordinate transformations. In addition, the final EM fields/voltages/conductivities are more accurately calculated by using a bilinear interpolation to replace the past equal-weight arithmetic mean when logging points are not located at FD grid nodes. More benchmark exercises have been performed, and the new SPFD scheme has been validated by other independent codes. We also found that the borehole-correction (BHC) processing (Hou et al. 2010) could be used for checking the new SPFD validity in some 3-D cases if other independent 3-D solutions are not available for comparisons. After all, this high-efficiency and practical SPFD scheme is applied for simulating MCI logs of some other fully 3-D models, modeling borehole and shoulder-bed effects, and for building the look-up table data needed in the MCI BHC-algorithm developments and data processing.

REFERENCES

1. Davydycheva, S., V. Druskin, and T. Habashy, "An efficient finite-difference scheme for electromagnetic logging in 3D anisotropic inhomogeneous media," *Geophysics*, Vol. 68, 1525–1536, 2003.
2. Gao, G., C. Torres-Verdin, and S. Fang, "Fast 3D modeling of borehole induction measurement in dipping and anisotropic formations using a novel approximation technique," *Petrophysics*, Vol. 45, 335–349, 2004.
3. Hou, J. and M. Bittar, "Fast finite-difference simulation of 3D borehole EM fields using scattered potentials," *SEG Seventy-nine Annual Technical Conference*, 2009.
4. Hou, J. and M. Bittar, "Correction for the Borehole effect of multi-component array induction log data," *PIERS Proceedings*, 403–409, Cambridge, USA, July 5–8, 2010.
5. Newman, G. A. and D. L. Alumbaugh, "Three-dimensional induction logging problems, Part 2: A finite difference solution," *Geophysics*, Vol. 67, 484–491, 2002.
6. Wang, T. and S. Fang, "3-D electromagnetic anisotropy modeling using finite differences," *Geophysics*, Vol. 66, 1386–1398, 2001.

Method of Measuring the Range from the UWB Borehole Logging Tool to the Oil-water Contact

M. I. Epov[1], **V. L. Mironov**[2], **and K. V. Muzalevskiy**[2]

[1]Trofimuk Institute of Petroleum Geology and Geophysics, SB, RAS, Russia
[2]Kirensky Institute of Physics, SB, RAS, Reshetnev Siberian State Aerospace University, Russia

Abstract— The oil production technologies with the use of horizontal drilling employ geosteering borehole logging tools [1]. Recently, research and development on geosteering technologies based on borehole GPR have been actively carried out [2]. In this paper, a method was worked out to determine the distance from the borehole, horizontally drilled through oil stratum, to the oil-water contact (OWC), using the mathematical model [3, 4] for an ultra-wideband electromagnetic pulse borehole radar (BHR). We simulated pulse shape voltages at the outputs of two receiving antennas spaced along the borehole to determined their specific delay times relative to the pulse driver of the transmitting antenna. On the basis of the results of this modeling a simple formula was derived allowing to calculate the distance from the BHR to the OWC, provide the spacing between the receiving antennas and delay times are available. In modeling, the values of complex dielectric permittivity of the oil saturated rock and water saturated rock were estimated based on the dielectric model substantiated in [5].The proposed method was experimentally tested using a laboratory prototype model of the BHR with the pulse duration 2 ns and a specific laboratory set up to physically simulate the oil-water boundary environment, which had dimensions of $1.5\,\mathrm{m} \times 0.6\,\mathrm{m} \times 1.5\,\mathrm{m}$. Having not used any a priori information about permittivity values for both the oil and water saturated rocks, the error of the distance determined proved to be of 2.2%.

REFERENCES

1. Antonov, Y .N., M. I. Epov, and K. N. Kayurov, "Electromagnetic isoparametric soundings — Innovation technique for vertical and horizontal boreholes in West Siberia," *Proceedings of V International Petroleum Conference and Exhibition*, 1, New Delhi, India, January 2003.
2. Ebihara, S. and M. Kiso, "Frequency spectrum change of borehole radar signals and blind separation," *Proceedings of Tenth International Conference on Ground Penetrating Radar*, Delft, The Netherlands, June 2004.
3. Epov, M. I., V. L. Mironov, K. V. Muzalevskiy, and I. N. Yeltsov, "UWB electromagnetic borehole logging tool," *Proceedings of IGARSS*, 3565–3567, Honolulu, USA, July 2010.
4. Komarov, S. A. and K. V. Muzalevskiy, "Method of discrete sources in the problem of pulse excitation of a vibrator in a layered medium," *Russian Physics Journal*, Vol. 50, No. 10, 1068–1070, 2007.
5. Epov, M. I., V. L. Mironov, S. A. Komarov, and K. V. Muzalevsky, "Nanosecond electromagnetic sounding of a fluid-saturated layered formation," *Russian Geology and Geophysics*, Vol. 48, No. 12, 1054–1060, 2007.

Modified Diagonal Tensor Approximation Algorithm for Three-dimensional GPR Forward Scattering

Yueqin Huang[1, 2], **Jianzhong Zhang**[1], **and Qing Huo Liu**[2]

[1]College of Marine Geoscience, Ocean University of China, China
[2]Department of Electrical and Computer Engineering, Duke University, USA

Abstract— The diagonal tensor approximation (DTA) method has been proved to be valid for high-contrast EM problems [1], thus can be applied to simulate GPR forward scattering. However, due to the iterative process to calculate the diagonal tensor coefficients (DTC), the computational efficiency of the DTA method is severely limited.

To improve the efficiency, a further approximation is introduced by simplifying the nonlinear iterative process of DTC calculation into a linear step. The detailed modification is implemented as follows. Firstly, we make use of the closed-form expression of the first iteration, which contributes most to the algorithm accuracy, for DTC calculation and to guarantee the effectiveness of the method. Secondly, consider a wideband GPR system. The frequency dependence of the DTC can be removed by approximating the coefficients at different frequencies with those evaluated at the center frequency. With the linear and frequency independent properties in modified DTC calculation, the efficiency of the DTA method can be greatly improved. The corresponding algorithm is separately deduced in both space and spectrum domains.

As for the algorithm described in spectrum domain, the dyadic Green's function is included for deduction. One will encounter several singularity points when real frequencies are used in the computation of the dyadic Green's function. To solve this problem, complex frequencies are used by adding a fixed value as the imaginary part. Besides, the non-uniform FFT [2] method is applied for fast implementation.

Several numerical results will be presented to illustrate the effectiveness of the proposed method for GPR forward scattering.

REFERENCES

1. Song, L.-P. and Q. H. Liu, "A new approximation to three-dimensional electromagnetic scattering," *IEEE Trans. Geosci. Remote Sensing Lett.*, Vol. 2, No. 2, 238–242, 2005.
2. Liu, Q. H. and N. Nguyen, "An accurate algorithm for nonuniform fast Fourier transform (NUFFT's)," *IEEE Trans. Microwave and Guided Wave Lett.*, Vol. 8, No. 1, 18–20, 1998.

Fast Three-dimensional GPR Backward Scattering Based on Wideband Diagonal Tensor Approximation

Yueqin Huang[1, 2], **Jianzhong Zhang**[1], **and Qing Huo Liu**[2]

[1]College of Marine Geoscience, Ocean University of China, China
[2]Department of Electrical and Computer Engineering, Duke University, USA

Abstract— With emphasis on environmental and engineering applications of GPR technique, it has become important to implement and evaluate methods for three-dimensional GPR backward/inverse scattering. Both the linear and the nonlinear approaches at present are valid for GPR inversion, but with different characteristics. The linear inversion method is based on Born approximation [1], which approximate the total EM field by the incident field inside the computational domain. It is fast and easy, but only performs well for low-contrast problems. The nonlinear inversion methods usually contain an iterative process so that the predefined cost function is a minimum. This kind of methods can provide good results for general problems, but is time-consuming, especially for three-dimensional cases. In our work, we aim to extend the applicability of the efficient Born approximation method to high-contrast problems.

With the developed Born approximation method which is called the diagonal tensor approximation [2], a two-step scheme for GPR inversion is proposed. In the first step, for simple implementation, we further introduce the wideband approximation where the diagonal scattering coefficients is evaluated by a specified value calculated at the center frequency. Thus the first step is a linear process and can be calculated with the efficient NUFFT method [3]. It is noting that the first step is essentially the traditional Born approximation inversion method. The second step is an emendatory process of the output of the first step. The equations in the second step can be solved with the BiCGS-FFT method for fast calculation.

Several numerical results will be presented to show the improvement of our proposed method for GPR backward scattering.

REFERENCES

1. Hansen, T. B. and P. M. Johansen, "Inversion scheme for ground penetrating radar that takes into account the planar air-soil interface," *IEEE Trans. Geosci. Remote Sensing Lett.*, Vol. 38, No. 1, 496–506, 2000.
2. Song, L.-P. and Q. H. Liu, "A new approximation to three-dimensional electromagnetic scattering," *IEEE Trans. Geosci. Remote Sensing Lett.*, Vol. 2, No. 2, 238–242, 2005.
3. Liu, Q. H. and N. Nguyen, "An accurate algorithm for nonuniform fast Fourier transform (NUFFT's)," *IEEE Trans. Microwave and Guided Wave Lett.*, Vol. 8, No. 1, 18–20, 1998.

UWB Borehole Logging Tool to Explore the Electrical and Structural Properties of Near-wellbore Fluid-filled Areas

M. I. Epov[1], **V. L. Mironov**[2], **K. V. Muzalevskiy**[2], **and I. N. Yeltsov**[1]

[1]Trofimuk Institute of Petroleum Geology and Geophysics SB RAS, the Russian Federation
[2]Kirensky Institute of Physics, SB RAS
Reshetnev Siberian State Aerospace University, the Russian Federation

Abstract— Currently, there is a search for new technologies suitable to explore the electrical and structural properties of a spatially inhomogeneous near-wellbore area running through the fluid-filled rock [1]. Petrophysical interpretation of the data attained with these technologies allows to derive the oil saturation factor, porosity, permeability, and fluid mobility of oil in the fluid-filled rock. At present, some technologies of this kind, which employ the electromagnetic sounding at frequencies from 1 kHz to several MHz, are widely used in the oil mining industries [2]. However, as shown in [3], some promising methods for sounding the near-wellbore area are expected to evolve from applying for this purpose the ultra-wideband (UWB) electromagnetic pulses with nanoseconds time duration. In this paper, we studied the feasibility for the UWB electromagnetic logging tool (UBELT) considered in [4] to be applied for detecting the size of the zone of penetration of mud filtrate in the parent rock of oil and gas reservoir and measuring the dielectric spectra of this zone. To this end, with the use of the mathematical model for the UBELT worked out in [4], there were studied the amplitude, shape, and time delay for the pulses at the output of receiving antennas, spaced along the borehole, as a function of the ranges between the receiving and transmitting antennas, as well as the time duration and shape of the pulses at the input of the transmitting antenna. Such computer simulations were carried out to cover a number of realistic radial profiles for the petrophysical properties of the near-wellbore area. In this case, the radial profiles of respective complex dielectric constant were calculated on the basis of the dielectric model substantiated in [5], provided the temperature, salinity of brine water, and the petrophysical parameters of the near-wellbore area are known. There were studied correlations between the time shape and delay of the sounding pulses on the one hand and the petrophysical parameters of the near-wellbore area on the other hand. The complex dielectric spectra in the near-wellbore area were also shown to be measured with the use of the UBELT proposed.

REFERENCES

1. http://www.slb.com/ds.aspx.
2. Antonov, Y. N., M. I. Epov, and K. N. Kayurov, "Electromagnetic isoparametric soundings — Innovation technique for vertical and horizontal boreholes in West Siberia," *Proceedings of V International Petroleum Conference and Exhibition*, 1, New Delhi, India, January 2003.
3. Liu, S. and M. Sato, "Electromagnetic logging technique based on borehole radar," *IEEE Transactions on Geoscience and Remote Sensing*, Vol. 40, No. 9, 2083–2092, 2002.
4. Epov, M. I., V. L. Mironov, K. V. Muzalevskiy, and I. N. Yeltsov, "UWB electromagnetic borehole logging tool," *Proceedings of IGARSS*, 3565–3567, Honolulu, USA, July 2010.
5. Epov, M. I., V. L. Mironov, S. A. Komarov, and K. V. Muzalevsky, "Nanosecond electromagnetic sounding of a fluid-saturated layered formation," *Russian Geology and Geophysics*, Vol. 48, No. 12, 1054–1060, 2007.

Session 1A5
Extended/Unconventional Electromagnetic Theory, EHD (Electro-hydrodynamics)/EMHD (Electro-magneto-hydrodynamics), and Electro-biology

Charge Continuity Equation in the Adjoint Fields

Zi-Hua Weng
School of Physics and Mechanical & Electrical Engineering
Xiamen University, Xiamen 361005, China

Abstract— The algebra of quaternions can be used to describe the scalar invariants and some conservation laws in the gravitational field. Meanwhile the algebra of octonions can be used to demonstrate the scalar invariants in the case for coexistence of the electromagnetic field and gravitational field, including the conservation of mass and the conservation of charge. Those results are only dealt with the quaternion operator, but the octonion operator. In the octonion space, the operator should be extended from the quaternion operator to the octonion operator.

Making use of the octonion operator, the gravitational field demonstrated by the octonion operator will generate an adjoint field. The source of adjoint field includes the adjoint mass and the adjoint linear momentum. In general, the adjoint mass and its movement can not be observed by the conventional experiments. However, when the adjoint mass is combined with the ordinary mass to become one sort of particles, their movements will be accompanied by some effects. Moreover, this kind of adjoint mass may influence the distribution of electric charge.

By means of the octonion operator, the electromagnetic field described by the octonion operator may originate its adjoint field. The source of adjoint field includes the adjoint charge and the adjoint electric current. Similarly the adjoint charge and its movement can not be observed by the usual tests. Nevertheless, when the adjoint charge is combined with the ordinary charge to become the charged particles, their movements will be consorted with some effects. And this kind of adjoint charge may be considered as one kind of candidate for the dark matter.

The paper discusses the impact of adjoint fields on the conservation laws in the gravitational and electromagnetic fields, by means of the features of octonions. When the adjoint field can not be neglected, it will cause the predictions to departure slightly from the known conservation laws, which include the mass continuity equation and the charge continuity equation. The adjoint field of electromagnetic field has an effect on the mass continuity equation, and that of gravitational field on the charge continuity equation. The study claims that the adjoint fields may exert an influence on some conservation laws in the gravitational and electromagnetic fields.

ACKNOWLEDGMENT

The author is grateful for the financial support from the National Natural Science Foundation of China under grant number 60677039.

A Generalized Variational Principle of Linear Elastic Materials with Voids

Ji-Huan He
National Engineering Laboratory for Modern Silk, College of Textile and Engineering
Soochow University, 199 Ren-ai Road, Suzhou 215123, China

Abstract— Governing equations for linear elastodynamics analysis of material with voids are reviewed and then cast in the framework of variational statement. Starting from a trial-functional with unknown functions, a family of variational principles is derived through a systematic procedure, including Hellinger-Reissner-like principle and Hu-Washizu-like principle.

Main Result: We write down a general variational principle

$$J(u_i, \sigma_{ij}, \varepsilon_{ij}, \varphi, h_i, g) = \int_0^t \iiint_\Omega L \mathrm{d}\Omega \mathrm{d}t \tag{1}$$

where

$$\begin{aligned} L &= \frac{1}{2}\rho u_i^{'2} + u_i(\sigma_{ij,j} + \rho \bar{f}_i) + \frac{1}{2}\rho k \varphi^{'2} + \varphi(h_{i,i} + g + \rho l) + \varepsilon_{ij}\sigma_{ij} \\ &\quad - \left(\frac{1}{2}\varepsilon_{ij}C_{ijkl}\varepsilon_{kl} + \frac{1}{\xi}\varepsilon_{ij}\beta_{ij}g - \frac{1}{2\xi}\varepsilon_{ij}\beta_{ij}\beta_{mn}\varepsilon_{mn}\right) + \frac{1}{2\alpha}h_i h_i - \frac{1}{2\xi}g^2. \end{aligned} \tag{2}$$

Making the above functional stationary, we can obtain equations of motion; constitutive equations; and geometrical equations of the problem.

REFERENCES

1. Nunziato, J. W. and S. C. Cowin, "A nonlinear theory of elastic materials with voids," *Arch. Rational Mech. Anal.*, Vol. 72, 175–201, 1979.
2. Cowin, S. C. and J. W. Nunziato, "Linear elastic materials with voids," *J. Elasticity,* Vol. 13, 125–147, 1983.
3. Clarletta, M. and A. Scalia, "On uniqueness and reciprocity in linear theroelasticity of materials with voids," *J. Elasticity*, Vol. 32, 1–17, 1993.
4. Dhaliwal, R. S. and J. Wang, "Domain of influence theorem in the theory of elastic materials with voids," *Int. J. Engineering Science,* Vol. 32, No. 11, 1823–1828, 1994.
5. Iesan, D., "A theory of thermoelastic materials with voids," *Acta Mech.,* Vol. 60, 67–89, 1986.
6. He, J. H., "Coupled variational principles of piezoelectricity," *Int. J. Engineering Sciences*, Vol. 39, No. 3, 323–341, 2000.
7. He, J. H., "Variational theory for linear magneto-electro-elasticity," *International Journal of Non-Linear Science and Numerical Simulation*, Vol. 2, No. 4, 309–316, 2001.

Using Numerical Analysis for NMR Coils Optimalization

D. Nespor, K. Bartusek, and P. Fiala
Department of Theoretical and Experimental Electrical Engineering
Brno University of Technology, Kolejni 2906/4, Brno 612 00, Czech Republic

Abstract— RF coils create a B_1 field which rotates the net magnetization in a pulse sequence. They also detect the transverse magnetization as it precesses in the XY plane. Most RF coils on NMR systems are of the saddle coil design and act as a transmitter of the B_1 field and receiver of RF energy from the sample. We can find one or more RF coils in a probe.

Each of these RF coils has to resonate, it means they must efficiently store energy, at the Larmor frequency of the nucleus being examined with the NMR system. All NMR coils are composed of an inductor, or inductive elements and a set of capacitive elements. The resonant frequency f_r of an RF coil is determined by the inductance and capacitance of the inductor-capacitor circuit.

RF coils which are used in NMR systems need to be tuned for the specific sample being studied. An RF coil has a bandwidth or specific range of frequencies at which it resonates. When a sample is placed in the RF coil the conductivity and dielectric constant of the sample affect the resonance frequency. If this frequency is different from the resonance frequency of the studied nucleus, the coil will not efficiently set up the B_1 field and will not efficiently detect the signal from the sample.

The B_1 field of an RF coil must be perpendicular to the B_o magnetic field. Another requirement for the RF coil in NMR system is that the B_1 field needs to be homogeneous over the volume of the sample. In case of low homogeneity, spins will be rotating by a distribution of rotation angles and obtained spectra will be distorted [1, 2].

Paper contains a description of B_1 field homogeneity computing. Basic model is a simply planar one-turn coil. This model is solved analytically and numerically [3, 4]. It was made a measurement in NMR system too. All results were compared. Hence, the correctness was verified. The next step was computing and size optimalization for maximum B_1 field homogeneity of the saddle coils. The final step was special shaped coils computing.

ACKNOWLEDGMENT

The work described in the paper was financially supported by the research project GA102/09/0314, research plan MSM 0021630513 and project of the BUT Grant Agency FEKT-S-10-13.

REFERENCES

1. Mispelter, J., M. Lupu, and A. Briguet, *NMR Probeheads for Biophysical and Biomedical Experiments*, Imperial College Press, 57 Shelton Street, Convent Garden London WC2H 9HE, 2006, ISBN 1-86094-637-2.
2. Brown, M. A. and R. C. Semelka, *MRI Basic Principles and Applications*, Printed in the United States of America, 2010, ISMB 978-0-470-50098-9.
3. Stratton, J. A., *Teorie Elektromagnetického Pole*, Státní nakladatelství technické literatury v Praze, 1961, Tipe number L25a-D-5III/5397.
4. Dědek, L. and J. Dědková, *Elektromagnetismus*, Vysoké uení technické v Brně, Published by VUTIUM, Kounicova 67a, 1996, ISBN 80-214-1106-6.

Limits to the Measurement of the Magnetic Susceptibility Using NMR Method

P. Marcon[1], **K. Bartusek**[2], **and M. Cap**[1]

[1]Department of Theoretical and Experimental Electrical Engineering
Brno University of Technology, Kolejni 2906/4, Brno 612 00, Czech Republic
[2]Institute of Scientific Instruments, Academy of Sciences of the Czech Republic
Kralovopolska 147, Brno 612 64, Czech Republic

Abstract— The paper deals with modeling of magnetic induction in non-ferromagnetic substances. For finding of the limits of the NMR magnetic susceptibility measurement method was set up a model in COMSOL environment. Results of the COMSOL model were processed in MATLAB. Non-ferromagnetic cylinders were placed in the center of the cube shaped static magnetic field $B_0 = 4.7\,\mathrm{T}$. Material of the specimen react with the static magnetic field and create a local changes of this field close to the specimen surface. Changes of the static magnetic field hold the possibilities to calculate the magnetic susceptibility of the used material. As an input for magnetic susceptibility calculation is possible to use 1D or 2D results of magnetic field modeling. More about this method you can see in [1] and [2].

Nevertheless, mentioned methods in [1] and [2] have some limitations. In this article will be discuss what under conditions is possible to use 1D and 2D method. Primarily, we were focused on possibilities of the magnetic susceptibility calculation from any cut of the specimen. Consequently, the influence of the relation between specimen length and neighborhood dimensions on the accuracy of the magnetic susceptibility calculation. As a specimen materials were used the varied size aluminum and copper cylinders. Examined limits of the NMR method of magnetic susceptibility measurement are very important for next improvement of this method.

REFERENCES

1. Bartusek, K., M. Cap, P. Marcon, and J. Mikulka, "Magnetic susceptibility modeling using ANSYS," *Progress In Electromagnetics Research Symposium*, Marrakesh, Morocco, March 20–23, 2011.
2. Steinbauer, M., *Mereni Magneticke Susceptibility Technikami Tomografie Magneticke Resonance*, VUT v Brne, FEKT, Brno, 2006.
3. Vladingerbroek, M. T. and J. A. Den Boer, *Magnetic Resonance Imaging*, Springer-Verlag, Heidelberg, Germany, 1999, ISBN 3-540-64877-1.
4. Bartusek, K., Z. Dokoupil, and E. Gescheidtova, "Mapping of magnetic field around small coils using the magnetic resonance method," *Measurement Science and Technology*, Vol. 18, 2223–2230, 2007.
5. Bartusek, K., Z. Dokoupil, and E. Gescheidtova, "Magnetic field mapping around metal implants using an asymmetric spin-echo MRI sequence," *Measurement Science and Technology*, Vol. 17, No. 12, 3293–3300, 2006.
6. Fiala, P., "Finite element method analysis of a magnetic field inside a microwave pulsed generator," *2nd European Symposium on Non-lethal Weapons*, Ettlingen, SRN, May 13–15, 2003.

Sensitivity of the Diffusion Coefficients Measurement to Gradient Field Changes

P. Marcon[1], **K. Bartusek**[2], **and M. Cap**[1]

[1]Department of Theoretical and Experimental Electrical Engineering
Brno University of Technology, Kolejni 2906/4, Brn 612 00o, Czech Republic
[2]Institute of Scientific Instruments, Academy of Sciences of the Czech Republic
Kralovopolska 147, Brno 612 64, Czech Republic

Abstract— The paper deals accuracy of the diffusion coefficient measurement. Diffusion coefficients were measured by the pulse filed gradient spin echo (PFGSE) method. Tube with deionized water was used as a sample for measurement of the tomograph. *b*-factor value as well as the diffusion coefficients of the measured sample is dependent on the gradient field. As a result is presented relationship between diffusion measurement accuracy and changes of the magnetic field. In this article is presented graph of this dependence. Due to this course is possible to configure the gradient field and measure the diffusion coefficient with higher accuracy.

The experiments were carried out on an MR tomograph system 4.7 T/120 mm (i.e., 200 MHz for 1H nuclei). Actively shielded gradient coils yield a maximum gradient field magnitude of 180 mT/m. As a specimen was used the injection syringe filled by sulphate water solution. The data measured were processed in the MAREVISI and MATLAB programs.

REFERENCES

1. Johansen-Berg, H. and T. E. J. Behrens, *Diffusion MRI: From Quantitative Measurement to in vivo Neuroanatomy*, Elsevier, China, 2009, ISBN 978-0-12-374709-9.
2. Bartusek, K. and E. Gescheidtova, "MR Measurement technique of rapidly switched gradient magnetic fields in MR tomography," *Applied Magnetic Resonance*, (IF 0,665), Vol. 29, No. 12, 675–686, 2006, ISSN 0937-9347.
3. Mansfield, P. and B. Chapman, "Active magnetic screening of gradient coils in NMR imaging," *Journal of Magnetic Resonance*, Vol. 66, 1986.
4. Bartusek, K., *Special Methods of Diffusion Coefficients Measurement by Use of Nuclear Magnetic Resonance*, Inaugural thesis, Brno Univeristy of Technology, Brno, 2007, ISSN 1213-418X.
5. Bartusek, K. and E. Gescheidtova, "MRI method of diffusion measurement in heterogeneous materials," *Measurement Science and Technology*, (IF 1,297), Vol. 19, 2008, ISSN 0957-0233.
6. Gescheidtova, E., R. Kubasek, Z. Smekal, and K. Bartusek, "Digital filter banks in MR measurement of gradient magnetic fields," *Applied Magnetic Resonance*, (IF 0,706), Vol. 33, 399–417, 2008, ISSN 0937-9347.
7. Bartusek, K. and E. Gescheidtova, "Testing the quality of magnetic gradient fields for studying self-diffusion processes in biological specimens by magnetic resonance methods," *Measurement Science and Technology*, (IF1,118), Vol. 17, 2256–2262, 2006, ISSN 0957-0233.
8. Mikulka, J., K. Bartusek, and E. Gescheidtova, "Perimeter measurement of spruce needles profile using MRI," *PIERS Proceedings*, 1128–1131, Beijing, China, March 23–27, 2009.
9. Marcon, P. and K. Bartusek, "Errors in diffusion coefficients measurement," *PIERS Proceedings*, 1035–1039, Cambridge, USA, July 5–8, 2010.

Evaluation of Errors in Manual Image Processing

J. Mikulka, **E. Gescheidtová**, **and K. Bartušek**
Department of Theoretical and Experimental Electrical Engineering
Brno University of Technology, Kolejni 4, Brno 612 00, Czech Republic

Abstract— Manual image processing is still the most used approach for evaluating of various parameters and properties of observed objects. This approach has advantages and disadvantages. The main advantage is direct use of processing person knowledge. The main disadvantage is time demand and in case of use of improper approach is high error rate.

The article describes kinds of errors which appears in biomedical image processing and possibilities of their evaluation. The research is focused mainly on evaluation of number of objects in image (cells, neurons, tissues). The issue of manual segmentation is also described within the meaning of bounding interesting areas for further processing (area evaluation, visualization).

In the first case (counting the objects) a tiredness and decreased concentration is expected in long-term manual image processing and thus increasing of error rate. In case of manual segmentation and bounding searched area adds to tiredness effect the error of inaccurate boundary determination.

There are described traditional methods of image processing in medical practice. Furthermore, the methodology of automatic and semiautomatic image processing is proposed. Impacts to speed, accuracy and entire efficiency are discussed.

Multiple Reflection from Layered Heterogeneous Medium

R. Kadlec, E. Kroutilová, and P. Fiala
Department of Theoretical and Experimental Electrical Engineering
Brno University of Technology, Kolejní 2906/4, Brno 612 00, Czech Republic

Abstract— The paper presents the problem of algorithm design of propagation, reflection and refraction of the electromagnetic waves on a layered medium. Analytic solution of this issue is very intricate and time demanding. This method is suitable for specific purposes of detail analysis of general issue. Numerical methods are more suitable for analysis of the reflection and the refraction of electromagnetic waves on layered heterogeneous medium. Fundamental law for analysis of the reflection and the refraction of electromagnetic waves on boundary line between two materials are Snell's law for electromagnetic waves. The paper deals with problem of complex angle of refraction in losing medium. In non-lossy environment is interpretation of Fresnel relations a Snell's law is simple. For a layered heterogeneous medium, an algorithm was prepared for the reflection on several layers in MatLab program environment. Method describing in this paper are suitable for analysis of beam refraction to the other side from the perpendicular line during the passage through the interface. This phenomenon is occurring in metamaterials. This is material with negative parameters constitute a group of media that possesses a negative value of relative permittivity or relative permeability or both.

ACKNOWLEDGMENT

The research described in the paper was financially supported by the research program MSM 0021630516 and research plan MSM 0021630513, Ministry of Defence of the CR, Ministry of Industry and Trade of the CR (Diagnostics of Superfast Objects for Safety Testing, FR-TI1/368), Czech Science Foundation (102/09/0314) and project of the BUT Grant Agency FEKT-S-10-13.

REFERENCES

1. Dedek, L. and J. Dedková, *Elektromagnetismus. 2*, 232, VITIUM, Brno, 2000, ISBN 80-214-1548-7.
2. Moss, C., *Numerical Metods for Electromagnetic Wave Propagation and Scattering in Comlex Media*, 240, 2004, available from http://portal.acm.org/citation.cfm?id=1023429.
3. Stratton, J. A., *Teorie Elektromagnetického Pole*, STNL, Praha, 1961.
4. Fiala, P., "Finite element method analysis of a magnetic field inside a microwave pulsed generator," *2nd European Symposium on Non-Lethal Weapons*, SRN, Ettlingen, May 13–15, 2003.
5. Fiala, P., R. Kadlec, P. Drexler, and P. Dohnal, "Tuned periodical structures — Model, experiments in thz band applied in safety application," *PIERS Proceedings*, 1022–1026, Cambridge, USA, July 5–8, 2010.

Stochastic Models of Electrodynamics

Pavel Fiala and Martin Friedl
Faculty of Electrical Engineering and Communication
Department of Theoretical and Experimental Electrical Engineering
Brno University of Technology, Kolejní 2906/4, Brno 612 00, Czech Republic

Abstract— The article presents the transient task numerical modelling of the electrodynamic process in gas with a pulsed electric field. Within the numerical model, non-linear electric properties of gas are respected and, by the help of a non-deterministic stochastic model, the possibility of an electric charge generation is analyzed. The authors examine the problem of electric charge probability evaluation; on the basis of testing the tip-tip disposition, a comparison of individual instances of the probability function evaluation is provided.

ACKNOWLEDGMENT

The funding of the project was supported by the Ministry of Industry and Trade of the CR (Diagnostics of superfast objects for safety testing, FR-TI1/368), Ministry of Education, Youth and Sports of the CR, and by institutional resources from the related Research Design — Electronic Communication Systems and New Generation Technologies (ELKOM) MSM0021630513, GAČR 102/09/0314.

REFERENCES

1. Fiala, P., "Finite element method analysis of a magnetic field inside a microwave pulsed generator," *2nd European Symposium on Non-Lethal Weapons*, SRN, Ettlingen, May 13–15, 2003.
2. Fiala, P. and P. Drexler, "Measurement methods of pulsed power generators," *4th European Symposium on Non-Lethal Weapons*, SRN, Ettlingen, May 21–23, 2007.
3. Stratton, J. A., *Teorie Elektromagnetického Pole*, STNL, Praha, 1961.

EMHD Models Respecting Relativistic Processes of Trivial Geometries

Pavel Fiala, **Zoltán Szabó**, **and Martin Friedl**
Faculty of Electrical Engineering and Communication
Department of Theoretical and Experimental Electrical Engineering
Brno University of Technology, Kolejní 2906/4, Brno 612 00, Czech Republic

Abstract— The authors report on the numerical modelling of a flying object dynamic task with a view to the evaluation of effects emerging on the flying object surface. An exact evaluation of magnetic field distribution in the configuration of the sensor enables us to determine correctly the instantaneous values of the object movement parameters. Thus, it is possible to improve the measurement of characteristics of fast moving objects in a given medium (air or fluid).

From the formal point of view, several perspectives are utilized to facilitate the topic analysis, and these aspects of evaluation can be identified within the regions of legal ethics, medicine, or military tactics as well as engineering and technology. In relation to the problem of protection against undesirable phenomena like terrorism, it is necessary to mention the fact that there exists long-term research focused on the institution of NATO and its member armies; this research mainly pertains to the determination and practical use of non-lethal or wounding means and methods in all constituent parts of protection and defense. The armies of European countries participate systematically in the process of non-lethal weapons development and integration within the respective armament systems.

ACKNOWLEDGMENT

The funding of the project was supported by Ministry of Industry and Trade of the CR (Diagnostics of superfast objects for safety testing, FR-TI1/368), Ministry of Education, Youth and Sports of the CR, and by instiutional resources from the related Research Design — Electronic Communication Systems and New Generation Technologies (ELKOM) MSM0021630513, GAČR 102/09/0314.

REFERENCES

1. Krüger-Sprengel, F., "Legal adaptation of non-lethal capabilities in new conflict scenarious," *2nd European Symposium on Non-Lethal Weapons*, SRN, Ettlingen, May 13–15, 2003.
2. Fiala, P., "Finite element method analysis of a magnetic field inside a microwave pulsed generator," *2nd European Symposium on Non-Lethal Weapons*, SRN, Ettlingen, May 13–15, 2003.
3. Fiala, P. and P. Drexler, "Measurement methods of pulsed power generators," *4th European Symposium on Non-Lethal Weapons*, SRN, Ettlingen, May 21–23, 2007.
4. Groll, J. H. and C. Pick, "Assessment of Non-Lethal-Weapons (NLW)," *4th European Symposium on Non-Lethal Weapons*, SRN, Ettlingen, May 21–23, 2007.
5. Stratton, J. A., *Teorie Elektromagnetického Pole*, STNL, Praha, 1961.

A Solar Element with Controlled Efficiency

P. Fiala and D. Nešpor
Faculty of Electrical Engineering and Communication
Department of Theoretical and Experimental Electrical Engineering
Brno University of Technology, Kolejní 2906/4, Brno 612 00, Czech Republic

Abstract— We present the numerical modelling of a periodic motive structure and, utilizing the properties of metamaterials, propose the model of an elementary solar cell which is capable of exploiting a high rate of solar radiation for a selected region of the Earth. The process of solar radiation exploitation is not based on the principle of the photoelectric effect in semiconductors.

ACKNOWLEDGMENT

The funding of the project was supported by Ministry of Industry and Trade of the CR (Diagnostics of superfast objects for safety testing, FR-TI1/368), Ministry of Education, Youth and Sports of the CR, and by institutional resources from the Research Design — Electronic Communication Systems and New Generation Technologies (ELKOM) MSM0021630513, GAČR 102/09/0314.

REFERENCES

1. Fiala, P., "Finite element method analysis of a magnetic field inside a microwave pulsed generator," *2nd European Symposium on Non-lethal Weapons*, SRN, Ettlingen, May 13–15, 2003.
2. Fiala, P. and P. Drexler, "Measurement methods of pulsed power generators," *4nd European Symposium on Non-lethal Weapons*, SRN, Ettlingen, May 21–23, 2007.
3. Stratton, J. A., *Teorie Elektromagnetického Pole*, STNL, Praha, 1961.

Fusion of the T1, T2 Weighted and Perfusion Weighted Images for Peritumoral Region Evaluation

M. Cap[1], **E. Gescheidtova**[1], **P. Marcon**[1], **K. Bartusek**[1, 2], **and A. Sprlakova**[3]

[1]Department of Theoretical and Experimental Electrical Engineering
Brno University of Technology, Kolejni 2906/4, 612 00 Brno, Czech Republic
[2]Institute of Scientific Instruments, Academy of Sciences of the Czech Republic
Kralovopolska 147, 612 64 Brno, Czech Republic
[3]Faculty Hospital Brno, Department of Radiology, Jihlavska 20, 625 00 Brno, Czech Republic

Abstract— Differential diagnosis of a high-grade glioms and solitary metastases is in some cases inconclusive. Investigators in several studies have demonstrated that in perfusion MRI (magnetic resonance imaging) of high-grade glioms and solitary metastases are differences. Analysis of the peritumoral region could be more useful then the analysis of the tumour itself. Precise evaluation of these differences in peritumoral region gives as a chance for tumour diagnosis.

Differential diagnosis of a high-grade glioms and solitary metastases is in some cases inconclusive. Investigators in several studies have demonstrated that in perfusion MRI (magnetic resonance imaging) of high-grade glioms and solitary metastases are differences. Analysis of the peritumoral region could be more useful then the analysis of the tumour itself. Precise evaluation of these differences in peritumoral region gives as a chance for tumour diagnosis.

Differential diagnosis of the high-grade glioms and solitary metastases in the peritumoral region is highly dependent on the precise match of T1W, T2W and the PWI images. The designed method promises more accurate diagnosis and the best type of therapy as a consequence.

REFERENCES

1. Law, M., S. Cha, E. A. Knopp, G. Johnson, J. Arnett, and A. W. Litt, "High-grade gliomas and solitary metastases: Differentiation by using perfusion and proton spectroscopic MR imaging," *Radiology*, 715–21, 2002.
2. Hakyemez, B., C. Erdogan, N. Bolca, N. Yildirim, G. Gokalp, and M. Parlak, "Evaluation of different cerebral mass lesions by perfusion-weighted MR imaging," *J. Magn. Reson. Imaging*, 817–24, 2006.
3. Rollin, N., J. Guyotat, N. Streichenberger, J. Honnorat, V. A. Tran Minh, and F. Cotton, "Clinical relevance of diffusion and perfusion magnetic resonance imaging in assessing intra-axial brain tumors," *Neuroradiology*, 150–9, 2006.
4. Cianfoni, A., R. Calandrelli, P. De Bonis, A. Pompucci, L. Lauriola, and C. Colosimo, "Nocardia brain abscess mimicking high-grade necrotic tumor on perfusion MRI," *Journal of Clinical Neuroscience*, Vol. 17, No. 8, 1080–1082, 2010.
5. Mikulka, J., E. Gescheidtova, and K. Bartusek, "Modem edge-based and region-based segmentation methods," *32nd International Conference on Telecommunications and Signal Processing*, 89–91, Dunakiliti, Hungary, 2009.

Session 1P1a
Fiber Micro/Nano-Photonic Components and Fiber Sensors

Thermal Properties of Light-controllable Photonic Liquid Crystal Fibers

Jia-Hong Liou, **Ta Lin**, **and Chin-Ping Yu**
Department of Photonics, National Sun Yat-Sen University, Kaohsiung 80424, Taiwan, R.O.C.

Abstract— Optical properties of photonic crystal fibers (PCFs) are hard to be tuned for the fixed geometry after the fabrication. To achieve thermally or electrically modulation in PCFs, one can infiltrate liquid crystals into PCFs to form photonic liquid crystal fibers (PLCFs). Recently, light-controllable PLCFs have been proposed by filling a photoresponsive liquid crystal mixture consisting of nematic E7 liquid crystal and photochromatic 4-methoxyazobenzene (4MAB) into PCF structures. However, the temperature effects on the photoresponsive PLCFs have not been studied yet. To measure the thermal characteristics of the PLCFs, we placed a photoresponsive PLCF on a temperature controller to vary the ambient temperature. After the PLCF was irradiated by a blue laser for 25 seconds, the transmission spectrum was collected by an optical spectrum analyzer (OSA). At room temperature, the transmission spectrum had a red shift after blue-laser irradiation due to the anisotropic LC mixture was switched to the isotropic phase, which was resulted from the photo-induced isomerization of 4MAB. If we raised the temperature from 26.4°C to 38.3°C, the viscosity coefficient of the liquid crystal was reduced and the phase structure of the LC mixture can be rapidly changed from anisotropic to isotropic by the blue laser. However, when the operation temperature reached 42.5°C, which was the phase transition point of the photoresponsive LC mixture, the phase structure of the LC mixture became isotropic before irradiation and the transmission spectrum cannot be changed by blue-laser exposure. The measured results show that the response time of the light-controllable PLCFs can be reduced by raising the operation temperature near the phase transition point of the photoresponsive LC mixture.

Design Approach of Liquid-filled Dispersion-flattened Photonic Crystal Fibers

Jui-Ming Hsu[1, 2] **and Der-Li Ye**[1]

[1]Department of Electro-Optical Engineering, National United University, Miaoli 360, Taiwan, R.O.C.
[2]Optoelectronics Research Center, National United University, Miaoli 360, Taiwan, R.O.C.

Abstract— We propose liquid-filled dispersion-flattened photonic crystal fibers (LF-DFPCFs) based on an available photonic crystal fiber (PCF) LMA-5, which is a product of NKT Photonics. Instead of changing the geometric structure, we fill specific liquids with different index into some cladding-holes of the PCF to design a broadband zero-dispersion PCF. As everyone knows, it is not everyone can fabricate a particular geometric structure of dispersion-flattened photonic crystal fiber. As an alternative approach, it is simpler and more convenient by selecting an available PCF as a frame and filling some liquids to achieve a dispersion-flattened fiber. After several simulation procedures, we found out the altering-tendency of waveguide dispersion when the hole-index of each layer was changed. According to these altering-tendencies, we designed a structure with appropriate waveguide dispersion to nullify material dispersion on the wavelength window as wide as possible. Figure 1 indicates the simulation model of the proposed LF-DFPCF structure. The geometric parameters of this model are based on that of LMA-5, while some liquids with different index are filled in the cladding-holes located at three layers nearest the solid-core. Figure 2 shows the chromatic dispersion behavior of the proposed LF-DFPCF. The wavelength window for which the fiber dispersion remains between 0 ± 1 ps/nm-km is from 1262 to 1722 nm. The flattened zero-dispersion bandwidth is approximately 460 nm. Furthermore, instead of using an artificial, dispersionless liquid, we select some available oils to redesign an actual LF-DFPCF. In this case, the Sellmeier equation for background silica and the Cauchy equations for liquids are all took into account. Finally, the chromatic dispersion behavior of the actual LF-DFPCF shows that the bandwidth of ultra-flat dispersion values between 0 ± 1.5 ps/nm-km is about 532 nm.

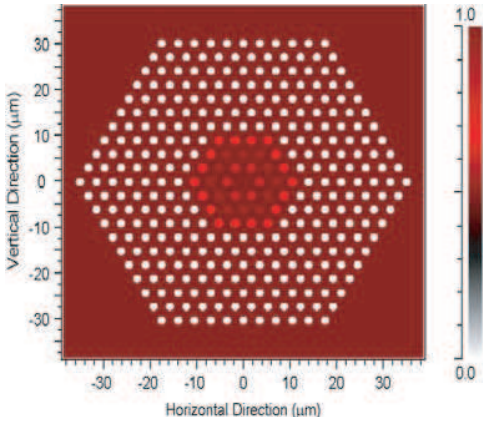

Figure 1: Simulation model of the proposed LF-DFPCF, which is based on an available PCF-LMA-5.

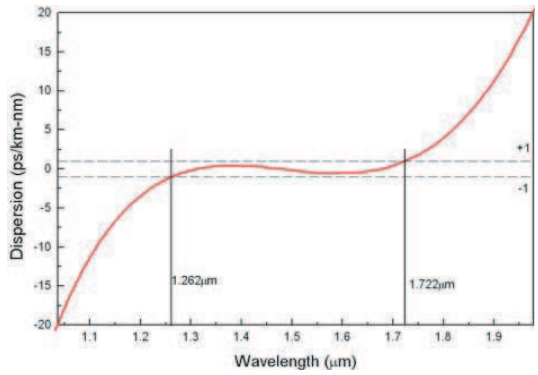

Figure 2: Dependence of chromatic dispersion on wavelength for the proposed LF-DFPCF.

A High Q Tellurite Microtoroid on Hollow Core Silica Fiber Post by a Flame Melting Technique

Yu-Hsin Hsieh[1], **Nan-Kuang Chen**[1, 2], **Junjie Zhang**[3], **and Sien Chi**[4, 5]

[1]Department of Electro-Optical Engineering, National United University, Miaoli 360, Taiwan, R.O.C.
[2]Optoelectronics Research Center, National United University, Miaoli 360, Taiwan, R.O.C.
[3]Shanghai Institute of Optics and Fine Mechanics, Chinese Academy of Science, Shanghai 201800, China
[4]Department of Photonics, National Chiao Tung University, Hsinchui 300, Taiwan, R.O.C.
[5]Department of Photonic Engineering, Yuan Ze University, Chungli 320, Taiwan, R.O.C.

Abstract— In contrast to the conventional microtoroid made of semiconductor materials based on the photolithography method, we demonstrate a simple and novel fabrication method for the microtoroid made of a rare-earth-doped glass based on a flame melting method for the first time. In this work, we use a perpendicularly cleaved hollow core fiber (HOF) with the initial inner diameter (ID) of at 10 µm and the initial outer diameter (OD) of 125 µm as the base of tellurite microtoroid. The ID and OD can be further modified by the flame tapering or chemical etching to the desired values. A melted tellurite glass is applied on the end surface of HOF and the glass is then automatically shaped into a donut by surface tension force. The melting point of the tellurite glass is much lower than that of the silica. Therefore, the tellurite glass can be very easy to be attached against the end surface of the HOF to form a microtoroid. Moreover, the

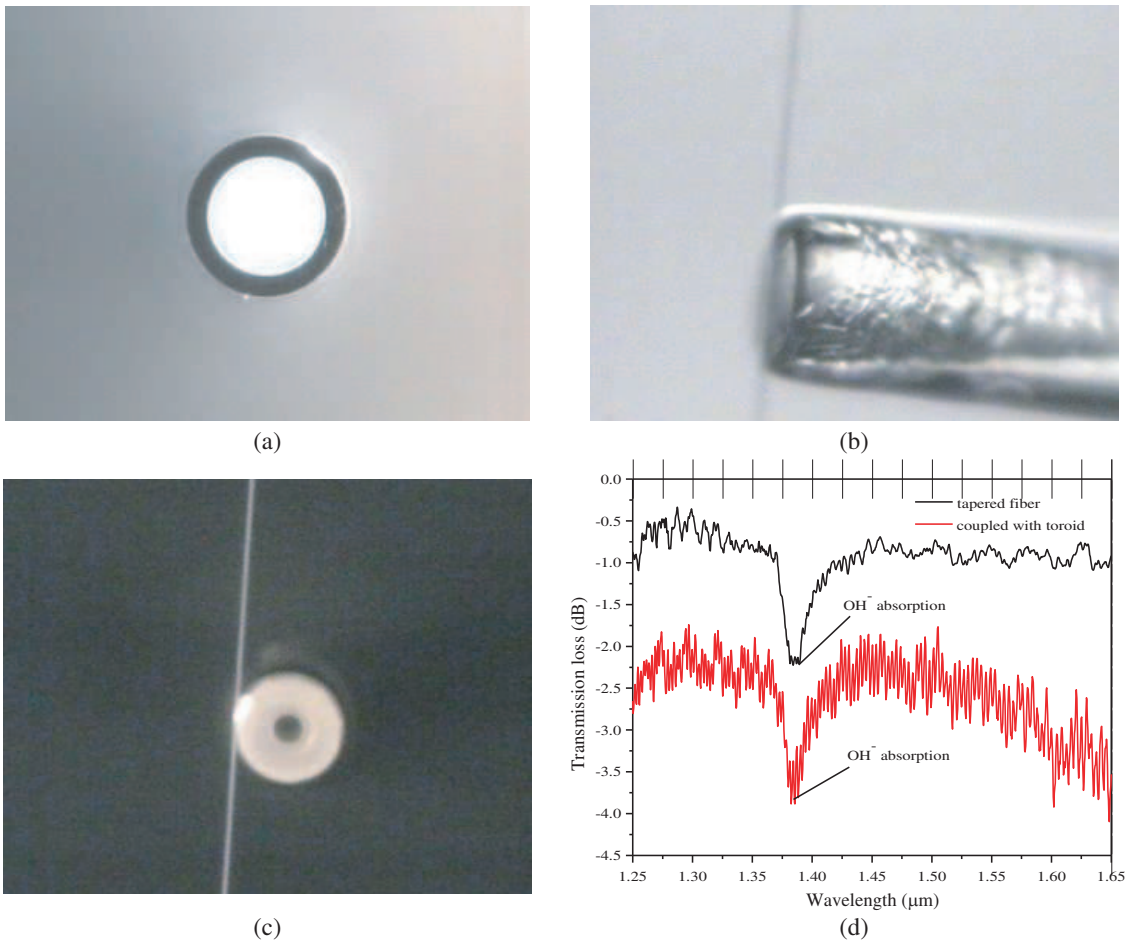

Figure 1: Photomicrograph of (a) etched silica hollow pillar with $D = 52\,\mu m$ and $w = 9.4\,\mu m$, (b) tapered-fiber-coupled Tm3+-doped tellurite microtoroid on silica hollow pillar, (c) tapered-fiber-coupled microtoroid with $D = 14.2\,\mu m$, $w = 20.6\,\mu m$, and $d = 2.8\,\mu m$, (d) spectral responses of the Tm3+-doped tellurite microtoroid.

index of tellurite glass is higher than 2 and which is good for a low-loss microtoroid with a small dimension. The silica post is not influential to the waveguiding of microtoroid due to the high index contrast between silica and tellurite glass. A white light source spanning 1250–1650 nm wavelength range is launched into a tapered fiber with a waist diameter of about 2–3 μm to deliver the specific wavelengths into microtoroid by side-contacting the microtoroid when the phase matching conditions are satisfied. The diameter and waveguide width of microtoroid are determined by the HOF and can be as small as 25 μm and 5 μm, respectively. The experimental results show that the coupling is successful and many resonant peaks can be observed from the spectral responses. The insertion losses can be less than 5 dB whereas the extinction ratios can be above 15 dB. This flame melting method is highly promising for microtoroid made of various kinds of glass and is advantageous to microtoroid lasers made of active glass material in the near future.

A High Extinction Ratio Micro-Fabry-Perot Resonator Using Thin Tellurite Glass Film over a Ge-diffused Core

Yu-Hsin Hsieh[1], **Nan-Kuang Chen**[1, 2], **and Junjie Zhang**[3]

[1]Department of Electro-Optical Engineering, National United University, Miaoli 360, Taiwan, R.O.C.
[2]Optoelectronics Research Center, National United University, Miaoli 360, Taiwan, R.O.C.
[3]Shanghai Institute of Optics and Fine Mechanics, Chinese Academy of Science, Shanghai 201800, China

Abstract— We demonstrate reflection-type micro Fabry-Perot resonators by using high-index thin tellurite glass film ($< 15\,\mu m$) at the cleaved fiber end with extinction about 34 dB. The key issues for making high finesse FP resonators are collimating input lights, two parallel high reflection interfaces, and low absorption loss cavity medium. Compared with the silica, tellurite glass has a refractive index of higher than 2 and is a good candidate to mate with silica or air to form a high reflection interface. In this work, the tellurite glass is melted by a butane flame at about 500°C and then applied on the cleaved singlemode fiber (SMF-28) end. Owing to the strong cohesion of this high index material, the tellurite glass molecules are easy to cluster into a mass and then move toward the other side of fiber end along the cladding surface. A fractional amount of the tellurite glass remained on the fiber end tends to be shaped into a spherical end face by itself due to the surface tension. The best extinction ratio can be higher than 39 dB and the thinnest thickness of micro Fabry-Perot cavity is 9.75 μm only. The free spectral range is from 20 nm to 33 nm contingent on the wavelengths. This high extinction ration micro Fabry-Perot resonator can be promising in biosensing and mechanical diagonasing applications. In future works, a micro-molding technique could be further employed to make a more perfect and longer tellurite glass rod for micro Fabry-Perot resonators with very small free spectral range.

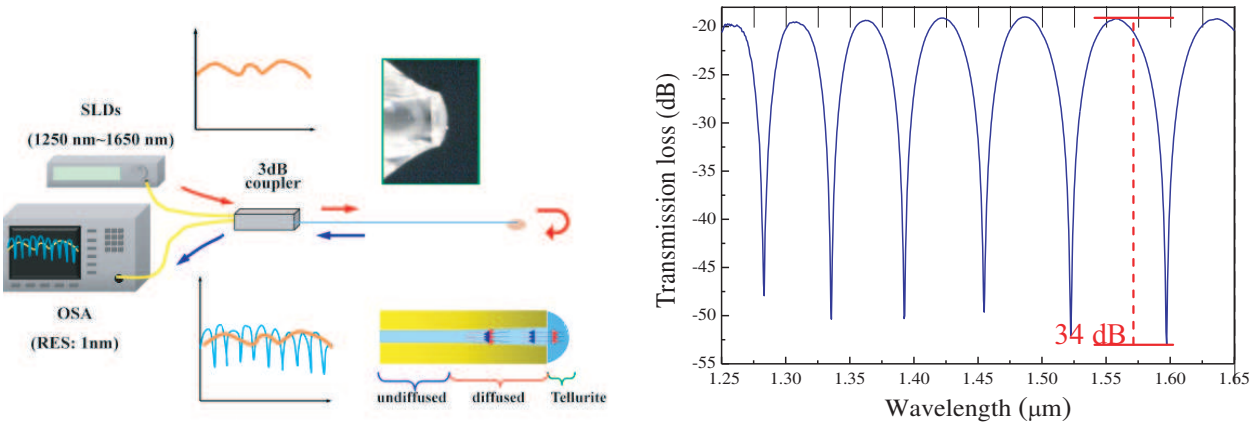

(a) (b)

Figure 1: (a) Experimental set-up of our micro-Fabry-Perot resonator. (b) Extinction ratio for micro-Fabry-Perot resonator can be as high as 34 dB.

Ultracompact In-line Mach-Zehnder Interferometer Made by Tapering a Hollow Optical Fiber

Shen-Wei Shen[1], **Nan-Kuang Chen**[1, 2], **and Junjie Zhang**[3]

[1]Department of Electro-Optical Engineering, National United University, Miaoli 360, Taiwan
[2]Optoelectronic Research Center, National United University, Miaoli 360, Taiwan
[3]Shanghai Institute of Optics and Fine Mechanics, Chinese Academy of Science, Shanghai 201800, China

Abstract— We demonstrate an ultracompact fiber optic Mach-Zehnder interferometer (MZI) using a novel concatenated structure, single-mode-fiber (SMF) — hollow optical fiber (HOF) — SMF. The HOF, composed of central air-hole and silica cladding, plays the key role of providing two optical paths, the leaky waveguide modes through the central air hole and the diverging radiation channel along the pure silica cladding. In fabrication, the HOF has an air core with a diameter of 5 µm. We tapered the HOF using a traveling-flame tapering rig. The fiber is heated and stretched to create a uniform narrow waist with a diameter of 125 µm joined to the untapered fiber by taper transitions of length. The inner diameter (ID) and outer diameter (OD) of the capillary were 1.32 µm and 33 µm, respectively. A white-light source comprising multiple superluminescent diodes (SLD) is launched into the tapered structure. When the input beam from SMF1 arrives at the HOF, a portion of the beam (E_1) is launched into the central air hole and the remnant annular portion (E_2) is incident into the pure silica clad. Accumulating optical path differences along the HOF, E_1 and E_2 recombine at SMF2, where the interference occurs to modulate the transmission response. To investigate the interference characteristics of tapered fiber, a taper-drawn silica microfiber with a uniform waist of about 33 µm in diameter, is placed in close contact with a piece of HF wafer. The whole length of the tapered region (including the uniform waist and conical tapers at both sides) is about 12.67 mm. Both sides of the as-drawn microfiber are continuously connected to the standard fibers for light launching and collecting. With the increasing etching time, periodic transmitted intensity responses may occur. The spectral response of the MZI is shown in Fig. 1, in which a clear interference is observed. The ultracompact in-line MZI demonstrated show advantages of compact size, wideband applicability, simple structure, and compatibility with miniaturized fiber devices.

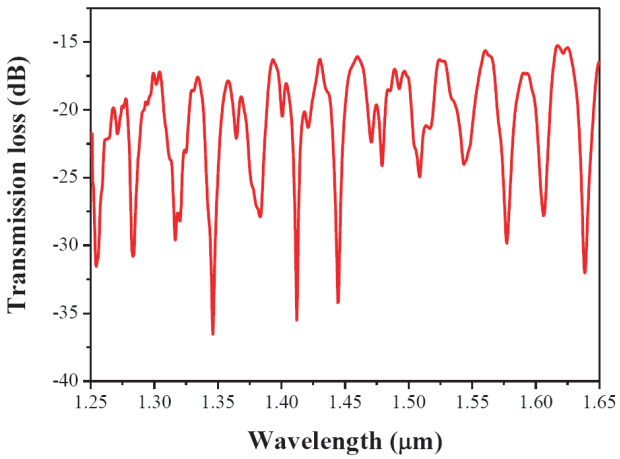

Figure 1: Transmission spectrum of the MZI with the core diameter of 1.32 µm

Fiber-based Optical Biosensing Using Tunable Near-infrared Supercontinuum Light Source

Chien-Hsiang Fan[1], **Chen-Han Huang**[1], **Hsiang-Ying Lin**[2], **and Hsiang-Chen Chui**[1]

[1]Institute of Electro-Optical Science and Engineering, National Cheng Kung University, Taiwan
[2]Institute of Biomedical Engineering, National Cheng Kung University, Taiwan

Abstract— We report using the conventional single mode fiber without tapering to generate the similar near infrared supercontinuum light. Femtosecond pulses from an unamplified Ti:sapphire laser were spectrally broadened into a supercontinuum. The unamplified Ti:sapphire laser (Spectra-Physics, Model 3960) emitted 84 fs. On the other hand, most of measure the absorption spectrum and other characteristics of materials or nanoparticals by using commercial instrument of light source. Therefore, we also report that the absorption spectrum of nanoparticals can be measured by the homemade tunable similar near-infrared supercontinuum light source from single mode fiber. Most important of all, this light source has many features better than the conventional light source such as high repetition rate, high peak power, and low optical damage. It is the simple and cost-effective way to generate a near-infrared light source to serve spectral measurement and achieve the bio-sensing. In this work, we demonstrated the near-infrared similar supercontinuum light generated by the conventional single mode fiber which main propagate light wavelength is 850 nm. And this light source can be tune by changing the center wavelength from Ti:sapphire mode-locked laser. The spectrum range of frequency broaden is thus increase to near 200 nm. And measuring the absorption spectrum of material and nanopartical can be achieved by using this near-infrared similar supercontinuum light.

Multiphoton Flow Cytometry in Whole Blood and *in Vivo* with a Double-clad Fiber Probe

Yu-Chung Chang[1], **Jing Yong Ye**[4], **Thommey Thomas**[3], **Zhengyi Cao**[3], **Alina Kotlyar**[3], **James R. Baker, Jr.**[3], **and Theodore B. Norris**[2, 3]

[1]Department of Electrical Engineering, National Changhua University of Education
Changhua 500, Taiwan
[2]Center for Ultrafast Optical Science, University of Michigan
2200 Bonisteel Blvd., Ann Arbor, MI 48109, USA
[3]Michigan Nanotechnology Institute for Medicine and Biological Sciences
Department of Internal Medicine, University of Michigan, Ann Arbor, MI 48109, USA
[4]Department of Biomedical Engineering, University of Texas at San Antonio
One UTSA Circle, San Antonio, TX 78249-1644, USA

Abstract— Circulating tumor cells in the blood stream are sensitive indicators for metastasis, disease prognosis, and therapy surveillance. Circulating cells have usually been monitored via extraction from blood, and more recently *in vivo* using free-space optics. To noninvasively detect circulating cells *in vivo*, much endeavor has been made in both one-photon and multiphoton excitation scheme. However, because of the scattering and absorption of biological tissue, only peripheral blood vasculature can be accessed by these free-space detection techniques. The sampled blood volume is thus too small to practically identify the rare CTCs for clinical use. Besides, in order to keep the laser focus on the blood vessel, the object has to be immobilized or anesthetized, which limits the acquisition time. We demonstrate the application of a two-photon-fluorescence optical fiber probe for the detection of cells in whole blood and in deep tissue *in vivo*. A sensitive single-fiber probe was utilized as a minimally invasive technique to access large blood vessels deep inside the body to increase the sampling rate. A double-clad fiber was used to enhance the detection sensitivity. Two-channel detection was employed to enable simultaneous measurement of multiple fluorescent markers. Because the fiber probe circumvents scattering and absorption from whole blood, the detected signal strength from fluorescent cells was found to be similar in PBS and in whole blood. The detection efficiency of cells labeled with the membrane-binding dye DiD was demonstrated to be the same in PBS and in whole blood. A high detection efficiency of green fluorescent protein (GFP)-expressing cells in whole blood was also demonstrated. To characterize *in vivo* detection, DiD-labeled untransfected and GFP-transfected cells were injected into live mice and the circulation dynamics of the externally injected cells was monitored in real time. The detection efficiency of GFP-expressing cells *in vivo* was consistent with that observed *ex vivo* in whole blood. The ability to efficiently detect GFP-expressing cells will further assist the study of cancer metastasis on mouse models.

Session 1P1b
Nano Scale Electromagnetics

Microwave Properties of Nanocrystalline and Microcrystalline of $La_{(1-x)}Sr_xFe_{(1-y)}Mn_{y/2}Ti_{y/2}O_3$ Based Powders by Mechanical and Ultrasonic Assisted Milling

Mas Ayu Elita Hafizah and A. Manaf
Postgraduate Program of Materials Science, Faculty of Mathematics and Natural Science
Universitas Indonesia, Jl. Salemba Raya No. 4, Jakarta 10430, Indonesia

Abstract— Microwave absorber of nanocrystalline (mean grain size < 100 nm) and microcrystalline of $La_{0.5}Sr_{0.5}Fe_{0.5}Mn_{0.25}Ti_{0.25}O_3$ powders prepared by mechanical and ultrasonic assisted milling were studied. The dielectric properties and absorption characteristics as evaluated by vector network analyzer of the absorber materials are discussed in terms of micostructure point of view. Microstructurally, powders of mechanically alloyed have coarser particle sizes of more than 1 micron in average. A realatively broadeninng particle size distribution which indicated a large variation was observed. As mechanically milled powder materials were sonically milled in a 40 kHz sonic bath for 1 hour the particle size distribution was improved significantly. The average particle size reduced to at least less than half of obtained from mechanically milling and fall down into a nano regime as evalauated by a Zetasizer Nano'S'. The XRD difraction trace for powder materials indicated that the material can be a single phase material which depend on the solid state reaction temperature. Particles with a homogenous size were clearly observed from micrographs obtained from electron microscope studies. In this paper, results of microwave characterization including calculated value for material impedance and reflection loss in the frequency range 1–20 GHz are discussed.

The Use of Magnetic Spectroscopy in the Investigation of the Magnetic Viscosity of Nanoparticles at Microwave Frequencies

P. C. Fannin[1] **and C. N. Marin**[2]

[1]Department of Electronic and Electrical Engineering, Trinity College, Dublin 2, Ireland
[2]Faculty of Physics, West University of Timisoara, Bd. V. Parvan no. 2, Timisoara, Romania

Abstract— The magnetic moment, m, of uniaxial single domain superparamagnetic particles has two anti-parallel equilibrium positions separated by a potential barrier. Under certain conditions the moment may switch over the potential barrier, its action often being treated as a 'binary magnetic' switching action. However, the switching does not happen instantaneously and parameters which influences this action in the particles include the magnetic viscosity, η_m, And the interwell and intrawell relaxation times, τ_N, and τ_0, respectively. In order to determine these parameters it is necessary to determine values for the Landau and Lifshitz damping parameter, α, the gyromagnetic constant, γ, and the anisotropy constant K of the nanoparticles. In this paper by means of polarised, ac complex susceptibility measurements over the frequency range. 100 MHz to 6 GHz, we evaluate these parameters for three colloidal suspensions of nanopaticles in isoparm and determine which particle is most suited for use in a switching environment.

Session 1P2
Transformation Optics and Cloaking

Making Macroscopic Objects Invisible

Baile Zhang[1, 2], **Yuan Luo**[1, 2], **and George Barbastathis**[1, 2]

[1]MIT Alliance for Research and Technology (SMART) Centre, Singapore 117543, Singapore
[2]Department of Mechanical Engineering, Massachusetts Institute of Technology
Cambridge, MA 02139, USA

Abstract— Invisibility cloaking has attracted more and more attention in the past few years. Significant progress has been made during the exploration of invisibility cloaks. However, previous experiments of invisibility cloaking can hide only about one-wavelength large objects and thus must be done under a microscope. How to see the invisibility effect with the naked eye, i.e., to cloak a macroscopic object in visible light, is still a crucial challenge.

There are two main diculties in the fabrication of cloak materials — anisotropy and inhomogeneity. The previously proposed quasiconformal mapping strategy attempted to solve anisotropy in order to facilitate metamaterial implementation. However, in conventional optical lens fabrication, the inhomogeneity is more dicult to implement than anisotropy. For example, historically, there have been a lot of successful applications of anisotropic optics, such as Nicol prism that was invented in 1828, while implementing gradient-refractive-index (GRIN) optical elements was quite limited until late last century when modern manufacturing technologies made it possible. By applying the transformation optics principle into conventional optical lens fabrication, we demonstrated the first realization of macroscopic invisibility cloaking at visible wavelengths. The cloak is implemented with calcite, a common anisotropic optical material. Since calcite itself is transparent in visible light, the concern of energy loss for metamaterials does not exist in this case, nor the bandwidth limitation associated with metal ingredients. To our knowledge, in our experiment invisibility was demonstrated for the first time by seeing through the cloak directly. It is, therefore, closest to the idealized concept of a cloak — being invisible to the eye.

Invisibility Cloak with an Opening

Thomas Ako[1, 2], **Min Yan**[1], **and Min Qiu**[1, 3]

[1]Laboratory of Photonic and Microwave Engineering
School of Information and Communication Technology
Royal Institute of Technology, Electrum 229, Kista 16440, Sweden
[2]Currently with the Liquid Crystals and Photonics Group
Department of Electronics and Information Systems, Ghent University
Sint-Pietersnieuwstraat 41, Gent 9000, Belgium
[3]State Key Laboratory of Modern Optical Instrumentation and Institute of Advanced Nanophotonics
Department of Optical Engineering, Zhejiang University, Hangzhou 310027, China

Abstract— Previous 2D cloak designs mostly have a closed annular shape. In such designs, it is not possible to insert or retrieve objects into or from the cloaking domain. We call this inconvenience as the matter-exchange bottleneck. In many practical cloaking applications it is however desirable for objects to be able to freely enter or leave the cloaking device. In this paper, we propose an open cloak designed with an analytical procedure. Its geometry and in turn material parameters all have analytical expressions, which is advantageous for optimization purposes from design point of view. The open cloak is realized with a transformation function which expands a point at the origin in electromagnetic space to a finite area in physical space in a highly anisotropic manner. A section of the cloak along a certain angular direction has permittivity and permeability values very close to 1; therefore it can be safely removed without causing heavy electromagnetic scattering. We verify the designed cloak, both with and without an opening, using full-wave finite-element simulations. Such a cloak facilitates matter exchange between the cloak's interior and exterior without significantly deteriorating the cloak's invisibility performance, overcoming the matter exchange bottleneck inherent to most previously proposed cloaks.

An Invisibility Cloak Using Silver Nanowires

Huanyang Chen
School of Physical Science and Technology, Soochow University, Suzhou, Jiangsu 215006, China

Abstract— We design a well-performed invisible cloak based on an empirical revised version of the reduced cloak by using the parameter retrieval method together with an analytical effective medium approach. The designed cloak can be realized by silver nanowires embedded in a polymethyl methacrylate host.

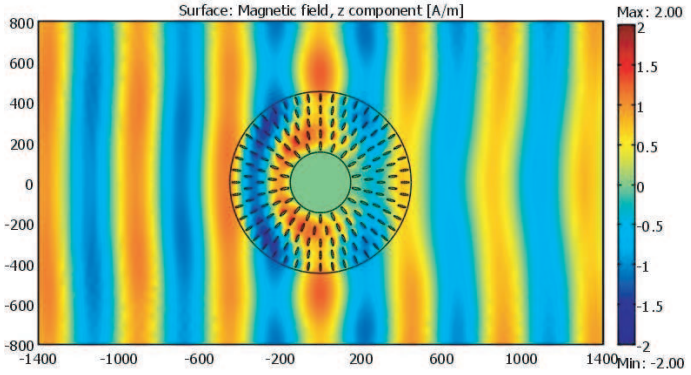

Figure 1: The total field pattern of the designed cloak with silver nanowires embedded in a polymethyl methacrylate host.

REFERENCES

1. Xie, Y., et al., http://arxiv.org/abs/0805.1328.

Concealing an Electromagnetic Sensing System Using Three Kinds of Isotropic Homogeneous Single-negative Materials

Xuefeng Zhu, **Xinye Zou**, **Qian Chen**, **Bin Liang**, **and Jian-Chun Cheng**
Key Laboratory of Modern Acoustics, MOE, Department of Physics, Institute of Acoustics
Nanjing University, Nanjing 210093, China

Abstract— A perfect non-blinded cloak consisting of multi-layers of single-negative materials is proposed to cloak an electromagnetic sensor. The numerical results show that the multi-layer structure can make a sensor undetectable but capable of receiving external signals, using only three different kinds of isotropic single-negative materials. This may significantly facilitate the experimental realization of electromagnetic sensor cloaking device and is of fundamental importance in a wide range of optics and engineering applications.

Low Scattering Cylindrical Invisibility Cloak with Wide Frequency Band

Su Xu[1, 2] **and Hongsheng Chen**[1, 2]

[1]The Electromagnetics Academy at Zhejiang University, Zhejiang University
Hangzhou 310027, China
[2]The Department of Information Science & Electronic Engineering, Zhejiang University
Hangzhou 310027, China

Abstract— Invisibility cloaks have attracted scientists' interests recently. However, it's difficult to realize invisibility cloak in practice due to the requirement of high anisotropic extreme values and continuous inhomogeneity. Here, we present a wideband cylindrical invisibility cloak. It is realized by non-resonnant metamaterials. The parameters are optimized by a Radar Cross Section (RCS)-oriented program. Closed rings (CRs) are used to realize cylindrical cloak as the unit cells of non-metamaterials. Experiments measurements are carried out both in waveguide and in free space. We measure an array of multiple discrete perfect electric conductor (PEC) cylinders with our invisibility cloaks at different incident angles. Our cloaks are quasi-3D invisibility cloaks to certain extend, shown by the experimental results. The relative bandwidth of the cloak is 10%, which shows a wider frequency band compared with those based on resonant metamaterials. The parameters in our method are relatively easy to be realized. Our study proposed an effective and robust way of realizing a low scattering cloak.

Experimental Realization of an Invisible Gateway by Transmission-line Medium

Chao Li[1], **Xiankun Meng**[1], **Xiao Liu**[1], **Fang Li**[1], **Guangyou Fang**[1], **Huanyang Chen**[2], **and C. T. Chan**[3]

[1]Key Laboratory of Microwave and Electromagnetic Radiation
Institute of Electronics, Chinese Academy of Sciences (IECAS), Beijing 100190, China
[2]School of Physical Science and Technology, Soochow University, Suzhou, Jiangsu 215006, China
[3]Department of Physics, William Mong Institute of Nano Science and Technology
Hong Kong University of Science and Technology, Clear Water Bay, Hong Kong, China

Abstract— Transformation optics has provided effective approaches for controlling electromagnetic (EM) waves and developing EM devices to obtain desired and unprecedented EM behaviors. One of the most notable examples is invisible cloaks, in which an excluded region for EM waves is produced to hide objects by coordinate transformation. Recently, the combination of the complementary media concept with the transformation optics has motivated a series of illusion optics devices, such as the super-scatter, anti-cloak, invisible gateway, and the special cloak that can conceal an object outside the cloak shell. However, such effects are limited to theoretical analysis and numerical simulations. Using a transmission-line (TL) medium, we realized the first experimental demonstration of a two dimensional illusion optics device, an "invisible gateway", which is an open channel that appears to be blocked for waves in a certain frequency band. The performance of the device is predicted by ADS simulation and measured with an Agilent E5071C vector network analyzer (VNA). The wave blockage properties of the open channel are quantitatively analyzed. Good agreement between the simulation and the experiment is obtained, which confirm the functionalities of the device. It also found that such a device works for a rather broadband. The experimental demonstration in this paper will be helpful for future design of other electromagnetic "illusion devices" at microwave frequencies.

Light Pulses in Maxwell's Fish Eye

T. Tyc
Institute of Theoretical Physics and Astrophysics, Masaryk University, Brno, Czech Republic

Abstract— In the last few years, perfect imaging with positive refraction has been attracting an increasing attention. It has been shown both theoretically [1, 2] and experimentally [3, 4] on the prototype of a perfect lens, Maxwell's fish eye, that a positively-refracting perfect lens has the capability of unlimited resolution. This could open the way to constructing new optical devices and instruments with sub-wavelength imaging, which could revolutionarize the optics industry.

It has also been shown [5] that in order to achieve this unlimited resolution, a suitable outlet must be placed to the position of the image so that the energy can be removed from the system. Without the outlet, the resolution is subject to the usual diffraction limit. This is caused by interference of the incoming converging wave near the image with the diverging wave into which the converging wave changes after passing through the image point.

Apart from knowing what happens to a monochromatic wave in Maxwell's fish eye, it is also important to analyze propagation of light pulses in the device. We investigate various aspects of light pulse formation and its propagation through the image point in Maxwell's fish eye in both two and three dimensions. We show that in three dimensions the outgoing wave obtains an additional phase jump of pi, which can be interpreted as Gouy phase. We show that in a two-dimensional fish eye, a pulse that is very well localized in time upon emission will arrive at the image point still localized, but the localization is worse than that of the emitted pulse. This is caused by the intrinsic dispersion of waves propagating in two dimensions, but this dispersion is even stronger in Maxwell's fish eye index profile than in case of a constant refractive index. We show this both by numerical simulations and analytically, by comparing the spectrum of eigenfrequencies in Maxwell's fish eye profile and for a 2D optically homogeneous disk surrounded by a mirror. We also show that in the absence of the outlet, converging sharply localized wave in 2D fish eye changes into a wave with a completely different shape, which is a typical feature for waves propagating in two dimensions.

REFERENCES

1. Leonhardt, U., *New J. Phys.*, Vol. 11, 093040, 2009.
2. Leonhardt, U. and T. G. Philbin, *Phys. Rev. A*, Vol. 81, 011804, 2010.
3. Ma, Y. G., C. K. Ong, S. Sahebdivan, T. Tyc, and U. Leonhardt, arXiv:1007.2530, 2010.
4. Gabrielli, L. H., U. Leonhardt, and M. Lipson, arXiv:1007.2564, 2010.
5. Leonhardt, U., arXiv:1010.4161, 2010.

Plasmonic Luneburg and Eaton Lenses

Jason Valentine[1], **Thomas Zentgraf**[2], **Yongmin Liu**[2], **Maiken H. Mikkelsen**[2], **and Xiang Zhang**[2]

[1]Department of Mechanical Engineering, Vanderbilt University
2301 Vanderbilt Place, PMB 351592, Nashville, TN 37235, USA
[2]NSF Nanoscale Science and Engineering Center, University of California
3112 Etcheverry Hall, Berkeley, CA 94720, USA

Abstract— Recently, it has been proposed to apply transformation optics to plasmonic systems, aiming to manipulate the propagation of surface plasmon polaritons (SPPs) in a prescribed manner [1–3]. While the rigorous transformation optics approach requires spatial modulation of both the metal and dielectric, it was proposed that only transforming the dielectric medium is sufficient to mold the propagation of SPPs [1, 2]. Furthermore, the transformed dielectric materials can be isotropic and non-magnetic, if a prudent transformation scheme is applied. In this case, the local effective index of SPPs is varied gradually and thus we term the approach gradient index (GRIN) plasmonics.

Here we will present the design and demonstration both a GRIN plasmonic Luneburg lens which is capable of focusing surface plasmon polaritons and an Eaton lens which bends surface plasmon propagation at 90°. Instead of modifying the cladding dielectric with discrete structures, we present an approach where slow changes in the thickness of an isotropic dielectric cladding layer is used to manipulate the local effective index of SPPs [2]. In such a way, the propagation of SPPs can be controlled without modifying the metal surface or adding discrete structures on the metal which can scatter light. The elements are realized by spatially varying the height of a thin dielectric, Poly (methyl methacrylate) (PMMA), on top of a Gold surface. This is achieved using grey scale electron beam lithography in which the dose of exposure is spatially varied to yield a variable height structure.

To validate the device performance using fluorescent imaging, dye was incorporated into the PMMA before spinning. This allows the SPPs to be imaged as they move through the device, demonstrating clear focusing in the case of the Luneburg lens and SPPs bending at 90° in the Eaton lens. To further validate the Luneburg lens performance, leakage wave microscopy was utilized to better visualize SPP propogation both inside and outside of the lens. Characteristic fringe patterns due to the interference of the directly transmitted light and the leakage radiation of the SPPs clearly shows the phase front of the SPP being focused at the lens surface.

REFERENCES

1. Huidobro, P. A., et al., *Nano Lett.*, Vol. 10, 1985–1990, 2010.
2. Liu, Y., et al., *Nano Lett.*, Vol. 10, 1991–1997, 2010.
3. Renger, J., et al., *Opt. Exp.*, Vol. 18, 15757–15768, 2010.

Investigation of Broadband Flat Antennas Using Transformation Electromagnetics

W. Tang, **C. Argyropoulos**, **E. Kallos**, **and Y. Hao**
Department of Electronic Engineering, Queen Mary, University of London
Mile End Road, London, E1 4NS, United Kingdom

Abstract— Transformation electromagnetics provides a practical approach to control electromagnetic fields at will, due to the form invariance in Maxwell's equations. Based on this principle, novel devices such as the invisible cloak have been proposed. A discretized coordinate transformation technique, accompanying the proposal of the carpet cloak, offers the possibility to realize broadband cloaking devices composed of dielectrics. The extension of this technique is tested in this paper for designing novel devices in antenna systems. Flat reflectors are generated from conventional parabolic reflectors by converting their curved profiles into flat boundaries. To avoid the loss and narrow bandwidth issues typically present in resonant metamaterials, appropriate approximations and simplifications are introduced to reduce the devices into a cluster of dielectrics with the size about half the wavelength at central operating frequency. Careful design procedure guarantees the similarity between the flat reflectors and the conventional ones in terms of non-dispersive, isotropic, broadband, and lossless properties, while confers the former the advantages of flat profiles and small volumes. Multiple coordinate transformation is also applied to control the radiation patterns and realize beam steerable flat reflectors. Numerical modelling using the Finite-Difference Time-Domain (FDTD) method is carried out to verify the performances of the reflectors. Simulation results have demonstrated that the flat reflectors with dispersive permittivities have very similar radiating performance compared to the conventional ones at target frequency. When the dispersive permittivities are neglected, the flat reflectors achieve a broad bandwidth over 8 GHz to 12 GHz, at price of slightly increased side lobes around the central frequency. Steerable beams are also observed in the simulations. A flat dielectric lens is designed from the conventional convex lens as another example. Its focusing performance, as well as the radiation pattern when fed by a point source, is proved through simulations. The flat lens has been realized using microstrip lines and tested at X band.

A Chirality Switching Device Designed by Transformation Optics

Yuan Shen, **Kun Ding**, **Wujiong Sun**, **and Lei Zhou**
State Key Laboratory of Surface Physics
Key Laboratory of Micro and Nano Photonic Structures (Ministry of Education)
Fudan University, Shanghai 200433, China

Abstract— Switching the chirality is our dreams due to the importance of it which originates from asymmetric synthesis [1]. It is not easy to achieve because the structure needs to be changed mechanically. However, people can use optical ways to "change" the chirality of certain objects effectively, for example a mirror transforms a right-handedness object to a left-handedness image. In recent years the propose of Transformation Optics [2–6] has provided a convenient way to do this, but such an approach surfers the limitations that the device is object-depended and the objects hidden inside the device must be transparent.

In viewing these previous effects, we find it still highly challenging to design a chirality-switching device. So in this paper we show that an optical device can be designed based on Transformation Optics [2–6], such that an object hidden inside would exhibit a reversed chirality (i.e., from left-handedness to right-handedness) for an observer at the far field. Distinct from a perfect mirror which also creates a chirality-reversed image, our device makes the original object completely invisible to the far field observer. Numerical simulations are employed to demonstrate the functionalities of the designed devices in both two- and three-dimensional spaces, as shown in the following figure [7].

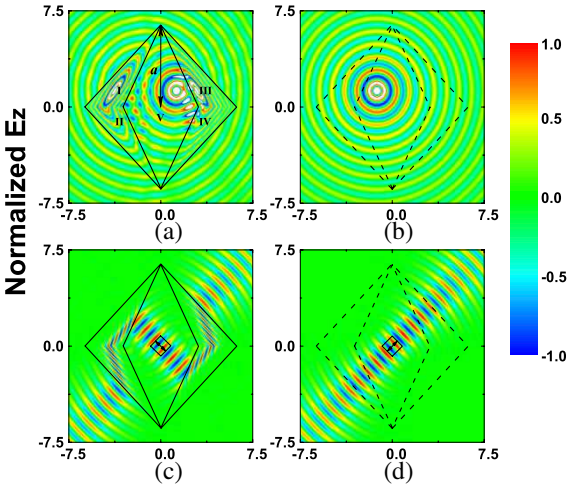

Figure 1: (a) Radiation pattern of a line source placed inside the 2D device. (b) Radiation pattern of a line source placed in free space, at the mirror-re ection position of the source. (c) Radiation pattern of a directional source inside the device, which emits rays only along two directions $\vec{k} = \pm(-\frac{\sqrt{2}}{2}, \frac{\sqrt{2}}{2}, 0)k_0$. (d) Radiation pattern of another direction source placed in free space, which emits rays only along two directions $\vec{k} = \pm(\frac{\sqrt{2}}{2}, \frac{\sqrt{2}}{2}, 0)k_0$.

REFERENCES

1. Lin, G. Q., Y. M. Li, and A. S. C. Chan, *Principles and Applications of Asymmetric Synthesis*, John Wiley & Sons, New York, 2001.
2. Leonhardt, U., *Science*, Vol. 312, 1777–1780, 2006.
3. Pendry, J. B., D. Schurig, and D. R. Smith, ibid, 312, 1780–1782, 2006.
4. Leonhardt, U. and T. G. Philbin, *Progress in Optics*, Vol. 53, Chap. 2, Elsevier, Amsterdam, 2009.
5. Chen, H. Y., C. T. Chan, and P. Sheng, *Nat. Mater.*, Vol. 9, 387–396, 2010.
6. Bergamin, L., *Phys. Rev. A*, Vol. 80, 063835, 2009.
7. Shen, Y., K. Ding, W. Sun, and L. Zhou, *Opt. Express*, Vol. 18, No. 20, 21419, 2010.

The Effective Medium Approximation of Metamaterials

Y. Lai[1], **Y. Wu**[2], **C. T. Chan**[3], **P. Sheng**[3], **and Z. Q. Zhang**[3]

[1]Department of Physics, Soochow University, 1 Shizi Street, Suzhou 215006, China
[2]Division of Mathematical and Computer Sciences and Engineering
King Abdullah University of Science and Technology, Thuwal 23955-6900, Saudi Arabia
[3]Department of Physics, Hong Kong University of Science and Technology
Clear Water Bay, Kowloon, Hong Kong, China

Abstract— Metamaterials [1, 2] are artificial electromagnetic materials that can produce intriguing and unique material responses which are not readily available in natural materials. A significant theoretical advance of metamaterials is transformation optics, which have broad scientific and practical implications like negative refraction, superlens, hyperlens, cloaking, illusion optics, etc.. In the applications designed by transformation optics, metamaterials can be approximately viewed as effective electromagnetic media with effective parameters beyond the normal range of natural materials, such as having certain values (even negative or zero), having new types of anisotropy, etc.. Due to the resonant nature of metamaterials, their effective parameters vary significantly with tiny structure or frequency change. Therefore, an efficient and accurate effective medium theory is vital in all metamaterial design and applications.

Previous effective medium theories developed in the quasistatic limit [3] cannot be applied to metamaterials, which works at a much higher frequency. Various approaches have been developed to obtain the effective parameters of metamaterials, including retrieving parameters from transmission and reflection coefficients [4], the coherent potential approximation method [5, 6], and a homogenization method by field averaging [7]. In this work, we propose a simple and efficient way to obtain the effective parameters of metamaterials, which is based on the physical picture of eigenfield averaging and matching on boundaries. The effective parameters obtained by this method can accurately reproduce the band structure dispersions near the center of the Brillouin Zone at rather high frequencies. This principle also applies to acoustic and elastic metamaterials. Finally, necessary conditions for metamaterials to have a good effective medium approximation will also be discussed.

REFERENCES

1. Smith, D. R., J. B. Pendry, and M. C. K. Wiltshire, "Metamaterials and negative refractive index," *Science*, Vol. 305, 788–792, 2004.
2. Liu, Z., et al., "Locally resonant sonic materials," *Science*, Vol. 289, 1734–1736, 2000.
3. Choy, T. C., *Effective Medium Theory*, Oxford University Press, Oxford, 1999.
4. Smith, D. R., S. Schultz, P. Markos, and C. M. Soukoulis, "Determination of effective permittivity and permeability of metamaterials from reflection and transmission coefficients," *Phys. Rev. B*, Vol. 65, 195104, 2002.
5. Wu, Y., J. Li, Z. Q. Zhang, and C. T. Chan, "Effective medium theory for magnetodielectric composites: Beyond the long-wavelength limit," *Phys. Rev. B*, Vol. 74, 085111, 2006.
6. Liu, Z., C. T. Chan, and P. Sheng, "Analytic model of phononic crystals with local resonances," *Phys. Rev. B*, Vol. 71, 014103, 2005.
7. Smith, D. R. and J. B. Pendry, "Homogenization of metamaterials by field averaging," *J. Opt. Soc. Am. B*, Vol. 23, 391, 2006.

Epsilon-near-zero Metamaterials with Defects

Yadong Xu and Huanyang Chen
School of Physical Science and Technology, Soochow University, Suzhou, Jiangsu 215006, China

Abstract— We find that total reflection and even total transmission can be obtained in a waveguide with epsilon-near-zero (ENZ) metamaterials by adjusting the geometric sizes and material properties of embedded defects.

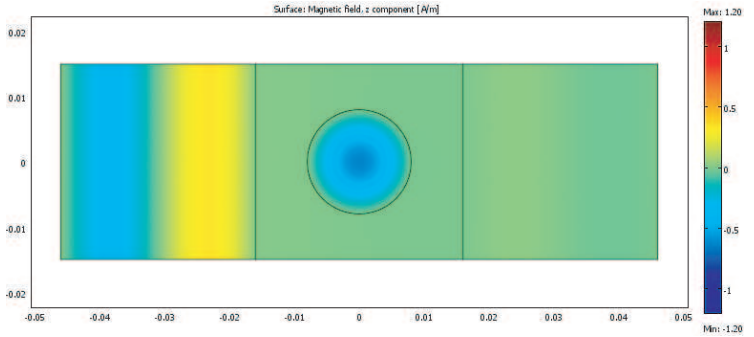

(a)

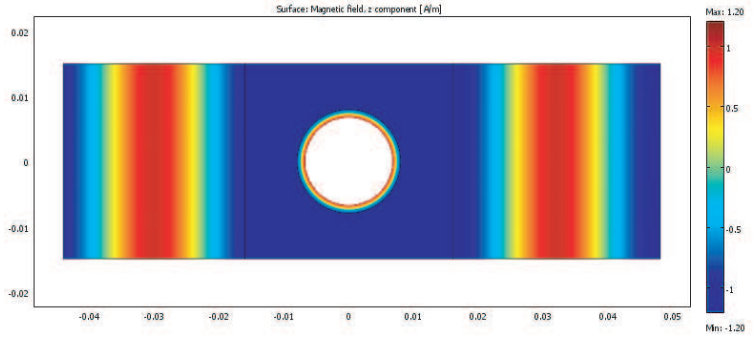

(b)

Figure 1: (a) Total reflection: the magnetic distribution of an ENZ medium with a dielectric cylindrical defect with $\varepsilon_2 = 2.06$ and $\mu_2 = 1$. (b) Total transmission: the magnetic distribution of an ENZ medium with a dielectric cylindrical defect with $\varepsilon_2 = 2.4$ and $\mu_2 = 1$.

REFERENCES

1. Xu, Y. and H. Chen, http://arxiv.org/abs/1012.5213.

A Boundary Integral Method to Remote Optical Cloaking and Illusions by Active Sources

J. J. Xiao[1, 2], Y. Lai[2, 3], H. H. Zheng[2], and C. T. Chan[2]

[1]Department of Electronic and Information Engineering
Key Laboratory of Network Oriented Intelligent Computation
Shenzhen Graduate School, Harbin Institute of Technology, Shenzhen 518055, China
[2]Department of Physics and William Mong Institute of NanoScience and Technology
The Hong Kong University of Science and Technology, Clear Water Bay, Hong Kong, China
[3]School of Physical Science and Technology, Soochow University, Suzhou, Jiangsu 215006, China

Abstract— We propose a scheme using active sources from devices that can create optical illusion effects. From a set of boundary integral equations, we show that coherent active sources can create a nearly "silent" domain which can conceal any objects inside and at the same time make the whole system look like a redesigned illusion outside a virtual boundary. Therefore an object outside of the devices can be made to look like another object, in the sense of optical scattering. Invisibility is a special case in which the concealed object is transformed to a volume of air. The boundary integral equations are numerically solved to give the fields and field gradients, which can be related to monopoles and dipoles on continuous curves which define the boundary of the active devices. Although there may exist severe limitations for realization of such a scheme, we discuss several possible ways to set up the active sources and their efficiency as the source number varies.

Session 1P3a
Remote Sensing of the Earth, Ocean, and Atmosphere

Estimation of Turbulent Fluxes with Geostationary Operational Environmental Satellites Data

Tongren Xu[1, 2], **Shunlin Liang**[2], **and Shaomin Liu**[1]

[1]State Key Laboratory of Remote Sensing Science, School of Geography
Beijing Normal University, Beijing 100875, China
[2]Department of Geography, University of Maryland, College Park, MD 20742, USA

Abstract— Accurate estimations of turbulent fluxes are critical for climate change research, planning, and management of water resources. A number of methods have been developed to estimate turbulent fluxes. Ground measurements, remote sensing method and land surface model can estimate turbulent fluxes in different way. However, the monitoring network for ground measurements is not sufficient for global coverage; the remote sensing data are instantaneous, estimating the daily, monthly, and annual flux values may cause errors; the land model output is strongly contaminated by uncertainties within the model parameters, model structures, and forcing data; this has adversely affected the development and application of land surface models. Considering these issues, it's necessary developing a series of techniques combining these methods to estimate turbulent fluxes in continuous temporal and spatial scales. Data assimilation is one such technique and is one of the most advanced approaches to improve land surface model predictions using different sources of data.

In this study, a data assimilation scheme is developed based on the ensemble Kalman filter (EnKF) algorithm and the common land model (CoLM); soil moisture and model parameters are simultaneously optimized to improve the estimates of turbulent fluxes. Land surface temperature (LST) is retrieved from geostationary operational environmental satellites (GOES) data, and assimilated into CoLM. The data assimilation results are validated at six observation sites in the United States that include grassland, cropland, and forestland cover types. Data assimilation results indicate that in addition to improvements in the prediction of turbulent fluxes, model uncertainties are also reduced as a result of the assimilation of GOES LST retrieval data. The effects of MODIS and GOES temporal resolution data on data assimilation results are studied. The assimilation results indicate that the average RMSE values for GOES temporal resolution data are smaller than that for MODIS temporal resolution data. During the assimilation time period, the soil moisture obtained from assimilation closely agrees with the observed values, and the four vegetation parameters show distinct seasonal variations.

Experimental Study of Thermal Anomaly before Earthquake Due to Gas Releasing from Crust

Shanjun Liu[1], **Lixin Wu**[1, 2], **Xin Liu**[1], **and Bo Tang**[1]

[1]Institute for Geo-informatics & Digital Mine Research
Northeastern University, Shenyang 110819, China
[2]Academe of Disaster Reduction and Emergency Management
Beijing Normal University, Beijing 100875, China

Abstract— Some violent earthquakes appear satellite thermal infrared anomaly around epicenter before earthquake, and generally the anomaly distributes along the geological structure. The reported increase of surface temperatures reaches 2–4°C, occasionally higher. Usually, the anomaly appears one month to several days before the earthquake. Several viewpoints have been put forward to interpret the thermal anomaly before earthquake, one of them is earth releasing gas to result in the thermal anomaly before earthquake.

In this paper, a group of physical simulation experiments were carried out to verify the viewpoints of earth releasing gas to result in the thermal anomaly before ocean earthquake. In the experiments a cylinder whose diameter was about 70 cm and the height was about 120 cm was used to contain water, and three kinds of gases, C_2H_2, CO_2 and vapor are respectively produced by three different chemical experiment to simulate the gas releasing from the ocean bottom due to the action of earthquake. A thermal imaging system, VarioSCAN 3021ST with temperature precision 0.03°C and 360×240 pixel was applied to detect the temperature field change of water surface when the gas was releasing from the water.

The experimental results showed that after 4 seconds of chemical reaction the gas went up to the water surface from the bottom of the container, and in the same time the temperature of water surface began to increase 0.4–1.1°C. After that the temperature varied a little but the high-temperature area enlarged. The high-temperature area was accordant with the gas releasing area. If comparing the experimental result with the actual satellite thermal anomaly before earthquake it can be found that two phenomena are similar but the aptitude of temperature increase in the simulation experiment is smaller than that in actual earthquake thermal anomaly.

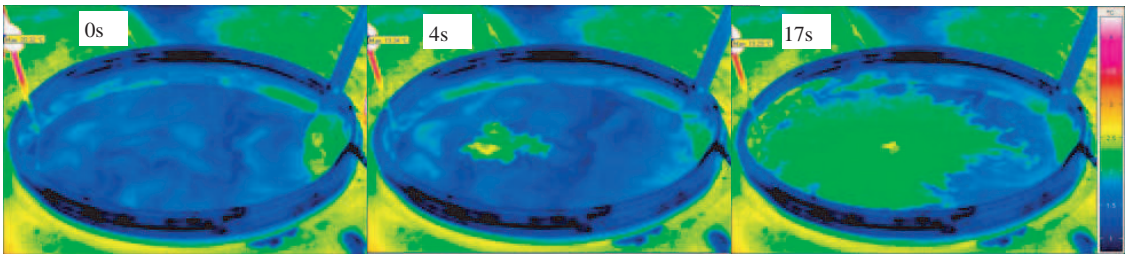

Figure 1: Temperature field variation of water surface in the process of gas releasing.

Results of the SMOS Data Validation over a Steppe and Forest Area in Siberia

P. P. Bobrov[1], **O. V. Kondratieva**[1], **V. L. Mironov**[2,4], **E. Shvetsov**[3], **A. I. Sukhinin**[3,4], **and A. S. Yashchenko**[1]

[1]Omsk State Pedagogical University, Omsk, Russia
[2]Kirensky Institute of Physics, SB RAS, Krasnoyarsk, Russia
[3]Sukachev Institute of Forest, SB RAS, Krasnoyarsk, Russia
[4]Reshetnev Aerospace State University, Krasnoyarsk, Russia

Abstract— In 2010–2011 we performed a field measurement aiming at validation of the SMOS radiobrightness data relative to those attained with the use of ground-based measurement. The test site was located in the southern part of the Omsk Region West Siberia at the interface of the steppe and forest landscape zones. The measurements were carried out for both the bare soil and the grass covered soil surfaces. Analysis of the data measured in the Summer 2010 showed for the SMOS and ground based radiobrightness time dependences, the latter having been taken over a bare soil plot, to be in good agreement, with deviation of the one from the other not exceeding the value of 6 to 8 K. This proves the SMOS footprint observed to consist of either bare or low and dry vegetation areas. Some difference between the SMOS and field measurements could be caused by the following factors. First, the heterogeneity in terms of soil moisture over the SMOS footprint observed could account for such a difference in radiobrightnesses. Second, the variation of the footprint size observed could also contribute in that difference. During the ground-based measurement in the case of grass covered plot, we registered a noticeable excess of the H-polarization radiobrightness over that related to the V-polarization radiobrightness, which may be attributed to the anisotropic permittivity of the grass layer. Such a phenomenon was sometimes registered regarding the SMOS radiobrightnesses observed. Using the radiobrightnesses measured in the field, we retrieved the topsoil moisture time dependences in the course of 2010 summer/autumn period. During this period of time, the moistures measured with the thermostatic-weighted method for a field plot and those retrieved from the SMOS radiobrightnesses were found to be of 3–8% and 2–4%, respectively. In autumn 2010, we carried out field measurements of the radiobrightness in the case of frozen topsoil. Once the soil moisture was too low during this measurement, in contrast to the results disscussed in [1, 2], the daily fluctuations of the radiobrightness, in the limits of ~ 15 K, were entirely caused by the respective fluctuations of the thermodynamic temperature, in the limits of ~ 18 K. Later, in the 2010–2011 winter period of time, we also carried out the measurement of radiobrightness in the case of soil surface covered with a snow layer. In general, the SMOS and in field measured radiobrightnesses were found to be in satisfactory agreement. We plan to proceed with this research in the Spring 2011 to study effect of snow melting on the SMOS radiobrightness fluctuations.

REFERENCES

1. Bobrov, P. P., V. L. Mironov, and A. S. Yashchenko, "Diurnal dynamics of soil brightness temperatures observed at frequencies of 1.4 and 6.9 GHz in the processes of freezing and thawing," *Journal of Communications Technology and Electronics*, Vol. 55, No. 4, 395–403, 2010.
2. Mironov, V. L., P. P. Bobrov, P. V. Zhirov, S. V. Krivaltsevitsh, A. S. Jaschenko, and R. D. De Roo, "Radiobrightness dynamics of freezing/thawing processes for different soils," *IEEE Geoscience and Remote Sensing Symposium and the 28th Canadian Symposium on Remote Sensing*, Vol. 6, 3015–3018, Denver, Colorado, USA, 2006.

Wave Attenuation in Sand and Dust Storms at 10.5 GHz

Hsing-Yi Chen[1], **Xiao-Ying Dong**[2], **and Dong-Hui Guo**[2]

[1]Department of Communications Engineering, Yuan Ze University
135, Yuan-Tung Road, Chung-Li 32003, Taiwan
[2]Department of Electronic Engineering, Xiamen University
Xiamen, Fujian 361005, China

Abstract— Sand and dust storms can affect microwave and millimeter-wave links due to the attenuation and cross-polarization produced by storm particles. Numerous calculations of wave attenuation in sand and dust storms are based on Rayleigh scattering approximation or Mie scattering theory. Attenuation calculated by Rayleigh scattering approximation is suitable for particles much smaller than a wavelength. The Mie scattering theory is elegant and still famous in today's research of scattering and absorption by spherical particles. However, calculations of wave attenuation in sand and dust storms by Rayleigh scattering approximation and Mie scattering theory do not include the multiple scattering effect or mutual interaction phenomenon. Sand and dust particles are randomly distributed in the air. Their geometries can not be classified as spheres, ellipsoids, cubes, or otherwise. In this paper, the attenuation and phase delay due to sand and dust storms are obtained by using the effective material property technique and general formulation of the complex propagation factor. The validity of attenuation is verified by Ghobrial et al.'s formula. It is found that the attenuation decreases sharply as the visibility increases. It is also proven that the attenuation is negligible except for very dense storms. The effective material property technique and general formulation of the complex propagation factor have shown a quick and easy way of calculating the attenuation and phase delay due to sand and dust storms, which otherwise requires complicated and expensive methods of calculation and measurement.

Bistatic Reflectometry and Refractometry Using GNSS Signals in the Earth's Surface and Atmosphere

Shuanggen Jin[1] **and Guiping Feng**[1, 2]

[1]Shanghai Astronomical Observatory, Chinese Academy of Sciences, Shanghai 200030, China
[2]Graduate University of the Chinese Academy of Sciences, Beijing 100049, China

Abstract— The Global Navigation Satellite System (GNSS) has been a very powerful and important contributor to all scientific questions related to precise positioning on Earth's surface, particularly as a mature technique in geodesy and geosciences. With the development of GNSS as a satellite microwave (L-band) technique, more and wider applications and new potentials are explored and utilized. Recently the versatile and available GNSS signals have been found to image the Earth's surface environments as a new, highly precise, continuous, all-weather and near-real-time remote sensing tool. In this paper, the recent results of GNSS remote sensing in the atmosphere, ocean, land and hydrology are presented, such as determining the atmospheric and ionospheric parameters and ocean height, wind speed and wind direction of ocean surface, soil moisture, ice and snow thickness. Furthermore, the future developments and new applications of GNSS remote sensing are presented and discussed.

Accelerated Melting of Antarctic Ice-sheet Observed from 7 Years of Satellite Gravimetry

Guiping Feng[1, 2], **Shuanggen Jin**[1], **and Liangjing Zhang**[1, 2]

[1]Shanghai Astronomical Observatory, Chinese Academy of Sciences, Shanghai 200030, China
[2]Graduate University of the Chinese Academy of Sciences, Beijing 100049, China

Abstract— Ice sheets are frozen fresh-water reservoirs with volume change related to the temperature and snowfall, which affect and are affected by changes in Earth's climate. It also plays a role in the global energy balance. However, due to the lack of in situ measurements, it is very difficult to monitor global high temporal-spatial ice-sheet variability in recently global warming, e.g., in the Antarctic. The Gravity Recovery and Climate Experiment (GRACE) mission with twin satellites launched in March 2002 can estimate monthly detailed Earth's gravity field which can be converted into the total terrestrial water storage (TWS), mainly reflecting ice sheets mass variations in the Antarctic. Therefore, the GRACE offers a unique opportunity to quantify ice-sheet mass variations. In this paper, accelerated melting of Antarctic ice-sheets is investigated from 7 years of monthly GRACE solutions (2003–2010).

Session 1P3b
Subsurface Imaging and Detection Technology, GPR

Infrared Imaging Detection of Hidden Danger in Mine Engineering

Shanjun Liu[1], **Zhongyin Xu**[1], **Lixin Wu**[1, 2], **Baodong Ma**[1], **and Xin Liu**[1]

[1]Institute for Geo-informatics & Digital Mine Research
Northeastern University, Shenyang 110819, China
[2]Academe of Disaster Reduction and Emergency Management
Beijing Normal University, Beijing 100875, China

Abstract— Thermal infrared (TIR) imaging is an all-weather, full-area, noncontact, and nondestructive technology. It has been successfully applied in the indoor and outdoor thermographic inspection of the defects of solid materials and building structures in the engineering scale. However, its use for detecting mine hidden danger is new.

In this paper, TIR imaging detection experiments were conducted in some mines of China to detect the mine safety problems, such as the landslide, high-stress area of underground mine and leakage of tailing pond etc. A thermal imaging system, VarioSCAN 3021ST with temperature precision 0.03°C and 360×240 pixel was applied to detect the temperature field of objects.

The experimental results showed that:

(1) In the high stress area of rock the infrared radiation temperature is higher. Hence, TIR imaging technology can detect the high-stress area of rock, which is very important for preventing the happening of rock burst.
(2) In the area of loose rock block the infrared radiation temperature is lower. Hence, TIR imaging technology can detect the loose rock block in the roof of laneway, which is very important for preventing the happening of collapse of roof rock occurring at underground mines.
(3) When water seeps from fracturing rock the infrared radiation temperature will became low. The experimental result indicates TIR imaging technology can detect the leakage of tailing pond, which is very important for preventing the happening of the break of tailing dam.
(4) In the landslide area of opencast mine the pattern of infrared radiation temperature field is different from that of the surrounding rock area. The experimental result indicates TIR imaging technology can detect the landslide of mine, which is very helpful for preventing the happening of landslide disaster.

Magnetic Anomaly Detection in Ferromagnetic Material

J. Atzlesberger and B. G. Zagar
Institute for Measurement Technology, Johannes Kepler University, Austria

Abstract— The proposed paper discusses a non-destructive testing (NDT) technique based on the magnetic flux leakage (MFL) method [1], which is able to detect magnetic anomalies in ferromagnetic material. These anomalies can be caused for example by thickness variation of the inspected test specimen [2], corrosion [3], residual stresses [4], cracks [5], flaws, non-metallic inclusions [6] and/or surface-defects. The goal is the detection of very small inhomogeneities not only on the surface but also anywhere in the cross section of magneto-conductive objects by scanning their surfaces using low-cost GMRs (giant magneto resistance) [7] at rather high scanning speeds (up to 3 m/s) in order to enable an automatic inspection and to minimize test time. The measured magnetic flux density variations due to the expected inhomogeneities are down to only some nT (depending on the inhomogeneity size and position) on a DC-level of some mT, therefore all parameters affecting the system's sensitivity (geometrical arrangement, sensors and electronics, signal acquisition, signal processing, etc.) have to be optimized in order to get a robust and highly sensitive measuring system. For the optimization of the magnetic circuit and the investigation of the measuring system's behaviour due to variation of different parameters FEM-simulations are used. As a pilot survey, some test specimen were prepared (by inserting artificial inhomogeneities into otherwise homogeneous, isotropic magneto conductive objects) and inspected with a prototype measuring system. Depending on the causes of the magnetic anomalies, the magnetic field strength images (obtained by 2-dimensional surface scans), may exhibit characteristical error patterns. For example a crack usually causes a very sharp but extended field anomaly in one direction (depending on the crack length and orientation) whereat corrosion usually appears as extensive region. By using appropriate digital image processing algorithms (in particular pattern recognition algorithms) the fault detection probability can be increased and the false alarm rate reduced, furthermore inhomogeneities which should not be considered can be ignored.

ACKNOWLEDGMENT

The authors gratefully acknowledge the partial financial support for the work presented in this paper by the Austrian Center of Competence in Mechatronics (ACCM).

REFERENCES

1. Blitz, J., *Electrical and Magnetic Methods of Non-destructive Testing*, 2nd Edition, Chapman & Hall, London, 1997.
2. Niese, F., "Wall thickness measurement sensor for pipeline inspection using EMAT technology in combination with pulsed eddy current and MFL," *ECNDT*, 2006.
3. Coughlin, C. R., et al., "Effects of stress on MFL responses from elongated corrosion pits in pipeline steel," *NDT&E International*, Vol. 33, 118–188, 2000.
4. Ricken, W., "GMR and eddy current sensor in use of stress measurement," *Sensors and Actuators*, 42–45, 2001.
5. Göktepe, M., "Non-destructive crack detection by capturing local flux leakage field," *Sensors and Actuators*, 70–72, 2001.
6. Atzlesberger, J. and B. Zagar, "Magnetic flux leakage measurement setup for defect detection," *Proc. of the Eurosensors XXIV*, Linz, Austria, September 2010.
7. Hauser, H., et al., "Magnetoresistors," *Magnetic Sensors and Magnetometers*, 129–171, 2001.

A New Analytical Method for Calculation of Eddy Current Distribution and Its Application to a System of Conductor-slab and Rectangular Coil

T. Itaya[1], **K. Ishida**[2], **A. Tanaka**[3], **N. Takehira**[2], **and T. Miki**[4]

[1]Suzuka National College of Technology, Japan
[2]Tokuyama College of Technology, Japan
[3]Ube National College of Technology, Japan
[4]Yamaguchi University, Japan

Abstract— This study proposes an analytical method for the eddy current distribution analyses, and provides the eddy current distribution in conductor slab with rectangular coils arranged perpendicular to the slab. Our analytical method utilizes double Fourier transform to derive a set of equations for determining the eddy current distribution. The eddy current density is derived from the analytical solution called "stream function". The spatial distribution of eddy current, which is dependent upon the excitation frequency, speed of moving conductor and conductor thickness, is successfully obtained. Our analytical method is usable for calculations of varieties of eddy current problems, and we demonstrate the eddy current distributions in a conductor slab facing to a rectangular coil.

Development of Spot Welding Evaluation Using a Magnetic Flux Leakage Method

Kosuke Miyake[1], **Kenji Sakai**[1], **Toshihiko Kiwa**[1],
Yoshinobu Hirano[2], **Mitsuaki Matsumoto**[2], **and Keiji Tsukada**[1]

[1]Okayama University, Japan
[2]Ohashi Engineering Co. Ltd, Japan

Abstract— Spot welding is widely used in automobile and aircraft body welding process. A fast and precise spot welding test is very important to assure product safety and quality control in productivity. Ultrasonic inspection, radiographic examination, and the infrared inspection have been used as the current method in spot welding test. However, these methods are expensive, and required skilled technicians, thus a low cost and high-efficient method is expected. In this study, we developed a spot welds evaluation technique using magnetic flux leakage flaw detection methods. The developed system consists of a coil for applying a magnetic field is applied to the sample measurement, ferrite core for a strong magnetic field, and a magneto resistance sensor (MR sensor) to detect magnetic flux leakage.

We measured and analyzed spot-welded samples which were joined by two iron plates. In addition, several samples were prepared by varying their welding time. We analyze measurement results to create a two-dimensional mapping using an image analysis system. By measuring the applied field and the parallel magnetic component, the results showed that for a sample with long weld time, the measured magnetic strength was strong, However, for a sample with short weld time, the measured magnetic strength was weak. This can be caused by the forming of low-permeability martensite at the welding spots and the difference in the amount of the formed martensite could be the influence of the experimental results. From this, by measuring the field strength at the spot welds, weld evaluation is possible.

To prove reliability in this method, tensile strength tests were made and measured weld strength showed that a correlation between the weld strength and the strength of stray fields at the spot weld joint was obtained. Using this developed system, mechanical strength of the welding spot can be determined by its magnetic flux leakage. Moreover, employing two-dimensional analysis technique, pattern of magnetic flux leakage changes can be visually analyzed.

Development of AC Magnetic Susceptibility Meter Using HTS-SQUID

Satoshi Maeda[1], **Yoshitatsu Yamaguchi**[1], **Kenji Sakai**[1], **Toshihiko Kiwa**[1], **Akira Tsukamoto**[2], **Seiji Adachi**[2], **Keiichi Tanabe**[2], **Akihiko Kandori**[3], **and Keiji Tsukada**[1]

[1]Department of Electrical & Electronic Engineering, Division of Industrial Innovation Sciences
Graduate School of Natural Science & Technology, Okayama University
3-1-1 Tsushimanaka, Kita-ku, Okayama 700-8530, Japan
[2]SRL-ISTEC, Japan
[3]Advanced Research Laboratory, Hitachi Ltd., Japan

Abstract— Magnetic susceptibility meters using Low-T_c Superconductor Superconducting Quantum Interference Device (LTS-SQUID) cooled by liquid helium have been widely used. LTS-SQUID has a high sensitivity of a few femtotesla, however, the measuring systems using LTS-SQUID need large cooling system with liquid helium for superconducting magnetic coil and LTS-SQUID. Recently, we developed a high sensitive High-T_c (HTS-) SQUID comparable to LTS-SQUID. Therefore, we have developed a compact AC magnetic susceptibility meter using HTS-SQUID operable liquid nitrogen temperature. The developed system consists of a Helmholtz coil exposing AC magnetic field to sample, a detection coil in order to detect sample signal, input coil which is directly-coupled to the detection coil and inductively coupled to SQUID for signal transferring, and 2-layer magnetically shield which is used to protect the HTS-SQUID for a stable work. The detection coil was designed to be a first-order differential coil in order to reduce static ambient magnetic fields and to improve the system output stability. The detection method is that the first-order differential coil detects the secondarily magnetic field generated from the sample exposed to low frequency magnetic field lower than 1 kHz. The signal of the sample was measured with lock-in amplifier, and analyzed to magnetic field strength and phase.

As an application of the developed system, we measured moisture content of mortar. The mortar was prepared by mixing standard sand, Portland cement, and water. The moisture content of the mortar is greatly related to the mortar strength and should be mixed in the proper amount of moisture content, which was from 11 to 13wt%. From the measurement results, the moisture content of the mortar is related to the magnetic field strength obtained by the developed system. Therefore, it was concluded that the developed system can be used as a moisture content evaluation.

Probabilistic Classification for Electromagnetic Demining — Issues and Advances towards Real Implementations

F. Viani[1], **L. Lizzi**[1], **P. Rocca**[1], **M. Balma**[2], **and A. Massa**[1]

[1]ELEDIA Research Group at DISI, University of Trento, Via Sommarive 14, I-38123 Trento, Italy
[2]Selex Galileo S.p.A., Str. Privata Aeroporto, I-10077 San Maurizio C.se, Torino, Italy

Abstract— Underground imaging through non-invasive techniques is of huge interest in civil and humanitarian frameworks ranging from the demining of dangerous areas contaminated with unexploded ordnances and landmines up to water leakages in underground water infrastructures.

In such a framework, approaches based on learning-by-examples (*LBE*) methods [1] proved their reliability and computational effectiveness thanks to the reduced computational burden (after the off-line training phase) that enables real-time estimations of both single and multiple buried targets [2–4]. Instead of deterministically determining locations and number of the unknown targets, the probabilistic classification thorugh LBE-methods defines a probability risk-map of the target-presence starting from the samples of the electromagnetic field at the air-soil interface collected through a suitable RF receiver. The spatial resolution of the targets within the region under test is increased fully exploiting the iterative synthetic zooming strategy iteratively performed on the '*Regions-of-Interest*' (RoIs) of the probability map where a higher presence-probability has been previously estimated [5].

Because of the flexibility of the approach, the fusion of heterogeneous data (i.e., data acquired with infrared and optical sensors besides microwave devices) is also exploited by means of suitably defined *support vector machine* (SVM) classifiers to further improve detection accuracy as well as resolution level. Moreover, an *incremental learning* strategy extending [6] is proposed to avoid (a) the customization of detection-system to a specific set of soils and targets, (b) a strong dependence of the classification performances on the environmental changes, and (c) the need of very large datasets in the initial training phase. More specifically, the incremental learning adaptively enables the discarging of past unreliable/unadequate training data and the inclusion of significant samples. Besides the training time reduction, such a process allows a fast re-adaptation of the classifier to the time-varying conditions of the scenario under test with enhanced generalization capabilities.

REFERENCES

1. Vapnik, V., *Statistical Learning Theory*, Wiley, New York, 1998.
2. Massa, A., A. Boni, and M. Donelli, "A classification approach based on SVM for electromagnetic sub-surface sensing," *IEEE Trans. Geosci. Remote Sens.*, Vol. 43, 2084–2093, Sep. 2005.
3. Bermani, E., A. Boni, S. Caorsi, and A. Massa, "An innovative real-time technique for buried object detection," *IEEE Trans. Geosci. Remote Sens.*, Vol. 41, No. 4, 927–931, Apr. 2003.
4. Lizzi, L., F. Viani, P. Rocca, G. Oliveri, M. Benedetti, and A. Massa, "Three-dimensional real-time localization of subsurface objects – From theory to experimental validation," *Proc. 2009 IEEE Int. Symp. Geosci. Remote Sens.*, 121–124, Cape Town, South Africa, Jul. 13–17, 2009.
5. Lizzi, L., M. Pastorino, F. Viani, and A. Massa, "3D electromagnetic subsurface imaging by means of a multi-resolution classification approach," *2010 Int. Symp. Electrom. Theory*, 175–178, EMTS, Berlin, Germany, Aug. 16–19, 2010.
6. Karasuyama, M. and I. Takeuchi, "Multiple incremental decremental learning of support vector machine," *IEEE Trans. Neural Networks*, Vol. 21, No. 7, 1048–1060, Jul. 2010.

Session 1P4a
Computational Techniques and Inverse Scattering Problems

High Performance 2D and 3D Approaches for Adjoint Variable Method Suitable for Inverse Problems

Ahmed Gomaa Radwan[1, 2]

[1]Cairo University, Egypt
[2]King Abdullah University of Science and Technology (KAUST), Saudi Arabia

Abstract— We present a novel efficient 2D and 3D computational approach for sensitivity analysis using the Adjoint Variable Method (AVM) combined with Time Domain Transmission-Line-Modeling (TD-TLM) using only one extra TD-TLM simulation. This approach is based on computing the necessary variables. The total variables needed are decreased by a rate of 80% in the 2D case and 83% in the 3D cases as compared with the conventional technique. This improvement will certainly reduce the necessary physical memory needed and will speed up the solution process by a considerable factor. By using these techniques, we can study the sensitivity analysis of larger discontinuous bodies inside the partially computational or completely computational domain. A Comparison table and examples are introduced to emphasis the importance of these techniques.

Reconstruction of Target Properties for Different Distributions Using Transient Adjoint Technique

Ahmed G. Radwan[1, 2]

[1]Faculty of Engineering, Applied Engineering Mathematics Department, Cairo University, Egypt
[2]King Abdullah University of Science and Technology (KAUST), Thuwal, Saudi Arabia

Abstract— Inverse electromagnetic scattering problems are computationally serious due to the complexity related with these problems. The most convenient way to solve inverse problems is by optimization techniques, which require some sensitivity analysis. This paper discusses the sensitivity analysis and the inverse problem solution using the Adjoint Variable Method (AVM) integrated with Transmission Line Modeling (TLM) and the gradient-based optimization technique to detect the properties of each cell inside the targets. The properties (ϵ_r, σ, μ_r) of each target is assumed to have certain distribution such as Gaussian, Poisson, exponential, chi-square, and gamma distributions. A comparison table is introduced with many different examples showing multiple obstacles having different distributions. Sensitivity analyses and inverse problem solutions are shown for different cases to recover the unknown parameters of the dielectric discontinuities through a given transient field.

Electromagnetic Inverse Scattering of Perfectly Electric Conductors by the Subspace-based Optimization Method

Xiuzhu Ye and Xudong Chen
National University of Singapore, Singapore 117576, Singapore

Abstract— A novel reconstruction method of perfectly electric conductors by a subspace-based optimization method (SOM) is presented in this paper. The key point in applying this method is discretizing the whole domain into square mesh and representing the scatterers by using the current line segments. Therefore, apart from the information that the unknown scatterer is PEC, no other prior information such as the number of the scatterers, the approximate locations or the centers is needed.

The SOM studies the spectral property of the singular values of the mapping from the induced current to the scattered field. And then split the induced current into two parts, the deterministic part which is uniquely determined by the mapping from the domain to receiver and scattered field, and the ambiguous part which is solved by optimization. Such process greatly reduces the number of unknowns involved in the optimization. The subspace-based optimization method for PEC scatterers is found to be more complex than its counterpart for dielectric scatterer that is also known as the medium scatterer.

A continuous-variable optimization method is further proposed to accelerate the convergence of the proposed SOM method. Several numerical examples are presented to verify our method. The proposed continuous-variable optimization method is found to behave more continuously in both the selection of the regularization parameters and the reconstruction pattern.

In particular, a combination of a line type object and a rectangular shape object is successfully reconstructed. To the best of our knowledge, the proposed algorithm is the first one that is able to reconstruct both closed-contour and line-shape obstacles, without a prior information of the total number of obstacles.

Reordering Techniques for Efficient Solution of Preconditioned Formulation of FE-BI Equations

Chao-Fu Wang and Fu-Gang Hu
Temasek Laboratories, National University of Singapore
#09-02, 5A Engineering Drive 1, 117411, Singapore

Abstract— Total electromagnetic (EM) scattering from a cavity structure within a general body can be described as an integration of interior scattering, exterior scattering, and scattering yielded through the interaction and coupling between fields on the interior surfaces of cavity and exterior of general body. The interior scattering is from interior surfaces of cavity and the exterior scattering is from exterior of the general body. This specific feature of the total scattering from a cavity structure naturally motivates us to develop numerical methods through dividing its computational domain into two parts in accordance to the aperture and cavity walls: cavity domain, and non-cavity domain which encloses the cavity domain. With this configuration, a preconditioned formulation of the finite element — boundary integral (FE-BI) equations with domain decomposition method (DDM) has been proposed for modeling the total scattering from cavity structure [1]. In the proposed method, the powerful higher order FE-BI method [2–4] is used to handle cavity domain and lower order one is used to handle non-cavity domain [5]. The employment of the Robin transmission condition (RTC) plays a key role in relating the fields in the interior and exterior regions of the cavity and mortar element technique [6] allows us to use tetrahedral elements with vector basis functions of different order in the two sub-domains [1]. Combination of these equations with that obtained from FEM and the combined field integral equation (CFIE) yields a complete system of equations, namely FE-BI-DDM matrix equation. It can be preconditioned using the effective and robust finite element-Robin transmission condition-absorber boundary condition (FE-RTC-ABC) preconditioner. To efficiently solve this preconditioned FE-BI-DDM matrix equation using fast algorithm with ILU decomposition, we have successfully implemented the FE-RTC-ABC preconditioner using two reordering techniques, reverse Cuthill-McKee (RCM) algorithm [7, 8] and METIS [9], to minimizing the bandwidth and profile of the preconditioner. Numerical simulation carried out for practical cavity structures illustrates the capability of the proposed method. More discussion and numerical results will be presented at the conference.

REFERENCES

1. Hu, F. G. and C. F. Wang, "Preconditioned formulation of FE-BI equations with domain decomposition method for calculation of electromagnetic scattering from cavities," *IEEE Trans. Antennas Propagat.*, Vol. 57, 2506–2511, Aug. 2009.
2. Jin, J. M., *The Finite Element Method in Electromagnetics*, 2nd Edition, Wiley, New York, 2002.
3. Liu, J. and J. M. Jin, "A special higher order finite-element method for scattering by deep cavities," *IEEE Trans. Antennas Propagat.*, Vol. 48, 694–703, May 2000.
4. Hu, F. G., C. F. Wang, and Y. B. Gan, "Efficient calculation of interior scattering from large three-dimensional PEC cavities," *IEEE Trans. Antennas Propagat.*, Vol. 55, No. 1, 167–177, Jan. 2007.
5. Liu, J. and J. M. Jin, "A highly effective preconditioner for solving the finite element-boundary integral matrix equation of 3-D scattering," *IEEE Trans. Antennas Propagat.*, Vol. 50, No. 9, 1212–1221, Sep. 2002.
6. Lee, S.-C., M. N. Vouvakis, and J.-F. Lee, "A non-overlapping domain decomposition method with non-matching grids for modeling large finite antenna arrays," *J. Comput. Phys.*, Vol. 203, 1–21, 2005.
7. Wang, C. F., "Efficient implementation of FE-RTC-ABC preconditioner for FE-BI equations with DDM," *APMC*, 2009.
8. Cuthill, E. and J. McKee, "Reducing the bandwidth of symmetric matrices," *Proc. 24th Nal. Conf. Assoc. Comput. Machinery*, 157–172, ACM Publ. P-69, Brandon Press, NJ, 1969.
9. Karypis, G. and V. Kumar, "A fast and highly quality multilevel scheme for partitioning irregular graphs," *SIAM J. Sci. Comput.*, Vol. 20, No. 1, 359–392, 1999.

A Novel Imaging Method for Inverse Scattering Problem Using Stepped-frequency Waveforms

Wei Yan, Nai-Zhi Wang, Amna Ajaz, and Jia-Dong Xu
School of Electronic and Information, Northwestern Ploytechnical University, Xi'an, Shaanxi, China

Abstract— Previously, many algorithms have been used to reconstruct an unknown object from backward scattering data. For the object on a turntable in microwave chamber, inverse synthetic aperture radar (ISAR) method is often used to acquire the image of the object. In this paper, circular synthetic aperture radar (CSAR) algorithm is applied to inverse scattering problem of the object. It can utilize the scattering sampled data of a 360 degree rotation of the objects on the turntable system. Compared to traditional ISAR method, CSAR algorithm can provide the reflective image of the target with high resolution. First, it transforms the scattering field to spatial frequency domain, and compensates the difference in height between the plane of antenna and the turntable. Then, circular spectrum theory is used to obtain the spatial frequency domain of the objects. After FFT transformation, the reflective image of the objects, which is also the spatial domain of the objects, is reconstructed. The point spread function (PSF) is given for the objects in the middle of turntable system. Finally, the simulations for the model of a plane are done both by CSAR algorithm and ISAR method. The results show that the method in this paper has high resolution. Then, an experiment with a metal plate on the turntable is done in microwave chamber at X band. The results form experiment is compared with the simulation of the same model, which shows the algorithm in this paper has high accuracy using stepped-frequency waveforms.

Mathematics behind the Fractional-order Smith Chart

A. G. Radwan[1, 2], **A. Shamim**[2], **and K. N. Salama**[2]

[1]Engineering Mathematics Department, Cairo University, Egypt
[2]Physical Sciences and Engineering
King Abdullah University of Science and Technology, Saudi Arabia

Abstract— Many practical measurements are related to the Smith chart such as input impedance, reflection coefficients, scattering parameters, and noise figure. The fractional-order Smith chart was introduced in our previous work. Many interesting features and properties that generalize the conventional Smith chart need to be explored. For example, it was shown that all the Smith chart circles (resistance and reactance) are actually pairs of identical circles. Moreover, the conventional Smith chart is considered now as a special case from this family of charts when the fractional order $\alpha = 1$. In this paper, we will discuss the major differences between the fractional-order impedance/admittance Smith charts relative to the conventional smith chart. Many analytical formulas with derivations will be introduced for the first time, quantity analysis with respect to the real and imaginary reflection coefficients, as well as sensitivity analysis with respect to the fractional-order parameter. In addition, the mathematics behind the single element fractional-order matching techniques will be emphasized with numerical techniques. This Smith chart can by used later for inverse.

Session 1P4b
Scattering and Inverse Problem

Algorithm Improvement for Real Time ILIDS Analysis in Airborne Research

Huanhuan Shen[1], **Marc Brunel**[1], **Gérard Grehan**[1], **Arnaud Querel**[2], **Pascal Lemaitre**[2], **and Emmanuel Porcheron**[2]

[1]UMR 6614 CORIA CNRS, Université de Rouen, France
[2]IRSN/DSU/SERAC/LECEV, Saclay, France

Abstract— Our objective is to develop an airborne optical spectrometer for atmospheric water droplets measurements (droplets diameters in the range 20–200 micrometers). The technique used is Interferometric Laser Imaging Droplet Sizing (ILIDS) which provides the instantaneous size and spatial distribution of transparent and spherical particles in a section of a flow [1, 2]. In ILIDS, the images of the droplets are captured with a CCD camera positioned in a non-focal plane (out-of-focus imaging). The camera records the interferometric pattern of the laser light scattered by the particles. This pattern results from the interference between the light reflected at the droplet surface and the light refracted within the droplet. Each droplet is thus associated to a circular fringe pattern whose frequency is linked to the droplet diameter. In our airborne system, the analysis must be fast enough to perform real-time processing during a flight through clouds. In order to realize a high-speed analysis of ILIDS interferograms, a Fourier analysis based on fast-Fourier transforms has been developed. Experimentally, a frequency-doubled pulsed Nd : YAG laser is extended using a cylindrical lens in order to create a laser sheet. The ILIDS scattered field is recorded at a scattering angle of 66° (which allows to obtain the best fringe contrast). As the camera is not perpendicular to the laser sheet, the images suffer some aberrations: focusing properties are indeed not identical on both right hand-side and left hand-side of the images. A Scheimpflug apparatus has thus to be added to correct this property [3].

In the present paper we show that our high speed analysis can be improved to avoid the use of a Scheimpflug apparatus. The Scheimpflug is indeed an obstacle to the compact integration of the whole system in an airborne device. We present in this communication a numerical alternative. We show how ILIDS images can be numerically modified to correct the image distortion introduced by the scattering angle, instead of using a Scheimpflug system.

The communication will be organized as follows: we will first recall the principle of our airborne ILIDS system, and the principle of the algorithm that has been developed for real time analysis. In a second time, we will present the principle of the image distortion that can be done numerically to avoid the introduction of a Scheimpflug system in the set-up. Performances of this alternative will be discussed.

ACKNOWLEDGMENT

This work is supported by the European EUFAR project.

REFERENCES

1. König, G., K. Anders, and A. Frohn, "A new light-scattering technique to measure the diameter of periodically generated moving droplets," *J. Aerosol Sci.*, Vol. 17, 157, 1986.
2. Glover, A. R., S. M. Skippon, and R. D. Boyle, "Interferometric laser imaging for droplet sizing: A method for droplet-size measurement in sparse spray systems," *Appl. Opt.*, Vol. 34, 8409, 1995.
3. Quérel, A., P. Lemaitre, M. Brunel, E. Porcheron, and G. Gréhan, "Real time global interferometric laser imaging for droplet sizing (ILIDS) analysis for airbone research," *Measurement Science and Technology*, Vol. 21, 015306, 2010.

Subspace-based Optimization Method for Reconstructing Extended Scatterers from Measured Phaseless Data

L. Pan, X. Chen, and S. P. Yeo
Department of Electrical and Computer Engineering
National University of Singapore, Singapore 117576, Singapore

Abstract— The electromagnetic inverse scattering technique has attracted much interest in a diversity of imaging-related applications, such as remote sensing, biomedical diagnosis, nondestructive testing and military surveillance. One of the main challenges in the practical application of inverse scattering technique lies in the fact that that the phase is generally more difficult to measure than the amplitude. As a matter of fact, accurate knowledge of the phase information involves far more sophisticated measurement equipments, especially as the working frequency increases. Furthermore, researchers have reported that the accuracy of phase measurements cannot be guaranteed for operating frequencies approaching the millimeter-wave band and beyond, due to the fact that the phase data is more prone to noise corruption during measurement than the amplitude data. Consequently, the adoption of phaseless (intensity-only) inverse scattering techniques is mandatory at optical frequencies, and strongly suggested at microwave frequencies.

In this paper, we use the phaseless measurement data (i.e., intensity data of the total field with no phase information) from the Fresnel database [1] to test the subspace-based optimization method (SOM) [2, 3]. Based on spectrum analysis, the contrast source is partitioned into two orthogonally complementary portions (viz., deterministic and ambiguous portions). The original SOM's procedure [2, 3] to obtain the deterministic portion has to be modified in order to accommodate the lack of phase information while the ambiguous portion is determined by another nonlinear optimization.

REFERENCES

1. Geffrin, J.-M., et al., "Free space experimental scattering database continuation: Experimental set-up and measurement precision," *Inverse Problems*, Vol. 21, S117, 2005.
2. Chen, X., "Application of signal-subspace and optimization methods in reconstructing extended scatterers," *Journal of the Optical Society of America A*, Vol. 26, 1022–1026, 2009.
3. Pan, L., K. Agarwal, Y. Zhong, S. P. Yeo, and X. Chen, "Subspace-based optimization method for reconstructing extended scatterers: Transverse electric case," *Journal of the Optical Society of America*, Vol. 26, 1932–1937, 2009.

An Improved Inverse Scattering Transform for DNLS$^+$ Equation under Nonvanishing Boundary Condition

Guo-Quan Zhou[1, 2]

[1]Department of Physics, Wuhan University, Wuhan 430072, China
[2]Department of Mathematics, The University of Vermont, Burlington, VT 05401, USA

Abstract— A revised and rigorously proved inverse scattering transform (IST for brevity) for the derivative nonlinear Schrödinger (DNLS$^+$) equation with nonvanishing boundary condition (NVBC) and normal group velocity dispersion is proposed by introducing a suitable affine parameter in Zakharov-Shabat integral kern; the explicit breather-type one soliton solution has been derived, which can reproduce the one pure soliton at the degenerate case and the the one bright soliton solution at the limit of vanishing boundary, verifying the validity of the improved IST.

Glare Point Reconstruction in Digital Holographic Microscopy for Droplet Characterization

Huanhuan Shen[1], **Marc Brunel**[1], **Sébastien Coetmellec**[1], **Gérard Grehan**[1], **Denis Lebrun**[1], **Xuecheng Wu**[2], **and Kefa Cen**[2]

[1]UMR 6614 CORIA CNRS, Université de Rouen, France
[2]State Key Laboratory, Zhejiang University, China

Abstract— Digital in-line holography can bring many informations in particle analysis. In the last decade, many configurations have been tested. In particular, the development of numerical anamorphous reconstruction has brought much progress to in situ characterizations of flows in pipes and micropipes [1, 2]. Of main importance is now the possibility to distinguish clearly opaque, semi-transparent or transparent particles in a flow. Some first works have been done through digital in-line phase contrast experiments [3], but much has still to be done. For the characterization of transparent or semi-transparent objects, the digital off-axis holography has important potentialities. It should indeed allow to determine simultaneously the position, the diameter, the real and imaginary parts of the refractive index of particles present in a flow.

We present in this communication our studies carried out in the domain of off-axis numerical holographic microscopy. Combining Generalized Lorenz-Mie Theory (GLMT) to compute the field scattered by transparent droplets and digital holography [4], we show that a numerical reconstruction based on the fractional Fourier transform allows to characterize the particle in terms of diameter of the droplet, position and refractive index.

The configuration under study is as follows: a laser illuminates some droplet. A camera records the hologram made by interference of a reference wave and of the laser light scattered by the particle. This pattern results essentially from the interference between the reference wave and both the light reflected at the droplet surface and the light refracted within the droplet. These two ways act as if two laser sources were issued from the droplet (i.e., the glare points). Using GLMT, we compute theoretical off-axis numerical holograms. In a second step, a fractional-order Fourier reconstruction is done and we show that the two glare points can be reconstructed. This reconstruction process allows then to determine characteristics of the droplets as position, diameter and refractive index.

In this communication, we will first present the principle of our GLMT calculations to predict numerical holograms, and our technique of numerical reconstruction using the fractional-order Fourier transformation. The results concerning the reconstruction of the glare points and the droplet characterization will then be detailed.

REFERENCES

1. Verrier, N., S. Coëtmellec, M. Brunel, and D. Lebrun, "Digital in-line holography in thick optical systems: Application to visualization in pipes," *Appl. Opt.*, Vol. 47, No. 22, 4147–4157, 2008.
2. Verrier, N., C. Rémacha, M. Brunel, D. Lebrun, and S. Coëtmellec, "Micropipe flow visualization using digital in-line holographic microscopy," *Opt. Express*, Vol. 18, No. 8, 7807–7819, 2010.
3. Brunel, M., S. Coëtmellec, D. Lebrun, and K. Aït Ameur, "Digital phase contrast with the fractional Fourier transform," *Appl. Opt.*, Vol. 48, No. 3, 579–583, 2009.
4. Wu, X., G. Gréhan, S. Meunier-Guttin-Cluzel, L. Chen, and K. Cen, "Sizing of particles smaller than 5 μm in digital holographic microscopy," *Optics Letters*, Vol. 34, No. 6, 857–859, 2009.

Temporal Backscattering of Forests: Ground Measurements

C. Albinet[3], **P. Borderies**[3], **T. Koleck**[1, 2], **F. Rocca**[4], **S. Tebaldini**[4], **T. Le Toan**[2], **and L. Villard**[2]

[1]CNES, Toulouse, France
[2]CESBIO, Toulouse, France
[3]ONERA, Toulouse, France
[4]POLIMI, Milan, Italy

Abstract— This abstract deals with ground experiments related to the future spaceborne BIOMASS mission for global forest biomass estimation.

Tropical forests present the major part of the world forest biomass and their changes in biomass by deforestation and/or by forest regeneration affect strongly the terrestrial carbon budget. To measure with accuracy tropical forest biomass and its temporal change is one of the objectives of the BIOMASS mission [1], a candidate for the European Space Agency 7th Earth Explorer Mission.

The possible retrieval algorithms currently developed for BIOMASS are based on the use of backscatter measurements derived from intensity, polarimetry and interferometry. However, these quantities are subject to evolution with the life cycle and the meteorological conditions at very different time scales, ranging from a few minutes to days, months ... with the possibility that their changes may affect the inversion algorithms. A ground experiment has been set up to follow systematically these evolutions. It has been installed over a temperate tree and also over a tropical forest in French Guiana. Based on the use of a Vector Network Analyzer and adequate antennas, it may deliver P band polarimetric, interferometric impulse responses and 2D (range/height) imaging.

In the presentation the set up will be described and their implementation in both sites discussed first. Then, some results about both site measurements will be displayed and the preliminary conclusions expound.

REFERENCES

1. BIOMASS Phase 0 Report for Assessment, European Space Agency, Nov. 2008, ref. SP1313/2.

Efficient Partial Concealment of Convex Conductive Body

A. M. Lebedev and A. I. Fedorenko
Institute for Theoretical and Applied Electromagnetics, Russian Academy of Sciences, Russia

Abstract— The solution to the problem of partial concealment of convex surface of big conductive body through the application of radar absorbing material (RAM) is discussed; the surface curvature radius is supposed to be much greater than the radar wave length. The task is to reduce the radar signature, characterized by backscattering radar cross section (further RCS for short), in relatively small interval of partial concealment $\Delta\varphi_{PC}$, which is supposed to be much smaller than the angular interval of normal to the surface direction variation $\Delta\varphi_N$. Precisely, the following is required: 1) angular interval of RAM coating $\Delta\varphi_{RAM}$ must only slightly exceed $\Delta\varphi_{PC}$ and, correspondingly, constitute only a small part of $\Delta\varphi_N$, 2) RCS reduction in angular interval $\Delta\varphi_{PC}$ must be about R_P times, where R_P is the coefficient of power reflection from RAM on the metal surface. Such solution to the problem of partial concealment should be considered efficient.

Even upon condition that good or ideal RAM is used, there exist two obstacles to the solution, each of them relates to the finiteness of RAM coating. Firstly, not more than 6dB RCS reduction at the end-points of RAM coating angular interval can be obtained (hence the difficulty in providing sharp RCS reduction with variation of angle). Secondly, the boundaries of uncoated surface virtually determine the backscattering within the interval of the desired concealment, and it can only be overturned if $\Delta\varphi_{RAM} \gg \Delta\varphi_{PC}$.

The problem is proved to be solved via introduction of gradual transition RAM-conductor; the classical apparatus of Fresnel zones is applied. The condition on gradual transition extent, which provides $\Delta\varphi_{RAM} \to \Delta\varphi_{PC}$ and explicit threshold-type reduction of RCS in R_P times within the angular interval $\Delta\varphi_{PC}$, was obtained.

Session 1P5
Novel Mathematical Methods in Electromagnetics

Some Helicities in Electromagnetic Fields

Zi-Hua Weng
School of Physics and Mechanical & Electrical Engineering
Xiamen University, Xiamen 361005, China

Abstract— The concept of the helicity was originated by C. F. Gauss's studying of the orbits of the comet and the asteroid in the astronomy. Recently it is extended to the researches regarding the double helix structure of DNA molecular chain, the solar electromagnetic field, the fluid dynamics, the meteorology and the topology etc. In the astronomy the helicity can be used to investigate the helical structure of the solar magnetic field, including the magnetic helicity, the current helicity, the cross helicity, and the kinetic helicity. In the fluid dynamics the helicity can be used to illustrate the vorticity fields, the kinetic helicity, and the enstrophy. It is found that the helicity will impact the inertial mass density and the mass continuity equation.

The algebra of quaternions was invented by W. R. Hamilton, and was first used by J. C. Maxwell to describe the features of the electromagnetic fields. Later the quaternion is used to represent the physical properties of the gravitational fields. The quaternion space for the gravitational field is independent to that for the electromagnetic field. These two quaternion spaces are perpendicular to each other, and are combined together to become one octonion space, which is related to the algebra of octonions. The latter was invented by A. Cayley etc. Consequently the octonions can be used to depict the features of the gravitational field and the electromagnetic field simultaneously, including the mass continuity equation, the inertial mass, and the helicity etc.

In the electromagnetic field and gravitational field, the octonion operator can draw out directly the physical properties of two fields, including the field potential, the field strength, the field source, the linear momentum, the angular momentum, the energy, the torque, the power, the force, and some helicities of the rotational objects and the spinning charged objects etc. In terms of the octonions, the helicity in the electromagnetic and the gravitational fields can be found in the definition of the field source and the force-power. The helicities cover all known helicity terms in the classical theories, including the magnetic helicity, the current helicity, the cross helicity, the kinetic helicity, the field energy, the enstrophy, and some new helicity terms.

It should be noted that the study for the helicity terms with different kinds of operators examined only some simple cases in the electromagnetic field and gravitational field. Despite its preliminary features, this study can clearly indicate the helicity terms and the enstrophy are only some simple inferences of the field strength helicity and the field source helicity. They will impact the inertial mass density and the mass continuity equation in the electromagnetic and gravitational fields. For the future studies, the research will concentrate on only the predictions about some new cross helicity terms related to different physical quantities in the case of the high velocity curl and the strong strength in the electromagnetic field and gravitational field.

ACKNOWLEDGMENT

The author is grateful for the financial support from the National Natural Science Foundation of China under grant number 60677039.

Finite Element Mesh Partitioning Using a Bubble Inspired Algorithm

Peng Liu[1] and Chao-Fu Wang[2]

[1]Key Laboratory of Wave Scattering and Remote Sensing Information (Ministry of Education)
Fudan University, Shanghai 200433, China
[2]Temasek Laboratories, National University of Singapore
5A, Engineering Drive 1, #09-02, Singapore 117411, Singapore

Abstract— To solve large-scale problems of real life on parallel computers, solution methods based on the concept of divide and conquer provide very attractive efficiency and robustness in finite element (FE) computations, such as domain decomposition method and multifrontal method. Both methods require their mesh space to be partitioned into a specified number of subdomains in a way that most closely reaches the following goals: (1) the profile of interface equation system connecting adjacent subdomains is minimized, (2) the profile of subdomain equation system is minimized, and (3) the computational load within the subdomain is the same in all subdomains.

Growing process of clusters of soap bubbles and interface between them reveals many interesting properties, such as the total area of the interface being a minimum and every single bubble also has the minimal surface area. All of these properties are governed by one of the most fundamental physical principles: minimization of energy. Following this physics of nature and constituting 'analogue computers' of bubbles can help us in solving the NP-hard mathematical problem of mesh partitioning, which will be the necessary first step of the domain decomposition based FE algorithms.

This paper presents a novel FE mesh partitioning algorithm, namely bubble inspired algorithm. Unlike those previous diffusion BUBBLE and Center-oriented Bubble methods, this newly proposed algorithm employs the physics mechanisms of real bubbles, including nucleation, spherical growth, bubble-bubble collision, reaching critical state, and the final competing growth. The realization of foaming process of real bubbles in the algorithm enables us to create partitions with good shape and without having to specify large number of artificial controls. The minimum edge cut can be simply achieved by increasing the volume of each bubble in the most energy efficient way. Moreover, the order, in which an element is gathered into a bubble, delivers the minimum number of surface cells at every gathering step, thus the optimal numbering of elements in each subdomain has naturally achieved. These two features have huge payback in terms of solver efficiency, as most efficient FE solvers, like multifrontal method, need to loop over all elements in the local subdomain condensation phase and the global interface solution phase. Experiments conducted on various structured and unstructured meshes clearly show that the obtained results are consistently better than the classical kMetis library in terms of the edge cut, partition shape and partition-connectivity.

Comparative Analysis of the Dynamic Stark Effect in Spectra of Rare Gas Atoms and Ions

E. V. Koryukina[1] and V. I. Koryukin[2]

[1]Tomsk State University, Lenin Avenue 36, Tomsk 634050, Russia
[2]Siberian State Medical University, Moscow Road 2, Tomsk 634050, Russia

Abstract— In this work, theoretical *ab initio* calculations and comparative analysis of splitting and shifts of energy levels of rare gas atoms and ions in an alternating circularly polarized electric field are performed. Electric fields of such polarization are generated in an inductive high-frequency discharge, under laser excitation and in collisions with charged particles at ultralow energies. Study of the Stark effect in spectra of rare gas atoms and ions is a topical problem, because rare gases are widely used in plasma physics.

In the circular polarized electric field, the non-stationary Schrödinger equation from which energies and wave functions of atoms in the electric field are determined is reduced to the stationary one. In traditional works, the stationary Schrödinger equation is solved in the framework of perturbation theory. However, it is much more convenient to solve this equation by the method of energy matrix diagonalization [1]. This method, free from limitations inherent in perturbation theory, is suitable for a wide range of frequency and strength of the electric field.

The suggested theoretical approach was implemented in a special software package written in FORTRAN. As the basis functions, the *ns*-, *np*-, *nd*-, and *nf*-states with principal quantum numbers n up to 10 were chosen. Calculations of the energy matrix of atoms in the electric field were performed using the *Jl*-coupling scheme for the Ne, Ar, and Kr atoms and using the *LS*-coupling scheme for the He atom. In calculations of the energy matrix of the Ne^+ and Ar^+ ions, the *ns*-, *np*-, and *nd*-states were computed using the *LS*-coupling scheme, while the *nf*-states were calculated using the *Jl*-coupling scheme. The behavior of all examined *ns*-, *np*-, *nd*-, and *nf*-states was investigated versus changes in the frequency ω and strength F of the electric field as well as versus changes in the nucleus charge Z.

The computations performed have allowed us to reveal the following regularities in the behavior of energy levels of atoms in the electric field:

- The dependence of the energy level shifts on the electric field strength is quadratic. Moreover, the sequence of levels in the electric field depends monotonically on the principal quantum number of an electron from the external shell;
- A decrease in splitting of the energy levels with an increase in the electric field frequency;
- Even and odd energy levels of He and Ne atoms are shifted toward opposite directions with an increase in the electric field strength. For all considered Z, the *ns*-levels are shifted toward the IR region, and the *nf*-levels are shifted toward the UV region.

The behavior of the energy levels in the electric field was also investigated for Ne^+ and Ar^+ rare gas ions.

It should be noted that quadratic dependence of the energy level shifts on the electric field strength is well known from perturbation theory. The rest of the regularities in the behavior of energy levels of atoms and ions depending on changes in the electric field strength, frequency, and nucleus charge Z have been obtained for the first time. The established regularities allow us to determine the behavior of spectral lines of rare gas atoms and ions in electric fields of arbitrary frequency and strength.

REFERENCES

1. Koryukina, E. V., *J. Phys. D: Appl. Phys.*, Vol. 38, 3296–3300, 2005.

Differential Forms and Decomposable Media

I. V. Lindell[1], **L. Bergamin**[2], **and A. Favaro**[3]

[1]Aalto University, Finland
[2]KB&P GmbH, Switzerland
[3]Imperial College London, UK

Abstract— Differential forms allow a most convenient way to express different relations of the electromagnetic fields in four-dimensional representation. The Maxwell equations take the compact form [1]

$$\mathbf{d} \wedge \mathbf{\Phi} = 0, \qquad \mathbf{d} \wedge \mathbf{\Psi} = \boldsymbol{\gamma}, \tag{1}$$

where $\mathbf{\Phi} = \mathbf{B} + \mathbf{E} \wedge \mathbf{d}\tau$ and $\mathbf{\Psi} = \mathbf{D} - \mathbf{H} \wedge \mathbf{d}\tau$ are two field two-forms (six-dimensional quantities) and $\boldsymbol{\gamma} = \boldsymbol{\rho} - \mathbf{J} \wedge \mathbf{d}\tau$ denotes the four-dimensional charge-current source. The medium condition becomes

$$\mathbf{\Psi} = \overline{\overline{\mathsf{M}}} | \mathbf{\Phi}, \tag{2}$$

where the medium dyadic $\overline{\overline{\mathsf{M}}}$ is a quantity involving 36 parameters in general.

In the present paper a class of decomposable media (DCM) is defined in terms of the four-dimensional formalism. In particular, the medium dyadic $\overline{\overline{\mathsf{M}}}$ is restricted by the requirement that the fields in the medium can be decomposed in two sets: the A-field and the B-field, where the two field components are defined by orthogonality conditions with respect to two chosen bivectors, $\mathbf{A}$ and $\mathbf{B}$, as

$$\mathbf{\Phi} = \mathbf{\Phi}_A + \mathbf{\Phi}_B, \qquad \mathbf{A} | \mathbf{\Phi}_A = 0, \quad \mathbf{B} | \mathbf{\Phi}_B = 0. \tag{3}$$

It is shown that the DCM class can be defined by requiring that the medium dyadic satisfy a dyadic equation of the second order, or in a special case, of the first order. Actually, the DCM class can be split in three subclasses, two of which, denoted by QDCM and PDCM, arise from the solutions of the second-order equation and the third, denoted by SDCM, from the solution of the first-order equation. The QDCM and PDCM are shown to equal the previously studied classes of generalized Q-media [2] and generalized P-media [3] with an addition of an extra axion term. The special case, SDCM, defines another class of decomposable media, not studied previously.

Dispersion equations are derived for each of the three subclasses and the corresponding eigenpolarizations are shown to satisfy the orthogonality conditions (3) corresponding to the decomposition of the field.

REFERENCES

1. Lindell, I. V., *Differential Forms in Electromagnetics*, Wiley, New York, 2004.
2. Lindell, I. V. and H. Wallén, "Generalized Q-media and field decomposition in differential-form approach," *Journal of Electromagnetic Waves and Applications*, Vol. 18, No. 8, 1045–1056, 2004.
3. Lindell, I. V., L. Bergamin, and A. Favaro, "The class of electromagnetic P-media and its generalization," *Progress In Electromagnetics Research B*, Vol. 28, 143–162, 2011.

Asymptotics of Physical Solutions to the Lorentz-Dirac Equation for a Planar Motion in Constant Electromagnetic Fields

P. O. Kazinski[1, 2] **and M. A. Shipulya**[1]

[1]Tomsk State University, Tomsk, Lenin ave. 36, 634050, Russia
[2]Institute of Monitoring of Climatic and Ecological Systems
Tomsk, Academichesky ave. 10/3, 634055, Russia

Abstract— The Lorentz-Dirac (LD) equation has an ill fame to suffer from the various type inconsistencies. The latter come from the higher derivative Schott term entering the LD equation and appear as the blowing up (runaway) and acausal solutions. However, despite of its undesirable features, we have to accept the LD equation as a correct one in its range of applicability by the following reasons. First, as it was shown in the seminal paper by Dirac [1] and then more elaborately in [2], the LD equation stems from the energy-momentum conservation law provided a charged particle is sufficiently small and possesses neglible higher multipoles of a charge distribution. Second, under these assumptions the LD equation is a minimal evolutionary equation describing a radiation reaction which complies with all the symmetries of the model: the Poincare and reparameterization invariance. Furthermore, having made certain approximations, the LD equation was derived in the context of quantum electrodynamics (see, e.g., [3]), where the LD equation can be considered as a leading quasiclassical asymptotics to the Schwinger-Dyson equations for an electron. Therefore, the LD equation makes a physical sense and, under certain conditions, its solutions should give rise to predictions which can be observed in experiments. It is clear that the LD equation is valid in the range of energies and field strengths where the quantum corrections are neglible in comparison with the classical contribution. Rough general estimates of this range can be found, e.g., in [4, 5], and the more accurate analysis for the particular case of a constant homogeneous magnetic field is presented in [6].

We present a study of planar physical solutions to the Lorentz-Dirac equation in a constant electromagnetic field. In this case, we reduced the Lorentz-Dirac equation to the one second order differential equation. We obtained the asymptotics of physical solutions to this equation at large proper times. It turns out that, in the crossed constant uniform electromagnetic field with vanishing invariants, a charged particle goes to a universal regime at large times. We found the ratio of momentum components which tends to a constant determined only by the external field. This effect is essentially due to a radiation reaction. There is no such an effect for the Lorentz equation in this field.

ACKNOWLEDGMENT

We appreciate Prof. V. G. Bagrov for stimulating discussions on the subject. The work is supported by the Russian Ministry of Education and Science, contract No. 02.740.11.0238, the FTP "Research and Pedagogical Cadre for Innovative Russia", contracts No. P1337, P2596, and the RFBR grant 09-02-00723-a.

REFERENCES

1. Dirac, P. A. M., "Classical theory of radiating electrons," *Proc. Roy. Soc. London A*, Vol. 167, 148, 1938.
2. Teitelboim, C., "Splitting of the Maxwell tensor: Radiation reaction without advanced fields," *Phys. Rev. D*, Vol. 1, 1572, 1970.
3. Krivitskii, V. and V. Tsytovich, "Average radiation-reaction force in quantum electrodynamics," *Sov. Phys. Usp.*, Vol. 34, 250, 1991.
4. Klepikov, N. P., "Radiation damping forces and radiation from charged particles," *Sov. Phys. Usp.*, Vol. 28, 506, 1985.
5. Shen, C. S., "Radiation and acceleration of a relativistic charged particle in an electromagnetic field," *Phys. Rev. D*, Vol. 17, 434, 1978.
6. Bagrov, V. G., G. S. Bisnovatyi-Kogan, V. A. Bordovitsyn, A. V. Borisov, O. F. Dorofeev, V. Y. Epp, V. S. Gushchina, and V. C. Zhukovsky, *Synchrotron Radiation Theory and Its Development*, World Scientific, Singapore, 1999.

Spectral Theory of Beam Scattering by Random Curved Surfaces for Imaging Laser Radar

Yasumitsu Miyazaki
Department of Media Informatics, Aichi University of Technology
50-2 Manori, Nishihasama-cho, Gamagori 443-0047, Japan

Abstract— Fundamental theory of scattering characteristics of laser beam wave has been studied for optical beam waveguide, optical resonator and optical beam circuit element. Particularly, reflection and scattering characteristics by curved surface of lens waveguide are typical examples. The author showed analytical theory of boundary value problem for beam wave scattering by general curved surfaces. Recently, we studied beam wave scattering theory concerning distance control system between driving automobiles and shape image recognition system using millimeter wave sensors. With the shape image recognition system of objects using millimeter electromagnetic waves, the system using laser radar is considered as effective autocruising system. In this paper, statistical scattering theory by random curved surface using spectral function is discussed. This theory is fundamental for laser radar sensors and applicable to optical ray tracing and CG.

Gaussian laser beam waves with temporal Gaussian impulse radiated from laser radar incident to complicated targets are considered. Spatial and temporal spectral functions are introduced using transverse wave number spectrum for the spatial space and angular frequencies for time domain. Spatial spectral functions concerned with Hermite-Gaussian eigenfunctions are expressed for incident and scattering electromagnetic fields. Asymptotic expressions are derived for the incident Gaussian beam, and reflected and scattered waves, using parameters of beam waist and beam spot size. Radiating optical beam packets from laser radars and reflected beam packets of temporal Gaussian pulse form and spatial Gaussian beam form are expressed as Fourier components for time coordinates and as spectral functions expanded by Hermite-Gaussian functions for space coordinates. Incident, reflected and scattered fields are studied using beam mode expansions derived by Hermite-Gaussian spectral functions.

Scattered and transmitted waves are discussed using eigenfunction orthogonalities, satisfying boundary conditions on complicated target shape for spectral functions of incident, reflected and transmitted waves. Boundary conditions of objects are applied to derive reflected and scattered fields for spectral components. Based on temporal and spatial characteristics of laser beam wave scattering, image recognition of object targets are shown with computer image processing.

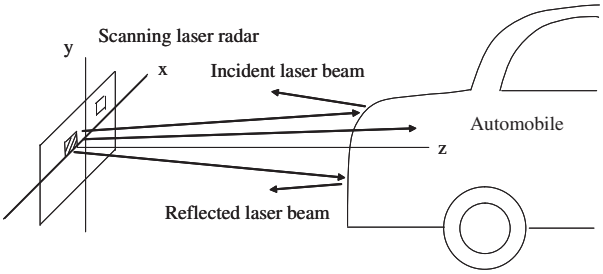

Figure 1: Automobile laser radar.

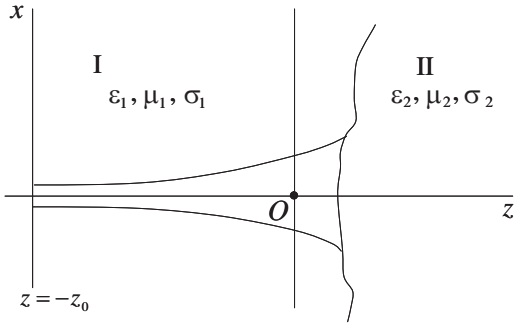

Figure 2: Reflection and scattering of laser beam wave by random curved surface.

REFERENCES

1. Akao, Y. and Y. Miyazaki, "Reflection and mode conversion of beam wave through a curved interface between dielectrics and thick dielectric lens," *Trans. of IECE, Japan*, Vol. 51-B, No. 1, 25–31, 1968.
2. Tanaka, M. and Y. Miyazaki, "Microwave simulation characteristics of electromagnetic wave scattering by automobile," *Trans. of IECE, Japan*, Vol. J66-B, No. 8, 1005–1012, 1983.
3. Miyazaki, Y., "Electromagnetic scattering theory of car body imaging using scanning millimeter wave radar," *PIERS Proceedings*, 1423–1428, Beijing, China, March 23–27, 2009.

Magnetoelectric Near Nields

E. O. Kamenetskii, **R. Joffe**, **and R. Shavit**
Microwave Magnetic Laboratory, Department of Electrical and Computer Engineering
Ben Gurion University of the Negev, Beer Sheva, Israel

Abstract— In a source-free subwavelength region of electromagnetic (EM) fields there can exist a local relation between the time-varying electric and magnetic fields differing from the electric-magnetic coupling in regular-propagating free-space EM waves. To distinguish such field structures we term them as magnetoelectric (ME) fields. We show that there exist point sources of microwave ME fields — the ME particles. These particles are represented by small quasi-2D ferrite disks with the magnetostatic-resonance spectra [1, 2]. Because of dynamics of the magnetization motion in a ferrite disk, characterizing by azimuth symmetry breaking, small ferrite particles with the magnetostatic-resonance spectra originate free-space microwave fields — the ME fields — with unique symmetry properties. There are the fields with the helicity effects and the power-flow-density vortices in a subwavelength region of a free-space electromagnetic field. ME fields have the "electric-magnetic democracy" very distinctive from the "electric-magnetic democracy" in free-space propagating-wave Maxwellian fields.

A small ferrite-disk particles with magnetostatic-resonance oscillations — the ME particles — can be represented as a rotating magnetic dipole and an electric moment normal to a disk plane [3, 4]. This gives a very peculiar mechanism of scattering of microwave EM fields by such a particle. In contrast to small metal particles with electrostatic (plasmon) resonances, where there is a strong localization of electric fields [5], in small ferrite particles with magnetostatic (magnon) resonances one has a strong localization of both magnetic and electric fields [6, 7].

We give a theoretical background of properties of the electric and magnetic fields inside and outside of a ferrite particle with the magnetostatic-resonance spectra resulting in appearance of microwave ME fields. We show results of numerical studies of microwave ME fields.

REFERENCES

1. Kamenetskii, E. O., *J. Phys. A: Mathematical and Theoretical*, Vol. 40, 6539, 2007.
2. Kamenetskii, E. O., *J. Phys.: Condens. Matter*, Vol. 22, 486005, 2010.
3. Sigalov, M., E. O. Kamenetskii, and R. Shavit, *J. Phys.: Condens. Matter*, Vol. 21, 016003, 2009.
4. Kamenetskii, E. O., M. Sigalov, and R. Shavit, *J. Appl. Phys.*, Vol. 105, 013537, 2009.
5. Tribelsky, M. I. and B. S. Luk'ynchuk, *Phys. Rev. Lett.*, Vol. 97, 263902, 2006.
6. Kamenetskii, E. O., M. Sigalov, and R. Shavit, *Phys. Rev. A*, Vol. 81, 053823, 2010.
7. Kamenetskii, E. O., R. Joffe, and R. Shavit, e-print, arXiv:1012.3621, 2010.

Propagation of TE-waves through a Nonlinear Metamaterial Layer with Arbitrary Nonlinearity

D. V. Valovik
Penza State University, 40 Krasnay Street, Penza 440026, Russia

Abstract— During many years propagation of TE- and TM-waves through nonlinear layers are intensively investigated [1–3]. Here, we obtain a dispersion equation (DE) for TE-waves propagating through a layer where permittivity is an arbitrary function of squared electric field intensity. From this DE constants of propagation can be numerically obtained. Using this DE nonlinear metamaterial can be studied as well. For the cases of TE- and TM-waves and Kerr nonlinearity see [4, 5].

Let us consider electromagnetic waves propagating through a homogeneous isotropic nonmagnetic dielectric layer filled by media with arbitrary nonlinearity. The layer is located between two half-spaces $x < 0$ and $x > h$ in Cartesian coordinate frame $Oxyz$. The half-spaces are filled with isotropic nonmagnetic medium containing no sources and with constant permittivities ε_1 and ε_3, respectively (ε_1 and ε_3 are arbitrary real values). Everywhere below μ is the permeability of free space.

Electromagnetic field harmonically depends on time $\vec{\tilde{E}}(x,y,z,t) = \vec{E}_+(x,y,z)\cos\omega t + \vec{E}_-(x,y,z)\sin\omega t$; $\vec{\tilde{H}}(x,y,z,t) = \vec{H}_+(x,y,z)\cos\omega t + \vec{H}_-(x,y,z)\sin\omega t$, where ω is circular frequency; $\vec{E}_+$, $\vec{E}_-$, $\vec{H}_+$, $\vec{H}_-$ are real required functions. Form complex amplitudes: $\vec{E} = \vec{E}_+ + i\vec{E}_-$; $\vec{H} = \vec{H}_+ + i\vec{H}_-$. Below time multipliers are omitted.

Electromagnetic field $\vec{E}$, $\vec{H}$ satisfies Maxwell equations $rot\vec{H} = -i\omega\varepsilon\vec{E}$, $rot\vec{E} = i\omega\mu\vec{H}$, continuity condition of tangential components at the interfaces $x = 0$, $x = h$ and radiation condition at infinity: electromagnetic field exponentially decays at $|x| \to \infty$ in the regions $x < 0$ and $x > h$.

The permittivity inside the layer has the form $\varepsilon = \varepsilon_2 + f\left(|\vec{E}|^2\right)$, where ε_2 is arbitrary real constant.

We seek solutions to the Maxwell equations in the entire space.

Consider TE-waves $\vec{E} = (0, E_y, 0)^T$, $\vec{H} = (H_x, 0, H_z)^T$. It is easy to show that components of electromagnetic field do not depend on y. Waves propagating along media interfaces z harmonically depend on z. It implies that components of electromagnetic field have the form: $E_y = E_y(x)e^{i\gamma z}$, $H_x = H_x(x)e^{i\gamma z}$, $H_z = H_z(x)e^{i\gamma z}$.

We perform the normalization the Maxwell equations in accordance with the following formulas $\tilde{x} = kx$, $\frac{d}{dx} = k\frac{d}{d\tilde{x}}$, $\tilde{\gamma} = \frac{\gamma}{k}$, $\tilde{\varepsilon}_j = \frac{\varepsilon_j}{\varepsilon_0}$ ($j = 1, 2, 3$), $\tilde{f} = \frac{f}{\varepsilon_0}$, where $k^2 = \omega^2\mu\varepsilon_0$ and ε_0 is the permittivity of free space. Introduce the notations $E_y(\tilde{x}) \equiv Y(\tilde{x})$, $Y'(\tilde{x}) \equiv Z(\tilde{x})$ and omitting tilde from the Maxwell equations we get the system of equations which we are studying

$$\begin{cases} Y' = Z, \\ Z' = (\gamma^2 - \varepsilon)Y; \end{cases} \quad \text{where } \varepsilon = \begin{cases} \varepsilon_1, \ x < 0; \\ \varepsilon_2 + f(Y^2), \ 0 < x < h; \\ \varepsilon_3, \ x > h. \end{cases}$$

We look for real values of γ and $Y(x) \in C(-\infty;+\infty) \cap C^1(-\infty;+\infty) \cap C^2(-\infty;\ 0] \cap C^2[0;h] \cap C^2[h;\ +\infty)$.

Introduce new variables $\tau(x) = \varepsilon_2 + Y^2(x)$, $\eta(x) = \frac{Z(x)}{Y(x)}$. It can be proved that DE has the form

$$h = -\int\limits_{-\sqrt{\gamma^2-\varepsilon_3}}^{\sqrt{\gamma^2-\varepsilon_1}} Q(\eta)d\eta + N\int\limits_{-\infty}^{+\infty} Q(\eta)d\eta, \quad N = \pm1, \pm2, \ldots,$$

where $Q(\eta) = \left(\gamma^2 - \varepsilon_2 - f(\tau - \varepsilon_2) - \eta^2\right)^{-1}$; $\tau = \tau(\eta)$ is expressed from the equation $(\tau - \varepsilon_2)\eta^2 + \varphi(\tau - \varepsilon_2) = (\tau(h) - \varepsilon_2)(\gamma^2 - \varepsilon_3) + \varphi(\tau(h) - \varepsilon_2)$; $\varphi(\tau - \varepsilon_2) = \int(\varepsilon_2 - \gamma^2 + f(u))du\Big|_{u=\tau-\varepsilon_2}$, and $\tau(h)$ is known as $Y(h)$ is supposed to be known (initial condition).

REFERENCES

1. Eleonskii, P. N., L. G. Oganes'ants, and V. P. Silin, *Sov. Phys. JETP*, Vol. 35, No. 1, 44, 1972.
2. Joseph, R. I. and D. N. Christodoulides, *Optics Letters*, Vol. 12, No. 10, 826, October 1987.
3. Shürmann, H. W., V. S. Serov, Y. V. Shestopalov, *Physical Review E*, Vol. 58, No. 1, 1040, July 1998.
4. Valovik, D. V. and Y. G. Smirnov, *Journal of Communications Technology and Electronics*, Vol. 53, No. 8, 883, 2008.
5. Valovik, D. V., *Journal of Communications Technology and Electronics*, Vol. 56, No. 5, 2011 (in appear).

Stopband and Resonance Characteristics of Cylindrical Electromagnetic Bandgap Structures

Vakhtang Jandieri[1] and Kiyotoshi Yasumoto[2]

[1]School of Electrical Engineering and Computer Science, Kyungpook National University
Daegu 702-701, Republic of Korea
[2]Kyushu University, 2-13-11 Mainosato, Koga, Fukuoka 811-3114, Japan

Abstract— Periodic dielectric or metallic structures are a subject of continuing interest because of their wide use for microwave and optical wave components. A periodic array of circular rods is typical of a discrete periodic structure. The electromagnetic response is characterized by the scattering properties of the individual rod and the multiple interactions among the rods periodically situated. Various analytical or numerical techniques have been developed over the years to formulate the electromagnetic guidance and scattering from the periodic arrays. However, the previous pertinent efforts have been mostly concerned with the planar arrays. Recently, the cylindrically periodic structures have received a growing attention because of their potential applications to the designs of photonic crystal fibers and directive antennas or beam-switching antennas.

In this paper, we shall investigate the frequency response of cylindrical electromagnetic bandgap structures shown in Fig. 1. It consists of N-layered cylindrical arrays of circular rods situated in a homogeneous background medium. The M_ν circular rods with radius r_ν are periodically distributed on each of N-concentric circular rings with radii $R_\nu (\nu = 1, 2, 3, \ldots, N)$. The number M_ν of rods is chosen to be $M_\nu/R_\nu = M_1/R_1$ so that the structure has the common transversal period $2\pi R_1/M_1$. The circular rods should be identical along one ring but those on different rings need not be necessarily identical in material properties and dimensions. Fig. 1 shows a typical example of three layered structure with $M_1 = 12$, $M_1 = 24$, and $M_3 = 36$. We assume the initial excitation by a line source which is located at the center of the structure and is parallel to the cylinder axis. The cylindrical bandgap structure acts as a resonant cavity to the source. The transmission spectra of the field radiated from the line source through the cylindrical structure are analyzed using the semi-analytical approach, which has been formulated [1, 2] for layered cylindrical arrays of circular rods. It is demonstrated that the directivity of radiation of the line source is closely related to the resonance characteristics in the transmission spectra of the cylindrical array.

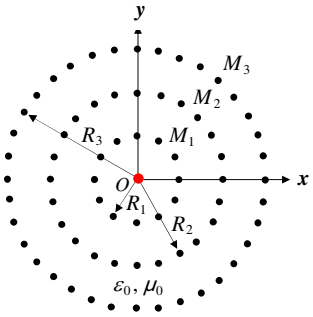

Figure 1: Cross sectional view of a three-layered cylindrical array formed by M_ν circular rods periodically distributed on each of concentric circular rings with radii R_ν ($\nu = 1, 2, 3$), where $M_1 = 12$, $M_2 = 24$, $M_3 = 36$, $R_2 = 2R_1$, and $R_3 = 3R_1$. A line source parallel to the cylinder axis is located at the origin of the structure.

REFERENCES

1. Yasumoto, K., "Semi-analytical approach for a specific microstructured fiber," *PIERS Online*, Vol. 5, No. 1, 95–100, 2009.
2. Jandieri, V. and K. Yasumoto, "Electromagnetic scattering by layered cylindrical arrays of circular rods," *IEEE Transactions on Antennas and Propagation*, 2011, accepted for publication.

Exact Solution for the Magnetic Force between a Thick Circular Coil and a Thick Elliptic Coil

John T. Conway
University of Agder, Norway

Abstract— In cylindrical coordinates (r, ϕ, z), the vector potential induced by a circular loop of radius R_1 and current I amps has only an azimuthal component. If the current loop lies in a plane $z = z_1$, then the vector potential induced in a parallel plane $z = z_2$ can be written as an integral of Bessel functions of the form [1]:

$$A_\phi(r, z_2) = \frac{\mu_0 I R_1}{2} \int_0^\infty J_1(sR_1) J_1(sr) \exp(-s\,|z_2 - z_1|) ds. \tag{1}$$

In some recent papers [2–5] this formulation has been exploited to perform inductance calculations for circular coils of various types, not necessarily coaxial. From Equation (3) it can be shown that the mutual inductance between two coaxial loops of radii R_1 and R_2, which lie in the respective planes $z = z_1$ and $z = z_2$, can be written in the form:

$$M_{21} = \mu_0 \pi R_1 R_2 \int_0^\infty J_1(sR_2) J_1(sR_1) \exp(-s\,|z_2 - z_1|) ds. \tag{2}$$

For the non coaxial case, where the centres of the loops are displaced by a perpendicular distance p, then Equation (4) generalizes to give:

$$M_{21} = \mu_0 \pi R_1 R_2 \int_0^\infty J_0(sp) J_1(sR_2) J_1(sR_1) \exp(-s\,|z_2 - z_1|) ds. \tag{3}$$

Equations (4) and (5) can be integrated in the radial and axial directions to give the mutual inductance of two thick coils [4].

Equation (4) for the coaxial case has recently been generalized to give the mutual inductance of a circular loop of radius R_1 and a coaxial elliptic loop with semi-minor and semi-major axes a and b respectively in the form:

$$\begin{aligned} M_{21} \;=\; & \mu_0 \pi R_1 \left(\frac{a+b}{2}\right) \int_0^\infty J_0\left(s\frac{b-a}{2}\right) J_1(sR_1) J_1\left(s\frac{a+b}{2}\right) \exp(-s\,|z_2 - z_1|) ds \\ & -\mu_0 \pi R_1 \left(\frac{b-a}{2}\right) \int_0^\infty J_0\left(s\frac{a+b}{2}\right) J_1(sR_1) J_1\left(s\frac{b-a}{2}\right) \exp(-s\,|z_2 - z_1|) ds. \end{aligned} \tag{4}$$

Equations (5) and (4) both involve products of three Bessel functions, but it is to be noted that Equation (4) applies only for the coaxial case. Remarkably, the mathematical structure of Equation (4) allows it to be integrated axially and with repect to coil thickness for precisely the kind of elliptic coils which can exist in practice. The same mathematics also allows the axial force to be calculated for such coils and the paper will present these results. From symmetry considerations, there is no radial force or torque in this case.

REFERENCES

1. Conway, J. T., "Exact solutions for the magnetic fields of solenoids and current distributions," *IEEE Trans. Magn.*, Vol. 37, No. 4, 2977–2988, 2001.
2. Conway, J. T., "Inductance calculations for noncoaxial coils using Bessel functions," *IEEE Trans. Magn.*, Vol. 43, No. 3, 1023–1034, 2007.
3. Conway, J. T., "Noncoaxial inductance calculations without the vector potential for axisymmetric coils and planar coils," *IEEE Trans. Magn.*, Vol. 44, No. 4, 453–462, 2008.
4. Conway, J. T., "Inductance calculations for circular coils of rectangular cross section and parallel axes using Bessel and Struve functions," *IEEE Trans. Magn.*, Vol. 46, No. 1, 75–81, 2010.
5. Conway, J. T., "Mutual inductance for an explicitly finite number of turns," *Progress In Electromagnetics Research B*, Vol. 28, 273–287, 2011.

Backscattering Diagrams of Inhomogeneous Currents on Generic Elongated Irregularities of Surface

A. M. Lebedev and A. I. Fedorenko
Institute for Theoretical and Applied Electromagnetics, Russian Academy of Sciences, Russia

Abstract— Physical optics (PO) method is the base for complex object scattering calculation. Preparation of 3D model of the object is quite a solvable problem. However, the question remains to take into account the diffraction effects of nonlocal origin, in particular due to the elongated irregularities on the surface of the object. That is of principal importance for directions, where scattering is far from specular.

The elongated irregularities are characterized by constant or slowly varying cross section. Part of the diffraction effects due to the elongated irregularities can be estimated with GTD and PTD methods (geometrical and physical theory of diffraction methods). However, these methods are based on canonical solution of 2D problem of ideal wedge scattering, and thus can only be applied to relatively small subset of elongated irregularities — namely sharp metal wedges with close to plane sides. As it is shown in this work, minor deviations in geometry of the wedge, for example, edge rounding with radius more than 1/20 wavelength, result in substantial variation of backscattering diagram (BSD), compared to the BSD of ideal wedge.

By definition, inhomogeneous current is the difference between really existing and PO currents. That is why exactly the fields, generated by inhomogeneous currents, form diffraction effects of nonlocal origin. The PTD advantage is the development of apparatus of elementary edge waves (EEW) generated by inhomogeneous currents. The task to work out the variant of PTD, where the EEW fields of inhomogeneous currents on elongated irregularities of arbitrary cross section are found from numerical solution of 2D problem, is of our interest. Application of numerical variant of PTD will lead to principal widening of the scope of elongated irregularities, for which calculations with PTD will be possible. Currently this task is solved step by step.

In this work, the BSD of inhomogeneous currents on generic elongated irregularities were investigated, using 2D models. The following types of elongated irregularities were studied: the straight and rounded end of the plate, the wedge with coating on one or both sides, the joint of surface portions. Angular dependence of 2D BSD simultaneously gives the EEW backscattered field distribution in plane perpendicular to the elongated irregularity. It was shown, that BSD of generic elongated irregularities are the smooth functions, suitable for approximation.

Session 1P6
Spin Physics in Low Dimensional Systems

Conservation Laws and Spin Motive Force in Magnetic Nanostructures: Part 1

Sadamichi Maekawa[1, 2]

[1]Advanced Science Research Center, Japan Atomic Energy Agency, Tokai 319-1195, Japan
[2]CREST, Japan Science and Technology Agency, Tokyo 102-0075, Japan

Abstract— In magnetic nanostructures, there are two conservation laws between the conduction electrons and the magnetic moment [1]. The first is the angular momentum conservation which brings about the spin angular momentum transfer between them. The other is that of energy between them. The magnetic energy stored in the conduction electrons is released as the spin motive force. The spin-motive force is derived by extending the Faraday's law of electromagnetism. The non-conservative force acting on the spins of conduction electrons causes the work, which brings about the spin-motive force [2]. A variety of the phenomena due to the spin motive force [3, 4] are presented.

REFERENCES

1. *Concepts in Spin Electronics*, S. Maekawa, Ed., Oxford University Press, 2006.
2. Barnes, S. E. and S. Maekawa, *Phys. Rev. Lett.*, Vol. 98, 246601, 2007.
3. Ohe, J., S. E. Barnes, H. W. Lee, and S. Maekawa, *Appl. Phys. Lett.*, Vol. 95, 123110, 2009.
4. Hai, P. N., S. Ohya, M. Tanaka, S. E. Barnes, and S. Maekawa, *Nature*, Vol. 458, 489, 2009.

Conservation Laws and Spin Motive Force in Magnetic Nanostructures: Part 2

Sadamichi Maekawa[1, 2]

[1]Advanced Science Research Center, Japan Atomic Energy Agency, Tokai 319-1195, Japan
[2]CREST, Japan Science and Technology Agency, Tokyo 102-0075, Japan

Abstract— In magnetic nanostructures, there are two conservation laws between the conduction electrons and the magnetic moment [1]. The first is the angular momentum conservation which brings about the spin angular momentum transfer between them. The other is that of energy between them. The magnetic energy stored in the conduction electrons is released as the spin motive force. The spin-motive force is derived by extending the Faraday's law of electromagnetism. The non-conservative force acting on the spins of conduction electrons causes the work, which brings about the spin-motive force [2]. A variety of the phenomena due to the spin motive force [3, 4] are presented.

REFERENCES

1. *Concepts in Spin Electronics*, S. Maekawa, Ed., Oxford University Press, 2006.
2. Barnes, S. E. and S. Maekawa, *Phys. Rev. Lett.*, Vol. 98, 246601, 2007.
3. Ohe, J., S. E. Barnes, H. W. Lee, and S. Maekawa, *Appl. Phys. Lett.*, Vol. 95, 123110, 2009.
4. Hai, P. N., S. Ohya, M. Tanaka, S. E. Barnes, and S. Maekawa, *Nature*, Vol. 458, 489, 2009.

Spin Orbit Interaction and Spin Accumulation in Quantum Dot System: Part 1

Yasuhiro Tokura
NTT Basic Research Laboratories, NTT Corporation, Kanagawa, Japan

Abstract— In the future device based on spintronics, one manipulates the electron's spin as well as its charge. This may potentially be applied for quantum information processing. Spin-orbit interaction (SOI) can provide intriguing transport properties through quantum dots (QDs). For example, the repulsion of two levels in a QD with different spins near their crossing condition clearly shows the strength and its vector character of the SOI [1]. Quite importantly, these features can be tuned by the gate voltage.

The spin can acquire a (non-Abelian) phase by SOI in the transport process, which is especially critical in the low-temperature coherent transport. These features are already proposed to constitute spin filters or analyzers by nanostructure interferometers with finite SOI [2]. We extend the study on the interferometer made of QDs [3, 4] for finite SOI interaction [5] and show the condition (finite bias and intrinsic asymmetry) of polarizing and accumulating spins. We also argue the technical issue how to detect these features.

REFERENCES

1. Takahashi, S., R. S. Deacon, K. Yoshida, A. Oiwa, K. Shibata, K. Hirakawa, Y. Tokura, and S. Tarucha, *Phys. Rev. Lett.*, Vol. 104, 246801, 2010.
2. Aharony, A., Y. Tokura, G. Z Cohen, O. Entin-Wohlman, and S. Katsumoto, unpublished.
3. Hatano, T., T. Kubo, Y. Tokura, S. Amaha, S. Teraoka, and S. Tarucha, *Phys. Rev. Lett.*, Vol. 106, 076801, 2011.
4. Tokura, Y., H. Nakano, and T. Kubo, *New J. Phys.*, Vol. 9, 113, 2007.
5. Kubo, T., Y. Tokura, and S. Tarcuha, *Physics Procedia*, Vol. 3, 1225, 2010.

Spin Orbit Interaction and Spin Accumulation in Quantum Dot System: Part 2

Yasuhiro Tokura
NTT Basic Research Laboratories, NTT Corporation, Kanagawa, Japan

Abstract— In the future device based on spintronics, one manipulates the electron's spin as well as its charge. This may potentially be applied for quantum information processing. Spin-orbit interaction (SOI) can provide intriguing transport properties through quantum dots (QDs). For example, the repulsion of two levels in a QD with different spins near their crossing condition clearly shows the strength and its vector character of the SOI [1]. Quite importantly, these features can be tuned by the gate voltage.

The spin can acquire a (non-Abelian) phase by SOI in the transport process, which is especially critical in the low-temperature coherent transport. These features are already proposed to constitute spin filters or analyzers by nanostructure interferometers with finite SOI [2]. We extend the study on the interferometer made of QDs [3, 4] for finite SOI interaction [5] and show the condition (finite bias and intrinsic asymmetry) of polarizing and accumulating spins. We also argue the technical issue how to detect these features.

REFERENCES

1. Takahashi, S., R. S. Deacon, K. Yoshida, A. Oiwa, K. Shibata, K. Hirakawa, Y. Tokura, and S. Tarucha, *Phys. Rev. Lett.*, Vol. 104, 246801, 2010.
2. Aharony, A., Y. Tokura, G. Z Cohen, O. Entin-Wohlman, and S. Katsumoto, unpublished.
3. Hatano, T., T. Kubo, Y. Tokura, S. Amaha, S. Teraoka, and S. Tarucha, *Phys. Rev. Lett.*, Vol. 106, 076801, 2011.
4. Tokura, Y., H. Nakano, and T. Kubo, *New J. Phys.*, Vol. 9, 113, 2007.
5. Kubo, T., Y. Tokura, and S. Tarcuha, *Physics Procedia*, Vol. 3, 1225, 2010.

Electrical Control of Anisotropic Spin-orbit Interaction in InAs Self-assembled Quantum Dots: Part 1

A. Oiwa[1], **R. S. Deacon**[1], **S. Takahashi**[1], **Y. Kanai**[1], **K. Yoshida**[1], **K. Shibata**[2], **K. Hirakawa**[2], **Y. Tokura**[3], **and S. Tarucha**[1]

[1]Department of Applied Physics, University of Tokyo, Tokyo, Japan
[2]Institute of Industrial Science, University of Tokyo, Tokyo, Japan
[3]NTT Basic Research Laboratories, NTT Corporation, Kanagawa, Japan

Abstract— Spin-orbit interaction (SOI) plays crucial roles for creating and relaxing spins in semiconductor low dimensional systems for applications to the spintronics and quantum information technologies. The electrical control of SOI offers the novel methods to manipulate electron spins and has not been realized in semiconductor quantum dots (QDs).

First we have quantitatively evaluated the SOI energy by measuring anit-crossings between two states with different orbitals and spins in excited state spectroscopy and also splitting of Kondo zero-bias anomaly in InAs self-assembled QDs. It has been found that the SOI energy is strongly anisotropic with respect to the direction of the external magnetic field reflecting the dot confinement potential. Then we have demonstrated for the first time the electrical control of the SOI energy using the side-gate lately coupled to the QD. The anisotropic side-gate would affect the lateral confinement potential of the QD, leading to a change of the SOI energy. We also show that the applied side-gate voltage tunes the g-factor of electrons in the QD.

ACKNOWLEDGMENT

This work is partially supported by Grant-in-Aid for Research S (No. 19104007), JST strategic Int. Coop. Program, CREST JST, Special Coordination Funds for Promoting Science and Technology, MEXT, and QuEST grant (HR-001-09-1-0007).

Electrical Control of Anisotropic Spin-orbit Interaction in InAs Self-assembled Quantum Dots: Part 2

A. Oiwa[1], **R. S. Deacon**[1], **S. Takahashi**[1], **Y. Kanai**[1], **K. Yoshida**[1], **K. Shibata**[2], **K. Hirakawa**[2], **Y. Tokura**[3], **and S. Tarucha**[1]

[1]Department of Applied Physics, University of Tokyo, Tokyo, Japan
[2]Institute of Industrial Science, University of Tokyo, Tokyo, Japan
[3]NTT Basic Research Laboratories, NTT Corporation, Kanagawa, Japan

Abstract— Spin-orbit interaction (SOI) plays crucial roles for creating and relaxing spins in semiconductor low dimensional systems for applications to the spintronics and quantum information technologies. The electrical control of SOI offers the novel methods to manipulate electron spins and has not been realized in semiconductor quantum dots (QDs).

First we have quantitatively evaluated the SOI energy by measuring anit-crossings between two states with different orbitals and spins in excited state spectroscopy and also splitting of Kondo zero-bias anomaly in InAs self-assembled QDs. It has been found that the SOI energy is strongly anisotropic with respect to the direction of the external magnetic field reflecting the dot confinement potential. Then we have demonstrated for the first time the electrical control of the SOI energy using the side-gate lately coupled to the QD. The anisotropic side-gate would affect the lateral confinement potential of the QD, leading to a change of the SOI energy. We also show that the applied side-gate voltage tunes the g-factor of electrons in the QD.

ACKNOWLEDGMENT

This work is partially supported by Grant-in-Aid for Research S (No. 19104007), JST strategic Int. Coop. Program, CREST JST, Special Coordination Funds for Promoting Science and Technology, MEXT, and QuEST grant (HR-001-09-1-0007).

Fermionic Theory for Low Dimensional Quantum Antiferromagnets with Spin $S > 1/2$: Part 1

Zheng-Xin Liu, **Yi Zhou**, **and Tai-Kai Ng**
Hong Kong University of Science and Technology, China

Abstract— The fermion representation for $S = 1/2$ spins is generalized to spins with arbitrary magnitudes. The symmetry properties of the representation is analyzed where we find that different path integral representations are needed for spin models with integer and half-odd-integer spin magnitude S, respectively because of a fundamental difference in the structure of the Hilbert space for integer and half-odd-integer spins. In particular, we show that mean-field theories based on representations with particle-hole symmetry applied to one dimensional (1D) antiferromagnetic Heisenberg models produce results in agreement with Haldane's conjecture. For integer open spin chains, we show that Majorana fermion edge states exist in our mean field theory. Preliminary results on application of our mean-field theory to spin models in 2-dimension triangular and kagome lattices will also be discussed. Some comments on the relation between our mean-field theory and different topological orders in low-dimensional spin systems will be given.

Fermionic Theory for Low Dimensional Quantum Antiferromagnets with Spin $S > 1/2$: Part 2

Zheng-Xin Liu, **Yi Zhou**, **and Tai-Kai Ng**
Hong Kong University of Science and Technology, China

Abstract— The fermion representation for $S = 1/2$ spins is generalized to spins with arbitrary magnitudes. The symmetry properties of the representation is analyzed where we find that different path integral representations are needed for spin models with integer and half-odd-integer spin magnitude S, respectively because of a fundamental difference in the structure of the Hilbert space for integer and half-odd-integer spins. In particular, we show that mean-field theories based on representations with particle-hole symmetry applied to one dimensional (1D) antiferromagnetic Heisenberg models produce results in agreement with Haldane's conjecture. For integer open spin chains, we show that Majorana fermion edge states exist in our mean field theory. Preliminary results on application of our mean-field theory to spin models in 2-dimension triangular and kagome lattices will also be discussed. Some comments on the relation between our mean-field theory and different topological orders in low-dimensional spin systems will be given.

Semiclassical Dynamics of Magnon Wavepacket and Magnon Hall Effect in Ferromagnets: Part 1

S. Murakami[1, 2] **and R. Matsumoto**[1]

[1]Tokyo Institute of Technology, Ookayama, Meguro-ku, Tokyo 152-8551, Japan
[2]PRESTO, Japan Science and Technology Agency, Honcho, Kawaguchi, Saitama 332-0012, Japan

Abstract— In electron systems, various kinds of Hall effects are attributed to Berry curvature in momentum space. This Berry curvature involves derivative of the Bloch wavefunction with respect to the wavenumber, and it is determined by the band structure. In a semiclassical picture it gives rise to electron velocity perpendicular to the electric field, causing the Hall effect.

In my talk we study dynamics of a magnon wavepacket, in analogy to electronic systems. Here magnons include both quantum-mechanical magnons by spin exchange and magnetostatic spin wave in the classical electromagnetic theory. In the vicinity of the boundary of the magnet, the confining potential exerts a force to the wavepacket perpendicular to the boundary, and it causes an anomalous velocity along the boundary due to the magnon Berry curvature. This anomalous velocity gives rise to the magnon current along the edge. We find that the magnon wavepacket undergoes two types of rotational motions: self-rotation and edge current of magnon.

Such magnon edge current causes thermal Hall effect of magnon. The magnon thermal Hall conductivity is calculated by two methods: The semiclassial theory based on edge current, and the linear response theory. We obtained the same result from the two methods. Our result contains new correction terms to the previous works, and these correction terms are attributed to the orbital motions of magnon wavepackets. We discuss two materials $Lu_2V_2O_7$ and YIG as an example.

Semiclassical Dynamics of Magnon Wavepacket and Magnon Hall Effect in Ferromagnets: Part 2

S. Murakami[1, 2] **and R. Matsumoto**[1]

[1]Tokyo Institute of Technology, Ookayama, Meguro-ku, Tokyo 152-8551, Japan
[2]PRESTO, Japan Science and Technology Agency, Honcho, Kawaguchi, Saitama 332-0012, Japan

Abstract— In electron systems, various kinds of Hall effects are attributed to Berry curvature in momentum space. This Berry curvature involves derivative of the Bloch wavefunction with respect to the wavenumber, and it is determined by the band structure. In a semiclassical picture it gives rise to electron velocity perpendicular to the electric field, causing the Hall effect.

In my talk we study dynamics of a magnon wavepacket, in analogy to electronic systems. Here magnons include both quantum-mechanical magnons by spin exchange and magnetostatic spin wave in the classical electromagnetic theory. In the vicinity of the boundary of the magnet, the confining potential exerts a force to the wavepacket perpendicular to the boundary, and it causes an anomalous velocity along the boundary due to the magnon Berry curvature. This anomalous velocity gives rise to the magnon current along the edge. We find that the magnon wavepacket undergoes two types of rotational motions: self-rotation and edge current of magnon.

Such magnon edge current causes thermal Hall effect of magnon. The magnon thermal Hall conductivity is calculated by two methods: The semiclassial theory based on edge current, and the linear response theory. We obtained the same result from the two methods. Our result contains new correction terms to the previous works, and these correction terms are attributed to the orbital motions of magnon wavepackets. We discuss two materials $Lu_2V_2O_7$ and YIG as an example.

Helical Magnetostatic-mode Resonances in Quasi-2D Ferrite Disks

E. O. Kamenetskii
Microwave Magnetic Laboratory, Department of Electrical and Computer Engineering
Ben Gurion University of the Negev, Beer Sheva, Israel

Abstract— Recent studies of magnetostatic (MS) oscillations in quasi-2D ferrite disks show special topological properties of MS modes. In these "big" magnetic systems (having sizes about tens of micrometers — the scales at which a role of the exchange fluctuations is negligibly small) one can observe peculiar MS-vortex eigenstates [1–3]. The dynamical symmetry breaking effects and the vortex solutions in MS oscillations are strongly connected with understanding physics of magnetic dipole-dipole interactions in low-dimensional magnetic systems. The magneto-dipole interactions, normally weak enough to be ignored in bulk magnetic materials, play an essential role in stabilizing long-range magnetic order in quasi-2D systems. Such interactions represent a topical problem in a condensed matter theory. Classically, distant magnetic dipolar fields can be modeled as a sum of the fields produced by the magnetic dipoles. In this approximation, the dipole fields are considered as "pure static" magnetic fields. The simplest possible numerical models of magneto-dipole interactions in FMR structures involve a discrete lattice of classical spins and direct summation of their magnetic fields. Another classical approach in analyzing a long-range mechanism of the dipole-dipole interaction is based on consideration of a magnetic medium as a continuum. For small magnetic samples with strong temporal dispersion, RF magnetic field is expressed as $\vec{H} = -\nabla\psi$, where ψ is a MS potential. The spectral solutions are obtained from the "pure static" Green-function integral problem and approximate boundary conditions for RF magnetization $\vec{m}$, generalized from the exchange boundary conditions. It is known, however, that the classical interpretation of interaction between magnetic dipoles cannot explain the reason for magnetic ordering. The spectral problem for long-range dipolar-mode fields with the boundary conditions imposed on the RF magnetization cannot be considered as the self-conjugate spectral problem. The known classical models of MS oscillations leave open the question of long-range phase coherence in eigenmodes with magneto-dipole interactions (in neglect of the exchange fluctuations). Contrary to the above classical models of magneto-dipole interactions in confined magnetic there exists the Walker's model based on the egenvalue-problem formulation for a "*fictitious*" MS-potential *wave* function $\psi(\vec{r}, t)$. The boundary conditions are imposed on the MS-potential field and not on the RF magnetization. The MS-mode spectral properties shown in Refs. [1–3] are based on postulates about a physical meaning of MS-potential functions $\psi(\vec{r}, t)$ as complex scalar wave functions with energy-eigenstate orthogonality conditions. Recently, it was shown that the MS-mode oscillations in a quasi-2D ferrite disk are characterized by helical resonances [4]. There are macroscopically entangled states associated with geometric phases. We discuss symmetry properties of MS-mode oscillations and interaction of these oscillations with external electromagnetic fields. There is a very peculiar mechanism of scattering of microwave electromagnetic fields by ferrite-disk particles with helical MS-mode resonances [3, 5].

REFERENCES

1. Kamenetskii, E. O., *J. Phys. A: Mathematical and Theoretical*, Vol. 40, 6539, 2007.
2. Sigalov, M., E. O. Kamenetskii, and R. Shavit, *J. Phys.: Condens. Matter*, Vol. 21, 016003, 2009.
3. Kamenetskii, E. O., M. Sigalov, and R. Shavit, *Phys. Rev. A*, Vol. 81, 053823, 2010.
4. Kamenetskii, E. O., *J. Phys.: Condens. Matter*, Vol. 22, 486005, 2010.
5. Kamenetskii, E. O., R. Joffe, and R. Shavit, E-Print, 2010, arXiv:1012.3621.

Room-temperature Ferromagnetism Characterization on Nano-scale Structures in GaN:Mn by Magnetic Force Microscope

Xianzhe Jiang, **Fafa Zhang**, **Yuhao Zhang**, **Zhiyuan Lin**, **Cunda Wang**, **and Guoyi Zhang**
State Key Laboratory of Artificial Microstructure and Mesoscopic Physics, School of Physics
Peking University, Beijing 100871, China

Abstract— Room temperature ferromagnetism with Curie temperature above 380 K was observed in GaN:Mn thin films grown by metal-organic chemical vapor deposition. To clarify the origin of the ferromagnetism, we studied both dislocation pits and pre-fabricated artificial microstructures on epitaxial GaN:Mn thin films, using a Digital Instruments NanoScope IIIa-D3000 MFM with the spatial resolution of 20 nm and a perpendicularly magnetized Fe-Pt high coercivity tip, assisted with mathematical simulation.

Considering the extremely weak magnetic field of the DMS, we focused mainly on the sloping faces of the sample, where magnetic signals may release and can be detected. An isolated GaN:Mn island with trapezium-shaped cross section was fabricated by focused ion beam and dislocation pits were also observed under both atomic force microscopy (AFM) and MFM modes.

The MFM images of the artificial microstructures exhibited an anti-symmetric pattern and did not support the presence of any magnetic clusters. Corresponding simulation results, under the assumption of uniform magnetization along the sample wafer plane, were in good agreement with experimental data of magnetic charge density from the response of magnetic tip of MFM. To confirm the hypothesis of magnetism distribution, we searched the whole GaN:Mn surface and found a $5 \times 5\,\mu m^2$ area with well dispersed dislocation pits which were similar to regularly reported threading dislocations.

The corresponding MFM image reveals that the magnetic signal of the isolated pits is characterized by a double-polar anti-symmetric pattern. The polarity of all dislocation pits, exhibiting the same direction, demonstrates the long range magnetic order in GaN:Mn sample. The consistency of experiment and simulated results confirmed the intrinsic ferromagnetism and its uniform distribution in GaN:Mn films.

Session 1P7
Poster Session 1

Parallelized FDTD-TDPO Algorithm Based on MPI Platform

Xiangqin Zhu[1], **Jianguo Wang**[1, 2], **and Libing Cai**[1]

[1]Northwest Institute of Nuclear Technology, Xi'an 710024, China
[2]School of Electronic and Information Engineering, Xi'an Jiaotong University
Xi'an 710049, China

Abstract— A parallelized FDTD-TDPO algorithm based on MPI (Message Passing Interface) platform is presented in this paper for simulation of reflector antennas, which can not be done on a personal computer due to over long time and prohibitive computation resources.

Firstly, the initial parameters of the reflector and its feed are read by root process. The initial parameters of reflector include related frequency, the aperture size, the focal length of the reflector, and the total number of triangular meshes on the reflector's surface, etc.. The initial parameters of the reflector's feed include related frequency of the feed, sizes of discrete cell in three dimension, the target boundary of the feed for FDTD method, the number of kinds of matter composed of the feed, and the electromagnetic parameters of every matter, etc..

Secondly, the computing tasks are divided and the corresponding parameters are broadcasted into corresponding sub-domains by root process. Load balancing needs to be considered when computing task is divided.

Thirdly, the near-magnetic fields of the feed in each subdomain are computed by FDTD method. And at the same time the currents on meshes of the reflector are computed by those near-fields based on Kirchhoff surface integral representation in each subdomain.

Lastly, the radiation fields of reflector are computed by TDPO method by means of the currents.

There's no interaction of the currents on meshes on the reflector when TDPO method is used to compute the radiation fields of reflector, that is, each process shouldn't keep synchronous to avoid communication conflict until root process gathers data from all processes at last.

The speedup factor and efficiency for parallel FDTD-TDPO code are measured on high performance computers. The computational results are in good agreement with those obtained by FDTD-TDPO method using single process. In addition, numerical results show that the speed up ratio is approximately equal to N, where N is the number of processes.

Design of a Novel Terahertz Antenna with Fan-scanning Beam

Xiang Gao, Chao Li, and GuangYou Fang
Institute of Electronics, Chinese Academy of Sciences, Beijing 100190, China

Abstract— Imaging at terahertz frequencies has many advantages, such as easy to penetrate obscuring materials and capable of obtaining relatively good spatial resolution. To exploit the potential of terahertz imaging, two main approaches have been used to realize a practical imager. One is the focal-plane-array system, in which high frame rates can be achieved because the entire image is acquired at once; the other is the scanned-antenna approach, which is able to build up an image over a two-dimensional plane by mechanically scanning an antenna with a single receiver. However, the two approaches are limited because of the high cost or the long scanning time. To overcome the above shortcomings, a novel approach is to develop an imaging system with beams-scanning function. In this paper, based on the multi-reflector quasi-optics, a novel terahertz antenna with fan-scanning beam is designed. The antenna consists of a pyramidal horn feed and two cylindrical reflectors, one of which is a fixed elliptical main-reflector to generate a thin fan beam and the other is a rotating sub-reflector to realize the beam scanning function. All these components are embedded between two parallel metal plates. To design and optimize such an antenna, a Reversed Ray Tracing Algorithm (RRTA) was introduced to minimize the aberration of the antenna and to determine the optimum positions and dimensions of the sub-reflector and the pyramidal horn. To verify and further optimize the performance of the antenna, a modified Physical Optics method based on Discrete Real Mirror Image theory (DRMI-PO) was developed to efficiently analyze the field patterns of the antenna with enough precision and reasonable computation complexity. Finally, a prototype of the fan-beam antenna was fabricated and measured at 0.2 THz. Good agreement between the analytical and experimental results was obtained, which validates the effectiveness of the systematic design method proposed in this paper.

A Fan-beam Millimeter-wave Antenna Based on Modified Luneberg Cylindrical Lens

Changzhou Hua[1, 2], **Xidong Wu**[1], **Nan Yang**[1], **Huixian Wu**[1], **Bo Li**[1, 2], **and Wen Wu**[2]

[1]Department of Information Science and Electronic Engineering, Zhejiang University
Hangzhou 310027, China
[2]Ministerial Key Laboratory of JGMT, Nanjing University of Science and Technology
Nanjing 210094, China

Abstract— A new design of lens antenna at millimeter-wave frequencies is introduced with special focus on ease of manufacturing and reliability. The system is composed of a modified Luneberg cylindrical lens and a feed antenna. The modified Luneberg cylindrical lens is designed by using the technique of parallel plates propagating the TE_{10} mode. It consists of two parallel plates with the space between plates only filled with air dielectric. The thickness of the air dielectric is designed to vary with the normalized radius r, to give the desired index of refraction $n = N_0\sqrt{2 - \delta r^2}$. A planar linear tapered slot antenna (LTSA) is inserted into the air region between the parallel plates at the edge of the lens as a feed antenna. The cylindrical lens system is analyzed through a combined ray-optics/diffraction theory. CST-MWS is then used to examine the property of the antenna. For this prototype, 3 dB E- and H-plane beamwidths of 9° and 68° is obtained at design frequency of 30 GHz, and the sidelobe level in the E-plane is −19.8 dB. It is also found that an aperture efficiency of 55% can be achieved. Due to its spherical symmetry, the proposed modified Luneberg cylindrical lens can be used to launch multiple beams by implementing an arc array of planar LTSA elements at the periphery of the lens. Beam scanning can be achieved by switching among the feed antenna elements. A 15-element antenna array with a −3 dB beam crossover and a scan angle of 135° is demonstrated. The designed 15-element array results in virtually no gain loss over the entire 135° scan angle, which proves to be a wide scan-angle antenna at millimeter-wave frequencies. The proposed antenna can be easily extended to a new design for higher mm-wave frequencies, and is well suitable for scanning fan-beam applications, such as aircraft landing systems.

A Dual Frequency Rectangular Dielectric Resonator Antenna Fed by a Coaxial Probe

Huixian Wu[1], **Xidong Wu**[1], **Changzhou Hua**[1, 2], **and Nan Yang**[1]

[1]Department of Information Science & Electronic Engineering
Zhejiang University, Hangzhou 310027, China
[2]Ministerial Key Laboratory of JGMT
Nanjing University of Science & Technology, Nanjing 210094, China

Abstract— A dual frequency dielectric resonator antenna (DRA) is presented for 19.5 GHz and 30.0 GHz dual band wireless communications. The proposed DRA is fed by a coaxial probe and has a rectangular dielectric resonator with a rectangular patch antenna on the top. The dielectric constant of the DRA is chosen to be 12. The rectangular dielectric resonator provides the first resonance frequency at 19.5 GHz while the patch antenna resonates at the second frequency 30.0 GHz. To get a satisfied design, a simple and efficient analysis procedure is implemented. The effects of the size of the dielectric resonator and patch antenna on the input impedance and operating frequencies are discussed. The effects of position of the coaxial probe and the length of the probe are also studied. The whole structure is simulated by using CST Microwave Studio. Finally, the length, width and height of the dielectric cuboid are optimized to be 2.5 mm, 2.5 mm and 2.0 mm, respectively, and the size of the patch antenna is 2.0 mm $*$ 2.0 mm. The gains of this antenna are both 5.6 dB at 19.5 GHz and 30.0 GHz. The simulated results show this type of antenna produces dual band that the frequency ratio of the two resonating frequencies is relatively large, which is quite difficult to realize. Such a structure can be used in satellite communication to solve the problems that the traditional antenna has, for example high ohmic loss at high frequency and the influence of machining accuracy on antenna performance.

A Matching Circuit with Genetic Algorithms for LNA Applications

Ming-Huei Chen, **Ming-Chih Huang**, **Hao-Hui Chen**, **and Cheng-Yu Tasi**
Department of Electronic Engineering
National Kaohsiung First University of Science & Technology, Kaohsiung, Taiwan, R.O.C.

Abstract— There are great advances in wireless local area network (WLAN) communications and world interoperability for microwave access (WiMAX) communication systems have become more advantages on boardband speed. Hence, the development of front-end subsystem such as antennas, matching circuit, and low noise amplifier (LNA) has become an attractive research in modern communication. In response this trend, the optimization GA scheme is used to determine a proper matching circuit topology and overcome the interface problems.

Genetic algorithms (GAs) first introduced by Holland in 1975, has been widely used in science and engineering problem. It also proves to be useful for solving complex electromagnetic problems. A good review section can be found [1]. In this research, the probabilities of mating (crossover) and mutation operator are selected. The optimum techniques with GA are also applied by a ranking selection method and fitness function with S_{11} to reduce the computation time for evaluation of the microwave circuits.

Due to the increasing demand in the wireless communications industries, an efficient optimum design to a small size, light weight, and low cost on applications is important for WiMAX and WLNA. In this work, a LNA is first utilized for the separating 2.4 GHz or 5.2 GHz LNA. The circuit of LNA is simulated using an RF circuit simulator, ADS(Agilent Technologies). An RF transistor, START540 is used for each stage of the amplifier and the specification, once the antenna (ANT), multiplexer and the LNA are separately implemented and tested to be within the required performance, their circuit layouts can be merged for the construction of front-end 2.4/5.2 GHz subsystem. The prediction of final design for 2.4 GHz matching circuit and 5.2 GHz are presented. The mini entity of LNA and matching circuit is made by FR4, $\varepsilon_r = 4.4$ and $h = 0.8$ mm. The prediction final results in operating bands to practical at 2.4/5.2 GHz, the optimum matching circuit value have a good gains and low noise.

REFERENCES

1. Lai, M.-I., and S.-K. Jeng, "Compact microstrip dual-band bandpass filters design using genetic-algorithm techniques," *IEEE Trans. on Microwave Theory and Techniques*, Vol. 54, No. 1, 160–168, Jan. 2006.

A Triple-band Monopole Antenna with Genetic Algorithms for WLAN and WiMAX Applications

Ming-Huei Chen, **Hao-Hui Chen**, **Sung-Te Lin**, **and Ming-Chih Huang**
Department of Electronic Engineering, National Kaohsiung First University of Science & Technology
Kaohsiung, Taiwan, R.O.C.

Abstract— Since Federal Communication Commission (FCC) released the 3.1–10.6 GHz band for commercial applications in 2002, ultrawideband (UWB) technology has received great attention in various high-data-rate mobile systems. Hence, the development of UWB components such as antennas, filters, and amplifiers has become an attractive research in modern communication. Although the UWB technology covers the frequency band ranging from 3.1 to 10.6 GHz, to prevent the possible interference with other wireless communication networks, thus are great advances in WLAN and WiMAX communication systems have become more advantages on board-band speed. For the WLAN systems, it works on 2.4–5.0 GHz bands, which are commonly used all over the world to satisfy the IEEE 802.11a and 802.11b standard, many related produces are designed to be capable dual-band operations in the 2.4 GHz band and 5.2 GHz band. And an additional this topic realizes a third band with a bandwidth of 80 MHz at 3.5 GHz for WiMAX. In response this trend, the optimization technique is used to determine a proper microstrip line topology and overcome the interface problems, thus the optimum design flow will be subscribed to find an optimum plan path antenna in this research.

Genetic algorithms (GA) first introduced by Holland in 1975, has been widely used in science and engineering problem. It also proves to be useful for solving complex electromagnetic problems. A good review section can be found in Refs. [1] and [2]. Due to the increasing demand in the wireless communications industries, an efficient optimum design to a small size, light weight, and low cost on applications is important for WLAN and WiMAX. In this work, the optimum design flow has been contributed, such a given geometry of monopole plan path antenna as an approach form is first simulated by the GA to a result for IE3D that can be presented by S_{11}. Next feedback to GA is evaluated by the fitness function. Normally, the iteration of the optimum design flow has to get an optimum antenna with the GA. Using the layout tool and circuit milling machine can be combined to realize the triple band of monopole plan path antenna with FR-4 and 0.8 mm as shown in Fig. 1.

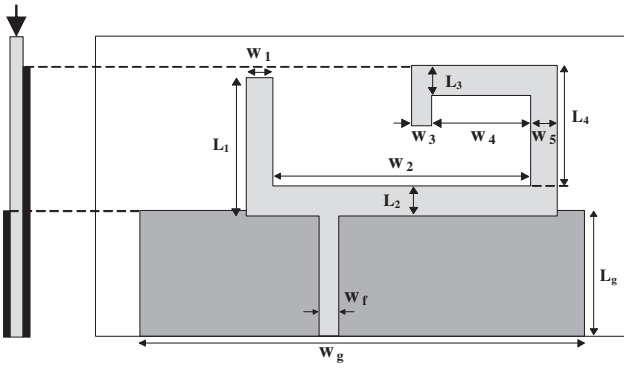

Figure 1: Pattern of a triple-band monopole antenna.

REFERENCES

1. Baena, J. D., et al., "Equivalent-circuit model for split-ring resonators and complementary split-ring resonators coupled to planar transmission lines," *IEEE Trans. Microw. Theory Tech.*, Vol. 53, 1451–1461, Apr. 2005.
2. Kim, J. H. and W. S. Park, "Dual-band antenna design using genetic algorithm-generated topology," *Microwave and Optical Technology Letters*, Vol. 52, No. 5, 1170–1174, May 2010.

A Circularly Polarized Rectenna for Wireless Power Transmission

Jwo-Shiun Sun, **Ren-Hao Chen**, **and Shao-Kai Liu**
Graduate Institute of Computer and Communication Engineering
National Taipei University of Technology, Taipei 10608, Taiwan

Abstract— Design of a circularly polarized rectenna (rectifying antenna) for wireless power transmission applications involving wireless power transfer to low power consumption wireless device is proposed. In order to build the rectenna, a CP wide-slot antenna and a finite ground coplanar waveguide circuit both with good impedance matching, have been developed. In addition, the size of the wide-slot antenna is smaller than the conventional slot antenna up to 60% when the meander line structure is adopted. The rectenna is the voltage-doubler rectifier with the low-pass filter for efficiency optimization and higher order harmonics re-radiation elimination. The maximum RF-to-DC conversion efficiency of the rectenna achieved 75% when the RF power of 15 dBm is received with a load resistance of 2 kΩ at free space. The experimental results prove that the proposed rectenna is suitable for the WPT applications.

Use of Frequency Selective Surface to Prevent SAR and Improve Antenna Performance of Cellular Phones

Han-Nien Lin[1], **Ke-Wen Lin**[2], **and Sheng-Chun Chen**[1]

[1]Department of Communications Engineering, Feng-Chia University
100 Wen-Hua Rd., Taichung 40724, Taiwan, R.O.C.
[2]Department of Electrical Engineering, National Chiao-Tung University
1001 University Road, Hsinchu 300, Taiwan, R.O.C.

Abstract— The purpose of this study is to design the low-cost planar inverted-F antenna (PIFA) applicably built in cellular phones with finite integration technique (FIT) for simulation of surface current distribution, radiation efficiency, radiation pattern, and gain. The prototype antenna is constructed with aluminum foil and low-cost FR4 PCB substrate. The antenna is designed with quarter wavelength ($\lambda/4$) of resonant frequencies and fed with $50\,\Omega$ matching microstrip. It owns the industrial demanding characteristics of light weight, compactness, low profile, and easy fabrication. The target frequency band is designed for the following cellular phone systems: GSM (Global system for mobile communication: 880–960 MHz), DCS (Digital communication system: 1.71–1.88 GHz, PCS (Personal communication system: 1.85–1.99 GHz), and IMT-2000 (3G: (1.92–2.17 GHz). However, since the bio-effect of specific absorption rate (SAR) by cellular phone gains popular concern, we also try to utilize the unique band-stop or band-pass features of frequency selective surface (FSS) to reduce the SAR. Finally, we design the finite size 2-dimensional periodic structure to integrate with antenna for SAR reduction by decreasing backward radiation. The result shows that the integrated PIFA-FSS module not only reduces the SAR but also improve the antenna gain and radiation efficiency of the cellular phone.

Receiving Performance Enhancement of Active GPS Antenna with Periodic Structure

Han-Nien Lin[1], **Ke-Wen Lin**[1, 2], **Chung-Wei Kuo**[3], **and Yu-Jie Huang**[1]

[1]Department of Communications Engineering, Feng-Chia University
100 Wen-Hua Road, Taichung 40724, Taiwan, R.O.C.
[2]Department of Electrical Engineering, National Chiao-Tung University
1001 University Road, Hsinchu 300, Taiwan, R.O.C.
[3]Ph.D. Program in Electrical and Communications Engineering
Feng-Chia University, 100 Wen-Hua Road, Taichung 40724, Taiwan, R.O.C.

Abstract— The purpose of this study is to design the high gain active GPS antenna module and analyze the performance improvement implemented with periodic structure. Since the utilization of high-impedance surface of periodic structures as reflector not only significantly reduces the antenna profile with phase enhancement, but it will also enhance its gain and directivity performance. We first investigated the electromagnetic radiation suppression characteristic of Electromagnetic Band-Gap (EBG) structure and utilized the microstrip measurement method to verify the simulation result for required stopband and performance. In this study, we design microstrip antenna and periodic structure with center frequency at 1.575 GHz for Global Positioning System (GPS) to investigate the effect with applications of EBG structure on antenna. Microstrip antenna has the industrial demanding characteristics of light weight, low profile, and easy integration with circuits on PCB. We investigated surface wave suppression and axial ratio improvement with the antenna surrounded by matching resonant EBG structure. Finally, we design the front-end low noise amplifier (LNA) with center frequency at 1.575 GHz to integrate with antenna to further improve GPS receiving sensitivity.

Finite Different Ground Shapes Printed Spiral Antennas for Multi Wide Band Applications Using PPPC Feeding Scheme

A. A. Jamali[1], **A. Gaafar**[1], **and A. A. Abd Elaziz**[2]

[1]Department of Electronics and Communications Engineering, AAST, Egypt
[2]Department of Electronics and Communications Engineering, MUST, Egypt

Abstract— In the era of modern wireless communication systems, antennas capable of operating at broad frequency band range are increasingly demanded. Various antenna design which enable antennas with low profile, light weight, enhanced dual or wideband frequency capabilities have been developed. However, such antennas mostly need a large size of ground plane which increases manufacturing cost. In this paper, three printed spiral antennas are proposed taking into account elimination the presence of ground plane under the radiating element for not to affect on the spiral radiation characteristics and bandwidth enhancement. This can be done through choosing L, U and rectangular shape as a finite ground plane. The proposed antennas consists of two FR4 (dielectric constant of 4.65 and thickness of 1.5 mm) layers with foam (dielectric constant of 1.05 and thickness of 1.6 mm) layer inserted between them. Upper layer, two arms spiral antenna placed on its top where the lower one has microstrip phase shifter etched on the surface and finite ground plane on its bottom. Parallel-plane perpendicular-current (PPPC) feed method will be used through connecting the spiral antenna arms with the microstrip phase shifter using shorted vias. Gain, directivity, bandwidth and other antenna parameter are studied using the IE3D Method of moments based software. For the rectangular ground plane shape spiral antenna we notice that the measured reflection coefficient better than the computed one where it occupy the ranges from 3.0625 GHz to 3.8125 GHz, 4.812 GHz to 5.6875 GHz, 6.5 GHz to 6.937 GHz and 7.125 GHz to 8.6875 GHz. For the L ground plane shape spiral antenna the measured reflection coefficient extends from 9.44 GHz to 10 GHz and 11.0625 GHz to 13 GHz. For the U ground plane shape spiral antenna we notice that the measured reflection coefficient extends from 2.6875 GHz to 3.75 GHz, 7.5 GHz to 8.06 GHz and 9.2 GHz to 13 GHz. the proposed structures have an arm width of 0.5 mm and the structures occupy an area of radius 10.5 mm for the spiral element with $4 \times 5\,\text{mm}^2$ for the rectangular shape and radius of 8.5 mm for the spiral with ground plane occupy $23 \times 35\,\text{mm}^2$ for the U shape and $20 \times 35\,\text{mm}^2$ for the L shape respectively. The antennas are fabricated and its measured results are discussed. Finally, the proposed antennas are cheap, compact and introduce a suitable antenna gain, directivity and bandwidth suitable for multi wide band applications especially Ku band.

Dual-band Printed Monopole Antenna with 1-D EBG Ground Plane

S. H. Kim, **D. J. Kim**, **J. Y. Lee**, **B. H. Shin**, **and J. H. Jang**
School of Information and Communications, WCU Department of Nanobio Materials and Electronics
Gwangju Institute of Science and Technology (GIST)
261 Cheomdan-gwagiro, Buk-gu, Gwangju 500-712, Korea

Abstract— The dual-band printed monopole antenna was designed and realized at the corner of a rectangular one-dimensional electromagnetic bangap (1-D EBG) ground plane. Two monopole antennas are placed on the two different edge of the ground plane with different polarization and fed by a port at the corner of the rectangular ground plane. The lengths of the two monopoles are also different, which leads to the different resonant frequencies. When each monopole is positioned horizontally close to an ordinary ground plane, the antenna cannot radiate energy efficiently. In order to make the antenna radiates efficiently, 1-D EBG structures with different energy bandgaps were inserted at the different edges of the ground plane. The improved radiation efficiency of the dual-band 1-D EBG backed antenna is due to the in-phase reflection characteristics within a certain frequency band, which are similar characteristics of a 2-D mush-room like EBG structure.

The designed antenna covers DCS 1800 (1.71 GHz∼1.88 GHz), PCS (1.85 GHz∼1.99 GHz), and WLAN 802.11 b/g (2.4 GHz∼2.4835 GHz) frequency band. Because the frequency bands of the antenna are within the operating bandwidth of each 1-D EBG structure, the degradation of the radiation performance of the antenna was minimized. The radiation efficiency was measured to be higher than 70% within all the operating frequency bands. Also, the radiation pattern is y-directive in the lower frequency band and the radiation pattern is x-directive in the higher frequency band, because of the effect of the 1-D EBG ground plane. The designed antenna could be applied to rectangular type wireless communication devices supporting 3G and WLAN environments, such as tablet personal computers or laptop computers.

Asymmetrical Dipole-like UWB Antenna

The-Nan Chang
Tatung University, Taiwan

Abstract— The printed UWB antenna could be a monopole in various shapes such as a circular disc, an ellipse, etc. Alternatively, a wide slot embedded with various tuning stubs such as a T-stub [1] or a U-stub [2] could also be served as a UWB antenna. In [3], a circular hole is cut out from a ground plane and is fed by a circular open-ended microstrip line. In [4], a split rectangular ring is cut out from a ground plane and is fed by a fork-like microstrip line.

In this symposium, we investigate a new UWB antenna fed directly by a coaxial line. The antenna is an asymmetrical dipole built on a single printed circuit board. One arm of the dipole is bent in U-shape to save space. A 50 ohm coaxial line is used to feed the antenna, with its signal line connected to one arm of the dipole and its shielding ground connected to the U-shaped arm. The antenna has a size of 34 mm × 27 mm with a measured 10 dB return loss bandwidth from 3.07 GHz ∼ 11.4 GHz. Measured antenna peak gain in horizontal plane is between 0 dBi to 4.3 dBi.

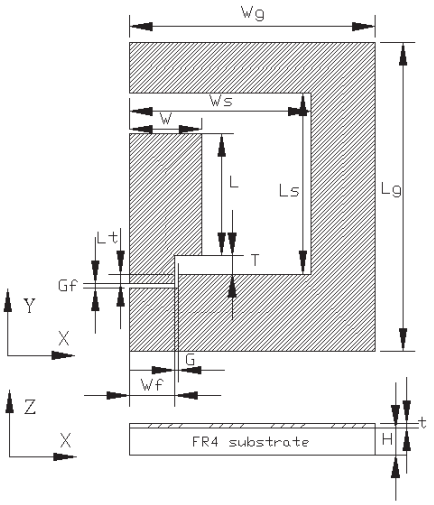

Figure 1.

REFERENCES

1. Chang, T.-N. and M.-C. Wu, "Band notched design for UWB antennas," *IEEE Antenna and Wireless Propagation Letters*, Vol. 7, 636–639, 2008.
2. Chair, R., A. A. Kishk, and K. F. Lee, "Ultrawide-band coplanar waveguide-fed rectangular slot antenna," *IEEE Antennas and Wireless Propagation Letters*, Vol. 3, 227–229, 2004.
3. Kharakhili, F. G., M. Fardis, G. R. Dadashzadeh, A. K. A. Ahmadi, and N. Hojjat, "Circular slot with a novel circular microstrip open ended microstrip feed for UWB applications," *Progress In Elecrtomagnetics Research*, Vol. 68, 161–167, 2007.
4. Sadat, S., M. Fardis, F. G. Gharakhili, and G. R. Dadashzadeh, "A compact microstrip square-ring slot antenna for UWB applications," *Progress In Elecrtomagnetics Research*, Vol. 67, 173–179, 2007.

Wideband Antenna Design by the Stacked Koch Fractal Structures

Homayoon Oraizi and Shahram Hedayati
Department of Electrical Engineering, Iran University of Science and Technology, Iran

Abstract— In this paper, a novel multiband stacked microstrip antenna is introduced, which is composed of an active patch, under which three parasitic patches are placed. The geometry of each patch is shaped as a Koch fractal of third generation. The antenna feed is made of a coaxial probe, which passes through a cylindrical cavity also shaped into a Koch fractal. In order to obtain wider frequency bandwidths, the active and parasitic patches on different substrates are displaced with respect to each other. Wide and multiband frequency characteristics are achieved for the radiation patterns and impedance matching. Another configuration is proposed for modifying performance of the stacked Koch antenna (SKA), wherein a space-filling slot in the form of Hilbert fractal geometry is cut into the active patch. High-directivity microstrip antennas comprising a driven patch and at least one parasitic element placed on the same plane, operate at a frequency larger than the fundamental mode of the driven patch in order to obtain a resonance frequency with a high-directivity broadside radiation pattern. The gap defined between the driven and parasitic patched is used to control the resonance frequency where the high-directivity behavior is obtained.

A Compact Planar Microstrip-Fed Feed Patch Antenna Using High Permittivity Substrate

C. H. Hsu[1], **C. H. Lai**[2], **and Y. S. Chang**[1]

[1]Department of Electrical Engineering, National United University, Taiwan
[2]Department of Electronic Engineering, National United University, Taiwan

Abstract— A compact-size Microstrip-Fed Feed Patch antenna is investigated by employing high-permittivity and low-loss substrate (i.e., high $Q \times f$ value) for 1.9-GHz application. The antenna was fabricated on ZnO-doped $Nd(Co_{1/2}Ti_{1/2})O_3$ ($\varepsilon_r = 27.4$, $Q \times f$ value of 147,000 GHz) substrate. The high permittivity and low-loss ceramic substrate (ZnO-doped $Nd(Co_{1/2}Ti_{1/2})O_3$) was used to reduce the microstrip antenna dimension on patch size. The proposed antenna occupies a size of 2.25 cm^2 and obtains the operation bandwidth of about 10 MHz. Good antenna gain and CP radiation patterns have also been observed. The measured results of the performance of the antenna are presented.

Design of Microstrip Antenna with Modified Annular-ring Slot for GPS Application

C. F. Tseng, **S. C. Lu**, **and Y. C. Hsu**
Department of Electronic Engineering, National United University, Taiwan

Abstract— A circularly polarized annular ring slot antenna with broadband impedance and circularly polarized bandwidth characteristics has been presented in this paper. By introducing proper asymmetry in the annular ring slot structure in the form of two pairs of slits, and feeding the ring slot using a 50 Ω microstrip line, the bandwidth is increased, and the circularly polarized antenna is also formed for GPS application. The measured results agree with the simulation, showing that the proposed antenna has a wide return loss and AR bandwidth (AR $<$ 3 dB) of more than 40% referred to the resonant frequency 1.575 GHz. The measured radiation patterns are stable and symmetric with respect to the broadside direction. Moreover, a prototype antenna with an average gain of 3.2 dBi over a CP bandwidth is shown.

Miniaturized Ultra-wideband Circular Metallic Plate Antenna Suspended by Shorting Pins

Homayoon Oraizi and Mehdi Hamidkhani
Department of Electrical Engineering, Iran University of Science and Technology, Narmak, Iran

Abstract— In this paper, a microstrip antenna composed of a square patch with mitred corners on a low dielectric substrate together with two smaller square parasitic patches on a substrate with high permitivities is introduced, which tends to reduce the size of the antenna, generate circular polarization and increase the frequency bandwidth. The high permittivity substrate under the parasitic patches causes strong surface waves to appear on the antenna and decrease its radiation efficiency. Defected ground structures are made to counter the generation of surface waves and also reduce the size of microstrip antenna. This antenna with favourable characteristic is presented for applications in mobile systems.

Design of UHF RFID Passive Tag Antenna Pasted on a Large Metal Structure

Shih-Chung Tuan[1], **Hsi-Tseng Chou**[2], **Kuo-Lun Hung**[2], **and Jen-Chung Chu**[2]

[1]Dept. of Communication Eng., Oriental Institute of Technology, Pan-Chiao, Taiwan
[2]Dept. of Communication Eng., Yuan Ze University, Chung-Li 320, Taiwan

Abstract— In this paper, we present a new design of patch-type antenna using a loop circuit located inside the antenna structure to excite the antenna, which has potential to resolve the problem arising from the situation when the antenna is pasted on a large metal ground. The problem of large metal structures to the RFID tag antenna arises because most of the RFID uses electrical dipole-type antennas. In this case, the presence of large metal structure will short the antenna and reduce the radiation field strength. The proposed antenna structure is a magnetic type. The proposed design concept intends to optimize the field distribution within the substrate between the patch and ground, and therefore may reduce significantly the antenna size. Experimental study showed that the antenna may be used to enhance the reading range to be more than 3 meters.

A Low Profile Printed Tri-band Antenna Using Multi-band Artificial Magnetic Conductor Ground Plane

Fuguo Zhu[1], **Steven Gao**[1], **and Jiadong Xu**[2]

[1]Surrey Space Centre, University of Surrey, Guildford, GU2 7XH, Surrey, UK
[2]School of Electronics and Information, Northwestern Polytechnical University, Xi'an 710072, China

Abstract— This paper presents the design, simulation, implementation and measurement results of printed tri-band antenna. A novel artificial magnetic conductor (AMC) ground plane is designed and integrated with the antenna. This leads to an antenna which has a low profile and can achieve multi-band operations and have a unidirectional radiation pattern. The unit cell of the AMC ground plane consists of a square ring with a square patch inside it. The AMC ground plane exhibits a characteristic of in-phase reflection in two frequency regions. Simulations show that the reflection phase of the AMC ground plane depends on the square patch and square ring patch respectively and thus can be adjusted easily. To prove the concept, a prototype tri-band antenna with this AMC ground plane is designed, fabricated and measured. The results will be useful for applications in portable devices which require a compact antenna for multiple wireless systems.

A Planar Monopole Antenna for DVB-H/GSM Applications

I.-Tseng Tang[1], **Simon Li**[2], **Ding-Bing Lin**[3], **and Cheng-Yu Chen**[2]

[1]Department of Greenergy, National University of Tainan, Tainan, Taiwan
[2]Department of Electrical Engineering, National University of Tainan, Tainan, Taiwan
[3]Institute of Computer and Communication Engineering, National Taipei University of Technology
Taipei, Taiwan

Abstract— This paper is to design the miniaturized digital video broadcasting (DVB) antenna. The proposed monopole antenna consists of the C character and dual-L shape strips. The antenna bandwidth includes DVB-H (518 $\sim$ 862 MHz) and GSM (862 MHz $\sim$ 1.04 GHz) bands. The antenna characteristics including return loss and radiation patterns were analyzed and discussed.

Introduction: The rapid progress of personal wireless communications has made it possible for a multimedia mobile handset to cope with both the digital video broadcasting and global system for mobile communication. Owing to covering wideband bandwidth (470 $\sim$ 960 MHz), we propose a novel antenna structure to satisfy this issue.

Antenna Design: Antenna structure and design: Fig. 1 shows the geometry and configuration of the proposed antenna. The proposed antenna is to fabricate on a low-cost FR-4 substrate with dielectric constant $\varepsilon_r = 4.4$, loss $\tan\delta = 0.02$, and thickness $h = 0.8$ mm, and fed by a 50-Ω microstrip line of width 1.5 mm. The antenna consists of the C character and two L-shape strips connected the C character. The C character has the outer circle radius 18 mm and the inner circle radius 9 mm. Two circles yield two different electric paths to satisfy the bandwidth requirements. Fig. 2 shows that the simulated return loss of the proposed monopole antenna. The input impedance is well matched as the 5-dB return loss bandwidth covers the DVB bands (518 $\sim$ 862 MHz) and GSM bands (862 MHz $\sim$ 1040 MHz).

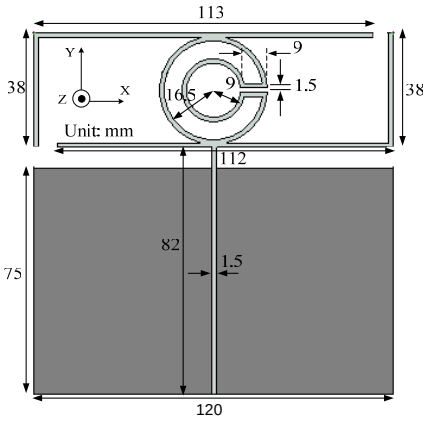

Figure 1: Geometry and configuration of the proposed antenna.

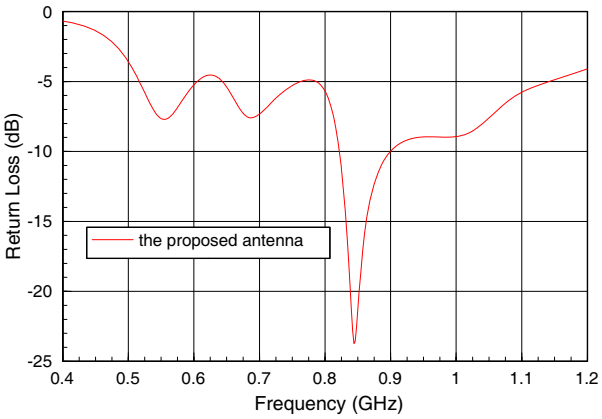

Figure 2: Effects of the stub length L_4 on the return loss.

REFERENCES

1. Li, R. L., B. Pan, J. Papapolymerou, J. Laskar, and M. M. Tentzeris, "Low-profile broadband planar antennas for DVB-H, DCS-1800, and IMT-2000 applications," *IEEE Antennas 2nd Propagation Society International Symposium*, 4729–4732, 2007.
2. Zhou, S., J. Guo, Y. Huang, and Q. Liu, "Broadband dual frequency sleeve onopole antenna for DTV/GSM pplications," *Electronics Letters*, Vol. 45, 766–768, 2009.

A Wide Bandwidth Rectangular Dielectric Resonator Antenna for LTE 4G Handset Front-end

I-Tseng Tang, Simon C. Li, Ding-Bing Lin, C. H. Syu, and Bo-Yuo Chen
Graduate Institute of Communication Engineering, National University of Tainan, Taiwan

Abstract— A new wideband rectangular dielectric resonator antenna is proposed. The rectangular dielectric resonator is excited by a monopole antenna. The antenna provides an impedance bandwidth of 95% for VSWR ≤ 2.5. A monopole antenna conformed standard ($2.05 \sim 5.8$ GHz) characteristics including return loss and radiation patterns were analyzed and discussed. A 2.6 GHz CMOS LTE 4G handset receiver front-end using merged folded cascoded (MFC) circuit scheme is also proposed.

Introduction: Recently, the dielectric resonator antenna has been extensively studied owing to its numerous advantages such as high radiation efficiency, low weight, miniature size. The shapes of DRAs are various and different, such as hemispherical, cylindrical and rectangular. DRAs can be excited by different feeding method, such as coaxial feed, microstrip line and co-planar lines. The DRAs can be completed low profile due to high dielectric permittivity of the materials.

Antenna Design: Figure 1 shows the geometry and configuration of the proposed antenna. The proposed antenna is to fabricate on a low-cast FR-4 substrate with dielectric constant $\varepsilon_r = 4.4$,

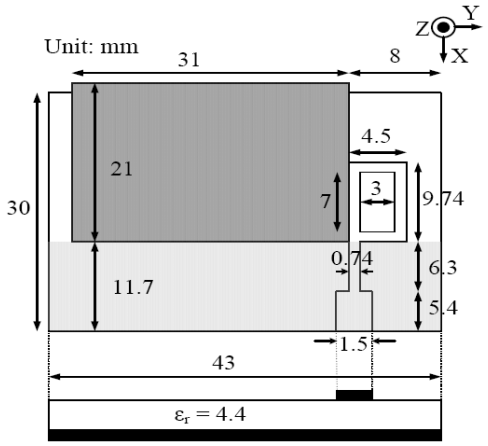

Figure 1: Geometry and configuration of the proposed antenna.

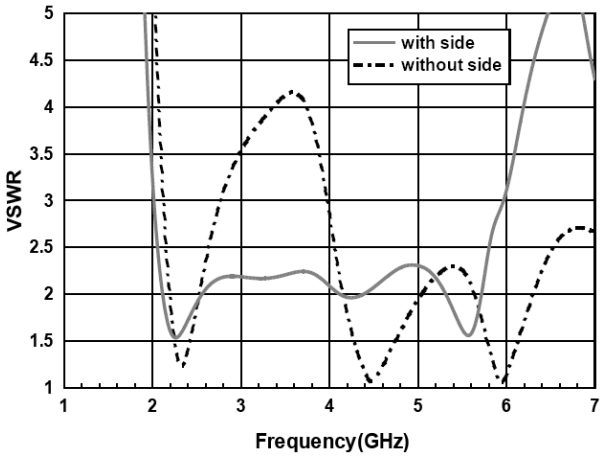

Figure 2: Effects of the dielectric resonator with and without side stub.

Table 1: Performances of MFC front-end for 4G LTE handset.

LTE Front-End Characteristics	This work	
	2.6 GHz	unit
Supply	1	V
Forward Gain	13.7	dB
Conversion Gain	5.0	dB
$P_{in\text{-}1\text{dB}}$	−24.5	dBm
IIP3	−1.67	dBm
Isolation (RF Port)	−27.2	dB
Isolation (LO Port)	−26.4	dB
Isolation (IF Port)	−13.0	dB
Noise Figure	5.6	dB
Power Consumption	1.97	mW

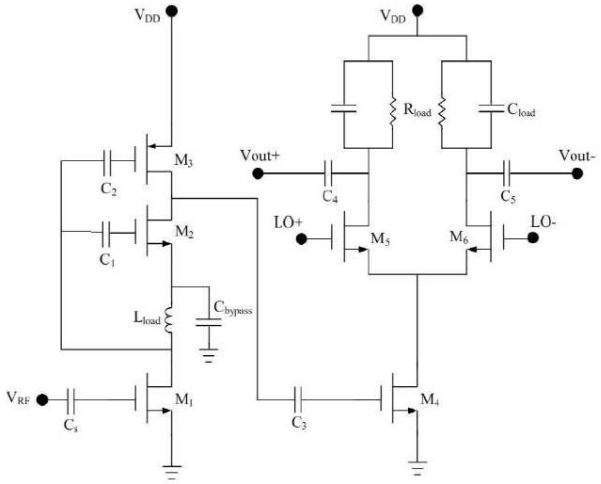

Figure 3: Proposed merged folded-cascoded (MFC) front-end for 4G LTE handset.

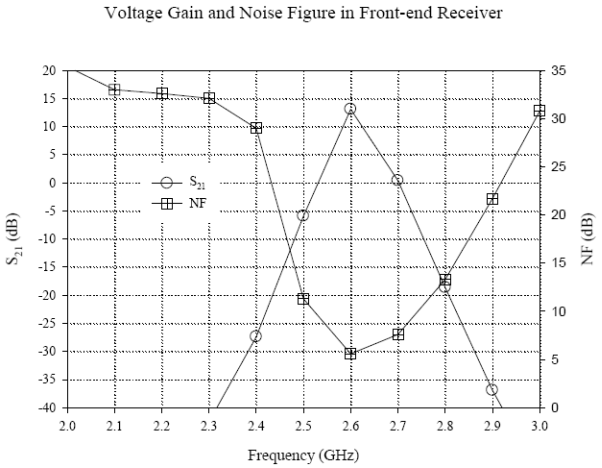

Figure 4: Voltage gain and noise figure of MFC front-end.

loss $\tan\delta = 0.02$, and thickness $h = 0.8\,\text{mm}$. A rectangular dielectric resonator is inserted a substrate with a size of $43 \times 30\,\text{mm}^2$. The dimension of dielectric resonator is $31 \times 21 \times 5.08\,\text{mm}^3$ with a permittivity of $\varepsilon_r = 9.8$. The dielectric resonator antenna is excited by a $50\,\Omega$ microstrip feed line. In order to an impedance matching, the monopole is connected to the feed connector to achieve enhanced input impedance matching over the preferred bandwidth. Besides, setting a stub beside the dielectric resonator can be improved the impedance matching. Just like the method of step impedance matching. Fig. 2 shows the effects of the dielectric resonator with and without side patch.

4G LTE Front-end Design: A 2.6 GHz CMOS LTE receiver front-end using merged folded cascoded (MFC) circuit scheme [3] is proposed. The MFC front-end achieves a forward gain of 13.7 dB and a noise figure of 5.6 dB at 10 MHz with 1.97 mA bias current from a 1-V power supply. In order to reduce power consumption, the dc current path from the power supply to the LNA is replaced by a stacked mixer transconductance stage. In this scheme, the LNA operates by only reusing the dc bias current of the stacked mixer. Fig. 3 shows the proposed merged folded-cascoded (MFC) front-end for 4G LTE handset. Voltage gain and noise figure of MFC front-end are shown in Fig. 4. The performances of merged folded-cascoded (MFC) front-end for 4G LTE handset. are summarized in Table 1.

ACKNOWLEDGMENT

Authors would appreciate the financial support from National Science Council of Taiwan, NSC 99-2221-E-024-019.

REFERENCES

1. Sulaiman, M. I. and S. K. Khamas, "A singly fed rectangular dielectric resonator antenna with a wideband circular polarization," *IEEE Antennas and Wireless Propagation Letters*, Vol. 9, 2010.
2. Liang, X.-L. and T. A. Denidni, "Cross-T-shaped dielectric resonator antenna for wideband applications," *Electronics Letters*, Vol. 44, No. 20, 2008.
3. Jarvinen, J. A. M., et al., "2.4-GHz receiver for sensor applications," *IEEE J. Solid-State Circuits*, Vol. 40, No. 7, 1426–1433, Jul. 2005.

A Monopole Antenna for Digital Video Broadcasting and GSM900 Applications

I.-Tseng Tang[1], **Simon Li**[2], **Ding-Bing Lin**[3], **and Ming-Jhe Wu**[2]

[1]Department of Greenergy, National University of Tainan, Tainan, Taiwan
[2]Department of Electrical Engineering, National University of Tainan, Tainan, Taiwan
[3]Institute of Computer and Communication Engineering
National Taipei University of Technology, Taipei, Taiwan

Abstract— A simple monopole antenna associated with a rectangular radiating strip and a controllable stub for DVB-H (Digital Video Broadcast for Handheld) application is presented. The simulated impedance bandwidth defined by return loss ≤ -6 dB is from 520 to 1140 MHz. This proposed antenna with broadband matched impedance, stable radiation patterns and good antenna gains can be suitable for communication products of DVB-H and GSM900 applications.

Introduction: Recently, digital video broadcasting-handheld (DVB-H) has made it possible to deliver broadcast television or other multimedia services to a mobile or handheld device. The DVB standard is designed to operate in UHF bands of IV and V (470–862 MHz). The content of this paper is focused on the analysis and research based on this DVB antenna. This paper proposed a simple idea of printed monopole antenna for DVB (470–860 MHz) and GSM900 application.

Antenna Design: Figure 1 shows the geometry and configuration of the proposed simple monopole antenna for DVB and GSM900 applications. This antenna has been printed on FR4 substrate with the relative permittivity (ε_r) of 4.4, loss $\tan\delta = 0.02$ and the substrate thickness of 0.8 mm, and is fed by a 50-Ω CPW transmission line with a fixed metal strip width of 1.5 mm. The ring-shaped radiating strip operates at its about half wavelength ($\lambda/2$) mode as the fundamental resonant mode for achieving wideband operation. Also, the controllable strip AB generates the second resonant mode at its half wavelength ($\lambda/2$) mode for GSM900 applications. Fig. 2 shows the simulated return loss for the proposed antenna with different length L. As the simulated return loss against frequency for various length $L = 50$ and 60 mm, the second resonant mode for the center frequency is varied from 890 to 980 MHz. The radiation patterns are displayed with traditional 8-shape in E-plane, and omni-directional in H-plane.

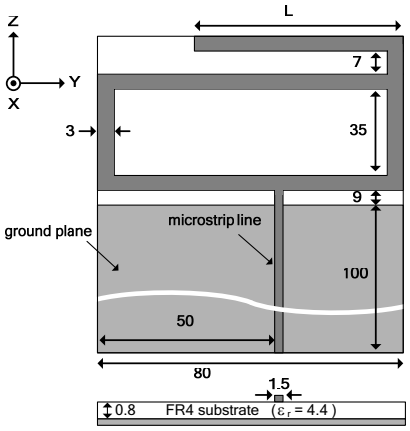

Figure 1: Geometry and configuration of the proposed antenna (unit: mm).

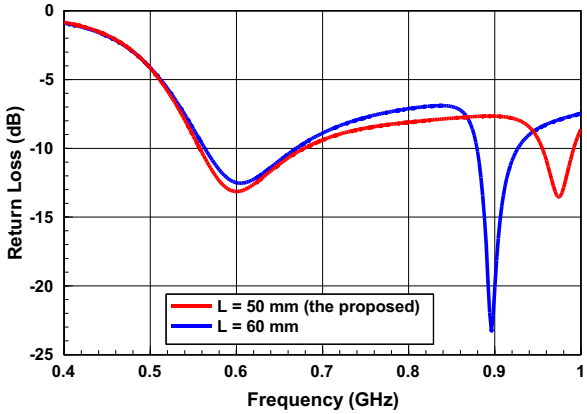

Figure 2: Simulated return loss for the proposed antenna with different length L.

REFERENCES

1. Huang, C.-Y., B.-M. Jeng, and C.-F. Yang, "Wideband monopole antenna for DVB-T applications," *Electronics Letters*, Vol. 44, No. 25, December 4, 2008.
2. Hsu, C.-K. and S.-J. Chung, "A wideband DVB forked shape monopole antenna with coupling effect for USB dongle application," *IEEE Transactions on Antennas and Propagation*, Vol. 58, No. 9, September 2010.

Design of Elliptical Microstrip Patch Antenna Using ANN

Amit Agrawal, D. Vakula, and N. V. S. N. Sarma
National Institute of Technology, Warangal, India

Abstract— Microstrip patch antenna is used for high-performance spacecraft, aircraft, missile and satellite applications, where size, weight, cost, performance, ease of installation, and aerodynamic profile are constraints. These patch antennas are low-profile, conformable to planar and non-planar surfaces, simple and inexpensive to manufacture using modern printed circuit technology. They are also mechanically robust when mounted on rigid surfaces and compatible with MMIC designs. When a particular patch shape and excited mode are selected they are very versatile in terms of resonant frequency, polarization, radiation pattern, and impedance.

In this work, elliptical microstrip antennas are the ones under consideration as their geometry presents greater potentials for a variety of electrically small low-profile antenna applications. The elliptical shape has several advantages like providing large flexibility in the design, more degrees of freedom compared to the circular geometry and circular polarization is achieved with single feed. The feed position is located along the 45° line between the major and minor axis of the elliptical patch. The radiated fields cause two modes that are perpendicular to each other and have equal amplitude, but are 90° out of phase. An elliptical patch antenna with optimum dimensions acts as a Circular Polarized wave radiator.

Elliptical patch geometry is perhaps least analyzed regular shape geometry due to involvement of Mathieu's and modified Mathieu's function in mathematical analysis. The involvement of these functions makes mathematics of elliptical patch geometries extremely difficult. There are various methods available for the calculation of resonant frequency for elliptical patch antenna. These methods obtain resonant frequency for even (f_e) and odd (f_o) modes as the function of input variables, which are the height of the dielectric substrate (h), dielectric constant of the dielectric material (ε_r), and antenna dimensions (major axis and the ratio of minor to major axis). But reverse calculation of the antenna dimensions from the inputs like frequencies (f_e, f_o), height (h) and dielectric constant (ε_r) is not available in the literature. A novel technique to design an elliptical microstrip patch antenna by using artificial neural networks (ANN) is presented in this paper. ANN is developed to calculate antenna dimensions.

The neural network design aims at utmost simplicity and self-organization. The present work uses radial basis function (RBF) ANN network. The RBF network is similar to a general feed-forward network trained using the back-propagation algorithm, i.e., Feed-Forward Back Propagation (FFBP) network. RBF network has three layers of neurons, namely input, hidden and output. Each neuron in the hidden layer operates as the Gaussian transfer function, as against the sigmoid function of the FFBP. The RBF network is one of the approaches which show a great promise in this sort of problems because of its faster learning capacity.

The ANN model is built to obtain antenna dimensions from the function of input variables, which are resonant frequency, the height of the dielectric substrate (h), dielectric constants of the dielectric material (ε_r). In order to make such model, network weights are to be found. Finding the RBF weights is called network training. By using set of input-output pairs, called training set, the network parameters are optimized in order to fit the network outputs to the given inputs. The proposed model requires less training time and is more accurate in prediction as compared to other networks. After training, the RBF network can be used with data whose underlying statistics is similar to that of the training set, known as testing set. A trained neural network can be used for high-level design, providing fast and accurate answers to the task it has learned. For the purpose of training and testing, data set is generated by using IE3d simulation software. Here simulation is done for two different h values 0.3125 cm and 0.1575 cm and frequency ranges from 1 to 3 GHz. Network topology design contains 4 input nodes, 15 hidden nodes and 2 output nodes.

The results obtained by using ANN for elliptical microstrip patch antennas are in good agreement with available simulated results. The various possible dimensions and different dielectric values are obtained to achieve high bandwidth and single feed circular polarization. By designing antenna on low permittivity substrate, a much higher bandwidth may be achieved. ANN models are simple, easy to apply, and very useful for antenna engineers to predict both patch dimensions and resonant frequency.

GPS Antenna Design and Measurement

Kuo-Liang Wu[1], **Jwo-Shiun Sun**[1], **Y. D. Chen**[2], **and Guan-Yu Chen**[1]

[1]Department of Electronic Engineering, National Taipei University of Technology, Taiwan
[2]Antenna and EMC Laboratory, HTC Corporation, Taiwan

Abstract— A meander line antenna (Fig. 1) has several meander line sections so as to shorten the length from the corresponding monopole antenna in this design. In high performance meander line antenna for GPS and A-GPA applications, where size, profile, and performance are of major considerations, shorter length of antenna are desirable.

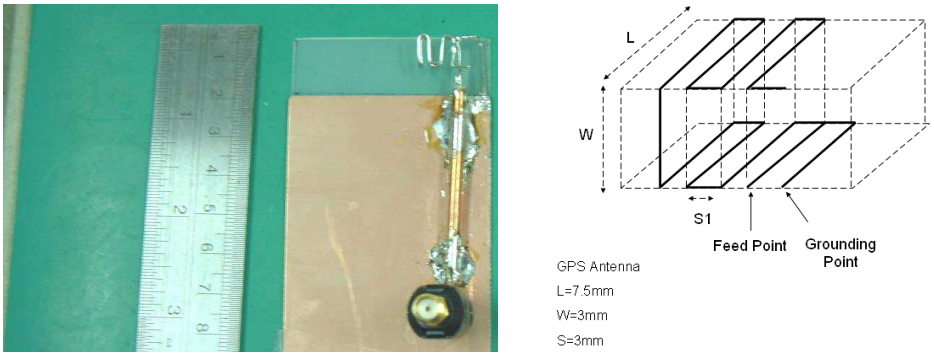

Figure 1: The proposed GPS antenna.

A Novel Fractal Patch Antenna for UWB Applications

Xue-Yong Zhang, **Shao-Bin Liu**, **Chun-Zao Li**, **Bo-Rui Bian**, **and Xiang-Kun Kong**
College of Electronic and Information Engineering
Nanjing University of Aeronautics and Astronautics, Nanjing 210016, China

Abstract— A novel fractal antenna is proposed for ultra-wideband (UWB) systems. We introduce a three-stage Sierpinski fractal geometry as the radiating element. The proposed antenna has compact dimension of 15 mm × 20 mm × 1.6 mm. The designed antenna has a wide bandwidth of more than 8.6 GHz (2.5–11.1 GHz) for a return loss of less than 10 dB. Also, the proposed antenna gives bidirectional pattern in the E plane and omni directional radiation pattern in the H plane over its whole frequency band of interest. In the paper, some parametric studies on the effect of the antenna on return loss are also done. So, the proposed antenna is considered a good candidate for UWB applications.

Flexible Antenna for Mobile Handsets

Ho-Jun Lee, Jae-Young Lee, and Kyu-Bok Lee
Convergence Communication Components Research Center
Korea Electronics Technology Institute, R. O. Korea

Abstract— In this paper, we proposed a novel design of flexible antenna for mobile handsets. A flexible antenna is meant to be a part of the clothing used for communication purposes, which includes tracking and notebook and mobile phone. The proposed antenna configuration is shown in Figure 1. Antennas in this paper are simulated by using the Ansoft simulation software high-frequency structure simulator (HFSS). A prototype of this antenna was fabricated on Taconic TLY substrate with thickness $h = 0.254\,\text{mm}$ and dielectric constant $\varepsilon_r = 2.17$. The measurements of electrical characteristics such as radiation patterns, VSWR, and return loss of the implemented antenna were conducted in an anechoic chamber equipped with a HP 8510C network analyzer and far field measurement system. Figure 2 shows return loss (S_{11}) characteristics. The measured impedance bandwidth of the antenna is from 2.385 to 2.5 GHz for VSWR < 2. Figure 3 shows a photograph of the fabricated antenna. We manufactured the antenna based on the results of optimized simulation results and measured characteristics of the suggested antenna in the anechoic chamber. Details of the proposed antenna designs are described, and typical experimental results are presented and discussed.

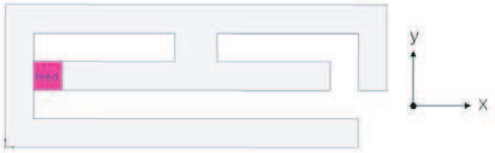

Figure 1: Proposed antenna.

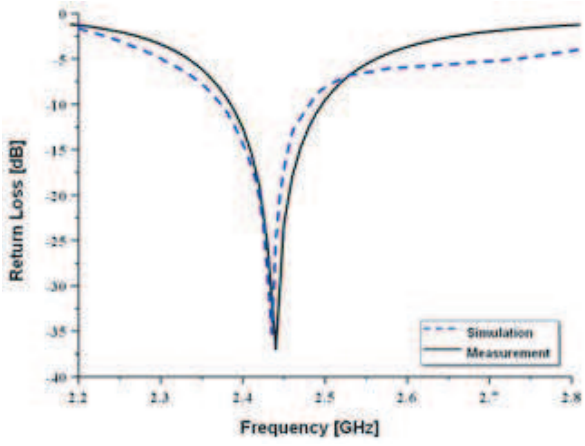

Figure 2: Measured return loss.

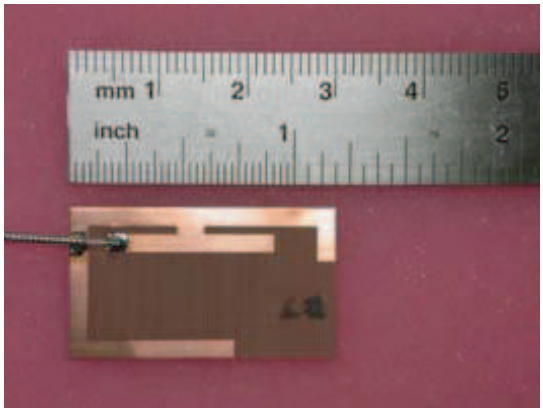

Figure 3: Photograph of the fabricated antenna.

REFERENCES

1. Choi, S. H., T. J. Jung, and S. Lim, "Flexible antenna based on composite right/left-handed transmission line," *Electronics Letters*, Vol. 46, No. 17, Aug. 2010.

WLAN Antenna Design and Measurement

Chien-Pang Chou[1], **Jwo-Shiun Sun**[1], **Y. D. Chen**[2], **and Guan-Yu Chen**[1]

[1]Department of Electronic Engineering, National Taipei University of Technology, Taiwan
[2]Antenna and EMC Laboratory, HTC Corporation, Taiwan

Abstract— A high performance monopole antenna (Fig. 1) fabricated using a folded wire line with loading effect as radiator is presented. A prototype of the proposed monopole antenna with a compact area size of 19.5 mm × 6 mm is implemented, and the multi-band WLAN antenna shows a wide operating bandwidth of about 560 MHz and 3550 MHz for low band and high band, bandwidth, making it easy to cover the IEEE 802.11a, IEEE 802.11b, IEEE 802.11g and IEEE 802.11n (MIMO) bands for wireless communication and future 4 G wireless operation of a mobile VoIP/VoWLAN handset phone.

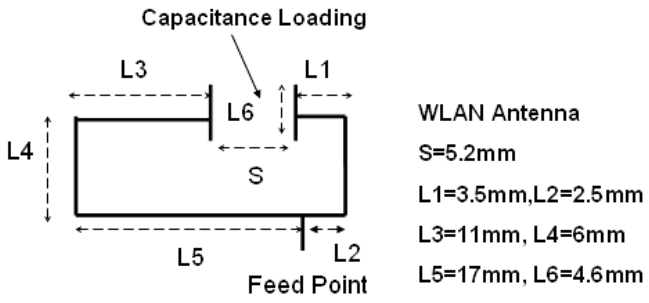

Figure 1: Dual wideband monopole antenna with capacitance-loading.

Cellular Antenna Design and Measurement

Chien-Pang Chou[1], **Y. D. Chen**[2], **Jwo-Shiun Sun**[1], **and Guan-Yu Chen**[1]

[1]Department of Electronic Engineering, National Taipei University of Technology, Taiwan
[2]Antenna and EMC Laboratory, HTC Corporation, Taiwan

Abstract— A high performance monopole antenna is designed (Fig. 1). A prototype of the proposed monopole antenna with a compact area size is implemented, and the antenna shows a wide operating bandwidth for low band and high band bandwidth, making it easy to cover the GSM, EDGE, CDMA, CDMA 2000, W-CDMA and UMTS band for wireless communication and 2.5 G/3 G dual mode operation of a mobile handset phone.

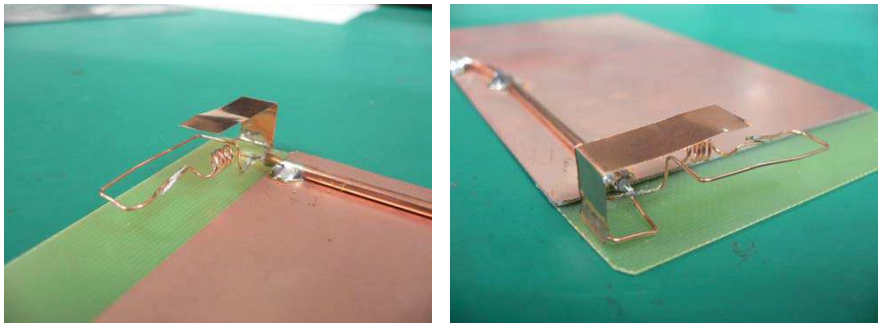

Figure 1: Dual wideband monopole antenna design.

Investigating the Effect of Nonlinearity on Adaptive Arrays

Cheng-Nan Hu
Communication Research Center (CRC), Oriental Institute of Technology
No. 58, Sec. 2, Sihchuan Rd, Ban-Ciao City, Taipei County, Taiwan, R.O.C.

Abstract— With witness the 4G wireless evolution, one can experience the technology competition between *Mobile WiMAX* and *LTE* (*Long Term Evolution*). One of the enabling technologies to the focused issue, "Convergence and Competition on the Way toward 4G", from the wireless communication prospects by various viewpoints of the contributing authors [1, 2], is the "Beam forming architecture" to support space-division multiple access (*SDMA*) [3]. This approach enables multiple users within the same radio cell to be accommodated on the same frequency and time slot. The beam forming technologies are used to modify its time, frequency, and spatial response by using internal feedback controlling the amplitude/phase weighting of the adaptive array [4]. However, realization of the beam-forming techniques poses high linearity demands on RF/IF up-/down-conversion chain because the inter-modulation products (IMPs) due to nonlinear distortion will degrade the radiation pattern, resulting in the poor signal quality. This study modeling the multi-modulated input signals for multi-carrier power amplifier (MCPA) at up-/down-conversion chain is introduced. The nonlinearity effects of the MCPAs on an 8-element adaptive array are investigated to assess the radiation pattern deviation due to the phantom lobes [5] generated by IMPs at MCPA.

A Differential Multi-band CMOS Low Noise Amplifier with Gain Flatness Performance and Bandwidth Enhancement

San-Fu Wang[1], **Jan-Ou Wu**[2], **Hua-Pin Chen**[1], **and Yang-Hsin Fan**[3]

[1]Department of Electronic Engineering, Ming Chi University of Technology
Taipei 243, Taiwan, R.O.C.
[2]Department of Electronic Engineering, De Lin Institute of Technology
Tucheng, Taipei, Taiwan, R.O.C.
[3]Department of Computer Science and Information Engineering
National Taitung University, Taitung, Taiwan, R.O.C.

Abstract— In this paper, a differential multi-band CMOS low noise amplifier (LNA) is proposed that is operated within a range of 1300 MHz $\sim$ 3000 MHz with input matching capacitor switching and gain flatness enhancement technique. Traditional multiband LNAs have poor performances on gain flatness performance. Therefore, we propose a new multiband LNA which obtain good gain flatness performance by integrating the characteristics of the transistor transconductance and LC resonant load. The new LNA can also achieve a tunable frequency at different matching capacitance conditions. The simulation results show that the maximum gain is between 16 and 19.7 dB, the NF is less than 2.5 dB, and the 1-dB compression point is about -5.86 dBm. The LNA consumes 17.5 mW under 1.8 V supply voltage in TSMC 0.18-µm RF CMOS process.

Performance Analysis in Using Repeaters with Coordination among Base Stations for LTE-A Systems

Hsien-Wei Tseng[1], **Yang-Han Lee**[2], **Ming-Hsueh Chuang**[3], **Wei Chien**[4], **Chih-Yuan Lo**[2], **and Yu-De Liao**[1]

[1]Computer and Communication Engineering, De Lin Institute of Technology, Taiwan, R.O.C.
[2]Electrical Engineering, Tamkang University, Taiwan, R.O.C.
[3]Electronic Engineering, National Taiwan University of Science and Technology, Taiwan, R.O.C.
[4]Electronic Engineering Department, De Lin Institute of Technology, Taiwan, R.O.C.

Abstract— LTE-A technique will play an important roll in the next generation wireless communication system due to it has the advantages of high transmission rate and wide communication bandwidth especially it has high quality throughput when the uses is moving in high velocity. The system performance and parameters characteristics resulting from utilizing LTE-A technique will be provided to the system designers as the references to the development of future IMT-Advanced wireless communication system. When the system bandwidth becomes wider the system utilization performance will be varied widely and becomes inefficiency because the number of users served in the system coverage areas will be varied and the signal transmission environments are changed. It needs to adopt coordination technique among base stations so as to effectively utilize the system resources and to improve the signal purity in its transmission. It has many advantages when considering coordination among base stations such as the reduction of system interference, the improvement of diversity effect and the increase of system gain at the receiver terminal etc. However, it has the requirement of increasing system bandwidth when the coordination among base stations is considered. In this paper when the coordination among base stations are implemented the following system characteristics such as the system capacity, the required system bandwidth, the effect on the users and the performance difference when FDD or TDD technique is implemented etc. will be investigated. Specifically it will also consider the system performance when Femto cells or Repeaters are included in the system. When the data characterizing the system performance are generated and studied they can be provided as references in the base stations installations and they can also be provided as the procedures of how and when to coordinating among various base stations. With Femto cells and Repeaters are included in the system they can be used to simulate the indoor transmission environments and to provide better services to users.

Approximate Outage Probability Expressions for Evaluating Cooperative Communications

Chengkun Sun, **Takashi Kodama**, **and Hua-An Zhao**
Department of Computer Science and Electrical Engineering, Kumamoto University, Japan

Abstract— Cooperative communication systems have emerged as a significant concept to improve reliability and throughput in wireless systems. In this paper, we focus on amplify and forward protocols where the relay node simply amplifies and retransmits the analog waveform received from the source node. This simple protocol was shown to increase the diversity order, allowing single-antenna nodes to cooperate and achieve performance like a real MIMO system. We mainly discuss the performance of Amplify-and-Forward (AF), Decode-and-Forward (DF) and Hybrid Amplify-or-Decode and Forward (HADF). Especially, we derive some approximate expressions of outage probability for all of the relaying protocols. These approximate expressions are proved to be better than some existing ones, in other words our approximations are much closer to the truth value. In our research, we select the results of outage probabilities calculated by Monte Carlo Method (MCM) as the reference for the reason that results by MCM is the nearest to the truth value. We show analytically and experimentally that our expressions are better than some existing approximate expressions in high-SNR. The simulation results and our analysis show the accuracy and concision of our propositions. Besides, the approximate expressions are useful to the analysis of outage probability when we investigate the performance of relaying protocols.

The RF Energy Transmission System Using Electric Resonance

Jung-Ick Moon, **In-Kui Cho**, **Seong-Min Kim**, **Je-Hoon Yun**,
Byun Woo Jin, **and Jae Ick Choi**
ETRI, South of Korea

Abstract— In this paper, wireless power transmission system using electric coupling instead of magnetic resonance is proposed. Since 2007, many researchers have developed the wireless power transmission using magnetic coupling or magnetic resonance [1]. However, the magnetic field has a great tendency to circulate. From this reason, it is difficult to shield an electric device from the magnetic field and to focus the magnetic energy on a point.

The capacitor is a good and small power transmission component. As we know, the capacitor is composed of two metal plates which have the opposite electric pole with each other. With some inductors we could make the electric resonance circuit and transfer most of energy with the desired frequency band from the transmitting device to the receiving one easily. Besides, electric field could be block with metal object. The wireless power transmission system using electric resonance circuit and its applications are shown in Figure 1. And the impedance tuning technique and its performance are shown.

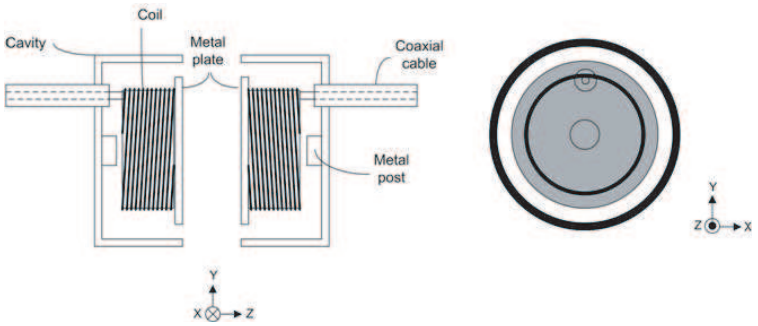

Figure 1: The structure of the proposed energy transfer system.

ACKNOWLEDGMENT

This work was supported by the IT R&D program of MKE/KCC/KEIT. [10035181-2010-01, Development of RF energy Transmission under 100Watts and Harvesting Technology].

REFERENCES

1. Choi, S. W. and M. H. Lee, "Coil-capacitor circuit design of a transcutaneous energy transmission system to deliver stable electric power," *ETRI Journal*, Vol. 30, No. 6, Dec. 2008.

The Design of the Compact and Wireless Desktop Using Wireless Power Transmission

Jung-Ick Moon, **In-Kui Cho**, **Seong-Min Kim**, **Je-Hoon Yun**,
Byun Woo Jin, **and Jae Ick Choi**
ETRI, South of Korea

Abstract— Since 2007, many researchers have developed the wireless power transmission using magnetic coupling or magnetic resonance [1]. In this paper, the design of the compact and wireless desktop using wireless power transmission (WPT) is shown.

As shown in Fig. 1, to transfer the high power energy into the compact desktop, the wireless power transmission technology using magnetic resonance was used.

The resonance frequency and transmitting power is 1.85 MHz and 85 W, respectively. And there is a wooden wall and the distance (d) both tx-coil and rx-coil is 17 cm. Both coils are made of a copper-pipe and have two layers to increase inductance. The compact desktop is composed of a LED monitor, wireless keyboard, mouse and video signal receiver. The power consumption of the desktop is about 38 W and the entire efficiency of this WPT system is 41%.

The receiving module is composed of RF rectifier, overvoltage protection (OVP) with active dummy load and DC to DC converter. The OVP plays an important role in the impedance match.

Finally, the strength of the magnetic field nearby the wireless desktop was measured and analyzed.

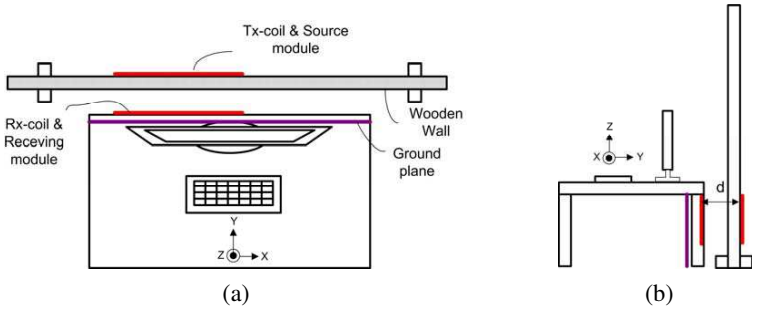

Figure 1: The configurations of the compact wireless desktop using wireless power transmission.

ACKNOWLEDGMENT

This work was supported by the IT R&D program of MKE/KCC/KEIT. [10035181-2010-01, Development of RF energy Transmission under 100Watts and Harvesting Technology].

REFERENCES

1. Choi, S. W. and M. H. Lee, "Coil-capacitor circuit design of a transcutaneous energy transmission system to deliver stable electric power," *ETRI Journal*, Vol. 30, No. 6, Dec. 2008.

A Low Power Transceiver for Medical Implantable Applications

Jin-Sup Kim
Wireless Communication Research Center, Korea Electronics Technology Institute, R. O. Korea

Abstract— A low power MICS-band transceiver is proposed and implemented using 0.18 µm CMOS technology. The architecture of the proposed low power transceiver is shown in Figure 1. The frequency band at 402–405 MHz allocated to MICS by FCC is used for transmission in the air. This system has following characteristics: 10 channels with 300 kHz bandwidth, low output power and full-integrated that is suitable for implantable applications. In conventional transceiver, the Weaver or Hartley structure is normal choice. In this work, we used the complex filter for low power operation in transceiver. The BFSK receiver's sensitivity is −90 dBm for a 500 kbps signal and 5.5 mA current consumption. The nominal output power of the transmitter is −5 dBm.

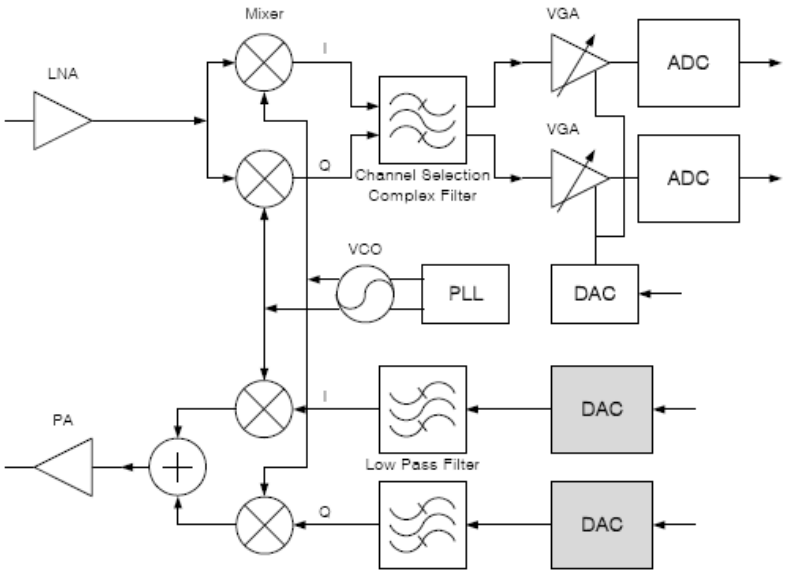

Figure 1: Block diagram of the proposed MICS transceiver.

Improvement of Source Stirring to Field Uniformity in Reverberation Chamber

Shuang Li[1], **Jianguo Wang**[1, 2], **Haiyan Xie**[1], **and Xicheng Lu**[1]

[1]Northwest Institute of Nuclear Technology, P. O. Box 69-12, Xi'an 710024, China
[2]School of Electronic and Information Engineering, Xi'an Jiaotong University, Xi'an 710049, China

Abstract— Traditional reverberation chambers (RCs) are excited by the continuous wave, with one or two mechanical stirrers in the chamber to change the boundary conditions of the cavity continually. While, current high power microwave sources generate very short pulses. The duration of such pulses are far less than the time of mechanical moving. Thus it is not suitable to use mechanical stirring method to research the effects of the electromagnetic pulse (EMP) on the subsystems such as the electronic or electric equipments in the RC. However, the way of source stirring, without mechanical tuning equipments, is feasible to stir the field distribution in the RC by changing the positions of the excitation sources.

This article mainly studies the influence of source stirring on the field uniformity in RC under short pulse excitation. Firstly, the factors that may affect the field distribution are summarized, according to the Maxwell's equations in ideal rectangular resonators. And the the source's position is proved to be an important one among those factors. Then the focus is on the effects of moving the sources consecutively on the electromagnetic field characteristics, especially the effects on the field uniformity under different moving steps during one moving period. As a statistical process, the main attention is paid to the maximum and the standard deviation of electric field strength and the isotropy as well. The results show that the maximum of electronic field strength can reach as high as 6.7 kV/m and the standard deviation of the field distribution falls below 3 dB after stirring the sources. Additional, the isotropy is improved. Therefore, the method of source stirring can improve the field uniformity effectively and it is useful to make a homogenous electromagnetic field environment.

Notebook EMI Noise Analysis and WLAN TIS Performance Improvement with Periodic Structure

Han-Nien Lin[1], **Ming-Cheng Chung**[1], **and Ming-Shan Lin**[2]

[1]Department of Communications Engineering, Feng-Chia University
100 Wen-Hua Rd., Taichung 40724, Taiwan, R.O.C.
[2]Section of EMC, Bureau of Standards, Metrology & Inspection
M.O.E.A., Taipei, Taiwan, R.O.C.

Abstract— Cloud computation and always-connected Internet gains the most industrial attention for the past few years. Meanwhile, with the development of IC technologies advancing toward higher operating frequencies and the trend of miniaturization on wireless communication products, the circuits and components are placed much closer than ever before. The system with highly integrated high-speed digital circuits and multi-radio modules are now facing the challenge from performance degradation by even more complicated platform EMI noisy environment. The EM noises emitted by unintentionally radiated interference sources may severely impact the receiving performance of antenna, and thus result in the severe performance degradation of wireless communications. Therefore, we have investigated and analyzed the EMI noise characteristics of commonly embedded digital devices for further high performance wireless communications design. Since the CAMERA or CMOS camera module is most adopted to the popular mobile devices like cellular phone or Netbook, we hence focus on EMI analysis of the built-in camera module by application of IEC 61967-3 method. To improve the wireless communication TIS performance on notebook computer, we first investigated the EMI noise from the built-in camera module and analyzed the impact of various camera modes on performance with throughput measurement. We then utilized the near-field EM surface scanner to detect the EMI sources on notebook and locate the major noise sources around antenna area with 2-D hot-spot distribution plot. Finally, we designed and implemented periodic structures for isolation on the notebook computer to effectively suppress noise source-antenna coupling and improve the receiving sensitivity of wireless communication system.

Grey Relational Clustering Applied to FPGA System Routing with Minimal Wire Length and Delay

Jan-Ou Wu[1], **Yang-Hsin Fan**[2], **and San-Fu Wang**[3]

[1]Department of Electronic Engineering, De Lin Institute of Technology, Tu-Cheng, Taipei, Taiwan, R.O.C.
[2]Department of Computer Science and Information Engineering, National Taitung University
Taitung, Taiwan, R.O.C.
[3]Department of Electronic Engineering, Ming Chi University of Technology
Taipei, Taiwan,, Taiwan, R.O.C.

Abstract— This paper proposes *grey relational clustering to hierarchical routing* (GRCHR) to solve physical routing problems for *field programmable gate array* (FPGA). The study comprises of four stages to achieve routed timing constraints with minimal wire length and delay. In the first stage, the predominant method exploits the *grey relational clustering of hierarchical* (GRCH) approach that consists of grey relational analysis theory and *grey local topology modification* (GLTM) technology to satisfy the demanding placement requirements. In the second stage, the global routing strategy applies line-probe hightower and matching-based segmentation technology to attain a set of shorter nets and wires for routing regions. In the third stage, the detail routing scheme adopts dogleg router algorithm to decrease routing track number in routing channel and assigns the connection block and switch block in channel routing. Furthermore, we compute Elmore delay model to obtain minimal delay within the assigned routing regions. Finally, the effectiveness of the proposed approach is demonstrated by assessing MCNC benchmarks via *versatile place and route* (VPR) tool for verification.

Design of Reaction Cavity for a Microwave-assisted Synthesis System

Myungsik Kim, **Jongmin Kim**, **and Kwangsoo Kim**
Sogang University, Republix of Korea

Abstract— This paper focuses on the microwave assisted synthesis system for the automatic preparation system of positron emission tomography (PET) radiopharmaceuticals. Recently, many microwave assisted chemical synthesis system has been developed, since the system has several advantages such as the reaction acceleration, the enhanced physicochemical properties, and so on. However, most systems are the microwave generation part and the reaction part all-in one then it is hard to apply to the already developed systems, specially the radiolabelling applications in the limited space of a hot-cell. Also, the radiated microwave power over several hundred watts can affect to the electronic circuits in the preparation system. For the problem, we developed a stand-alone compact reaction cavity, which is connected to the power controllable magnetron using flexible cable. The cavity is a doughnut-shape and an electrical field is radiated to the middle hole, to which a vial is inserted. In order to prevent the radiated microwave from affecting to neighboring electronic circuits, an electromagnetic shield made using a metallic net is developed. The cavity is designed not to be affected by the existences of the inserted vial and the shield. The cavity is simulated using HFSS and the resonance properties are tested using network analyzer E8357A. The experiment results using a vial with radius of 22 mm and height of 38 mm, which is used in the preparation system show that the water in the vial is heated in shorter time than the conventionally used electric heating system.

Evaluation of Electromagnetic Shielding Effectiveness

Ping Li[1], **Yueyan Shan**[2], **and Junhong Deng**[3]

[1]Advanced Materials Technology Centre, Singapore Polytechnic, 500 Dover Road, 139651, Singapore
[2]National Metrology Centre (NMC), A*STAR, 1 Science Park Drive, 118221, Singapore
[3]EEC Centre, TUV SUD PSB Pte Ltd., 1 Science Park Drive, 118221, Singapore

Abstract— Electromagnetic shielding effectiveness (SE) is the ratio of power received with and without a material present for the same incident power. It is usually expressed in decibels by the following equation:

$$SE = 10 \log \frac{P_1}{P_2} \text{ (decibels, dB)} \tag{1}$$

where: P_1 = received power with the material present, and P_2 = received power without the material present.

If the receiver readout is in units of voltage, use the following equation:

$$SE = 20 \log \frac{V_1}{V_2} \text{ (decibels, dB)} \tag{2}$$

where: V_1 and V_2 are the respective voltage levels with and without a material present.

According to these equations, SE will have a negative value if less power is received with the material present than when it is absent. In practical application, SE will always use positive value, omitting the negative sign.

There is often a confusion to explain the measured SE in dB with respect to the corresponding attenuation to the transmitted power. For example, if we measured SE=17dB, is it adequate to shield against electromagnetic interference? What is the meaning behind the 17 dB SE?

Based on the energy loss or power attenuation, we derived the following equation:

$$attenuated\ energy\ (\%) = \left(1 - 10^{\frac{-SE\,(\mathrm{dB})}{10}}\right) \times 100\% \tag{3}$$

Equation (3) explains that the attenuated energy in percentage can be calculated from the shielding effectiveness SE in dB expression when a material present. Table 1 lists the common useful relationship between shielding effectiveness SE expressed in dB and the energy loss expressed in percentage %. It is clear that when SE = 17 dB, the attenuated energy is 98% of the incident energy. These relationships are very useful in the evaluating of the measured SE and the practical effectiveness of the shielding materials.

Table 1.

SE (dB)	5	8	10	15	17	20	25
k (linear)	1.7783	2.5119	3.162	5.6234	7.08	10	17.7828
Ar	0.6838	0.8415	0.9	0.9684	0.98	0.99	0.9968
energy loss %	68.38	84.15	90	96.84	98	99	99.68
SE (dB)	28	30	35	40	50	60	70
k (linear)	25.1189	31.6228	56.2341	100	316.228	1000	3162.278
Ar	0.9984	0.999	0.9997	0.9999	0.99999	0.999999	1
energy loss %	99.84	99.9	99.97	99.99	99.999	99.9999	99.99999

ACKNOWLEDGMENT

This research is supported by Innovation Fund granted by Singapore Ministry of Education (MOE2010-IF-1-018).

Simulations and Analysis of the Corner Geometry and Its Influence on the Electromagnetic Behavior of Components and Structures: Comments on GTEM and Other Microwave Guided Structures Designs

H. X. Araújo and L. C. Kretly
University of Campinas, Brazil

Abstract— The electromagnetic analytical treatment of corner geometry on electronic circuits, RF systems or microwaves components is normally neglected and sharp corner is a constant geometry that empires on the simulation work and design procedure. This fact arises from the simplicity of analysis of the sharp geometry compared to the rounded ones. In large dimensions, this approximation is acceptable, but it is inaccurate in the region of the corners and these singularities impact the performance of the implemented structure or device.

Generally, in the literature the corner is analyzed on the electrostatic regime and not on the propagation one.

In this paper, simulation shows what are the extend and influence of actual corners, rounded due to mechanical manufacturing process on the behavior of electromagnetic systems.

Concerning these differences between sharp and round corners, the investigation was carried out for a GTEM — Gigahertz Transverse Electromagnetic Chamber, specifically the APEX (from the Latin, the highest point; the vertex, it is the first sector of the GTEM chamber) and a horn

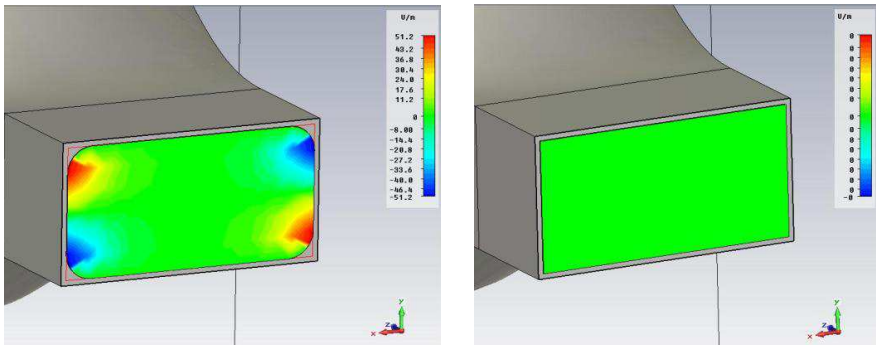

(a) (b)

Figure 1: Electrical field distribution on x direction. (a) Rounded corner structure, (b) sharp corner structure.

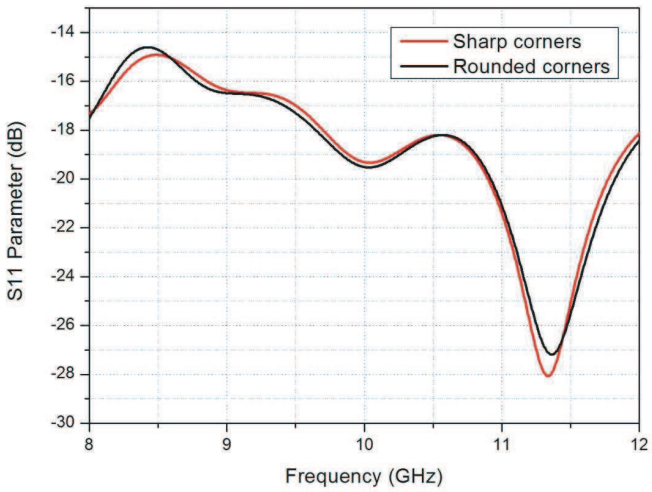

Figure 2: S_{11} parameter — The shift between the two corner geometries response.

antenna. A commercial simulator, based on the Finite Element method (FEM) is used with very accurate models to identify the influence of the rounded corners on the propagation regime. To be sure that the simulation tool is doing a refined numerical solution, a close up of the meshing at the corner was verified. The simulated results show that the numerical analysis is compatible with the analytical solution for electrostatic fields presented in several works. Also, they show a non-negligible sensitivity of S_{11} parameter when comparison of sharp and rounded corners are done. As a conclusion, the designer must evaluate the tradeoff between excessive computation costs and the accuracy needed by the system when faced with actual round corners and sharp ones.

Session 2A1
Generation, Propagation and Application of Coherent and Partially Coherent Beams with Special Beam Profile and Polarization 1

The Number of Degrees of Freedom of Aberrated and Non Aberrated Images Generated by Coherently- or Incoherently Illuminated Objects

Bernhard J. Hoenders[1] and Yangjian Cai[2]

[1]Centre for Theoretical Physics and Zernike Institute for Advanced Materials
University of Groningen, Nijenborg 4, 9747 AG Groningen, The Netherlands
[2]School of Physical Science and Technology, Soochow University, Suzhou 215006, China

Abstract— An important problem in information optics is the calculation of the number of statistically independent parameters characterising the image generated by an imaging device like an optical microscope. This number is very important because it is a measure of the information content of the image. Gabor made the following famous conjecture with respect to this number, known as the Number of Degrees of Freedom (NDF), which in his own words, reads as:

"Assume that the object area, large compared with the square of the wavelength, is limited by a black screen. Assume also that there is a similar limitation in the aperture plane at a great distance from the object plane. Then, in the domain limited by these two black screens there exist S independent solutions of the wave equation $\nabla^2 u + k^2 u = 0$*, that is to say, solutions with* $u = 0$ *immediately behind the black screens and S is given by the formula*:

$$S = \lambda^{-2} \iiiint dx_o dy_o d(\cos\alpha_x) d(\cos\alpha_y), \tag{1}$$

x_o *and* y_o *are the coordinates in the object plane, and* $\cos\alpha_x$ *and* $\cos\alpha_y$ *are the direction cosines of the geometrical optical rays leaving the object plane. Any progressive wave through the object area and through the aperture can be expanded in terms of these S eigensolutions, with no more than S complex coefficients*".

(The aperture plane is the focal plane in case of imaging with an ideal microscope). Although proofs of this conjecture exist for apertures with rectangular- or circular shape, no proof exist for arbitrarily shaped apertures. A *constructive* proof of Gabor's conjecture is presented for arbitrarily shaped apertures, based on the explicit construction of the distribution of the statistically independent sampling points in the image plane.

The NDF for aberrated and partially coherent images are also calculated. It is shown that some aberrations like coma and distortion can even *increase* the NDF, thus increasing the information content of the image wave function, whereas other aberrations like defocusing or spherical abberation do not change the NDF of the image wave function.

An ongoing debate is concerned with the question whether or not the NDF of a image generated by an incoherently radiating object is two times the NDF of freedom generated by a coherently radiating object. We show that the images in both cases have exactly the same number of NDF, i.e., the same information content. The proof is based on a new sampling theorem in terms of the point spread function pertinent for incoherent imaging instead of using the point spread function pertinent for coherent imaging used by the Whittaker-Shannon-Kotel'nikov-Cauchy sampling theorem. The method can be generalised for the analysis of the information content of images generated by partially coherent radiating objects.

Flat-topped Field Correlations in Extremely Strong Turbulence

Yahya Baykal
Electronic and Communication Engineering Department, Çankaya University
Öğretmenler Cad. No. 14, Yüzüncüyıl, Balgat 06530, Ankara, Turkey

Abstract— In extremely strong turbulent horizontal atmospheric optical links, field correlations of flat-topped Gaussian incidence are evaluated. Field correlations are represented versus the diagonal distance at the receiver plane, for variations in the number of beams forming the flat-topped structure, receiver points, source sizes, link lengths, structure constants and the wavelengths. Our results in extremely strong turbulence are compared to their free space counterparts which only reflect the diffraction patterns at the receiver plane. The effects of the inner scale of turbulence on the field correlations in extremely strong turbulence are examined in detail and it is observed that the size of the inner scale in extremely strong turbulence can considerably influence the field correlations of flat-topped beams.

A Three-zone Ternary Phase Superresolving Diffractive Optical Element

Yaoju Zhang, Chaolong Fang, and Xianjie Wang
College of Physic and Electronic Information Engineering, Wenzhou University
Wenzhou 325035, Zhejiang, China

Abstract— Diffractive optical elements (DOEs) have been widely used to optimize the optical field distribution of far- and near-field optical microscopy systems. DOEs can be divided into three types of amplitude, phase, and amplitude-phase hybrid DOEs. Recently, some binary amplitude and phase diffractive optical elements have been designed to increase the resolution and depth of focus of near-field microscopy and optical storage systems [1–3]. However, if a superresolving DOE is designed into binary amplitude or binary phase types, the intensity of the focused spot will be largely decreased, which is very disadvantageous for the near-field optical storage where the intensity of recording spot is originally very small without DOEs. In this paper, a three-zone ternary phase DOE is designed to improve the resolution of near-field optical storage systems with a solid immersion lens. The design is based on the vector diffraction theory and the MATLAB optimization toolbox is used in calculation. Compared with the case without a DOE, the resolution of the near-field optical storage system with the designed DOE is improved by 20% about, the sidelobe intensity is limited within 10% about, and the intensity of spot descends merely 20% about. These distribution features are better than those with a three-zone binary phase DOE.

REFERENCES

1. Zhang, Y., H. Xiao, and C. Zheng, "Diffractive super-resolution elements applied to near-field optical data storage with solid immersion lens," *New J. Phys.*, Vol. 6, 75, 2004.
2. Liu, C. and S.-H. Park, "Numerical analysis of an annular-aperture solid immersion lens," *Opt. Lett.*, Vol. 29, No. 15, 1742–1744, 2004.
3. Zhang, Y., "A new three-zone amplitude-only filter for increasing the focal depth of near-field solid immersion lens systems," *J. Mod. Opt.*, Vol. 53, No. 13, 1919–1925, 2006.
4. Zhang, Y., "Three-zone phase-only filter increasing the focal depth of optical storage systems with a solid immersion lens," *Appl. Phys. B*, Vol. 85, No. 1, 97–103, 2007.

Experimental Study of the Propagation of a Partially Coherent Beam in Turbulent Atmosphere

Fei Wang and Yangjian Cai
School of Physical Science and Technology, Soochow University, Suzhou 215006, China

Abstract— We carry out an experimental study of the propagation of a partially coherent beam in thermal induced turbulence. The effect of the initial spatial coherence length of partially coherent beam on scintillations and beam wandering are studied experimentally. It is found that degrading the coherence of laser beam can lead to the decrease of the scintillation and beam wandering effect, which is useful in many applications, such as free-space optical communication and remote sensing.

Scattering of a Partially Coherent Plane-wave Pulse

Chaoliang Ding[1], **Yangjian Cai**[2], **Yongtao Zhang**[1], **and Liuzhan Pan**[1]

[1]Department of Physics, Luoyang Normal College, Luoyang 471022, China
[2]School of Physical Science and Technology, Soochow University, Suzhou 215006, China

Abstract— In recent years the statistical properties of the light generated by scattering have been studied extensively due to their considerable interest in medical diagnostics and imaging, remote sensing of the atmosphere and ocean, and so on. However, in most cases, the treatment of scattering of the field was confined to the case that the incident field is statistically stationary. Using the model of partially coherent pulses proposed by Friberg et al., we investigate the scattering of a partially coherent plane-wave pulse on a Gaussian-correlated, quasi-homogeneous random medium. The analytical expressions for the temporal coherence length and the pulse duration of the scattered field are derived. We demonstrate that the scattering-induced changes in the temporal coherence length and the pulse duration may be used to determine the correlation function of the scattering potential of the medium.

Experimental Generation of a Partially Coherent Dark Hollow Beam by a Multimode Fiber

Chengliang Zhao and Yangjian Cai
School of Physical Science and Technology, Soochow University, Suzhou 215006, China

Abstract— We report the experimental generation of scalar and electromagnetic partially coherent dark hollow beams by coupling scalar or electromagnetic partially coherent beams into a multimode fiber with a suitable incidence angle. It is found that coupling efficiency of the multimode fiber, the coherence and the polarization of the generated partially coherent dark hollow beam are closely determined by the coherence of the input beam.

Computation of Forward Scattering by Noncoaxial Cylinder Using a Geometrical-optics Approach

Xiangzhen Li, **Xiang'e Han**, **and Paerhatijiang Tuersun**
School of Sciences, Xidian University, Xi'an 710071, China

Abstract— Within the framework of geometrical optics, we present an approximation method with which to calculate of scattering intensity distribution within a forward angular range 0°–60° for noncoaxial cylinder illuminated by a incident plane wave. Phases of scattering rays are exactly calculated to improve the approximation precision. On the basis of the above work, the forward scattering intensity distribution of noncoaxial cylinder is calculated by the geometrical-optics approximation. The influence of the scattering intensity distribution caused by the distance between the two cylinders' axes is analyzed. The scattering intensity distributions of different size noncoaxial cylinders are calculated and the effective size range of this approximation algorithm is analyzed. The result shows that the approximation algorithm works effective for noncoaxial cylinder with large size parameters but fails to give good approximation results at scattering angles at which refractive rays are absent.

Degree of Polarization of Random Electromagnetic Vortex Beams in Atmospheric Turbulence

Jinhong Li[1], **Meiling Duan**[2], **Yamei Luo**[3], **and Jilin Wei**[1]

[1]Department of Physics, Taiyuan University of Science and Technology, Taiyuan 030024, China
[2]Department of Physics, North University of China, Taiyuan 030051, China
[3]Department of Biomedical Engineering, Luzhou Medical College, Luzhou 646000, China

Abstract— Using the extended Huygens-Fresnel principle and the quadratic approximation of the phase structure function, and taking the random electromagnetic Gaussian Schell-model (GSM) vortex beams as a typical example of random electromagnetic vortex beams, the analytical expressions for the cross-spectral density matrix of random electromagnetic GSM vortex beams with topological charge $m = +1$ propagating through atmospheric turbulence are derived, and used to study the degree of polarization of random electromagnetic GSM vortex beams in atmospheric turbulence and to compare the results of random electromagnetic GSM vortex-free beams. The influence of vortex and atmospheric turbulence on the degree of polarization is analyzed. The validity of our results is interpreted physically.

Nonparaxial Properties of a Stochastic Electromagnetic Beam

Lina Zhang, **Fei Wang**, **and Yangjian Cai**
School of Physical Science and Technology, Soochow University, Suzhou 215006, China

Abstract— The concept of the degree of paraxiality introduced recently for monochromatic fields is extended to the domain of stochastic electromagnetic fields. Analytical expression for the degree of paraxiality of a stochastic electromagnetic Gaussian Schell-model (EGSM) beam is derived. It is found that the nonparaxial properties of an EGSM beam is determined by the degree of polarization, r.m.s. widths of the spectral densities and of the correlation functions of its source. One can modulate the degree of paraxiality of an EGSM beam by a linear polarizer.

Propagation Properties of a Laser Array Beam in Turbulent Atmosphere

Yangsheng Yuan, **Yangjian Cai**, **and Chengliang Zhao**
School of Physical Science and Technology, Soochow University, Suzhou 215006, China

Abstract— Based on the extended Huygens-Fresnel integral and the Wigner distribution function, analytical expressions for the propagation factor and the scintillation index of a radial phase locked laser array beam are derived. As an application example, the propagation properties, such as the propagation factor and the scintillation index, of a radial laser array beam in turbulent atmosphere are studied in detail. It is found that a radial laser array beam has advantage over a Gaussian beam for overcoming or reducing the negative influence of turbulence, which is useful in free-space optical communications.

High-power Partially Coherent Fiber Laser Beams Propagating in Real Environment

Rumao Tao, **Lei Si**, **Yanxing Ma**, **Yongchao Zou**, **and Pu Zhou**
College of Optoelectric Science and Engineering
National University of Defense Technology, Changsha 410073, China

Abstract— The performance of high-power partially coherent fiber laser beams propagating in real environment is investigated. Partially coherent fiber laser beams has the advantage of unsensitive to the effect of turbulence compared with coherent beams. For high-power fiber laser application, the effect of thermal nonlinearities of lenses in the collimating system can't be neglected besides the geometrical aberrations, which will degrade the optical quality of laser beams and result in a large spreading angle decreasing the laser energy concentrating in the far-field. The influence of turbulence, atmosphere extinction and beam jittering on the laser energy concentrating must also be considered. The theoretical mode including the influence of the above factors is established in the paper. The laser energy concentrating in the far-field is calculated and analyzed based on the theoretical mode. For a high-power fiber laser system, there exists a best laser energy concentration. The dependence of average power in the bucket on propagation distance in typical atmosphere environment is obtained. The investigation presents a reference for application of high power fiber laser system.

Session 2A2
Photonics and Metamaterials with Chirality

Intrinsic and Extrinsic Chirality in Metamaterials

E. Plum, V. A. Fedotov, and N. I. Zheludev
Optoelectronics Research Centre and Centre for Photonic Metamaterials
University of Southampton, Southampton SO17 1BJ, United Kingdom

Abstract— It has been known since Louis Pasteur's pioneering work in 1848 that optical activity, i.e., the ability to rotate the polarization plane of light, can be observed in intrinsically 3D-chiral substances (e.g., consisting of helical molecules). Almost 160 years passed until it was discovered that also intrinsic 2D chirality (e.g., think of flat spirals) leads to a fundamental electromagnetic effect, the directionally asymmetric transmission of circularly polarized waves [1].

While chiral effects in natural materials are relatively weak, intrinsic 2D and 3D chirality in metamaterials lead to very large effects. In particular, optical activity, which is associated with different refractive indices for right-handed and left-handed circularly polarized waves, can become so large that it drives the refractive index negative for one circular polarization [2].

Even more intriguingly, we recently found that in metamaterials neither optical activity nor asymmetric transmission require materials with intrinsic chirality. This is possible in the presence of extrinsic 2D and 3D chirality associated with the entire experimental arrangement including the direction of incidence onto a non-chiral structured interface [3, 4].

We will give an overview over the concepts of intrinsic and extrinsic 2D and 3D chirality and the resulting electromagnetic phenomena illustrated by recent experimental results.

REFERENCES

1. Fedotov, V. A., P. L. Mladyonov, S. L. Prosvirnin, A. V. Rogacheva, Y. Chen, and N. I. Zheludev, "Asymmetric propagation of electromagnetic waves through a planar chiral structure," *Phys. Rev. Lett.*, Vol. 97, 167401, 2006.
2. Plum, E., J. Zhou, J. Dong, V. A. Fedotov, T. Koschny, C. M. Soukoulis, and N. I. Zheludev, "Metamaterial with negative index due to chirality," *Phys. Rev. B*, Vol. 79, 035407, 2009.
3. Plum, E., X.-X. Liu, V. A. Fedotov, Y. Chen, D. P. Tsai, and N. I. Zheludev, "Metamaterials: Optical activity without chirality," *Phys. Rev. Lett.*, Vol. 102, 113902, 2009.
4. Plum, E., V. A. Fedotov, and N. I. Zheludev, "Asymmetric transmission: A generic property of two-dimensional periodic patterns," *J. Opt.*, Vol. 13, 024006, 2011.

Nonlinear Goos-Hänchen Effect in the Gap of Photonic Crystals Containing Single-negative Materials

Dongliang Gao and Lei Gao
Department of Physics, Suzhou University, Suzhou 215006, China

Abstract— Nonlinear Goos-Hänchen effects for one-dimension photonic crystals containing single-negative (SNG) materials and a Kerr-type nonlinear defect are investigated. Both positive and negative bistable GH shifts are found near the defect mode frequency of the zero-phase (zero-ϕ_{eff}) gap. And with the increase of the incident angle, the hysteretic curve will do some appropriate changes. We numerically explain this phenomenon by investigating the relation of the phase and incident angle.

REFERENCES

1. Wang, L. G., H. Chen, and S. Y. Zhu, *Phys. Rev. B*, Vol. 70, 245102, 2004.
2. Jiang, H. T., H. Chen, H. Q. Li, Y. W. Zhang, and S. Y. Zhu, *Phys. Rev. E*, Vol. 69, 066607, 2004.
3. Jiang, H. T., H. Chen, H. Q. Li, and Y. W. Zhang, *J. Appl. Phys.*, Vol. 98, 013101, 2005.
4. Goos, F. and H. Hänchen, *Ann. Phys.*, Vol. 1, 333, 1947.
5. Goos, F. and H. Hänchen, *Ann. Phys.*, Vol. 5, 251, 1949.
6. Li, C. F., *Phys. Rev. Lett.*, Vol. 91, 133903, 2003.
7. Guan, G. S., H. T. Jiang, H. Q. Li, Y. W. Zhang, and H. Chen, *Appl. Phys. Lett.*, Vol. 88, 211112, 2006.

Goos-Hänchen Shift of the Reflected Wave through an Anisotropic Metamaterial Containing Metal/Dielectric Nanocomposites

Yanyan Huang and Lei Gao
Department of Physics, Suzhou University, Suzhou 215006, China

Abstract— Goos-Hänchen (GH) shift of a transverse-magnetic (TM) wave reflected from a semi-infinite anisotropic metamaterial consisting of aligned metallic nanowires in a dielectric matrix is investigated. With the stationary phase method, we discuss the influence of the incident wavelength and the volume fraction on the GH shift from metamaterials. Numerical results show that for metamaterials with positive refraction, GH shift is greatly enhanced near the pseudo-Brewster angle for small absorption, and enhanced GH shift takes place at close-to-grazing incidence for large absorption. In addition, for positive metamaterials with weak absorption, one can realize the transition from negative GH shift to positive GH shift adjusting the incident wavelength. However, the transition of the enhanced GH shifts from positive to negative occurs by adjusting the volume fraction of the metal for the negative metamaterial. In addition, numerical simulations are performed for a Gaussian-shaped beam to demonstrate the validity of the stationary-phase approach. In the end, by using COMSOL simulation, a comprehensive understanding is given and the above analysis are confirmed.

REFERENCES

1. Shi, L. H., L. Gao, B. W. Li, and S. L. He, *Phys. Rev. B*, Vol. 76, 045116, 2007.
2. Shi, L. H. and L. Gao, *Phys. Rev. B*, Vol. 77, 195121, 2008.
3. Cai, W. S., D. A. Genov, and V. M. Shalaev, *Phys. Rev. B*, Vol. 72, 193101, 2005.
4. Gao, L., Z. Y. Li, K. W. Yu, and B. Hu, *Phys. Rev. E*, Vol. 64, 036615, 2001.

Magnetostatic-mode Near-field Scanning Microwave Microscopy for Chirality Measuring

R. Joffe, E. O. Kamenetskii, and R. Shavit
Microwave Magnetic Laboratory, Department of Electrical and Computer Engineering
Ben Gurion University of the Negev, Beer Sheva, Israel

Abstract— The imaging of an object by a standard optical microscope is limited by its minimum size (resolution limit) that can be only slightly smaller than the wavelength of light used for imaging. This resolution limit is called as the "Abbe barrier" [1]. Using the near-field scanning optical microscopy (NSOM), enables one to overcome the resolution limit by utilizing evanescent electromagnetic waves. That is why the NSOM gained popularity in recent years.

The implementation of near-field imaging in microwave frequencies, in general, and by the near-field scanning microwave microscopes (NSMMs), in particular, have created the opportunity for a new class of electrodynamics experiments of materials and integrated circuits [2, 3]. In this paper, we propose to use a thin-film ferrite disk with magnetostatics (MS) oscillations as an effective sensor for the NSMM. Spectral characteristics of the MS oscillations in a ferrite disk underlie the main physical properties of the proposed microwave microscope. Since the characteristic sizes of the MS oscillations are much less than the free-space electromagnetic wavelength at the same frequency [4], the proposed NSMM should give extremely high resolution compared to the known NSMMs based on standard microwave resonators. By a proper excitation, a ferrite-disk MS-wave resonator exhibits a multiresonance high-Q-factor spectrum. Compared to microwave structures with single-frequency resonances in usual NSMMs, use of the MS-mode rich-spectrum resonances in microwave microscopy will give more detailed amplitude and phase information of the selected object. In recent experiments [5], it was shown that the resonance peak positions in a spectrum of MS modes in a ferrite disk are very sensitive to the dielectric properties of a material placed on a surface of a ferrite.

Recently, it was shown that MS-mode resonances in a normally magnetized ferrite disk are characterized by unique rotating-field behaviors and power flow density vortices [6, 7]. Due to specific interactions between magnetic oscillations in a ferrite disk and the incident electromagnetic wave, one observes the field vortices not only inside a ferrite disk, but also in a near-field region outside a ferrite disk. Such interactions result in strong concentration of energy of the electromagnetic field in the vicinity of a ferrite disk [8, 9]. Strong concentration of electromagnetic energy and special symmetry properties of the fields near MS-mode sensors will allow effective microwave measurement of material parameters on nanometer-length scales. One of the interesting and important implementations of the proposed MS-mode NSMM will be microwave measuring of chirality in chemical and biological objects.

REFERENCES

1. Born, M. and E. Wolf, *Principles of Optics*, Pergamon, Oxford, 1986.
2. Anlage, S. M., et al., e-print, arXiv:cond-mat/0001075, 2000.
3. Rosner, B. T. and D. W. van der Weide, *Rev. Sci. Instrum.*, Vol. 73, 2505, 2002.
4. Stancil, D. D., *Theory of Magnetostatic Waves*, Springer-Verlag, Berlin, 1993.
5. Sigalov, M., E. O. Kamenetskii, and R. Shavit, *J. Appl. Phys.*, Vol. 104, 053901, 2008.
6. Sigalov, M., E. O. Kamenetskii, and R. Shavit, *J. Phys.: Cond. Matt.*, Vol. 21, 016003, 2009.
7. Kamenetskii, E. O., M. Sigalov, and R. Shavit, *J. Appl. Phys.*, Vol. 105, 013537, 2009.
8. Kamenetskii, E. O., M. Sigalov, and R. Shavit, *Phys. Rev. A*, Vol. 81, 053823, 2010.
9. Kamenetskii, E. O., R. Joffe, and R. Shavit, e-print, arXiv:1012.3621, 2011.

Chirality and Anisotropy Induced Fano Resonances

Cheng-Wei Qiu[1] and Jianwen Dong[2]

[1]Department of Electrical and Computer Engineering
National University of Singapore, Republic of Singapore
[2]State Key Laboratory of Optoelectronic Materials and Technologies
Sun Yet-Sen University, Guangzhou, China

Abstract— Composite materials with chirality and (or) anisotropy give us a new paradigm of achieving intrigue Fano resonance. In this talk, we will first propose a 3D spiral photonic crystal structure with controllable phase shift. The paradoxical high Right-handed (RH) transmission is found surprisingly in RH polarization gap, which is owing to Fano resonances derived from mode interference. The intrinsic mechanism of such a paradox is interpreted by mode coupling theory by analyzing Fourier spectra and chirality of eigenmodes. Then other paradigm to achieve asymmetric Fano resonance is proposed by manipulating radial anisotropy instead of manipulating frequency. A fast-switching radiation pattern is observed in association with Fano resonance under a tiny perturbation of the anisotropy. At different resonant modes (symmetrical or asymmetrical), the corresponding bifurcation and singularities of Poynting vector are investigated for the potential use in calculation of heating, radiation pressure and trapping, etc.

Goos-Hänchen Shifts of the Reflected Waves from a Cold, Inhomogeneous and Magnetized Plasma Slab

Guoding Xu[1], **Taocheng Zang**[1], **Tao Pan**[1], **and Lei Gao**[2]

[1]Department of Physics, Suzhou University of Science and Technology, Suzhou 215009, China
[2]Jiangsu Key Laboratory of Thin Films, Department of Physics, Soochow University, Suzhou 215006, China

Abstract— We discuss theoretically the Goos-Hänchen (GH) shifts of the reflected waves from a cold, inhomogeneous and magnetized plasma slab by using the invariant imbedding approach. Aiming at the linear and parabolic electron density profiles, we demonstrate numerically the dependences of the co- and cross-polarized GH shifts on the angle of incidence, external static magnetic field and the thickness of the plasma slab. The results show that the different electron density profiles of plasma can result in the very different dependences of the GH shifts on the angle of incidence, external magnetic field and the slab's thickness; the GH shifts can be switched between the considerably large positive and negative values under certain conditions. Particularly, without altering the structure of the plasma slab, the GH shifts can be manipulated by modifying the angle of incident or the external static magnetic field.

Design and Simulation of Optical Planar Chiral Metamaterial

Fang-Qing Yang, Jie Li, and Jian-Feng Dong
Institute of Optical Fiber Communication and Network Technology
Ningbo University, Ningbo 315211, China

Abstract— The double-layer twisted metallic wires and twisted conjugated gammadion planar chiral metamaterial working in near-infrared frequency range have been designed and optimized. Their transmission and reflection spectra for left-handed circularly polarized (LCP) and right-handed circularly polarized (RCP) wave are obtained from numerical simulations. Obvious resonance dips of the transmission spectra at the frequencies of 245 THz and 270 THz for twisted metallic wires structure, and at the frequencies of 145 THz and 305 THz for twisted conjugated gammadion structure are observed. Their circular dichroism spectra, ellipticity angle, polarization azimuth rotation angle are calculated from simulated transmission and reflection spectra. The results show that the larger circular dichroism and exceptionally strong optical activity are found at the resonance frequency regions for the two structures. Their maximum polarization azimuth rotation angle θ can reach 140° and 95°, respectively. Especially, at ellipticity angle $\eta = 0°$, the rotated angles are about 70° and 10°, respectively. $\eta = 0°$ corresponds a pure optical activity effect, i.e., for the linearly polarization incident wave, the transmission wave will still be linearly polarization, but with a rotated angle θ. Then the effective parameters of the two planar chiral metamaterials, including relative permittivity, relative permeability, chiral parameter and refractive index, are retrieved from simulated transmission and reflection spectra. Note that the negative refractive indexes of the LCP and RCP waves of the two structures can be realized at the resonance frequency regions. Their numerical results demonstrate that the negative refractive index of the chiral metamaterial is due to a large chiral parameter which does not require simultaneously negative permittivity and negative permeability. Because of the excellent optical properties of proposed chiral metamaterials, they may have potential applications in the optical functional materials and optical polarization devices.

Achieving All-optical Diode through Non-symmetrical Nonlinear Cavity and the Effect of Photon Tunneling

Yong-Feng Gao[1], **Yun-Tuan Fang**[2], **and Ming Zhou**[3]

[1]School of Mechanical Engineering, Jiangsu University, Zhenjiang, Jiangsu 212013, China
[2]Department of Physics, Zhenjiang Watercraft College, Zhenjiang, Jiangsu 212003, China
[3]Center for Photon Fabrication Science and Technology
Jiangsu University, Zhenjiang, Jiangsu 212013, China

Abstract— Basing on the effect of photon tunneling, we have studied the transmission properties of a non-symmetrical nonliear cavity through transfer matrix method. It is found that a unidirectional diode-like transmission occurs with this structure. For the same incident frequency and incident intensity, while light is at switch-up status for left incidence, the light is at switch-down status for right incidence.

Magneto-optical Photonic Band-gap Structures with Optimized Characteristics

Othman Sidek, **Muhammad Hassan Bin Afzal**, **and Shahid Kabir**
Collaborative μ-Electronic Design Excellence Centre (CEDEC)
Universiti Sains Malaysia, Malaysia

Abstract— Magneto optical photonic band-gap structures (MO-PBG) consist of cyclic dielectric structures in such a way that they have a strong impact on the transmission of electromagnetic waves. They act similar to the way that the sporadic prospective in semiconductor crystals affects the electron movement by defining permitted and prohibited electronic energy bands. This paper investigates the properties of MO-PBG structures, which hold recurrent interior regions of high and low dielectric constants in such a way that transmission through this specific type of structure definitely depends on the wavelength. This paper also provides a thorough review of different types of MO-PBG structures. These structures are simulated and their characteristics and results compared with related reference values. Finally, a front-end program is introduced, which will help users to understand, measure and evaluate the different characteristics of these structures in order to select the most suitable structure with optimized characteristics for further applications.

Session 2A3a
EM Scattering Models and Applications

Velocity Curl and Theorems in Electromagnetic Fields

Zi-Hua Weng
School of Physics and Mechanical & Electrical Engineering
Xiamen University, Xiamen 361005, China

Abstract— The concept of the linear momentum was originated by some great scientists. The linear momentum of the particle and the conservation of linear momentum were first introduced by R. Descartes. Further the concept of linear momentum was extended from the particle to the electromagnetic field and gravitational field, and covered the quantum mechanics. The concept of the angular momentum includes that in the gravitational and electromagnetic fields, and is an important concept in the physics with numerous applications. The paper claims that the theorems will be impacted by the velocity curl and field potential etc.

The gravitational field and electromagnetic field both can be illustrated by the quaternion, and their quaternion spaces may be combined together to become the octonion space. In other words, the features of gravitational field and electromagnetic field can be described with the algebra of octonions simultaneously. With the algebra of quaternions and octonions, we can deduce some theorems and conservation laws in the gravitational field and electromagnetic field. And it is found that the velocity curl and the field strength in the gravitational field and electromagnetic field have the effect on the theorems and conservation laws regarding the linear momentum.

In the quaternion spaces, we obtain the theorem of linear momentum and the conservation of linear momentum from the quaternion definition of the force. Similarly, from the quaternion definition of the torque, we have the theorem of angular momentum and the conservation of angular momentum. It is found that the gravitational strength has an influence on the theorems and conservation laws regarding the linear momentum. In the octonion compounding spaces, we can obtain the conservation laws and theorems similarly, and find the field potential and its integral have the influence on the theorems and conservation laws about the angular momentum.

It should be noted that the study for the conservation laws and the theorems of physical quantities examined only some simple cases in the electromagnetic field and gravitational field. Despite its preliminary characteristics, this study can clearly indicate the conservation laws and theorems are only some of simple inferences due to the low velocity curl and weak strength of electromagnetic and gravitational fields. For the future studies, the research will focus on only some predictions about the conservation laws and theorems with the high velocity curl and strong strength in the electromagnetic and gravitational fields.

ACKNOWLEDGMENT

The author is grateful for the financial support from the National Natural Science Foundation of China under grant number 60677039.

Ewald-Oseen Extinction Modeling on Si Nano-rod Scattering Induced Surface Depolarized Reflection

Yung-Hsiang Lin and Gong-Ru Lin
Graduate Institute of Photonics and Optoelectronics, Department of Electrical Engineering
National Taiwan University, Taipei 106, Taiwan, R.O.C.

Abstract— Si nano-rod is an important research topic since it induces unique optical and electronic properties, which plays a key role on the future technologies. The polarized light could suffer multiple scattering in inhomogeneous materials to cause depolarization phenomenon. The phenomenon has a great impact on the spectroscopic and imaging performance, however, the influence is relatively difficult to formulate with present models. In this work, light scattering and depolarized reflection of linearly polarized incident light from the large-area vertically aligned Si nano-rod surface obtained by metal-particle-catalytic wet etching method are investigated. The degree of multiple scattering is characterized by observing the scattering angle and reflected Haze ratio (light diffusivity/total transmittance) of Si nano-rod surface. A serious divergence reflection beam from the nano-rod surface is observed, the scattering angle of the reflection beam from Si nano-rod surface is much broader than that from the Si wafer. As lengthening the rod length from 190 to 2760 nm, the scattered pedestal of the reflection beam broaden from 6° to 34° and from 7° to 34.67° under TE and TM-incidences, respectively. The reflected Haze ratio increases from 5% to 22% and 3% to 21% under TE and TM-incidences, respectively. The complex polarization factor (defined as $E_{\mathrm{TM/TE}}/E_{\mathrm{TE/TE}} = (I_{\mathrm{TM/TE}}/I_{\mathrm{TE/TE}})^{1/2}$ at TE-mode incidence or $E_{\mathrm{TE/TM}}/E_{\mathrm{TM/TM}} = (I_{\mathrm{TE/TM}}/I_{\mathrm{TM/TM}})^{1/2}$ at TM-mode incidence, where E and I are the electric field and optical intensity of the reflection beam, respectively) of a linearly polarized light reflected from the Si nano-rod surface is characterized to realize the correlation between nano-rod length and depolarization level. A serious depolarized reflection from the Si nano-rod surface is observed with its increasing complex polarization factor by lengthening Si nano-rod. The complex polarization factor increases from 0.54 to 0.86 and from 0.42 to 0.84 under TE and TM-mode incidences with lengthening rod length from 190 to 2760 nm.

The small perturbation modeling established by Vesperinas is utilized to describe the depolarized reflection from the Si nano-rod surface. The model is based on the vector formulation which developed from the Ewald-Oseen extinction theorem. According to the theoretical analysis, the complex polarization factor of the reflection beam is a function of surface corrugation and the second-order polarization transformation would depolarize the reflection beam from highly corrugated Si nano-rod surface. In addition, the higher complex polarization factor is obtained under TE-mode incidence, because the TE-mode incidence with its polarization is perpendicular to the orientation of the Si nano-rod, which inevitably causes a severer depolarization effect.

The complex polarization factor of the reflection beam increases with broadening scattering angle and enlarging reflected Haze ratio. The linear polarized wave would suffer a multiple scattering and is perturbed by the Si nano-rod roughen surface. The quantitative analyses demonstrate that electromagnetic wave in the etched sample with longer rod length would suffer critical multiple scattering, therefore, a severe depolarization effect would be existed in the reflection beam.

Comparative Strengths of a Pseudo-spectral Time Domain Method in Numerical Simulation of Single Particle Optical Scattering

R. Lee Panetta, **Chao Liu**, **and Ping Yang**
Department of Atmospheric Sciences, Texas A&M University, USA

Abstract— We are interested in numerical simulation of single particle optical scattering properties of atmospheric aerosols in the regime of large particle size parameter. Because calculations quickly become quite demanding of cpu time once the size parameter passes 10, it is important to develop efficient numerical methods. We have experimented with a range of methods, including finite difference time domain, DDA, finite difference frequency domain, and most recently pseudo-spectral time domain.

In this talk we present results on the relative efficiencies of pseudo-spectral, finite difference time domain, and DDA methods. Our test case considers a homogeneous spherical particle, a case in which exact solutions for the phase matrix elements are available. We consider a range of sizes and indices of refraction, at selected wavelengths in the visible and IR range. We find that the pseudo-spectral time domain method is more efficient (uses less cpu time for a given accuracy) than the finite-difference time domain method under all circumstances. The DDA method is superior to the pseudo-spectral method for small particles and indices of refraction less than 1.5, but as the size parameter increases into our range of interest, and as indices of refraction increase, the pseudo-spectral method becomes superior. We will comment on some questions regarding the optimal choice of spectral cut-off and related issues of accuracy.

An Extended Study on Retrieval of Sea Ice Parameters Using Multipolarization Data

Y. J. Lee[1], **W. K. Lim**[2], **and H. T. Ewe**[1]

[1]Universiti Tunku Abdul Rahman, Malaysia
[2]Multimedia University, Malaysia

Abstract— In recent times, research on data retrieval using remote technology for a myriad of purposes, such as yield prediction of crops and environment monitoring, has been on the rise. Such technology, however, require the development of suitable inverse models to correctly calculate the required information from radar backscatter data. There have been numerous reports on the development of inverse models using various techniques and theories for the purpose of sea ice parameter retrieval. Recently, an inverse model for the retrieval of sea ice thickness using Radiative Transfer Theory had been developed by the authors and the model also incorporates the Dense Medium Phase and Amplitude Correction Theory for better accuracy in the calculation and the Levenberg-Marquardt Optimization for estimating the required information. While far from perfect, the model was found to have been successful in estimating sea ice thickness from the use of single polarization radar backscatter data (HH) from RADARSAT. In this paper, the attempt to extend the use of the developed inverse model to retrieve sea ice parameters other than sea ice thickness, such as volume fraction, is reported. The results of this study will provide essential information on the potential of the inverse model towards the retrieval of other sea ice parameters and to provide ideas for further improvements. In addition, the further incorporation of multi-polarization radar backscatter data into the earlier study shall be discussed in this paper. The comparison of utilizing a combination of data from RADARSAT and ENVISAT for sea ice thickness retrieval instead of using just RADARSAT shall be presented. The results from this study shall be used as an indication on whether single or multi-polarization data works better with the developed inverse model.

Effects of Precipitation on Backscattering and Emission from Sea Surface

Saibun Tjuatja[1], **Jiamel Li**[2], **and Xiaolong Dong**[2]

[1]Wave Scattering Research Center, Department of Electrical Engineering
The University of Texas at Arlington, UTA, Box 19016, Arlington, TX 76019-0016, USA
[2]National Microwave Remote Sensing Laboratory, Center for Space Science and Applied Research
Chinese Academy of Science, No. 1, Nan'ertiao, Zhongguancun, Haidian Distrist, Beijing 100080, China

Abstract— The effects of precipitation on backscattering and emission from sea surface at c- and Ku-band are investigated in this study. Scattering and emission model for sea surface with precipitation that accounts for the effects of rain column will be presented. The rain column is modeled as many sublayers with different physical characteristic determined by the vertical precipitation profile. Each sublayer is assumed to be statically homogeneous. Sea surface scattering is modeled using the IEM model [1] for moderate roughness cases and the Kirchhoff modeled [2] for large roughness cases. Multiple scattering within and interactions between the rain layer, cloud-precipitation transition layer and sea surface are accounted for in the matrix doubling formulation [3]. Brief description of the scattering phase matrix formulation for the model is provided in the following subsection. Model analyses, including quantitative analysis of rain effects on sea state sensing, and comparisons with published data will be given at the presentation.

The Scattering Phase Matrix for Sea Surface with Precipitation:

Figure 1 shows the model structure for sea surface with precipitation. At the C- and Ku-Band, scattering from the cloud layer is negligible compared to the responses from the rain column and sea surface; the effect of cloud is not considered in this study. The rain layer (an inhomogeneous medium) is discretized vertically into N sublayers. Each sublayer within the inhomogeneous medium is assumed to be statistically homogenous. The scattering characteristics of sublayer n are described by the backward and forward scattering phase matrices, denoted by $\mathbf{S}_n$ and $\mathbf{T}_{n'}$, respectively, for $-Z$ incident direction, $\tilde{\mathbf{S}}_n$ and $\tilde{\mathbf{T}}_n$ for $+Z$ incident direction.

The total scattering phase matrix of the sea surface with precipitation, $\mathbf{S}_T$, is determined using the following algorithm [4]:

1. Determine the volume-scattering phase-matrix set for each sublayer, $\bar{\mathbf{P}}_i = \{\mathbf{S}_i, \mathbf{T}_i, \tilde{\mathbf{S}}_i, \tilde{\mathbf{T}}_i\}$ where $i = 1, \ldots, N$, using the matrix-doubling method.
2. Determine the volume scattering phase-matrix set for the rain layer, $\bar{\mathbf{P}}_R = \{\mathbf{S}_R, \mathbf{T}_R, \tilde{\mathbf{S}}_R, \tilde{\mathbf{T}}_R\}$, using $\bar{\mathbf{P}}_R = \bar{\mathbf{P}}_1 \otimes \bar{\mathbf{P}}_2 \otimes \ldots \otimes \bar{\mathbf{P}}_N$ where $\otimes$ denotes matrix doubling operation.
3. Determine the effective reflected and transmitted scattering phase matrices for the cloud-rain interface: $\mathbf{R}_{cr}$ and $\mathbf{Q}_{cr}$ for $-Z$ incidence, and $\tilde{\mathbf{R}}_{cr}$ and $\tilde{\mathbf{Q}}_{cr}$ for $+Z$ incidence. Determine the effective reflected scattering phase matrix for the sea surface, $\mathbf{R}_w$.

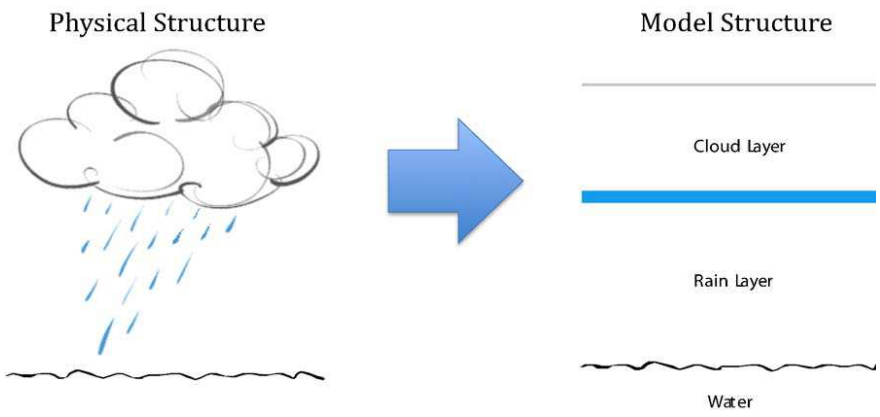

Figure 1: Physical and model structures for sea with precipitation.

4. The total scattering phase matrix for the sea surface with precipitation is determine by

$$\mathbf{S}_T = \mathbf{R}_{cr} + \tilde{\mathbf{O}}_{cr}\left(\mathbf{I} - \tilde{\mathbf{T}}_R\mathbf{R}_w\mathbf{T}_R\tilde{\mathbf{R}}_{cr}\right)^{-1}\tilde{\mathbf{T}}_R\mathbf{R}_w\mathbf{T}_R\mathbf{Q}_{cr}$$

The scattering coefficients for the sea surface with precipitation are obtained from $\mathbf{S}_T$ using the method described in [5].

REFERENCES

1. Fung, A. K. and K. S. Chen, "An update on the IEM surface backscattering model," *IEEE Geoscience and Remote Sensing Letters*, Vol. 1, No. 2, 75–77, 2004.
2. Ulaby, F. T., R. K. Moore, and A. K. Fung, *Microwave Romote Sensing*, Ch. 13, Vol. 3, Addison-Wesley, 1986.
3. Ulaby, F. T., R. K. Moore, and A. K. Fung, *Microwave Romote Sensing*, Ch. 12, Vol. 3, Addison-Wesley, 1986.
4. Tjuatja, S., A. K. Fung, and M. S. Dawson, "An analysis of scattering and emission from sea ice," *Romote Sensing Reviews*, Vol. 7, 83–106, 1993.
5. Fung, A. K., *Microwave Scattering and Emission Models and Their Applications*, Ch. 8, Artech House, Norwood, MA, 1994.

An Efficient Meshless Method for Solving Electromagnetic Volume Integral Equations

M. S. Tong
Department of Electronic Science and Technology, Tongji University, Shanghai, China

Abstract— Meshless or meshfree methods represent the effort of reducing meshing costs in the numerical solution of problems and have received an extensive attention in mechanical engineering due to the practical need for solving the problems with moving boundaries, such as extrusion molding process, growth of cracks, and propagation of interfaces between solids and liquids. Traditionally, meshless methods employ discrete nodes to replace meshes in the geometric description of objects and this can lead to a great reduction of costs in geometric discretization because generating a set of nodes without connection is usually much easier than generating meshes. Meshless methods are also desirable for solving electromagnetic (EM) problems though they have not been paid a sufficient attention. For example, the widely used method of moments (MoM) with the Rao-Wilton-Glisson (RWG) basis function for solving EM surface integral equations (SIEs) require high-quality meshes and remeshing could be frequently encountered for complex structures because of the existence of unqualified meshes. In addition, the solution of inverse scattering problems for reconstructing unknown objects also requires remeshing involved geometries because their profiles are refined or changed iteratively. There have been some publications addressing the meshless methods for EM applications in recent years, but they mainly deal with differential equations for static or quasi-static problems and also only deal with the SIEs in the integral equation approach.

The integral equation method in EM includes the numerical solutions for SIEs or volume integral equations (VIEs). Though SIEs are preferred whenever available, the VIEs are indispensable for inhomogeneous structures or inverse scattering problems. Solving VIEs requires the volumetric elements in discretization and tetrahedral elements are usually preferred to match arbitrary geometric shapes. However, volumetric discretization is much harder than surface discretization in general and special commercial software for mesh generation is definitely needed even for very simple geometries. Therefore, it would be great if one can avoid the use of volume elements in the numerical solutions.

In this work, we develop a meshless method for solving the VIEs. The method transforms the volume integrations over a domain into boundary (surface) integrations plus a one-dimensional (1D) line integral so that the direct volume integrations over volume domains can be avoided and the volumetric discretization is not necessary. To facilitate the evaluation of boundary integrals, the original domain represented with the object is expanded to a cylinder circumscribing the object and the involved integrands are redefined. The above transformation is based on the Green-Gauss theorem and is only valid for nonsingular integrals. Since the integral kernels with the double gradient of Green's function in the VIEs are hypersingular, we need to exclude a small cylinder including the observation node and the transformation is performed for the remaining part. For the singular integrals over the small cylinder, we derive the solution with the strategy of singularity subtraction as for Nyström method. Numerical examples for EM scattering by dielectric objects are presented to illustrate the scheme and the solutions are compared to the available analytical solutions or conventional MoM counterparts.

Electromagnetic Scattering from a Corn Canopy

Yang Du[1], **Wenzhe Yan**[1], **J. C. Shi**[2], **Zeng-Yuan Li**[3], **and Er-Xue Chen**[3]

[1]Department of Information Science and Electronic Engineering, Zhejiang University, China
[2]Institute of Remote Sensing Applications, Chinese Academy of Sciences, China
[3]Research Institute of Forest Resources Information Technique, Chinese Academy of Forestry, China

Abstract— The ability to retrieve and monitor soil moisture and vegetation water content (VWC) is of great importance. Yet accurate retrieval of such information from microwave observations presents a big challenge, which calls for the development of high fidelity scattering models.

In the literature, a "discrete scatter" approach was usually deployed, which attempted to determine first the scattering behavior of the individual constituent of the canopy, then that of canopy as a whole by summing up either incoherently [1] or coherently [2, 3].

To simplify the problem, constituents of the canopy are modeled as canonical geometrical objects. For corn canopy, the stalks are modeled as dielectric circular cylinders with finite length, and the leaves are represented as thin dielectric disks with elliptic cross section. Since scattering from each of the canonical object serves as the base for further "assembling", it is expected to be accurately determined. However, mush is still desired in this regard.

For a dielectric cylinder of finite length, in studying its scattering behavior the generalized Rayleigh-Gans approximation (GRGA) [4] is usually applied, which approximates the induced current in a finite cylinder by assuming infinite length. This method is valid for a needle shaped scatterer with radius much smaller than the wavelength. Yet caution must be taken even at L band when EM scattering from the stalk of a corn plant is to be evaluated using GRGA. It is also well known that GRGA fails to satisfy the reciprocity theorem [2].

In the evaluation of scattering amplitude of leaves, the GRGA method is usually used. However, caution must be taken here. At C band the wavelength is 5.6 cm, which is comparable to the length of minor axis of corn leaves, which presents an unfavorable condition in applying GRGA and thus appreciable error is expected in the predicted scattering amplitude.

When corn canopy is at its early stage of growth, or when the incidence angle is not large, contribution from the underlying ground is appreciable and thus its accurate prediction is important. Yet this roughness effect has not been adequately addressed in canopy scattering models, where what is typically applied is conventional analytical method such as Kirchhoff approximation (KA), or the small perturbation method (SPM) [5], or the more advanced yet still improvement-needed integral equation method (IEM) [6]. In this study, we choose to apply a more rigorous treatment of the rough surface contribution using the recently advanced EAIEM model by the authors [7].

With the advancement of several scattering models of dielectric cylinder and disks and of rough surfaces, it is the aim of this paper to investigate if a coherent combination of these constituent models can improve predictive power of the resultant canopy scattering model.

To be more specific, in analyzing electromagnetic scattering from a dielectric cylinder of finite length, we use the new approach that we have recently proposed [8], where a long cylinder is divided into a cluster of N identical sub-cylinder by using $N-1$ hypothetic surfaces, for each the T matrix can be calculated stably in the numerical sense. The boundary conditions at the hypothetic interface are treated carefully. A system of equations is set up for each sub-cylinder, and the overall system of equations is coupled and linear, thus can be solved by appropriate iterative method.

Moreover, the VPM method is found to be applicable to dielectric cylinders of arbitrary length as long as the T matrix is attainable for the elementary sub-cylinder. The applicable relative dielectric constant can go up to 70 (real part), which is normally the upper bound for corn stalks at C band. The radius of the cylinder can be as high as 5 wavelengths, a feature of the model that is expected to be useful for forest applications [9].

Scattering from rough surface is treated using the EAIEM model [7], which is a unifing model recently developed by us for electromagnetic scattering from a Gaussian rough surface with small to moderate heights. It is based on the integral equation formulation where the spectral representations of the Greens function and its gradient are in complete forms, a general approach similar to those used in the advanced integral equation model (AIEM) [10]. Yet this new model can be regarded as an extension to these two models on two accounts: first it has made fewer

and less restrictive assumptions in evaluating the complementary scattering coefficient for single scattering, and second it contains a more rigorous analysis by the inclusion of the error function related terms for the cross- and complementary scattering coefficients, which stems from the absolute phase term in the spectral representation of the Greens function.

The proposed coherent scattering model will be validated at both L and C bands. At C band we acquired some RADARSAT-2 data of several test fields of corn canopy in Jiangsu province, China, in 2009, and carried out simultaneousmeasurement campaigns to collect the *in situ* ground truth. At L band high quality AIRSAR measurement data are available along with detailed ground truth in the literature [1] and will be used in the current work.

REFERENCES

1. Chauhan, N. S., D. M. Le Vine, and R. H. Lang, "Discrete scatter model for microwave radar and radiometer response to corn: Comparison of theory and data," *IEEE Trans. Geosci. Remote Sensing*, Vol. 32, 416–426, Mar. 1994.
2. Yueh, S. H., J. A. Kong, J. K. Jao, R. T. Shin, and T. Le Toan, "Branching model for vegetation," *IEEE Trans. Geosci. and Remote Sensing*, Vol. 30, No. 2, 390–401, Mar. 1992.
3. Du, Y., Y. Luo, W.-Z. Yan, and J. A. Kong, "An electromagnetic scattering model for soybean canopy," *Progress In Electromagnetics Research*, Vol. 79, 209–223, 2008.
4. Karam, M. A., A. K. Fung, and Y. M. M. Antar, "Electromagnetic wave scattering from some vegetation samples," *IEEE Trans. Geosci. Remote Sensing*, Vol. 26, 799–808, Nov. 1988.
5. Tsang, L., J. A. Kong, and R. T. Shin, *Theory of Microwave Remote Sensing*, Wiley-Interscience, New York, 1985.
6. Fung, A. K., Z. Q. Li, and K. S. Chen, "Backscattering from a randomly rough dielectric surface," *IEEE Trans. Geosci. Remote Sensing*, Vol. 30, No. 2, 356–369, Mar. 1992.
7. Du, Y., "A new bistatic model for electromagnetic scattering from randomly rough surfaces," *Waves in Random and Complex Media*, Vol. 18, No. 1, 109–128, Feb. 2008.
8. Yan, W. Z., Y. Du, H. Wu, D. W. Liu, and B. I. Wu, "EM scattering from long dielectric circular cylinder," *Progress In Electromagnetics Research*, Vol. 85, 39–67, 2008.
9. Yan, W. Z., Y. Du, Z. Y. Li, E. X. Chen, and J. C. Shi, "Characterization of the validity region of the extended T-matrix method for scattering from dielectric cylinders with finite length," *Progress In Electromagnetics Research*, Vol. 96, 309–328, 2009.
10. Chen, K. S., T. D. Wu, L. Tsang, Q. Li, J. C. Shi, and A. K. Fung, "Emission of rough surfaces calculated by the integral equation method with comparison to three-dimensional moment method simulations," *IEEE Trans. Geosci. Remote Sensing*, Vol. GE-41, No. 1, 90–101, Jan. 2003.

Session 2A3b
Remote Sensing of Water Cycle Related Components 1

Sea Surface Salinity and Wind Retrieval Algorithm Using Passive-active L-band Microwave Data

Simon H. Yueh and Mario J. Chaubell
Jet Propulsion Laboratory, California Institute of Technology, Pasadena, USA

Abstract— Aquarius is a combined passive/active L-band microwave instrument developed to map the salinity field at the surface of the ocean from space. The measurement principle is based on the response of the L-band (1.413 GHz) sea surface brightness temperatures (T_B) to sea surface salinity. To achieve the required 0.2 psu accuracy, the impact of sea surface roughness (e.g., wind-generated ripples) on the observed brightness temperature has to be corrected to better than a few tenths of a degree Kelvin. To this end, Aquarius includes a scatterometer to help correct for this surface roughness effect.

To quantify the benefits of combining passive and active microwave sensors for ocean salinity remote sensing, the Jet Propulsion Laboratory (JPL) Passive/Active L-band Sensor (PALS) was used to acquire data over a wide range of ocean surface wind conditions during the High Ocean Wind (HOW) Campaign in 2009. The PALS brightness temperatures and the radar σ_0 from the campaign show response to ocean surface wind speed as well as direction. The brightness temperature changes are about 0.2 to 0.3 K for every one m/s change in wind speed. In addition, there is significant wind direction dependence for high winds (> 10 m/s), about 0.5 K peak to peak at 9 m/s wind speed and 1.5 K at 24 m/s wind speed.

The wind direction effects will introduce significant errors. For example, a directional variation of 0.7 Kelvin will result in a salinity retrieval error of about 1 practical salinity unit (psu) for warm waters at 25 degrees C and greater than 2 psu error for cold waters at 5 degrees C. The current approach for Aquarius salinity retrieval algorithm requires the use of ancillary ocean wind direction from the National Centers for Environmental Prediction (NCEP) to enable the correction. Any errors in the NCEP analyses, particularly for high winds or near the front, as well as temporal mismatch with the Aquarius sampling may not allow the directional effects to be accurately removed using ancillary wind data. It is highly desirable to have an algorithm using the Aquarius data itself to correct the effects of both wind speed and direction.

We develop an algorithm to retrieve the salinity together with the wind speed and direction to eliminate the need of ancillary NECP wind analyses. The algorithm minimizes a weighted least square error (LSE) measure, which signifies the difference between measured and modeled brightness temperatures and radar backscatter. Our algorithm uses the conjugate gradient method to search for the local minima of the LSE. We carried out a set of simulations to test the feasibility and accuracy of the optimization algorithm. We simulated the radiometer and radar measurements. Gaussian random noises were added with standard deviation equal to noise equivalent delta T (NEDT) or radar detection noise (k_{pc}). Our simulations show that we can use the passive and active microwave data together to accurately retrieve sea surface salinity along with the wind speed and direction. The RMS errors for the retrieved salinity and wind speed are nearly independent of wind direction. At 25 deg C, the RMS SSS error is about 0.3 psu at 15 m/s wind speed, fairly close to the error expected from the net effects of 0.1 K for ΔT and 0.5 m/s error for wind speed. It is also shown that the retrieved wind speed and direction derived from this algorithm will be very accurate, thus allowing Aquarius to provide coincident ocean surface wind products.

Estimation of Soil Moisture with the Combined L-band Radar and Radiometer Measurements

Jian-Cheng Shi
Institute for Remote Sensing Applications, Datun Rd., Chaoyang District, Beijing 100101, China

Abstract— Soil moisture is a key parameter in numerous environmental studies, including hydrology, meteorology, and agriculture. It plays an important role in the interactions between the land surface and the atmosphere, as well as the partitioning of precipitation into runoff and ground water storage. Therefore, the spatial and temporal dynamics of soil moisture are important parameters for various processes in the soil-vegetation-atmosphere-interface. The Soil Moisture Active Passive (SMAP) with both Active/Passive L-band instruments has been approved by NASA for monitoring global soil moisture and freeze/thraw. The SMAP instrument combines radar and radiometer subsystems. The radar operates with VV, HH, and HV transmit-receive polarizations, and uses separate transmit frequencies for the H (1.26 GHz) and V (1.29 GHz) polarizations. The radiometer operates with V, H and U (third Stokes parameter) polarizations at 1.41 GHz.

In attempt to use the active or passive microwave remote sensors for estimation of soil moisture, we are mainly facing two common problems: effects of surface roughness and vegetation cover. Natural variability and the complexity of the vegetation canopy and surface roughness significantly affect the sensitivity of backscattering and brightness temperature to soil moisture. Backscattering and brightness temperature signals from vegetated areas is a function of water content and its spatial distribution as determined by vegetation structure and underlying surface conditions including surface roughness parameters and dielectric properties. Due to the limited observations from either passive or active measurements alone, an ill condition, the number of measurements and equations are less than the number of unknowns, is expected. It results in the uncertainties in estimation of soil moisture.

In this study, we develop a combined active/passive technique to estimate surface soil moisture with the focus on the short vegetated surfaces. We first simulated a database for both active and passive signals under Hydros's sensor configurations using the radiative transfer model with a wide range of conditions for surface soil moisture, roughness and vegetation properties that we considered as the random orientated disks and cylinders. Using this database, we developed 1) the techniques to estimate surface backscattering and emission components and 2) the technique to estimate soil moisture with the estimated surface backscattering and emission components. We will demonstrate these techniques with the model simulated data and its validation with the airborne PALS image data from the soil moisture SGP'99 and SMEX'02 experiments.

Surface Soil Moisture Retrieval from the Temporal Evolution of Surface Temperature for Bare Surface

Wei Zhao[1, 2, 3] **and Zhao-Liang Li**[1, 2]

[1]State Key Laboratory of Resources and Environment Information System
Institute of Geographical Sciences and Natural Resources Research, CAS, Beijing 100101, China
[2]LSIIT, UdS, CNRS, Bld Sebastien Brant, BP10413, 67412 Illkirch, France
[3]Graduate University of Chinese Academy of Sciences, Beijing 100049, China

Abstract— Land surface soil moisture (SSM) has an important role for groundwater recharge, agriculture, soil chemistry, and climate forecasting. Many recent scientific research efforts have aimed toward a predictive-understanding of SSM over space and time using thermal infrared remote sensing method, and most of them are based on the instantaneous observations of land surface temperature (LST). However, the information embedded in the temporal variation of LST has been less considered or discussed. The present study aims to find the interaction between the temporal variation of LST and SSM and then propose a method to retrieval SSM with geostationary satellite remote sensing data. Due to the absence of accurate SSM at a large scale, NOAH land surface model (LSM) is used to provide the temporal evolution of the LST under different soil types and SSM conditions for cloud free days, and bare soil surface is only discussed. Two empirical models (linear form and second-degree polynomial) are proposed with the two LST temporal variables TN (the LST rising rate normalized by the difference in the net surface shortwave radiation during the mid-morning) and t_d (the time at which the daily maximum temperature occurred) to estimate SSM. The root mean square errors (RMSE) of the SSM retrieved using linear and second-degree models with simulated data are found to be $0.029\,\mathrm{m}^3/\mathrm{m}^3$ and $0.024\,\mathrm{m}^3/\mathrm{m}^3$ respectively. The results show that the coefficients of variables in both models are independent of the atmospheric conditions and soil types, but the constant term in both models varies with atmospheric forcing data. This study also indicates that the SSM of bare soil surfaces can be estimated with high accuracy if the constant term is obtained. A preliminary validation is conducted with in-situ measurements and the results are very encouraging.

Calibration on AMSR-E Soil Moisture Retrievals Based on SMOS Soil Moisture Product

Jinyang Du and Jiancheng Shi
The Institute of Remote Sensing Applications, Chinese Academy of Sciences
P. O. Box 9718, Beijing 100101, China

Abstract— Soil moisture is a crucial parameter for understanding earth science processes including land-atmosphere interaction, global circulation, and carbon cycling. Space-borne microwave sensors have been used for monitoring large-scale soil moisture for decades to satisfy these needs. Advances have been made towards the goal of routinely providing accurate satellite-based soil moisture products, in particular using moderately low frequency instruments, such as the Advanced Microwave Scanning Radiometer-EOS (AMSR-E) (Njoku et al., 2003; Koike et al., 2000). Moreover, significant improvements in frequency and spatial resolution with the ESA L-band Soil Moisture and Ocean Salinity (SMOS) Mission have been achieved and led to most accurate soil moisture estimation since SMOS launch in 2009.

Meanwhile, time series of soil moisture are available for more than 30 years including AMSR-E soil moisture products generated by NASA since 2002. By introducing L-band estimations from SMOS and future NASA's Soil Moisture Active-Passive (SMAP) Mission, it is possible to correct vegetation and/or surface roughness effects at X-band and rebuild more accurate time-series soil moisture for AMSR-E. In this work, a high-order radiative transfer model with AIEM model incorporated is first used to simulate vegetation and soil emission signals at X and L-band under a variety of vegetation/soil conditions. It is found that vegetation optical thickness at X-band is well related with that at L-band and it is possible to estimate vegetation optical thickness at X-band by its estimation at L-band. On the other hand, microwave vegetation index (Shi et al, 2008), which can be calculated directly from X and Ku-band AMSR-E observations, has been proved to be correlated with vegetation parameters only. We further establish the relationships between vegetation optical thickness at X-band and microwave vegetation index based on available observations from SMOS and AMSR-E. The relationships are finally used to correct vegetation effects and rebuild historical time-series soil moisture using AMSR-E observations.

Session 2A4
Time Modulated Antenna Arrays

Real-Time Nulling with 4D Arrays for Cognitive Radio

L. Poli, **P. Rocca**, **G. Oliveri**, **and A. Massa**
ELEDIA Research Group@DISI, University of Trento, Via Sommarive 14, I-38123 Trento, Italy

Abstract— Time-modulated arrays (TMAs), unlike classical phased arrays where each radiating element is excited by narrowband signals, are based on the use of time pulses to modulate the signals transmitted by the elements. The application of time as an additional degree of freedom in the design of antennas was firstly conceived in [1] and then significantly extended over the years both from the theoretical [2] and from the experimental viewpoint [3–5] therefore yielding increased flexibility for communication as well as radar systems Their recent success is related to the continuous improvement of the speed of RF switches and to the development of effective ptimization strategies able to control/reduce the power losses in the sideband radiation [6, 7] generated by the on-off commutation of the RF switches. In this framework, TMAs are currently seen as one of the possible breakthrough for next generation wireless communications Indeed, modern implementation of TMAs enable the remote reconfigurability of the antenna features (mainlobe steering, sidelobe shaping, footprint) by means of modulation sequences applied to programmable switches included in the antenna beam forming network. Accordingly, such technology has extended the concept of Software/Cognitive Radio to the physical layer of wireless communication arrays.

Although the latest advancements in TMAs [8], such technology cannot be still considered as a suitable alternative to phased arrays in many practical applications. In this work, an innovative strategy for the synthesis of TMAs able to adapt in real-time to the surrounding environment to increase the reliability of the communication system in presented. More specifically, the on-off sequence modulating the static excitations is properly optimized by means of an approach based on the Particle Swarm Algorihm to maximize the signal to noise-plus-interference ratio (SINR) at the receiver in a time varying scenario where several interferences from different directions impinge on the antenna. The power losses in the sideband radiation are also properly reduced to increase the efficiency of the overall system.

REFERENCES

1. Shanks, H. E. and R. W. Bickmore, "Four-dimensional electromagnetic radiators," *Canad. J. Phys.*, Vol. 37, 263–275, Mar. 1959.
2. Brégains, J. C., J. Fondevila, G. Franceschetti, and F. Ares, "Signal radiation and power losses of time-modulated arrays," *IEEE Trans. Antennas Propag.*, Vol. 56, No. 6, 1799–1804, Jun. 2008.
3. Kummer, W. H., A. T. Villeneuve, T. S. Fong, and F. G. Terrio, "Ultra-low sidelobes from time-modulated arrays," *IEEE Trans. Antennas Propag.*, Vol. 11, No. 6, 633–639, Jun. 1963.
4. Tennant, A. and B. Chambers, "Two-element time-modulated array with direction-finding properties," *IEEE Antennas Wireless Propag. Lett.*, Vol. 6, 44–65, 2007.
5. Li, G., S. Yang, and Z. Nie, "A study on the application of time modulated antenna arrays to airborne pulsed doppler radar," *IEEE Trans. Antennas Propag.*, Vol. 57, No. 5, 1579–1583, May 2009.
6. Yang, S., Y. B. Gan, and A. Qing, "Sideband suppression in time-modulated linear arrays by the differential evolution algorithm," *IEEE Antennas Wireless Propag. Lett.*, Vol. 1, 173–175, 2002.
7. Poli, L., P. Rocca, L. Manica, and A. Massa, "Handling sideband radiations in time-modulated arrays through particle swarm optimization," *IEEE Trans. Antennas Propag.*, Vol. 58, No. 4, 1408–1411, Apr. 2010.
8. Poli, L., P. Rocca, G. Oliveri, and A. Massa, "Adaptive nulling in time-modulated linear arrays with minimum power losses," *IET Microw. Antennas Propag.*, Vol. 5, No. 2, 157–166, 2011.

Exploiting Time-modulated Arrays for Harmonic Beamforming in Advanced Communications and Radar Systems

L. Poli, **P. Rocca**, **G. Oliveri**, **and A. Massa**
ELEDIA Research Group @ DISI, University of Trento, Via Sommarive 14, Trento I-38123, Italy

Abstract— The use of multi-beam antennas is nowadays of interest in several practical applications both in communications and radar systems. Multiple beams can be suitably exploited to manage several communication links over different spatial sectors and/or over multiple frequency bands or to find and localize targets at the same time in the antenna field of view. In this framework, solutions based on parabolic reflectors or reflectarrays equipped with an array of feeders and switchable/reconfigurable phased arrays of direct radiating elements have been effectively proposed. More recently, there has been a renewed interest towards the use of time-modulated arrays (TMAs) [1] for the simultaneous generation of multiple patterns thanks to the easy reconfigurability of their radiation diagrams by modifying the on-off binary sequence which controls a set of radio-frequency (RF) switches used in the antenna architecture to modulate the static element excitations. The patterns are generated by the periodic commutations of the RF switches at harmonic frequencies defined at multiple of the pulse repetition frequency from the antenna working frequency. Although such sideband radiation has been generally considered as power losses to be minimized [2–4], in others cases they have been properly exploited to generate patterns of the same shape pointing at different angular directions for electronic beam scanning applications [5] as well as for the estimation of the directions of arrival [6], or to localize and track objects by synthesizing sum and difference patterns for monopulse radar [7].

However, to further exploit the capabilities of TMAs the possibility to obtain multiple beam patterns with different shapes and characteristics on the harmonics is considered since such solution in nowadays requested in advanced systems for communication purposes as well as radar applications. The optimization of the pulse sequence has been carried out by means of a global optimization strategy based on the Particle Swarm Optimization [8].

REFERENCES

1. Shanks, H. E. and R. W. Bickmore, "Four-dimensional electomagnetic radiators," *Canad. J. Phys.*, Vol. 37, 263–275, Mar. 1959.
2. Yang, S., Y. B. Gan, and A. Qing, "Sideband suppression in time-modulated linear arrays by the differential evolution algorithm," *IEEE Antennas Wireless Propag. Lett.*, Vol. 1, 173–175, 2002.
3. Fondevila, J., J. C. Brégains, F. Ares, and E. Moreno, "Optimizing uniformly excited linear arrays through time modulation," *IEEE Antennas Wireless Propag. Lett.*, Vol. 3, 298–301, 2004.
4. Poli, L., P. Rocca, L. Manica, and A. Massa, "Handling sideband radiations in time-modulated arrays through particle swarm optimization," *IEEE Trans. Antennas Propag.*, Vol. 58, No. 4, 1408–1411, Apr. 2010.
5. Li, G., S. Yang, Y. Chen, and Z. Nie, "A novel electronic beam steering technique in time modulated antenna arrays," *Progress In Electromagnetic Research*, Vol. 97, 391–405, 2009.
6. Li, G., S. Yang, and Z. Nie, "Direction of arrival estimation in time modulated antenna arrays with unidirectional phase center motion," *IEEE Trans. Antennas Propag.*, Vol. 58, No. 4, 1105–1111, Apr. 2009.
7. Tennant, A. and B. Chambers, "Two-element time-modulated array with direction-finding properties," *IEEE Antennas Wireless Propag. Lett.*, Vol. 6, 64–65, 2007.
8. Poli, L., P. Rocca, G. Oliveri, and A. Massa, "Harmonic beamforming in time-modulated linear arrays," *IEEE Trans. Antennas Progag.*, in press.

Sideband Level Suppression Improvement via Splitting Pulses in Time Modulated Arrays under Static Fundamental Radiation

E. Aksoy and E. Afacan
Department of Electrical & Electronics Engineering
Gazi University, Maltepe, Ankara, Turkey

Abstract— In this work, an idea which can be used for minimisation of sideband level (SBL) of a time-modulated array (TMA) is presented. The idea is based on splitting pulses while the total switch-on durations remain constant which provides an additional degree of freedom in design and it is shown that lower SBL can be achieved under static fundamental radiation. Also it is shown with an example that the general opinion that maximum level of sideband radiation occurs in first sideband is not always true.

In [1] and [2] it is shown that under static fundamental radiation a SBL minimisation method or control can be made by varying the starting instants of pulses and a -19.5 dB SBL is achieved in [2] via a method called pulse shifting which is approximately 7 dB better than achieved in [1]. If the same conditions (i.e., -30 dB Chebyshev array) are considered and switching sequence is optimized via pulse splitting using *DE/best/1/bin* as described and used in [3] with algorithm parameters of population size $P = 50$, crossover probability $Cr = 0.6$ and mutation factor $F = 0.6$, the resultant switching scheme is given in Fig. 1. Moreover, maximum SBL of first 30 harmonics and the radiation pattern related to Fig. 1 is given in Fig. 2.

As it can be seen from Fig. 2 SBLs can be lowered to a value (≈ -22.51 dB) below -19.5 dB which is found in [2] by splitting pulses.

In this study, an idea about controlling the maximum level of harmonic radiations via splitting pulses while the total switchCon durations are constant is presented. Two different examples are given to illustrate the effectiveness of this approach. This approach provides an additional degree of freedom in design and it is shown with first example that SBL suppression capability seems to be better than other published works. Also splitting pulses provides an independent control of each harmonic frequency. Finally, it is illustrated that first sideband level is not always greater than other harmonics.

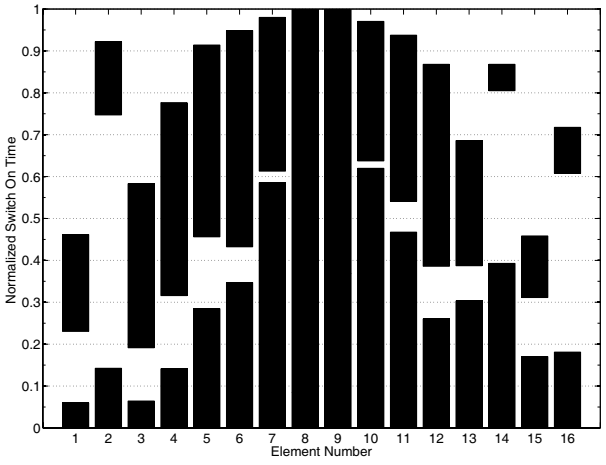

Figure 1: On-off time sequence of 16 element -30 dB Chebyshev pattern optimized to reduce SBLs.

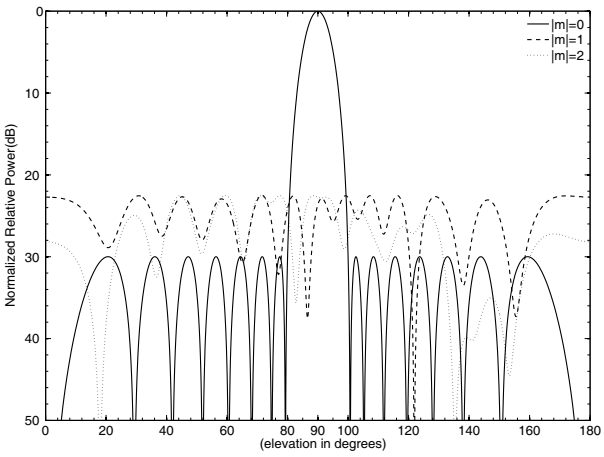

Figure 2: Radiation patterns related to Fig. 1.

REFERENCES

1. Tennant, A. and B. Chambers, "Control of the harmonic radiation patterns of time-modulated antenna arrays," *Proc. IEEE AP-S Int. Symp.*, S. Diego, California, USA, July 5–12, 2008.
2. Poli, L., P. Rocca, L. Manica, and A. Massa, "Pattern synthesis in time-modulated linear arrays through pulse shifting," *IET Microw. Antennas Propag.*, Vol. 4, No. 9, 1157–1164, 2010.
3. Aksoy, E. and E. Afacan, "Planar antenna pattern nulling using differential evolution algorithm," *Int. J. Electron. Commun.*, Vol. 63, 116–122, 2009.

Generalized Representation of Sideband Radiation Power Calculation in Arbitrarily Distributed Time-modulated Planar and Linear Arrays

E. Aksoy and E. Afacan
Department of Electrical & Electronics Engineering, Gazi University, Maltepe, Ankara, Turkey

Abstract— In this study, grid independent general representation of formulation of sideband radiaditon power calculation in time-modulated planar and linear arrays is aimed. It is shown that both distinct formulations can be written in one form which provides an expectation about conformal case.

Recently a useful formulation which gives the total radiated power associated to the harmonic frequencies of a time modulated linear array is published by Brégains et al. [1]. After this work Poli et al. applied this same idea to rectangular grid planar arrays [2]. Both of these formulations provide calculation simplicity when the harmonic radiation is concerned but they are still in distinct forms.

In this study, generalization of formulation originally given in [2] which is constructed on idea given in [1] to a grid independent form with linear cases is aimed while trying to keep the original notation as much as possible.

For

$$g_n(t) = \begin{cases} 1, & 0 < |t| \leq \frac{\tilde{t}_n}{2} \\ 0, & \text{otherwise} \end{cases}, \tag{1}$$

both formulations may be written in one form which is:

$$\begin{aligned} P_{SR} &= 2\pi \sum_{<n>} |I_n|^2 [\tau_n(1-\tau_n)] \\ &\quad + 2\pi \sum_{\substack{m,n=0 \\ m\neq n}}^{N-1} |I_m||I_n| \cos\left(\Delta_{mn}^{\beta}\right) [\tau_{mnMinVal} - \tau_m\tau_n] \frac{\sin(kd_{mn})}{kd_{mn}}. \end{aligned} \tag{2}$$

It must be noted that these formulations are valid if there exist only one pulse per period which are symmetric around $t = 0$. If there exist more than one pulse in each period Eq. (2) must be extended to a new general form.

In this paper a general representation of total power loss calculation for planar and linear arrays and some comments about power loss calculations are presented. It is shown that both distinct formulations given in published works can be combined and written in one form. This form also provides an expectation about the conformal case.

REFERENCES

1. Brégains, J. C., J. Fondevila-Gómez, G. Franceschetti, and F. Ares, "Signal radiation and power losses of time-modulated arrays," *IEEE Trans. Antennas Propag.*, Vol. 56, No. 6, 1799–1804, 2008.
2. Poli, L., P. Rocca, L. Manica, and A. Massa, "Time modulated planar arrays — Analysis and optimisation of the sideband radiations," *IET Microw. Antennas Propag.*, Vol. 4, No. 9, 1165–1171, 2010.
3. Watson, G. N., "A treatise on the theory of Bessel functions," Cambridge University Press, London, 1922.

Synthesis of Pencil-beam Patterns with Time-modulated Concentric Circular Ring Antenna Arrays

L. Zheng, **S. Yang**, **Q. Zhu**, **and Z. Nie**
School of Electronic Engineering, University of Electronic Science and Technology of China (UESTC)
Chengdu 611731, China

Abstract— In this paper, a method for the synthesis of pencil beam patterns from time modulated circular ring antenna arrays is presented, based on the differential evolution (DE) algorithm. The time modulation approach is applied to the uniformly excited concentric circular ring array (CCRA) to suppress the sidelobe level with fixed beamwidth. The CCRA contains many concentric circular rings of different radii and number of elements, which give rise to different radiation patterns. The technique proposed in this paper proceed by time weighing the rings in the array with each ring controlled by a high speed RF switch, where all elements in an individual ring are weighted in time intervals by the same value and the weight values of different rings are optimized by the DE algorithm. The fitness function to be minimized is to obtain the desired pencil beam pattern with minimum SLL and sideband level (SBL). According to the additional variable of time, the sidelobe level can be further reduced as compared to the conventional concentric circular ring arrays, while keeping the amplitude excitations uniform. Some examples synthesized from the proposed method are compared with some published results. Numerical results show that the achievable performance of the approach in suppressing the SLL with an improvement of about 7.6 dB, which is more attractive than the conventional amplitude weighing method. Meanwhile, the SBLs were suppressed to below −20 dB, which is a sufficiently small SBL for the reduction of the inherent power loss due to time modulation. As compared to the amplitude weighing method, the difficulty of the amplitude control technique is overcomed by the switch-on time intervals, which can be more precisely and more easily implemented. The method is very useful and can be applied to the design of time modulated planar arrays with other array geometrical profiles.

Sideband Suppression with Sub-sectional Optimized Time Steps in Time Modulated Linear Arrays

Q. Zhu, **S. Yang**, **L. Zheng**, **and Z. Nie**
School of Electronic Engineering, University of Electronic Science and Technology of China (UESTC)
Chengdu 611731, China

Abstract— The inherent characteristic of time modulated antenna arrays is that there are many sideband signals spaced at multiples of the modulation frequency. To improve the efficiency of low/ultra-low sidelobe level (SLL) time modulation antenna arrays, the sideband levels (SBL) need to be suppressed as low as possible. This paper presents a novel approach, namely, the time modulated antenna arrays with sub-sectional optimized time steps, to suppress the SBL while realizing low/ultra-low SLL. The approach divides the time modulation period T_p into several subsections, and the "switch-on" and "switch-off" time in each subsection is optimized by the differential evolution (DE) algorithm.

In the first section of this paper, a brief review of the past approaches to suppress the SBL is given. In the second section, the theory of the new approach is presented. Relevant equations and figures are present. In the third section, the approach is illustrated through a 16-element linear array with uniform and non-uniform amplitude excitations. Numerical results show that for a -30 dB SLL 16-element time modulated linear arrays with uniform excitations, the SBL can be suppressed to less than -27.5 dB. For the design of a -40 dB SLL 16-element time modulated linear arrays with $1 : 0.25$ static excitation amplitude ratio, the SBL can be suppressed to less than -39.5 dB.To compare the new approach with published approaches such as the binary optimized time sequences or pulse shifting approach, numerical results of past approaches are also given. As compared to the published approaches, the proposed approach can be used to reduce the SBL significantly. The study shows that the proposed approach is more robust for the synthesis of low/ultra-low SLL patterns with lower SBL.

From Time Modulated Antenna Arrays to Four-dimensional Antenna Arrays — An Overview

Shiwen Yang, Quanjiang Zhu, and Zaiping Nie
School of Electronic Engineering, University of Electronic Science and Technology of China (UESTC)
Chengdu 611731, China

Abstract— The time modulated antenna array is extended to four-dimensional (4-D) antenna array, and their theoretical development and application studies are overviewed. By introducing a fourth dimension — time — into conventional antenna arrays, 4-D antenna arrays can be formed and much flexibility is available in the design of high performance antenna arrays.

The time modulated antenna arrays can be considered as one type of 4-D antenna arrays, which have the property of variable aperture sizes of the antenna arrays due to time modulation. Other forms of 4-D antenna arrays include the moving phase center antenna arrays. 4-D antenna arrays are not only suitable for the design of low/ultra-low sidelobes with very low amplitude ratios or even uniform amplitude excitations, but also can be used for the synthesis of shaped patterns including flat-top patterns or cosec square patterns. The sideband suppression is an important issue in the design of 4-D antenna arrays, thus there are many studies focused on the sideband suppression. Moreover, topics such as the directivity or gain estimation of the 4-D antenna arrays, the full wave simulation of the 4-D antenna arrays are also reviewed.

Recently, more and more studies are focused on the practical application of the 4-D antenna arrays. Many studies show that 4-D antenna arrays have distinct advantages in many application areas as compared to the conventional antenna arrays, including the direction of arrival (DOA) estimation, adaptive beam forming (ABF), airborne pulsed Doppler radar, phased array beam scanning without phase shifting, etc.. The overview in this paper demonstrates that 4-D antenna arrays are very promising for many applications, due to the additional freedom introduced into the conventional antenna arrays.

Session 2A5a
Information Optics and Photonics

A Fast 3D System for AR Film Thickness Measurement of Single Crystalline Silicon Solar Cells

H. N. Yen and H. C. Wang
Department of Electronic Engineering, St. John's University, Taiwan

Abstract— For increasing marketing competence, silicon solar cell manufacturers have adopted optical inspection techniques in production lines to perform product classification and statistical process analysis. The product classification is based on overall photoelectric conversion efficiency of the solar cell itself. Two factors directly influence the overall photoelectric conversion efficiency of the solar cell, i.e., composed materials and anti-reflection (AR) film coating on substrate. Since film thickness variation of the AR layer will induce color change on the surface of solar cell, a cost-effective three dimensional (3D) system is proposed to perform fast AR film thickness measurement of single silicon crystalline solar cells.

The proposed system first uses a color CCD to capture the red-green-blue color image of inspected single silicon crystalline solar cell, and transforms it to hue-saturation-lightness image format. And then the area and boundary of different hue-value images are calculated and sorted with the image thresholding and label operation. Besides, with the corresponding measurement procedure on specified hue-value regions of using a precise height measurement instrument, such as the wavelength scanning profiler, the regression equation between the hue value and AR film thickness is obtained, and then implemented into the proposed 3D system to perform large area scanning AR film thickness measurement of single silicon crystalline solar cells. Compared to the optical ellipsometry, the measurement speed of the proposed system is fast. It take only 0.1 seconds to finish the AR film thickness measurement of a 12.5 cm × 12.5 cm solar-cell image, and the measurement accuracy can reach 3 nm.

GPU-based Computing in Digital Holographic Microscopy

Han-Yen Tu[1, 2], **Yi-Ta Lee**[1, 2], **and Chau-Jern Cheng**[1, 2]

[1]Department of Electronic Engineering, St. John's University, Taipei 25135, Taiwan
[2]Institute of Electro-Optical Science and Technology, National Taiwan Normal University
Taipei 11677, Taiwan

Abstract— This paper presents a fast computation and processing for off-axis digital holographic microscopy (DHM) based on graphic processing unit (GPU). DHM is a highly effective imaging technique capable of reconstructing the three-dimensional (3-D) structure by retrieving the amplitude and phase information of the specimen. To obtain the 3-D profile of the specimen, the wrapped phase derived from their reconstructed image of digital holograms is required to be unwrapped to a continuous phase. This phase unwrapping procedure is a computation intensive and can be accelerated by GPU in a personal computer. For achieving enormous calculations of image reconstruction, phase unwrapping algorithms and improving the computational speed for their practical applications, we have performed the preceding computation and processing of DHM through GPU, which can effectively accelerate the computation performance with the parallel computing architectures and algorithms. Further, we perform accurate 3-D profile of the specimen by the use of filtering algorithm adjusting the contrast of reconstructed images. The proposed GPU-based DHM provides the potential for significant speed-up of numerical calculation compared to the counterpart of the central processing unit (CPU) and the cost-effective computational capability of 3-D profile measurement in real time and on-line processing.

Multimodality Imaging of Digital Holographic Microscopy

Xin-Ji Lai[1], **Yu-Chih Lin**[1], **Han-Yen Tu**[2], **and Chau-Jern Cheng**[1]

[1]Institute of Electro-Optical Science and Technology, National Taiwan Normal University
Taipei 11677, Taiwan
[2]Department of Electrical Engineering, Chinese Culture University, Taipei 11114, Taiwan

Abstract— We propose and demonstrate multimodality imaging of digital holographic microscopy for measuring the complex wavefront (amplitude and phase) and the state of polarization through the specimen simultaneously. The digital holographic microscopy has been widely investigated and has great potential for applications such as measuring whole wavefronts of the specimen because it can quantitatively assess all information in a complex wavefront derived from a digital hologram. In contrast to traditional microscopy techniques like confocal laser scanning microscopy, atomic force microscope and scanning electron microscope, digital holographic microscopy permits a non-destructive, non-invasive and low energy penetration measurement with full-field information of the specimen and can directly observe the multimodality images of the specimen with single hologram acquisition. In this study, the reconstructed phase and amplitude images can be derived from a digital hologram and quantitatively exhibit the topography or refractive index distribution of the specimen, including live cells and micro-optics. The state of polarization through the specimen can also be measured by using the incidence light with two orthogonal polarizations going through the specimen to form the polarization-encoded digital holograms, in which two wavefronts of different polarization states can be numerically reconstructed in form of amplitude and phase. Thus, the Jones vector representation of the specimen can be synthesized and determined by calculating the amplitude and phase distribution of the two orthogonal polarization state of the wavefronts. The multimodality imaging of digital holographic microscopy can measure not only the three-dimensional structure but also the birefringence characters of the specimen and provide the potential functional studies and dynamic investigations in biological living cells.

GPU-based Computer-generated Hologram for Three-dimensional Display

Yi-Ta Lee[1], **Han-Yen Tu**[2], **and Chau-Jern Cheng**[1]

[1]Institute of Electro-Optical Science and Technology, National Taiwan Normal University
Taipei 11677, Taiwan
[2]Department of Electronic Engineering, St. John's University, Taipei 25135, Taiwan

Abstract— We proposes and demonstrates a new technique for producing the computer-generated hologram (CGH) by using the graphic processing unit (GPU), which can dramatically accelerate the computation speed of numerical calculation. Also, we develop a holographic printer system to output the CGH on a photo-sensitive plate for the optical reconstruction as a three-dimensional display. In this study, CGH is made by simulating the interference phenomenon between object wave and reference wave using numerical calculation. Traditional computation based on central processing unit (CPU) for making CGH is a computation-intensive and time-consuming procedure, because the digital computer embedded a CPU is a serial processing such that it is not suited for huge pixel number of calculation and processing in a hologram. In contrast to CPU, GPU can provide parallel processing architecture of numerical calculation to accelerate the computation and improve the quality of the holographic reconstruction. In this study, we present the GPU-based system for making CGH of a three-dimensional object (10,000 points), which can offer the speedup of 25 times faster than that in CPU. Further, the holographic printer system can output the CGH with the size of $5 \times 5\,\mathrm{cm}^2$ and the pixel pitch of less than $1\,\mu\mathrm{m}$ on a photo-sensitive plate. The achievable viewing angle of the three-dimensional display is about 30 degree, which is suitable to human eye vision. The analytical study and preliminarily experimental results are presented and discussed.

Digital Holographic Microscopy Based on Graphic Process Unit

Han-Yen Tu[1], **Yi-Ta Lee**[2], **and Chau-Jern Cheng**[2]

[1]Department of Electrical Engineering, Chinese Culture University, Taipei 11114, Taiwan
[2]Institute of Electro-Optical Science and Technology, National Taiwan Normal University
Taipei 11677, Taiwan

Abstract— This paper presents a fast computation and processing for off-axis digital holographic microscopy (DHM) based on a graphic processing unit (GPU). DHM is a highly effective imaging technique capable of reconstructing the three-dimensional (3-D) structure by retrieving the amplitude and phase information of the specimen. To obtain the 3-D profile of the specimen, numerous calculations for image reconstruction are required. For achieving enormous calculations of image reconstruction and improving the computational speed for their practical applications, we have performed the preceding computation and processing of DHM through the GPU. This method leads to effectively accelerate the computation performance with the parallel computing architecture and algorithm. Further, we perform accurate 3-D profile of the specimen by the use of filtering algorithm adjusting the contrast of reconstructed images. The proposed GPU-based DHM provides the potential for significantly speed-up of numerical calculation compared to the counterpart of the central processing unit (CPU). The high-speed cost-effective computational capability derives 3-D profile measurement in real time and on-line processing.

A Study of Optical Design of Blu-ray Pickup Head System with Liquid Crystal Element

Chih-Ta Yen[1], **Hui-Chen Yeh**[2], **Yi-Chin Fang**[3], **and Jui-Hsin Hsu**[3]

[1]Department of Electrical Engineering, National Formosa University, Yunlin, Taiwan
[2]Advanced Optical Design Center
National Kaohsiung First University of Science and Technology, Taiwan
[3]Department of the Mechanical and Automation Engineering
National Kaohsiung First University of Science and Technology, Taiwan

Abstract— This study proposes a new optical design and compensation method of Blue Ray pick up head system with liquid crystal optics. Fundamental methodology are given that a hole-patterned electrode liquid crystal optics with input of external voltage, which generates a symmetric non-uniform electrical field in the liquid crystal layer, will direct liquid crystal molecules into the appropriate gradient refractive indices distribution, then resulting in convergence or divergence of specific light beam. Liquid crystal optics delivers fast compensation through optical design when errors occur.

According to specification from Blue-ray Disc White paper, different types of pick up head system with LC liquid optics, Diffractive Optics and simulation are studied in this research. Simulation work will be done by Code V software and tolerance as well. Different tolerance such as de-focus, tilt, de-center and their related compensation are further analyzed in this research. The results show that optical design with liquid crystal optics as a compensation device achieves success. Aberrations are eliminated up to 46% compared to traditional ones.

A Study of Optical Design of Miniature Zoom Optics with Liquid Lenses

Cheng-Mu Tsai[1], **Yi-Chin Fang**[2], **Cheng-Lun Chung**[2], **Wei-Ting Li**[2], **and Je-Yi Huang**[2]

[1]Department of Computer and Communication, Kun Shan University
No. 949, Dawan Rd., Yongkang District, Tainan City 710, Taiwan, R.O.C.
[2]Institute of Electro-Optical Engineering
National Kaohsiung First University of Science and Technology
No. 2, Jhuoyue Rd., Nanzih District, Kaohsiung City 811, Taiwan, R.O.C.

Abstract— A new optical design of 2X miniature zoom optics with liquid lens elements are proposed in this research. Two liquid lenses are applied to minimize the overall length of miniature zoom optics. Due to complexity of conventional zoom method with complicated mechanical cam system, zoom optics with liquid optics will play the role in the further because no more complicated opto-mechanical system will be required. In other words, focus, zoom and zoom compensation will be replaced by electronics of liquid optics, which might significantly minimize volumetric size of zoom optics. Liquid lenses are optical components especially designed to perform focusing in high quality and small form factor imaging systems. They can either be used as an add-on on a stand alone fixed focus lens module to convert it into an auto-focus module; or be integrated within the auto-focus lens module at design stage. Besides, liquid lens could be as a vari-focal component, which takes advantage of reduce the size of the optical zoom lens. This research presents some optical design with decent performance, which represents success of miniature zoom optics with liquid optics.

Session 2A5b
Broadband Optical Access

Adaptive Loading Algorithms Evaluations for IMDD SMF System-based Optical OFDM Transceivers

E. Giacoumidis[1], **J. L. Wei**[2], **E. Hugues Salas**[2], **J. M. Tang**[2], **and I. Tomkos**[1]

[1]Networks and Optical Communications (NOC) Group
Athens Information Technology (AIT), Athens, Greece
[2]School of Electronic Engineering, Bangor University, Bangor, Wales, UK

Abstract— Detailed investigations of the effectiveness of three widely adopted optical orthogonal frequency division multiplexing (OOFDM) adaptive loading algorithms, including power loading (PL), bit loading (BL), and bit-and-power loading (BPL), are undertaken, over < 100 km single-mode fibre (SMF) system without incorporating inline optical amplification and chromatic dispersion (CD) compensation. It is shown that the BPL (PL) algorithm always offers the best (worst) transmission performance. The absolute transmission capacity differences between these algorithms are independent of transmission distance and launched optical power. Moreover, it is shown that in comparison with the most sophisticated BPL algorithm, the simplest PL algorithm is effective in escalating the OOFDM SMF links performance to its maximum potential. On the other hand, when employing a large number of subcarriers and a high digital-to-analogue (DAC)/analogue-to-digital (ADC) sampling rate, the sophisticated BPL algorithm has to be adop

Diversity Statistics of Free Space Optical Links Affected by Rain

S. Zvanovec
Department of Electromagnetic Field, Czech Technical University in Prague, Czech Republic

Abstract— Free Space Optics (FSO) bring many advantages to modern communication including larger frequency bandwidth and substantially higher available data rates, immunity to interferences, free license, higher safety of transmission due to narrow optical beams etc. [1]. Rain does not introduce the main negative influence affecting optical systems, the fog prevails causing instant drops of links [2], nevertheless as it was published in [3] substantial rain attenuations can be observed. Therefore there is a need to solve rain influence even in the region where raindrops are several orders larger than wavelengths (comparing to millimeter wavelength links).

A propagation simulation tool to study a performance of FSO heterogeneous terrestrial networks under different signal propagation conditions and with various configurations has been developed. In order to obtain precise fading statistics, the rain database from a four year period was utilized including 50 km × 50 km rain scans from Czech meteoradars (rain rate distributions with 1 km grid resolution and 1 minute time steps). For the case of the scenarios employing two optical wireless links affected by time-space variable rain intensities, resulted statistics of diversity gains will be discussed in the paper. Focus will be given on angular separations and link length ratio dependencies. Implementation of FSO in heterogeneous networks covering large urban areas will be discussed as well.

REFERENCES

1. Bouchet, O., et al., *Free Space Optics: Propagation and Communication*, ISTE Ltd, London, 2006.
2. Colvero, C. P., et al., "FSO systems: Rain, drizzle, fog and haze attenuation at different optical windows propagation," *SBMO/IEEE MTT-S International Microwave and Optoelectronics Conference, IMOC 2007*, 563–568, 2007.
3. Carbonneau, T. H. and D. R. Wisely, "Opportunities and challenges for optical wireless; the competitive advantage of free space telecommunications links in today's crowded marketplace," *Wireless Technologies and Systems: Millimeter-Wave and Optical*, Vol. 3232, 119–128, 1998.

Effect of ADC on the Performance of Optical Fast-OFDM in MMF/SMF-based Links

E. Giacoumidis[1], **S. K. Ibrahim**[2], **J. Zhao**[2],
J. L. Wei[3], **J. M. Tang**[3], **A. D. Ellis**[2], **and I. Tomkos**[1]

[1]Networks and Optical Communications (NOC) Group
Athens Information Technology (AIT), Athens, Greece
[2]Photonics Systems Group, Tyndall National Institute and Department of Physics
University College Cork, Cork, Ireland
[3]School of Electronic Engineering, Bangor University, Bangor, Wales, UK

Abstract— Based on a recently proposed novel technique known as optical fast orthogonal frequency-division multiplexing (FOFDM), which has twice the bandwidth efficiency compared to conventional OFDM, investigations are undertaken into the impact of an analog-to-digital converter (ADC) involved in FOFDM signals over unamplified intensity-modulation and direct-detection (IM/DD) multimode-fiber (MMF) and singlemode-fiber (SMF) based links. It is evaluated, for the first time, two important issues: 1) The impact of signal quantization and clipping effects for identification of a set of ADC parameters using various FOFDM single-dimensional modulation formats; 2) The FOFDM ADC parameters are compared with the corresponding ADC parameters of a conventional OFDM over both MMF and SMF links. It is shown that FOFDM and conventional OFDM over MMF/SMF links have similar optimum ADC parameters for a targeted BER of 10^{-3}.

Improved Transmission Performance of Adaptively Modulated OFDM Signals Using Quantum Dot Semiconductor Optical Amplifier Intensity Modulators

A. Hamié[1], M. Hamze[1,3], J. L. Wei[2], J. M. Tang[2], and A. Sharaiha[3]

[1]Arts, Sciences, and Technology University of Lebanon (AUL)
Hamra, Commodore Street, Beirut, Lebanon
[2]School of Electronic Engineering, Bangor University, Dean Street, Bangor LL57 1UT, UK
[3]Laboratoire RESO, Ecole Nationale d'Ingénieurs de Brest, Brest, France

Abstract— Wavelength division multiplexed-passive optical networks (WDM-PONs) are promising for providing "future-proof" technical solutions to satisfy the exponentially increasing end-users' bandwidth demand. In intensity modulation and direct detection (IMDD) optical orthogonal frequency division multiplexing (OOFDM) transmission systems, the potential of using semiconductor optical amplifier intensity modulators (SOA-IMs) to achieve desired cost-effective and colorless OOFDM transmission has been reported in [1, 2], in which, however, 20 dBm optical powers input to the SOA-IMs are required.

In this paper, the feasibility of utilizing quantum dot semiconductor optical amplifier intensity modulators (QD-SOA-IMs) are explored numerically, for the first time, in SSMF-based IMDD adaptively modulated OOFDM (AMOOFDM) systems. It is shown that QD-SOA-IMs can not only considerably improve the OOFDM transmission performance but also reduce the required optical powers by approximately 10 dB compared to SOA-IMs. In addition, QD-SOA-IMs also have very fast dynamic gain responses in a range of picoseconds, implying that QD-SOA-IMs can offer higher modulation bandwidths than conventional SOA-IMs. A theoretical QD-SOA-IM model is developed based on assumptions that all QDs are identical and uniform, and that there is only one confined energy level in the conduction and valence band of each dot [3]. The transmission system considered here is illustrated in Fig. 1(a).

To maximize the transmission performance of the system, numerical simulations are first performed to identify the optimum operating conditions of QD-SOA-IMs in terms of peak to peak driving currents, bias currents and optical input powers. Fig. 1(b) shows comparisons of the obtained capacity versus reach performance for SOA-IMs, QD-SOA-IMs and ideal intensity modulators for 20 dBm CW optical input powers. For transmission distances of up to 140 km, QD-SOA-IMs always offer an increased transmission capacity in comparison to SOA-IMs. In particular, for transmission distances of less than 20 km, the QD-SOA-IM enabled transmission performance is very similar to that corresponding to the ideal intensity modulator, leading to the performance of 38 Gb/s over 20 km. In addition, our simulation results also show that QD-SOA-IMs subject to an input optical power as low as 10 dBm can support better performance compared to SOA-IMs subject to an input optical power as high as 20 dBm. Such results are valuable for cost-effective OOFDM transceiver design.

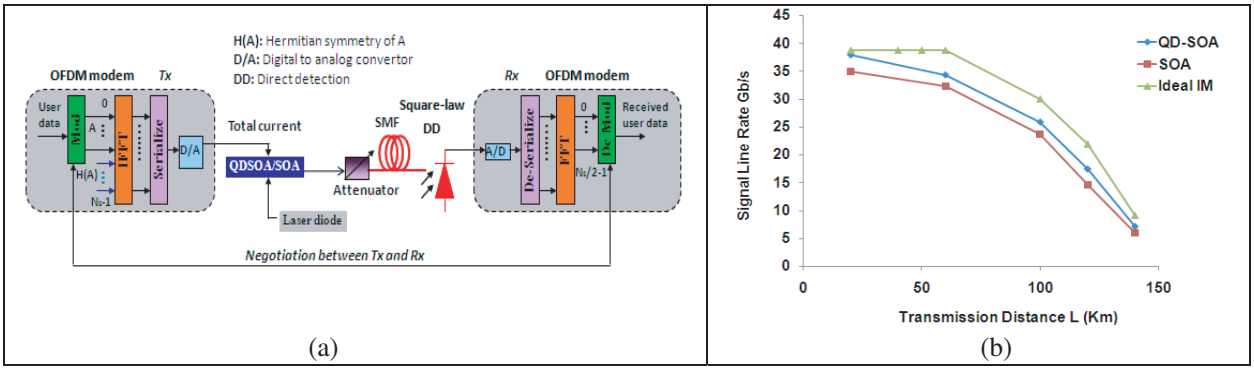

Figure 1: (a) Transmission system diagram together with block diagrams of the AMOOFDM transmitter and receiver, (b) Signal Line Rate versus the reach performance for QD-SOA, SOA, and Ideal IM for 20 dBm CW optical input power.

REFERENCES

1. Wei, J. L., A. Hamié, R. P. Gidding, E. Hugues-Salas, X. Zheng, S. Mansoor, and J. M. Tang, "Adaptively modulated optical OFDM modems utilizing RSOAs as intensity modulators in IMDD SMF transmission systems," *Optics Express*, Vol. 18, No. 8, 8556, April 12, 2010.
2. Wei, J. L., A. Hamié, R. P. Giddings, and J. M. Tang, "Semiconductor optical amplifier-enabled intensity modulation of adaptively modulated optical OFDM signals in SMF-based IMDD systems," *Journal of Lightwave Technology*, Vol. 27, No. 16, August 15, 2009.
3. Sun, H., Q. Wang, H. Dong, and N. K. Dutta, "XOR performance of a quantum dot semiconductor optical amplifier based Mach-Zehnder interferometer," *Optics Express*, Vol. 13, No. 6, 1892, March 21, 2005.

Bandwidth Efficient Hybrid Wireless-optical Broadband-access Network (WOBAN) Based on OFDM Transmission

Redhwan Q. Shaddad[1,2], **Abu Bakar Mohammad**[1], **and Abdulaziz M. Al-Hetar**[2]

[1]Photonic Technology Center, InfoComm Research Alliance, Universiti Teknologi Malaysia, Malaysia
[2]Communication and Computer Engineering Department
Faculty of Engineering and Information Technology, Taiz University, Yemen

Abstract— In this paper, a simple and bandwidth efficient hybrid wireless-optical broadband access network (WOBAN) based on orthogonal frequency division multiplexing (OFDM) is proposed and designed. It is an optimal combination of an optical backhaul and a wireless front-end for an efficient access network. The bandwidth efficient WOBAN based on OFDM provides an effective solution to eliminate intersymbol interference (ISI) caused by dispersive channels. There are two factors considered important here; multipath fading in wireless link and dispersion effects in fiber link. The physical layer performance is analyzed in terms of bit error rate (BER), error vector magnitude (EVM), and signal-to-noise ratio (SNR). An 8 Gb/s data rate has been achieved by the optical backhaul along optical fiber length of 20 km. The wireless front-end access point supports data rate up to 240 Mb/s along an outdoor wireless link.

Session 2A6a
Computational Techniques

FDTD Analysis of Signal and Interference Characteristics in Multi-channel Propagation over Forests for WiMAX Communication

Yasumitsu Miyazaki[1], **Nobuo Goto**[2], **and Koichi Takahashi**[1]

[1]Department of Media Informatics, Aichi University of Technology
50-2 Manori, Nishihasama-cho, Gamagori 443-0047, Japan
[2]Institute of Technology and Science, The University of Tokushima
2-1 Minamijosanjima-cho, Tokushima 770-8506, Japan

Abstract— WiMAX wireless communication has been rapidly developed for broadband mobile communication. Mobile WiMAX communication system uses microwave carrier of 2.5 GHz frequency band and modulation is OFDM mainly. By using OFDM technique, WiMAX provide high speed and reliable communication against multi pass interferences due to the presence of obstacles in communication channels. To design excellent high performance mobile communication systems, accurate evaluation of communication system is indispensable. By using parallel FDTD, we studied fundamental characteristics of microwave propagation and scattering in urban area [1, 2]. We also studied wave propagation and scattering by forest and trees using two-dimensional FDTD [3]. The effects of multiple scattering and attenuation of microwave by forest are severe factors of high speed wireless communications.

In this paper, signal and interference characteristics of WiMAX communication signal in more realistic forest model are numerically analyzed using three-dimensional FDTD method. The incident wave is a WiMAX communication wave given by equivalent current

$$J_y(\mathbf{r}_t, t) = s(t) \sin\left[(\omega_c + m\omega_0)\, t\right] \mathbf{J}(\mathbf{r}_t) \tag{1}$$

$$\mathbf{J}(\mathbf{r}_t) = \exp\left\{-\left(\frac{x - x_0}{S}\right)^2\right\} \exp\left\{-\left(\frac{y - y_0}{S}\right)^2\right\} \delta(z - z_0) \tag{2}$$

where $(x_0,\ y_0,\ z_0)$ is a center of incident beam, S is a beamspot size at $z = z_0$, $\omega_c = 2\pi f_c$, $f_c = 2.5\,\mathrm{GHz}$ is a carrier frequency, $\omega_0 = 2\pi f_0$, $f_0 = 1/T = 50\,\mathrm{MHz}$ is a interval of carrier frequency and mf_0 is a sub carrier frequency. The OFDM system provides high-speed data rate by synthesizing multi sub carriers. $s(t)$ is a sequence of transmission code. Total analysis region of FDTD is shown in Fig. 1. Fig. 2 shows a block diagram of communication system. $h(t)$ is a transfer function which contains noises generated by propagation channel and interference signals from other user's terminal. In case of WiMAX, multiple sub carrier are used for signal modulation to realize reliable high data rate communication. WiMAX provides connection service to multi users simultaneously, the interference of signals from multi users at base station is considered. For evaluation of transmission characteristics under this environment, SNR, CNR and BER are calculated by time response obtained using FDTD and to improve the transmission characteristics, design of digital signal processing and digital filter for recognition and separation of each desired signal from received signals contaminated by noise interference are discussed.

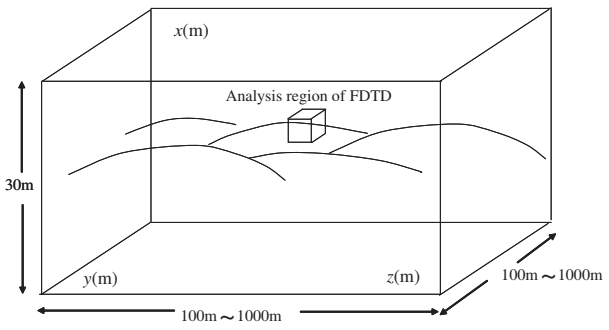

Figure 1: 3-dimensional total analysis region of propagation over forests.

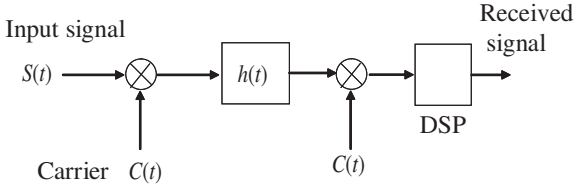

Figure 2: Block diagram of digital communication system for OFDM.

REFERENCES

1. Selormey, P. and Y. Miyazaki, *Trans. IEE Japan*, Vol. 119-C, No. 1, 97–104, 1999.
2. Rodriguez, G., Y. Miyazaki, and N. Goto, *IEEE Trans. Antennas & Propagat.*, Vol. 54, No. 3, 785–796, 2006.
3. Miyazaki, Y., T. Takada, and K. Takahashi, *Trans. IEE Japan*, Vol. 130-C, No. 4, 637–643, 2010.

Effect of an External Magnetic Field on Multipactor on a Dielectric Surface

Libing Cai[1], **Jianguo Wang**[1, 2], **Xiangqin Zhu**[1], **Yue Wang**[1], **Chun Xuan**[1], **and Hongfu Xia**[1]

[1]Northwest Institute of Nuclear Technology, P. O. Box 69-12, Xi'an 710024, China
[2]School of Electronic and Information Engineering, Xi'an Jiaotong University, Xi'an 710049, China

Abstract— As the high power microwave (HPM) technology advances, the power and pulse duration of the HPM source increase substantially, the breakdown of the dielectric window of the feed of HPM source has been becoming the major factor of limiting the transmission and radiation of HPM. It involves many basic physical phenomena, such as the field electron emission, multipactor, and electron-irradiated outgassing, etc. These phenomena cause the further gas breakdown in the gas layer near dielectric surface. The occurrence of breakdown is the final result of complicated physical mechanisms mentioned above. In the process of the breakdown, the multipactor plays a key role, and it decides the velocity of outgassing and the formation of the gas layer which is the necessary condition of final gas breakdown.

In this paper, the effect of external magnetic field on multipactor is studied by particle-in-cell (PIC) simulation, and the suppression of multipactor by external magnetic field is investigated. The multipactor discharge under different external magnetic field is simulated by the program. The simulation results show that the external magnetic affects the multipactor by changing the motion of multipactor electrons. In a half-period, the drift force pulls the electrons back to dielectric surface, and pushes the electrons away from dielectric surface in the other half-period. When the external magnetic field exceed a certain value, the multipactor will be cut off in a half-period, which means the velocity of outgassing is half of the case of no external magnetic field, and the delay time of breakdown will be increased to two times. For the HPM pulse with same width, the dielectric window would get fourfold power capability. As the increase of the strength of external magnetic field, the intension of multipactor will be decreased in the other half-period, which means the dielectric window would get a higher power capability.

Asymptotic Analysis of the Scattering of Light by an Imperfection Core in a Waveguide System

Akira Komiyama
Osaka Electro-Communication University, Hatsu-cho, Neyagawa-shi 572-8530, Japan

Abstract— In an ordered waveguide system composed of identical cores mode waves are extended over the entire system. Light launched into a core at the input end of the waveguide system propagates in a certain specific direction. The amplitude of light decreases in proportion to $z^{-\frac{1}{2}}$, where z is the distance along the waveguide axis.

In a disordered waveguide system composed of randomly different cores in size mode waves are localized and are concentrated into a narrow region of several cores [1]. In a two-dimensional system all modes are localized. When one of core is illuminated at the input end of the waveguide system several localized modes are excited and propagate through the system. The average amplitude of light decreases exponentially with increasing distance [2]. However, the physical meaning is unclear.

In this paper, an asymptotic expansion of the amplitude of the scattered wave by an imperfection core in a waveguide system is derived and the direct wave is partially canceled by the scattered wave and the shadow takes place. The amplitudes of the direct and scattered waves decrease in proportion to $z^{-\frac{1}{2}}$ and in the shadow region the amplitude of the sum of both waves decreases in proportion to $z^{-\frac{3}{2}}$. It is expected that in a disordered waveguide system the direct wave is completely canceled by the scattered wave and the average amplitude of light decreases exponentially.

REFERENCES

1. Komiyama, A., *Opt. Comm.*, Vol. 151, 25–30, 1998.
2. Komiyama, A., *IEICE Trans. Electron.*, Vol. E93-C, 46–51, 2010.

Plasmon Bio-sensor Based on Metal Grating with High Resolution and Wide Measurement Range

Ziqian Luo, **Taikei Suyama**, **and Yoichi Okuno**
Kumamoto University, Japan

Abstract— A metal grating has an interesting property known as the resonance absorption [1]. This is caused by excitation of surface plasmon waves and is accompanied by an abrupt change of diffraction efficiency [1–3]. A grating-based plasmon biosensor utilizing phase detection is presented. Yasuura's mode-matching method [4, 5] is used as the method of solution.

Figure 1(a) shows the schematic representation of diffraction by a layered grating made of Al and having an over-coating made of Au.

Without changing the structure parameters but only the incident angle, the measurement range can be shifted in a wide range while the sensor resolution can remain 5×10^{-8} refractive index units. The superior limit of resolution is predicted to be 10^{-9} refractive index units according to the simulation result shown as Fig. 1(b). Considering a trade-off between high sensitivity and experimental practicability, an optimizing advisement of experiment setting, which can enhance the diffraction efficiency to at least 10^{-3} and remain the sensitivity as 7.5×10^{-7}, is proposed for the future experiment.

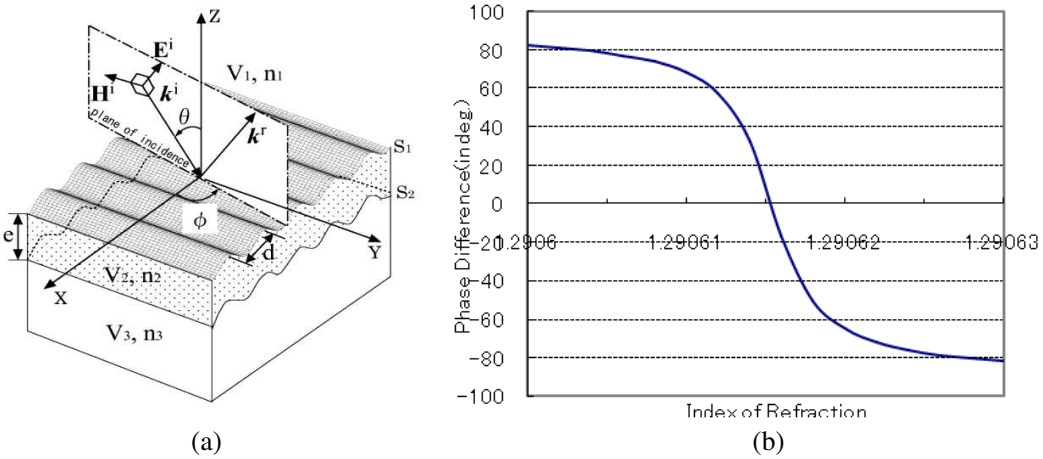

Figure 1: (a) Schematic representation of diffraction by a metal grating and (b) phase response with $\theta = 17.2°$, $\phi = 12.6°$.

REFERENCES

1. Raeter, H., "Surface plasmon and roughness", *Surface Polaritons*, V. M. Argranovich and D. L. Mills, eds., Chap. 9, 331–403, North-Holland, New York, 1982.
2. Nevière, M., "The homogeneous problem," *Electromagnetic Theory of Gratings*, R. Petit, ed., 123–157, Springer-Verlag, Berlin, 1980.
3. Barnes, W. L., T. W. Preist, J. R. Sambles, N. P. K. Cotter, and D. J. Nash, "Photonic gaps in the dispersion of surface plasmons on gratings," *Phys. Rev. B*, Vol. 51, 11164–11167, 1995.
4. K. Yasuura and T. Itakura, "Approximation method for wave functions (I), (II) and (III)", Kyushu Univ. Tech. Rep., 38, 1, 72–77, 1965; 38, 4, 378–385, 1966; 39, 1, 51–56, 1966.
5. Okuno, Y. and H. Ikuno, "Yasuura's method, its relation to the fictitious source methods, and its advancements in solving 2-D problems," *Generalized Multipole Techniques for Electromagnetic and Light Scattering*, Th. Wriedt, ed., 111–141, Elsevier, Amsterdam, 1999.

Finite-width Excitation and Impedance Models

Y. H. Lo[1], **L. Jiang**[1], **Y. P. Chen**[1] **and W. C. Chew**[1, 2]

[1]The University of Hong Kong, Hong Kong, China
[2]University of Illinois, Urbana-Champaign, USA

Abstract— We present a new feed model for the method of moments (MoM) formulation for the electric field integral equation (EFIE). This new model is formulated around an accurate model which enables a physical excitation with a finite size, in order to replace the commonly-used but inaccurate delta-gap model. Moreover, the new model does not require a magnetic frill-current around the excitation as in the previous models; hence it does not require the use of the K-operator for solving the MoM problem. Moreover, the model we employ here allows the implementation of lumped impedance inserted. This is achieved by a modification of the excitation formulation and a correction of the MoM matrix elements.

In the feed model, the excitation is provided by an electric field which is the result of a magnetic frill-current enclosing the feed volume [1]. The voltage applied across the feed is provided by the incident electric field, which is itself induced from the magnetic frill-current around it. In our model, we simplify the implementation by assuming that the electric field would be generated by the magnetic-frill to a good approximation that provides the correct applied voltage. Therefore the electric field is defined without using K-operator [2, 3]. This way, we simplify the implementation process, especially regarding the singularity treatment. We prove from the calculation of the port impedance using a half-wavelength strip antenna that the model provides correct results. Variational formulation can also be applied here to further enhance accuracy.

By treating lumped elements as a special form of excitation, our model allows insertion of lumped impedances. The inserted elements are essentially loads that cause a drop in voltage, which is similar to a reverse excitation. The voltage drop of such a load is dependent on the current which is the unknowns of the MoM problem. Therefore the current dependent coefficients are transferred into the corresponding elements in the impedance matrix. Similar technique has been applied previously with the delta-gap model [4] and we show here that it can also be applied here although slightly in a more complicated fashion. Note that in our model, the resulting impedance matrix becomes asymmetric since the elements to be corrected are not limited to the diagonal ones as in the previous delta-gap formulation.

REFERENCES

1. Jordan, E. C. and K. G. Balmain, *Electromagnetic Waves and Radiating Systems*, Prentice-Hall Inc., 1968.
2. Cui, T. J. and W. C. Chew, "Accurate model of arbitrary wire antennas in free space, above or inside ground," *IEEE Trans. Antennas Propag.*, Vol. 48, No. 4, 482–493, Apr. 2000.
3. Chew, W. C., M. S. Tong, and B. Hu, *Integral Equation Methods for Electromagnetic and Elastic Waves*, Morgan and Claypool, 2009.
4. Jiao, D. and J.-M. Jin, "Fast frequency-sweep analysis of RF coils for MRI," *IEEE Trans. Biomed. Eng.*, Vol. 46, No. 11, 1387–1390, 1999.

Propagation Characteristics of Dielectric Waveguides with Arbitrary Inhomogeneous Media along the Middle Layer

Ryosuke Ozaki and Tsuneki Yamasaki
Department of Electrical Engineering, College of Science and Technology, Nihon University, Japan

Abstract— Propagation of light in periodic structure waveguide is both theoretical and practical interest in many areas of physics and engineering. For example, there are such as integrated optics, optical waveguide filter, and other optical devices. In periodic structure such as photonic crystal structure, it is known frequency stop band occurs. Consequently, in the design of photonic crystal structure with periodic constant same as optical wavelength, it is important to investigate the stop band region. On the other hand, it can be controlled optical constants by the development of manufacturing technology of semiconductor and optical devices. Thus, many analytical and numerical techniques have been proposed that are applicable to dielectric gratings having arbitrary structures. To deal with multilayered dielectric gratings such as photonic crystal structure, it is necessary to analyze the multilayered periodic arrays. In multilayer method, as the inhomogeneous region is divided into an assembly of stratified thin layers with modulated index, the size of the matrix depends on the number of layers. In our method, the order of characteristic matrix equation depends on the modal truncation number, but it does not depend on the number of layers. Therefore the range of applicability for the periodic structures is much wider than that of the other method. Especially, it is effective method for the guiding problems such as multilayered periodic array. However the guiding problem is reported by various numerical techniques, the propagation characteristic is not investigated in detailed in the Bragg region. In recent paper, we proposed an improved method to analyze the scattering problem of dielectric gratings with the dielectric rectangular cylinders in the middle layer.

In this paper, we apply the improved method for the guiding problem of dielectric waveguide with arbitrary inhomogeneous media along the middle layer introduced the defect layers, and analyzed the propagation characteristics of dielectric waveguide composed of dielectric circular cylinders and the arbitrary inhomogeneous media in the middle layer.

Numerical results are given for the complex propagation constants and distribution of poynting vector in the dielectric circular cylinder and dielectric triangular cylinders as the inhomogeneous media in the middle layer for both TE_0 and TM_0 modes.

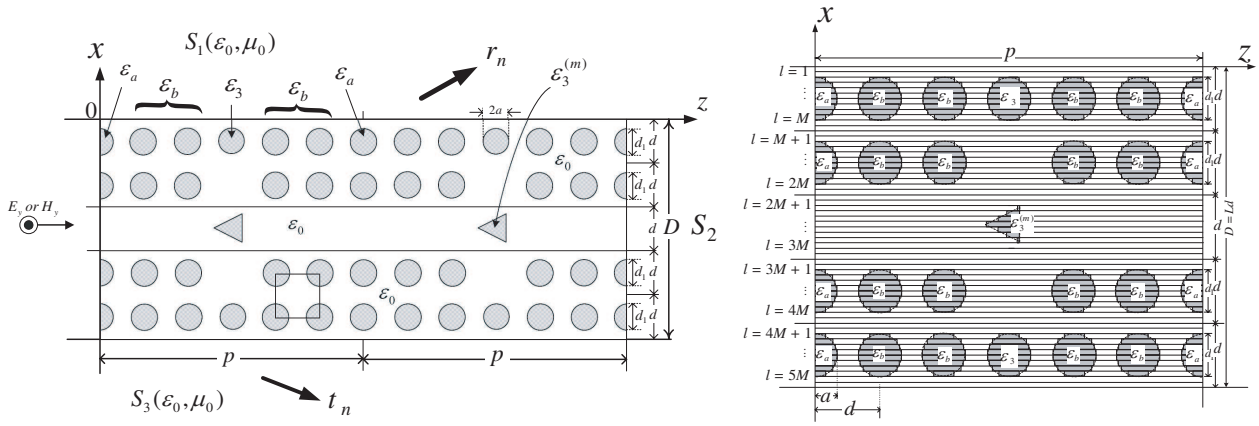

Figure 1: Structure of dielectric waveguides with arbitrary inhomogeneous media along the middle layer.

Session 2A6b
Computational Electromagnetics, EM Method and Simulation 1

Generalized Modal Expansion of Electromagnetic Fields in Unbounded Media

Q. I. Dai[1], **W. C. Chew**[1, 2], **Y. G. Liu**[1], **B. O. Zhu**[1], **and L. Jiang**[1]

[1]The University of Hong Kong, Hong Kong, China
[2]University of Illinois, Urbana-Champaign, USA

Abstract— Eigenmode expansion theory has been widely used in the study of electromagnetic (EM) problems as a powerful analysis tool. Most of the previous works on eigenmode expansion have such a limitation that they are system specific [1]. Here, we present a generalized modal expansion analysis for unbounded media which results in a unified treatment.

We start with an arbitrary bounded EM problem at a given excitation frequency. We show that different implementations of the boundary condition, such as perfect electric conductor (PEC), perfect magnetic conductor (PMC) and periodic boundary condition (PBC), will not affect the generality of our conclusion. When the governing operator in the Helmholtz equation is symmetric or self-adjoint, we seek the field due to any excitation in terms of the system's complete and orthogonal eigenmodes. When the governing operator is nonsymmetric or non-selfadjoint, we form a biorthogonal system by constructing an auxiliary operator with respect to the original operator [2, 3]. In fact, when the medium is symmetric or self-adjoint, it is a special case of the above since the auxiliary operator will be the same as the original problem. These biorthogonal eigenmodes and related eigenvalues can be numerically solved for by finite difference (FD), finite element method (FEM) or integral equation (IE). Thus, the EM field under source excitation can be expanded by employing the complete biorthogonal eigenmodes.

The unbounded case can be obtained by letting the boundary approach to infinity. When this happens, the discrete modes due to the boundary condition become a continuum while the trapped modes due to the inhomogeneity of the medium stay almost the same. Hence, we obtain the eigenmode expansion of an excited field in terms of discrete and continuum modes.

Furthermore, we can arrive at a reduced modal representation of a general excitation problem where only several modes dominate. Such generalized modal expansions can provide physical insight into the working of many electromagnetic structures, such as microstrip antennas, small antennas, and metamaterial-inspired structures. They also provide physical insight into the frequency behavior of the solution, as well as arriving at a reduced representation of a highly complex problem.

REFERENCES

1. Collin, R. E., *Field Theory of Guided Waves*, IEEE Press, 1991.
2. Chen, C. H. and C. D. Lien, "The variational principle for non-self-adjoint electromagnetic problems," *IEEE Transactions on Microwave Theory and Techniques*, Vol. 28, No. 8, 878–886, Aug. 1980.
3. Chew, W. C., *Waves and Fields in Inhomogeneous Media*, IEEE Press, 1995.

A Matrix Representation of Dyadic Green's Function for Modeling General Dielectric Objects Embedded in a Layered Medium

Yongpin Chen[1], **Weng Cho Chew**[1, 2], **and Lijun Jiang**[1]

[1]Department of Electrical and Electronic Engineering
University of Hong Kong, Pokfulam, Hong Kong, China
[2]Department of Electrical and Computer Engineering
University of Illinois at Urbana-Champaign, Urbana, IL 61801, USA

Abstract— Electromagnetic scattering from general dielectric objects embedded in a planarly layered medium is an important research topic. The applications include: geophysical exploration, remote sensing, detection of unexploded ordnance, light absorption enhancement in solar cell, improvement of out-coupling efficiency in LED design, lithography, etc. For homogeneous dielectric objects, the surface integral equation (SIE) method based on layered medium Green's function (LMGF) is the most favorable one since the number of unknowns can be drastically reduced compared to other methods, such as the volume integral equation (VIE) method or finite element method (FEM). There are several ways of deriving the LMGF, for example, the transmission line analog, Ez-Hz formulation, Hertz potential approach, etc.

Recently, a matrix-friendly formulation of the LMGF based on the vector wave functions has been proposed in the electric field integral equation (EFIE) for modeling perfect electric conducting (PEC) objects. In this formula, the spatial derivatives in the dyadic Green's function have been partially moved to both basis and testing functions, to make the coordinate-space singularities of the Green's function as weak as possible.

In this paper, we extend this formulation to model general dielectric objects. Different from the PEC case, in order to derive the proper SIE by applying the extinction theorem, four different dyadic Green's functions are required to connect the electric/magnetic current sources to the electric/magnetic fields. Duality properties of these Green's functions and their corresponding spectral counterparts are investigated in details. Matrix representation of these Green's functions is formulated by invoking integration by parts and the properties of Fourier-Hankel transforms. The line integral issues for objects straddling different layers are further analyzed based on the continuity of the propagation factors. Several numerical results are demonstrated to validate this formulation.

Improved Hybrid MoM-PO Method with Iterative Framework

Z. L. Liu and C. F. Wang
Temasek Laboratories, National University of Singapore, Singapore

Abstract— A novel hybrid Method of Moments — Physical Optics (MoM-PO) with iterative process between the MoM and PO is presented to analyze electrically large structure with small features, such as large platform equipped with several antennas. MoM is fit for modeling of complex objects with fine features but limited to electrically small and medium-sized objects. PO method can be used to compute approximate scattering of large targets, but unsuitable for describing the Electromagnetic (EM) wave behavior on detailed structure components, such as antenna sources and small features of antennas. A remedy is to combine MoM with PO. To apply the hybrid MoM-PO method, the whole EM problem domain is divided into MoM- and PO-regions according to the EM characteristics of the structure. Small feature objects and sources should be contained in the MoM-region, and the rest is considered in the PO-region. The difficulty of hybrid MoM-PO method is how to efficiently and accurately treat the interaction between the EM fields on MoMand PO-regions. In traditional hybrid MoM-PO method, the contribution of the PO-region is coupled into the impedance matrix of MoM. However, this traditional scheme is not efficient and flexible. The original MoM impedance matrix is disturbed by PO contribution, and the resultant matrix equation is hard to be solved by the existing fast algorithms due to its ill-conditioned numerical behavior. To break through the limitation of the traditional hybrid MoM-PO method for efficient simulation of electrically large and complex EM problem, a novel hybrid MoM-PO method is proposed based on a new framework and iterative process to physically combine the MoM and PO solutions. The newly proposed hybrid MoM-PO method has been successfully formulated using integral equations and carefully implemented. It provides a very good base for further development to solve real EM problems with reasonable accuracy. More discussion on the method and results will be presented at the conference.

Study and Modeling of Electromagnetic Interference in the Neonatal Monitoring Systems

Elagiri-Ramalingam Rajkumar[1, 2]

[1]VIT University, TN, India
[2]Institut de Recherche en Systèmes Electroniques Embarqués (IRSEEM)
Technopôle du Madrillet, Avenue Galilée, BP 10024
Saint Etienne du Rouvray 76801, France

Abstract— In this paper, we examine the electromagnetic interference [1, 2] in the neonatal monitoring systems and propose a methodology to calculate the coupling between single board computer acquisition system and the transmission cables associated. Due to signal frequency range, the EEG signals acquired from the neonates are very low and easily subject to surrounding perturbations. This will lead to lot of artifacts and the signal preprocessing and amplification are often getting into unnecessary errors. In order to avoid these errors it is necessary to study the electromagnetic interference and compatibility of the devices and the transmission cables. From the literature [3, 4] and the results obtained from statistical analysis in the function of base station signals with bedside monitoring systems indicates the percentage of the error increases with increase in radiated power level of the medical equipments. We understand that close proximity of components, devices and cables are subjected to radiated coupling and inducing the electrical components. In medical applications, it is evident that these emissions from the devices/implants are playing vital in performance of the device; this study will enhance the continuous bedside cerebral metabolic monitoring devices.

REFERENCES

1. Taylor, C. D., R. S. Sattewhite, and C. W. Harrison, "The response of a terminated twowire transmission line excited by a non-uniform electromagnetic field," *IEEE Transactions on Antenna Propagation*, Vol. 13, No. 6, 987–989, Nov. 1965.
2. Trigano, A. J., A. Azoulay, M. Rochdi, and A. Campillo, "Electromagnetic interference of external pacemakers by walkie-talkies and digital cellular phones: Experimental study," *Pacing Clin. Electrophysiol.*, Vol. 22, No. 4, 588–593, Apr. 1999.
3. Scavino, G., L. Proietti, and V. Barbaro, "Electromagnetic interference to infusion pumps from GSM mobile phones," *Proc. 26th Annu. Int. Conf. IEEE EMBS*, Vol. 2, 3515–3518, Sep. 2004.
4. "Electromagnetic compatibility of medical devices with mobile communications," Medical Devices Bulletin DB9702, Medical Devices Agency, London, U.K., 1997.

A Comparison and Validation of Two and Three Dimensional Dipoles in the Calculation of Radiated Coupling

Elagiri-Ramalingam Rajkumar, **Abhishek Ramanujan**, **Mohamed Bensetti**, **and Anne Louis**
Institut de Recherche en Systèmes Electroniques Embarqués (IRSEEM)
76801 Saint Etienne du Rouvray, France

Abstract— In modern automotive applications, where cables and electronic components are found in close proximity, it is indispensible to study the induced coupling onto the cable due to the emission by the electronic circuit/components. The emission from the electronic components can be represented by an equivalent behavioral model based on a set of elementary 2D dipoles [1]. The work in [2] has illustrated a technique to compute the radiated coupling on the cables with the use of these 2D dipoles in the frequency domain. The Partial Element Equivalent Circuit (PEEC) method is a commonly used approach to solve combined circuit and electromagnetic problems in the time and frequency domain [3]. In the context of modeling the radiated coupling in the timeCdomain, this method is an interesting candidate to calculate the coupled voltage on a cable due to an external electromagnetic source. In IRSEEM, a preliminary method is developed to calculate the distribution of currents in the groundplane [4]. This method calls for a 3D representation of the problem under study. In order to adapt the 2D emission model representation in PEEC, a 3D equivalent dipole has been analyzed. Different configurations of 3D dipole are tested and compared with 2D configuration.Good correlation is obtained between the 3D and 2D dipole configurations. This will be the basis for the implementation of the radiated coupling through PEEC formulation.

REFERENCES

1. Ramanujan, A., Z. Riah, A. Louis, and B. Mazari, "Modeling the electromagnetic radiations of passive microwave components using a near-field scanning method," *IEEE Trans. EMC*, 2010.
2. Leseigneur, C., P. F. Lopez, C. Arcambal, D. Baudry, and A. Louis, "Near-field coupling model between electronic systems and transmission line," *IEEE Int. Symp. EMC*, 22–27, Ft. Lauderdale, USA, Jul. 25–30, 2010.
3. Ruehli, A. E. and A. C. Cangellaris, "Application of the partial element equivalent circuit (PEEC) method to realistic printed circuit board problems," *Proc. IEEE Int. Symp. EMC*, 182–187, Aug. 1998.
4. Duval, F., "Gestion du cablage des masses electroniques dans un vehicule automible," Thesis, University of Rouen, 2007.

Session 2A7
Poster Session 2

A Spherical Left-handed Metamaterial with Innate Isotropy

Jia Liu[1], **Gang He**[1], **and Wei Gu**[2]

[1]Science College, Air Force Engineering University, Xi'an 710051, China
[2]Department of Electronic Information and Computer Technologies
Engineering & Technical College, Chengdu University of Technology, Leshan 614300, China

Abstract— A spherical left-handed metamaterial with innate isotropy is proposed in this paper. The unit cell of the left-handed metamaterial consists of six labyrinth resonators, three crossed continuous wires and a dielectric sphere. The labyrinth resonator can eliminate the bianisotropy and electromagnetic coupling related to the split-ring resonator. Effective material parameters of the left-handed metamaterial were retrieved from S parameters. The negative refraction behavior of the left-handed metamaterial was simulated, which is consistent with the retrieved refractive index.

A Direction-selective Metamaterial Absorber with Polarization-insensitive Property

Jia Liu[1], **Gang He**[1], **and Wei Gu**[2]

[1]Science College, Air Force Engineering University, Xi'an 710051, China
[2]Department of Electronic Information and Computer Technologies, Engineering & Technical College Chengdu University of Technology, Leshan 614300, China

Abstract— We report the design of a direction-selective metamaterial absorber with polarization-insensitive property. Both theoretical and simulated results reveal that our absorber assuredly has a distinct absorption point with direction selectivity at 10.38 GHz, which are related to the resonance of the metamaterial and are influenced indistinctively by polarization. The retrieved impedance and the distributions of the surface current density show that the resonance of the metamaterial could be tuned to approximately match the impedance of the free space in order to minimize the reflectance at the absorption frequency. The distributions of the power loss indicate that the absorber is an excellent electromagnetic wave collector: the wave is first trapped and reinforced in certain specific locations and then completely consumed. This metamaterial absorber may have applications in many scientific and technological areas.

A Three-dimensional Left-handed Metamaterial Composed of Spiral Resonators and Crossing Continuous Wires

Wei Gu[1], **Jia Liu**[2], **and Gang He**[2]

[1]Engineering & Technical College, Chengdu University of Technology, Leshan 614300, China
[2]Science College, Air Force Engineering University, Xi'an 710051, China

Abstract— A three-dimensional left-handed metamaterial composed of spiral resonators (SRs) and crossing continuous wires is presented in this paper. The SRs can reduce the size of the left-handed metamaterial and weaken its electromagnetic coupling. The transmission property of the left-handed metamaterial was demonstrated and the constitutive parameters were retrieved from S parameters. The negative index of the lefted-handed metamaterial is verified by simulating its refraction behaviour.

An Hybrid MoM-CG Method to Analyze Electromagnetic Scattering

H. Belhadj, S. Mili, and T. Aguili
Sys'Com Lab, National Engineering School of Tunis, Tunisia

Abstract— A hybrid method based on the moment method [1] combined to the conjugate gradient (CG) algorithm [2] is presented in this paper to analyze electromagnetic scattering. In fact, the most idea was to exploit the advantages of the CG algorithm, which is an iterative method, and to use it, when the moment method fails to solve a matrix system due to ill conditioning.

The structure studied was, the Cantor iris located in the cross section of a parallel-plates EMEM waveguide. The aim was to compute the current density of the considered structure when illuminated by some active modes [3]. Boundary conditions are synthetically expressed by the Generalized Equivalent Circuit GEC method [4–6] which translates the relations between electric and magnetic fields into an equivalent circuit.

The moment method has been used to solve the equation based on the impedance operator. When the structure is excited by its first active mode: the TEM mode, the moment method converges perfectly to the solution also was the CG method [7]. However, when the guide is excited by some active modes, the moment matrix becomes badly scaled and ill conditioned so the result is inaccurate. The CG method is, then incorporated, and used in place of the matrix inversion on the MoM algorithm. Results obtained show the efficiency of this method comparing to the MoM.

REFERENCES

1. Harrington, R. F., *Field Computation by Moment Methods, IEEE Press Series on Electromagnetic Waves*, Syracuse University, 1993.
2. Hestenes, M. R. and E. Stiefel, "Methods of conjugate gradients for solving linear systems," *Journal of Research of the National Bureau of Standards*, Vol. 49, No. 6, 409–436, December 1952.
3. Mili, S., C. Larbi Aguili, and T. Aguili, "Study of fractal-shaped structures with pin diodes using multi-scale method combined to the generalized equivalent circuit modeling," *Progress In Electromagnetic Research B*, Vol. 27, 213–233, 2011.
4. Aguili, T., "Modélisation des composantes SFH planaires par la méthode des circuits équivalents généralisée," Thesis manuscript, National Engineering School of Tunis, Tunisia, 2000.
5. Baudrand, H., "Representation by equiavelent circuit of the integrals methods in microwave passive elements," *European Microwave Conference*, Vol. 2, 1359–1364, Budapest, Hungary, September 10–13, 1990.
6. Baudrand, H. and H. Aubert, *L'Electromagnétisme par les Schémas Equivalents*, Cepaduès éditions, 2003.
7. Belhadj, H., S. Mili, and T. Aguili, "New implementation of the conjugate gradient based on the impedance operator to analyze electromagnetic scattering," *Progress In Electromagnetic Research B*, Vol. 27, 21–36, 2011.

The Design of a Novel Quasi-omnidirectional Plannar Metamaterial Absorber

Chao Gu, **Shao-Bo Qu**, **Hua Ma**, **Jia-Fu Wang**, **Hang Zhou**, **Xin-Hua Wang**, **and Lei Lu**
Science College, Air Force Engineering University, Xi'an 710051, China

Abstract— In this paper, a novel quasi-omnidirectional plannar metamaterial absorber is presented. The unit cell of this absorber consists of a front electric resonator, a middle dielectric substrate and a back ring. Simulated S-parameter magnitude and absorbance show that this absorber has strong non-reciprocity absorption at 7.07 GHz. Simulated absorbance values under different polarization angles and different angles of incidence validate the quasi-omnidirectional absorption property of the absorber. Simulated surface currents and power losses at the absorption peak indicate that this absorber is an excellent electromagnetic wave collector: the wave is first trapped and reinforced at certain specific locations, and then mostly consumed. This absorber may have potential applications in devices such as bolometers.

Dual-band, Polarization-insensitive and Wide-angle Terahertz Metamaterial Absorber

Chao Gu, **Shao-Bo Qu**, **Hua Ma**, **Jia-Fu Wang**, **Hang Zhou**, **Xin-Hua Wang**, **and Lei Lu**
Science College, Air Force Engineering University, Xi'an 710051, China

Abstract— We present the design of a dual-band, polarization-insensitive and wide-angle metamaterial absorber in the terahertz regime. Theoretical and simulated results show that the absorber has two strong absorption peaks at 1.98 and 2.35 THz, which are polarization-insensitive, wide-angle and consistent with "fingerprints" of some explosives. The retrieved real parts of the impedance indicate that the impedance of the absorber could be tuned to match approximatively the impedance of the free space on the one side and do not match to the impedance of the free space on the other side at the two absorption peaks, resulting in the minimal reflectance, the minimal transmission and the highest absorbance. The simulated absorbance values under three different loss conditions indicate that high absorbance values at the two absorption peaks are collaborative effects of metallic absorption of the metal and dielectric loss of the substrate. This dual-band absorber may have potential applications in detection of explosives.

Effect of the Three-dimensional Wideband Antenna on Plane Wave Distribution

Feng Lu, **Li-Yuan Su**, **Li-Hua Shi**, **Yan-Xin Li**, **and Bi-Hua Zhou**
Engineering Institute of Corps of Engineers
PLA University of Science and Technology, Nanjing 210007, China

Abstract— In order to measure the electromagnetic field of three-dimensional (3-D), a three-dimensional (3-D) wideband antenna for transient electric field measurement is designed shown as Fig. 1.

All parts and its function of the three-dimensional (3-D) wideband antenna are analyzed. In the experiment, we are often concerned with the effect of the antenna on electromagnetic wave distribution. In order to simplify analysis, we assume that the electromagnetic wave is plane wave.

In this paper, the method of moment is used to model the effect of the antenna on plane wave distribution. In the numerical model, the angle of propagation is changed and the size of the antenna is also changed. From the numerical result, we find the law of effects of the antenna on plane wave distribution. At the same time, this work will offer theory direction of the antenna's optimized design.

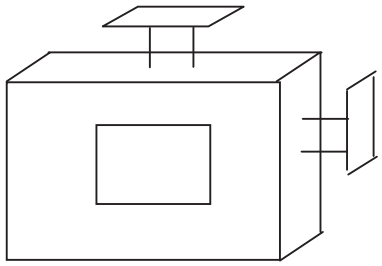

Figure 1: Three-dimensional (3-D) wideband antenna.

Sensitivity Analysis of Eddy Current Sensors Using Computational Simulation

R. Neugebauer[1], **W.-G. Drossel**[1], **P. Mainda**[1], **H.-J. Roscher**[1], **K. Wolf**[1], **and M. Kroschk**[2]

[1]Fraunhofer Institute for Machine Tools and Forming Technology IWU, Chemnitz/Dresden, Germany
[2]EAAT GmbH Chemnitz, Germany

Abstract— Eddy current sensors can detect the position and movement of metal parts without direct contact. The magnetic fields of these sensors can penetrate protective metal enclosures when designed and applied appropriately. Thus particularly robust solutions for industrial applications are possible, e.g., tracking objects electrically like conductive or ferromagnetic work pieces (device currently being tested) during a treatment process under difficult production conditions.

The disadvantage of a test set up where the sensor and the tested specimen are surrounded by equipment and enclosures is reduced sensor sensitivity, this combined with different test piece material properties and tolerances adversely influences the measurements. In order to evaluate the performance of an eddy current sensor, a sensitivity analysis for selected measurement frequencies are necessary. Experimental studies on the subject of sensor sensitivity under production conditions are difficult and usually not feasible due to the costs involved.

Therefore, using a virtual 3D model such effects were simulated using the finite element program ANSYS. The sensor output is the phase angle between voltage and current of the sensor coil. The use of the magnetic field strength to determine this phase angle yielded results in accordance with the experimental trends. The problem is the large differences in the geometric dimensions, such as the sensor size compared to effective magnetic air gaps.

Magnetic permeability and electrical conductivity are the relevant parameters for the eddy current sensors. In experimental tests, these parameters were determined, also as a function of temperature.

It was followed by the simulation of the sensor characteristics by varying different parameters affecting the sensor signal. The results obtained with element type SOLID117 were highly dependent on finite element meshing.

But requires significantly less computational effort than an element type SOLID236, which was used to verify selected results based on SOLID117 element type.

The result of the simulations is the influence of the considered parameters on the achievable accuracy in the detection of the device under test during the process of machining, individually or in combination.

An Effective Formulation Based on Approximated Electromagnetic (EM) Mathematic Models of Feed Antennas to Efficient Estimate the Performances of Rotationally Symmetric Parabolic Reflector Antennas

Shih-Chung Tuan[1] **and Hsi-Tseng Chou**[2]

[1]Department of Communication Engineering, Oriental Institute of Technology, Pan-Chiao, Taiwan
[2]Department of Communication Engineering, Yuan Ze University, Chung-Li 320, Taiwan

Abstract— In this paper, an effective formulation based on approximated electromagnetic (EM) mathematic models of feed antennas is developed to efficiently estimate the performances of rotationally symmetric parabolic reflector antennas including spillover and aperture efficiencies. The EM mathematic models employ cosine and sine functions with fractional powers to approximate the co-polarized and cross-polarized components of the fields radiated from the antennas to feed the reflectors, where the closed-form solutions of antenna performances are then obtained. In distinguishing from previous works where only cosine tapers with integer powers are employed to model the co-polarized components of feed's radiation with the cross-polarized components ignored, the present work is a broad extension and provides tremendous flexibility in the modeling of realistic feed antennas. Furthermore it allows one to estimate the impact on the antenna performance due to the existence of cross-polarized components, which had been previously ignored for a feed antenna with an ideal radiation pattern. Numerical examples are presented to demonstrate the analysis.

Stabilizing the Method of Moments for Dielectrics Using a Combined Charge and Current Formulation of the EFIE

J.-W. De Bleser, E. Van Lil, and A. Van De Capelle
ESAT, Katholieke Universiteit Leuven, Belgium

Abstract—

Introduction: The standard *Electric Field Integral Equation*, used in finding a full-wave solution to Maxwell's equations, is known to suffer from instability at low frequencies [1]. This is due to charge being eliminated from the equation via the Lorenz gauge, introducing a $1/\omega$ dependency. A possible solution for closed surfaces would be to explicitly calculate both charge and current using both incident fields. This has so far worked well for perfect conductors, so we now seek to apply it to more general materials.

Theory: The basis of this technique originates in (1) and the corresponding magnetic field equation, derived from Maxwell's equations extended with magnetic charges ρ_m and currents $\bar{J}_m$. Together with appropriate boundary conditions, they can be used to calculate the equivalent charge and current on the dielectric surface, and from these the fields in both media can be calculated. By explicitly including the charges ρ_e and ρ_m we avoid introducing a $1/\omega$ dependency, eliminating one source of instability. To implement this, appropriate basis and testing functions are required, as is a method for handing the integration of the green's functions.

$$\bar{E} = \frac{1}{\epsilon}\nabla \times \bar{A}_m(\bar{J}_m) - \nabla\phi_e(\rho_e) - \frac{d}{dt}\bar{A}_e(\bar{J}_e) \tag{1}$$

Results: The PEC code has successfully been verified with various different types of computations applied to a sphere and compared to analytical solutions. The dielectric extension is now being verified and has so far been tested for a static electric field. Figure 1 shows a first set of results. The equivalent surface charge and current distributions in Figure 1(a) closely match the analytical solutions. Figures 1(b) and 1(c), a plot of the azimuthal component of the total field and of the radial component of the total displacement field respectively, show that the boundary conditions are respected up to around one scale length of the mesh. The method is clearly stable at low frequency.

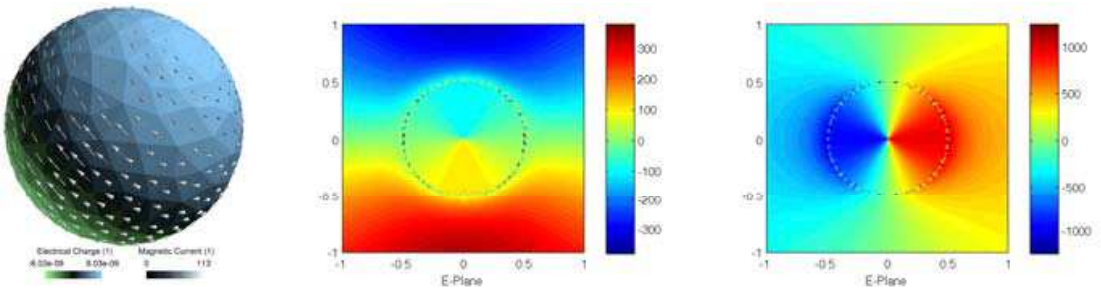

(a) (b) (c)

Figure 1: Simulation at DC of a $r = 0.5\,\mathrm{m}$ sphere with $\epsilon_r = 9$ and $E_0 = \eta_0$. (a) $\bar{J}_m$ and ρ_e. (b) Azimuthal $\bar{E}_{total}$. (c) Radial $\bar{D}_{total}$.

ACKNOWLEDGMENT

This research was funded by a Ph.D. grant from the IWT, the *Agency for Innovation through Science and Technology*, Belgium.

REFERENCES

1. Adams, R. J., "Physical and analytical properties of a stabilized electric field integral equation," *IEEE T. Antenn. Propag.*, Vol. 52, No. 2, 362–372, 2004.

Electromagnetic Properties at Millimeter Wavelength Range of Diamond Films Grown by DC arc Plasma Jet Technique

B. M. Garin[1], **V. V. Parshin**[2], **E. A. Serov**[2], **Ch. Ch. Jia**[3], **W. Z. Tang**[3], **and F. X. Lu**[3]

[1]Institute of Radio Engineering and Electronics of Russian Academy of Sciences, Fryazino Branch
1, Vvedensky Sq., Fryazino, Moscow Region 141190, Russia
[2]Institute of Applied Physics of Russian Academy of Sciences
46, Ulianov Str., Nizhny Novgorod 603950, Russia
[3]Beijing University of Science and Technology, 30, Cellege Str., Beijing 100083, China

Abstract— The diamond sample was prepared by using a DC arc plasma jet technique [1], operated under a gas-recycling mode. The flow rates of the gases H2 and CH4 were 8 L/min and 3 L/min, respectively, and the recycled portion of the gases amounted to about 90%. The voltage and current of the DC arc were 100 V and 130 A, respectively, and the deposition rate of the sample was about 10 mkm/hour. After the deposition, the sample was mirror-polished mechanically from the both sides. The disc is of diameter 18 mm and thickness 0.316 mm. The sample is transparent, but with a gray color. The in-plane thermal conductivity of the sample at room temperature, measured by photothermal deflection technique, is about 19 W/cm · K, that is closely to the highest possible in diamond (20–22 W/cm · K). It means that inner structure is rather perfect.

The refractive index and loss tangent of the sample were measured using a Fabry-Perot resonator with a high Q-factor (Q $\sim 10^6$) [2]. The measurements were made at the "resonant" frequency (201 GHz) of the disk when the disk optical thickness is equal to half-wavelength. The measured loss tangent is $\tan\delta = 3\cdot 10^{-3}$. The estimated accuracy of tan measurements is 10% for such disc. The measured refraction index was found from the measured resonant frequency of the dielectric plate: $n = 2.354(\pm 0.002)$. It differs essentially from the value previously measured in big set of CVD diamonds where $n = 2.380(\pm 0.001)$ (the later is near to the value for monocrystalline diamond). On the other hand a significant increasing of loss tangent with the frequency is observed relatively to $\tan\delta \sim 2\cdot 10^{-4}$ at 35 GHz (measured by a cylindrical cavity method).

The studied sample essentially differs from CVD diamonds studied earlier. In particular:

1. The refractive index is essentially less compared with usual CVD diamonds. It means that the density of sample is less. It combines with absence of big internal cavities. The latest can give additional advantage at terahertz (THz) range due to less scattering of electromagnetic wave.
2. The relative transparency combines with high deposition rate: 10 mkm/hour compared with 2–3 mkm/hour for usual high quality CVD diamonds.
3. The loss tangent increases with frequency whereas it decreases in usual CVD diamonds. It corresponds to the mechanism of loss induced by lattice disorder [3]. Whereas in usual CVD diamonds the loss in MM range is due to electric conductance in intergranular regions [4].

Such material is perspective for diamond coated copper-diamond composites in the high power electronics at MM and THz ranges.

REFERENCES

1. Lu, F. X., et al., "Large area high quality diamond film deposition by high power DC arc plasma jet operating at gas recycling mode," *Diamond and Related Materials*, Vol. 10, 1551, 2001.
2. Dryagin, Y. A. and V. V. Parshin, "A method to measure dielectric parameters in 50.5 mm wavelength band," *International Journal of Infrared and Millimeter Waves*, Vol. 13, No. 7, 1023–1032, 1992.
3. Garin, B. M., "One-phonon dielectric c losses by excitation of sound," *Sov. Phys. Solid State*, Vol. 32, No. 11, 1917–1920, 1990.
4. Garin, B. M., V. V. Parshin, S. E. Myasnikova, and V. G. Ralchenko, "Nature of millimeter wave losses in low loss CVD diamonds," *Diamond & Related Materials*, Vol. 12, No. 10–11, 1755–1759, 2003.

Calculation and Analysis of the Coupling Effects of High Voltage Transmission Lines in Joint-use Corridors Shared by Multi-systems

Jun Zhu, **Guangning Wu**, **Xiaobin Cao**, **Zihui Zhao**, **and Li Chen**
School of Electrical Engineering, Southwest Jiaotong University, China

Abstract— With the rapid development of economy and society, joint-use corridor shared by multi-system such as high voltage transmission lines, metal pipes, communication lines and railways has the characteristic of saving land, which is occupied by power, communication, transportation and energy transport systems. Meanwhile, in order to meet energy demand, the ultra-high voltage (UHV) transmission lines are gradually put into use, leading to the load current and fault current of transmission lines in joint-use corridors increased significantly. The investment of UHV transmission lines exacerbate the coupling effects between transmission lines and the interaction on each system in joint-use corridors, and the electromagnetic interference threatens the stability and reliability of each system in the corridors. In order to ensure each system operating safely in the corridor, many countries have started research work and have developed regulations and standards. In China, researchers mainly study on the coupling effects between AC and DC transmission lines, but only concerning parallel and infinitely long transmission lines. The research is very little for non-parallel/oblique approach and finitely long transmission lines. However, in practice, high voltage transmission lines in joint-use corridor are often constructed in the above situation. So it is necessary to study on the coupling effects of high voltage transmission lines which are constructed in various situation.

In this paper, first electromagnetic coupling mechanism between transmission lines in common corridor will be reviewed. The influence parameters such as length of parallel lines, distance between transmission lines, height of conductors are investigated. Then, coupling effects between AC and DC transmission lines which are parallel will be discussed. And a typical example is operated to analyze induced voltage and current on the maintenance line. At last, a new method will be proposed to calculate induced voltage and current on the transmission lines, which are non-parallel/oblique approach.

Design of Waveguide Filter with Rectangular Irises in Cylindrical Cavities

Uma Balaji
Electrical Engineering Technology, Farmingdale State College, Farmingdale, NY 11735, USA

Abstract— The filter described in this paper is composed of rectangular irises of finite thickness as a junction between two cylindrical cavities. Although closed form solutions for the susceptance of such junctions are available in literature this paper uses Mode matching method to analyze the discontinuity for scattering parameters. The filter which is composed of many such discontinuities is analyzed by cascading the scattering matrices of individual discontinuity.

The analysis of rectangular iris of finite length to a cylindrical cavity is based on the analysis of scattering at the junction of a smaller rectangular waveguide to a larger circular waveguide. The fields in the rectangular waveguide of this discontinuity are expanded in terms of the fundamental and higher order TE and TM modes with sinusoidal basis functions in rectangular coordinate system. In the larger circular waveguide the fields are expanded in terms of the fundamental and higher order TE and TM modes with basis functions that are product of Bessel functions with sinusoidal functions in cylindrical coordinate system. These functions are later expanded in terms of a series of complex exponential function in Cartesian coordinate system for the purpose of field matching. The mode matching method involves matching the tangential components of electric and magnetic field at the discontinuity. This is followed by using the principle of orthogonality of modes to arrive at set of equations that relate the incident field of unknown co-efficient on either sides of the discontinuity. The equations are rearranged and manipulated to obtain the generalized scattering matrix of the discontinuity. The generalized scattering matrices are cascaded to obtain the characteristic of the filter.

The filter that is described in this paper uses rectangular waveguide for input and output although the cavities are cylindrical. Hence the first discontinuity in the filter is from a larger rectangular waveguide to a smaller rectangular waveguide that forms the first iris. This type of discontinuity is also analyzed using mode matching method. The irises in the filter are arranged such that the discontinuity is symmetric all through the filter. This allows for applying symmetry in the analysis. Sufficient higher order modes have been used in the analysis of the discontinuity by testing for convergence of the scattering parameters. The filter has been designed and optimized in order to obtain the desired performance.

Design of the Wide Stopband CPW Bandpass Filter Using Cross Shaped Resonators

Jin-Sup Kim and Kyu-Bok Lee
Wireless Communication Research Center, Korea Electronics Technology Institute, Republic of Korea

Abstract— The wide-stopband CPW (Coplanar Wave Guide) filter is proposed and implemented using cross shaped resonators. The proposed filter is realized in double-sided structure, of which the top side provides the main filtering characterisitics by employing two coupled resonators. After optimization of this filter, a good bandpass behavior with transmission poles is theoretically realized and experimentally confirmed. Suppose the LCP (Liquid Crystal Polymer) substrate is flexible and it can be bent toward arbitrary angles. The measured response of the proposed CPW bandpass filter is shown in Figure 1. To validate the above design approach, the proposed filter was fabricated on LCP substrate with relative dielectric of 2.9 and thickness of 100 µm. The frequency response is specified with a pass band of 2.4–2.5 GHz, and with less than 1.5 dB insertion loss and more than 22 dB return loss. Its stopband is extended up to 40 GHz with an rejection greater than 23.25 dB.

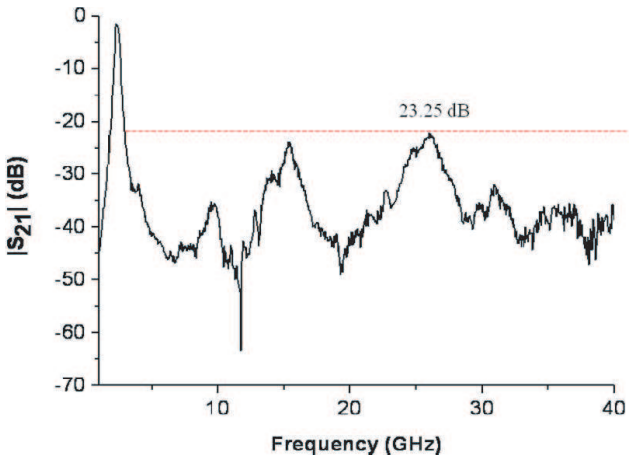

Figure 1: Measured response of the proposed CPW bandpass filter.

A CMOS Doubly Balanced Monolithic Passive Star Mixer with a Compact IF Extraction

Yi-Chang Lee, **Shih-Han Hung**, **Chih-Ming Lin**, **and Yeong-Her Wang**
Department of Electrical Engineering, Institute of Microelectronics
National Cheng-Kung University, No. 1 University Road, Tainan 701, Taiwan

Abstract— In order to make a star doubly balanced mixer (DBM) more compatible with conventional MMICs, many topologies have been proposed. However, the configurations of the previous star mixers were mostly based on a pair of symmetrical dual baluns, which may still have larger circuit dimensions. To overcome this problem, attention has been drawn to the design of miniature dual baluns using a new miniature dual balun. However, the DBM design still has a critical issue of IF extraction. For this reason, a novel configuration of doubly balanced passive mixer with a small chip size fabricated in a 0.18 µm CMOS process utilizes a LO spiral balun and a meandering RF dual balun to simplify the architecture of the conventional star DBM, while simultaneously satisfy the mixing mechanism of the star mixer is proposed. The proposed configuration is more compact in layout design and also more effective in improving the mixer's performance as compared to the conventional DBMs. Particularly, the RF dual balun formed with multiple coupled-line can not only excite the RF signal with a 180° relative phase difference into diodes, but provide an output port for IF extraction. It can be viewed the overall structure is symmetric, and the terminals of four outside strip-lines were connected together to construct an IF port. A major consideration in the design of the dual balun is the enhancement of the isolation between RF and IF port, which avoids the leak of RF signal from IF port, and vice versa. Owing to the anti-phase relationships of the RF signal, the IF port presents a virtual ground to the RF port. This intrinsic feature leads into the outside coupled-line of the dual balun to form a band-pass filter. Accordingly, it provides a transmission path for the RF signal. The proposed dual balun retains the native property, as well as includes the IF extraction circuit with inherence isolation. Furthermore, this work presents the meandering RF dual balun and the LO spiral balun, which employ a metal shielded transmission line in CMOS technique so as to surmount the lossy nature of silicon substrate, and achieve the miniaturized necessity.

From the measured results, the fabricated DBM exhibits wideband performance, superior isolations and high dynamic range. Performance enhancement and flexible layout design were possible with the proposed baluns as well, including IF extraction techniques. Owing to the utilization of the new 180° hybrid in the CMOS passive DBM provides the widest IF bandwidth of 18 GHz and smallest chip size of $0.4 \times 0.54\,\mathrm{mm}^2$, but maintains superior isolations and high linearity.

A Miniature 18–38 GHz pHEMT MMIC Frequency Doubler

W.-C. Chien[1], **C.-H. Liu**[2], **S.-H. Hung**[1], **Y.-C. Lee**[1], **and Y.-H. Wang**[1, 2]

[1]Institute of Microelectronics, Department of Electrical Engineering
National Cheng-Kung University, No. 1 University Road, Tainan 701, Taiwan
[2]Institute of Electro-Optical Science and Engineering
National Cheng-Kung University, No. 1 University Road, Tainan 701, Taiwan

Abstract— A compact 18–38 GHz frequency doubler is proposed and implemented using a 0.15 µm pHEMT technology. The circuit configuration is composed of a spiral balun, two common-source transistors, and a band pass filter, which are integrated with a bias and a dc-isolated capacitor. Two identical common-source configurations, which act as the doubler, and the bias circuits, are integrated in the planar spiral balun and the band pass filter. The planar spiral balun and the band pass filter are connecting to the gate and the drain of the transistor, respectively. The dc-isolated capacitor was used to ensure the gate bias return path between the transistor and the balun. Further, the two pHEMT transistors were operated in the class-B region to achieve higher second harmonic signal than the class-A region and good fundamental frequency rejection because of the balanced topology. The topology of the doubler can thus be simplified to reduce the use of the bias components, such as the inductor. The compact configuration with core chip size of 0.847×0.59 $(0.5)\,\mathrm{mm}^2$ can then be achieved. The measurements were performed under the balanced transistors, which were biased for maximum second harmonic output and optimum flatness of output power. The pHEMT devices were operated under a drain voltage of 1.7 V and a gate voltage of −1.1 V. As the measured results show, the fabricated frequency doubler shows a broad bandwidth of 71.4%, with the conversion loss between 0.5 to 5 dB at input frequency of 9 to 19 GHz The conversion gain was relatively high even without a buffer amplifier. In a similar frequency range, the pHEMT doubler shows competitive performance as compared with other reported pHEMT MMIC doublers. It is possible for this pHEMT doubler, with smaller chip size, better fundamental rejection ratio, and higher output power compared with those of previous works, to be fabricated.

Investigations on the Design of All-dielectric Frequency Selective Surfaces

F. Yu[1], **S. B. Qu**[1, 2], **Z. Xu**[2], **J. F. Wang**[1], **Y. M. Yang**[1], **X. H. Wang**[1], **H. Zhou**[1], **and Y. Q. Li**[1]

[1]Department of Mathematics and Physics, College of Science
Air Force Engineering University, Xi'an, Shaanxi 710051, China
[2]Electronic Materials Research Laboratory, Key Laboratory of the Ministry of Education
Xi'an Jiaotong University, Xi'an, Shaanxi 710049, China

Abstract— Metallic parts are indispensable to traditional frequency selective surfaces. However, for millimeter waves, because of surface wave skin effect, the loss of metal-containing FSS is so large that the performance is badly affected. Besides, metal materials are quite unfavourable for high-temperature resistence and corrosion-resistant requirements. Based on the Mie scattering theory and dielectric resonant characteristics, all-dielectric metamaterials frequency selective surfaces were proposed. The article adopt different dielectric constants and different period dielectric structure to achieve desired frequency selective properties.

The Design of A Broad Band Third-order Frequency-Selective Surfaces

Yuqing Li[1], **Zhiping Pei**[1], **Shaobo Qu**[1, 2], **Zhuo Xu**[2], **Jiafu Wang**[1], **Hang Zhou**[1], **Chao Gu**[1], **and Fei Yu**[1]

[1]College of Science, Air Force Engineering University, Xi'an 710051, China
[2]Electronic Materials Research Laboratory, Key Laboratory of Ministry of Education
Xi'an Jiao-Tong University, Xi'an 710049, China

Abstract— In view of high order band-pass frequency selective surface (FSS) has the advantages of stable performance, flat passband and low insertion loss, we proposed a third-order FSS in this paper.

The proposed FSS is composed of four metallic layers separated from one another by three dielectric layers. Numerical results show that such FSS has a third-order response which leads to a quite flat, smooth passband and very low insertion loss. Its 3 dB bandwidth is about 6.75 GHz and relative bandwidth is 43%. Moreover, the FSS keep stable performance under different incident angles and polarization states. The FSS owns its advantages to these merits, which is suitable for modern communication, hybrid-radomes, etc.

Versatile DVCC-based Universal Voltage-mode Biquadratic Filter

Hua-Pin Chen, Yen-Hung Lin, Wen-Hsuan Wu, and Chun-Lin Li
Department of Electronic Engineering, Ming Chi University of Technology, Taiwan, R.O.C.

Abstract— This paper introduces a versatile DVCC-based universal voltage-mode filter with three inputs and three outputs. The proposed circuit employs two differential voltage current conveyors as active elements together with two grounded capacitors and two resistors. Either applications two-input three-output or three-input single-output can be realized in the same configuration. It is more versatile than the universal one with single input and three outputs or the universal one with three inputs and single output. In the operation of two-input three-output, the lowpass, bandpass highpass and bandreject can be realized simultaneously. In the operation of three-input single-output, the lowpass, bandpass, highpass, bandreject and allpass can be realized from the same configuration without any inverting-type voltage input signals or double input voltage signals. The proposed circuit maintains the following advantages: (i) the employment two grounded capacitors ideal for integrated circuit implementation, (ii) no need to impose component choice, (iv) no need to employ inverting-type voltage input signals, and (v) low active and passive sensitivity performances. HSPICE simulations with TSMC 0.18 μm 1P6M CMOS technology and 0.9 V supply voltages to verify the theoretical results.

High-input Impedance Tunable Voltage-mode Multifunction Biquadratic Filter Using All-grounded Passive Elements

Hua-Pin Chen, **Shih-Hsuan Yuan**, **Wei-Yen Huang**, **and Yu-Hsin Lin**
Department of Electronic Engineering, Ming Chi University of Technology, Taiwan, R.O.C.

Abstract— This paper introduces a high-input impedance tunable voltage-mode multifunction biquadratic filter. The proposed biquadratic filter with single input and five outputs employing two active components and all grounded passive elements. The circuit is very simple, consisting of one single-output differential difference current conveyor (DDCC), one dual-output inverting second-generation current conveyor (ICCII), three grounded resistors and two grounded capacitors. The filter can realize highpass, bandpass and lowpass filtering responses, simultaneously. It is widely used in various parts such as communication, measurement, instrumentation and control system. The proposed circuit offers the following advantages: (i) using grounded capacitors attractive for integration and absorbing shunt parasitic capacitance, (ii) using grounded resistors at X terminal of DDCC/ICCII suitable for the variations of filter parameters and absorbing series parasitic resistances at X terminal of DDCC/ICCII, (iii) high input impedance good for cascadability, (iv) no need to change the filter topology, (v) no need to component-matching conditions, (vi) orthogonal tunable of the resonance angular frequency and quality factor, and (vii) low active and passive sensitivity performances. HSPICE simulations with TSMC 0.18 μm 1P6M CMOS technology and ±0.9 V supply voltages to verify the theoretical results.

Versatile CCII-based Universal Current-mode Biquadratic Filter

Hua-Pin Chen, **Kai Chen**, **Chun-Yeh Chen**, **and Ming-Shan Chen**
Department of Electronic Engineering, Ming Chi University of Technology, Taiwan, R.O.C.

Abstract— New versatile universal current-mode filter with three inputs and three outputs using three multiple-output second-generation current conveyors, two grounded resistors and two grounded capacitors is proposed. Either applications single-input three-output or three-input single-output can be realized in the same configuration. It is more versatile than the universal one with single input and three outputs or the universal one with three inputs and single output. Unlike the previous1y works, it is highly flexible and easy to design. In the operation of single-input three-output, the lowpass, bandpass and bandreject can be realized simultaneously while the highpass and allpass responses can be easily obtained by connecting appropriated output currents directly without using additional stages. In the operation of three-input single-output, the lowpass, bandpass, highpass, bandreject and allpass can be realized from the same configuration without any inverting-type current input signals or double input current signals. The proposed circuit maintains the following advantages: (i) the employment two grounded capacitors ideal for integrated circuit implementation, (ii) high output impedance good for cascadability for the current-mode circuits, (iii) no need to impose component choice, (iv) no need to employ inverting-type current input signals, and (v) low active and passive sensitivity performances. HSPICE simulations with TSMC 0.18 µm 1P6M CMOS technology and ±0.9 V supply voltages to verify the theoretical results.

Sensitivity of Fabry-Perot Resonator Based Measurements of Gas Absorptions

P. Piksa, **S. Zvanovec**, **and P. Cerny**
Department of Electromagnetic Field, Czech Technical University in Prague, Czech Republic

Abstract— Microwave high-resolution spectroscopy provides the basic experimental data for molecular physics [1, 2]. The microwave measurements then unable to resolve standardly the hyperfine structures of rotational lines. Joint research teams of Department of Electromagnetic Field of the Faculty of Electrical Engineering of the Czech Technical University and Laboratory of High-Resolution Molecular Spectroscopy at the Department of Analytical Chemistry of the Institute of Chemical Technology, Prague are equipped with two millimeter/submillimeter wave spectrometers operating in the spectral intervals from 50 to 600 GHz [3] and from 20 to 120 GHz [1], respectively, for absorption and emission spectra measurements. A new spectrometer based on time-domain Fourier transform is developed within the frame of above mentioned cooperation for a sensitive detection of the rotational free induction decay following polarization by the short pulse.

A Fabry-Perot interferometer is very common tool enabling an enhancement of the sensitivity of the absorption as well as emission measurements in the region of microwave spectroscopy [1] especially due to an apparent lengthening of the optical path length by means of multiple reflections. In order to reach maximum sensitivity of gas attenuation measurements and to propose optimal parameters of the new developed spectrometer, the coupling characteristics of several resonator based measurement approaches were analyzed. Three types of millimeter wave resonator deployments were investigated — the first based on a radial feeding of a resonator cavity, second one using axially alignment feeding with two ports (transmission measurement) and the last having one axial port feeding (reflection measurement method). Based on both analytically derived relations and results form simulations, the optimal setting of coupling will be proposed in the paper. Analytical results covering a wide range of couplings were validated by spectroscopic measurements of particular gases attenuations.

REFERENCES

1. Zvánovec, S., et al., "The use of the Fabry-Perot interferometer for high resolution microwave spectroscopy," *Journal of Molecular Spectroscopy*, Vol. 256, 141–145, 2009.
2. Townes, C. H. and A. L. Schawlow, *Microwave Spectroscopy*, Dover Publications, New York, 1975.
3. Kania, P., et al., "Pressure shifts of acetonitrile ground state parameters," *Journal of Molecular Structure*, Vol. 795, 209–218, Aug. 21, 2006.

Microstrip Diplexer Using High Permittivity Substrate

C.-H. Hsu[1], **H.-H. Tung**[1], **C.-K. Hsu**[1], **J.-S. Lin**[2], **and H.-W. Yang**[3]

[1]Department of Electrical Engineering, National United University, Taiwan
[2]Department of Mechanical Engineering, National United University, Taiwan
[3]Department of Materials Science and Engineering, National United University, Taiwan

Abstract— A planar microwave diplexer with using cross-coupled compact hairpin filter is proposed. Miniaturization hairpin resonator is realized by using an interdigital structure having parallel coupled lines. The full-wave simulator IE3D is used to design the interdigital hairpin resonator, and to calculate the coupling coefficient of the basic coupling strictures. The response of the fabricated diplexer using $(Mg_{1/2}Co_{1/2})Al_2O_4$ substrate is designed at a GSM/DSC system. The compact size and the performance of this class of diplexer have been demonstrated.

A Broadband Balun Using Meander Line

C. F. Tseng and S. C. Lu
Department of Electronic Engineering, National United University, Taiwan

Abstract— In this study, a broadband branch-line balun with meander lines is presented. It is implemented by using meander line structure to improve the size and performance of the conventional branch-line balun. The parametric analysis of the proposed balun is carried out using the available electromagnetic solver IE3D. Using the meander line structure, experimental measurements show that the fabricated balun has an amplitude imbalance of 0.09 dB and a phase imbalance of 0.24° operation at 1.98 GHz. Moreover, the proposed balun is found to occupy only 58% of the conventional branch-line balun's area.

A Novel Multilayer Dual-mode Substrate Integrated Circular Cavity (SICC) Filter with Power Divider

Zhigang Zhang, **Yong Fan**, **and Yonghong Zhang**
Extreme High Frequency Key Laboratory, School of Electronic Engineering
University of Electronic Science and Technology of China, Chengdu, China

Abstract— A novel millimeter-wave multilayer dual-mode filter with power divider is developed based on the substrate integrated waveguide circular cavity (SICC). The novel dual-mode SICC filter/power divider with arc-shaped coupling slots has been designed for Ka-band application. The multilayer dual mode filter/power divider has been firstly realized only by adjusting arc-shaped coupling slots located in metal layers.

Simulated results show that excellent impedance matching at all three ports, amplitude and phase balance at the two output ports, and out-of-band rejection are observed at the operating band. Meanwhile, it is possible to control the return loss, bandwidth and rejection level by adjusting the size of the coupling slots. This novel filter/power divider is very compact and has the advantages of return loss, very low insertion loss, high selectivity.

Design of a Bandpass Filter Using Parallel Coupled Stepped Impedance Resonator Using the Novel Method of Lines

Eman G. E. Ouf[1], **Hossam A. Saker**[1], **Esmat A. F. Abdallah**[1], **and Hadia M. El-Hennawy**[2]

[1]Microstrip Department, Electronics Research Institute, Egypt
[2]Electronic and Communication Department, Ain Shams University, Egypt

Abstract— The main objective of this paper is to design and analyze a filter at 4 GHz, with bandwidth of 200 MHz to be used in a portable transceiver system. The filter should have short length and suppression of first harmonic to obtain a wide stopband. The analysis is applied using the novel method of line. Also, this analysis is developed by nonequidistant discretization to reduce the discretization window. Based on this algorithm, bandpass filters using parallel coupled stepped impedance resonators are designed and examined. Also, a bandpass filter using the conventional parallel coupled line was designed and examined by this algorithm, to be our reference for comparison. The bandpass filter using parallel coupled stepped impedance resonator was fabricated using thin film technology and photolithographic technique, where good agreement is found between the numerical and experimental results. The filter length is reduced by about 23% compared to the conventional one and the first harmonic was attenuated by about 22 dB.

REFERENCES

1. Hunter, I., *Theory and Design of Microwave Filters*, 201–212, Electromagnetic Wave, IEE Press, 2001.
2. Song, K., Y. Z. Yin, X. Yang, J. Y. Deng, and H. H. Xie, "Compact LPF with pair of coupling slots for wide stopband suppression," *IEEE Electronics Letters*, Vol. 46, No. 13, Jun. 2010.
3. Makimoto, M. and S. Yamshita, "Compact bandpass filters using stepped impedance resonators," *Proc. IEEE*, Vol. 67, 16–19, Jan. 1979.

Design of On-chip Stacked Spiral Inductors with Variable Metal-line Width

Hao-Hui Chen[1], **Ming-Huei Chen**[1], **and Young-Huang Chou**[2]

[1]Department of Electronic Engineering
National Kaohsiung First University of Science and Technology, Kaohsiung, Taiwan
[2]Department of Electronic Engineering, Huafan University, Taipei, Taiwan

Abstract— On-chip spiral inductors (Fig. 1(a)) are particularly essential and extensively used in various radio frequency integrated circuits (RFICs) such as mixers, amplifiers, and oscillators. To facilitate the analysis and design of RFICs, much research has been devoted to the investigation of RFIC spiral inductors. Among these researches, the improvement of the quality factor (Q-factor) of an inductor and the reduction of the spiral layout area are two important design concerns that have received much attention. In general, the Q-factor of an inductor is governed by the losses of the metal strip and substrate. Various techniques have been reported to improve the Q-factor by reducing the metal or substrate loss. One possible approach is the variable line-width design [1]. As shown in Fig. 1(b), this technique modifies a conventional spiral inductor with fixed line width to be the one with the line width increasing from the inner to the outer coils. By narrowing the width of the inner coils, the losses due to the eddy-current on the metal strip, which is induced by the time-varying magnetic flux passing through the metal lines and is significant in the inner coils, can be alleviated. The metal loss is therefore reduced leading to the increase of the Q-factor. On the other hand, an on-chip inductor usually required a relatively large layout area to obtain the desired inductance. The layout area can be reduced by the three-dimensional (3-D) stacked architecture design [2]. The stacked inductor is formed by connecting the spiral metal coils deposited on two (or more) metal layers. It can be treated as a series connection of inductors, and the layout area can be therefore reduced to achieve the same inductance. However, the stacked architecture design can also degrade the Q-factor performance due to the parasitic capacitance between the adjacent metal spirals. In this work, a miniature on-chip stacked inductor with improved Q-factor is proposed. As shown in Fig. 1(c), this design is implemented by connecting the spiral metal coils deposited on the top metal layer and the adjacent lower layer. Such a stacked architecture can save the required layout area for a desired inductance. In addition, the variable line-width technique is utilized to reduce the metal resistance and improve the Q-factor. By adopting the variable line-width technique and stacked architecture design simultaneously, the inductor chip area can be greatly reduced while the Q-factor would be effectively improved. Several Si-based spiral inductors have been tested. The results and the detailed designs will be presented and discussed in the symposium.

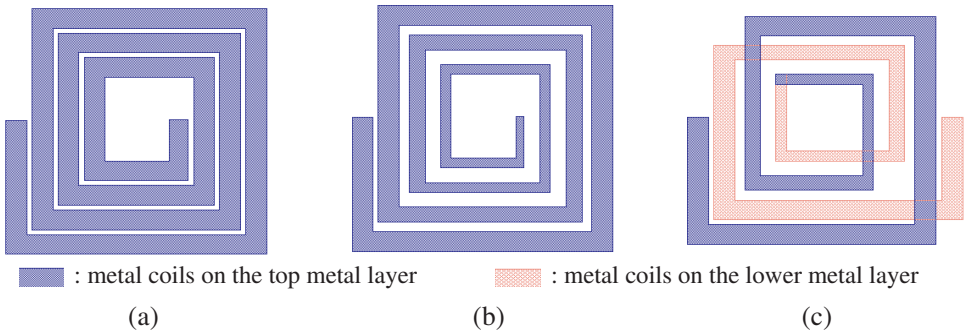

Figure 1: Miniature on-chip inductor design with improved Q-factor: (a) conventional planar spiral inductor, (b) planar inductor with variable line width, and (c) stacked inductor with variable line width.

REFERENCES

1. Hsu, H.-M., "Improving the quality factor of a broadened spiral inductor with arithmetic-progression step width," *Microw. Opt. Tech. Lett.*, Vol. 45, 118–120, Apr. 2005.
2. Zolfaghari, A., A. Chan, and B. Razavi, "Stacked inductors and transformers in CMOS technology," *IEEE J. Solid-State Circuits*, Vol. 36, 620–628, Apr. 2001.

A High-Q CMOS Tunable Notch Filter

Sen Wang and Bo-Zong Huang
Department of Electronic Engineering, National Taipei University of Technology, Taipei, Taiwan

Abstract— A high-Q CMOS tunable notch filter incorporating a semi-passive inductor is presented in this paper. The semi-passive inductor uses a tapped-inductor feedback to achieve a negative resistance, and then compensate the resistive losses of the inductor. Compared with conventional transformer feedback architectures, the proposed technique not only compensates resistive losses with low-power consumption but also provides a high-inductance inductor. The simulated peak Q of the semi-passive inductor based on a standard 0.18 µm CMOS process is about 150 at 9.7 GHz, and the Q factor at 7 GHz is above 50 which is further applied to a notch filter design. The notch filter can be operated from 6.84 GHz to 7.86 GHz with 1.02 GHz tuning range, and the Q factors of the filter with less than 1.2 mW power consumption are above 240 demonstrating a good notching performance. The feasibility of the proposed semi-passive inductor is believed that it is well suited for further practical RF designs such as bandpass filters or VCOs.

Novel Millimeter-wave Power Combining Utilizing Wafer Level Packaging Technology

Yingqian Huang, **Xinyi Hu**, **Jinfang Zhou**, **Zhiguo Shi**, **and Kangsheng Chen**
Department of Information Science & Electronic Engineering, Zhejiang University, Hangzhou, China

Abstract— It is extremely difficult to obtain high output power with silicon based processes, which presents one of the greatest challenges for realizing fully integrated transceivers, especially at millimeter-wave frequencies. For this reason, various power combining methods have been proposed to achieve higher power levels.

In this paper, a novel power combining method suitable for millimeter-wave applications is presented. The power combining network is synthesized in package utilizing wafer level packaging technology, with an array of power sources of moderate output power capability assumed to be distributed on chip, which means applying further combining in addition to existing on-chip power combining scheme for potentially even higher output power is possible.

The power combining network is composed of more basic power combining units, each consisting of one substrate integrated waveguide (SIW) resonator coupling four λ-4 standing-wave resonators, which can be synthesized using two quarter-wavelength vertical vias with one end open and the other end shorted. For power combining purpose, the open end of each λ-4 resonator is connected to the differential output of one on-chip power source, while the shorted end is realized using one of the two metal plates of the SIW resonator. The coupling between the SIW resonator and λ-4 resonators is through slotting on the metal plate to allow magnetic leakage so that oscillation in λ-4 resonators will excite the SIW resonator to oscillate. As the quality factor of the SIW resonator is much larger than those of λ-4 resonators, energy is mainly confined in the cavity of the SIW resonator so that power combing is achieved.

Example design for 60 GHz application is detailed in the paper with simulation results using commercial CST software showing the effectiveness of the power combining method.

Input Signal Distribution Using Coupled $\lambda/2$ Standing-wave Oscillators for Coherent Power Combining

Yingqian Huang, **Xi Zi**, **Jinfang Zhou**, **and Kangsheng Chen**
Department of Information Science & Electronic Engineering, Zhejiang University, Hangzhou, China

Abstract— One of the key challenges to realize a fully integrated transceiver using silicon based processes is the limited output power achievable, especially at millimeter-wave frequencies. Higher output power can be obtained by using various power combining schemes, which typically sum the output power of N identical amplifying stages coherently. Thus to ensure efficient power combining, the input signal must be distributed to all the amplifying stages on the chip with equi-phase and equi-magnitude. While Wilkinson power splitter has been employed for this purpose in the literatures, it becomes bulky and inefficient when N is large, which severely limits the number of outputs that can be combined.

In this paper, a network of coupled λ-2 standing-wave oscillators is employed to distribute the input signal. Proposed formerly for global clock distribution, theoretically, differential signals of equi-frequency, equi-phase, and equi-magnitude can be obtained by taping onto specific points in the network. It should be noted, however, that the network is especially suited for input signal distribution purpose here, since the specific power combining scheme assumes that a grid of N amplifying stages resides on the chip, which matches to the tap points in a perfect way.

A 30 GHz prototype network comprised of four coupled λ-2 standing-wave oscillators using TSMC 0.18 µm CMOS process has been design. Post-layout simulation results are presented showing that no distinguishable difference in frequency, phase, and amplitude is observed for the multiple output differential signals. The chip has a total area (including pads) of $800 \times 990\,\mu m^2$ and has been submitted for fabrication.

An Investigation of Second-Harmonic Shifting Characteristic of Stepped-Impedance Resonators

S. Theerawisitpong[1], **T. Suzuki**[2], **and Y. Utsumi**[2]

[1]Faculty of Technical Education, Rajamangala University of Technology Thanyaburi
39 Moo 1, Rangsit-Nakorn Nayok Road, Klong Hok, Thanyaburi, Pathumtani 12110, Thailand
[2]Department of Electrical and Electronic Engineering, Nippon Institute of Technology
4-1 Gakuendai, Miyashiro-machi, Minami Saitama-gun, Saitama-ken 345-8501, Japan

Abstract— Microstrip filters is increasingly attention in recent years because of several advantages, such as low cost, compactness, light weight, easy fabrication, and affordability for integrating with surface mount devices (SMDs). Simultaneously, second-harmonic suppression characteristic is also needed for those filters, which can be obtained with stepped-impedance resonator (SIR) technology [1–6]. Second-harmonic frequency of conventional filters using uniform impedance resonator (UIR) is typically at two times of resonant frequency ($2f_0$) but second-harmonic frequency of improved filters using SIR is shifted at three times of resonant frequency ($3f_0$). And, the length of SIR is also shorter than the length of UIR. Thus SIR technology has been widely applied to enables second-harmonic suppression characteristic of compact filters. However, a fact of this characteristic was disregard and was not clearly revealed in any reports.

In our study, second-harmonic frequency shifting of SIR has been investigated with respect to current density, impedance, and equivalent model, which are also compared with that of UIR. In particular, a fact of second-harmonic frequency shifting of SIR has been revealed in this paper, which is very easy to understand why the length of SIR shorter than the length of UIR and how second-harmonic frequency shifted. Furthermore, we also recommend a SIR physical chart which is used to determine the proper dimensions of SIR. By using this chart, the proper length and width of SIR can be easily determined by designing of required second-harmonic location.

Finally, we hope that the beneficial information reported in this paper could be useful for researchers to understand the second-harmonic frequency shifting characteristic of SIR technology.

REFERENCES

1. Kuo, J.-T. and E. Shih, *IEEE Trans. Microw. Theory Tech.*, Vol. 51, No. 5, 1554–1559, May 2003.
2. Lin, S.-C., Y.-S. Lin, and C. H. Chen, *Proc. 35th European Microwave Conference*, 931–934, 2005.
3. Wang, H. and L. Zhu, *IEICE Trans. Electron.*, Vol. E89-C, No. 3, 403–409, Mar. 2006.
4. U-Yen, K., et al., *IEEE Trans. Microw. Theory Tech.*, Vol. 54, No. 3, 1237–1244, Mar. 2006.
5. Kuo, J.-T., et al., *IEEE Trans. Microw. Theory Tech.*, Vol. 55, No. 8, 1747–1755, Aug. 2007.
6. Makimoto, M. and S. Yamashita, *Microwave Resonators and Filters for Wireless Communication: Theory, Design, and Application*, Springer, 2001.

A Novel Bandstop Resonator in Waveguide and Its Application for Suppressing the Spurious Responses with New Advantages to Typical Resonators

S. A. Hassani Gangaraj and M. Tayarani
Department of Electrical Engineering, Iran University of Science and Technology, Iran

Abstract— In this paper, a new structure for bandstop waveguide-type resonators is introduced. Because of the similarity between the shape of this resonator and the Greek letter Φ, this resonator is named Φ- shaped resonator. These resonators are located in the cross section of the waveguide. The direction of the electromagnetic waves and the position of these resonators are studied to obtain a good excitation. Various resonances of these structures are determined. Moreover a circuit model is proposed and the parameters of this model are extracted. As a consequence an array of these resonators is used to design a bandstop filter. The results are simulated with CST Microwave Studio 2009 and a rejection level of almost 35 dB is achieved. Finally, these resonators are used as a solution for suppressing the spurious response of inductive post filters. In this case two methods are examined. In the first method an array of these resonators are cascaded with the total structure of the inductive post filter and in the second method these resonators are located in the spaces between the posts. The results verify the performance of these resonators for suppressing the spurious responses.

Design of an UWB Bandpass Filter Using a Microstrip Five-mode Step-impedance Resonator

Zhewang Ma[1], **Akihito Beppu**[1], **Chun-Ping Chen**[2], **and Tetsuo Anada**[2]

[1]Graduate School of Science and Engineering, Saitama University
255 Shimo-okubo, Sakura-ku, Saitama-shi, Saitama 338-8570, Japan
[2]High-Tech Research Center, Kanagawa University, Japan

Abstract— Microstrip multi-mode step-impedance resonators (SIRs) are small in size and simple in structure for the design and fabrication of UWB filters, and can realize easily fractional bandwidth larger than 100%. Up to date, UWB filters using two-mode, three-mode, and four-mode microstrip SIRs have been reported. However, it is found that these filters using only one SIR failed to realize attenuations large enough in the stopband, and multiple SIRs are required to satisfy FCC's spectrum mask. This results in more complicated design and larger filter size. In this paper, we try to design an UWB bandpass filter by using a microstrip five-mode step-impedance resonator. The target is to realize filter characteristics that can meet FCC's spectrum mask by using only one five-mode SIR. The filter will be then more compact compared with previous UWB filters using cascaded multi-mode SIRs. The resonance characteristics of the microstrip five-mode SIR are investigated first. Then analysis of the equivalent transmission line circuit of the resonator filter is implemented, and a novel equal-ripple response function realizable by this filter is derived, which is expressed by a combination of Chebysheve functions of the first kind. Based on the ideal response function, an efficient optimization algorithm is developed to determine the equivalent circuit parameters and physical dimensions of the filter. An example filter with a midband frequency of 6.85 GHz and an equal-ripple FBW of 105% is designed. The final microstrip filter shows passband return loss better than 12dB, and sharp skirt property that meets FCC's indoor limit favorably.

Novel RF Front-end Module with Power Management Technique by Dynamic Supply

C. I. Lee[1, 2], **Y. T. Lin**[1], **Y. H. Chen**[2], **and W. C. Lin**[1]

[1]Department of Electrical Engineering, National Sun Yat-Sen University, Taiwan, R.O.C.
[2]Institute of Communications Engineering, National Sun Yat-Sen University, Taiwan, R.O.C.

Abstract— Novel RF front-end module consisting of low noise amplifier (LNA), power amplifier (PA), and parallel directed switches in a 0.18-μm CMOS technology is presented. A crucial power management technique with the dynamic supply is utilized in this paper. The novel on-chip class-E PA with a current reuse and double primary transformer (DPTF) structure can reduce the power consumption and maintain the module performance simultaneously. A new pulse bias approach is employed for the PA and the LNA is biased by the DC sources. The transmitter (Tx) and receiver (Rx) modes are controlled by the dynamic supply and parallel directed switches. The narrower signal pulse width can reduce more consumption power in the whole period. Therefore, we analyze the pulse width and bias level influence on the system performance. Furthermore, our low power circuit topologies are also analyzed and applied. The crucial DPTF applied in the PA can significantly increase the power added efficiency (PAE) when the lower DC bias level is applied. The presented LNA with a differential inductor in parallel with the input network can provide the noise matching needed and increase the transducer gain in order to achieve the optimal power consumption and the transducer gain in the Rx mode. The excellent isolation between the Tx and Rx mode is obtained with our new parallel directed switch. The post-simulation result shows the gain, output power, and PAE are 10 dB, 10 dBm and 30%, respectively in the Tx mode. In the Rx mode, this proposed module exhibits the noise figure, gain, and input 1 dB compression point ($IP_{1\,dB}$) are 3 dB, 10 dB, and −16 dBm, respectively.

A Novel Power Management Technique Applied in the Low Power Transceiver

C. I. Lee[1, 2], **Y. T. Lin**[1], **J. J. Chen**[1], **and W. C. Lin**[1]

[1]Department of Electrical Engineering
National Sun Yat-Sen University, Taiwan, R.O.C.
[2]Institute of Communications Engineering
National Sun Yat-Sen University, Taiwan, R.O.C.

Abstract— This paper presents a new power management technique with pulse-driven power supply for a non-contact vital-sign medical monitoring system. The presented radio frequency (RF) front-end module is implemented by the circularly polarized (CP) antenna, single pole double through (SPDT) switch, low noise amplifier (LNA), and power amplifier (PA). The class-E power amplifier by this new pulse-driven method can work well in the transmitter (Tx) mode. All these components are integrated on the printed circuit board (PCB). The proposed structure can achieve only 50% power consumption of the ZigBee system for the green energy application. It is obvious that this structure driven by the narrower pulse width signal can consume much less power in the whole period comparing to the DC power supply. However, the experimental result shows that this pulse bias with extremely short pulse width may cause the severe distortion for this module. Therefore, we need to focus on the optimum design for the whole RF frond-end performance. The front-end module has the gain of 9.5 dB, output power of 9 dBm, and power added efficiency (PAE) of 30% in the Tx mode. For the 1 ms pulse period and 0.1 ms pulse width, the power consumption is 21.8 mW. On the other hand, in the Rx mode, the performance of the architecture exhibits the noise figure of 2.5 dB and gain of 14 dB.

A Low-voltage and Low-power Low Noise Amplifier for Ku-band Application

Cheng-Chi Yu[1], **Jiin-Hwa Yang**[2], **Lien-Chi Su**[1], **Heng-Yi Lee**[1], **and Chang-Chih Chen**[1]

[1]Department of Communications Engineering, Feng-Chia University
100, Wen-Hua Rd., Taichung 407, Taiwan, R.O.C.
[2]Ph.D. Program in Electrical and Communications Engineering
Feng-Chia University, 100, Wen-Hua Rd., Taichung 407, Taiwan, R.O.C.

Abstract— A low-voltage and low-power low noise amplifier (LNA) for Ku-band (12–18 GHz) application is proposed in this paper. The LNA can be used in receiver front-end for Direct Broadcasting Satellite (DBS) system. In order to decrease the power consumption and provide sufficient gain for the LNA at 12–18 GHz operation, a two-stage wide-band amplifier topology is presented in this circuit. In the first stage, a filter type matching network with an on-chip transformer is used as the input matching network for better noise improvement and power matching. The main goals of this stage are to achieve the required bandwidth and reduce the chip area. In the second stage, a current-reused circuit is used to reduce the power consumption. In addition, a series-peaking inductor between the current-reused circuit and output matching network is adopted to improve more flat gain.

The proposed LNA chip is fabricated by a TSMC 0.18 µm CMOS process. The chip occupies a die area of 0.67 mm^2 (0.73 mm $*$ 0.91 mm). On-wafer measurement was used to measure the characteristics of the LNA. The results show that gain (S_{21}) of 10.63 $\sim$ 14.77 dB, noise figure (NF) of 3.7 $\sim$ 4.8 dB and 1-dB compression points ($P_{1\,\mathrm{dB}}$) from -17 to -11 dBm between 12–18 GHz. The total power consumption is only 7.68 mW under 0.8 V power supply voltage. The good performances of the LNA make it suitable for Ku-band application.

A Broadband Low Noise Amplifier for X-band Applications

Cheng-Chi Yu[1], **Jiin-Hwa Yang**[2], **Hsiao-Hua Yeh**[1], **and Lien-Chi Su**[1]

[1]Department of Communications Engineering, Feng-Chia University
No. 100, Wen-Hua Rd., Seatwen, Taichung 407, Taiwan, R.O.C.
[2]Ph.D. Program in Electrical and Communications Engineering, Feng-Chia University
No. 100, Wen-Hua Rd., Seatwen, Taichung 407, Taiwan, R.O.C.

Abstract— A broadband low noise amplifier (LNA) for X-band (8–12 GHz) applications is proposed in this study. The proposed LNA circuit is composed of three-stage NMOS transistors which construct a cascade configuration. The design can achieve wide-band matching and higher gain at the same time. In order to perform the proposed operating bandwidth, the operating frequencies of each stage are designed at 8 GHz, 10 GHz and 12 GHz, respectively. A source inductor is used in this circuit to improve impedance matching. Furthermore, in order to reduce chip area, authorized-layout inductors are presented in this design to replace the conventional inductors provided by the process. An obvious size reduction is obtained by these topologies.

The proposed LNA chip is fabricated by TSMC 0.18 µm CMOS process. The chip occupies a die area of 0.45 mm^2 (0.73 mm* 0.62 mm) only. On-wafer measurement was used to measure the characteristics of the LNA. The results shows that gain (S_{21}) of 15.1 $\sim$ 20.1 dB, noise figure (NF) of 2.82 $\sim$ 3.11 dB, and 1-dB compression points ($P_{1\mathrm{dB}}$) from -27 to -21 between 8–12 GHz. The total power consumption is 12.45 mW under a power supply voltage of 0.75 V. The good performances of the LNA make it suitable for X-band application.

Effect of Buffer Layer Thickness on the Surface Impedance of Un-patterned Superconducting Films Operating in Microwave Frequencies

Heng-Tung Hsu[1] and Chien-Jan Wu[2]

[1]Department of Communications Engineering, Yuan Ze University
135 Yuan-Tung Road, Chung-Li 320, Taiwan, R.O.C.
[2]Institute of Electro-Optical Science and Technology, National Taiwan Normal University
162, HePing East Road Section 1, Taipei 116, Taiwan, R.O.C.

Abstract— Microwave properties of high-T_c superconductors (HTSC) have been intensively studied with applications of HTSC in the fields of microwave passive devices. The main advantage of adopting superconducting films for fabrication of microwave devices lies in the reduction of power dissipation and thus the enhancement of the system performance. These devices have been proven to have better performance than those with ordinary conductors. In this paper, we study theoretically the effect of buffer layer thickness on the surface impedance of un-patterned high-T_c YBCO films operating in microwave frequencies. We calculate theoretically the effective surface impedance of the structure that is realistically characterized by a HTSC thin film, a buffer layer, a dielectric substrate and a gold ground plane. It should be noted that since HTSC have better conductivity than ordinary conductors at superconducting state, the finite conductivity of the gold ground layer must be included. Starting with the vector decomposition of Maxwell's equations, scalarized field components can be related to voltage and current on the equivalent transmission line models to be adopted for impedance calculations. In the scattering of plane waves by such a structure, the occurrence of substrate resonance was observed under certain conditions. Simulation results revealed that the existence of buffer layer had major effect on the occurrence of substrate resonance. Moreover, the effect was more pronounced when the operating frequency is in the vicinity of the resonance frequency of the structure.

A Tri-band Bandpass Filter Using Short-stub Loaded SIR

Xuehui Guan[1,2], **Fang Wen**[1], **Wei Fu**[1], **Haiwen Liu**[1], **Guohui Li**[2], **and Lu Zhu**[1]

[1]College of Information Engineering, East China Jiaotong University, Nanchang 330013, China
[2]Key Laboratory of Specialty Fiber Optics and Optical Access Networks
Shanghai University, Shanghai 200072, China

Abstract— A novel compact triple-passband bandpass filter is presented in this paper. A short-stub is loaded to a stepped-impedance resonator (SIR), and the first three resonant frequencies can be controlled easily. The resonant frequencies are set at designed frequency band by changing the length of the loaded stub and the impedance ratio of the SIR. Two resonators are coupled and three passbands are achieved. The input and output port are coupled to the resonator by utilizing pseudo-inter-digital structure, increasing the coupling strength. Based on the proposed resonator, a two-pole microstrip triple-passband bandpass filter with central frequencies 1.5 GHz, 2.4 GHz and 5.78 GHz is designed for GPS and WLAN application. Four transmission zeros are realized at 1.3 GHz, 2.1 GHz, 3.7 GHz, and 6.2 GHz, which improve the selective in the transition band and attenuation in the stopband. The schematic of the proposed filter and its frequency response are shown in Fig. 1 and Fig. 2. Experimental results verify the proposed scheme.

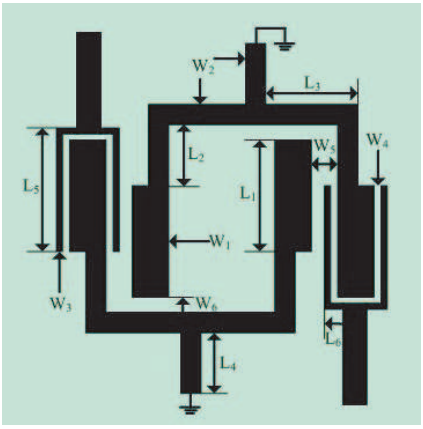

Figure 1: Schematic of the proposed filter.

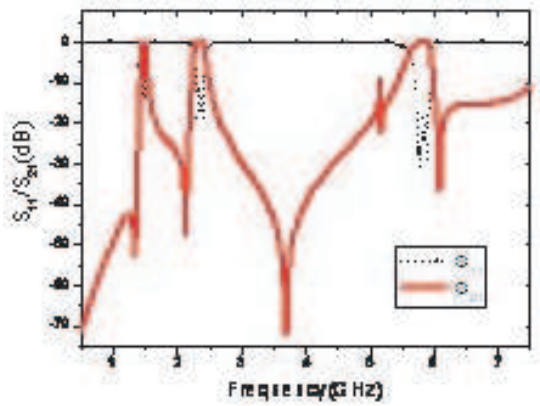

Figure 2: Simulated frequency response.

Waveguide-based Meniscus Thin Lens for Broadband MM-wave Power Combining Applications

Nan Yang, **Huaicheng Zhao**, **Xidong Wu**, **and Jinfang Zhou**
Department of Information Science & Electronic Engineering, Zhejiang University, China

Abstract— A meniscus thin lens integrated in a rectangular waveguide is presented for broadband high-efficiency power combining applications. The combiner structure is composed of ten side-by-side input waveguides, a meniscus thin lens with a matching layer, an E-plane sectoral horn, and an output waveguide. The electromagnetic fields are launched from a standard rectangular waveguide WR-28 with a feed horn. A meniscus thin lens is used to transform the cylindrical wavefront to planar wavefront, which is then splitted into ten-way output fields. These output fields have a uniform phase and amplitude. In the parallel rectangular waveguides, the mm-wave power is coupled into a microstrip line by a detailed-designed antipodal finline and then amplified by commercial monolithic-microwave integrated-circuit (MMIC) power amplifiers. The amplified power is then collected and combined in a reverse way, i.e., the electromagnetic fields are retransformed by another finline and then converged into rectangular waveguide by meniscus thin lens and horn. In this design, all the waveguides are standard rectangular waveguides WR-28. This article introduces the working principles of the power combiner in detail and analyzes its parameters' effects, especially the focal length diameter ratio (f/D) by using CST Microwave Studio. A matching layer for the meniscus thin lens is introduced to improve the combing efficiency. The power combiner shows a very high efficiency, the peak of which is 93.5%, and the bandwidth of 80% efficiency is up to 11.5 GHz, nearly the entire Ka band. Besides the conventional advantages of spatial power combiner, this design also leads to growth potential since more power can be achieved by merely cascading several power combiners together.

Session 2P1
Generation, Propagation and Application of Coherent and Partially Coherent Beams with Special Beam Profile and Polarization 2

Sub-cycle Pulse with Arbitrary Envelope

Jian Zheng, **Enming Qiu**, **and Qiang Lin**
Institute of Optics, Department of Physics, Zhejiang University, Hangzhou 310027, China

Abstract— In recent years, the great progress in generation of ultrashort laser pulses has made the shortest electromagnetic pulses which consist of one or less optical cycles (measured full-width at half-maximum of the pulse's envelope) possible. From the terahertz band, to the visible spectrum and the extreme ultra-violet band, the single-cycle pulses start a new era for ultrafast science. The theoretical description of the single-cycle pulses and their applications has caught the interests of many researchers. In this paper, the popularly used vector potential definition is found to be inapplicable in the sub-cycle regime. New expressions for sub-cycle pulses with arbitrary envelopes are derived from the oscillating dipole model. The sub-pulses are found to chirp intrinsically and the form of their chirps is envelope dependent. Being an analytical expression, the expressions are applicable to pulses with arbitrary pulse width. The expressions are then applied to the study of high harmonic generation (HHG) of atomic hydrogen in intense sub-cycle pulses. It is found that the envelope form plays a crucial role in the case of sub-cycle pulses than few-cycle pulses. A reduction of the cutoff energy occurs as the pulse width goes down to sub-cycle. The amount of the reduction is envelope dependent. The blueshift of the center frequency due to envelope-dependent intrinsic chirp is considered as the cause of the reduction.

REFERENCES

1. Lin, Q., J. Zheng, J. Dai, I.-C. Ho, and X.-C. Zhang, "Intrinsic chirp of single-cycle pulses," *Phys. Rev. A*, Vol. 81, 043821, 2010.
2. Lin, Q., J. Zheng, and W. Becker, "Subcycle pulsed vector beams," *Phys. Rev. Lett.*, Vol. 97, 253902, 2006.
3. Corkum, P. B. and F. Krausz, "Attosecond science," *Nature Phys.*, Vol. 3, 381, 2007.

Beam Propagation Factor of Truncated Gaussian Schell-model Beams in Turbulence

Xiaoling Ji and Xiaoqing Li
Department of Physics, Sichuan Normal University, Chengdu 610068, China

Abstract— A method of studying the beam propagation factor (i.e., M^2-factor) of truncated partially coherent beams both in free space and in turbulence has been proposed, i.e., the method of the window function being expanded into a finite sum of complex-valued Gaussian functions. Taking the Gaussian Schell-model (GSM) beam as a typical example of partially coherent beams, the analytical formula of the M^2-factor of truncated GSM beams in turbulence has been derived, and the results for non-truncated GSM beams in turbulence and truncated GSM beams in free space have been readily obtained as special cases of that of truncated GSM beams in turbulence. It is shown that the M^2-factor of truncated GSM beams in turbulence depends on the propagation distance z, the truncation parameter δ, the coherence parameter α, and the refraction index structure constant C_n^2. The M^2-factor decreases as δ and α increase. However, the M^2-factor in turbulence is more sensitive to δ than that in free space. In particular, the non-truncated fully coherent beam has the smaller M^2-factor than the truncated partially coherent beams. The M^2-factor increases with increasing propagation distance z due to turbulence. The stronger the strength of turbulence is, the larger the M^2-factor is. On the other hand, the M^2-factor of truncated partially coherent beams with smaller δ is more affected by turbulence. Furthermore, for the non-truncated case the M^2-factor is less sensitive to turbulence than that for the truncated case. In addition, the effect of turbulence on the M^2-factor of truncated GSM beams is less sensitive to the coherence parameter α than that of non-truncated GSM beams.

Radiation Force of Hightly Focused Gaussian Beam on Gold Nano-particles

F. Y. Jiang, K. K Huang, and X. H. Lu
Department of Physics, Institute of Optics, Zhejiang University, Hangzhou 310027, China

Abstract— The numerical calculation has theoretically demonstrated that the gold nano-particles could really be trapped by the highly focused Gaussian beams. Through analyses we obtain the radius range of gold nanoparticles for a given optical tweezer.

Since Ashkin realized the optical tweezer in his lab in the 1986 [1], this approach has been widely used in biology, chemistry and physics. The particle is considered as a simple point dipole in the electromagnetic field, for the particle is much smaller compared with the wavelength, so the force exerted on the particle can be calculated [2].

For the metallic particles in Rayleigh regime, the larger polarizability implies larger scattering force, absorption force and gradient force at the same time. In this report, we investigate the distribution of radiation force exerted on the gold nanoparticles detailedly. We analyze the optical system and calculate the radiation force distribution of the highly focused Gaussion beams on the gold nanoparticle. We analyze the trapping stability and give the radius range of the gold nanoparticles which could be trapped.

The polarizability can be calculated as expression:

$$\alpha = \left[\frac{\varepsilon_n + 2\varepsilon_h}{a^3(\varepsilon_n - \varepsilon_h)} - \frac{4i\varepsilon_h^{\frac{3}{2}}\pi^2}{3\lambda^3} \right]^{-1}, \tag{1}$$

where ε_n is the dielectric function of the metallic particle, ε_h is the dielectric function of the host solution, λ is the wavelength of the light.

Our analyses theoretically demonstrate the gold nanoparticle could be stably trapped by highly focused fundamental Gaussian beams. Compared with the dielectric particles, we fin the large dielectric function and large polarizability of gold nanoparticles are the direct reason for metallic nanoparticles to be trapped. Our theory results are quite agreed with the experiment before.

REFERENCES

1. Ashkin, A., et al., *Optics Letters*, Vol. 11, 288, 1986.
2. Harada, Y. and T. Asakura, *Optics Communications*, Vol. 124, 529, 1996.

Evolution Properties of a Stochastic Electromagnetic Beam in a Gaussian Cavity

Shijun Zhu and Yangjian Cai
School of Physical Science and Technology, Soochow University, Suzhou 215006, China

Abstract— With the help of a tensor method, analytical propagation formula for the cross-spectral density matrix of a stochastic electromagnetic beam in a Gaussian cavity is derived. As an application example, the evolution properties of the propagation factor and the degree of polarization of an electromagnetic Gaussian Schell-model (EGSM) beam in a Gaussian cavity are studied numerically. It is found that we can modulate the properties of an EGSM beam by a Gaussian cavity, which is useful in many applications, such as free-space optical communications, laser radar system, optical trapping and optical imaging, where stochastic electromagnetic beams are required.

Focusing Properties of a Partially Coherent Pulse

Yiming Dong, **Yangjian Cai**, **and Chengliang Zhao**
School of Physical Science and Technology, Soochow University, Suzhou 215006, China

Abstract— Propagation of a linearly polarized partially coherent pulse through a high numerical aperture thin lens is formulated. The tight focusing properties, such as the degree of polarization, the intensity distribution, and the degree of coherence, of a partially coherent pulse are investigated in detail. It is found that the focusing properties of a partially coherent pulse are closely related with the initial coherence and the numerical aperture of the thin lens.

Phase Singularities of Focused High-order Hermite-Gaussian Beams

Yongtao Zhang, **Chaoliang Ding**, **Zhiguo Zhao**, **and Liuzhan Pan**
Department of Physics, Luoyang Normal College, Luoyang 471022, China

Abstract— The phase singularities of high-order Hermite-Gaussian beams focused by an aperture lens are studied. Numerical calculation results are given to illustrate the dependence of phase singularities on the truncation parameter and beam order. The reorganization process of phase singularities of focused high-order Hermite-Gaussian beams with increasing truncation parameter is illustrated by numerical examples.

Laser Radar System with a Partially Coherent Beam

Gaofeng Wu, **Yangjian Cai**, **and Fei Wang**
School of Physical Science and Technology, Soochow University, Suzhou 215006, China

Abstract— Analytical propagation for a partially coherent beam passing through paraxial $ABCD$ optical systems operating through turbulent atmosphere is investigated with the help of the $ABCD$ matrices and the generalized Huygens-Fresnel integral. As an application example, we study the laser radar system with a partially coherent beam. We found that the laser radar system induces the changes of the coherence and beam width of a partially coherent beam. By measuring these changes, we can determine the parameters of the structure function of the target.

The Effect of Spherical Aberration on the Spectral Stokes Singularities of Tightly Focused Partially Coherent Anomalous Hollow Beams

Yamei Luo[1], **Jinhong Li**[2], **and Bihua Tang**[1]

[1]Department of Biomedical Engineering, Luzhou Medical College, Luzhou 646000, China
[2]Department of Physics, Taiyuan University of Science and Technology, Taiyuan 030024, China

Abstract— The spectral Stokes singularities of partially coherent radially polarized anomalous hollow beams focused by a high numerical aperture (NA) objective in the presence of spherical aberration is studied in detail by using the vector Debye formula. It is shown that there exist s_{12}, s_{23}, and s_{31} spectral Stokes singularities. The variation of the spherical aberration, truncation parameter and half angle of the aperture lens will result in the motion, pair creation and annihilation, and changes in the degree of polarization of s_{12}, s_{23}, and s_{31} spectral Stokes singularities, and the handedness reversal of s_{12} singularities (C-points). The creation and annihilation occur for a pair of s_{12} singularities with opposite topological charge but same handedness, and for a pair of oppositely charged s_{23} or s_{31} singularities, which is similar to the aberration-free case. The collision of an s_{12} singularity with an L-line ($s_3 = 0$ contour) leads to a V-point, which is located at the intersection of contours of $s_{12} = 0$ and $s_{23} = 0$ (or $s_{31} = 0$) and is unstable. A small perturbation leads to the handedness reversal and changes in the degree of polarization of the C-point. In the process the topological relationship holds true. The results have been illustrated numerically and are compared with the results of previous work.

Spatio-temporal Coupling of a Stochastic Electromagnetic Pulse

Min Yao[1, 2] **and Yangjian Cai**[1]

[1]School of Physical Science and Technology
Soochow University, Suzhou 215006, China
[2]Centre for Optical and Electromagnetic Research
Zhejiang University, Hangzhou, 310058, China

Abstract— The interaction of a stochastic electromagnetic pulse with linear optical elements is analyzed with the help of the matrix optics. A 6×6 order matrix describing transformation of a six-dimensional state vector including four spatial and two temporal positions within the field is used to derive conditions for spatio-temporal coupling. An example is included which deals with a spatio-temporal coupling in a stochastic electromagnetic pulse on reflection from a reflecting grating. Dependence of the spatio-temporal coupling on the degree of polarization and the structure of the grating is explored in detail.

Propagation of Nonparaxial Gaussian Schell-model Electromagnetic Beams through an Aperture

Haixia Wang, **Chaoliang Ding**, **Yongtao Zhang**, **and Liuzhan Pan**
Department of Physics, Luoyang Normal College, Luoyang 471022, China

Abstract— Based on the generalized Rayleigh-Sommerfeld diffraction integrals, the analytical expression for the 3×3 cross-spectral density matrix of nonparaxial Gaussian-Schell model (GSM) electromagnetic beams propagating through a circular aperture is derived and used to formulate the spectral density (intensity), degree of polarization and spectral degree of coherence of electromagnetic beams at the z plane. The effect of f-parameter, self- and cross-correlation lengths on the intensity, the degree of polarization and the spectral degree of coherence of electromagnetic beams are stressed. The results are illustrated by numerical examples.

Spectral Stokes Singularities of Nonparaxial Partially Coherent Elliptical Gaussian Vortex Beams Diffracted at a Half-plane Screen

Shangbin Zheng, **Yamei Luo**, **and Yuan Zhu**
Department of Biomedical Engineering, Luzhou Medical College, Luzhou 646000, China

Abstract— Based on the generalized vector Rayleigh-Sommerfeld diffraction integrals, the analytical expression for the cross-spectral density matrix has been derived and used to study the dynamic behavior of spectral Stokes singularities of nonparaxial partially coherent elliptical Gaussian vortex beams diffracted at a half-plane screen. It is shown that the motion, pair creation and annihilation of spectral Stokes singularities are dependent on a controlling parameter, such as spatial correlation length, the off-axis displacement parameter, or the waist width ratio of elliptical Gaussian vortex beams. The analytical results are illustrated numerically. The results obtianed in this paper about studying on some new effects in nonparaxial beam diffraction and propagation provide a method for generating spectral Stokes singularities and are further enrichment and extension of the research range of singular opticsand can be useful for practical applications of optical vortices.

Session 2P2
Electromagnetic Resonances in Photonic/Plasmonic Crystals and Transformational Metamaterials

Dirac Cones Induced by Accidental Degeneracy in Photonic Crystals and Zero Refractive Index Materials

Xueqin Huang[1], **Yun Lai**[2], **Zhi Hong Hang**[1], **and C. T. Chan**[1]

[1]Department of Physics, Hong Kong University of Science and Technology, Hong Kong, China
[2]Department of Physics, Soochow University, China

Abstract— Electronic and photonic systems with Dirac cones in the band structure possess amazing wave transport properties. Materials with a zero refractive index also possess very interesting wave manipulation characteristics. These two seemingly unrelated classes of material are actually related in a subtle way. We show that by employing accidental degeneracy, dielectric photonic crystals can be designed and fabricated which exhibit Dirac cone dispersion at the center of the Brillouin zone at a finite frequency. Many interesting properties intrinsic to a Dirac cone dispersion can be realized. Multi-frequency component oscillations can be observed in our system, which bear similarity to the Zitterbewegung phenomenon, the dynamic behavior of trembling motion of electrons in electronic systems. We also have a new understanding to this Zitterbewegung-like phenomenon, which applies to other photonic systems with a Dirac cone dispersion. Moreover, by applying effective medium theory, we relate the same dielectric photonic crystal to a material with effectively zero permittivity and permeability. A zero refractive index metamaterial is one in which waves do not experience any spatial phase change and such peculiar material has many interesting wave manipulating properties. We numerically and experimentally demonstrate in the microwave regime that such dielectric photonic crystals with reasonable dielectric constants do manipulate waves as if they have near zero refractive indices at and near the Dirac point frequency. Especially, we experimentally demonstrate the transmission through a channel made up with such photonic crystals can be tuned by changing the size and position of an embedded object.

Strong Photon-plasmon Coupling in a Layered Waveguide

A. Castanié, D. Felbacq, and B. Guizal
Laboratoire Charles Coulomb, UMR-CNRS 5221, Université de Montpellier 2, France

Abstract— It is shown that it is possible to realize the strong coupling of a guided mode with a plasmon in a waveguide coated by a lossy metal. Despite the losses, it is shown that it is possible to define precisely a density of states and to construct a spectral measure. The structure of the modes is analyzed as well as the density of states. The possibility of designing a spaser based on this structure is investigated.

The strong coupling of plasmons with excitons in a layered structure was investigated in [1–3]. It is a phenomenon that is interesting both from the point of view of fundamental quantum physics as well as from the point of view of technology. Indeed, it can realize spatial Rabi oscillations [4] and is useful for an efficient extraction of light. In this work, we investigate a somewhat related phenomenon: the strong coupling of a plasmon with a guided mode in a planar structure. From a mathematical point of view, it is shown that, despite the presence of losses, and the consecutive loss of self-adjointness, a complete spectral analysis can be obtained, with a proper definition of the density of states [5] and a expansion of the resolvent upon modes. The asymptotics when the layer of metal is very thin or very thick are investigated. From a numerical point of view, a algorithm based on Cauchy integrals is given for the extraction of the complex dispersion relation. It is to be noted that the dispersion relation $F(k,\omega) = 0$ admits an analytic extension to the double complex plane $\mathbb{C}^2$. More precisely, it is shown that the plasmon lives on a Rieman surface of genus 0. The consequences are analyzed in the frequency and temporal domain, by showing that all the points of the Riemann surface are accessible by the proper use of an incident pulse. From the point of view of applications, the possibility of amplification of a plasmon [6] is investigated in the situation when the waveguide is filled with quantum dots. Various models are used: a classical simple one using a permittivity with an imaginary part properly chosen, a semi-classical model based on the Maxwell-Bloch system and finally a fully quantized (Jaynes-Cumming) model.

ACKNOWLEDGMENT

The financial support of the Institut Universitaire de France is gratefully acknowledged.

REFERENCES

1. Bellessa, J., et al., "Giant Rabi splitting between localized mixed plasmon-exciton states in a two-dimensional array of nanosize metallic disks in an organic semiconductor," *Phys. Rev. B*, Vol. 80, 033303, 2009.
2. Bellessa, J., C. Bonnand, J. C. Plenet, and J. Mugnier, "Strong coupling between surface plasmons and excitons in an organic semiconductor," *Phys. Rev. Lett.*, Vol. 93, 036404, 2004.
3. Chern, R.-L. and D. Felbacq, "Artificial magnetism and anticrossing interaction in photonic crystals and split-ring structures," *Phys. Rev. B*, Vol. 79, 075118, 2009.
4. Centeno, E. and D. Felbacq, "Rabi oscillations in bidimensional photonic crystals," *Phys. Rev. B*, Vol. 62, 10101, 2000.
5. Felbacq, D. and R. Smali, "Density of states for finite photonic crystals," *Phys. Rev. B*, Vol. 67, 085105, 2003.
6. Bergman, D. J. and M. I. Stockman, "Surface plasmon amplification by stimulated emission of radiation: Quantum generation of coherent surface plasmons in nanosystems," *Phys. Rev. Lett.*, Vol. 90, 027402, 2003.

Cancellation of Reflection and Transmission at Metamaterial Surfaces

Xinhua Hu[1], **Jiong Yang**[2], **and Jian Zi**[2]

[1]Department of Material Science and Laboratory of Advanced Materials, Fudan University Shanghai 200433, China

[2]Department of Physics and Surface Physics Laboratory, Fudan University, Shanghai 200433, China

Abstract— Based on analytical derivations and numerical simulations, we show that both reflection and transmission can be canceled at the surface of a metamaterial (MM) with a metal-dielectric stratified structure. Strong anisotropic absorption and the surface direction are found to play important roles in this phenomenon. For the angle between the surface and the layers of MMs above a critical value, only reflection is eliminated and transmission is permitted. Since they are not related to resonance, the phenomena can occur in a broad frequency range.

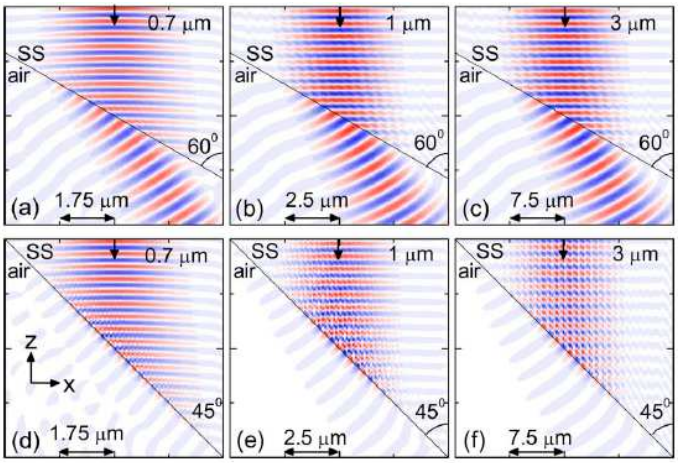

REFERENCES

1. Yang, J., et al., *Optics Letters*, Vol. 35, No. 16, 2010.
2. Yang, J., et al., *Physical Review B*, Vol. 80, 125103, 2009.

Fabrication of Photonic Crystals by Holographic Lithography Using Single Refracting Prism and Spatial Light Modulator for Phase Control

Kam Sing Wong
Department of Physics, Hong Kong University of Science and Technology, Hong Kong, China

Abstract— As being able to produce defect-free, nanometer-scale structures over large area uniform photonic crystals (PhCs) in a single step fabrication, holographic lithography (HL) has shown to be a very economic and powerful tool and might hold the key to volume producing of photonic structures. In the previous demonstrations, however, multiple beams forming the interference pattern were obtained by two independent optical elements and steps: splitting the laser output into multiple beams either by a dielectric beam splitter or a grating; and then superposing them at the exposure area by another specially designed prism. This fabrication strategy can introduce alignment complexity and inaccuracies due to differences in the optical path length and angles among the interfering beams as well as vibrational instabilities in the optical setup. We now have demonstrated another approach for easy fabrication of 2D and 3D photonic crystal microstructures, based on beam splitting and overlapping by a single refracting prism. 3- and 4-beam interference pattern is generated and recorded in a photosensitive polymer to produce high quality 2D and 3D microstructures. This method enables splitting of an incoming laser beam into multiple beams and at the same time, recombining them by the same optical element. Thus, anti-vibration equipment and complicated optical alignment system to adjust the angles between the interfering beams are not required, leading to a very simple optical setup. In the context of mass production, this method is much more practical and robust, and able to produce PhCs over larger and more uniform area than those previous demonstrations by two independent-element setups [1]. This method is extended to two-photon excitation using femtosecond laser pulses where highly nonlinear absorption enable one to make high contrast and large aspect ratio structures [2] This two-photon based HL technique is particularly suitable for making 3D PhCs and quasicrystals with complex and fine structure details.

One major problem of above standard HL technique is that it is very difficult to incorporate defect structure in a precise way inside the PhC. We have now developed a technique using liquid crystal spatial light modulator to control the intensity and phase of each interference beams [3], thus enabling us to make complex 2D defects within the PhC in a single step process. With this phase controlled HL, line defects, zigzag waveguide and microcavity point defect can be embedded in 2D or 3D PhC. Detail study of the optical properties and SEM measurements of some 3D and 2D PhC structures will be reported in the conference.

ACKNOWLEDGMENT

This work is partially supported by the Research Grants Council of Hong Kong (project # 603908, 604409) and HKUST RPC10SC13.

REFERENCES

1. Wu, L., et al., *Appl. Phys. Lett.*, Vol. 86, 241101, 2005.
2. Zhong, Y., et al., *J. Appl. Phys.*, Vol. 107, 074311, 2010.
3. Li, J., et al., *Opt. Express*, Vol. 16, 12899, 2008.

Influence of Spherical Anisotropy on the Optical Properties of Plasmon Resonant Metallic Nanoparticles

Yaxian Ni and Lei Gao
Department of Physics, Suzhou University, Suzhou 215006, China

Abstract— We demonstrate the features of the dipole and quadrupole resonant modes in extinction spectra of spherically anisotropic nanoparticles based on the full-wave scattering theory. It is found that in a core-shell nanosphere, the introduction of spherical anisotropy in the core leads to the blue shift in resonant wavelengths for small nanoparticles, while for large particles (the core radius is larger than 90 nm) the dipole resonant wavelength keep unchanged with the variation of spherical anisotropy. In addition, the peak strength for the dipole and quadrupole modes are also studied. Numerical simulations show that the strong localization of electric fields can be further enhanced and tuned by adjusting the spherical anisotropy in the core. In contrast, the anisotropy introduced in the shell results in blue shift for small nanoparticles but red shift for nanoparticles with larger size. The tunability of plasmon resonant shifts in extinction spectra and tailored localization of enhanced fields are revealed.

REFERENCES

1. Qiu, C. W., L. W. Li, T. S. Yeo, and S. Zouhdi, *Phys. Rew. E*, Vol. 75, 026609, 2007.
2. Liu, D. H., C. Xu, and P. M. Hui, *Appl. Phys. Lett.*, Vol. 92, 181901, 2008.
3. Oldenburg, S. J., R. D. Averitt, S. L. Wsetcott, and N. J. Halas, *Chem. Phys. Lett.*, Vol. 288, 243, 1998.
4. Wang, H., G. P. Goodrish, F. Tam, C. Oubre, P. Nordlander, and N. J. Halas, *J. Phys. Chem. B*, Vol. 109, 11083, 2005.
5. Liu, C., C. C. Mi, and B. Q. Li, *IEEE Trans. Nanobiosci.*, Vol. 7, 206, 2008.
6. Alam, M. and Y. Massoud, *IEEE Trans. Nanotechnol.*, Vol. 5, 265, 2006.

Sharply Asymmetric Reflection from Magnetic Metamaterials and its Potential Applications

Shiyang Liu[1], **Wanli Lu**[2], **Zhifang Lin**[3], **and S. T. Chui**[4]

[1]Institute of Information Optics, College of Mathematics Physics and Information Engineering
Zhejiang Normal University, Jinhua, Zhejiang 321004, China
[2]State Key Laboratory of Surface Physics, Department of Physics
Fudan University, Shanghai 200433, China
[3]Key Laboratory of Micro and Nano Photonic Structures, Ministry of Education
Fudan University, Shanghai 200433, China
[4]Bartol Research Institute, University of Delaware, Newark, DE 19716, USA

Abstract— Plasmonic materials are capturing increasing interest due to their promising applications ranging from nanophotonics, nonlinear optics, to biosensing, and even medical therapy. Most efforts hitherto have been devoted to investigate the electric surface plasmons (ESP) originating from the collective resonance of electronic density wave and hosted by metallic building blocks. The symmetry of Maxwell's equations with respect to the magnetic and electric degrees of freedom enables a symmetric type of phenomenon in magnetic systems, which is known as "magnetic surface plasmon" (MSP). However, it has not been well investigated as the ESP in metallic materials.

In this presentation, we demonstrate a dramatically molded reflection of electromagnetic (EM) wave from magnetic metamaterials (MM) consisting of ferrite rods with the operating frequency located near the MSP resonance. It can be found that on one side of the source the reflected field nearly cancels the incoming field, giving rise to a shadowy region near the MM surface, while on the other side the reflected field considerably enhances the incoming field, resulting in a brightened region. This phenomenon arises from the coupling of EM wave to MSP resonance states which exhibit giant circulations going only in one direction due to the broken time reversal symmetry in MM. Possible applications are manifested in designing a robust one-way waveguide, a 90° beam bender, and a beam splitter, which are shown to work even in deep subwavelength scale. In this case the wavelength λ of the propagating wave is nearly 30 times of the characteristic size (lattice constant a) of MM.

Optical Force in Magnetic Plasmon Cavities

H. Liu[1, 2], **Jack Ng**[2], **S. B. Wang**[2], **Z. F. Lin**[2, 3], **Z. H. Hang**[2], **C. T. Chan**[2], **and S. N. Zhu**[1]

[1]National Laboratory of Solid State Microstructures, Department of Physics
Nanjing University, Nanjing 210093, China
[2]Department of Physics and Nano Science and Technology Program
Hong Kong University of Science and Technology, Clearwater Bay, Hong Kong, China
[3]Department of Physics, Fudan University, Shanghai, China

Abstract— It is well known that metamaterials exhibit artificial magnetic plasmon resonance, and such responses can be realized in the visible or infrared frequency range based on LC resonance effect. In our former works, various coupled magnetic plasmon modes were reported in

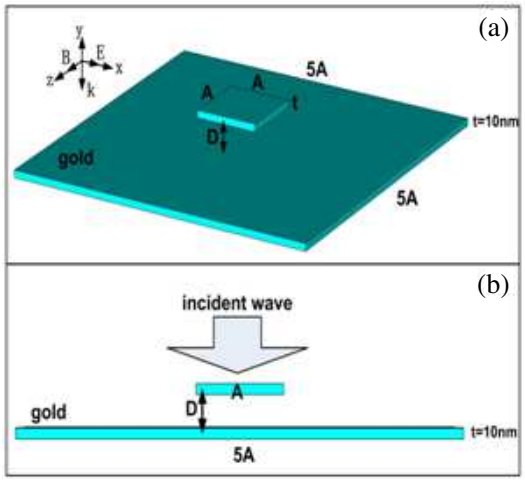

Figure 1: Schematic of nanocavity with two gold patches.

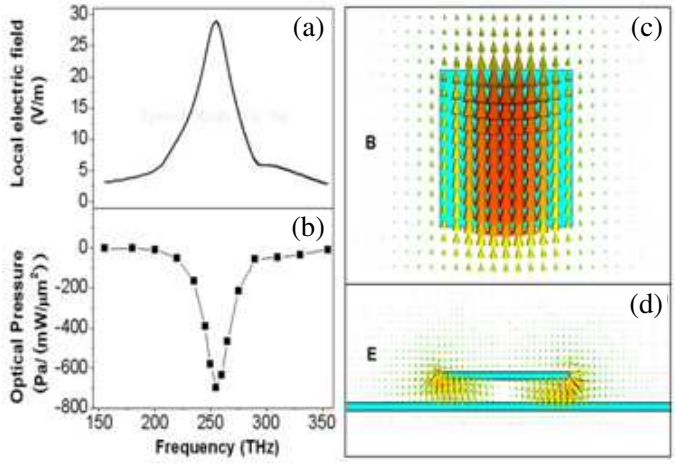

Figure 2: The frequency dependence of (a) local electric field between two patches and (b) optical pressure between two patches (with $A = 200\,\text{nm}$, $D = 30\,\text{nm}$); (c) Magnetic field (on y-cut middle layer) and electric field (on z-cut middle layer) at the resonance frequency.

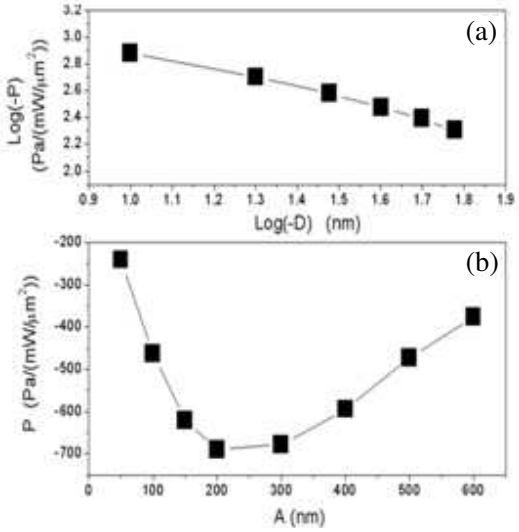

Figure 3: (a) The log-log relationship between optical pressure P and distance D (with $A = 600\,\text{nm}$); (b) The dependence of optical pressure P on the size parameter A (with $D = 30\,\text{nm}$).

stereometamaterials [1, 2], one-dimensional meta-chains of split-ring resonators (SRR) [3], nano-rods [4], nano-sandwiches [5], slit-hole resonators (SHRs) [6] and some other systems [7].

In this work [8], we designed a magnetic plasmon cavity system comprising a patch and a slab (see Fig. 1). A strong magnetic plasmon resonance mode could be excited in this structure (see Fig. 2). At the resonance, the kinetic energy of conduction electrons is found to induce a strong negative optical pressure (see Fig. 3). A Lagrangian model is proposed to describe the salient features. The mechanism and theoretical model reported in this paper could have potential applications in many other subwavelength optomechanical plasmonic structures, such as selective optical trapping [9].

REFERENCES

1. Liu, H., D. A. Genov, D. M. Wu, Y. M. Liu, Z. W. Liu, C. Sun, S. N. Zhu, and X. Zhang, "Magnetic plasmon hybridization and optical activity at optical frequencies in metallic nanostructures," *Phys. Rev. B*, Vol. 76, 073101, 2007.
2. Liu, N., H. Liu, S. N. Zhu, and H. Giessen, "Stereometamaterials," *Nature Photonics*, Vol. 3, 157–162, 2009.
3. Liu, H., D. A. Genov, D. M. Wu, Y. M. Liu, J. M. Steele, C. Sun, S. N. Zhu, and X. Zhang, "Magnetic plasmon propagation along a chain of connected subwavelength resonators at infrared frequencies," *Phys. Rev. Lett.*, Vol. 97, 243902, 2006.
4. Cao, J. X., H. Liu, T. Li, S. M. Wang, Z. G. Dong, and S. N. Zhu, "High sensing properties of magnetic plasmon resonance in the double-rod and tri-rod structures," *Appl. Phys. Lett.*, Vol. 97, 071905, 2010.
5. Zhu, Z. H., H. Liu, S. M. Wang, T. Li, J. X. Cao, W. M. Ye, X. D. Yuan, and S. N. Zhu, "Optically pumped nanolaser based on two magnetic plasmon resonance modes," *Appl. Phys. Lett.*, Vol. 94, 103106, 2009.
6. Liu, H., T. Li, Q. J. Wang, Z. H. Zhu, S. M. Wang, J. Q. Li, S. N. Zhu, Y. Y. Zhu, and X. Zhang, "Extraordinary optical transmission induced by excitation of a magnetic plasmon propagation mode in a diatomic chain of slit-hole resonators," *Phys. Rev. B*, Vol. 79, 024304, 2009.
7. Liu, H., Y. M. Liu, T. Li, S. M. Wang, S. N. Zhu, and X. Zhang, "Coupled magnetic plasmons in metamaterials," *Phys. Status Solidi B*, Vol. 246, 1397, 2009 (Review Paper).
8. Liu, H., J. Ng, S. B. Wang, Z. F. Lin, Z. H. Hang, C. T. Chan, and S. N. Zhu, "Strong light-induced negative optical pressure arising from the kinetic energy of conduction electrons in plasmonic cavities," *Phys. Rev. Lett.*, 2011 (accepted).
9. Zheng, Y. J., H. Liu, S. M.Wang, T. Li, J. X. Cao, L. Li, C. Zhu, Y. Wang, S. N. Zhu, and X. Zhang, "Selective optical trapping based on strong plasmonic coupling between gold nano-rods and slab," *Appl. Phys. Lett.*, 2011 (accepted).

Observation of Backscattering-immune Tunnelling States without External Magnetic Fields

Jian-Wen Dong[1], **Wen-Jie Chen**[1], **Zhi Hong Hang**[2], **C. T. Chan**[2], **and He-Zhou Wang**[1]

[1]State Key Laboratory of Optoelectronic Materials and Technologies
Sun Yat-Sen University, Guangzhou 510275, China
[2]Department of Physics, The Hong Kong University of Science and Technology
Hong Kong, China

Abstract— A strategy is proposed to realize robust transport in time reversal (TR) invariant photonic sys-tem. By both numerical simulation and microwave experiment, we demonstrate that a chiral photonic mode in a 3D dielectric photonic crystal is immune to scattering of impurities, and the phenomenon bear some similarity to robust transport of electrons in topological insulators. In particular, the robust one way transport does not require an external field, which is distinct from the previous findings employing two dimensional magnetic photonic crystals with explicit time reversal breaking by an external field. The chirality based robust transport has the obvious advantage that it can be realized in non-magnetic dielectric materials and thus has a clear roadmap to optical frequencies, and it does not require any external field.

Interaction between Resonating Elements in Conventional and Dielectric Metamaterials

Elena Semouchkina
Michigan Technological University, USA

Abstract— The performance of metamaterial structures is usually analyzed by using the effective medium approach and is based on the assumption that waves "do not see" metamaterial particles and propagate in a metamaterial as in a uniform medium. Considering metamaterials homogenized due to subwevelength dimensions of their resonating particles and lattice parameter, this approach assumes uniform excitation of all particles at a single resonance frequency and identical orientation of the excited magnetic/electric dipoles. Such approach is used to justify close-packing of resonators in metamaterials.

Here the results of full-wave simulations of resonance responses of metamaterial structures incorporating multiple unit cells are presented. Amplitude and phase distributions of electric and magnetic fields in metamaterial samples are analysed. The simulated scattering parameters spectra of the structures are compared to the experimental data. The structures under consideration include as conventional metamaterials comprising arrays of split-ring resonators and cut wires, so metamaterials composed of dielectric resonators. The latter present a perspective low-loss alternative to conventional metallic metamaterials, especially for applications at mm-wave and higher frequencies.

The conducted studies have revealed drastic interactions between partcles in both types of metamaterials that do not allow for consideration of these structures as homogenized media. In particular, it was demonstrated that due to overlapping of resonance fields coupled resonators can create additional paths for wave transfer. The patterns of these paths can change with frequency and form self-organized networks with symmetry that depends on the resonance mode and particle arrangement. These phenomena are able to modify the mechanism of wave propagation in conventional metamaterials and cause unusual transmission and negative refraction in metamaterials comprising dielectric resonators, even resonators of just one type.

The performances of shell-type cylindrical cloaks consisting of either metallic or dielectric resonator arrays and designed by using the coordinate transformation approach have been studied by using full-wave simulations of true multi-resonator structures in contrast to the models comprising material layers with prescribed parameters. The latter models, which are typically used for the analysis of metamaterial cloaks, cannot account for interactions between the building elements. The performed simulations revealed strong interaction between elements in the shells formed by concentric arrays of closely packed split-ring-resonators, a drastic splitting of their resonance response, and the formation of a wide resonance band. A design of an infrared invisibility cloak composed of glass resonators which accounts for inter-resonator coupling is presented. In this design, the distances between resonators and between arrays have been carefully chosen to keep overlapping of the resonance fields of elementary resonators under control. An opportunity to homogenize the resonator responses in arrays and to realize radial dispersion of the effective permeability requested by the transformation optics is demonstrated. The performed simulations confirmed the cloaking effect.

Subwavelength Electromagnetic Diode: One-way Response of Cascading Nonlinear Meta-atoms

Yuancheng Fan, **Jin Han**, **Zeyong Wei**, **Chao Wu**, **Yang Cao**, **Xing Yu**, **and Hongqiang Li**
Physics Department, Tongji University, Shanghai 200092, China

Abstract— We propose a scheme for subwavelength electromagnetic diode by employing cascading nonlinear meta-atoms. One-way response is conceptually demonstrated on a microwave transmission line comprising of three metallic ring resonators acting as meta-atoms and a varactor as the nonlinear medium inclusion. Experiments show that our implementation can operate simultaneously as forward diode and backward diode at different frequencies. A transmission contrast of up to 14.7 dB was achieved between forward and backward transmission. Subwavelength size of our diode ($\sim \lambda/4$) should be useful for miniaturization of integrated optical nanocircuits.

Tuning Trapped-mode Resonances in a Planar Metamaterial

J. H. Shi[1], **E. Plum**[2], **V. A. Fedotov**[2], **and N. I. Zheludev**[2]

[1]College of Science, Harbin Engineering University, Harbin 150001, China
[2]Optoelectronics Research Center, University of Southampton, Southampton SO17 1BJ, UK

Abstract— Metamaterials have attracted a tremendous amount of attention in recent years since it was fabricated to exhibit simultaneously negative values of effective permeability $\mu_{eff}(\omega)$ and permittivity $\varepsilon_{eff}(\omega)$ at microwave frequencies. Our interests in metamaterials are to develop low-loss metamaterials supporting high quality resonances. The excitation of trapped modes depends on metamaterials' structures and polarization as well as the incident angle. At normal incidence, the trapped-mode resonance is not allowed for the symmetric structural metamaterials. We demonstrated the trapped-mode resonance in symmetric planar metamaterials at oblique incidence.

Metamaterials that were used in our research consisted of identical subwavelength metallic inclusions structured in the form of symmetrically split rings (SSR), which were arranged in a periodic array and placed on a thin dielectric substrate. SSR patterns can be etched from 35 μm copper cladding covering FR4 PCB substrate of 1.5 mm thickness. Each copper split ring had the radius of 6 mm and width of 0.8 mm and occupied a square translation cell of 15×15 mm. Such periodic structure does not diffract normally incident electromagnetic radiation for frequencies lower than 20 GHz. Transmission of a single sheet of this metamaterial can be measured in an anechoic chamber under normal or oblique incidence conditions using broadband horn antennas. We studied transmission of this structure in the 9–13 GHz spectral range where the trapped-mode resonance happened. To understand the resonant properties of this metamaterial, we also gave the simulated results based on FEM. The metal pattern is treated as a perfect conductor, while the substrate is assumed to be a lossy dielectric.

We demonstrate trapped-mode resonance in symmetric planar metamaterials at oblique angles of incidence both experimentally and theoretically. The transmission of metamaterials has been studied at different angles of incidence and the quality factor strongly depends on angle of incidence. There is a good agreement between the simulated and experimental results. The extrinsic trapped mode of symmetric metamaterials is excited by oblique incident electromagnetic wave, not resulting from the broken symmetry.

REFERENCES

1. Fedotov, V. A., M. Rose, S. L. Prosvirnin, N. Papasimakis, and N. I. Zheludev, "Sharp trapped-mode resonances in planar metamaterials with a broken structural symmetry," *Phys. Rev. Lett.*, Vol. 99, 147401, 2007.

Modelling of a Monolithic Pulse Reshaper Based on a Photonic Crystal Waveguide

T. Cao
Faculty of Electronic Information & Electrical Engineering
Dalian University of Technology, Dalian 116024, China

Abstract— 3D Finite Difference Time Domain (FDTD) and Finite Element (FE) frequency domain methods are used to study the propagation of arbitrary chirped pulses in Photonic Crystal (PhC) waveguides. An arbitrary chirped pulse is derived from a separate Semiconductor Optical Amplifier (SOA) model and is passed through a ministop band (MSB) in a Photonic crystal waveguide. Reasonably good agreement is shown between the FDTD and FE models and pulse compression of 3.25 : 1 is observed. Group delay has been calculated at both the output of the SOA and the PhC waveguide and shows how the non-linear chirp of the SOA output pulse interacts with the dispersion of the MSB.

Figure 1(a) shows a top view of the structure to be studied from our in-house FDTD user interface. This is a narrowed W3 waveguide in the Γ-K direction with a lattice constant of 480 nm and is 7.68 µm long. Figure 1(b) shows a comparison between the FDTD and FEMLAB modelled transmission around the MSB wavelength. The waveguide is excited by the fundamental TE mode (E_x is the dominant field component) of the input photonic wire waveguide. This feature enables realistic excitation of the structure and also allows overlap integrals to be performed at the output of the waveguide. Figure 1(c) shows the input and output pulses (w.r.t the PhC waveguide) for the case of 60 MW/cm^2 input power to the SOA for carrier wvalengths of 1518 nm and 1550 nm. The SOA output pulse has strong nonlinear frequency chirp due to Rabi oscillation.

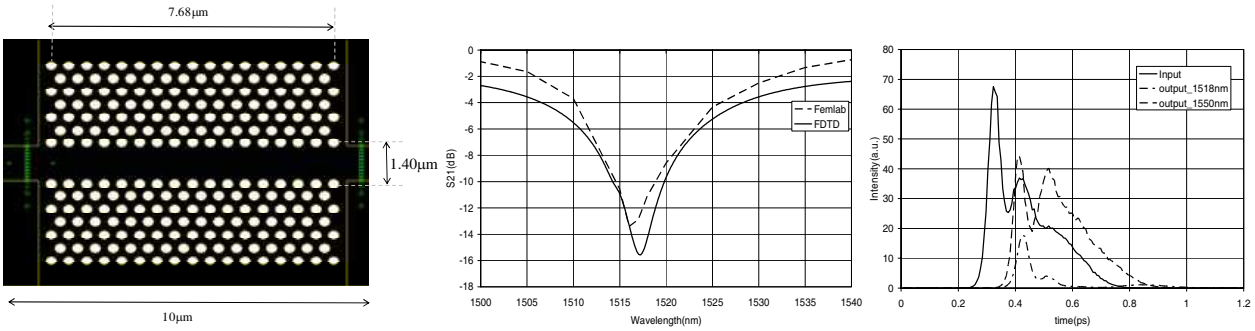

(a) (b) (c)

Figure 1: (a) FDTD model of a narrowed W3 PhC waveguide with $a = 480$ nm, $r/a = 0.329$, Γ-K direction, $n = 3.24$, length = 7.68 µm, FDTD mesh size in horizontal and vertical direction = 10 nm; (b) Modal FDTD transmission for waveguide of Figure 1(a); (c) Input and FDTD calculated output pulse from PhC waveguide, centre wavelength =1518 nm and 1550 nm, input pulse peak intensity is 60 MW/cm^2.

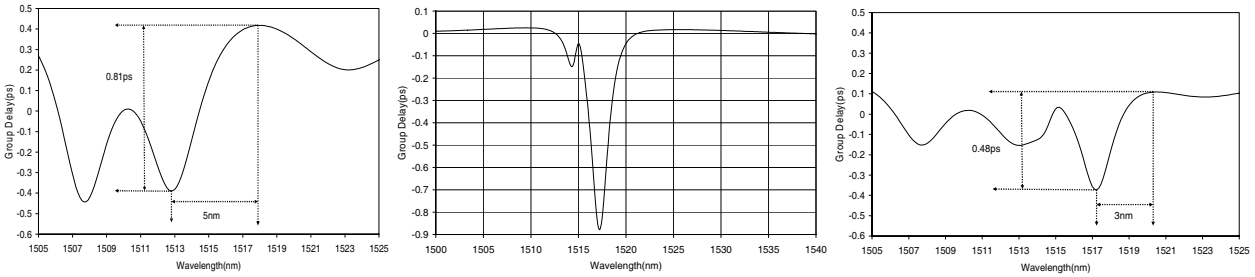

(a) (b) (c)

Figure 2: (a) The group delay of the input 150 fs non-linear chirp pulse, the carrier wavelength is at 1518 nm. (b) The group delay of the 10 µm long modified W3 for the round holes. (c) The group delay of the output 150 fs non-linear chirp pulse, the carrier wavelength is at 1518 nm.

Pulse compression can be clearly observed for the output pulse at 1518 nm and has been calculated to be 3.25 : 1.

We then investigate the Group Delay of the MSB and the linearly chirped pulses to explain the observed pulse compression phenomena at 1518 nm. The GD for the output a nonlinearly chirp pulse of the SOA is shown in Figure 2(a), It can be seen that across the spectral width of the pulse the GD varies nonlinearly as might be expected. Thus in simple dispersion compensation, a reverse identical slope is sort for the dispersive element in order to cancel out the group delay of the pulse. We next investigate the GD of the MSB, shown in Figure 2(b), Figure 2(c) shows the output pulse GD of PhC and It can be seen that the fast light region is now accelerating the trailing edge of the pulse reducing the overall pulse width.

Session 2P3
Remote Sensing of Water Cycle Related Components 2

Improve Geostationary IR Precipitation Estimation by Space-based Passive and Active Microwave Measurements

P. Zhang, **D. Y. Qin**, **H. Yang**, **Q. F. Lu**, **and R. You**
National Satellite Meteorological Center, China

Abstract— A new proposal will be introduced in this paper. The proposal aims to improve geostationary hourly IR precipitation estimation. The baseline is the FY-2D/E IR precipitation estimation algorithm. The additional information from the new techniques will be considered into the algorithm including polar active measurements, polar microwave measurements, ground-based Doppler Radar. The improved algorithm is expected to improve the validation of IR precipitation estimation compared with accumulated precipitation rate measured by ground station. At last a new database for precipitation from Fengyun 2 and 3 series measurements is expected to generate after reanalyzed remote sensing precipitation with the regional numerical weather prediction model.

The Preliminary Results from Assimilating Rain Rate Derived from Satellite

Q. Lu, **X. Yang**, **R. You**, **D. Qin**, **H. Yang**, **and P. Zhang**
National Satellite Meteorological Center of CMA, Beijing, China

Abstract— Inadequate specification of divergence and moisture in the initial conditions of numerical models results in the well-documented "spinup" problem. Observational studies indicate that latent heat release can be a key ingredient in the intensification of extratropical cyclones. As a result, the assimilation of rain rates during the early stages of a numerical simulation results in improved forecasts of the intensity and precipitation patterns associated with extratropical cyclones. Rawin observation is the important observation to record the precipitation; fortunately, the precipitation information could be quantitatively estimated from geostationary IR observation, Microwave observation and Radar observation. Here, a technique is described in which data from a variety of sources-passive microwave sensors, infrared sensors, and radar observations are combined to yield a continuous time series of rain rates, which may then be assimilated into a mesoscale model. Compared to the control simulation, assimilation simulation gives rise to a dramatic improvement in forecasts of precipitation patterns, sea level pressure fields, and geopotential height fields when information from all of the sources is combined to determine the rain rates.

An Initial Study on Assimilating Satellite-derived Total Precipitable Water in a Variational Assimilation System

Q. Lu, **X. Yang**, **C. Wu**, **J. Zheng**, **D. Qin**, **H. Yang**, **and P. Zhang**
National Satellite Meteorological Center of CMA, Beijing, China

Abstract— A variational assimilation system was used to examine the comparative impact of including satellite derived total column water vapour from IR and MW. The results show that the initial humidity field was improved by assimilating the satellite derived total column water vapour, especially over the rainfall areas, at the same time, the initial temperature field and the geopotential height field were also improved. The precipitation forecast difference between including and excluding the total column water vapour experiments was obvious during the assimilation time-window, and the precipitation forecast was also improved in the twenty-four hours precipitation forecast. More precipitation information can be obtained by introducing the satellite derived total column water vapour information into the variational assimilation system.

A Validation of Remotely Sensed Evapotranspiration Using In-situ Observations at Multi-scales in Hai River Basin, China

Zhenzhen Jia, **Shaomin Liu**, **and Ziwei Xu**
State Key Laboratory of Remote Sensing Science, School of Geography
Beijing Normal University, Beijing 100875, China

Abstract— A precise estimation of evapotranspiration from remote sensing is considered an essential need for global change science, water resource management and sustainable management of agriculture. So it has been well recognized that validation of remotely sensed evapotranspiration is indispensable, though there are many challenges. Hai River Basin in North China has been suffering the water crisis, thus a plan for water resources management based on remotely sensed evapotranspiration has been proposed by Global Environment Facility since 2004. Consequently, the accuracy of remotely sensed evapotranspiration is the significant issue.

In this study, a systematic and quantitative validation method was proposed and then carried out in Hai River Basin. The approach to validate regional evapotranspiration based on in-situ observations was investigated in three aspects: accuracy assessment of estimations, error source analysis, and uncertainties analysis in validation process. Crucial issues such as evapotranspiration measurements at various satellite pixel scales, observational data processing and quality control, a comprehensive validation procedure, validation pixel selection using footprint, and index system of accuracy assessment were advanced here. On this basis, validation of remotely sensed evapotranspiration in Hai River Basin was performed. Evapotranspiration products and related parameters derived from ETWatch system at both 30 m and 1 km resolutions in Hai River Basin from 2003 to 2009 were validated. Annual evapotranspiration over the basin was evaluated using calculations by water balance method; the estimations at typical landscapes were validated with the in-situ measurements from large aperture scintillometer, eddy covariance system and E601. Finally, spatio-temporal variation and differences between different landscapes of estimated evapotranspiration were studied.

Electromagnetic Models of Like-polarization and Cross-polarization in Radar Remote Sensing of Terrestrial Snow at X- and Ku-band for CoReH20 and SCLP Applications

Xiaolan Xu[1], **Leung Tsang**[1], **Wenmo Chang**[1], **and Simon Yueh**[2]

[1]University of Washington, Seattle, WA 98195-2500, USA
[2]Jet Propulsion Laboratory, California Institute of Technology, Pasadena, CA 91109, USA

Abstract— Snow water equivalent is an essential element in the global water cycle. Melting snow provides an important source of the fresh water for many places in the world. The global mapping of the snow storage will advance our knowledge of the climate systems. The satellite mission Cold Regions Hydrology High-resolution Observatory, (CoReH2O), was proposed by ESA. At the same time, NASA also recommended Snow and Cold Land process (SCLP) Satellite Mission in the Decadal Study. In this paper, we study the electromagnetic signatures on the active radar return signal based on both volume and surface scattering. The radar in CoReH2O mission operates at X and Ku band for both co-polarization and cross-polarization. The SCLP instrument has not been finalized, but is likely to have to have two frequencies and two polarizations.

In this paper, we study both volume scattering and surface scattering at X band and Ku band. Both co-polarization and cross polarization of surface scattering and volume scattering are studied. The studies are important as the relative contributions from surface and volume scattering need to be clearly understood in both CoReH2O and SCLP missions. The frequency and polarization dependences of surface and volume scattering should also be studied.

For surface scattering, we used the results based on 3D full wave simulations of Numerical Maxwell Model in 3 Dimensional (NMM3D) rough surfaces. The simulation is based on the Method of Moment. Several fast computation methods have been developed by UW group, including the Sparse Matrix Canonical Grid (SMCG) method the Physical Based Two Grid (PBTG) method and the multilevel UV method. There are two advantages of using the NMM3D. First of all, it can handle larger rms height than traditional small perturbation method. Secondly, both co-polarization and cross-polarization can be computed. In this paper, we computed random rough surface scattering due to the snow -ground interface using NMM3D.

For volume scattering, we use the model based on NMM3D using Foldy-Lax equations of densely packed sticky particles. The bicontinuous model is also used. Both models give cross polarization in addition to co-polarization. The surface and volume scattering are combined by the Dense Media Radiative Transfer equations with rough surface boundary conditions. The combined volume scattering and surface scattering are used in both X band and Ku band. Comparisons are made between the model results with Terra-SAR X band measurements and CLPX Ku band measurements.

Inversion of Snow Emission from Passive Microwave Time-series Observation Using Simulated Data

Lingmei Jiang[1, 2, 3] **and Jiancheng Shi**[2]

[1]State Key Laboratory of Remote Sensing Science, Beijing Normal University, China
[2]The Institute of Remote Sensing Applications, Chinese Academy of Sciences, China
[3]School of Geography, Beijing Normal University, China

Abstract— Terrestrial snow water equivalence (SWE) monitoring is important because it has strong climatological impacts of snow distribution on local, regional and hemispheric energy exchange and the hydrological significance of snowpack water storage. Passive microwave remote sensing mainly estimate snow depth and water equivalence based on the linear relationships between brightness temperature and snow depth. But these methods have limited to specific regional area that may not be representative of the prevailing land cover. The key issue with passive microwave remote estimates is the uncertainty resulted from its coarse footprint. Surface heterogeneity has caused great error on snow depth or SWE retrieval by passive microwave remote sensing. The purpose of this study is to investigate the effects of snow cover on snow water equivalence retrieval through parametric modeling simulation, and to extract snow signal from the total observation emission over a mixed-pixel composed of snow and bare soil surface. The snow layer is modeled as a closely packed irregular inhomogeneous layer above a homogeneous half space using DMRT_AIEM_MD model.

In this work, we firstly simulated surface emissivity of snow falling process with DMRT_AIEM_MD model, including non-snow surface, fully snow-covered, and partly snow-covered surface (e.g., from 100% snow fraction decreasing to 90%, 80%, 70% and to 10% in a passive microwave remote sensing pixel). The emissivity databases of fully snow-cover surface and snow-free surface have been generated covering a wide range of snow and bare natural surface, respectively. We assumed the surface totally covered with bare soil before snow falling. For a specific pixel, emissivity with snow-free patch in a mixed-pixel was also assumed almost the same with that before snow falling during the averaging period of three to five days in the model simulation. The averaging period is still needed to be determined by the actual snow falling process. If we have snow fraction known, we may calculate the snow signal from the total emission minus other land surface fraction multiplied its emissivity. The computed snow emission will be validated with the simulation values. And this technique is still needed to be further evaluated using the actual satellite microwave data.

An Experimental Study on Relationship between Snow Cover Fraction and Passive Microwave Brightness Temperature

Tao Che[1], **Liyun Dai**[1, 2], **and Xin Li**[1]

[1]Cold and Arid Regions Environmental and Engineering Research Institute, Chinese Academy of Sciences
Lanzhou, Gansu 730000, China
[2]Graduate University, Chinese Academy of Sciences, Beijing 100039, China

Abstract— Snow depth and snow equivalent water (SWE) are very important geophysical variables for the hydrologic study in cold regions. At present, passive microwave remote sensing is the most effective way on snow depth or SWE retrieval. However, within a footprint of AMSR-E, snow depth distribution is often not homogenous and snow sometimes can not cover the whole footprint, which leads to the low accuracy of snow retrieval. In fact, the inhomogeneity of snow depth and snow cover within one AMSR-E pixel makes the calibration and validation of snow depth and SWE more difficult. Therefore, it is significant to observe and understand the passive microwave brightness temperature (TB) features of inhomogeneous snow depth and snow cover distribution.

We investigated the relationship between snow cover fraction (SCF) and TB by two field snow experiments, in Northeastern China (Jilin Province) and in Northwestern China (Xinjiang Uygur Autonomous Region), respectively. Two ground based microwave radiometers at K (18.7 GHz) band and Ka (36.5 GHz)band were used to observe TB on the height of 1.5 m. The beam angle of radiometer is 15 degree, and the incidence angle is 50 degree. SFC was controlled by sweeping snow step by step within experimental site. The whole view field was divided into 8 parts with equivalent area to record the TB for each snow cover fraction, while snow physical variables were simultaneously measured, including snow depth, temperature, density, grain size, as well as temperatures at the interfaces of snow-air and snow-ground.

In Northeastern China, we observed on three types of snow covered land (e.g., bare soil, river ice and grassland) and analyzed the relationship between TB and SCF. The snow depth is about 5–6 cm. Results show that TB at Ka and K band increases with the reduction of SCF on grassland and bare soil, and decreases on river ice. Due to the scattering of snow, the TB at K band is higher than that of Ka band on the grassland and bare soil. With the reduction of SCF, the brightness temperature difference (TBD) decreases. When the snow is completely swept out, the TBD is negative. Due to the incoherent emissivity, the emissivity of snow-covered river ice is larger than that of river ice with snow free. Generally, the TB at K and Ka band vary linearly with SCF on all the three types of snow covered land.

In Northwestern China, we observed on two types of snow with the underlying surface of bare soil, and analyze the relationship between TB and SCF. The two different snow types are defined by snow depth, one is shallow snow depth (3 cm), and another is deep snow depth (30 cm). Results show that TB varies little with the SCF on the shallow snow and the TBD of K and Ka band is negative. Because the snow is very shallow, and it is fresh snow, the scattering of snow is very weak and contribute little to brightness temperature. On the deep snow, the TB at Ka band increases when the SCF reduction, but that varies little at K band. The main reason is that penetrability of K band is stronger than Ka band, and when snow is swept, the soil physical temperature decreased, and the raised TB from snow volume scatter reduction is counteracted by that from soil physical temperature reduction. So, we corrected the TB by considering the soil physical temperature. And found that the TB at both bands increase linearly with SFC reduction, and the TBD decrease with SFC.

Both field experiments showed the similar results that TB and TBD vary linearly with SFC. But there is not linear relationship between the TBD and snow depth, for the TBDs from different types of bare land are different. So, it is necessary to consider the brightness temperature features before snow when retrieving snow depth.

Trend of Terrestrial Water Storage Redistribution in China Detected by Recent Nine Years Satellite Gravity Observations

Zhi-Cai Luo[1, 2, 3], **Qiong Li**[1], **Kun Zhang**[1], **and Bo Zhong**[1, 2]

[1]School of Geodesy and Geomatics, Wuhan University, 129 Luoyu Road, Wuhan 430079, China
[2]Key Laboratory of Geospace Environment and Geodesy, Ministry of Education
Wuhan University, 129 Luoyu Road, Wuhan 430079, China
[3]State Key Laboratory of Information Engineering in Surveying, Mapping and Remote Sensing
129 Luoyu Road, Wuhan 430079, China

Abstract— The Gravity Recovery and Climate Experiment (GRACE) satellite mission, launched by NASA and the German Aerospace Centre (DLR) in 2002, has provided ten day to monthly measures of temporal gravity field with unprecedented accuracy, which can be used to estimate changes in terrestrial water storage. Using a hybrid filtering scheme with the combination of decorrelated filter P3M6 and 300 km Fan filter, we estimated the recent nine years terrestrial water storage variations for entire continent in China from GRACE temporal gravity filed models. The results from GRACE were also compared to those from CPC (Climate Prediction Center) and GLDAS (Global Land Data Assimilation System) hydrological models. After removed the periodic signals from the GRACE results, the long-term trend was given in the study. Moreover, several regions with prominent anomalies are revealed and analyzed in detail, and some valuable conclusions were drawn from the study.

The Web Site for Retreaving the Microwave Complex Permittivity Spectra of Moist Soils

V. L. Mironov[1], **A. M. Epikhin**[2], **S. V. Fomin**[1], **and L. G. Kosolapova**[1]

[1]Kirensky Institute of Physics, SB, RAS, Krasnoyarsk, Russia
[2]Digital Mind Development Ltd., Krasnoyarsk, Russia

Abstract— Moist soil dielectric models (MSDM) in the microwave band are an essential part of the software used in radar and radiometer remote sensing. These models are also needed for interpreting the data attained by TDRs and GPRs. To facilitate a remote excess to usage of MSDMs in the process of designing and testing respective remote sensing software, an internet site was designed in order to 1) ensure the on line analysis of dielectric data used in specific projects of remote sensing and 2) provide for a ready-made software library to be built in a general remote sensing software utilities, which use moist soil permittivity models as an important element for the inverse problems to be solved. This site offers such a service free of charge.

The software developed for this site is based on the measured permittivity data that are recognized as most reliable and have been used for developing the MSDMs employed in the contemporary radar and radiothermal remote sensing algorithms [1–4]. It provides moist soil complex permittivity values as a function of soil moisture (from dry to field capacity), electromagnetic frequency (from 0.3 to 26.5 GHz), soil temperature (from 10°C to 40°C), and percentage of clay in soil (from about zero to 76%). The MSDM software covers the soil types containing less then 5–7% of organic matter and classified as not saline. The software for calculating the complex permittivity employs the dielectric models [5, 6]. The error of predictions attained by these models is substantially decreased as compared with that of the well known in remote sensing Dobson model [2, 3] and is on the same order regarding the renowned Schmugge model [1]. Besides that, the Dobson and Schmugge models are valid in the narrower temperature range from 22°C to 24°C, and the Schmugge model accounts only for two frequencies, that is, 1.4 and 5.0 GHz.

The internet site developed is available at http://rsl.dmdevelopment.ru/. The deliveries of the site are presented in the form of tables and plots for the relative dielectric constant and loss factor as a function of soil moisture, frequency, and temperature, with the rest variables being fixed. The results provided can be downloaded from the site. In addition, the users can enter their own values of complex permittivity in order to quantitatively compare them with those displayed on the site graphs. Moreover, the users can download the dynamic linked library file "CalculationMethods.dll" to use it as a ready-made software library in their applications, if the environment Microsoft. NET Framework 4.0 is installed. The evolution of this site is planned to include other dielectric models and use the initial dielectric data measured over a broader assemblage of soils, frequencies, and temperatures, with frozen soils being considered as well.

REFERENCES

1. Wang, J. and T. Schmugge, "An empirical model for the complex dielectric permittivity of soils as a function of water content," *IEEE Trans. Geosci. Remote Sensing*, Vol. 18, No. 4, 288–295, 1980.
2. Dobson, M. C., F. T. Ulaby, M. T. Hallikainen, and M. A. El-Rayes, "Microwave dielectric behavior of wet soil — Part 1," *IEEE Trans. Geosci. Remote Sensing*, Vol. 23, No. 1, 25–34, 1985.
3. Dobson, M. C., F. T. Ulaby, M. T. Hallikainen, and M. A. El-Rayes, "Microwave dielectric behavior of wet soil — Part 2," *IEEE Trans. Geosci. Remote Sensing*, Vol. 23, No. 1, 35–46, 1985.
4. Curtis, J. O., C. A. Weiss, Jr. and J. B. Everett, "Effect of soil composition on dielectric properties," Technical Report EL-95-34, U.S. Army Corps of Engineers Waterways Experiment Station, Vicksburg, MS, December 1995.
5. Mironov, V. L., L. G. Kosolapova, and S. V. Fomin, "Physically and mineralogically based spectroscopic dielectric model for moist soils," *IEEE Trans. Geosci. Remote Sensing*, No. 7, 2059–2070, 2009.
6. Mironov, V. L. and S. V. Fomin, "Temperature and mineralogy dependable model for microwave dielectric spectra of moist soils," *PIERS Online*, Vol. 5, No. 5, 411–415, 2009.

Temperature Dependable Microwave Dielectric Model for a Pine Litter Thawed and Frozen

V. L. Mironov and I. V. Savin
Radiophysics of Remote Sensing Laboratory, Kirensky Institute of Physics
SB, RAS, Krasnoyarsk, Russia

Abstract— Forest floor strongly influences the radiobrightness temperature of forest land territories. Consequently, complex dielectric constant of the layer of leaf or needle debris must be taken into account in remote sensing algorithms to retrieve the moisture content of forest topsoil. So far, the dielectric constant models for litter have not been developed to the same extent as the dielectric models of moist soils have. In this area of research, there are published only a few papers. In particular, semi-empirical models of the complex permittivity are proposed for two types of litter which samples were taken from the leaf [2] and pine [3] forest floors. These models provide for the dielectric properties of thawed only litter, which limits their usage, particularly for the northern territories, where the topsoil is in the frozen state for a long time during the year.

In this paper, we developed a physically substantiated temperature dependable spectroscopic dielectric model of pine litter, which is characteristic for the pine forests in Siberia. The model covers the range of frequencies and temperatures stretching from 500 MHz to 15 GHz and from $+25^{\circ}$C to -30°C, respectively. The theoretical basis of this model have been developed in the case of shrub tundra soil, containing at least 90% organic matter [4]. The intrinsic variables in this model, on which the complex dielectric constant depends, are the litter moisture, electromagnetic frequency, temperature, and density of dry litter sample. Among the parameters of the model are included the parameters of the linear temperature dependence for the reduced complex refractive index of sample solids. The latter are supplemented by the parameters related to the exponential temperature dependences of water contents in a litter sample, regarding bound, film, and capillary types of litter water. In addition, the number of parameters of the model includes some physical characteristics for each type of litter water. This group of parameters consists of the low-frequency and high frequency limits of dielectric constant and ohmic conductivity, temperature coefficient of volume expansion, activation energy, activation entropy and the temperature coefficient of the increment of ionic conductivity. All the parameters of the dielectric model developed are derived from measurement the dielectric constant of moist litter samples. To describe the temperature dependence, the laws by Clausius-Mossotti, Debye, and the law of the ionic conductivity of solutions are used.

The error of the dielectric model with respect to the experimental data was determined using correlation analysis. In this case, the correlation coefficient (R) and standard deviation (sd) for the dielectric constant and dielectric loss factor were found to be: $R = 0.994$, $sd = 0.699$ and $R = 0.996$, $sd = 0.201$, respectively. Next, we plan to apply the developed method for constructing temperature dependable spectroscopic dielectric model for other types of litter.

REFERENCES

1. Grant, J. P., A. A. Van de Griend, M. Schwank, and J.-P. Wigneron, "Observations and modeling of a pine forest floor at L-band," *IEEE Transactions on Geoscience and Remote Sensing*, Vol. 47, No. 7, Part 1, 2024–2034, 2009.
2. Schwank, M., M. Guglielmetti, C. Matzler, and H. Fluhler, "Testing a new model for the L-band radiation of moist leaf litter," *IEEE Transactions on Geoscience and Remote Sensing*, Vol. 46, No. 7, 1982–1994, 2008.
3. Demontoux, F., B. Le Crom, G. Ruffi, J.-P. Wigneron, J. P. Grant, and V. L. Mironov, "Electromagnetic characterization of soil-litter media — Application to the simulation of the microwave emissivity of the ground surface in forests," *European Physical Journal — Applied Physics*, Vol. 44, 303–315, 2008.
4. Mironov, V. L., R. D. De Roo, and I. V. Savin, "Temperature-dependable microwave dielectric model for an arctic soil," *IEEE Transactions on Geoscience and Remote Sensing*, Vol. 48, No. 6, 2544–2556, June 2010.

Backscattering Measurements of River Surfaces at 35 GHz

Pierre Borderies
ONERA-DEMR, 2-Avue E. Belin, 31055-Toulouse-Cédex, France

Abstract— The paper proposed here consists in proximity experiments for measurements of continental water backscattering coefficient in KA Band and at nearly vertical incidence angle. The whole study aims at collecting such data with associating roughness as well as wind measurements, since few data are available on this topic. Also, very few data exist about the stationarity of backscattering, however it is a critical point for SAR processing at this frequency.

These proximity experiments have to be developed from a raised location above water surface (bridge, bank ...). To obtain an homogeneous incidence angle over the scene of interest, it was proposed to work either in the near field, tubular zone of a large reflector where the radiated wave is nearly plane, or in the far field where the radiated wave is locally plane.

The presentation will include several parts.

First one will describe the experimental set-up which has been implemented and the method of measurement and derivation of sigma0, with particular emphasis on the calibration strategy both in near field and in far field. Second one will present the preliminary experiments in laboratory, including the near field characterization of the antenna. Last section is about the results obtained both in laboratory as well as outside on real rivers. Last part presents the conclusion about the method of measurement and the results obtained.

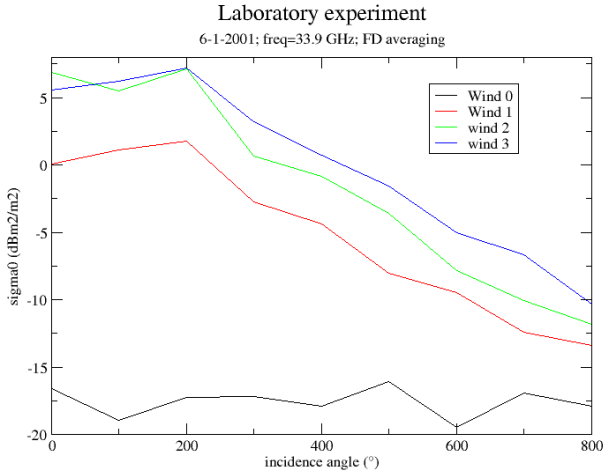

Figure 1: Laboratory experiment :Backscattering coefficient as a function of incidence angle in 1/100e of degree for 4 fan positions.

Data Cube Representation of Vegetated Surfaces Based on Physical Scattering Model for SMAP Mission

Xiaolan Xu[1], **Tien-Hao Liao**[1], **Leung Tsang**[1], **Seungbum Kim**[2], **and Eni Njoku**[2]

[1]Department of Electrical Engineering, University of Washington, Seattle, WA 98195-2500, USA
[2]Jet Propulsion Laboratory, California Institute of Technology, Pasadena, CA 91109, USA

Abstract— In this paper, we present forward model of the microwave backscattering from a vegetated terrain at L band for application in the upcoming SMAP (Soil Moisture Active and Passive) mission. The objective of the SMAP mission is to provide global measurements of soil moisture and its freeze/thaw state. These measurements will be used to enhance understanding of processes that link the water, energy and carbon cycles, and to extend the capabilities of weather and climate prediction models. A physical-based forward scattering model is essential to understand the relationship between the vegetated terrain and radar responses. To represent the vegetation layer, we include a layer of cylinders and disks above the rough surface. The cylinders are used to represent branches and the disks are used to represent leaves. The rough surface represents the soil interface. The data cube is formed by two surface parameters, which are soil moisture and rms height, and one vegetation parameter, vegetation water content. In addition, the radar acquisition is also sensitive to the physical structure of the vegetation. Thus, we have different data cube for different vegetation type. The data cubes have been validated by the field campaign data (SGP99, SMEX02 and SMAPVEX08).

For the layer of vegetation, distorted Born approximation is applied for the mean field calculation. The scattering cross section of the vegetation layer and its interaction with the underground soil surface were illustrated by half space Green's Function, which expressed explicitly as three scattering mechanisms. A) The direct volume scattering B) The double bounce effect as exhibited by bouncing first the vegetation layer and then the rough surface or vice versa. The effect on the interface of the vegetation layer and soil is considered by modifying the rough surface reflectivity using the coherent wave as computed by Numerical solution of Maxwell equations of 3 Dimensional simulations (NMM3D) of bare soil scattering and C) The rough surface scattering of the soil was calculated for by NMM3D.

The vegetation affects the backscattering in two ways, 1) the ratio of the HH/VV 2) the cross polarization (HV). In the bare soil model, the HH/VV ratio is smaller than 1. However, due to the different distribution of the scatterers in the vegetation layer, the HH/VV ratio usually larger than the bare soil. On the other hand, the anisotropic structures of the vegetation scatterers contribute more cross-polarization backscattering. The comparisons for these two factors of grassland and crop field (including corn, soybean and wheat) are demonstrated though the field campaign data mentioned above.

SMOS First Results Successes and Issues: Towards Global Soil Moisture and Sea Sea Salinity Maps

Y. H. Kerr[1], **P. Waldteufel**[2], **F. Cabot**[1], **P. Richaume**[1], **A. Mahmoodi**[3], **S. Delwart**[4], **J.-P. Wigneron**[6], **S. Mecklenburg**[4], **N. Reul**[5], **and J. Boutin**[7]

[1]CESBIO (CNES CNRS UPS IRD), Toulouse, France
[2]IPSL, Verrieres le Buisson, France
[3]Array Systems, Toronto, Canada
[4]ESA ESRIN, Frascati, Italy
[5]IFREMER, Brest, France
[6]INRA EPHYSE, Bordeaux, France
[7]LOCEAN, Paris, France

Abstract— SMOS, a L Band radiometer using aperture synthesis to achieve a good spatial resolution, was successfully launched on November 2, 2009. It was developed and made under the leadership of the European Space Agency (ESA) as an Earth Explorer Opportunity mission. It is a joint program with the Centre National d'Etudes Spatiales (CNES) in France and the Centro para el Desarrollo Teccnologico Industrial (CDTI) in Spain.

SMOS carries a single payload, an L band 2D interferometric, radiometer in the 1400–1427 MHz h protected band. This wavelength penetrates well through the vegetation and the atmosphere is almost transparent enabling to infer both soil moisture and vegetation water content over land and sea surface salinity over the oceans. SMOS achieves an unprecedented spatial resolution of 50 km at L-band maximum (43 km on average) with multi angular-dual polarized (or fully polarized) brightness temperatures over the globe and with a revisit time smaller than 3 days.

SMOS as been now acquiring data for over one year after the end of the commissioning phase. The data quality exceeds what was expected, showing very good sensitivity and stability. The data is however very much impaired by man made emission in the protected band, leading to degraded measurements in several areas including parts of Europe and of China. However, many different international teams are now addressing cal val activities in various parts of the world, with notably large field campaigns either on the long time scale or over specific targets to address the specific issues. These campaigns take place in various parts of the world, in different environments from the Antarctic plateau to the deserts, from rain forests to deep oceans. Actually SMOS is a new sensor making new measurements paving the way to new applications. However it also requires a very fine analysis of the data so as to validate both the approach and the retrieval quality, as well as for monitoring the evolution of the sensor. To achieve such goals it is very important to link efficiently ground measurement to satellite measurements through field campaigns and related airborne acquisitions as well as with other existing sensors.

This paper thus gives an overview of the science goals of the SMOS mission, a description of the main mission elements, and a foretaste of the first results including performances at brightness temperature as well as at geophysical parameters. It will include how the grond campaigns were elaborated to address the main cal Val activities accounting for SMOS specificities, in what context they were organized as well as the most significant results.

Session 2P4a
Antenna Array for Wireless Communications

Method of Moment Simulation of Noise Correlation in Antenna Arrays

Choon Hock Niow[1], **Hon Tat Hui**[1], **and Yantao Yu**[2]

[1]Department of Electrical and Computer Engineering, National University of Singapore, Singapore
[2]College of Communication Engineering, Chongqing University, Chongqing, China

Abstract— A new noise modeling method is proposed to calculate the correlated noise covariance matrix in antenna arrays using Method of Moments. This noise modeling method models the antenna array performing under a noisy environment in a more accurate manner. By obtaining the correlated noise covariance matrix from the proposed noise modeling method, compensation can be carried out more accurately to achieve better direction finding in a noisy environment.

The method consists of two parts. Firstly, signal sources with an equal magnitude and phase are spatially distributed around the circumference of the antenna array to simulate the signals coming from all directions and the actual current distributions in the antenna array are obtained using Method of Moment. Next, the current distributions obtained are recalculated together with the white Gaussian noise to obtain the correlated noise covariance matrix.

The correlated noise covariance matrix shows the presence of non-diagonal elements at different antenna separations. This is due to the mutual coupling between the antenna elements. The diagonal elements are also different in magnitude and phase. The different diagonal elements and the presence of non-diagonal elements in the correlated noise covariance matrix show that noises are correlated in the antenna array. This is different from the conventional uncorrelated noise covariance matrix where only diagonal elements are present and noises are assumed to be uncorrelated.

Computer simulations using the spatial smoothing MUSIC algorithm with coherent signals show that the correlated noise covariance matrix has a more accurate and realistic performance compared to conventional uncorrelated noise covariance matrix.

A Compact Printed Array with Increased Port Isolation

Yantao Yu
Chongqing University, China

Abstract— Antenna arrays with multiple ports are widely used in modern wireless communication systems, such as MIMO system, direction finding, etc. In mobile applications, the small physical sizes of the platform restrict the volume for the antennas and thus the use of compact arrays is required. In such a scenario, strong mutual coupling between closely spaced elements in compact antenna arrays may cause significant system performance degradation, such as reduction in gain, signal-to-noise ratio (SNR) and bandwidth. In this paper, an efficient technique to increase the isolation between the antenna ports is proposed. It utilizes the electromagnetic band-gap structure (EBG) to reduce the mutual coupling between antenna elements. Examples of printed monopole arrays are designed. Computational results are presented.

Study on the Decoupling of Stacked Phased Array Coils for Magnetic Resonance Imaging

Dandan Liang[1], **Hon Tat Hui**[1], **Tat Soon Yeo**[1], **and Yantao Yu**[2]

[1]Department of Electrical & Computer Engineering, National University of Singapore, Singapore
[2]College of Communication Engineering, Chongqing University, Chongqing 400044, China

Abstract— It has been suggested that multi-coil solenoid, which consists of an array of stacked surface coils, can be used in magnetic resonance imaging (MRI) applications to increase the signal-to-noise ratio (SNR) and consequently improve the image quality. However, due to the physical stacked design, mutual coupling effects occur and distort the array signals. A new compensation method has been proposed to remove the mutual coupling effect. It employs a set of newly defined mutual impedances to establish a compensation matrix through which the decoupled signals can be obtained. In this paper, the design of stacked phased array coils for MRI is described in details, and the decoupling method between the coil elements is clearly explained. Moreover, workbench experiments were conducted in a mimic MRI system with a cylindrical phantom acting for the loading purpose. A two-element stacked phased array has been designed as the receive-only coils under the radiation of a source coil placed above the cylindrical phantom. With the scattering parameters measured by a network analyzer, the new mutual impedances and compensation matrix were determined, and thereby decoupled signals were obtained. To demonstrate the robustness of the decoupling method, measurements were performed over a power deviation from −10 dBm to 10 dBm, a frequency deviation from 84.9 MHz to 85.1 MHz, and a deviation of the distance between the two coil elements from 0.5 cm to 3 cm. In each case, the derived decoupled signals were then compared with the ideally measured coupling free signals. From the comparison results, it is concluded that the new decoupling method can decouple the coupled signals effectively. Because of the robustness and flexibility in all the different experimental scenarios, the stacked phased array coil design together with the new decoupling method is proved to have a potential application in MRI.

Novel Wideband Microstrip Antenna Array with Double U-slots

Hong-Jun Wu[1], **Jie-Feng Xu**[1], **Xiao Hua**[1], **Shi-Lei Zhang**[1], **and Ying Wang**[2]

[1]Wenzheng College, Soochow University, Suzhou 215006, China
[2]School of Electronics and Information, Soochow University, Suzhou 215006, China

Abstract— A novel 2×2 microstrip patch antenna array is presented in this paper. With two cross-coupled slots etched in the radiating element, the proposed structure achieves wide band and high gain. Simple fabrication techniques can be used, since the radiating elements and the feeding network are placed on the same layer. Good agreement between the simulated and measured responses has been obtained. An impedance bandwidth of 20% and a gain of 11 dBi are achieved.

Dual-band Microstrip Antenna Array with EBG Structures

Jian-Jian Gu and Ying Wang
School of Electronics and Information, Soochow University, Suzhou 215006, China

Abstract— In this paper, a novel dual-band microstrip antenna array with electromagnetic band gap (EBG) structures is presented. The EBG structures help to separate the feed lines for the two bands, thus the two different groups of arrays of patch antennas operate individually at their particular frequencies, simultaneously. Improved gain and radiation patterns at both frequencies have been achieved.

A Compact Printed Multi-band Antenna for Laptop Applications

Cheng-Chi Yu[1], **Jiin-Hwa Yang**[2], **Chang-Chih Chen**[1], **and Wen-Chao Hsieh**[1]

[1]Department of Communications Engineering, Feng-Chia University
No. 100, Wen-Hua Rd., Seatwen, Taichung 407, Taiwan, R.O.C.
[2]Program in Electrical and Communications Engineering, Feng-Chia University
No. 100, Wen-Hua Rd., Seatwen, Taichung 407, Taiwan, R.O.C.

Abstract— This study proposes a compact printed multi-band antenna, which has the advantages of simple structure, small size, easy fabrication, and making integration within thin laptop. The main operating frequencies of the proposed antenna are at GPS (1.575 GHz), WLAN (2.4, 5.2 GHz), Bluetooth (2.45 GHz) and WiMAX (2.5, 3.5, 5.5 GHz) bands. The main structure of the antenna is composed of T-shape monopole and grounded inverted L-shape branch. The T-shape monopole excites 1.575 GHz and 2.4 GHz operating frequency bands. And, the grounded inverted L-shape branch not only can excite 3.5 GHz operating band but also can be used for impedance matching, which can tune the bandwidth of each operating band. Finally, the 5.5 GHz operational frequency of WiMAX can be excited by adding a stub on the T-shaped monopole branch. Therefore, a multi-band antenna for laptop applications is achieved.

The proposed antenna was fabricated on an FR4 substrate with a thickness of 1.6 mm and a relative permittivity of 4.4. The antenna occupies a small area of $9 \times 47\,\text{mm}^2$ only. This antenna is fed on the T-shape monopole antenna by a 50-Ω coaxial cable. The measured result shows that the 10 dB return loss is satisfied at each operating band, and has a good agreement with simulated result. Moreover, the gain, radiation efficiency and radiation pattern of each operating center frequency were also measured. They demonstrate very good performances. The gain is about $-1.23 \sim 5.4$ dBi and the radiation efficiency ranges from 67% to 95%. The measured radiation pattern is similar to general monopole antenna. The characteristics of the antenna make it attractive for practical application in laptops.

A Novel Compact EBG Structure for Mutual Coupling Reduction in a Patch Array

Haoyun Fei, **Huipin Guo**, **Xueguan Liu**, **and Ying Wang**
School of Electronic and Information Engineering, Soochow University, Suzhou 215021, China

Abstract— The mutual coupling among array antenna elements, often has serious effects on antenna arrays' performance, such as reducing the antenna element's efficiency, changing the radiation pattern, destroying antenna's polarization characteristic and so on. So mutual coupling must be considered in design of array antennas, especially for phase arrays. The mutual coupling among array antenna elements is mainly through space coupling and surface coupling. As for planar antenna arrays, surface wave propagation is an important reason for mutual coupling. High impedance surface EBG structure has certain bandgap which block surface wave propagation, thus can reduce mutual coupling. Traditional high impedance surface EBG structure adopts Mushroom structure, which has big size, and less adjustable parameters. Therefore, a novel compact structure, which is called C-EBG is studied in this paper. C-EBG structure has a simple unit with the shape like letter 'C'. Compared with Mushroom structure, C-EBG structure has smaller size, more adjustable parameters, including outer ring radius, inner radius, aperture radius and unit spacing. What's more, it has various arrangement patterns, including symmetrical structure, asymmetric structure, anti-symmetry distribution structure, and so on. Each pattern has its own bandgap characteristic. After studying the bandgap characteristics of various layouts and structural parameters' influence on mutual coupling, we finally obtain a suitable pattern for this usage, which is the reverse symmetric distribution C-EBG structure. In order to observe the performance of this EBG structure, we design a two-element patch antenna, whose center frequency is 2.4 GHz, and the proposed EBG structure is placed between elements. The whole structure parameters are optimized by using HFSS simulation software and a power divider is also designed which is used to measure the antenna. After simulation, we made a sample shown in Fig. 1. The test results indicated that the two-element patch antenna with the C-shaped EBG structure has a better performance than the one without EBG. The main lobe gain has been increased 1.3 dB, the side lobe level has been reduced 4.1 dB, and front-back ratio is enhanced 5.4 dB. This C-EBG structure has the advantages of compact, simple-shaped and easy for fabricating. It is very suitable for mutual coupling reduction in patch array antennas and provides a new option for phased array antenna design.

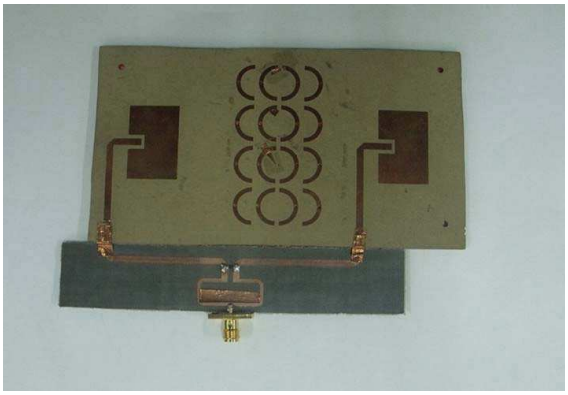

Figure 1: Photo of manufactured sample.

Session 2P4b
Antenna and Array Design and Simulation Techniques 1

Simulation of a Conformal Reconfigurable Fractal Tree Antenna with Adaptive Multi Beam and Frequency Characteristics

Huseyin Altun[1], **Erdal Korkmaz**[1], **and Bahattin Turetken**[2]

[1]Department of Electrical and Electronics Engineering, Fatih University, Istanbul, Turkey
[2]The National Research Institute of Electronics and Cryptology (UEKAE), Tubitak, Gebze, Turkey

Abstract— In radar and modern communication systems the demand on multi functional antennas is increasing. The requirements for these antennas are the abilities to have multi radiation patterns, adapting the operating frequency and polarization, keeping the physical dimensions and positioning unaltered. Reconfigurable antennas with switching capability used as a multiple input multiple output (MIMO) system have been used in recent years to fulfill these requirements. For switching mechanism usually PIN diodes are used since they have several crucial properties such as low insertion loss, good isolation, low power handling and low cost. By means of switches with compatible antenna elements the antenna and its feed structure can be physically reconfigured to provide radiation pattern, frequency band and polarization diversity. Although a reconfigurable antenna can take any shape we will focus on fractal antennas. The term fractal means broken or irregular fragments to describe a family of complex shapes that possess an inherent self-similarity in their geometric structure. As a result of small observation in the nature a lot of example for fractal can be seen as trees, clouds, snowflakes, leaves, galaxies and much more. Fractal tree structures can be applied into antenna design to produce multiband characteristics. This paper presents the design and analysis of a conformal fractal tree reconfigurable antenna having adaptive multi beam radiation patterns and adaptive operation frequency characteristics. The designed antenna is reconfigured by using of PIN diode switches. For biasing the diodes the biasing lines are used which can adversely affect the antenna characteristics. The optimization in biasing and integration of these switches into the antenna is also discussed.

Performance Investigation of Antenna Array with FSS Radome

Wenhua Yu[1, 2] **and Wenxing Li**[1]

[1]Harbin Engineering University, Harbin, China
[2]2COMU, State College, PA 16801, USA

Abstract— In this paper, we investigate the performance of an antenna array with a FSS radome. The antenna array includes 8 elements and the radome with FSS coating. The MoM speeded up with FFT and CGM analyzes the planar FSS structure, and the FDTD method is used to simulate the curved FSS structure and antenna system. The antenna array is embedded in the real environment and performance is analyzed.

Convergence and Sidelobe Suppression Properties of Array Antenna

James Jen, **Meng Qian**, **Zekeriya Aliyazicioglu**, **and H. K. Hwang**
Electrical and Computer Engineering, California State Polytechnic University-Pomona
3801 W. Temple Ave., Pomona, CA 91768, USA

Abstract— This paper investigates the performance of beam pattern forming employing the Minimax algorithm. The antenna beam pattern and its convergence rate depend on the relative weight and step size. The simulation results show the converging time of the array antenna is relatively insensitive to the relative weight and a fast step size decay rate speeds up the converging time. A 244 element nonuniformly spaced array antenna is used in this simulation study.

Stacked Coupled Circular Microstrip Patch Antenna for Dual Band Applications

Pradeep Kumar and Nitasha Bisht
Department of Electronics and Communication Engineering
Jaypee University of Information Technology, India

Abstract— In this paper, the design of the stacked coupled circular microstrip antenna is presented for dual frequency operations. The two circular patches are isolated by a substrate. The lower patch is the feed patch and the upper patch is excited by coupling. The designed antenna is simulated and optimized using CST Microwave Studio simulator. The designed antenna produces two resonances at 3.4233 GHz and 3.7395 GHz. For both resonances the return loss is less than −10 dB. The radiation pattern of the designed antenna is also shown. The designed stacked coupled circular microstrip antenna produces broadside radiation pattern.

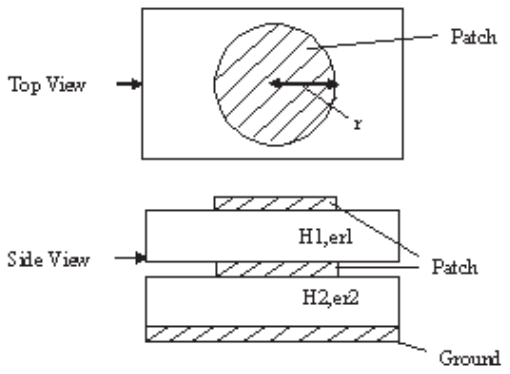

Figure 1: Geometrical configuration of stacked coupled circular microstrip antenna.

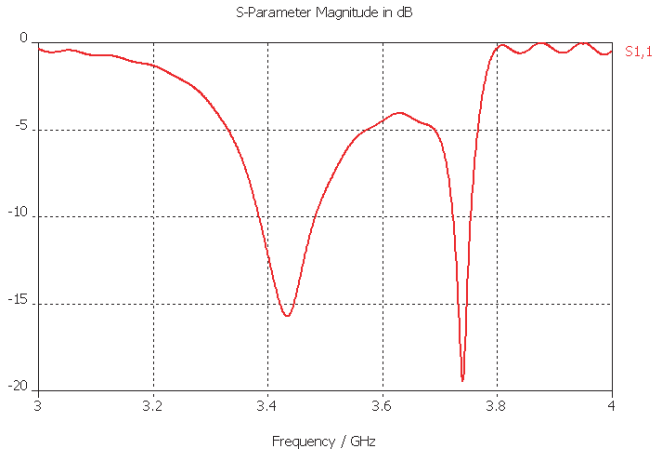

Figure 2: Return loss of the proposed antenna.

Session 2P5
Electromagnetic Nondestructive Evaluation (NDE) Methods for Industrial and Medical Applications

Electromagnetic Imaging in Nondestructive Evaluation: Industrial and Medical Applications

Yiming Deng[1], **Zhiwei Zeng**[2], **and Xin Liu**[1]

[1]University of Colorado Denver, Denver, CO 80204, USA
[2]Department of Aeronautics, Xiamen University, Xiamen, Fujian 361005, China

Abstract— Nondestructive electromagnetic imaging (EM Imaging) techniques are used in both engineering and clinical fields to determine the state or internal conditions of structures and human body on the basis of information contained in measured signals and images without the use of destructive approaches. Conventional Electromagnetic nondestructive evaluation (NDE) methods like eddy current, magnetic flux leakage, etc. usually do not form images directly unless time consuming mechanical scanning is involved. Furthermore, one-dimensional NDE signals and related signal processing techniques suffer from the difficulties in interpretation and visualization. An extensive review of the state-of-the-art NDE EM Imaging techniques is presented including the recent developments in several fast imaging applications developed by the authors: Magneto Optic (MO) imaging, Giant Magneto Resistive (GMR) imaging and Microwave-induced Thermoacoustic Hybrid (MTH) imaging methods. Both MO imaging and GMR imaging offer much higher sensitivity that allow detection of defects located deep in the test object comparing to conventional eddy current testing. MO imaging is a technology, based in part on the Faraday rotation effect that uses eddy current induction techniques along with a MO sensor, which generates real-time analog images of the magnetic fields associated with induced eddy currents interactions with structural anomalies. GMR imaging sensor is unipolar in nature and is sensitive to the magnetic fields along the easy axis of the sensor. The local magnetic fields measured by the GMR sensors are converted into electric voltages, which are also associated with the induced current interactions with structural anomalies. Physics and potential medical applications using the newly developed MTH imaging system will also be discussed. Both numerical simulation and experimental results will be presented for all three EM Imaging techniques.

Review of Finite Element Method for Simulating Eddy Current Testing

Zhiwei Zeng[1], **Yiming Deng**[2], **and Xin Liu**[2]

[1]Department of Aeronautics, Xiamen University, Xiamen, Fujian 361005, China
[2]University of Colorado Denver, Denver, CO 80217, USA

Abstract— The finite element method (FEM) has been one of the most important numerical methods in many engineering fields, such as structural analysis, fluid dynamics, and electromagnetics. This is because of its special properties including the capability of modeling complex problems and resultant sparse and banded stiffness matrix yielding efficient solution. The FEM was introduced for simulating eddy current testing (ECT) in the 1970s. In that era, two-dimensional and axis-symmetric ECT problems were simulated. The role of FEM in understanding the physical phenomena of remote field eddy currents showed the merit of FEM. Research in applying three-dimensional (3-D) FEM in ECT simulation started in the early 1980s. Since then, various formulations using different potentials, such as magnetic vector potential, electric scalar potential, magnetic scalar potential, current vector potential, and reduced potentials, have been applied in eddy current computation. Nowadays, the FEM has become an important tool in the research and development of ECT. Examples include the use of 3-D FEM in the parametric studies of magneto-optic imaging and the use of FEM in training operators inspecting steam generator tubes in nuclear power plants. The paper reviews the FEM formulations and introduces examples of using FEM in ECT simulation.

Domain-decomposition Finite Element Method for Eddy Current Modeling

Rongguang He, **Lin Huang**, **and Zhiwei Zeng**
Department of Aeronautics, Xiamen University, Xiamen, Fujian 361005, China

Abstract— The conventional finite element methods (FEM) use one mesh to discretize all the objects including conductors and magnetic materials, which results in inefficient simulation in terms of labor, computer memory, time of solution, and even worse, noisy signals. A novel numerical method, named domain-decomposition finite element method (DDFEM), is proposed to overcome the above problems. The proposed method divides the solution domain into several subdomains and therefore can greatly reduce meshing complexity and computation resource requirement, which makes modeling flexible and efficient. Particularly, the method is very useful in eddy current modeling involving multiple objects and is crucial for the research in areas such as eddy-current nondestructive evaluation and electrical machines. An important application of the new method is the development of a model for simulating magneto-optic imaging, a technique for nondestructively testing aircraft skin structures including multilayer aluminum plates and fasteners.

The Use of RBF Based on Ant Colony Algorithm and Fisher Ratio for Eddy Current Nondestructive Detecting System

Xiaoyun Sun[1], **Donghui Liu**[2], **and Aihua Li**[3]

[1]College of Electrical and Electronics Engineering, Shijiazhuang Tiedao University, Shijiazhuang, China
[3]College of Electrical Engineering and Information Science, Hebei University of Science and Technology Shijiazhuang 050018, China
[2]Department of Electrical Engineering, Mechanical Engineering College, Shijiazhuang 050003, China

Abstract—

Introduction: The traditional neural network method is difficult to recognizing defect signals quantitatively in eddy current nondestructive detecting, RBF network is used to detect defect signal. RBF network training is divided into two parts. Firstly, the selection of RBF centers and rasis function width. Secondly, the estimation of the weight. A new algorithm which combines ant colony algorithm and Fisher ratio is adopted to optimize RBF network.

RBF Center Selection Based on Ant Colony Algorithm and Fisher Ratio: Ant colony algorithm (ACA) is a novel population-based meta-heuristic framework for solving difficult discrete optimization problems, inspired by the foraging behavior of real ant colonies [1].

The specific procedure of RBF center selection based on ant colony algorithm and Fisher ratio is is summarized as follows:

(1) Obtain initial centers using ant colony algorithm. At first, deposit the ants with different attribution on every sample, and then distribute samples to clustering centers. In this process, ants deposit pheromone τ_{ij} from samples Xi to clustering center ci(k). When getting the optimal centers, ants find the food fountain too. We don't know the initial centers. So samples clustering process is equal to the processing of ants searching the most optimal paths [2–5].
(2) Optimize RBF network using Fisher ratio algorithm. Take the centers obtained from step 1 as the initial centers of fisher ratio algorithm. Then train RBF network. At last a simplified and optimal RBF network is obtained.

Conclusion: An improved RBF network based on ant colony algorithm and Fisher ratio algorithm is applied in eddy current quantiftive detecting. First, compute RBF initial centers and rasis function width according to the advantages of ant colony algorithm such as the parallel optimization characters and self-adaptive changing attenuation coefficient; second, optimize RBF network using Fisher ratio algorithm according to the advantages of Fisher ratio algorithm such as quick training and better clustering. The results show that the neural structure is simplified strongly, the precision is improved. Contrast with single ant colony algorithm, this method has much better recognition effect.

REFERENCES

1. Martens, D., M. De Backer, R. Haesen, et al., "Classification with ant colony optimization," *IEEE Transactions on Evolutionary Computation*, No. 5, 651–665, 2007.
2. Man, C., X. Li, and L. Zhang, "Radial basis function neural network based on ant colony optimization," *International Conference on Computational Intelligence and Security Workshops*, 59–62, 2007.
3. Wu, F. and Y. Zhao, "Radial basis function neural network based on ant colony clustering," *Journal of Xi'an Jiaotong University*, Vol. 40, No. 4, 386–389, 2006.
4. Jayaram, A. V. K., B. D. Kulkarni, S. Karale, et al., "Ant colony frame work for optimal design and scheduling of batch plants," *Computers and Chemical Engineering*, Vol. 7, No. 24, 1901–1912, 2000.
5. Mao, K. Z., "RBF neural network center selection based on fisher ratio class separability measure," *IEEE Trans. Neural Networks*, Vol. 13, No. 5, 1211–1217, 2002.

Invariant Analysis of Sensor-tilt Effect in Eddy Current NDE

G. Yang[1], **Y. Deng**[2], **Z. Zeng**[3], **X. Liu**[2], **L. Udpa**[1], **and Y. Yang**[1]

[1]Department of Electrical & Computer Engineering, Michigan State University, USA
[2]Departments of Electrical Engineering, Bioengineering and Radiology
University of Colorado Denver, USA
[3]Department of Aeronautics, Xiamen University, China

Abstract— In any NDE application, the measured signal received by sensors is decided by the flaw associated with operational parameters during inspection. The techniques of invariant pattern recognition have been studied to render NDE signals insensitive to operational variables and preserve or recover defect information. The invariant scheme and algorithms were addressed to facilitate Magnetostatic flux leakage NDE, which eliminated changes damaged the signal due to experimental variations and kept defect inspection identical [1]. The novel invariance analysis of eddy current signals during inspection of deep embedded cracks under fastener heads (CUF) in multi-layer structures has been presented in this paper.

The independent component analysis (ICA) [2] technique based transformation for sensor-tilt invariance of the eddy current (EC)-giant magnetoresistive (GMR) sensor system has been applied. The ICA-invariance analysis of GMR sensor-tilt effect using numerical model based parametric study is investigated. As shown in the Fig. 1, the crack signals measured under different GMR sensor-tilt conditions have been removed the difference and variance generated by the sensor tilt. The proposed ICA-invariance approach has shown the feasible invariance analysis of EC signals with advantage of avoiding large training processing. The analysis of feature invariance to sensor-tilt noise illustrated in the Fig. 1(b) will be presented along with implementation ICA-invariance transformation of experimental GMR signals. The processed crack signals insensitive to sensor-tilt noise also validated the reliable performance of EC-GMR system in detecting bottom cracks around fastener sites.

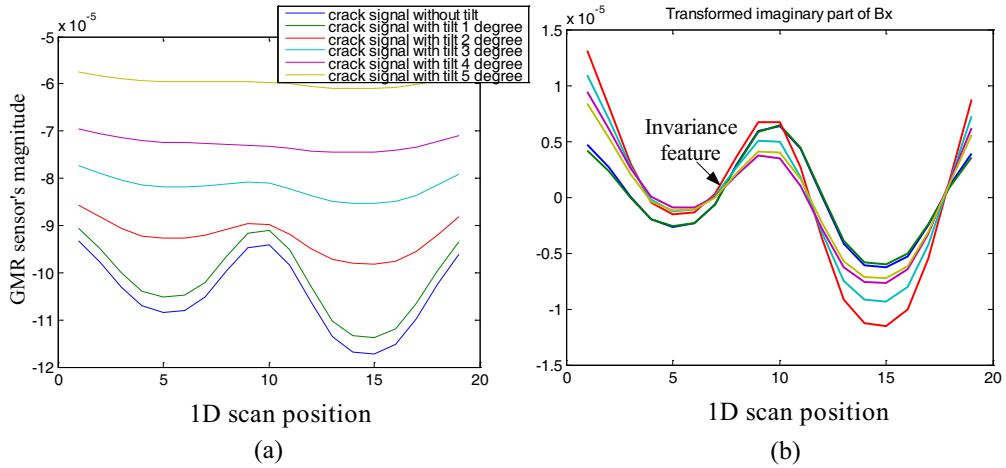

Figure 1: (a) The measured crack signals sensitive to sensor-tilt conditions. (b) The crack signals after the ICA-invariance transformation: insensitive to GMR sensor-tilt effect.

REFERENCES

1. Shreekanth Ammanji, M., "Invariance transformations for processing NDE signals," Ph.D. thesis, 1995.
2. Morabito, F. C., "Independent component analysis and feature extraction techniques for NDT/NDE data," *Materials Evaluation*, Vol. 58, No. 1, 85–92, 2000.

Multi-sensor Data Fusion System for Enhanced Analysis of Deterioration in Concrete Structures

Othman Sidek, **Shahid Kabir**, **and S. A. Quadri**
Collaborative μ-electronic Design Excellence Centre (CEDEC)
Engineering Campus, Universiti Sains Malaysia (USM), Penang, Malaysia

Abstract— Multisensor data fusion provides significant advantages over single source data. The use of multiple types of sensors plays an important role in achieving reasonable accuracy and precision. A novel integrated heterogenous multi sensor data fusion approach in structural health monitoring is proposed. The study concerns to find a simple and affordable monitoring strategy for Alkali-aggregate reaction (AAR), which is one of the root causes for structural deterioration in concrete. Many researchers have stated the process of gradual structural deterioration to be very complicated because of the random distribution of aggregate, the arising and growth of concrete crack shows remarkable abnormity and discontinuity. Although researchers have developed several test methods to identify potential reactivity of aggregate. There is no universally valid standard testing method for all cases of AAR. The conventional methods namely petrographic examinations, expansion tests, and chemical analyses are cost expensive and require high skilled person to carry out tests. More over they qualitatively determine the possibility of AAR presence but least quantitatively predict whether the AAR will be deleterious. In order to develop a monitoring strategy for AAR in small size concrete structures, it is necessary to simulate the AAR expansion and cracking within reasonable laboratory timescale. A standard method to accelerate AAR expansion is employed on four samples which are prepared with different level of alkali concentrations. Different sensor systems are used at surface and internal level. Acoustic sensor system, electro-mechanical system, optical systems are employed to obtain surface level damage. The internal level of damage is obtained by embedded sensors within the structure. Features extracted from heterogeneous sensors are fed to Decentralized Kalman filter. The fused global estimates and individual source estimates are fed to artificial neural network (ANN), which characterize and quantify the level of damage. The research is focused on establishing correlation among surface damage level, internal damage level and the amount of gel concentration in the structure. To emphasize the expected improved accuracy using data fusion, evaluations are done on efficiency and accuracy of single source data system comparing with the fused heterogeneous data.

Fiber Optic-based Sensing Approach for Corrosion Detection

Othman Sidek, **Shahid Kabir**, **and Muhammad Hassan Bin Afzal**
Collaborative μ-electronic Design Excellence Centre (CEDEC)
Engineering Campus, Universiti Sains Malaysia (USM), Penang, Malaysia

Abstract— Fiber-optic based sensing technology has shown remarkable progress in obtaining higher degree of accuracy for structural health monitoring of civil structures; especially, in concrete structures. In this work, a FOS based Enhanced Fiber Optic Corrosion Sensor is being applied in the concrete structures to sense, measure and obtain the level of corrosion in concrete structures and also quantify the corrosion level. A conventional Half-cell method is being applied on the similar accelerated concrete structures as a benchmark to evaluate and analyze the accuracy level of proposed EFOCS method of corrosion detection. Finally, a unique and special coating material (PDMS) is being applied on the EFOCS sensor for performance and accuracy enhancement. All data from three different methods has been collected, analyzed and evaluated and further scope of improvement also been discussed.

Industrial Applications of SonicIR Nondestructive Evaluation Method

Xiaoyan Han[1], **Golam Newaz**[2], **Lawrence D. Favro**[3], **and Robert L. Thomas**[3]

[1]Department of Electrical and Computer Engineering, Wayne State University, Detroit, MI 48202, USA
[2]Department of Mechanical Engineering, Wayne State University, Detroit, MI 48202, USA
[3]Department of Physics and Astronomy, Wayne State University, Detroit, MI 48202, USA

Abstract— Nondestructive Evaluation (NDE), also known as Nondestructive Testing (NDT) or Nondestructive Inspection (NDI), covers wide range of methods that can be used to determine the quality or integrity of structures/materials nondestructively. The commonly used methods include Ultrasonic, radiographic, electromagnetic, and optic ultrasound. NDE methods play important roles not only in the quality control of the finishing products but also during various stages of manufacturing. Therefore, NDE techniques have been widely adapted in manufacturing industries for decades. With the demands of low cost of products and services, fast, wide-area, and reliable NDE technology becomes more and more attractive. In this presentation, we'll present such a NDE technology: SonicIR Imaging and its application in industrial applications. SonicIR Imaging is a relatively new NDE technology that combines ultrasound excitation and imaging of thermal radiation. This technology was invented by the authors about a decade ago. The authors have received nine patents on it[1]. The underline physics in this technology is quite simple: a short pulse (typically a fraction of a second) of sound/ultrasound (in the range of tens of kilo-hertz) causes frictional rubbing between faying surfaces of defects such as cracks, the frictional heating is detected by thermal detectors or imagers to identify defects. The effect of such heating can be astonishing. The authors will present its industrial applications through some examples such as defect detection in metal structures and materials. Its advantages over traditional NDE methods will be described through the examples as well.

[1]US Patents: # 6,236,049, # 6,399,948; # 6,437,334; # 6,593,574; # 6,759,659; # 6,998,616; # 7,064,332, # 7,122,801, and # 7,199,367.

Artifact Mitigation in High Energy CT via Monte Carlo Simulation

Xuemin Jin and Robert Y. Levine
Spectral Sciences, Inc., USA

Abstract— The photon attenuation coefficient is a measure of how strongly a material absorbs or scatters light at a given wavelength. In an *idealized* experiment, the photon attenuation can be measured by using an infinitely narrow beam of incident monoenergetic photons and detecting the number of those photons traversing a material of known thickness. These particles are the so-called primary photons. In computerized tomography (CT), the raysum is a line integral of the extinction coefficient for the primary photons.

In practice, CT raysum measurements are far from ideal. For example, in nondestructive testing (NDT) with an accelerator-generated source, the incident photon flux is not monoenergetic but rather has the spectrum of bremsstrahlung photons created in the accelerator head. This polychromatic beam leads to the well-known beam hardening artifact in CT imaging, arising from the preferential absorption of low-energy photons. Beam hardening can cause the appearance of enhanced absorption on the periphery of an object. Furthermore, the electron-gamma shower (EGS) through the object of interest contains scattered photons and charged particles (electrons and positrons) that are incident onto the detector. The scatter can cause streaking effects across the reconstructed image. The detection and mitigation of scatter is important for CT imaging, and has been the focus of recent beam innovations.

The complexity of the EGS and the particular nature of CT raysum for primary photons motivate the use of Monte Carlo simulation to characterize the measurement process and to provide accurate mitigation of artifacts in CT imaging. In Monte Carlo simulation, photons and charged particle creation, annihilation, and scattering are stochastically accounted for in transit through the accelerator head and object of interest. In this study we use the EGS/BEAM code, and the polychromatic bremsstrahlung beam will be simulated by using an accelerator head model with 15 MeV electrons incident on a tungsten slab. The primary photons can be isolated from scatter photons and charged particle secondaries by assigning latch bits to particles at a scoring plane just before the detector. This is the key to assessing the degree of deviation from ideal CT raysum measurements and consequent artifact mitigation.

The key to mitigation of scatter and beam hardening artifacts is the energy-resolved photon attenuation of the target material, μ(E), as well as the difference of this attenuation for primary photons and for all-particle fluences. We evaluate μ(E) using Monte Carlo simulation with a monoenergetic pencil beam and material slabs of appropriate thickness. The extractions are performed with both primary photon and all-particle fluence, yielding two separate attenuations of the target material. It is found that the extracted attenuations in water and copper are very close to the measured values, demonstrating the simulation accuracy. The same simulation is performed on high-Z materials of aluminum, steel, and tungsten, and the energy-resolved attenuation, μ(E), is extracted for these materials within the energy range of 0.5–15 MeV.

The high energy (< 15 MeV) incident polychromatic γ-ray spectrum and the energy-resolved photon attenuations in high-Z materials are applied to derive the beam hardening correction in steel cylinders and pipes. Monte Carlo simulated pencil beam simulations of raysum projections are processed using latch bit filters to isolate exiting primary photons. The beam hardening correction is applied to this data, which is then interpolated to a uniform grid. Filtered back projections of the raysums are compared with and without the beam hardening correction. It is demonstrated that beam hardening artifacts can be successfully removed in tomographic reconstructions of high-Z dense materials such as steel.

Session 2P6
Electromagnetic Media and Wireless Propagation

Analysis of Depolarized Electromagnetic Waves Propagated through Random Media

Yukihisa Nanbu[1], **Mitsuo Tateiba**[2], **and Hosam El-Ocla**[3]

[1]Sasebo National College of Technology, Sasebo, Nagasaki 857-1193, Japan
[2]Ariake National College of Technology, Omuta, Fukuoka 836-8585, Japan
[3]Department of Computer Science, Lakehead University
955 Oliver Road, Thunder Bay, Ontario P7B 5E1, Canada

Abstract— Studies of the electromagnetic (EM) wave propagation through random media have been continued into the important development of remote sensing, various measurements, and satellite communications. It is mainly assumed in those studies that the fluctuating intensity of continuous random medium is so weak and the fluctuating scale-size is much larger than the wave length of EM wave. Therefore the scalar approximation has been used. When the optical path-length becomes large in long propagation in the random medium, however, then we have to consider the effect of depolarization of EM waves. In previous studies, quantitative analysis of the depolarization has not been investigated sufficiently.

To solve this depolarization problem, we first have derived an integral equation using the dyadic Green's function on the assumption that there exists a random medium screen of which the dielectric constant is fluctuating randomly. Next we have modified the integral equation on the assumption that the observation point is very far from the screen. Form this modified integral equation, the analytic expression of the depolarized EM wave has been given by using the perturbation method. Finally we have shown the first order perturbation of the depolarized EM wave and discussed quantitatively the depolarization of EM wave propagated through the random medium screen.

Anisotropic Properties of Graphene and BN Sandwiched Graphene Based on the First-principle Theory and Kramers-Kronig Relation

Junxia Wang[1, 2], **Yang Xu**[2], **and Hongsheng Chen**[1, 2]

[1]The Electromagnetics Academy at Zhejiang University
Zhejiang University, Hangzhou 310027, China
[2]Department of Information and Electronic Engineering
Zhejiang University, Hangzhou 310027, China

Abstract— In this work, we present a detailed and systematical study of anisotropic properties of monolayer graphene, bilayer graphene and BN sandwiched graphene without charge doping, including the conductance, permittivity, refractive index, transmittance, reflectance and absorance at different directions. We find the parameters exit big differences when we change the directions of incident wave, so we give the conclusion that the graphene is an anisotropic material. The calculation is based on the first principle theory and Kramers-Kroning relation.

Casimir Stresses in Slender Inhomogeneous Dielectric Media

R. W. Tucker[1, 2], **S. Goto**[1, 2], **and T. Walton**[1, 2]

[1]Physics Department, Lancaster University, Lancaster, UK
[2]The Cockcroft Institute, Daresbury, UK

Abstract— The role of quantum fluctuations in determining the behaviour of fabricated microstructures is becoming increasingly important in a wide area of science and technology. Quantum interactions of matter with the electro- magnetic field in renormalizable theories (QED) in an unbounded vacuum yield remarkably accurate predictions at the micro-scale. However, macroscopic predictions directly from QED that are induced by the presence of bulk macroscopic matter and material interfaces can be made with far less confluence since they depend critically on both geometric and constitutive modelling on macroscopic scales. In particular the effect of quantum states of the electromagnetic field on the behavior of isolated closed material micro-domains of polarisable matter that exhibit inhomogeneities remains an unsolved problem and an active area of current research. A new mathematical and computational technique for calculating quantum vacuum expectation values of energy, momentum and angular momentum currents and densities associated with electromagnetic fields in bounded domains will be presented. This technique will be used to analyze the effects of quantum fluctuations of such fields in inhomogeneous and anisotropic slender dielectric structures.

Electromagnetic Analysis of an in-car Complex Channel of Propagation by Means of Non Invasive Measurements and FDTD Based EM Simulations

J. G. Tartarin[1], M. Cheikh[2], J. David[3], and A. Morin[2]

[1]LAAS-CNRS & Universite de Toulouse, 7 av. du Col. Roche, Toulouse 31077, France
[2]Continental Automotive France SAS, 1 rue Paul Ourliac, Toulouse 31036, France
[3]LAPLACE, 2 rue Camichel, Toulouse 31000, France

Abstract— Automotive security requirements makes use of different RF systems (radar in free space with no obstacle, in-car RF links for evaluation of the tire state, ...). Among these systems, tire pressure monitoring systems (TPMS) allow a real time evaluation of the pressure for each tire of the car, by sending frames of data over a RF signal (@ F_{RF} = 434 MHz). The system can locate each tire around the vehicle, and a display screen on the dashboard close to the receiver alerts the driver when the pressure is lower or higher than the expected value. It is well established that RF propagation in a complex structure (electronic RF packages, indoor communications, ...) can be sensitive to local RF signal losses. In a car structure, the medium of propagation is made of 3D multi-scale modules, and the transmitters (sensors+RF) are moving around the rim according to the speed of the vehicle. As the structure of the car is made with many different dielectric or metal parts sizing from some wavelengths (λ_{RF} = 69 cm) to less than $\lambda_{RF}/20$ (i.e., lumped pieces), the RF propagation's channel is perturbed by a combination of dense multipath processes due to diffraction, diffusion, reflection (diffuse or specular), and waveguide transmission processes. The development of TPMS modules needs an accurate knowledge of the involved propagation phenomena, so that matched strategies can be developed to improve the reception rate of the sent frame (i.e., robustness of the TPMS). A fully experimental approach is not suited to develop optimized modules: this technique is time consuming, and cannot authorize studies versus variable parameters to understand the underlying phenomena managing the channel efficiency. Electromagnetic (EM) simulations stand as an efficient tool to shorten times of development, and to understand how the RF channel is established between the transmitter and the receiver. Moreover, it allows to determine the impact of the car design on the RF budget link, or to test the robustness of the TMPS system versus different options (change of tire manufacture, rim size, size and number of passengers, location and quantity of luggage). This paper presents different studies on simplified cars (Figure 1(a)) where the sizes and electric-metallic characteristics have been tuned, and also on complex realistic structures (cabriolet, berline car in Figure 1(b)). EM studies are also proposed on the source module to evidence the impact of the rim and tire, and the ground influence on the repartition of the power in the near field zone. From simulation over the whole car structure, it is shown that in-car transmission is largely perturbed as the EM field fades at local positions, whereas transmission by the lateral sides (or between ground and chassis) still keeps the field at acceptable

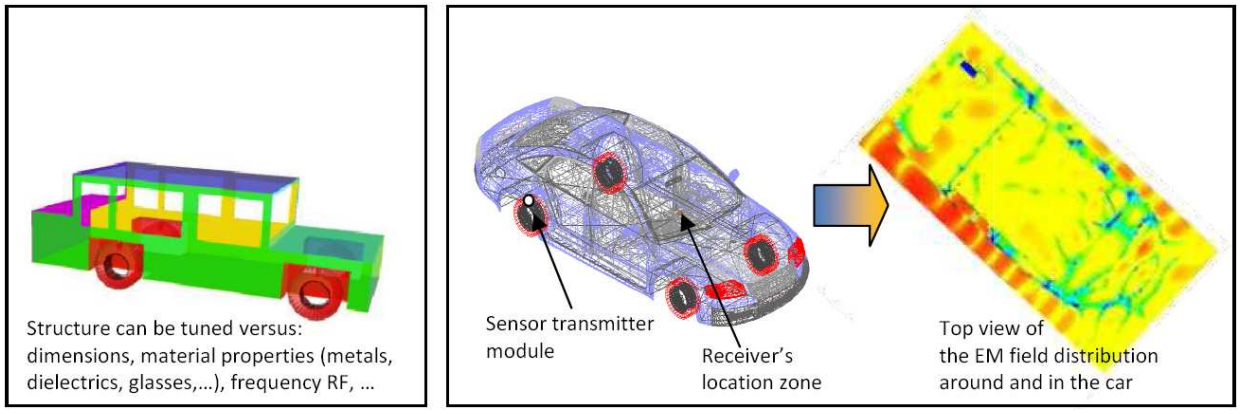

(a) (b)

Figure 1: (a) Simplified tunable car's structure. (b) Realistic models (meshing and EM simulations @ F_{RF} = 434 MHz).

levels. Then the receiver's 3D best location is studied accurately as the space (i.e., meshing) resolution must be very low. All these simulations are compared with measurements. From this work, different strategies are brought up (antenna diversity, polarization diversity, time diversity): improvements of more than 5 dB, up to 12 dB have been proposed on the TPMS efficiency, thanks to the knowledge of the RF fading profiles' behavior between the transmitters and the receiver.

Characterisation and Modelling of Ultra Wideband Radio Propagation Links for Low Power Body-centric Wireless Network

Qammer Hussain Abbasi, **Wenxuan Tang**, **Akram Alomainy**, **and Yang Hao**
Queen Mary, University of London, United Kingdom

Abstract— For wireless communication of medical implants to external sources, a compact and low power wearable node on the human body is required. Now-a-days demand for higher data rate and bandwidth becomes incredibly high, so researchers are looking towards a technology that has potential for higher data rate, larger bandwidth and low power wearable nodes. In this work, ultra wideband (UWB) on-body radio propagation channel characterisation has been investigated using a compact UWB antenna thoroughly and performance of various on-body links have been analysed on the basis of bit error rate (BER) for a specific value of outage threshold and therefore optimum locations for wearable devices have been identified with low power requirements.

In this study, measurements were performed in both an anechoic chamber and in an indoor environment for over one hundered different on body links. Half of the locations are for line of sight (LOS) and the other half for non-line of sight (NLOS) case as shown in Fig. 1(a). For all measurements transmitter (Tx) is fixed at left waist and receiver (Rx) is placed at different locations as shown in Fig. 1(a). Path loss model for both LOS and NLOS cases have been derived from the measured on-body channel data. Channel impulse responses (CIR) have been calculated for each on-body links and those calculated CIRs have been used in Multiband-OFDM based UWB to calculate BER performance for each link at a specified bit energy to noise (E_b/N_o) ratio. Finally on the basis of BER, different on-body links are categorized as good, bad or acceptable links at certain outage threshold (i.e., $1e^{-3}$). Also whole human body is divided in different sections for LOS and NLOS cases and on basis of system outage, recommendations have been given for putting wireless devices on the body. Fig. 1(b) shows BER variations of different on-body links in an indoor environment for a low value of (E_b/N_o). Result shows that variation of BER is dependent not only on the distance of Rx from Tx but also depends on the human body tissues and orientation between Tx and Rx.

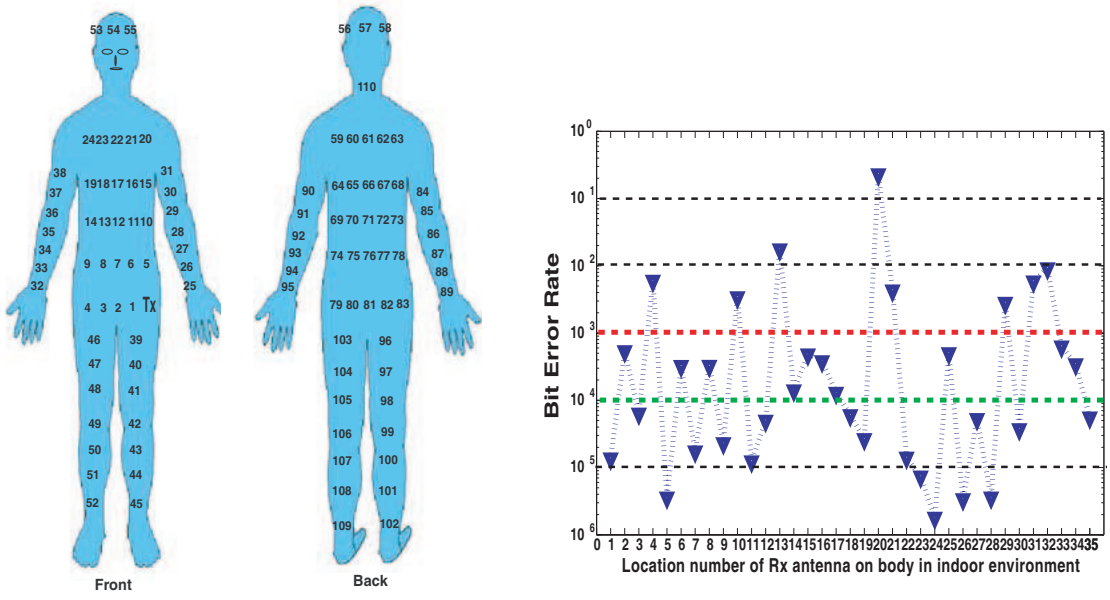

(a) (b)

Figure 1: Measurement setup and BER variations for various on-body links. (a) On-body locations used in the measurement campaign for UWB on-body radio channel characterisa. (b) BER variations for different locations on the body for $E_b/N_o = 4\,\text{dB}$ in an indoor environment

Received Signal Strength (RSS) Based Localization for WLAN Networks

Sreejith Sisupalan Lathikumari, **Suman K. Gunnala**, **and Saibun Tjuatja**
Wave Scattering Research Center, Department of Electrical Engineering
The University of Texas at Arlington UTA, Box 19016, Arlington, TX 76019-0016, USA

Abstract— Indoor localization based on Received Signal Strength has been a topic of Interest due to its relative simplicity in measurement and minimal hardware requirements. Much of the research in this field has been on developing an indoor propagation model. A generic indoor propagation model that fits all types of indoor environment has largely been unsuccessful due to the complex multipath environment present in indoor environments. This research focuses on a different aspect of localization. That is, if the estimated distances from three access points (APs) are given, how do we accurately estimate the target position (MS or mobile station). If the estimated distances are error free, if a circle is drawn with each AP as center and estimated distance to the target as radius, the three circles will intersect at a point as shown in Figure 1.

In presence of noise however the circles do not intersect at a point instead they intersect over an area as shown in Figure 2.

In such a situation a least square solution is the straightforward approach to solve the problem. The least square problem can be formulated as linear, nonlinear or iteratively weighted least square problem [1]. In this study, the performance of these techniques is compared to the weighted center of mass based approach given in [2]. The effect of using different weighting schemes is studied and their performances were evaluated using experimental data collected in different indoor environments. A brief description of the experimental setup is as follows

1. The experiment is conducted in a Hallway and an Atrium at the University of Texas at Arlington.
2. The Mobile station or target is kept at the center of the Hallway or Atrium and three Access points are arranged randomly as shown in Figure 3.
3. The Mobile station is stationary and is an active transmitter. The Access points (AP1, AP2 and AP3) are the receivers which record the signal statistics. The signal statistics around the three access points (1, 2, 3) are recorded.
4. The distance estimate from the Mobile station to the Access points are estimated using the dynamic propagation model method used in [3].
5. Linear, Non linear and iteratively weighted least square (IRWL) trilateration is used for estimating the position of MS. The variance of the range estimate is used as weighting factor for IRWL.

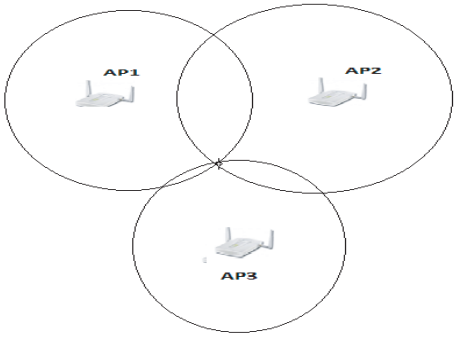

Figure 1: Trilateration without measurement error or noise.

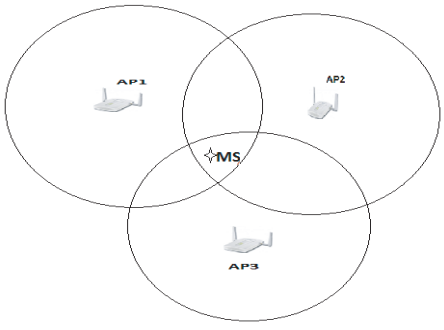

Figure 2: Trilateration with measurement error and noise (AP1, AP2, AP3 are the access points and MS is the Mobile Station or the target to be localized).

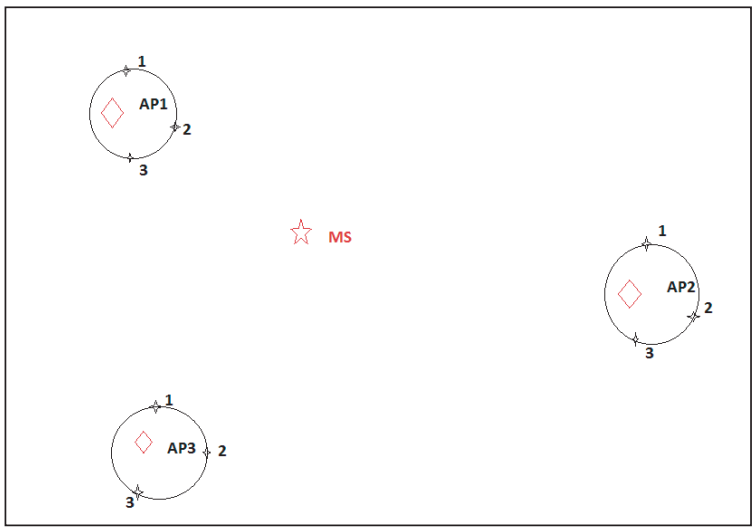

Figure 3: Experimental setup.

REFERENCES

1. Sharma, N. K., "Weighted center of mass based trilateration approach for locating wireless devices in indoor environment," *Proc. of the 4th ACM International Workshop on Mobility Management and Wireless Access (MobiWac 2006)*, 112–115, Terromolinos, Spain, Oct. 2006.
2. Navidy, W. and W. S. Murphy Jr, "Statistical method in surveying by trilateration," *Computational Statistics and Data Analysis*, Vol. 27, No. 2, Apr. 1998.
3. Mazuelas, S., et al., "Robust indoor positioning provided by real — Time RSSI in unmodified WLAN networks," *IEEE Journal of Selected Topics in Signal Processing*, Vol. 3, No. 5, Oct. 2009.

A Neural Network-ray Launching Technique for Coverage Prediction

Juan Pascual-García, José Víctor Rodríguez-Rodríguez, María Teresa Martínez-Inglés, José María Molina-García-Pardo, and Leandro Juan-Llácer
Department of Information and Communication Technologies (TIC)
Technical University of Cartagena (UPCT), Spain

Abstract— Wireless communications systems require accurate coverage prediction to achieve an appropriate deployment. Ray launching is one of the most precise techniques to calculate path loss for urban outdoor an indoor environments. Nevertheless, it is a very time consuming method. In [1] an efficient mechanism to evaluate the path loss in a limited area from a one point ray launching simulation was presented. This technique was two hundred times faster than the original ray launching method.

In order to use this fast technique in the whole area of interest is necessary to select the simulation points in a suitable way. Otherwise, large errors will occur in the coverage prediction. To allow fast and accurate prediction coverage in large areas the one simulation technique is incorporated into a neural network structure. The neural structure has three layers. The main layer is composed of several one point simulation units. Each unit (neuron) is able to calculate the path loss everywhere in the whole area, but is accurate only in a certain region of the area. For this reason, another layer groups the input points in different regions and connects each region to the appropriate neurons. Finally, the output layer performs a linear combination of the main layer neuron outputs. The neural network-ray launching technique was tested in a 60 GHz indoor environment. The simulation results show that the proposed method is precise and allows a drastic time reduction with respect to the original ray launching tool.

ACKNOWLEDGMENT

This work is funded by the Ministerio de Educación y Ciencia. Ref. TEC2010-20841-C04-03 project and the Fundación Séneca CARM Ref. 08818/PI/08 project.

REFERENCES

1. Ibernon-Fernández, R., J.-M. Molina-Garcia-Pardo, J.-V. Rodríguez-Rodríguez, and L. Juan-Llacer, "Predicting coverage in an area from a single simulation," *Proceedings of Antennas and Propagation Society International Symposium*, 727–730, Washington, USA, July 2005.

A Robust Indoor Wireless Localization

Hermawan Raharjo, **Si Wen Chen**, **and Pengty Ngor**
School of Electrical and Electronic Engineering, Nanyang Technological University, Singapore

Abstract— We propose a novel Non-Line-of-Sight localization algorithm by using Time-of-Arrival (TOA) and Angle-of-Arriva (AOA) measured at both mobile and reference devices in a three dimensional multipath environment. Gaussian neighborhood weighting is proposed to reduce uncertainties in mobile device's location. In this process, Gaussian neighborhood function is formulated and used to calculate weighted centroid of adjacent points. Monte Carlo simulations show that the proposed localization scheme is robust and outperforms previous NLOS localization scheme.

Channel Impulse Response Simulation Based on Propagation Graph Theory for High Speed Train Scenarios

Li Tian[1], **Quan Zuo**[1], **Junhe Zhou**[1], **Xuefeng Yin**[1], **Meisong Tong**[1], **Zhimeng Zhong**[2], **and Stan X. Lu**[2]

[1]College of Electronics and Information Engineering, Tongji University, Shanghai, China
[2]Huawei Technology Company, Xi'an, China

Abstract— Recently studies on wireless wideband communications on high-speed trains have received an extensive attention. Empirical characteristics of radio propagation channels in such vehicular environments are of importance for designing transmission techniques for high-data-rate communications. Conventional channel measurements usually require a mass of human and material resources and may be difficult to carry out in many cases. Furthermore, it is nontrivial to get sufficient amount of time-frequency-space samples of channel impulse responses using traditional measurement equipment due to the fast movement of trains in the scenarios of interest. It is then necessary to resort to numerical computational methods for analyzing the vehicular channels and constructing realistic stochastic channel models.

In this contribution, the propagation graph modeling approach is originally applied as a simulation-based method for predicting the channel characteristics in various scenarios. [1] First we collect geographical information of the propagation environments that are usually encountered in high-speed-train scenarios, and categorize into several typical scenarios, such as urban, suburban and rural. Then, similar to the ray-tracing approach, we determine the positions, visibility and mobility of scatterers according to the specific environments. By using the graph modeling approach, the channel impulse responses in time, frequency and space, are computed analytically.

The graph modeling emulates the interaction between electromagnetic wave and scatterers existing in a socalled random graph. The vertices of a graph represent scatterers and the edges connecting two scatterers models the wave propagation paths between them. When a graph is generated, the corresponding realization of the channel impulse response can be computed by exhaustively searching for propagation paths that connect the transmitters and the receivers. The obtained impulse response contains well-separated discrete components and the diffuse scattering components. The specular-to-diffuse transition is found to be consistent with the observed results in measurements. Since the propagation-graph-based method basically relies on the position and mobility information of random scatterers, it is applicable to analyze both the deterministic and stochastic channel characteristics.

In the full paper, we will first elaborate the propagation graph based channel modeling approach. Then, according to the analysis in our previous work [2], the graph model is modified slightly. Moreover, we will choose several scenarios as examples to illustrate the application of the method. The stochastic channel models obtained by using the method will be presented as well in the paper.

REFERENCES

1. Pedersen, T. and B. Fleury, "Radio channel modelling using stochastic propagation graphs," *IEEE International Conference on Communications*, 2733–2738, Glasgow, Scotland, 2007.
2. Zhou, J., X. Yin, L. Tian, M. Tong, Z. Zhong, and S. X. Lu, "Characterization of the random scattering induced delay power spectrum using born series," *2011 IEEE Symposium on Antennas and Propagation and USNC/URSI National Radio Science Meeting*, submitted, Spokane, Washington, USA, July 2011.

Session 2P7
Poster Session 3

Neural Model for Modeling of Dumbbell Shape Defected Ground Structure

Hamid Reza Dalili Oskouei and Jafar Khalilpour
University of Aeronautical Science & Technology, Tehran, Iran

Abstract— In recent years, neural networks have gained a lot of attention as fast and flexible tools for modeling, simulation, optimization and design of microwave device. In this paper, a new approach of neural networks is proposed to model the Dumbbell Defected ground structure (DGS). This structure is used in different parts of microwave systems such as filters, oscillators and power amplifiers.

It should be noted that the obtained results are in excellent agreement with simulation and measurement results.

A Novel Multilayer Dual-mode Substrate Integrated Circular Cavity (SICC) Filter with Two Arc-shaped Coupling Slots

Zhigang Zhang, **Yong Fan**, **Yujian Cheng**, **and Yonghong Zhang**
Extreme High Frequency Key Laboratory, School of Electronic Engineering
University of Electronic Science and Technology of China, Chengdu, China

Abstract— A novel millimeter-wave multilayer dual-mode filter is developed based on the substrate integrated waveguide circular cavity (SICC). A dual-mode SICC filter with two arc-shaped coupling slots has been designed for Ka-band application. The multilayer dual mode filter has been firstly realized only by adjusting two arc-shaped coupling slots located in metal layers. The position and size of the two coupling apertures can determine the coupling amount between two degenerate modes. Meanwhile, it is possible to control the return loss, bandwidth and rejection level by adjusting the size and relative position of the two arc-shaped slots. This novel filter is very compact and has the advantages of return loss, very low insertion loss, high selectivity.

Design of an LNA with Ultra Low Noise and Model Noise Temperature at 2.45 GHz

S. A. Burney and C. Qunsheng
College of Electronic Information Engineering
Nanjing University of Aeronautics and Astronautics, Nanjing 210016, China

Abstract— An LNA was designed that exhibits ultra low noise figure (NF) and noise temperature. Emphasis was given to achieve the minimum NF as offered by the device (transistor). The selected device uses E-PHEMT technology and has 0.25 micron gates allowing ultra low noise figure. Furthermore, the device is chosen because it requires minimum feedback for stability. It was found that this device comparatively exhibits reasonable tradeoffs. The VMMK-1218 characterizes high dynamic range, high gain and low NF that generates off of a single position DC power supply. The LNA has been systematically designed thus illustrating not only a simple structure and minimum NF but also exhibits excellent overall performance. The design methodology uses analytical approach. This allows us to control all the parameters of the project. Also with the help of visual aid softwares like 'Advance Design System' (ADS), it is possible to visualize, fine tune and optimize the physical dimensions to achieve the desired results. Previously, a Low Noise Amplifier at 2.45 GHz was designed that achieved NF of 0.3. The technique used in this paper employs a simultaneous procedure that compares results from two sources, namely inbuilt ADS functions and user equations; this combined information gives the designer added advantage. Even if software limitations restrict the designer to achieve the desired objective, the results from the user equations can be realized. Hence the designer can modify the values in the equations for optimum performance. This can be seen by the results achieved. The LNA has improved S_{11} value near -10 dB and output VSWR of 1.073 and obtained an excellent NF of 0.202 and model noise temperature of 13.8 K. This design has potential to serve in civil marine radar applications.

The Study of Statistical Properties for Rainfall and Rain-induced Attenuation in Xi'an, China

Houbao Shi, Shuhong Gong, and Kexiang Liu
School of Science, Xidian University, Xi'an, Shaanxi 710071, China

Abstract— The rain-induced attenuation has a great influence on the frequencies over 10GHz. Many research institutions or scholars have being working on that and have given several models, such as ITU-R model, Assis-Einloft Improve model and so on. These traditional models analysis year probability statistical properties, which is helpful for the technic of fixed power margin. However, rain-induced attenuation becomes greater at millimeter-wave frequencies, and rainfall events are often small probability in time and space, so it is a big challenge for power margin technic because of its cost-effective. Some scholars and research institutions recommend adopting adaptive power control technology to mitigate rain-induced attenuation. But self-adaptive power control need more accurate protection of link dynamic fade so that the self-adaptive control system can adjust transmit power and suppress the rain attenuation. It is very important to research the dynamic characteristics of rain-induced attenuation. In this paper, the year probability statistical properties of rain are analyzed based on the measurement data of 1 minute cumulative rainfall in Xi'an, China. And the results are compared with ITU-R model, Moupfuma model etc.. The dynamic characters of rain-induced attenuation are investigated using those measured data. The results given in this paper are significant for studying channel dynamic fade properties and Fade Mitigation Techniques (FMT).

ACKNOWLEDGMENT

This work has been supported by Natural Science Foundation of China 61001065 (NSFC: 61001065).

Inversion of Refractive Index in Marine Atmospheric Duct by Genetic Algorithm

X. L. Zhao, **Y. P. Wang**, **and L. H. Bao**
Tianshui Normal University, China

Abstract— Marine evaporation duct is a nearly permanent propagation mechanism due to the abrupt changes in the vertical temperature and humidity profiles just above the large ocean surface. Its existence greatly strengthens or degrades the capability of the naval Radar, Communication, and Electronic Support Measures (ESM) system. Environmental information based on the effective duct can accurately predict the EM-wave propagation, and exactly assess the performance of electronic weapons systems.

Based on the characteristic parameter of the atmospheric duct, such as modified refractivity, the ray-tracing technique and the parabolic equation by Fourier split-step method were introduced to analyze the anomalous propagation of electromagnetic wave in marine evaporation duct. The simulation results show that evaporation duct can significantly trap some radio rays to extend the propagation distance of EM wave and result in the appearance of radar blind zone. Therefore, the real-time, accurate forecasting and prediction of refraction index in atmospheric duct is key factor for performance evaluation and system design of electronic systems.

By Genetic Algorithm (GA) and Fourier split-step method (FSS) and for neutral layer of evaporation duct with the duct height 30m, Refractivity from Clutter (RFC) is used to predict and forecast the refractive index profile of evaporation duct. Inversion of atmospheric refractive index profile using radar sea clutter has an obvious advantage which can use ship-borne radar remote sensing equipment to estimate the current atmospheric refractive index profile of the vertical and horizontal distribution. Meanwhile, the inversion problem is converted to statistical estimation of parameters. In contrast with traditional meteorological measure, refractive index profile from radar sea clutter does not need to add additional measuring equipment, and real time, military secrecies is better. Therefore, the RFC technique is an efficient method to estimate atmospheric refractive index profile.

ACKNOWLEDGMENT

The authors acknowledge the financial support of NSFC (National Natural Science Foundation of China) grant No. 61002008, Foundation of Gansu Educational Committee grant No. 1008B-11 and 'QingLan' Talent Engineering Funds by Tianshui Normal University.

Subsurface Imaging with NIR Light Using Polarization Gating

M. Šormaz[1] and P. Jenny[2]

[1]Laboratory for Media Technology
Swiss Federal Laboratories for Materials Science and Technology (EMPA)
Überlandstrasse 129, 8600 Dübendorf, Switzerland
[2]Institute of Fluid Dynamics, Swiss Federal Institute of Technology Zürich (ETH)
Sonneggstrasse 3, 8092 Zürich, Switzerland

Abstract— In this paper a numerical study with the near infrared (NIR) laser light and polarization gating is used to show possible contrast improvement of the spherical inclusion hidden in the turbid medium. Inclusion has the same refractive index and scattering properties as surrounding medium but slightly higher absorption. Approach is based on time-resolved reflectance measurements and selection of photons with arc-like trajectories using polarization gating technique. Numerical studies performed for two turbid media, typically used to mimic biological tissues, reveal that coaxial setup of laser and detector is not suitable for detection of photons with arc-like trajectories. As well, the contrast improvement in ballistic-photon imaging strongly depends on the single-scattering phase function.

Radar Based Tomography System for Breast Tumor Imaging

V. Lalitha[1] **and E. R. Rajkumar**[2, 3]

[1]Department of Electronics and Communication
MNM Jain Engineering College, Thoraipakkam, Chennai 600033, India
[2]VIT University, India
[3]IRSEEM, France

Abstract— Breast cancer causes a number of deaths every year all over the world. There are a variety of imaging modalities for the detection of tumor in breast like mammography and thermography. The biggest disadvantage of mammography is that it uses X-rays which have high ionization property and is hence can cause radiation hazards to the human being. The disadvantage of thermography is the high cost and complexity of the system as well as imaging and image reconstruction techniques. Hence the need for a better and comparatively less complicated imaging system arises.

Here a radar based tomography system is proposed that can be used for imaging of breast and detection of tumors. An ultra wideband antenna is chosen which acts as both transmitter and receiver for radar. This antenna is chosen as it as a low profile and good transient characteristics [1]. A 3-D breast phantom is developed for the purpose of testing and validation of the system. The antenna is dipped in a coupling liquid of propylene glycol in distilled water so that its dielectric is similar to that of human breast [2]. In order to extract the tumor data, rotation subtraction algorithm is preferred over background subtraction method as it is more efficient in real-time application [3]. A mechanical gear-like system is used to rotate the antenna arrays in order to obtain data from various tomographic planes. These signals are received and processed and finally the image is reconstructed using iterative gauss-newton method. The development is in the process and with appropriate phantom design, the same can be validated.

REFERENCES

1. Son, S. H., N. Simonov, H. J. Kim, J. M. Lee, and S. L. Jeon, "Preclinical prototype development of a microwave tomography system for breast cancer detection," *ETRI Journal*, Vol. 32, No. 6, 901–910, December 2010.
2. Klemm, M., J. A. Leendertz, D. Gibbins, I. J. Craddock, A. Preece, and R. Benjamin, "Microwave radar-based differential breast cancer imaging: Imaging in homogenou breast phantoms and low contrast scenarios," *IEEE Transactions on Antennas and Propogations*, Vol. 58, No. 7, 2337–2344, July 2010.
3. Klemm, M., I. J. Craddock, A. Preece, J. Leendertz, and R. Benjamin, "Evaluation of hemispherical wideband antenna array for breast cancer detection," *Radio Science*, Vol. 43, RS6S06, 2008, doi: 10.1029/2007RS003809.

A Compressive Sensing Imaging Method for Simulated GPRs Data

Lu Zhu, **Haiwen Liu**, **Shan Wang**, **and Xuehui Guan**
School of Information Engineering, East China Jiaotong University, Nanchang 330013, China

Abstract— Recent advances in signal processing have focused on the use of sparse representations in various applications. A new field of interest based on sparsity has recently emerged: "compressed sensing (CS)". This theory is a new sampling framework that provides an alternative to the well-known Shannon sampling theory. A Compressive Sensing imaging method is presented ground penetrating radars (GPRs). It is enough to make measurements at only a small number of random projection to construct an image of the target space by solving a convex optimization problem which enforces sparsity through l1 minimization, thanks to that the GPRs target space is sparse, i.e., a small number of point like targets. This imaging strategy provides a simple coding or compression stage that only requires a low computational burden. Beyond the scope of GPRs data analysis, it presents a simple but illustrative comparison of CS with a standard wavelet-based compression scheme from a Simulated GPRs Data. Imaging results for simulated GPR data exhibit less clutter than the standard migration methods. The images also have increased resolution where closely spaced targets that cannot be resolved by the standard migration methods.

Pseudo Random Binary Sequence GPR Imaging via Compressive Sensing

Xin Xu[1, 2], **Wei Wang**[1, 2], **Zhiwei Lin**[1, 2], **Peng Zhang**[1, 2], **and Xiaojuan Zhang**[2]

[1]Graduate School, Chinese Academy of Sciences, Beijing, China
[2]Institute of Electronics, Chinese Academy of Sciences, Beijing, China

Abstract— In this paper, the Pseudo Random Binary Sequence Ground Penetrating Radar (PRBS-GPR) is investigated under the Compressive Sensing (CS) framework. We show that the bernoulli signal transmitted by PRBS-GPR has an inherent connection with CS theory, and sampling rate can be reduced without loss of resolution. The Restricted Isometry Property (RIP) of subsampled toeplitz bernoulli matrix is obtained by theoretical analysis, then exact reconstruction is guaranteed by some well-known theorems. Our analysis is not restricted on the bernoulli case, so extensions can be made to a larger class of noise modulated radar systems.

Short Electric-field Antennae as Diagnostic Tools for Space Plasmas

Jean Gabriel Trotignon and Jean Louis Rauch
Laboratoire de Physique et Chimie de l'Environnement et de l'Espace (LPC2E)
Centre National de la Recherche Scientifique (CNRS)
3A Avenue de la Recherche Scientifique, 45071 Orléans Cedex 02, France

Abstract— A technique, used in geophysical prospection to measure the ground permittivity, has been successfully transposed to space plasmas. The basic principle is to measure the self impedance of a single electric antenna or the mutual impedance between two sets of Hertz dipoles. Since the impedance of the probe depends on the dielectric properties of the medium in which the probe is immersed, characteristics of this medium can be determined, and in particular the density and temperature of thermal electrons. Natural waves are also investigated in a large frequency range including the electron cyclotron and plasma frequencies. Any electrode immersed in a plasma acquires a charge and perturbs the plasma in its immediate neighbourhood: an ion sheath is created and insulates the electrode partially from the unperturbed plasma. The way to get around this difficulty is to use four electrodes, two for transmitting and two for receiving. Transmitting electrodes are excited from a signal generator, while the receiving electrodes are connected to a voltmeter with a very high input impedance. The mutual impedance Z is by definition $Z = V/I$, where I is the transmitted current. Plasma properties may then be deduced from both the imaginary and real parts of Z. The quadripole probe technique have been used for many years on sounding rockets and spacecraft (GEOS, VIKING, ARCAD/AUREOL-3, MARS-96). Electric-field impedance measurements will be made on ROSETTA and BepiColombo and have been proposed for the L-class Cosmic Vision study EJSM/Laplace of ESA.

Absolute Determination of the Ion Density inside the Terrestrial Magnetosphere Using the Wave Propagation Properties Observed by WHISPER and STAFF Experiments on Board CLUSTER Satellites

J. L. Rauch[1], **J. G. Trotignon**[1], **F. Mazouz**[1], **N. Cornilleau-Wehrlin**[2], **and P. Robert**[2]

[1]LPC2E, 3A av. de la Recherche Scientifique, 45071 Orléans Cedex 2, France
[2]LPP, École Polytechnique, Palaiseau Cedex 91128, France

Abstract— The Wave of High frequency and Sounder for Probing of Electron density by Relaxation (WHISPER) performs the measurement of the electron density on the four satellites of the CLUSTER project. The two main purposes of the WHISPER experiment are to record the natural waves and to make a diagnostic of the electron density using the sounding technique. The various working modes and the fourier transforms calculated on board provide a good frequency resolution obtained in the bandwidth 2–83 kHz and a well instrumental adaptability to determine the electron density in various plasma.

The Spatio Temporal Analysis of Field Fluctuations (STAFF) consists of a three-axis search coil magnetometer to measure magnetic fluctuations at frequencies up to 4 kHz, a waveform unit (up to either 10 Hz or 180 Hz) and a Spectrum Analyser (up to 4 kHz). In this work, we will use the data coming from the wave form unit.

The aim of this presentation is to show the possibility to determine the ratio of the ion H+, He+, O+ species using the propagation characteristic of the ULF waves inside the plasmasphere. In a multicomponents plasma, the wave dispersion relation is strongly modified. The propagation modes are spitted into several parts with various polarizations. Cut-off and resonance frequencies appear whose the values are a tracer of the ratio of the density species. Moreover, crossover frequencies happen where the polarization right-handed become left-handed which allow us to have another way to evaluate the rate of the different species. STAFF waveform measurements of the three magnetic components in the ULF bandwidth give us an access to the total wave energy, polarisation properties and wave propagation direction. A carefully analysis of the spectra allow us to determine these characteristic frequencies. An interpretation is proposed with the aim to determine a realistic estimation of the ion density background using, in addition, the absolute electron density deduced of the active WHISPER data with the assumption of global plasma neutrality.

The Simulation of Reflectance Characteristics of Nanotube Array

Ming-Jer Jeng, **Bo-Yi Wu**, **and Liann-Be Chang**
Department of Electronic Engineering and Green Technology Research Center
Chang Gung University, Taiwan, R.O.C.

Abstract— The optical reflectance depends on the refractive index and surface condition of sample devices. In order to reduce optical reflectance, the nanotube or nanorod array is widely used to change effective refractive index and surface roughness. As well known, low-density vertically aligned nanotube arrays have a low refractive index and result in a very low reflectance. It can be used as an anti-reflection layer for solar cells. In this work, we study the reflective property of nanotube array by simulation. It is observed that the higher the nanotube height is, the lower the reflectance is. In addition, the large nanotube diameter also exhibits a low reflectance. This behavior will be related to surface roughness effects. For example, the simulation reflectance of nanotube array with various diameters and heights is studied by using silicon materials as nanotube array. The silicon nanotube array with a large diameter exhibits the lowest reflectance. It is interesting to note that bare silicon has high reflectance. Large nanotube diameter means that there is more silicon area on the surface. Its reflectance should be higher, but not from the simulation result. It indicates that an optimal size of nanotube array might exist for the same height. How to properly determine the nanotube diameters and heights needs more simulation to examine them. The further detailed study is under progress.

An Analytic Solution to the Scattering Fields of Shaped Beam by a Moving Conducting Infinite Cylinder with Dielectric Coating

Mingjun Wang[1, 2], **Huayong Zhang**[3], **Yingle Li**[1], **Jiadong Xu**[2], **and Ningjing Xiang**[1]

[1]Institute of E.M. Wave Propagation & Scattering, Xianyang Normal College, Box 103, 712000, China
[2]School of Electronic Information, Northwestern Polytechnical University, Xi'an, Shaanxi 710072, China
[3]School of Electronic Science and Technology, Anhui University, Hefei, Anhui 230039, China

Abstract— The coordinate transformations and the relation of wave vector and Electromagnetic fields and based on the generalized Lorenz-Mie theory (GLMT) that provides the general framework and expansion of the incident shaped beam in terms of cylindrical vector wave functions, an analytic solution to the electromagnetic scattering by coated moving infinite cylinders with high speed is constructed, for arbitrary incidence of a shaped beam. As an example, for a tightly focused Gaussian beam propagating perpendicular to the cylinder axis, the scattering characteristics that obviously demonstrate the three-dimensional nature are described in detail.

ACKNOWLEDGMENT

This works is partly supported by the National Natural Science Foundation of China (Grant No. 60801047, 60971079), China Postdoctoral Science Foundation funded project (Grant No. 20090-461308), the Natural Science Foundation of Shaanxi Province (2010JQ8016)and the Natural Science Foundation of Shaanxi Province education office, China (Grant No. 2010Jk897).

Radar and Optical Modelling of Forest Remote Sensing

C. Albinet[1], **P. Borderies**[1], **and S. Fabre**[2]

[1]Département Electromagnétisme et Radar
Office National d'Études et de Recherches Aérospatiales, ONERA, Toulouse, France
[2]Département Optique Théorique Appliquée
Office National d'Études et de Recherches Aérospatiales, ONERA, Toulouse, France

Abstract— Retrieval of bio-physical parameters of forests with remote sensing is nowadays a challenge. In particular, the biomass of the canopy and the soil moisture estimations are targets for this retrieval. It is well known that low frequency radars may furnish lots of characteristics of forests, and in particular P band is often proposed [1, 2] for biomass estimation, even if the response is strongly affected by soil moisture as well as branches ones. On the other hand, Optical signatures are often presented as able to deliver characteristic features of the forest vegetation, through for example LAI [3] versus NDVI, determination of specie [4]. Hopefully, using both sources of information through a fusion process should improve the determination of the characteristic parameters of the forest. To evaluate the potential of this combined approach, a focus is done in this paper on a parallel direct modelling approach in which the same forest scenario is simulated in polarimetric P band backscattering and in optics (visible and NIR).

A ground representation of a maritime pine forest as a function of growing age and consequently growing biomass is obtained thanks to a growth model depicted in [5], which delivers the statistical parameters of the trunks and branches in terms of sizes, locations and orientations. It is then used for MIPERS [6] computation of backscattering matrix and the position of all scatterers is then re-used as input for the optical model DART [7], with soils input data from [8].

REFERENCES

1. Le Toan, T., A. Beaudoin, J. Riom, and D. Guyon, "Relating forest biomass to SAR data," *IEEETGARS*, Vol. 30, No. 2, 403–411, March 1992.
2. Cloude, S. R. and K. P. Papathanassiou, "Polarimetric SAR interferometry," *IEEE Transactions on Remote Geoscience and Remote Sensing*, Vol. 36, No. 5, 1551–1565, September 1998.
3. Treuhaft, R. N., G. P. Asner, B. E. Law, S. Van Tuyl, "Forest leaf area density profiles from the quantitative fusion of radar and hyperspectral dara," *Journal of Geophysical Research*, Vol. 107, No. D21, 4568, 2002.
4. http://modis.gsfc.nasa.gov/.
5. Saleh, K., A. Porte, D. Guyon, P. Ferrazzoli, and J. P. Wigneron, "A forest geometric description of a maritime pine forest suitable for discrete microwave models," *IEEETGARS*, Vol. 43, No. 9, 2024–2035, September 2005.
6. ESA Contract No. 20449/06/NL/LvH, "Rigorous numeric techniques applied to microwave interaction with natural targets: volume scattering," CCN, 2010.
7. Martin, E., "DART: Modèle 3D multispectral et inversion d'images optiques de satellite — Application aux couverts forestiers," Ph.D. Dissertation, Université Paul Sabatier, July 25, 2006.
8. Lesaignoux, A., "Estimation de l'humidité de surface des sols nus à partir de l'imagerie hyperspectrale sur le domaine optique 0.4–14 µm," Ph.D. Dissertation, Institut Supérieur de l'Aéronautique et de l'Espace, December 16, 2010.

Quantifying Rice Map and Yield by Using Remotely-sensed Imagery

Yuei-An Liou and Hsueh-Chun Sha
Center for Space and Remote Sensing Research, National Central University
No. 300, Jung-Da Rd., Jung-Li 320, Taiwan

Abstract— Food supply is fundamental to sustain the mankind. Rice is a key component of the food supply as it is the most important staple food for a significant portion of the world's human population. Quantifying rice map and yield is hence of great importance in food supply management and policy making, as well as speaking of food security. In this study, it is aimed to develop a reliable scheme for monitoring rice area and estimating its yield by use of remotely sensed imagery. The MODIS 8-day composites reflectance 500 m and 250 m data (MOD09A1 & MOD09Q1) in 2006–2008 are applied. The indices that are sensitive to vegetation, water body, and land-use are derived from the satellite data. They include Normalized Difference Vegetation Index (NDVI), Enhanced Vegetation Index (EVI), and Land Surface Water Index (LSWI). Classification of rice from the other types of land-use is initially conducted and its area is subsequently found. Based on regression relationship between rice area and its yield, rice yield is then determined. The developed scheme is implemented in the southern counties of Taiwan, including Changhua, Yunlin, Chiayi, and Tainan. The results of quantified rice map and yield is satisfactory with errors less than 20% for all cases. Suggestions of improving the estimate accuracy are made by carefully examining the procedures of the scheme. It is expected the errors will be reduced by implementing the findings of this study.

Error of Moisture Retrieving from the SMOS Radiobrightness with the Use of the Temperature Dependable Soil Dielectric Model

V. L. Mironov[1], **L. G. Kosolapova**[1], **and F. Demontoux**[2]

[1]Kirensky Institute of Physics, SB, RAS, Russia
[2]IMS Laboratory, Bordeaux 1 University, France

Abstract— In connection with the European Space Agency's (ESA) Soil Moisture and Ocean Salinity (SMOS) mission, the evaluation of the error of soil moistures retrieved by 1.4 GHz radiometer has emerged as an especially important issue. To retrieve the moisture from the radiobrightness measured, a specific dielectric model must be applied, which links the radiobrightness to the wave frequency, moisture, temperature, and soil type. We have previously shown [1], that the error of moisture retrieved from the SMOS observation depends to a large extend on the specific dielectric model of moist soil used to resolve the respective inverse problem. This research concerned only the dielectric models that are valid in the narrow range of temperatures from 20 to 22°C. At the same time the real temperature of thawed topsoil may fluctuate in a much wider range. Recently, a temperature dependable soil dielectric model was developed [2] to take into account the fluctuations of temperature in the range from 10 to 40°C.

In this paper a statistical analysis similar to that of [1] to estimate the moisture error induced by imperfectness of the model proposed in [2] was carried out. The 95% confidence intervals were obtained, in which a true moisture is confined, relative to the value retrieved with the use of the temperature dependable dielectric model [2]. In this case a data set for complex dielectric constant measured in the range of temperatures 10 to 40°C was formed on the basis of those published in [3]. With this database available, the emission coefficients were calculated, using both the predicted and measured values of complex dielectric constant. As a result, the emission coefficient computed using the measured complex permittivities was compared with that calculated with the use of the temperature dependable dielectric model (emission coefficient predicted). We considered the emission coefficient corresponding to the radiobrightness observation in nadir. The moisture retrieving error was estimated as a relative deviation of the predicted soil moisture from the upper and lower boundaries of the 95% confidence intervals.

The error thus obtained was shown to reach the value of $\pm 0.05\,\mathrm{cm}^3/\mathrm{cm}^3$ while the soil moisture precision target for the SMOS mission is equal to $\pm 0.04\,\mathrm{cm}^3/\mathrm{cm}^3$. Thus, the need to improve the dielectric model of moist soil taking into account the temperature dependence is still an actual problem for running the SMOS project. Further, we plan to develop a specific dielectric model of moist soil at 1.4 GHz which is applicable to meet the SMOS project requirements in terms of moisture retrieving error.

REFERENCES

1. Mironov, V. L., Y. Kerr, J.-P. Wigneron, L. G. Kosolapova, F. Demontoux, and C. Duffour, "Statistical error for the moistures retrieved with the smos radiobrightness data, as induced by imperfectness of a dielectric model used," *IEEE Proceedings IGARSS*, 4430–4432, 2010.
2. Mironov, V. L. and S. V. Fomin, "Temperature and mineralogy dependable model for microwave dielectric spectra of moist soils," *PIERS Proceeding*, 938–942, Moscow, Russia, August 18–21, 2009.
3. Curtis, J. O., C. A. Weiss, Jr., and J. B. Everett, "Effect of soil composition on dielectric properties," Technical Report, EL-95-34, December 1995.

Topographic Normalization of Landsat TM Images in Rugged Terrain Based on the High-resolution DEM Derived from ASTER

Yanli Zhang[1, 2] **and Xin Li**[1]

[1]Cold and Arid Regions Environmental and Engineering Research Institute
Chinese Academy of Sciences, Lanzhou 730000, China
[2]College of Geography and Environment Science
Northwest Normal University, Lanzhou 730070, China

Abstract— A method for topographic correction for TM remote sensing image is presented in rugged terrain, with the help of high-resolution stereo image pairs provided by modern satellite sensors. Topographic effects and atmospheric factors interacted, and severely distorted the true information of surface nature characters. Some popular terrain correction models nowadays, such as the cosine model, Minnaert model, C model, SCS model and so on, are not a quantitative method. The mountain radiant transfer model with more strict physical meaning must be selected to remove terrain effects in mountainous quantitative remote application. However, because of its stringent requirements for digital elevation model DEM in the high precision and high resolution, it limited its development and wider application. Based on ASTER remote sensing stereo image pairs constituted by nadir images and backsight images, relatively high accuracy 15 m DEM data was obtained in the study area. Finally putting micro topographic factors and the main atmospheric parameters into Richter mountains radiation model, TM remote sensing image terrain correction was rapidly completed. The results show that this method has a remarkable ability to remove topographic and atmospheric effects, and also provides reliable basis data for surface parameters retrieval of quantitative remote sensing in the rugged terrain.

Mapping Surface Soil Moisture Using L-band Radiometer Observations in the Second Australian Airborne Cal/val Experiment for SMOS (AACES-2)

Shuguo Wang[1], **Xin Li**[1], **Tao Che**[1], **Xujun Han**[1], **Jeffrey Walker**[1], **Christoph Rüdiger**[1], **Sandy Peischl**[1], **and Nan Ye**[2]

[1]Cold and Arid Regions Environmental and Engineering Research Institute
Chinese Academy of Sciences, China
[2]Monash University, Australia

Abstract— Surface soil moisture is important in agronomic, hydrological, and meteorological processes at all spatial scales. The ability of inferring soil moisture by using passive microwave techniques has been intensively demonstrated. The second Australian Airborne Cal/val Experiment for SMOS (AACES-2) is a part of validation effort of the SMOS satellite performance in operational mode which took place on the central half of the 100 km × 500 km transect of the Murrumbidgee River catchment with a range of diverse soil moisture and land cover characteristics. The AACES-2 campaign was able to provide aircraft dual-polarized L-band radiometer observations at 1 km resolution by the Polarimetric L-band Multibeam Radiometer (PLMR). Intensive near-surface soil moisture sampling and other ground measurements were supported as well Retrieval of soil moisture using physically based models is a classic example of underdetermined problem due to a lack of credible known soil roughness distributions at a regional scale. Characterization of this roughness is therefore crucial for an accurate derivation of soil moisture based on backscattering models. This study aims to derive surface soil moisture by using a two-step inversion approach with the advanced integrated equation model (AIEM). Dependent on the dual-polarized L-band brightness temperature observations and extensive vegetation and ground temperature measurements, firstly, radiative transfer model needed main roughness parameters (standard deviation of surface height σ and correlation length cl) were calibrated by training data sets. Then, soil moisture retrieval was conducted based on the calibrated roughness beyond the calibration area. Globally, soil moisture estimates were obtained with errors around $0.05\,\mathrm{cm}^3\ \mathrm{cm}^{-3}$ (RMSE) across different land covers. It is demonstrated that the proposed method is feasible to achieve reliable estimation of soil water content.

Monitoring Aurora in Day Light Side of the Earth in Relation to Solar Plasma Flow

Shigehisa Nakamura
Kyoto University, Japan

Abstract— A note is introduced for problems on monitoring aurora in day light side of the earth in relation to the solar plasma flow. The solar plasma flow (the solar wind) distorts the geomagnetic field to form a magnetopause. The solar plasma flow at a super high speed so that a shock front is appeared just outside of the magnetosphere. It has been monitored the aurora in the day light side of the earth after the energy of the electron increased between the shock front and the magnetopause. This electron is the trigger of the red aurora (630.0 nm). On the basis of the surveys it is clarified that the polar cusp is a guide of the intruding electron of the solar plasma along the magnetic line into the upper atmosphere of the earth. This red aurora is induced after energy release of the oxygen at the altitude of 200 km or more above the earth surface at intruding electron (ca 500 km/sec). Now, it should be noticed that the energy release of the electron to activate the oxygen atom is an order of several KeV in the visible aurora curtain (557.7 nm) found in the dark night side of the earth. The author notes one case of the non-natural energy release producing a similar pattern in the subtropical zone of the ocean. Spacecraft monitoring of the planets in the solar system is noted referring to the updated data in short, because this monitoring must be only a part of the big scientific project.

Satellite Monitoring of Subglacial Volcano in Atlantic

Shigehisa Nakamura
Kyoto University, Japan

Abstract— This is a note to satellite monitoring of the subglacial volcano in the Atlantic. The satellite data are obtained by EUMETSAT and NASA. An eruption of a subglacial volcano in Iceland had issued volcanic ash, and the winds transferred the ash to the European Union in April 2010. This volcano is one of the volcanoes in the Atlantic. There are volcanoes in the north and south Atlantic. Some of them are in Azores Islands, in Canary Islands and Cape Verde Islands. Iceland is located on the zone of the mid-Atlantic ocean ridge, where the magma can be seen by an eye-watch technique directly on the island, though one of the subglacial volcanoes had an event of the ash scattering to the on-land area of the European Union. In this work, the author has to give his remark on the important notice about consideration of the chemical effects of the gasses bursted at the volcanic eruption. The volcanic ash pattern is well governed by the winds around the volcano. This event has had a strong impact to the global net-work of the air-line transportation. Now, the author introduces about the volcanic islands in the Atlantic, including the volcanoes in Azores Islands, in Canary Islands, and in Cape Verde Islands.

Satellite Monitoring of Aurora Oval on the Earth in Relation to Solar Winds

Shigehisa Nakamura
Kyoto University, Japan

Abstract— This work concerns on satellite monitoring of the aurora oval on the earth in relation to solar winds. First of all, a brief review is given for help of our understanding of what is seen in the solar-earth system. The mechanism of the aurora has to be studied in relation to the solar winds which affect to generate a disturbance on a boundary between the earth's magnetic field and the solar magnetic field. Electromagnetic understanding of the solar-earth system has been advanced to obtain a modeling of so-called MHD (magneto-hydrodynamics. Chapman (1964) had written about solar plasma flow around the earth's magnetic field. In the age of spacecraft monitoring of the planet Saturn, the satellite monitoring of the aurora might be the trigger for understanding the more detailed structure of the aurora. As the results of the research on the aurora of the planets in the solar system, satellite monitoring of the aurora must be contributive to give the next spacecraft monitoring of the planets for our advanced research.

Intensity Distribution of the Light in a Diffuse Sphere

Ailin Yang, Jian Zheng, and Qiang Lin
Institute of Optics, Department of Physics, Zhejiang University, Hangzhou 310027, China

Abstract— The interaction of a photon with an atom can be used to manipulate the atom. A famous example is the cooling and trapping of atom by laser beam. This technique relies on the resonant exchange of momentum between photons and atoms to control the external degrees of freedom of atoms and thus to reduce their kinetic energy [1]. Cooling and trapping of atoms in isotropic laser light in a vapor cell is a hot topic for a long time [2, 3]. The advantage of using an diffuse sphere to cool and trap atoms is that no laser beam alignment or collimation is needed, which simplifies the setup and nearly all the atoms in the cell can be cooled, whereas, in a standard optical molasses, only atoms within the crossing area of the six laser beams can be cooled [4, 5]. In this paper, we calculated the intensity distribution of laser beam in a diffuse sphere by algorithm of ray tracing based on light ray reflection and propagation in a diffuse sphere, and carry out a series of recursive cosine equations of reflected light for ray tracing. In our calculations, we assume the reflection obeys Lambert's cosine law. The results show that the intensity distribution of the light in the sphere is axially symmetric, and there are two maximum on the symmetry axis, which is in agreement with the result of the experiment. We also analyzed several parameters that may affect the distribution of the light in the sphere, such as diffuse reflection coefficient at the inner surface, diameter of aperture, etc.. It is shown that higher intensity-homogeneity can be obtained by using sphere with higher reflection coefficient, and smaller diameter of aperture. The results obtained in this paper could be useful for improving the laser cooling atoms system with diffuse sphere.

REFERENCES

1. Chu, S., J. E. Hollberg, J. E. Bjorkholm, A. Cable, and A. Ashkin, "Three-dimensional viscous confinement and cooling of atoms by resonance radiation pressure," *Phys. Rev. Lett.*, Vol. 55, 483, 1985.
2. Hansch, T. W. and A. L. Schawlow, "Cooling of gases by laser radiation," *Opt. Commun.*, Vol. 13, 68, 1975.
3. Ketterle, W., A. Martin, M. A. Joffe, and D. E. Pritchard, "Slowing and cooling atoms in isotropic laser light," *Phys. Rev. Lett.*, Vol. 69, 2483, 1992.
4. Guillot, E., P. E. Pottie, and N. Dimarcq, "Three-dimensional cooling of cesium atoms in a reflecting copper cylindert," *Opt. Lett.*, Vol. 26, 1639, 2001.
5. Cheng, H. D., W. Z. Zhang, H. Y. Ma, L. Liu, and Y. Z. Wang, "Laser cooling of rubidium atoms from background vapor in diffuse light," *Phys. Rev. A*, Vol. 79, 023407, 2009.

Time Reversal Method Based on Wavelet-analysis for Complex Environment

Qi Kong, **Guangze Yu**, **and Qingfan Shi**
Department of Science, Beijing Institute of Technology, Beijing 100081, China

Abstract— Time reversal (TR) algorithm as one of the electromagnetic inverse problems has now been a major method in computational electromagnetics. This method can infer location, shape and electromagnetic parameters of the unknown target without contact with it. Therefore TR algorithm is widely used in earthquake prediction, target recognition, ground penetrating radar, geophysical remote sensing, medical imaging, nondestructive testing and many other fields.

In this paper, we develop a new kind of TR method in which wavelet analysis is firstly introduced to deal with the electromagnetic time reversal processing. As a powerful signal analysis tool, the wavelet can improve the resolution of electromagnetic imaging by removing the clutter of electromagnetic noise. At first, the total processing signals are produced by finite-difference time domain (FDTD) method. The source signal is emitted by a transmitter. Next, the signals radiated from the scatter (target) are accepted by twenty antennas at different regions. To the complex environment, a cluster of obstacles near the received transmitters are settled. Then different kinds of wavelet basis are utilized to smooth and reduce the negative effect of the noise. Finally the processed signals are re-radiated so as to obtain the imaging. The results show that the wavelet analysis method can effectively suppress the noise and improve the image effect. The method leads stable, fast, reliable inversion imaging. Our method may be helpful to some areas such as the target detection, ground penetrating radar, medical imaging and many other fields.

RCS Reduction Assisted by Surface Plasmon Polaritons

Jiafu Wang[1, 2], **Shaobo Qu**[1, 3], **Duolin Zhang**[1], **Zhuo Xu**[3], **Hua Ma**[1, 3], **Song Xia**[3], **Xinhua Wang**[1], **Hang Zhou**[1], **Lei Lu**[1], **and Fei Yu**[1]

[1]College of Science, Air Force Engineering University, Xi'an, Shanxi 710051, China
[2]The Second Aviation College of Air Force, Huxian, Shanxi 710306, China
[3]Electronic Materials Research Laboratory, Xi'an Jiaotong University, Xi'an, Shanxi 710049, China

Abstract— We demonstrated that the RCS of a metallic cylinder can be drastically reduced based on surface plasmon polaritons. By enclosing the metallic cylinder with a plasmonic cover, surface plasmon polaritons can be excited on surface of the metallic cylinder. Due to the highly surface-confined property of surface plasmon polaritons, the otherwisely backscattered EM energy is transferred to other directions, even to the other side of the metallic cylinder, achieving enhanced transparency.

Polarization Changes of Stochastic Spatially and Spectrally Partially Coherent Electromagnetic Pulsed Beams in Turbulent Atmosphere

Zhiguo Zhao[1], **Jianguo Lu**[2], **Fengguo Fan**[3], **Haixia Wang**[1], **and Yongtao Zhang**[1]

[1]Department of Physics, Luoyang Normal College, Luoyang 471022, China
[2]Department of Primary Education, Jiaozuo Teachers College, Jiaozuo 454150, China
[3]Network Center, Shangqiu Teachers College, Shangqiu 476000, China

Abstract— In the recent decades, there has been substantial interest in studying the polarization properties of stochastic electromagnetic beams on propagation. However, most of studies have been restricted to the stationary beams. On the other hand, statistical optical pulses represent a wide class of partially coherent fields that find numerous applications as optical imaging and fiber optics etc. Recently, a scalar model of spectrally partially coherent pulses was introduced by Pääkkönen et al.. The propagation properties of spatially and spectrally partially coherent scalar pulses were studied by Turunen et al. Ding et al. extended the scalar model of spectrally partially coherent pulses to a vectorial one, and investigated the characterization of stochastic spatially and spectrally partially coherent electromagnetic pulsed beams, and whose changes in the spectral degree of polarization in dispersive media were studied in detail. In this paper, using the coherence theory of non-stationary fields and the method of two-time Fourier transform, the analytical expression for the spectral degree of polarization of stochastic spatially and spectrally partially coherent electromagnetic pulsed beams in turbulent atmosphere is derived, and used to study the polarization changes of stochastic electromagnetic pulsed beams propagating through turbulent atmosphere. The influence of pulse frequency and refraction index structure constant on the spectral degree of polarization is emphasized. It is shown that, in comparison with free-space case, the turbulent atmosphere plays an important role on the distribution of the spectral degree of polarization of stochastic electromagnetic pulsed beams propagating in turbulent atmosphere. The results obtained might find potential application for sensing, imaging and communication through the atmosphere.

The Frequency Dependence Problem of Conducting Cylinder Buried in a Half-space

Wei Chien[1] **Hsien-Wei Tseng**[2], **Kai-Xiang Huang**[1], **and Chi-Hsien Sun**[3]

[1]Electronic Engineering Department, De Lin Institute of Technology, Taiwan, R.O.C.
[2]Computer and Communication Engineering, De Lin Institute of Technology, Taiwan, R.O.C.
[3]Electrical Engineering Department, Tamkang University, Taiwan, R.O.C.

Abstract— Frequency dependence problem of conducting cylinder buried in a half-space is investigated. A conducting cylinder of unknown shape is buried in one half-space and scatters the incident wave from another half-space. By using measured scattered field, the image problem is reformulated into an optimization problem and solved by the genetic algorithm. Frequency dependence on image reconstruction is investigated and numerical results show that the reconstruction is quite good in the resonant frequency range. On the contrary, if the frequency is too high or too low, the reconstruction becomes bad. It is worth noting that the present work provides not only comparative information but quantitative information.

Far-field Diffraction Patterns Evolution of a Gaussian Laser Beam due to Thermo-optical Effect in Metal Nanocolloids

Yuri E. Geints[1], **Nicolay S. Panamarev**[2], **and Aleksey A. Zemlyanov**[2]

[1]Zuev Institute of Atmospheric Optics SB RAS, 1 Zuev square, Tomsk 634021, Russia
[2]Siberian Physical and Technical Institute, 1 Novosobornaya square, Tomsk 634050, Russia

Abstract— We report on the results of our systematic experimental investigations of the diffraction pattern (DP) formed due to CW low-power laser beam propagation through a cell with metal nanocolloids (NC). We have used different types of metal NC and for the first time have studied thoroughly the temporal dynamics and structural characteristics of far-field DP. The experimental data has shown that in the observation plane the dynamic diffraction structure was formed. It consists of several coaxial light and dark rings, whose diameters and number increased with time and varied depending on the type and concentration of the colloidal solution. The stable diffraction pattern with the fixed number of fringes is formed at the screen for periods of several seconds from the beginning of the exposure to laser radiation. The number of formed rings is inversely proportional to the optical thickness of the colloid and to the laser power also.

The experimental results have been interpreted theoretically from the viewpoint of thermal self-action of laser radiation in the absorbing medium. Colloidal silver nanoparticles serve as centers which efficiently absorb laser radiation and transfer the heat to the host liquid due to the thermal conductivity, thus giving rise to the temperature gradient across the laser beam. Since the thermo-optical nonlinearity of the liquid leads to the decrease in the refractive index of the medium at the places, where the medium temperature is higher, the nonlinear negative phase shift appears in the zone of the beam action. This phase shift acts on the radiation as a defocusing aberration lens and leads to the formation of fringes observed in the far-field diffraction zone.

Based on the analytical solution to the heat transfer equation of a homogeneous medium with a thermal source caused by the linear absorption of laser radiation, we have calculated the spatiotemporal profiles of temperature increments of silver nanocolloids. To determine the structure of the far field, we used the Fresnel-Kirchhoff integral in Fraunhofer approximation. This allowed us to derive formulae, which related the number of bright rings in the observation plane and the angular size of the entire diffraction pattern to thermophysical characteristics of the liquid solvent, volume fraction of the metal sol, and parameters of the laser beam.

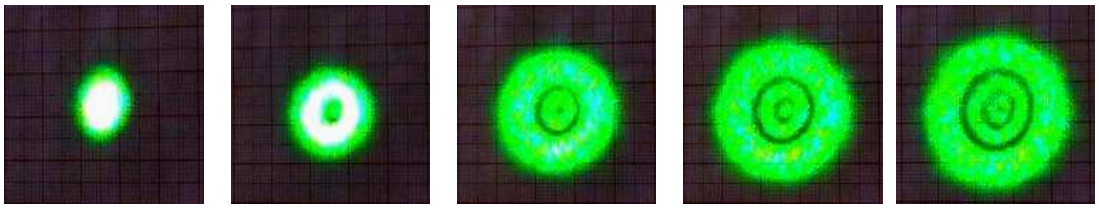

Figure 1: DP evolution of a laser beam passed through a cell (thickness 2 mm) with the glycerin solution of collargol (silver concentration 0.001%): (a) 0.01 s; (b) 0.15 s; (c) 0.5 s; (d) 1.1 s; (e) 3.5 s after beam passage.

Two-dimensional Linear Inversion Method for Phaseless EM Problem

Hu Zheng
University of Electronic Science and Technology of China, China

Abstract— Recently, phaseless imaging method has found its special applications in non-destructive imaging, medical imaging and other related areas of applications. The main bottleneck of phaseless imaging method is that it will take an excessive amount of time to repeat computing 'exact' filed. As it is known, when dealing with weak scatterers, the Born approximation may be used advantageously in many inversion algorithms. In this paper, the Born approximation is introduced in the PD-MRCSI method, which can degenerate the nonlinear inverse problem into a linear one and reduces the computation time drastically.

For weak scattering or Born approximation, the direct scattering problem can be modeled via two coupled contrast source integral relationship, in particular, the data equation and the state equation, explicitly,

$$f_k(r) = u_k^{inc}(r) + k_b^2 \int_D G(r,r')\,\omega_k(r')\,dr' \quad \text{for} \quad r \in S \tag{1}$$

$$u_k(r) = u_k^{inc}(r) \quad \text{for} \quad r \in D \tag{2}$$

For simplicity, Equation (1) is rewritten in more condensed form:

$$f_k = u_k^{inc} + G_S \omega_k, \quad r \in S \tag{3}$$

The state Equation (2), multiplying both sides of it with χ, can be expressed as

$$\omega_k = \chi u_k^{inc}, \quad r \in D \tag{4}$$

Introducing the following notations

$$f_{k,R} = \mathrm{Re}(f_k), \quad f_{k,I} = \mathrm{Im}(f_k), \quad u_{k,R}^{inc} = \mathrm{Re}\left(u_k^{inc}\right), \quad u_{k,I}^{inc} = \mathrm{Im}\left(u_k^{inc}\right)$$

$$G_{S,R} = \mathrm{Re}(G_S), \quad G_{S,I} = \mathrm{Im}(G_S), \quad \omega_{k,R} = \mathrm{Re}(\omega_k), \quad \omega_{k,I} = \mathrm{Im}(\omega_k)$$

we can get the representation of (3) as

$$f_{k,R} = u_{k,R}^{inc} + G_{S,R}\omega_{k,R} - G_{S,I}\omega_{k,I} \quad \text{and} \quad f_{k,I} = u_{k,I}^{inc} + G_{S,I}\omega_{k,R} + G_{S,R}\omega_{k,I}$$

Before introducing cost functional, we define $F(\omega_{k,n}, \chi_n)$ as a linear combination of the modified mismatch in data equation F_S and the mismatch in state equation F_D. Then the cost functional C can be expressed as

$$C(\omega_{k,n}, \chi_n) = F(\omega_{k,n}, \chi_n)\, F_{TV}(\chi_n) \tag{5}$$

with

$$\begin{aligned} F(\omega_{k,n}, \chi_n) &= F_S(\omega_{k,n}) + F_D(\omega_{k,n}, \chi_n) \\ F_S(\omega_{k,n}) &= \eta_S \sum_k \left\| M_k^2 - f_{k,R}^2 - f_{k,I}^2 \right\|_S^2 \\ F_D(\omega_{k,n}, \chi_n) &= \eta_D \sum_k \left\| \chi u_k^{inc} - \omega_{k,n} \right\|_D^2 \end{aligned}$$

Then the inverse scattering problem can be solved by minimization the cost functional. The optimization procedure used in this paper is to update the two sequences (contrast sources and contrast) alternately using conjugate gradient method by minimizing the cost functional.

An Improvement of QR-M MLD for MIMO Wireless Communications

Tatsuki Fukuda, **Tadaharu Takahashi**, **and Hua-An Zhao**
Department of Computer Science and Electrical Engineering, Kumamoto University, Japan

Abstract— Recently, we can see a lot of wireless systems in many kind of products such as computers, broadcast, and mobile phones. It means that we need higher-speed wireless systems. There are many technique for higher wireless communications, especially a lot of researches for the signal detection technique. In this paper, we propose a new detection method based on the QRM MLD, which is based on the algorithm of QR-M MLD with a tree structure. The nodes on first level represent the symbol candidate of the symbol transmitted by N_T-th antenna. The nodes on d-th level represent the candidates of the symbol transmitted from $(N_T - d + 1)$-th antenna. Each nodes have the M child nodes which represent the M constellation points, respectively. MLD method check the all of the nodes from first level to N_T-th level, so it takes a lot of times. QRM MLD method select M nodes for each level by selecting the nodes which have lower metrics. Our method selects the kM nodes by selecting the k nodes for each signal point, which have the smaller metrics in the set of $N(S)$ in the level. Here we refer to nodes corresponding to the constellation point S as $N(S)$. By this method, we have no chance to delete the correct symbol candidate for all level, and we think the bit error ratio (BER) performance get better than the other method. The simmulation results show the bit error ratio (BER) of our method is better than other methods. When the signal-to-noise ratio is high, it can be seen that our method is feasible and superior to other methods in terms of BER without increase in the computational complexity.

Experimental Validation that Optical Scintillation Obeys the Same Rules of Share Price Fluctuations

C. Yang[1,2], **X. Li**[2], **W. Jiang**[2], **and C. Rao**[2]

[1]School of Science, Xi'an Shiyou University, Xi'an 710065, China
[2]Institute of Optics and Electronics, Chinese Academy of Sciences, Chengdu 610209, China

Abstract— It is traditionally treated that when optical wave propagates through a turbulent atmosphere, the optical signal fluctuates randomly. However, this paper validates that this well-known theory is wrong by experiments. 3 optical propagation experiments are performed: ground-to-satellite-to-ground, horizontal propagation, and stellar observation. The experiments results show that: when it is observed in a small-scale period, the optical wave propagating through the atmosphere fluctuates randomly; but when it is observed in a large-scale period, the optical scintillation follows the same rules of share price fluctuations. Utilizing the techniques of share transaction to predict the optical scintillation has potential value for free-space optical communication system and laser transmitter system.

The Analysis of Paired Unequally Spaced Reapeated Alternate Unequally Spaced Allocation Channels for FDM Lightwave System

Ashira Jumpates, **Vissavavit Rachnarong**, **and Suthichai Noppanakeepong**
Faculty of Engineering, Department of Telecommunication Engineering
King Mongkut's Institute of Technology Ladkrabang, Ladkrabang, Bangkok 10520, Thailand

Abstract— This paper proposes the new technique to improve the conventional techniques in the channel allocations, in order to reduce transmission loss, in case of there are a large number of channel and each of channel is nearby. We have found this case in dense wavelength division multiplexing (DWDM) that is the cause of transmission loss called four-wave mixing due to the fiber nonlinear. The channel allocations that used to resolve this problem are equally spaced (ES), unequally spaced (US), repeated US (RUS), unequally spaced RUS (URUS) and paired URUS. This paper presents the new technique to arrange the channel allocation is called paired URAUS to avoid the four-wave mixing. From the simulation results, the new proposed technique has lower the effect of four-wave mixing than the conventional techniques and decrease bit error probabilities and bandwidth, containing higher channels, in DWDM transmission systems.

Generation of Diffraction-compensated Beams through a Phase Plate

Marc Brunel[1], **Huanhuan Shen**[1], **Driss Mgharaz**[1], **Sébastien Coetmellec**[1], **Qiulin Huang**[2], **and Kamel Ait Ameur**[3]

[1]UMR 6614 CORIA CNRS, Avenue de l'Université, BP 12, 76801 Saint-Etienne du Rouvray Cedex, France
[2]School of Electronic Engineering, Xidian University, Xi'an 710071, China
[3]CIMAP, ENSICAEN, CNRS, CEA/IRAMIS, Université de Caen, 14050 Caen Cedex, France

Abstract— The generation of non-diffracting beams has been much investigated for the last two decades [1, 2]. Many applications exist from metrology and classical optics to nonlinear optics. Different techniques exist to generate diffraction-free beams: they involve an annular aperture, a conical prism (axicon), a computer generated hologram, a spatial light modulator. Recently, we have reported another technique based on the diffraction of a gaussian beam by an opaque disk [3]. With this method we could generate a diffraction-compensated beam over more than 5 meters. The technique is applicable in the case of femtosecond laser pulses, and a compact configuration could be developed at the output of a pigtailed laser diode. Recent developments showed that the beam generated can be reasonably described by a non-diffracting J_0 Bessel [4]. The main disadvantage of this method concerns the relatively high losses induced by the opaque disk which stops the central part of the gaussian beam. Typically, the whole transmission through the opaque disk does not exceed 15 per cent.

This method would become particularly interesting if this difficulty could be solved. As the beam-shaping occurs by diffraction of a gaussian beam through a circular opaque disk (amplitude mask), we can wonder whether the use of a transparent diffractive optical element could lead to relatively similar results except losses. In this communication, we will consider a new configuration, where the opaque disk is replaced by a binary diffractive optical element, referred to in this paper as a circular phase plate and commonly involved in laser physics [5]. The phase plate will introduce a phase shift in the central part of the incident beam, but not stop this part of the beam. Losses will thus be much reduced. The dephasing area, which is circular, consists of a thin film of ITO (Indium Tin Oxide) disk of diameter D deposited on a silica substrate. In such a case, the losses induced by the diffracting element are only 8 percent. We will present in this communication the results obtained with this new configuration. The set-up will be as follows: a gaussian beam is focused in the vicinity of this circular phase plate: the phase plate is set beyond the focus point of a gaussian beam. The diffracted beam is then collimated using a collimating lens. A beam will be generated with a central spot which conserves its dimension over more than 1.1 meter. The results are well predicted theoretically.

In this communication, we will successively present the theoretical development, the optimization stage to design our set-up (in particular the optimization of the phase-mask characteristics), and the experimental results obtained. These latter will be compared successfully to theoretical simulations.

REFERENCES

1. Durnin, J., J. J. Miceli, Jr., and J. H. Eberly, *Phys. Rev. Lett.*, Vol. 58, 1499–1501, 1987.
2. McGloin, D. and K. Dholakia, *Contemp. Phys.*, Vol. 46, 15–28, 2005.
3. Brunel, M. and S. Coëtmellec, *J. Opt. Soc. Am. A*, Vol. 24, 3753–3761, 2007.
4. Huang, Q., S. Coëtmellec, A. Louis, F. Duval, H. Leblond, and M. Brunel, *Progress In Electromagnetics Research Symposium*, Marrakesh, Morocco, March 20–23, 2011.
5. Aït Ameur, K., F. Sanchez, and M. Brunel, *Opt. Commun.*, Vol. 184, 73–78, 2000.

Generation of Perfect 3D Dark Spots Using Double-ring Cylindrical Vector Vortex Beams

Yaoju Zhang, **Zhonghua Ma**, **and Youyi Zhuang**
College of Physics and Electronic Information, Wenzhou University, Wenzhou, Zhejiang 325035, China

Abstract— Three-dimensional (3D) dark spots or bottle beams surrounded by light at all direction are applied in many areas in optics, such as dark-spot optical traps for atoms they will seek the dark or the low-field region so that the field distribution will not substantially be disturbed by the presence of atoms [1, 2] and for microparticles whose refractive index is smaller than the ambience. In super-resolution fluorescence microscopy, a 3D dark spot is used as the erase beam [3].

Several methods have been used to produce 3D bottle beams that have an intensity null surrounded by light in all directions. In this paper, a 3D dark spot is generated by using a double-ring-shaped cylindrical vector vortex beam which can be considered as a vector superposition of a double-ring-shaped radially-polarized light and a double-ring-ring-shaped azimuthally-polarized light. When the vortex angle of the double-ring-shaped cylindrical vector vortex beam is equal to 0.25π, the volume of the 3D dark spot generated is very small ($V = 0.311\lambda^3$) and the uniformity of the light wall surrounding the dark spot is quite high ($U = 0.67$). Compared with the case of the corresponding double-ring-shaped radially-polarized light focusing ($U = 0.35$) [4], the uniformity of the light wall is largely improved. This small 3D dark spot with highly uniform light wall is very perfect for particle trapping and for super-resolution fluorescence microscopy.

REFERENCES

1. Kaplan, A., N. Friedman, and N. Davidson, "Optimized single-beam dark optical trap," *J. Opt. Soc. Am. B*, Vol. 19, No. 6, 1233–1238, 2002.
2. Isenhower, L., W. Williams, A. Dally, and M. Saffman, "Atom trapping in an interferometrically generated bottle beam trap," *Opt. Lett.*, Vol. 34, No. 8, 1159–1161, 2009.
3. Harke, B., C. K. Ullal, J. Keller, and S. W. Hell, "Three-dimensional nanoscopy of colloidal crystals," *Nano Letters*, Vol. 8, No. 5, 1309–1313, 2008.
4. Kozawa, Y. and S. Sato, "Focusing property of a double-ring-shaped radially polarized beam," *Opt. Lett.*, Vol. 31, No. 6, 820–822, 2006.

17.9% Efficiency Silicon Solar Cells by Using Spin-on Films Processes

Yi-Yu Lee, **Wen-Jeng Ho**, **Jhih-Kai Syu**, **Quan-Ru Lai**, **and Cheng-Ming Yu**
Institute of Electro-Optical Engineering, National Taipei University of Technology
1, Sec. 3, Chung-Hsiao E. Rd., Taipei 106, Taiwan

Abstract— In this paper, high performance of the n^+-p Si solar cell fabricated by spin-on film diffusion and spin-on film AR-coating processes are characterized with dark I-V and photo-illuminated I-V measurement. We developed and investigated the phosphorus diffusion process by using the spin-on film (SOF) and optimized rapid temperature annealing (RTA) techniques on single crystalline p-Si wafer to form an high-quality thin n^+-emitter. We also studied a broad-band low-reflectance multi-layer AR-coating ($SiO_2/TiO_2/TiO_2$) by using the SOF process. Furthermore, we successfully integrated both SOF processes to fabricate an n^+-p Si solar cell with excellent photovoltaic performances.

All samples used in the experiment were 525 μm thick, (100) oriented, $1 \sim 10\,\Omega$-cm, p-type (boron doped) Si wafer and the individual cell area was $0.1296\,cm^2$. After standard RCA cleaning, the samples are coated with the phosphorus diffusion source by used the spin-on technique. The samples are spun at a speed of 6000 rpm for 20 s, followed by a prebaking at 200°C for 5 min and at 400°C for 10 min on the hot plate. Then the sample was kept in RTA chamber at 900°C for 2 min for diffusion. After phosphorus diffusion, an Al (200 nm) film was evaporated onto the back side and annealed at 450°C as the back electrode. Subsequently, the front electrode of Ti/Al (20/200 nm) film was formed by evaporating and lifts-off processes. Finally, $SiO_2/TiO_2/TiO_2$ multi-layer AR-coating on the surface of cell was deposited by spin-on film process.

In summary, we demonstrated a high efficiency n^+-p Si solar cell fabricated by spin-on film diffusion and spin-on film AR-coating processes. Under AM1.5G, 25°C, and the cell without AR-Coating, the open circuit voltage (V_{oc}) of 0.54V, short-circuit current (I_{sc}) of 3.78 mA, fill factor (FF) of 0.74, and conversion efficiency (η) of 12.01% are presented. However, the improved performances of cell with spin-on multi-layer AR-coating ($SiO_2/TiO_2/TiO_2$) show that V_{oc} of 0.56 V, I_{sc} of 5.35 mA, FF of 78.46%, and η increased to 17.91% are obtained.

ACKNOWLEDGMENT

The authors would like to thank the financial support from the National Science Council under Grant NSC 99-2221-E-027-050-.

Fresnel Lenses Based on Blue Phase Liquid Crystals

Chi-Huang Lin, **Yu-Yin Wang**, **and Chen-Wei Hsieh**
Department of Physics, National Sun Yat-Sen University, Taiwan

Abstract— A polarization-independent and high diffraction efficiency Fresnel lens is developed based on blue phase liquid crystals (BPLCs). The BPLC Fresnel lens is characterized by its polarization-independent feature based on the Kerr effect of BPLCs induced by a vertical electric field. The small optical phase shift of BPLCs induced by the Kerr effect is suitable for Fresnel lenses to obtain high diffraction efficiencies of 41% and $\sim$ 34% in theory and in experiment, respectively. An electrically erasable memory effect of the focusing diffraction in the BPLC Fresnel lens at an applied voltage $V > 120\,\mathrm{V}$ is also demonstrated.

Switching of Dark Discrete Cavity Solitons

Keivan Mahmoud Aghdami[1], **Reza Kheradmand**[2], **and Roghayeh Karimi**[2]

[1]Physics Department, Payame Noor University, Tehran 19395-4697, Iran
[2]Research Institute for Applied Physics and Astronomy, University of Tabriz, Tabriz 51665-16, Iran

Abstract— The propagation of light in discrete system, such as waveguide arrays shows novel unique physical phenomena in comparison with beams propagating in usual continuous systems, For example, in discrete systems dark and bright discrete solitons have been generated simultaneously [1]. In the present work, we focus on the different orders of dark discrete cavity solitons (DDCSs), and we investigate possibility of switching and their co-existence by appropriate control Gaussian beam in both self focusing and de-focusing regime.

We consider an array of coupled nonlinear cavities with Kerr nonlinearity which is excited by an external driving field (Fig. 1). The evolution of field at the output of each cavity obeys a discrete nonlinear Schrodinger (DNLS) equation [2]:

$$i\frac{\partial u_n}{\partial T} + C(u_{n+1} + u_{n-1} - 2u_n) + (i + \Delta)u_n + \gamma|n_u|^2 u_n = \tilde{E}_{0n}e^{iqn} \tag{1}$$

where C and q correspond to the coupling constant and phase shift between adjacent cavities. Δ Define the detuning from cavity resonance. The nonlinear Kerr coefficient γ rescaled to $\gamma = \pm 1$, (-1 for the focusing and -1 for the self-defocusing case respectively). $\tilde{E}_{0n}$ is input field in the nth waveguide and is assumed as a superposition of plane wave with the amplitude E_0 and a Gaussian beam with the amplitude E_1, [3]

$$\tilde{E}_{0n} = \left(E_0 + E_1 e^{\frac{n^2}{w^2}} e^{i\phi}\right) \tag{2}$$

where w and ϕ specify the width and phase of Gaussian beam respectively.

Numerical methods are used to integrate coupled Equation (1) to simulate dynamics of light propagation in this system. Various orders of DDCSs with different width, shape and deep intensity have been observed (e.g., Figs. 1(b) and (c)). We manage to write and erase DDCSs in a given place on a homogeneous or pattern background and to switch different orders of DDCSs to each other by an appropriate Gaussian control beam.

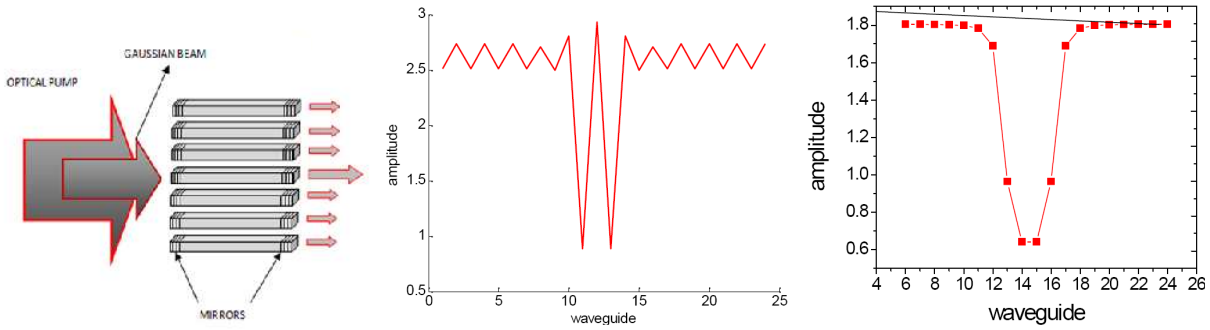

(a) (b) (c)

Figure 1: A array of coupled cavities that driven by a holding beam (a), Dark discrete cavity soliton in focusing (b) and defocusing regime (c).

REFERENCES

1. Lederer, F., G. I. Stegemanb, D. N. Christodoulides, G. Assanto, M. Segev, and Y. Silberberg, *Physics Reports*, Vol. 463, 1–126, 2008.
2. Egorov, O. A., F. Lederer, and Y. S. Kivshar, *Opt. Express*, Vol. 15, 4149, 2007.
3. Mahmoud Aghdami, K., R. Kheradmand, and R. Karimi, "Switching of multiples solitons in arrays of coupled cavities," *Jpn. J. Appl. Phys.*, to be published, 2011.

EIT-based Coherent Control Effect Sensitive to Probe Frequency and Control Field Intensity in a Periodic Layered Medium

Teh-Chau Liau[1], **Jin-Jei Wu**[2], **Jian Qi Shen**[3, 4], **and Tzong-Jer Yang**[2]

[1]Ph.D. Program in Engineering Science, College of Engineering
Chung Hua University, Hsinchu 30012, Taiwan, China
[2]Department of Electrical Engineering, Chung Hua University, Hsinchu 30012, Taiwan, China
[3]Centre for Optical and Electromagnetic Research
State Key Laboratory of Modern Optical Instrumentations
East Building No. 5, Zijingang Campus, Zhejiang University, Hangzhou 310058, China
[4]Joint Research Laboratory of Optics of Zhejiang Normal University and Zhejiang University
East Building No. 5, Zijingang Campus, Zhejiang University, Hangzhou 310058, China

Abstract— EIT (electromagnetically induced transparency) material can exhibit a large number of intriguing quantum optical effects relevant to light wave manipulation, which are expected to be beneficial for developing new technologies in quantum optics and photonics. A periodic layered medium with unit cells consisting of a dielectric and an EIT atomic vapor is suggested for light propagation manipulation. Such an EIT-based periodic layered medium exhibits a flexible frequency-sensitive optical response, e.g., a very small change in probe frequency can lead to a drastic variation in reflectance and transmittance, since such an EIT atomic system interacts with both control and probe fields, and destructive quantum interference caused by two-photon resonance occurs. The present EIT-based periodic layered structure can also lead to controllable optical processes depending sensitively on the external control field. The tunable and sensitive optical response induced by quantum interference of the EIT atomic system has useful applications, such as new photonic device design (e.g., optical switches, photonic transistors, logic and functional gates).

Manipulating Photonic Nanojet Parameters of Micron-sized Dielectric Microspheres

Yuri E. Geints, **Ekaterina K. Panina**, **and Alexander A. Zemlyanov**
Zuev Institute of Atmospheric Optics SB RAS, 1 Zuev square, Tomsk 634021, Russia

Abstract— The problem of overcoming the diffraction limit in the spatial resolution of wave microscopy devices, the necessity of a significant increase of the electromagnetic field strength in the region of its localization at the given radiation energy, and the micromanipulation of very small objects come recently to the forefront in connection with the development of nanophotonics studying optical fields and optical radiation behavior on a nanometer scale. One of the important aspects of this problem is the study of the structure of the optical field near a surface of slightly absorbing micron-sized particles from the viewpoint of the possibility of sub-diffraction focusing of the incident optical radiation. This effect, called the "photonic nanojet" (PNJ), was first noticed quite recently. The peculiarity of the PNJ from a spherical object is connected with the highest symmetry inherent to a sphere and providing for better focusing capability. Essentially, a PNJ corresponds to the specific spatial region within the external focal waist of the light wave diffracted on a transparent particle. It is located near the rear (shadow) side of the particle, extends to the distances of about several wavelengths in the environmental medium, and may have a sub-wavelength transversal dimension.

In this report we present the results of our systematic theoretical investigations of spatial and amplitude characteristics of PNJ formed in the vicinity of transparent dielectric microspheres exposed to the laser radiation. Based on the numerical calculation within the framework of the extended Mie theory for the optical radiation scattering on multilayered sphere, spatial and amplitude characteristics of the photonic jet of particles with a different size, optical properties, and structural composition were considered. In particular, for the first time the influence of the shell thickness and refractive index of composite two-layer microparticle on PNJ parameters were studied.

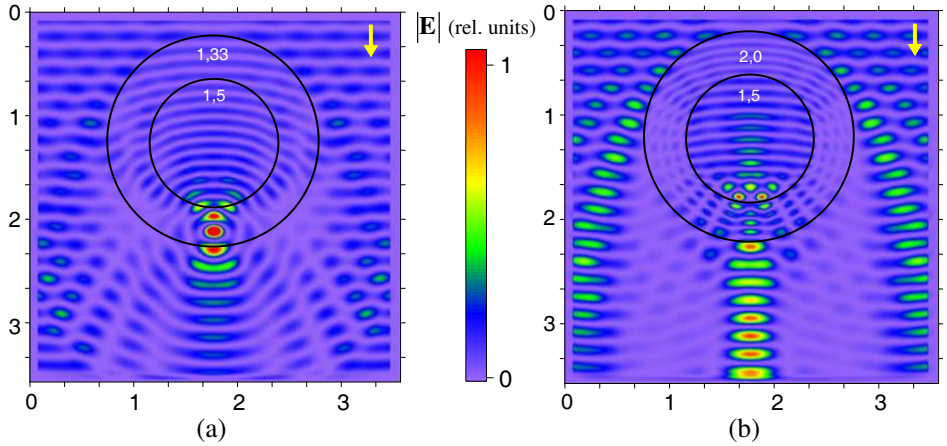

Figure 1: TFSF 3D-FDTD simulations of electric field amplitude $|E|$ spatial distribution in the vicinity of two-layered spherical particle (core + shell = 3 μm) with (a) $m_a = 1.5$ and $m_l = 1.33$ and (b) $m_l = 2.0$ illuminated by a plane wave (532 μm). The incident wave propagates from the top. The value of $|E|$ in each figure is normalized to its maximal value.

Influence of Stokes Pulse Shapes on SBS Slow Light in Fibers

Shanglin Hou[1], **Hongbing Li**[1, 2], **Yunbo Shang**[1], **Yanjun Liu**[1], **and Yongzhao Xu**[3]

[1]School of Science, Lanzhou University of Technology, Lanzhou, Gansu 730050, China
[2]School of Science, Nantong University, Nantong, Jiangsu 226007, China
[3]Institute of Electronic Engineering, Dong Guan University of Technology
Dongguan, Guangdong 523808, China

Abstract— In order to increase time delay and decrease pulse broadening via Stimulate Brillouin Scattering slow light, the coupled amplitude equations of Stimulated Brillouin Scattering in optical fibers were solved with fourth-order Runge-Kutta formula and characteristics, the influence of the edge sharpness, magnitude and duration of injected stokes pulse on time delay and pulse broadening factor was investigated. A method of optimizing time delay and pulse broadening factor was represented, namely, increasing the sharpness of stokes pulse appropriately. Comparing with using Gaussian-shaped pulse as injected stokes pulse, the similar time delay and less pulse broadening factor were obtained by this method. Theoretical analysis based on different power of injected stokes pulse proves that improving the sharpness of injected stokes pulse contributes a lot to reduce pulse broadening factor.

Measurement of the Verdet Constant in Different Mediums by Using Ellipsometry Technique

S. Suchat, **P. Viriyavathana**, **P. Jaideaw**, **N. Haisirikul**, **W. Kerdsang**, **and S. Petcharavut**
Physics Program, Faculty of Science and Technology
Phranakhon Rajabhat University, Bangkhen, Bangkok 10220, Thailand

Abstract— This experiment is designed to measure the Verdet constant V through Faraday Effect rotation of a polarized laser beam as it passes through different mediums, Flint Glass and water, parallel to the magnetic field B. As the B varies, the plane of polarization rotates and the transmitted beam intensity is observed. The angle through which it rotates is proportional to B and the proportionality constant is the Verdet constant times the optical path length. That by using ellipsometric parameters of under study was obtained. These are used to determine the Verdet constant for each medium and compared with standard known values. The experimental results are in good agreement with the corresponding theoretical analysis.

REFERENCES

1. Azzam, R. M. A. and N. M. Bashara, "Ellipsometric measurement of the polarization transfer function of an optical system," *J. Opt. Soc. Am.*, Vol. 62, 336–340, 1972.
2. Suchart, S. and R. Chitaree, "A novel optical fiber ellipsometer," *The IEEE Asia-Pacific Conference on Circuits and Systems*, 205–208, Chiangmai, Thailand, 1998.
3. Wen, H., M. A. Terrel, H. K. Kim, and M. J. F. Digonnet, "Measurements of the birefringence and Verdet constant in an air-core fiber," *Journal of Lightwave Technology*, Vol. 27, No. 15, 3194–3201, 2009.
4. Koerdt, C., G. L. J. A. Rikkenb, and E. P. Petrovc, "Faraday effect of photonic crystals," *Applied Physics Letters*, Vol. 82, No. 10, 1538–1540, 2003.
5. Jain, A., J. Kumar, F. Zhou, L. Li, and S. Tripathy, "Simple experiment for determining Verdet constants using alternating current magnetic fields," *Am. J. Phys.*, Vol. 67, No. 8, 714–717, 1999.

Session 3A1
Plasmonic Nanophotonics 1

Fabrication and Morphology Control of Metallic Micro/Nanostructures for Applications in Plasmonic Photonics

Xuan-Ming Duan, **Wei-Er Lu**, **Hong-Zhong Cao**, **Xian-Zi Dong**, **Yong-Liang Zhang**, **and Zhen-Sheng Zhao**
Laboratory of Organic NanoPhotonics (LaONP), Technical Institute of Physics and Chemistry Chinese Academy of Sciences, Beijing 100190, China

Abstract— Metallic micro/nanostructures have been applied in the fields including electronic and photonic devices. As an emerging technique to fabricate micro/nanostructures, multiphoton processing have been widely used to fabricate micro/nanometer-scaled patterns in the past decade as one of the recognized powerful lithography tools. A number of two-dimensional (2D) and three-dimensional (3D) microstructures have been successfully created using multiphoton processes toward photonic, electronic and plasmonic applications with polymers, dielectrics and metals. Progress has been made on patterning metal with the demonstration of 2D and 3D microstructures. However, comparing to the spatial resolution of nanometer scale achieved with polymers, obtaining the resolution in nanometer scale with laser photoreduction is still a hard challenge for fabricating continuous metallic structures. Furthermore, the metallic micro/nanostructures are composed of small nanoparticles, which would obstruct to develop the applications of the metallic micro/nanostructures in photonic and electronic devices. In this presentation, we will report the laser direct patterning of metal nanoparticles with the association of surfactant, which improve the resolution upon diffraction limit in the fabrication of metallic microstructure. With a post-treatment process with laser, the morphologies of metallic micro/nanostructures could be modified, which led to the smooth surface. The metallic micro/nanostructures with the smooth surface morphology functional devices could be expected to play an important role as plasmonic photonics interdisciplinary research fields, i.e., plasmonic photonics, nanoimaging, nanodetection, nanomanipulation and so on.

High Throughput Fabrication of Localized Surface Plasmonic Devices Using Ordered Porous Structures

Toshiaki Kondo[1], **Kazuyuki Nishio**[1, 2], **and Hideki Masuda**[1, 2]

[1]Kanagawa Academy of Science and Technology
5-4-30 Nishihashimoto Midori-ku, Sagamihara, Kanagawa 252-0131, Japan
[2]Department of Applied Chemistry, Tokyo Metropolitan University
1-1 Minamiosawa, Hachioji, Tokyo 192-0397, Japan

Abstract— Fabrication of ordered nanostructures of metals (Au, Ag) has attracted increasing interest due to its capability for the enhancement of electric fields of incident light based on the localized surface plasmon resonance (LSPR). The Use of materials with ordered porous structures of nanometer scales is effective for the fabrication of various types of functional plasmonic devices. For example, anodic porous alumina, which has ordered hole array structures, is useful as a starting material for the fabrication of functional plasmonic devices due to its unique geometrical structures [1]. Advantage of the use of anodic porous alumina for the preparation of is its controllability of the dimension of the structures besides its easiness of the preparation. In the present report, recent results of high throughput fabrication of plasmonic devices using porous structures will be presented [2–4]. The two dimensional (2D) and three dimensional (3D) ordered structures prepared from ordered porous structures were applied to the substrate for the measurement of surface enhanced Raman scattering (SERS). The optical properties of the obtained fine structures were analyzed theoretically by the FDTD method.

REFERENCES

1. Masuda, H. and K. Fukuda, *Science*, Vol. 268, 1466, 1995.
2. Kondo, T., T. Fukushima, K. Nishio, and H. Masuda, *Appl. Phys. Express*, Vol. 2, 125001, 2009.
3. Kondo, T., K. Nishio, and H. Masuda, *Appl. Phys. Express*, Vol. 2, 032001, 2009.
4. Nishio, K. and H. Masuda, *Angew. Chem. Int. Ed.*, Vol. 50, 1, 2011.

Surface Enhanced Raman Scattering Based on Gold Nanoparticles Decorated on Polymer Inverse Opal Crystals

Cheng Yi Wu[1], **Chia Chi Huan**[2], **Jia Sin Jhang**[1], **An Chi Liu**[1], **Chun-Chen Chiang**[2], **Ming-Lung Hsieh**[2], **Ping-Ji Huang**[2], **Le Dac Tuyen**[1, 6], **Le Quoc Minh**[5], **Tzyy Schiuan Yang**[2], **Lai-Kwan Chau**[2], **Hung-Chih Ka**[1], **and Chia Chen Hsu**[1, 3, 4]

[1]Department of Physics, National Chung Cheng University, Ming Hsiung, Chia Yi 621, Taiwan
[2]Department of Chemistry and Biochemistry, National Chung Cheng University
Ming Hsiung, Chia Yi 621, Taiwan
[3]Graduate Institute of Opto-Mechatronics, National Chung Cheng University
Ming Hsiung, Chia Yi 621, Taiwan
[4]Department of Photonics, National Sun Yat-Sen University, Kaohsiung 804, Taiwan
[5]Institute of Materials Science, VAST of Vietnam, Hoang Quoc Viet Road, Hanoi, Vietnam
[6]Hanoi University of Mining and Geology, Tu Liem, Hanoi, Vietnam

Abstract— A novel surface-enhanced Raman scattering (SERS) substrate based on Au nanoparticles decorated inverse opal (IO) photonic crystal (PhC) is presented. In addition to the enhancement contributed from Au nanoparticles, a desired Raman signal can be selectively further enhanced by appropriately overlapping the center of photonic bandgap of the IO PhC with the wavelength of the Raman signal. Furthermore, the lattice structure the IO PhC provides excellent control of the distribution of Au nanoparticles to produce SERS spectra with high uniformity. The new design of SERS substrate provides extra maneuverability for ultra-high sensitivity sensor applications.

Size Dependence of Nanoparticle-SERS Enhancement from Silver Film over Nanosphere (AgFON) Substrate

Wen-Chi Lin[1], **Lu-Shing Liao**[1], **Yi-Hui Chen**[2], **Hung-Chun Chang**[2], **Din Ping Tsai**[3, 4], **and Hai-Pang Chiang**[1, 4, 5]

[1]Institute of Optoelectronic Sciences, National Taiwan Ocean University, Keelung, Taiwan, R.O.C.
[2]Department of Electrical Engineering, Graduate Institute of Photonics and Optoelectronics
National Taiwan University, Taipei, Taiwan, R.O.C.
[3]Department of Physics, National Taiwan University, Taipei, Taiwan, R.O.C.
[4]Instrument Technology Research Center
National Applied Research Laboratories, Hsinchu, Taiwan, R.O.C.
[5]Institute of Physics, Academia Sinica, Taipei, Taiwan, R.O.C.

Abstract— Surface-enhanced Raman scattering has become a powerful tool for biological detection due to its high sensitivity [1, 2]. Many methods have been used to produce periodic structures that enhance SERS sensitivity, such as colloidal methods to produce silver nanoplates, electron beam lithography (EBL) to produce nanoparticles on substrates, oblique angle deposition (OAD) to fabricate nanorod arrays, and nanosphere lithography (NSL) to fabricate silver nanoparticle arrays. Among these techniques, NSL has several advantages including the applicability to different substrates, fast fabrication speed, and low-cost. This method can generate two particular kinds of structures, arrays of triangular nanoparticles with lift-off and nanoparticles without lift-off called "metal film over nanosphere" (MFON); in AgFON, the metal is silver.

Optimizing the conditions for SERS is important for enhancing the Raman intensity. Research on optimizing SERS with different substrate is of great interest. Many researchers have investigated ways to improve SERS, such as by using copper phthalocyanine thin films deposited onto Ag films by using underlayers of gas-evaporated Si particles, where the roughness depth is 100 Å and the maximum enhancement factor $\sim 1.5 \times 10^4$; the use of glycine for determining the SERS activity and changing the nanoparticles size as a function of PH and ionic strength, and estimating the corresponding enhancement factor (EF); etc. In addition, finite difference time domain (FDTD) calculations have been employed to explain the relationship between particle size and SERS activity.

In this paper, optimal SERS enhancement using AgFON was realized by controlling the nanosphere size. AgFON nanostructures were fabricated with different periods by using polystyrene nanospheres of various sizes. An AgFON substrate was dipped into Rhodamine 6G (R6G) dye solution for 24 hours. FDTD simulations of electric field distribution of AgFON with different nanosphere sizes revealed the relation between the localized surface plasmon (LSPR) around silver nanoparticles and the SERS spectrum. These results provide assistance in selecting nanoparticle size to maximize the sensitivity of SERS.

REFERENCES

1. Lin, W. C., H. C. Jen, C. L. Chen, D. F. Hwang, R. Chang, J. S. Hwang, and H. P. Chiang, "SERS study of tetrodotoxin (TTX) by using silver nanoparticle arrays," *Plasmonics*, Vol. 4, 187, 2009.
2. Lin, W. C., S. H. Huang, C. L. Chen, C. C. Chen, D. P. Tsai, and H. P. Chiang, "Controlling SERS intensity by tuning the size and height of a silver nanoparticle array," *Appl. Phys. A*, Vol. 101, 185, 2010.

Light Manipulation by Plasmonics Nanobump Structure

C. M. Chang[1], **C. H. Chu**[1], **M. L. Tseng**[1], **B. H. Chen**[1], **and Din Ping Tsai**[1, 2, 3]

[1]Department of Physics, National Taiwan University, Taipei 106, Taiwan
[2]Research Center for Applied Sciences, Academia Sinica, Taipei 115, Taiwan
[3]Instrument Technology Research Center, National Applied Research Laboratories, Hsinchu 300, Taiwan

Abstract— Surface plasmon polaritons (SPPs) which is quantization from surface collective electrons resonance forms the surface plasma propagating wave. Surface plasmon wave can be modified by the artificial subwavelength structure on metal surface, such as plasmonic waveguide with the gold slots [1] plasmonics lens with grating [2], SPPs focusing by the quarter-circle [3], and squeezing near-field light by metallic nanoparticles [4]. There are three basis mechanism processes to describe the SPP interaction with these subwavelength structures, namely SPP reflection, SPP transmission and scattering SPP in light [5]. These researches open up the possibility to manipulate light and overcome the diffraction limit of the traditional optics.

In this paper, we study the interaction of SPPs with plasmonic structure composed of nanobumps on gold thin film. The SPPs of the gold film surface is launched by attenuation total internal refraction (ATIR) method with Nd:YAG laser (wavelength 532 nm) Total internal reflection fluorescence microscopy (TIRFM) system is employed to bring out the plasmonic mode of the structure. The nanobumps are directly fabricated on the 30 nm thick gold film by femtosecond laser illumination(wavelength 800 nm, pulse duration 140 fs, exposure time 30 ms), and the size of each nanobump is 300 nm for diameter and 12 nm for height. The subwavelength nanobumps of plasmonic structure are protuberance for scattering the SPPs wave. We find that the scattering light is focused to spots which FWHM of intensity is 330 nm and the property of focusing spot depends on the geometry configuration of plasmonic structure. This research has potential to be applied in the area such as the integrated photonic circuit in the future.

ACKNOWLEDGMENT

This research is supported by financial aids from under grant number 99-2120-M-002-012 and 99-2911-I-002-127.

REFERENCES

1. Barnes, W. L., A. Dereux, and T. W. Ebbesen, *Nature*, Vol. 424, 824, 2003.
2. Zhao, C. L., J. Y. Wang, X. F. Wu, and J. S. Zhang, *Appl. Phys. Lett.*, Vol. 94, 2009.
3. Yin, L. L., V. K. Vlasko-Vlasov, J. Pearson, J. M. Hiller, J. Hua, U. Welp, D. E. Brown, and C. W. Kimball, *Nano Lett.*, Vol. 5, 1399, 2005.
4. Krenn, J. R., A. Dereux, J. C. Weeber, E. Bourillot, Y. Lacroute, and J. P. Goudonnet, *Phys. Rev. Lett.*, Vol. 82, 2590, 1999.
5. Zayats, A. V., I. I. Smolyaninov, and A. A. Maradudin, *Phys. Rep.*, Vol. 408, No. 3–4, 131–314, 2005.

Thermal Dynamics in a Plasmonic Metamaterial Absorber

Min Qiu[1, 2], **Jiaming Hao**[2], **Jing Wang**[2], **Yiting Chen**[2], **Xi Chen**[2], **and Min Yan**[2]

[1]State Key Laboratory of Modern Optical Instrumentation and Institute of Advanced Nanophotonics
Department of Optical Engineering, Zhejiang University, Hangzhou 310027, China
[2]Division of Optics and Photonics, Royal Institute of Technology (KTH)
Electrum 229, Kista 164 40, Sweden

Abstract— Plasmonic and metamaterial nanostructures are in most cases inevitably lossy at optical regime, mostly due to the fact that metallic materials absorb light. This is usually unwanted; however, absorption is sometimes important for certain applications, e.g., photothermal effects. Photothermal effects in plasmonic structures have given rise to many important applications, e.g., thermal cancer therapy, optical data storage, sensing, etc. Here, we theoretically designed and experimentally demonstrated a plasmonic metamaterial absorber, which can efficiently absorb light at near infrared wavelengths. Due to high absorption, the structure has interesting thermal dynamic effects, including localized heating. This can lead to new possibilities for all-optical thermal tuning, infrared imaging, micro-bolometer, thermal actuators, sensors, etc.

Plasmonic Enhancement on Molecular Fluorescence by Coreshell

Mao-Kuen Kuo[1], **Chuan-Li Liu**[1], **and Jiunn-Woei Liaw**[2]

[1]Institute of Applied Mechanics, National Taiwan University
1, Sec. 4, Roosevelt Rd., Taipei 106, Taiwan, R.O.C.
[2]Department of Mechanical Engineering, Chang Gung University
259 Wen-Hwa 1st Rd., Kwei-Shan, Tao-Yuan 333, Taiwan, R.O.C.

Abstract— The average enhancement factor (AEF) of a large number of coreshells ($Ag@SiO_2$ [1] and $Au@SiO_2$ [2]) on the fluorescence of molecules doped within the silica shell is studied theoretically by considering the random orientation and location of the molecules to evaluate the overall performance of coreshell. Due to the surface plasmon resonance of metallic nanoparticle, the fluorescence of the nearby molecule can be enhanced. Our results indicate that AEF of a coreshell is much less than the maximum EF. For example, AEF of a FITC-doped $Ag@SiO_2$ (radius of Ag core: 25 nm, thickness of silica shell: 15 nm) irradiated by a laser of 488 nm for FITC's emission at 518 nm is 2.406, which is much smaller than the maximum EF (30.114) of $Ag@SiO_2$ containing a single molecule with a radial orientation at its optimal position. $Ag@SiO_2$ is like a narrowband enhancer (400–430 nm), while $Au@SiO_2$ is a low-frequency enhancer with a cutoff wavelength of 590 nm. For Alexa 430-doped $Ag@SiO_2$ excited at 428 nm, AEF is 12.34 at the emission of 538 nm. In contrast, for Alexa 633-doped $Au@SiO_2$ (radius of Au core: 50 nm, thickness of silica shell: 25 nm) excited at 633 nm, AEF is 2.844 at the emission of 653 nm.

REFERENCES

1. Liaw, J.-W., C.-L. Liu, W.-M. Tu, C.-S. Sun, and M.-K. Kuo, "Average enhancement factor of molecules-doped coreshell ($Ag@SiO_2$) on fluorescence," *Opt. Express*, Vol. 18, No. 12, 12788–12797, 2010.
2. Liaw, J.-W., C.-L. Liu, W.-M. Tu, and C.-S. Sun, "Plasmonic enhancement of coreshell ($Au@SiO_2$) on molecular fluorescence," *J. Quantitative Spectroscopy & Radiative Transfer*, 2011 (in press).

Acousto-plasmonics and Surface Enhanced Raman Scattering Properties of Metal Nanoparticles

Adnen Mlayah[1], **Renaud Marty**[1], **Arnaud Arbouet**[1], **Christian Girard**[1], **Sudhiranjan Tripathy**[2], **Vivian Kaixin Lin**[2], **Siew Lang Teo**[2], **Enyi Ye**[2], **Ming Yong Han**[2], **and Lucien Saviot**[3]

[1]Centre d'Elaboration de Matériaux et d'Etudes Structurales CNRS
Université de Toulouse, 29 Rue J. Marvig Toulouse, 31055, France
[2]Institute for Material Research and Engineering/A*STAR, 3 Res. Link, 117602, Singapore
[3]Laboratoire Interdisciplinaire Carnot de Bourgogne CNRS
Université de Bourgogne, 9 Av. A. Savary, Dijon BP 47 870, France

Abstract— Raman scattering by acoustic vibrations of metal nano-objects has been addressed in several reports. In particular, the size and shape dependence of the acoustic vibrations and their Raman activity have been the subject of detailed experimental and theoretical investigations [1–6]. However, in most of the previously reported works, the scattering was excited in resonance with the surface plasmons of the nano-objects *themselves*. Hence, all established Raman activities and selection rules assume coupling between acoustic vibrations and surface plasmons of the same nano-object [6]. But are these selection rules still valid when considering the interaction between acoustic vibrations of spherical nanoparticles and surface plasmons that do not exhibit any spherical symmetry? Could we demonstrate and control the Acoustic Phonons SERS (AP-SERS) effect by engineering the surface plasmons?

Answering these questions requires separating the vibrational dynamics and the surface plasmon properties.

The studied system combines spherical gold nanoparticles, from a colloidal solution, and gold nanodisk trimers processed by electron beam lithography. The Raman probe wavelengths are chosen to selectively excite the surface plasmons of either the nanoparticles or the nanodisk trimers. The electromagnetic interaction among the gold nanodisks in the trimer configuration provides the localized electric near-fields at the origin of the AP-SERS. For excitation close to resonance with the localized surface plasmons of the nanodisk trimers we are able to detect several intense Raman bands generated by the spherical gold nanoparticles. Based both on vibrational dynamics calculations and Raman selection rules, the measured Raman bands are assigned to fundamental and overtones of the quadrupolar and breathing vibration modes of the spherical gold nanoparticles [2, 3, 6]. Simulations of the electric near-field intensity maps performed at the Raman probe wavelengths showed strong localization of the optical energy in the vicinity of the nanodisk trimers, thus corroborating the role of the interaction between acoustic vibrations of the spherical nanoparticles and surface plasmons of the NDTs. Acoustic Phonons Surface Enhanced

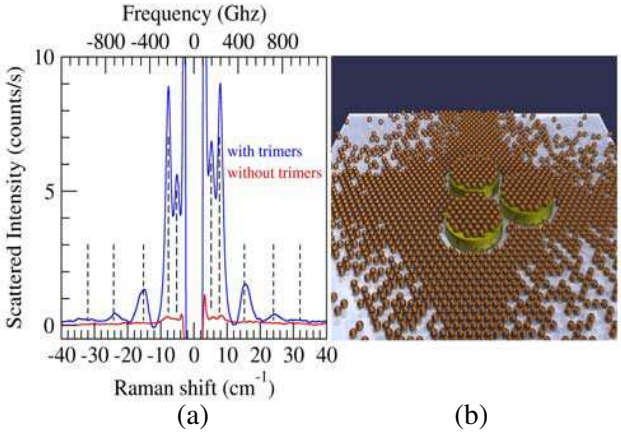

Figure 1: (a) Low-frequency Raman spectra showing the enhancement of scattering by acoustic vibrations of the spherical gold nanoparticles when the latter are located on the gold nanodisk trimers. (b) Schematic view of the nanoparticles and nanodisk trimers.

Raman Scattering (AP-SERS) is here demonstrated for the first time for such coupled plasmonic systems. This work paves the way to surface plasmon engineering for sensing the vibrational properties of nanoparticles.

REFERENCES

1. Weitz, D. A., et al., *Phys. Rev. Lett.*, 355, 1980.
2. Adichtchev, S., et al., *Phys. Rev. B*, 201402, 2009.
3. Nelet, A., et al., *Appl. Surf. Science*, 209, 2004.
4. Margueritat, J., et al., *Nano Lett.*, 2037, 2006.
5. Large, N., et al., *Nano Lett.*, Vol. 9, 3732, 2009.
6. Bachelier, G., et al., *Phys. Rev. B*, 205408, 2004.

Session 3A2a
Merging of Metamaterials and Natural Materials

Special Structured Photonic Crystals Based on Colloidal Crystals and Crystal Habits of Oxides

Ming Fu
Key Laboratory of Luminescence and Optical Information, Ministry of Education
Institute of Optoelectronic Technology, Beijing Jiaotong University, Beijing 100044, China

Abstract— The colloidal-crystal template method is proven to be a simple and efficient approach for fabricating photonic crystals with easily controlled periodicities. However, only inverse opal structures or nanobowl array films are made by the colloidal-crystal template (CCT) method. In fact, single-layer nanobowl arrays are inverse opal structures in which the thickness of the porous structures is controlled to be less than the radius of the microsphere The symmetry of fabricated structures using the CCT method is only determined by the shape of the template, which restricts the diversity of the photonic crystal properties. The use of a face-centered cubic (FCC) CCT to fabricate structures other than inverse opals is helpful. Therefore, we'd like to discuss several special structured oxide photonic crystals which are fabricated by the assistant of CCT and their growth habits, including zinc oxide nanomeshes, cuprous oxide particles, heterostructures, and inverse opals with defects.

ZnO nanomeshes can be fabricated from the nanosheet habit of ZnO by using CCT. ZnO nanomeshes with higher densities might show a prominent photonic reflection band. An important photonic band gap property different from inverse opal structure is exhibited because of the different symmetry of the fabricated free-standing nanomeshes. Furthermore, the nanoscale 2D porous shape makes the structure more flexible than the 3D macroporous structure. The symmetry of the nanomesh structure is more sensitive to outside forces. The current velocity-sensitive property of nanomeshes under water current is also studied because the photonic properties are different from those of the inverse opals. In addition, a broad photonic stop band can be measured from the photonic crystal heterostructures which are fabricated by ZnO nanomeshes and inverse opals templated by a single CCT. Further, Cu_2O crystals with various morphologies were fabricated by their habits and branching via the colloidal crystals. The CCT affects the branching of Cu_2O crystal. Inverse opals with extrinsic defects can be fabricated based on these structures with their growth habits.

Tunable Left-handed Material by Ferrite and Metallic Wire Array: Design and Realization

Rui-Xin Wu, **Yin Poo**, **Guang-Hua He**, **and Da-Yong Zhou**
School of Electric Sciences and Engineering, Nanjing University, Nanjing 210093, China

Abstract— Metamaterials especially the left-handed materials, have attracted much attention in recent years. They have some important applications, for instance, the perfect lens that overcome the resolution limit in conventional imaging systems, the invisible cloak that can hide objects from detection, and perfect absorbers that have high absorption with thin topologies [1–3]. For the applications, how to broaden the working frequency range is one of the main problems. Tunable metamaterial, which has changeable and reconfigurable properties, provide a practical way to solve the problem. Some possible implementations for the tunable metamaterials have been proposed. For example, photo capacitance effect was used to control the dynamic response of split ring resonators [4] The negative permittivity can be tuned by electric field, temperature and strain [5–7], and negative permeability can be controlled by magnetic field [8].

In this work, we design a composite by ferrite rod and metallic wire array and demonstrate the composite is a tunable left-handed material. We show the composite has both negative permittivity and negative permeability by retrieved equivalent permittivity and permeability, and the transmission spectra in magnetize states. We further prove the metamaterial has negative refraction by simulating the electric field distribution of the wave refracted from a wedge-shape composite. The index of refraction obtained by the Snell's law and the retrieval procedure are in good agreement, which quantitatively confirm the negative refractive index of the composite. We find the magnitude and the frequency range of the negative index are tunable in applied magnetic fields. The permeability and permittivity of the component materials, as well as the composite configuration, influence the tunabilty and the loss of the negative index. It is demonstrated that ferrite-wire structure is a lower loss tunable metamaterial. Experimentally, we fabricated a two-dimensional periodic composite made of MgMn ferrite rods and metallic wires, and demonstrated the LHM regime by the sample's abnormal transmission in bias magnetic fields. The experiments are in good agreement with simulations. We observed the abnormal transmission changed with the intensity of the bias magnetic field, showing the frequency tunable character of the LHM regime.

ACKNOWLEDGMENT

This work is supported by National Natural Science Foundation of China (No. 60771013 and 61071007).

REFERENCES

1. Pendry, J. B, *Phys. Rev. Lett.*, Vol. 85, 3966, 2000.
2. Schurig, D., J. J. Mock, B. J. Justice, et al., *Science*, Vol. 314, 977–979, 2006.
3. Landy, N. I., S. Sajuyigbe, J. J. Mock, D. R. Smith, and W. J. Padilla, *Phys. Rev. Lett.*, Vol. 100, 207402, 2008.
4. Boulais, K. A., D. W. Rule, S. Simmons, et al., *Appl. Phys. Lett.*, Vol. 93, 043518, 2008.
5. Ustinov, A. B., V. S. Tiberkevich, G. Srinivasan, et al., *J. Appl. Phys.*, Vol. 100, 093905, 2006.
6. Zhao, Q., B. Du, L. Kang, et al., *Appl. Phys. Lett.*, Vol. 92, 051106, 2008.
7. Kim, S. and V. Gopalan, *Appl. Phys. Lett.*, Vol. 78, 3015, 2001.
8. He, Y. X., P. He, S. D. Yoon, et al., *J. Magn. Magn. Mater.*, Vol. 313, 187–191, 2007.
9. Kang, L., Q. Zhao, H. J. Zhao, et al., *Opt. Express*, Vol. 16, 17269–17273, 2008.

THz Metamaterials by Stacked Subwavelength Hole Arrays

S. Wang[1,2], **F. Garet**[3], **E. Lheurette**[1], **J. L. Coutaz**[3], **and D. Lippens**[1]

[1]Institut d'Electronique de Micro-électronique et de Nanotechnologie
UMR CNRS 8520, Université des Sciences et Technologies de Lille
Avenue Poincaré BP 60069, 59652 Villeneuve d'Ascq Cedex, France
[2]College of Electronics and Information Engineering, Wuhan Textile University
Wuhan 430073, China
[3]IMEP-LAHC, UMR CNRS 5130, Université de Savoie
73376 Le Bourget du Lac Cedex, France

Abstract— We demonstrate THz metamaterials by stacked subwavelength hole arrays. High-transmissivity composite left/right-handed bulk metamaterials were fabricated in a multilayered dielectric/hole array technology and experimentally assessed at submillimeter wavelength (0.4–0.9 THz) by time domain spectroscopy. A wedge-type negative index metamaterial verified the negative refraction closed to $n = -1$ at around 0.5 THz experimentally. A flat lens with gradient negative index of refraction based on such dielectric/hole arrays and operated at THz was also proposed.

Electromagnetic (EM) metamaterials have atta-rcted much interest in the last decade owing to the possibility of guiding the EM waves by tailoring the effective parameters, permittivity ε and permeability μ [1]. Thus provides some practical applications including focusing with a flat lens [2] and invisibility cloaks [3]. Most of the experimental realizations have only been done in the microwave regime because of the relatively simple fabrication techniques which allows a large freedom to design the metamaterials. However, the extension of these studies in the terahertz (THz) or the optical regime is still challenging because of the standard fabrication methods (photolithography or electron beam lithography) allow only the possibilities to build planar structures with very limited number of layers but not bulk metamaterials. The so-called fishnet structure [4] was introduced as the substitute of the split ring resonator [5] and wire arrays [6] to operate at visible and terahertz frequencies, respectively.

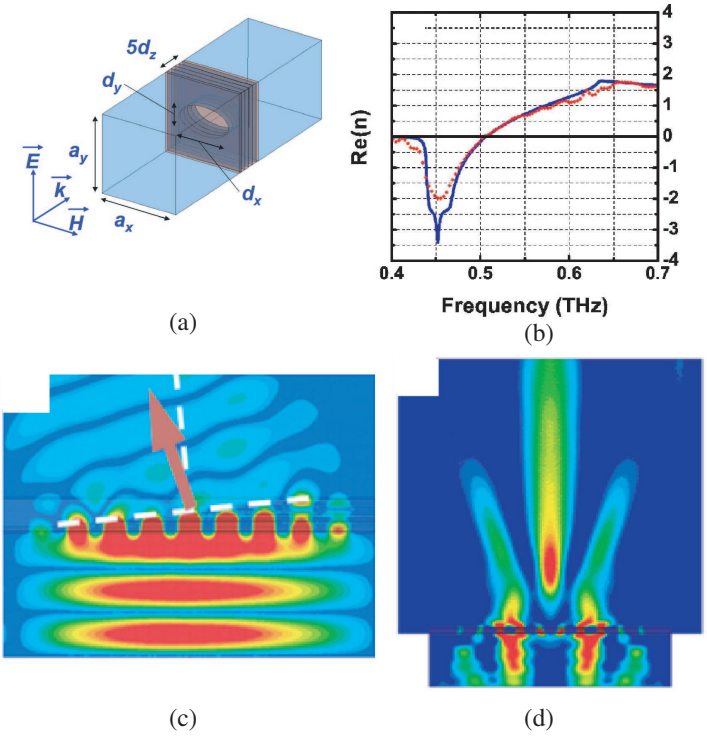

Figure 1: (a) A unit scheme of the metamaterials; (b) Index of the metamaterials as function of the frequency; (c) Electric field mapping of a ten stairs prism at 0.46 THz; (d) Electric field of a flat lens with gradient negative index at 0.5 THz.

In this paper, we present the metamaterials operating at THz fabricated by stacked hole arrays. Composite left/right-handed bulk metamaterials with high transimissivity were fabricated in a multilayered dielectric/hole array technology and experimentally assessed at submillimeter wavelength (0.4–0.9 THz) by time domain spectroscopy [7], see Figure 1(a). A wedge-type sample further demonstrates the negative refractive index at around 0.5 THz as shown in Figures 1(b) and (c) [8]. Finally, we propose a flat lens with gradient negative index of refraction operating at THz as Figure 1(d).

REFERENCES

1. Capolino, F., *Metamaterials Handbook*, CRC, Great Britain, 2009.
2. Aydin, K., et al., *Opt. Express*, Vol. 13, 8753, 2005.
3. Schurig, D., et al., *Science*, Vol. 314, 977, 2006.
4. Zhang, S., et al., *Opt. Express*, Vol. 13, 4922, 2005.
5. Pendry, J. B., et al., *IEEE Trans. Microw. Theory Tech.*, Vol. 47, 2075, 1999.
6. Pendry, J. B., et al., *Phys. Rev. Lett.*, Vol. 76, 4773, 1996.
7. Wang, S., et al., *J. Appl. Phys.*, Vol. 107, 074510, 2010.
8. Wang, S., et al., *Appl. Phys. Lett.*, Vol. 97, 181902, 2010.

Electrically Tunable Metamaterials Operating Under Normal Incidences

Fuli Zhang[1], **Qian Zhao**[2], **Jingbo Sun**[3], **Weihong Zhang**[4], **Ji Zhou**[3], **and Didier Lippens**[5]

[1]Key Laboratory of Space Applied Physics and Chemistry, Ministry of Education
School of Science, Northwestern Polytechnical University, Xi'an 710072, China
[2]State Key Lab of Tribology, Department of Precision Instruments and Mechanology
Tsinghua University, Beijing 100084, China
[3]State Key Lab of New Ceramics and Fine Processing
Department of Materials Science and Engineering, Tsinghua University, Beijing 100084, China
[4]Key Laboratory of Contemporary Design & Integrated Manufacturing Technology, Ministry of Education
Northwestern Polytechnical University, P. O. Box 552, 710072 Xi'an, China
[5]Institut d'Electronique de Microélectronique et de Nanotechnologie, CNRS 8520
Université des Sciences et Technologies de Lille, 59652 Villeneuve d'Ascq Cedex, France

Abstract— Electromagnetic metamaterial has undergone rapid development over past few years on account of its unique properties. As a kind of resonant restructure, metamaterial inevitably suffers from narrow bandwidth. The creation of tunable metamaterials, whose operational frequency could be adjusted to other desired frequency, is of great interest to overcome this limitation. Although various efforts were given to realize tunable metamaterial via capacitance variation by the incorporation of active devices such as varactor diode [1], semiconductors [2, 3], ferroelectric [4], and anisotropic materials [5, 6], these works are mainly focused on the metamaterial devices operating under grazing incidence. Here, we report on the proof-of-principle demonstration of voltage tunable metamaterial via liquid crystal technology operating under normal incidence at microwave frequencies.

Two types structures, one is composed of short wire pair [7] and the other one using fishnet [8] configuration, were used for the realization of the variation of effective permeability and effective index, respectively. The proposed active devices are a tri-layer structure assembled by two Teflon fibreglass layer stacked with one nematic LC layer in between. To apply a uniform bias field, the adjacent short wire elements were connected by short bars whereas it is no necessary for the fishnet pattern. For the short wire pair structures, it is found that by increasing bias voltage from 0 to 100 Volt, magnetic resonance frequency is continuously and reversibly shifted from 9.91 down to 9.55 GHz. Moreover, the effective permeability experiences the variation from negative to positive values. On the other hand, the left handed passband of fishnet structure can be reversibly shifted from 9.14 to 8.80 GHz, whereas the upper right handed passband is nearly unchanged. Such discrepancy is due to the different local electric field distribution for electric and magnetic resonances for fishnet structure. Furthermore, during LC molecular reorientation, magnetic resonance shift is accompanied by an effective index change of 1.1 within negative index regime.

REFERENCES

1. Chen, H., B.-I. Wu, L. Ran, T. M. Grzegorczyk, and J. A. Kong, "Controllable left-handed metamaterial and its application to a steerable antenna," *Appl. Phys. Lett.*, Vol. 89, 053509, 2006.
2. Degiron, A., J. J. Mock, and D. R. Smith, "Modulating and tuning the response of metamaterials at the unit cell level," *Opt. Express*, Vol. 15, 1115–1127, 2007.
3. Chen, H.-T., J. F. O'Harai, A. K. Azadi, A. J. Taylor, R. D. Averitt, D. B. Shrekenhamer, and W. J. Padilla, "Experimental demonstration of frequency-agile terahertz metamaterial," *Nat. Photonics*, Vol. 2, 295–298, 2008.
4. Hand, T. H. and S. A. Cummer, "Frequency tunable electromagnetic metamaterial using ferroelectric loaded split rings," *J. Appl. Phys.*, Vol. 103, 066105, 2008.
5. Xiao, S., U. K. Chettiar, A. V. Kildishev, V. Drachev, I. C. Khoo, and V. M. Shalaev, "Tunable magnetic response of metamaterials," *Appl. Phys. Lett.*, Vol. 95, 033115, 2009.
6. Zhao, Q., L. Kang, B. Du, B. Li, J. Zhou, H. Tang, X. Liang, and B. Zhang, "Electrically tunable negative permeability metamaterials based on nematic liquid crystals," *Appl. Phys. Lett.*, Vol. 90, 011112, 2007.

7. Zhang, F., W. Zhang, Q. Zhao, J. Sun, K. Qiu, J. Zhou, and D. Lippens, "Electrically controllable fishnet metamaterial based on nematic liquid crystal," *Opt. Express*, Vol. 19, 1563, 2011.
8. Zhang, F., Q. Zhao, W. Zhang, J. Sun, J. Zhou, and D. Lippens, "Voltage tunable short wire-pair type of metamaterial infiltrated by nematic liquid crystal," *Appl. Phys. Lett.*, Vol. 97, 134103, 2010.

Ultraviolet Negative Refraction in Graphite

Jingbo Sun, **Ji Zhou**, **Bo Li**, **and Feiyu Kang**
State Kay Lab of New Ceramics and Fine Processing, Department of Materials Science and Engineering
Tsinghua University, Beijing 100084, China

Abstract— In this work, we report a natural indefinite material of crystalline graphite that exhibits negative group refraction at ultra-violet region. A hyperbolic equifrequency contour was obtained from ellipsometry data at 254 nm and an all-angle negative refraction was verified experimentally. This indefinite permittivity is attributed to extremely strong anisotropy between the directions perpendicular and parallel to the atomic plane of the graphite structure, and the hybrid electronic transitions. As a homogenous material, it avoids severe wave scattering caused by the inner structure in those artificially engineered material. On the other hand, this natural negative-index avoids complicated design and fine fabrication techniques. Additionally, because graphite tends to be intercalated with many molecules, ions, or atomic clusters to form intercalation compounds, the frequency range and the index value of negative refraction can be tunable. This result not only explores a route toward natural negative-index materials, but also holds a promise for ultra-violet hyperlens, which may lead to a breakthrough in nanolithography for the next generation of electronics.

Anomalous Refractive Effects in Photonic Crystals Formed by Holographic Lithography

G. Y. Dong[1], **J. Zhou**[1], **X. L. Yang**[2], **and L. Z. Cai**[2]

[1]Department of Materials Science & Engineering, Tsinghua University, Beijing 100084, China
[2]Department of Optics, Shandong University, Jinan 250100, China

Abstract— Anomalous refractive effects of photonic crystals (PhCs) formed by holographic lithography (HL) can be modulated more easily than regular PhCs. The HL PhCs show the effective indices quite close to -1 for a wide range of incident angles with a larger all-angle left-handed negative refraction frequency range. The calculations and FDTD simulations have shown that the high-performance negative refraction properties can happen in the holographic structures for a wide filling ratio and can be modulated by changing the filling ratio easily. The symmetry mismatch between the incident wave and the Bloch modes of the holographic PhC is used to guide light efficiently. By properly designing the waveguide, backscattering loss can be significantly reduced. Due to the unique advantages of holographic photonic crystals, the serious problems of material loss and fabrication difficulty in left-handed material waveguides are also avoided. It is shown that high transmission efficiency is easily achieved in the frequency region with effective refraction index near zero. A dual-negative refraction effect based on overlapping bands in a two-dimensional hexagonal photonic crystal is proposed. Theoretical analysis and numerical simulation show that an incident plane wave launched into this photonic crystal under certain conditions excites dual negative refracted modes simultaneously with the same frequency and the same polarization state. This dual-negative refraction effect can be manipulated by adjusting the incident angle, dielectric constant and filling ratio. By utilizing this special effect, double focusing images of a point source and beam splitting can be realized. These unique features extend the possibly guiding ability of holographic PCW and promising potential in optical application.

Effective Circuit Model Analysis of Dielectric Metamaterials

Lingyun Liu[1, 2], **Jingbo Sun**[1], **Ji Zhou**[1], **and Bo Fu**[2]

[1]State Key Lab of New Ceramics and Fine Processing, Department of Materials Science and Engineering Tsinghua University, Beijing 100084, China

[2]School of Electrical and Electronic Engineering, Hubei University of Technology, Wuhan 430068, China

Abstract— We developed an effective series RLC model for the electromagnetic response of weakly absorbing dielectric sphere near the first magnetic dipole resonance. The effective magnetic properties of Mie resonance-based dielectric metamaterials were attained in terms of this model. This approach is intuitive and can give analytical dependence of the magnetic properties of the composite on the electromagnetic and geometric parameters of the constituting dielectric particles. We verified the model by use of numerical simulation and EMG based on accurate Mie theory. The important parameters of dielectric metamaterials, such as the magnetic resonance frequency and the relative broadness of negative magnetic permeability, are discussed in terms of this model.

Session 3A2b
Cloaked Material System and Electromagnetic Compatibility

Fabrication and Electromagnetic Wave Absorption Properties of Amorphous Fe-Si-B Microwires

Mangui Han, **Deifei Liang**, **JianLiang Xie,**, **and Longjiang Deng**
State Key Laboratory of Electronic Thin Films and Integrated Devices
University of Electronic Science and Technology of China, Chengdu 610054, China

Abstract— Glass coated Fe-based amorphous and nanocrystalline wires have been widely studied for their giant magnetoimpedance (GMI) effect, and have been mainly exploited for sensor developments, such as magnetic field sensors, position sensors, structural health monitoring etc [1]. Usually the reported methods of fabricating magnetic microwires include melt extraction method, Taylor-Ulitovsky method, Taylor method of producing glass-coated wire, the in-rotating-water quenching technique [2]. Recently, there was an ever increasing interest in studying their electromagnetic (EM) wave absorption properties due to their potential applications in anti-EM interference coatings, microwave darkrooms [3]. However, most of the high frequency properties investigations concentrate on glass coated ferromagnetic microwires with GMI (giant magnetoimpedance effect). It is well known that Fe-based nanocrystalline materials can be fabricated by properly annealing amorphous precursor alloy: nano scale α-Fe grains are embedded in an amorphous matrix [4]. Both amorphous and nanocrystalline Fe-base ferromagnetic alloys have good soft magnetic properties. Fewer efforts have been put on amorphous alloys, especially on the high frequency electromagnetic properties.

In this paper, we have prepared the amorphous Fe-base metallic microwires by a melt extract method. Magnetic hysteresis loop measurements show the microwires exhibit strong shape anisotropy. The dependence of permeability on frequency has been explained based on the assumption that the observed dispersion is due to the spin rotation mechanism. The dispersion of permittivity can be interpreted as the results of multi Lorentzian dispersion processes which might due to the inhomogenous microstructure. Single layer absorber made of the as-prepared microwires exhibit good microwave absorption properties when its thickness is larger than 4 mm. However the absorption bandwidth is found narrow.

ACKNOWLEDGMENT

This work is financially supported by the National Basic Research Program of China (973) (No. 2010CB334702), China National Funds for Distinguished Young Scientists (No. 51025208), the Fundamental Research Funds for the Central Universities (No. ZYGX2009J036) and the Basic Research Funds of National Defense Department (No. 9140A10030409DZ0228).

REFERENCES

1. Han, M., D. F. Liang, and L. J. Deng, *J. Mater. Sci.*, Vol. 40, 5573, 2005.
2. Chiriac, H. and T. Ovari, *Progr. Mater. Soc.*, Vol. 40, 333, 1996.
3. Qin, F. X., H. X. Peng, N. Pankratov, M. H. Phan, L. V. Panina, M. Ipatov, V. Zhukova, A. Zhukov, and J. Gonzalez, *J. Appl. Phys.*, Vol. 108, 044510, 2010.
4. McHenry, M. E., M. A. Willard, and D. E. Laughlin, *Prog. Mater. Sci.*, Vol. 44, 291, 1999.

Dielectric Device for Broadband Extraordinary Transmission in a Waveguide Using Transformation Electromagnetics

D. Bao, W. Tang, K. Z. Rajab, and Y. Hao
Department of Electronic Engineering, Queen Mary, University of London
Mile End Road, London, E1 4NS, United Kingdom

Abstract— There have been intensive studies on different technologies for guiding electromagnetic waves through sub-wavelength apertures, channels or waveguides in recent times. The theory of transformation electromagnetics provides a novel way to obtain extraordinary transmission (ET) over a broad frequency band. According to this theory, a physical space may have the same electromagnetic properties as a virtual space to the external observers if there is a satisfied relation between the coordinates of the two spaces. The main scheme to enhance the transmission is to build a physical space containing a sub-wavelength aperture, and a virtual space containing a much larger aperture comparable to the wavelength. By engineering the background medium in the physical space, the two spaces have the same electromagnetic properties to the environment, which means, the transmitted energy to the outer space through the sub-wavelength aperture is similar to that through the large aperture. In this way, the transmission is increased dramatically. Discrete coordinate transformation is utilized to decide the electromagnetic properties (the permittivity and the permeability) of the background medium in the physical space. When the coordinates are quasi-orthogonal, the physical space is reduced to be a small device composed of a few isotropic dielectrics which possesses a broad band performance at the price of an acceptable reduction of the transmission. Finite-Difference Time-Domain (FDTD) simulations are used to verify the significantly increased transmission through an aperture sized $0.2\,\lambda_0$. The ET device is further experimentally demonstrated in an X band waveguide. It is fabricated using commercially available nonmagnetic materials, with the relative permeability equals to unity and the relative permittivities range from 2.1 to 6. This device is put in front of a copper plate with a sub-wavelength slit inside the waveguide and the transmission coefficient is measured. The results have proved that the device can provide transmission with the $-3\,\mathrm{dB}$ bandwidth over more than 1 GHz, in a region which would otherwise be a stop band due to the sub-wavelength aperture in the X-band waveguide.

Cylindrical Electromagnetic Field Concentrators with Incident-direction Dependent Concentrating Ratio

Wei Li, **Jianguo Guan**, **and Wei Wang**
State Key Lab of Advanced Technology for Materials Synthesis and Processing
Wuhan University of Technology, Wuhan 430070, China

Abstract— Based on the optical transformation, a circular cylindrical electromagnetic field concentrator whose energy concentrating rate varies with the incident angle of the electromagnetic wave is proposed. The design is achieved by compressing an ellipse region in the original space into a smaller circular region in physical space. Since the space is compressed with different ratio in different direction, finally incident-angle-dependent filed concentrator is achieved. Numerical simulations are performed to demonstrate the properties and the wave incident angle dependent concentrating effect of the concentrator. The relationship between the wave incident angle and the concentrating rate is investigated and a corresponding analytical expression is given and verified. This wave incident angle dependent concentrator is thought to be of practical applications since it provides a very convenient route to continuously controlling the energy density by simply rotating the device.

Electromagnetic Cloaking with Dielectric Metamaterials

Elena Semouchkina
Michigan Technological University, USA

Abstract— The recently introduced coordinate transformation method has provided the mathematical foundation for designing an electromagnetic "invisibility" cloak based on a prescribed spatial variation of the constitutive parameters within the cloak shell. Employment of a reduced set of material parameters for TE/TM incident waves in cylindrical cloak designs requires only one radial component of the permeability/permittivity tensor to vary radially in the range between 0 at the surface of the hidden object and 1 at the outer surface of the shell, i.e., in the range providing the values of the wave phase velocity in the shell exceeding those in free space the more, the closer to the object the wave passes. As the result, the waves passing around the object along extended routes get an opportunity to arrive to the observer with the same phase as the waves propagating in free space along straight paths, making the hidden object invisible for the observer. In the previously reported in literature designs, the desired dispersion of the effective material parameters in cylindrical shells was typically provided by special arrangement of metal resonators in concentric arrays, so that the designed metamaterial structures responded at the resonance by the formation of radially directed magnetic or electric moments responsible for radial components of either the effective permeability or permittivity tensors. The different size of resonators in each of the concentric arrays had to be carefully chosen to obtain resonances at different frequencies that increased from the outer array to the inner one.

Here we present the designs of cylindrical cloaks composed of identical dielectric resonators, in which the desired dispersion of the effective relative permeability was obtained due to the controlled decrease of the density of resonators from the inner layer of the cloak to the outer layer, i.e., due to radial dispersion of air fractions in the shell. In particular, an infrared cloak design comprised of nano-sized glass resonators is presented. The designed spoke-like structure of this cloak allowed for avoiding as the problem of fabricating differently sized resonators at nanoscale, so the problem of obtaining magnetic resonance response in metallic structures at optical frequencies. One important issue that had to be resolved at the designing of this cloak was interaction between elementary resonance fields spreading beyond the boundaries of the resonator bodies, although the chosen chalkogenide glass had the record value of the relative permittivity for the optical range (above 11). Therefore, it was necessary to control the dimensions of field "halos" at the choice of minimal distance between resonators, in order to avoid strong inter-resonator coupling, as the latter could significantly change the dispersion of the permeability. The design of a microwave cloak comprised of ceramic resonators is also described. It was found that despite of the higher permittivity of the ceramic materials of the resonators (above 30), the interactions between the resonators in the shell also played a crucial role in the cloak performance. The performances of both the infrared and microwave cloaks have been studied by using full-wave simulations of true multi-resonator structures in contrast to the models comprising material layers with prescribed parameters. The latter models, which are typically used for the analysis of metamaterial cloaks, cannot account for interactions between the building elements. This work also demonstrates that interaction between resonators and consequent splitting of the resonance modes in metamaterial opens up an opportunity to broaden the frequency band of the cloak operation.

Session 3A3
Advanced Methods for Polarimetric Information Extraction

Urban Impervious Surfaces Estimation from RADARSAT-2 Polarimetric Data Using SVM Method

Xinwu Li, **Huadong Guo**, **Zhongchang Sun**, **and Guozhuang Shen**
Center for Earth Observation and Digital Earth, Chinese Academy of Sciences, Beijing 100094, China

Abstract— The urban impervious surface is a key environmental indicator in assessing urbanization impacts on the urban environmental and ecological conditions, and it has therefore attracted more interest recently in the remote sensing community. The main objective of this investigation is to explore potential to extract impervious surface in the dense urban areas from RADARSAT-2 fully PolSAR data. To compare the results, the SPOT-5 multispectral imagery is also used. A case study in the dense urban (Beijing, China) is conducted for this purpose by applying the support vector machine (SVM) algorithm to SPOT-5 imagery and RADARSAT-2 full PolSAR data. An accuracy assessment is performed using the high-resolution WorldView images with a spatial resolution of 0.5 m. The root mean square error (RMSE), the mean absolute error (MAE), and the coefficient of determination (R2) are calculated to validate the accuracy of impervious surfaces derived from the SPOT-5 image and RADARSAT-2 PolSAR data. For the SPOT-5 imagery, the RMSE, MAE, and R2 are 16.41%, 12.43%, and 0.8386, respectively. The RADARSAT-2 full PolSAR data yields results with an RMSE of 13.27%, an MAE of 9.98%, and an R2 of 0.8421. The results indicate that the result derived from RADARSAT-2 data is superior to that of SPOT-5 in impervious surface estimation. The results also demonstrate that the bore soil or water can be easily separated from the buildings or asphalt roads using RADARSAT-2 data, which is a difficult task for estimating impervious surface with optical remote sensing data. In addition, compared with optical image, the impervious surfaces covered by tree crowns can be easily extracted from the RADARSAT-2 PolSAR data in sparse trees area. Overall, our results demonstrate that PolSAR image can provide more efficient and useful polarmetric information and has enormous potential for extracting the impervious surfaces.

New Method for the $\pi/4$ Compact Polarimetric SAR Mode

J. J. Yin[1], **J. Yang**[1], **and Y. Yamaguchi**[2]

[1]Department of Electronic Engineering, Tsinghua University, Beijing 100084, China
[2]Faculty of Engineering, Niigata University, Niigata 950-2181 Japan

Abstract— Compact polarimetric synthetic aperture radar (SAR) is a dual-polarimetric system, which shows promise of reducing the complexity, cost, mass, and data rate of a SAR system. It allows fully polarimetric information reconstructed from compact polarimetry (CP) under some constrains. Two assumptions are required here for the reconstructing, one is the reflection symmetry, and the other is a relationship model between the co-polarized and cross-polarized channels. In this paper, an improved reconstruction algorithm is proposed according to both the assumptions, and two improvements are proposed. Since the helix scattering component is always used to take account of the non-reflection symmetric circumstance which mostly appears in complex urban area, helix scattering should be considered in the reconstruction algorithm, especially for the regions with strong orientation angle effects. A modified four-component model-based decomposition algorithm is proposed with a new volume scattering model. Then using the decomposed powers of the four components, an average relationship between the co-pol and cross-pol channels is developed. By the proposed method, the helix scattering component which is omitted by the original method is also extracted. Finally, the E-SAR L-band data acquired over Oberfaffenhofen in Germany are used to demonstrate the effectiveness of the proposed algorithm, as shown in Figure 1.

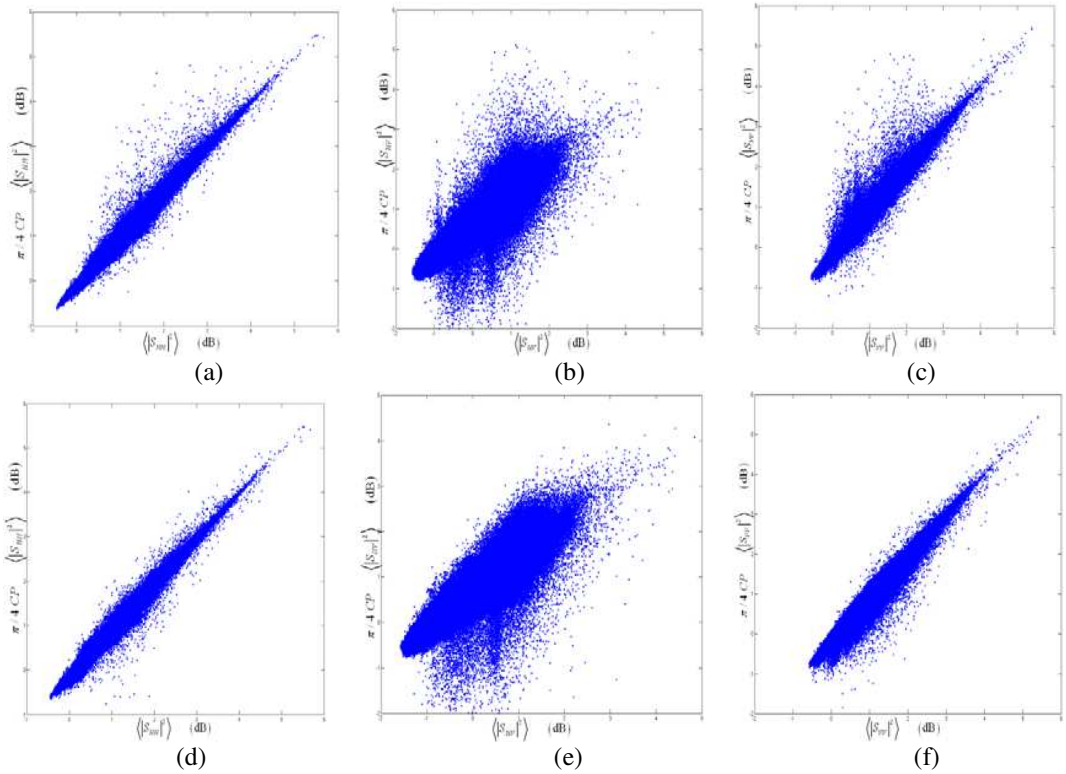

Figure 1: The reconstructed fully polarimetric data. On the abscissa are the original data; the ordinate indicates the reconstructed values. (a), (b), and (c) are the performance of the original FP reconstruction algorithm. (d), (e), and (f) are the performance of the proposed FP reconstruction algorithm. The scatter plots use all pixels of the Oberpfaffenhofen image.

Snow Line Detection for Glacial Areas with Polarimetric SAR Images

Zhen Li, **Lei Huang**, **Bangsen Tian**, **and Ping Zhang**
Center for Earth Observation and Digital Earth, Chinese Academy of Science
No. 9 Dengzhuang South Road, Haidian District, Beijing 100094, China

Abstract— Snow line in glacier area is sensitive indicators of climate fluctuations. The effects of climate warming are for instance evident in the continuous retreat of glaciers and decrease of snow area. In the paper, methods of snow classification, snow line identification for glacial area are presented with polarimetric SAR from RadarSat-2/SAR data in the Qinhai-Tibetan Plateau.

This study was performed around the Dongkemadi glacier, which lies in the eastern part of the Qinghai-Tibetan plateau. The altitude of the DD glacier ranges from 5275 to 6060 m, and on the XD glacier the altitude ranges from 5380 to 5926 m. The lengths of the DD glacier and the XD glacier are 5.4 km and 2.8 km, respectively. The warm season in the study area, when most of the yearly precipitation falls in the form of snow, spans from June to September every year. The C-band RADARSAT-2 full polarization SAR data in Aug. 30, 2009 is used in this study. We firstly generate a multi-look image with 2 looks in the azimuth direction and 1 look in the range direction, and performed the absolute calibration. Then, a refined Lee Sigma filter is used to suppress speckle noise, and then target decomposition is performed. Next, the SVMs and other classifiers are used for image classification. Following this procedure, a control points (CPs) based geo-rectification is performed on the classification map for land cover mapping. Finally, the snow lines of the major glaciers are extracted using the wet snow-ice boundary on the classification map, and the geo-rectified snow line map is produced. The results showed that the ice and the ground can be better separated in the $H/A/\bar{\alpha}$ decomposition feature space than in the backscattering coefficient feature space, and the combination of the $H/A/\bar{\alpha}$ decomposition and the support vector machines is an accurate and efficient method for polarimetric SAR image classification and snow line detection in glacial areas.

Metamodel-based Adaptive Use of a Coherent Polarimetric Backscattering Simulator for the Characterization of Forested Areas at Low Ffrequencies

A. Vasko[1, 4], **L. Thirion-Lefevre**[2], **S. Bilicz**[1, 4], **I. Champion**[3], **M. Lambert**[1], **and S. Gyimóthy**[4]

[1]L2S, UMR 8506, CNRS-SUPELEC, University Paris-Sud, France
[2]SONDRA/SUPELEC, France
[3]EPHYSE/INRA, France
[4]Budapest University of Technology and Economics, Hungary

Abstract— In the frame of forest observation, e.g., in the purpose of biomass retrieval, simple scattering models are used to perform inversion. For instance, the Random Volume over Ground (RVoG) model [1] derived from the work of Treuhaft et al. [2] is widely used to retrieve the mean height of the forest (see, e.g., [3] at X-band and [4] at P-band). However, the use of more complex scattering models (such as [5]) for inversion appears to be difficult due to several bottlenecks, such as the high number of descriptive parameters and the computational cost of the simulation.

In this paper, we propose the combined use of a coherent polarimetric backscattering simulator and some adaptive metamodeling tools to retrieve the mean forest height. In a first part, we present the metamodeling tools and the surrogate model derived from the coherent polarimetric backscattering simulator. In a second step, this surrogate model is applied to retrieve the forest height, considering a simple case for the forest description. The impact of the radar parameters (frequency, incidence angle, polarimetry) is investigated, namely to evaluate the accuracy we can expect on the retrieved quantity.

The metamodel imitates the true model at a much lower computational cost. Such tools are usually based on the sampling of the studied model: the numerical simulator is run at certain well-chosen input parameter combinations, then the metamodel consists in an interpolator, fitted to these samples. However, depending on the subsequent use of the metamodel, the choice of the samples must be adapted both to the modeled problem and the interpolation method in order to obtain a good performance of the metamodel. Beyond the approximation of the simulator, the metamodels can provide additional meta-information on the studied model. This knowledge might be represented by the repartition of the adaptively chosen samples within the domain of the feasible ones, or by the estimated uncertainty of the yielded interpolation. The available meta-information can be used to characterize the behaviour of the studied model to a certain extent, which might yield important conclusions on, e.g., the ill-posedness of the related inverse problem. The proposed metamodeling schemes have already been successfully used in electromagnetic non-destructive evaluation (see, e.g., [6, 7]), where the involved numerical simulators are also computationally demanding. Our main goal herein is to extend the use of these metamodeling techniques for the frame of forest characterization. In these adaptive metamodeling approaches, the kriging prediction plays an important role. Kriging was initially developed in geostatistics to model unknown spatial distributions based on some observations. By now, it has become a general tool of function approximation. The basic idea of kriging is to model the unknown function by a Gaussian random process, which is predicted as a linear combination of the available observations, via a stochastic framework. A considerable advantage of kriging over other techniques is the estimation of the prediction uncertainty, provided along with the prediction in a straightforward manner. In the metamodeling schemes, the use of kriging is twofold: the metamodel-building procedure can be accelerated via the interpolation of the involved auxiliary functions, or obviously, kriging can subsequently be fitted to the yielded samples to interpolate the observed data.

In this study, we consider the case of a French temperate managed forest whose structure and radar response have already been widely studied in [5] and [8], respectively. For the illustration of the ability of the metamodeling tools to perform inversion, we propose herein to focus on a simple description of the forest: only the dielectric trunks standing on a rough and dielectric surface are considered. This can be seen as a rough, but acceptable approximation at these frequencies. The permittivity of the trunks is derived using [?] and considering a constant gravimetric moisture around 54%. On the contrary, the permittivity of the ground is more sensitive to climatic conditions. Therefore, we consider a variation of the ground gravimetric moisture from 10% to 70%. The size of the trunks (diameter, height) are calculated using allometric equations [9] depending on the age of the forest. As a consequence, there are only four

input data for the metamodel: the age of the forest, the moisture of the ground, the frequency and the incidence angle. The output data are the full polarimetric backscattered fields. Considering a set of polarimetric backscattering coefficients obtained for a given radar configuration and derived from the backscattered fields, we address the inverse problem of determining the forest age and the ground moisture. The effect of the number of polarimetric channels and the radar parameters (frequency, incidence angle) on the performance of the inversion is investigated in particular.

REFERENCES

1. Cloude, S. R. and K. P. Papathanassiou, "Three-stage inversion process for polarimetric SAR interferometry," *Proc. Inst. Elect. Eng. Radar, Sonar Navig.*, Vol. 150, 125–134, 2003.
2. Treuhaft, R. N., S. Madsen, M. Moghaddam and J. J. van Zyl,, "Vegetation characteristics and underlying topography from interferometric data," *Radio Sci.*, Vol. 31, 1449–1485, 1996.
3. Garestier, F., P. Dubois-Fernandez, and K. P. Papathanassiou, "Pine forest height inversion using single-pass X-band Pol-InSAR data," *IEEE Trans. Geosci. Remote Sens.*, Vol. 46, 59–68, 2008.
4. Garestier, F., P. Dubois-Fernandez, and I. Champion, "Forest height inversion using high-resolution P-band Pol-InSAR data," *IEEE Trans. Geosci. Remote Sens.*, Vol. 46, 3544–3559, 2008.
5. Thirion, L., E. Colin, and C. Dahon, "Capabilities of a forest coherent scattering model applied to radiometry, interferometry and polarimetry at P- and L-bands," *IEEE Trans. Geosci. Remote Sens.*, Vol. 44, 849–862, 2006.
6. Bilicz, S., E. Vazquez, M. Lambert, S. Gyimóthy, and J. Pavo, "Characterization of a 3D defect using the Expected Improvement algorithm," *COMPEL*, Vol. 28, 851–864, 2009.
7. Bilicz, S., M. Lambert, and S. Gyimóthy, "Kriging-based generation of optimal databases as forward and inverse surrogate models," *Inverse Problems*, Vol. 26, 074012, 2010.
8. Sartore, M., et al., "Tree architecture in remote sensing analytical models: The Bray experiment," *International Journal of Remote Sensing*, Vol. 22, 1827–1843, 2001.
9. Saleh, K., et al., "A forest geometric description of a Maritime pine forest suitable for discrete microwave models," *IEEE Trans. Geosci. Remote Sens.*, Vol. 43, 2024–2035, 2005.
10. Hallikainen, M., et al., "Microwave dielectric behavior of wet soil. Part I: Empirical models and experimental observations," *IEEE Trans. Geosci. Remote Sens.*, Vol. GE-23, 25–34, 1985.
11. Peplinski, N. R., F. T. Ulaby, and M. C. Dobson, "Dielectric properties of soils in the 0.3–1.3 GHz range," *IEEE Trans. Geosci. Remote Sens.*, Vol. 33, 803–807, 1995.
12. Peplinski, N. R., F. T. Ulaby, and M. C. Dobson, "Corrections to dielectric properties of soils in the 0.3–1.3 GHz range," *IEEE Trans. Geosci. Remote Sens.*, Vol. 33, 1340, 1995.

Ship Detection Using Polarimetric Radarsat2

R. Touzi
Canada Centre for Remote Sensing, Natural Resources Canada
588 Booth St., Ottawa, Ontario, K1A 0Y7, Canada

Abstract— The added value of polarimetric SAR information was demonstrated for enhanced ship detection [1] and ship recognition [2] using C-band Convair-580 SAR [3]. The Touzi anisotropy was introduced in [1] for the optimum extraction of the polarimetric information to maximize ship-sea contrast. It was shown that fully polarimetric information permits a significant improvement of ship–sea contrast, in comparison with conventional (i.e., scalar) single-channel polarizations (i.e., HH, VV, or HV, at operational satellite synthetic aperture radar (SAR) incidence angles (20° –50°).

Three year ago, Radarsat2 (RS2) has been launched with operational polarimetric capabilities 9 m resolution at multiple incidence angles between (20°–50°). In this study, the Touzi anisotropy will be assessed for enhanced ship detection using Radarsat2 data collected over Gibraltar. AIIS data collected during the RS2 acquisitions will be used for ship identification. On the other hand, a new roll invariant scattering decomposition (ICTD), the Touzi decomposition, was introduced in [4, 5]. In contrast to the Cloude-Pottier's (ICTD) [6], which has been the most used method for target scattering classification, our ICTD characterizes uniquely the scattering type with three parameters; the symmetric scattering type magnitude α_s and phase $\phi_{\alpha s}$ and the target helicity [4]. The Touzi ICTD will be used to assess the potential of RS2 for ship detection. Comparison with the wave polarization anisotropy will be completed in term of ship-sea contrasts, for various RS2 illumination angles.

REFERENCES

1. Touzi, R., F. Charbonneau, R. K. Hawkins, and P. W. Vachon, "Ship detection and characterization using polarimetric SAR," *Canadian Journal of Remote Sensing*, Special issue on RADARSAT-2, Jun. 2004.
2. Touzi, R., R. K. Raney, and F. Charbonneau, "On the use of permanent symmetric scatterers for ship characterization," *IEEE TGRS*, Vol. 42, No. 10, 2039–2045, Oct. 2004.
3. Touzi, R., W. Boerner, J. S. Lee, and E. Luneberg, "A review of polarimetry in the context of synthetic aperture radar: Concepts and information extraction," *Canadian Journal of Remote Sensing*, Special issue on RADARSAT-2, 380–407, Jun. 2004.
4. Touzi, R., "Target scattering decomposition in terms of roll-invariant target parameters," *IEEE TGRS*, Vol. 45, No. 1, Jan. 2007.
5. Touzi, R., A. Deschamps, and G. Rother, "Phase of target scattering for wetland characterization using polarimetric C-band SAR," *IEEE TGRS*, Vol. 47, No. 9, 3241–3261, Sep. 2009.
6. Cloude, R. and E. Pottier, "A review of target decomposition theorems in radar polarimetry," *IEEE Trans. Geoscience Rem. Sens.*, Vol. 34, No. 2, 498–518, Mar. 1996.

Current Perspectives of Radar Polarimetry with Applications to Multiparameter POLSAR Remote Sensing of Earth, Ocean and Atmosphere

Wolfgang-Martin Boerner
University of Illinois at Chicago, 1021 Cedar Lane, Northbrook, IL, USA

Abstract— With the un-abating global population increase our natural resources are stressed as never before, and the global day/night monitoring of the terrestrial covers from the mesosphere to the litho-sphere becomes all the more urgent. Microwave radar sensors are ideally suited for space imaging because those are almost weather independent, and microwaves propagate through the atmosphere with little deteriorating effects due to clouds, storms, rain, fog aerosol and haze. Globally humidity, haze and aerosols next to cloudiness are increasing at a rather rapid pace, whereas only 20 years ago all of those covered 48% of the globe, today those have increased to about 62% and within another 20 years may exceed 80% for irreversible reasons. Thus, optical remote sensing from space especially in the tropical and sub-tropical vegetated belts is already and will become ever more ineffective, and microwave remote sensing technology must now be advanced strongly and most rapidly hand in hand with digital communications technology because operationally it is more rapidly available especially for disaster mitigation assistance.

The basic radar technologies to do the job at day and night are the multimodal Synthetic Aperture Radar (SAR) sensors, first developed for air-borne sensing implemented as for example in 1978 with the first space-borne digital Sea-Sat L-Band SAR which had severe limitations in that it was of fixed wide swath-width at a single arbitrary polarization (HH) and of rather poor 25 m resolution. In the meantime, fully polarimetric multi-modal high resolution SAR systems at multiple frequencies and incidence angles were introduced first with the multi-band AIRSAR of NASA-JPL culminating in the once-only pair of SIR-C/X-SAR shuttle missions of 1994 April and October, which laid the ground work for true day/night space remote sensing of the terrestrial barren and vegetated land and ocean covers using multi-band polarimetric SAR. Thereafter, the Canadian CCRS, the German DLR and the Japanese NASDA & CRL {now JAXA & NICT} took over introducing and steadily advancing the Convair-580, the E-SAR (now F-SAR) and Pi-SAR airborne highly advanced fully polarimetric sensors platforms, respectively.

These separate international multi-modal fully polarimetric and also interferometric airborne SAR developmental efforts culminated in a well coordinated group effort of three independent teams eventually launching and operating Fully Polarimetric Satellite SAR Sensors at L-Band (ALOS-PALSAR launched by JAXA/Japan in 2006 January — and to be followed by ALOS-PALSAR-2&3); at C-Band (RADARSAT-2 launched by CSA-MDA in 2007 December — to be followed by independent RADARSAT-3&4) and at X-Band (TerraSAR-X launched by DLR-Astrium in 2007 July with the follow-on tandem mission TanDEM-X launched in June 2010) . Thus, international collaboration on advancing day & night global monitoring of the terrestrial covers was demonstrated with the launch of the three fully polarimetric multi-modal SAR Satellites at L-, C-, X-Band and its first tandem satellite-pair update of the DLR TanDEM-X. Recently NASA-JPL is joining these global efforts again, and all of these efforts will be topped by the near-future joint DLR-JPL DESDynI/Tandem-L wide-swath, high-resolution fully polarimetric sensor implementation.

Polarimetric Signature and the Temporal Variation Analysis for Deforestation Mapping in Southwest China

Fengli Zhang[1], **Maosong Xu**[2], **Chou Xie**[1], **Zhongsheng Xia**[3], **Kun Li**[1], **Aimin Cai**[1], **Yun Shao**[1], **Xuejun Wang**[2], **and Ridha Touzi**[4]

[1]State Key Laboratory of Remote Sensing Science, Institute of Remote Sensing Applications Chinese Academy of Sciences, #3 Datun Road, Chaoyang District, Beijing 100101, China
[2]Academy of Forestry Inventory, Planning and Designing, State Forestry Administration (SFA) Beijing 100714, China
[3]Forest Resource Management and Conservation Station, Guizhou 550001, China
[4]Canada Centre for Remote Sensing, 588 Booth Street Ottawa, Ontario, K1A0Y7, Canada

Abstract— In the southwest of China, Synthetic aperture radar (SAR) has been gradually adopted for forestry inventory because the cloudy and rainy weather in this area has hindered the optical remote sensing too much. In early 2008, a severe snow swept south China with long lasting cold and frozen weather, not happened for last 50 years, which caused great damage on forest ecosystem in 18 provinces. Polarimetric SAR data contains more information of targets and has been expected more helpful for forest mapping. In this paper, polarimetric response and its temporal variation of deforestation areas caused by snow storm was analyzed using six temporal polarimetric RADARSAT-2 data and taking Zhazuo area in Guizhou Province as the study area, and method for deforestation mapping method based on polarimetric SAR data was studied.

Backscattering coefficient of normal forest and deforestation areas damaged by snow storm was first calculated, and then the temporal variation of backscattering coefficient was analyzed using the six temporal RADARSAT-2 images. And expeirments showed that backscattering coefficient of forest damaged by snow storm was significantly lower than that of forest not damaged.

Characteristics of polarimetric signature is helpful to analyze backscattering mechanism of targets. In this paper, polarimetric workstation (PWS) was adopted to analyze the polarization response of normal forest and deforestation areas damaged by snow storm. Using PWS, Cloude's parameters, entropy (H), anisotropy (A), α and β for normal forest and deforestation areas caused by snow storm were derived, and the temporal variation of polarimetric response for normal forest and deforestation areas damaged by snow storm was analyzed with the six polarimetric RADARSAT-2 images. And experiments show that α value of forest damaged by snow storm is generally higher than that of normal forest.

And polarimetric decomposition experiments showed that Freeman decomposition was more suitable for discrimination of deforestation areas. For the Freeman decomposition results, surface scattering of forest damaged by snow storm is higher than that of normal forest. So surface scattering component of Freeman decomposition is useful for identifying deforestation areas caused by snow storm.

Rice Monitoring Using Touzi Decomposition Based on Polarimetric SAR Data in Southwestern China

Kun Li[1], **Yun Shao**[1], **Ridha Touzi**[2], **Brian Brisco**[2], **and Fengli Zhang**[1]

[1]Institute of Remote Sensing Applications, Chinese Academy of Sciences (IRSA, CAS), China
[2]Canada Centre of Remote Sensing (CCRS), Canada

Abstract— Rice is one of the three largest food grains in the world, which provides food for more than one third of globe population. China is the largest rice producer with rough production of 193 million tons annually. Guizhou province is an important rice growing area in the southwest of China. However, due to its perennial cloud-coverage weather and undulating terrain, rice monitoring by remote sensing has great difficulties in this region. Synthetic Aperture Radar (SAR) has been proved to be a significant data source in rice monitoring. With the emergence of full polarimetric SAR data and advanced methods for information extraction, monitoring rice in this region has more possibility.

In this study, the objective is to assess the ability of polarization decomposition, a new kind of advanced method for polarimetric information extraction, in rice monitoring and derive a method for rice monitoring. Zhazuo, in the middle of Guizhou province, was selected as the test site. And four temporal Fine Quad-polarization (FQ) mode RADARSAT-2 data in this area was acquired in 2009, corresponding to the beginning of heading stage, milky stage, maturity stage and harvest of rice. Based on the four polarimetric SAR data, Touzi decomposition and Cloude-Pottier decomposition were conducted using Polarimetric Workstation (PWS). All the SAR parameters derived above were converted from slant to ground range, followed by an orthorectification. Then based on the ground data, rice fields were located on the images. And various SAR parameters of rice were extracted.

The preliminary results show that Touzi decomposition is more sensitive to rice and its growth than Cloude-Pottier decomposition, especially Touzi dominant scattering type magnitude, which is much more sensitive to rice than Cloude Alpha angle. Some other parameters of Touzi decomposition, such as dominant scattering type phase, medium scattering type helicity and orientation angle are also sensitive to rice information. As to Cloude-Pottier decomposition, only parameter Beta is sensitive to rice. In addition, Touzi parameters are very sensitive to the change of rice. Dominant scattering type magnitude and phase decreased gradually with the growth of rice, showing good regularity. Medium scattering type helicity and orientation angle are the most sensitive parameters to rice growth, however, their variations are not so stable. We need further more ground data to validate their variation.

Next we will quantitatively assess the accuracy of rice information extraction by Touzi decomposition. And we will focus on the physical meaning of Touzi parameters, combined the rice growth conditions, to find the reason why these parameters are much more sensitive to rice and its change.

Polarimetric Radar Response of Snow Covered Area Observed by ALOS PALSAR

Sang-Eun Park[1], **Y. Yamaguchi**[2], **and G. Singh**[1]

[1]Graduate School of Science and Technology, Niigata University
8050 Ikarashi 2-no-cho, Nishi-ku, Niigata 950-2181, Japan
[2]Department of Information Engineering, Niigata University
8050 Ikarashi 2-no-cho, Nishi-ku, Niigata 950-2181, Japan

Abstract— Terrestrial snow is a sensitive indicator of climate change, a significant storage component of the global water cycle, and affects weather and climate through several surface energy and mass exchange mechanisms. Microwave remote sensing has a great potential to detect parameter related to snow properties. Most previous studies have been carried out on the basis of the use of C-band or higher frequencies due to their higher sensitivity to snow properties. Because of the dynamic and diverse snow processes, however, integrated observation of snow-covered areas from multi-sourced data sets is essential for mapping and monitoring snow hydrology. This study discusses the capability assessment of L-band space-borne Synthetic Aperture Radar (SAR) for detection of seasonal snow covered areas. Particularly, the utilization of the fully polarimetric scattering observation can possibly offers an efficient and reliable means of collecting quantitative information on the seasonal changes of snow-cover. In this study, polarimetric ALOS PALSAR time-series data sets in the Niigata Prefecture, Japan have been investigated to evaluate the fully polarimetric signal scattered from snow-covered mountainous ecosystem. Results show that it is difficult to distinguish signal from snow-covered and snow-free forest using the single polarization measurement. But, changes in scattering mechanism across the various snow states can be identified from polarimetric indicators, such as the eigenvalue/eigenvector parameter sets, the optimization of polarization contrast enhancement, the surface to volume scattering contribution of the model-based scattering power decomposition. Experiment results illustrate how fully polarimetric SAR remote sensing can be a promising approach in monitoring, without a priori information, the spatio-temporal evolution of snow covered areas and their conditions such as the snow water equivalent.

Polarimetric L-band Palsar for Peatland Characterization

R. Touzi[1], **G. Gosselin**[1], **and R. Brook**[2]

[1]Canada Centre for Remote Sensing, Natural Resources Canada
588 Booth St., Ottawa, Ontario, K1A 0Y7, Canada
[2]Department of Ecosystem and Public Health, University of Calgary
3330 Hospital Drive NW Calgary, Alberta, T2N 4N1, Canada

Abstract— Canada has 25% of the world's wetlands and wetland management has become a critical issue in order to avoid or mitigate further loss of wetland area or function. Peatlands represent an important wetland class very sensitive to climate change. While it is well established that fens change naturally into bogs over time and that bogs can revert to fens, the observations over the last fifty years indicate that the rate of these changes has been significantly altered by climate change, isostatic uplift, fire, and goose grazing. This has been noted in the Hudson Bay Lowlands, which contains the most extensive wetlands and thickest peat deposits in Canada [1–3]. The region is home to unique concentrations of wildlife, most notably polar bears, caribou, and migratory birds. Bears rely on inland denning habitat, caribou are tied to peatland vegetation, and birds intensively graze coastal herbaceous salt marsh and fen. The loss of bogs will have important implications for polar bear denning habitat which is entirely within bogs with thick peat deposits [1–3]. Earth observation satellite and in particular all weather L-band polarimetric ALOS, should provide the required information for monitoring the impact of climate change on the integrity of peatlands in the Northern of Canada.

Two peatlands sites are considered in our investigation; Lac St Pierre (North of Montréal) and the Wapusk National Park in the Hudson Bay Lowlands of Manitoba. Two polarimetric ALOS acquisitions took place on Lac St Pierre at spring and fall seasons (May and Nov. 2007), during the calibration phase. Unfortunately, we were not lucky with the Wapusk site, and only acquisitions achieved at saturated water conditions are available because of the limitation of polarimetric window acquisitions.

In this study, the Touzi decomposition [4], which has been recently introduced for a unique and roll-invariant characterization of target scattering, is investigated for peatland characterization. In contrast to the Cloude-Pottier [5] decomposition, which uses a real entity to describe target scattering type, the Touzi decomposition characterizes uniquely the scattering type with a complex entity, whose both magnitude and phase have been shown very promising for wetland class characterization [6, 7]. In particular, the new target scattering phase has been shown to be very promising for separation of nutrient poor fens from bogs.

The results obtained with L-band PALSAR on Lac St Pierre confirm the excellent performance of the Touzi scattering phase. for detection of underneath peat water flow. While the scattering phase could detect the peat beneath water level change, the polarization radiometric scattering

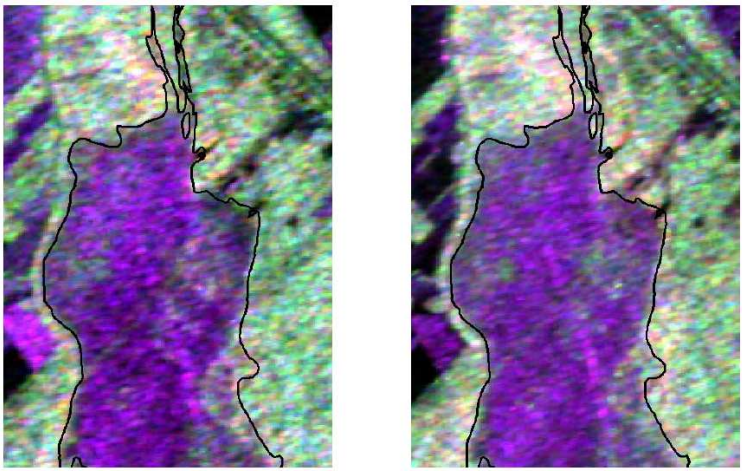

May 07 Nov. 07

Figure 1: HH-HV-VV.

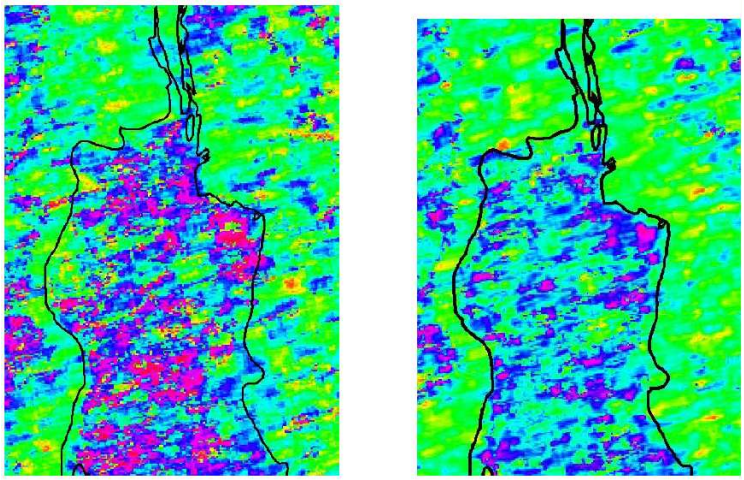

Figure 2: Touzi-phase.

information (provided by the Cloude α, the entropy H, and the multi-polarization (HH, HV, and VV)) is insensitive to the presence of underneath peat water, as seen in Figures 1–4. The Touzi phase can detect the presence of water flow beneath peat surface in bogs of thin peat (up to 1.4 m). However, the phase looks to be less sensitive to deep water in thick bogs (more than 2.8 m). As such, the phase looks very promising for providing information related to the peat thickness, and we would expect that this parameter should play a key role in monitoring the bog-fen transformation process related to climate change stress.

Unfortunately, the results above could not be confirmed with the Wapusk data sets collected under water and ice saturated conditions (June 2007). The phase is no more efficient under saturated water conditions, and only the polarization radiometric scattering information can be exploited. Like HV, the polarimetric scattering type permits detecting of the presence of water in swamps or treed bogs, but no useful information can be retrieved related to the presence of water underneath the peat. We would expect much better results with acquisitions that would be completed during summer dry conditions. We wish that JAXA will allow us to have a series of 45 days polarimetric acquistions collected between June and September.

Dark blue correspond to thick peat, whereas pink colour indicates shallower bog beneath water. No underneath water flow change is detected with HH-HV-VV.

REFERENCES

1. Brook, R. K. and N. C. Kenkel, "A multivariate approach to vegetation mapping of Manitoba's Hudson Bay Lowlands," *International Journal of Remote Sensing*, Vol. 23, 4761–4776, 2002.
2. Brook, R. K., "Forest and tundra fires in the Hudson Bay Lowlands of Manitoba," *Climate Change: Linking Traditional and Scientific Knowledge*, eds. R. Riewe & J. Oakes, Aboriginal Issues Press, Winnipeg, Manitoba, Canada, 2006.
3. Jano, A. P., R. L. Jefferies, and R. Rockwell, "The detection of vegetational change by multitemporal analysis of LANDSAT data: The effects of goose foraging," *Journal of Ecology*, Vol. 86, No. 1, 93–99, Feb. 1998.
4. Touzi, R., "Target scattering decomposition in terms of roll-invariant target parameters," *Proc. IEEE TGRS*, Vol. 45, No. 1, Jan. 2007.
5. Cloude, R. and E. Pottier, "A review of target decomposition theorems in radar polarimetry," *IEEE Trans. Geoscience Rem. Sens.*, Vol. 34, No. 2, 498–518, Mar. 1996.
6. Touzi, R., A. Deschamps, and G. Rother, "Wetalnd characterization using polarimetric Radarsat-2 capability," *Can. J. Rem. Sens.*, Vol. 33, No. 1, S56–S67, 2007.
7. Touzi, R., A. Deschamps, and G. Rother, "Phase of target scattering for wetland characterization using polarimetric C-band SAR," *IEEE TGRS*, Vol. 47, No. 9, 3241–3261, Sep. 2009.

Session 3A4
Antennas and Array Design and Simulation Techniques 2

Dual-band Circularly Polarized CPW-fed Circular Slot Antenna with Two Opened-ground Rings for GPS and WLAN Applications

Sheau-Shong Bor[1], **Chia-Yen Wei**[2], **Tian-Fu Hung**[2], **Ji-Chyun Liu**[3], **and Hai-Tao Sun**[1]

[1]Department of Electrical Engineering, Feng-Chia University, Taichung, Taiwan, R.O.C.
[2]Program in Electrical and Communications Engineering, Feng-Chia University, Taichung, Taiwan, R.O.C.
[3]Department of Electrical Engineering, Ching Yun University, Chung-Li, Tao-yuan, Taiwan, R.O.C.

Abstract— This paper presents a novel dual-band circularly polarized CPW-fed annular slot antenna embedded with two open-ground rings. The proposed antenna particularly features those two opened-ground rings facing in opposite directions around the annular slot and the CPW acting as the signal strip. The prototype is implemented on to a 0.8 mm-thick FR4 substrate with $\varepsilon_r = 4.4$. By way of adjusting the relevant parameters, we can obtain the dual band of frequencies at 1.57 GHz and 2.45 GHz individually. The ratio of 2.45 to 1.57 with frequencies is 1.56. Referring to the optimized antenna prototype, the measured 10 dB return loss impedance bandwidth are 19.68% for the 1.57 GHz lower band (RHCP) and 8.75% for the 2.45 GHz upper band (LHCP). The measured 3 dB axial-tobandwidth ratio for 1.57 GHz and 2.45 GHz frequency bands are 30.3% and 8.73%, and the antenna gain are 3.8 and 2.2 dBic respectively.

Compact Dual-band Monopole Antenna for WLAN/WiMAX Applications

Chia-Hao Ku[1], **Hsien-Wen Liu**[2], **Di-Yu Lin**[1], **and Yao-Xin Ding**[1]

[1]Department of Electrical Engineering, Ming Chi University of Technology, Taipei, Taiwan, R.O.C.
[2]Technological Research Center, Auden Techno Corp., Taoyuan, Taiwan, R.O.C.

Abstract— A novel, compact dual-band monopole antenna for WLAN and WiMAX applications is proposed in this paper. This antenna with a key-like slot is fabricated using a 0.8 mm-thick FR4 substrate, which only occupies a small area of $8\,(L) \times 8\,(W)\,\mathrm{mm}^2$ to be easily embedded inside a portable device as an internal antenna. By properly designing the key-like slot etched on the radiator, two operating frequency bands covering 2.39–2.51 GHz and 4.57–5.99 GHz can be achieved with our antenna. The resonant properties of the antenna are also tunable while various lengths and widths of the slot are adopted. Nearly omnidirectional coverage with stable receiving performance for actual applications can be obtained due to the antenna. Simulated and measured results are performed and analyzed. With a compact size, the proposed monopole antenna may well work as an internal antenna in a portable device for WLAN/WiMAX operations.

Synthesizing a High Gain Planar Array Antenna for Volume Scanning Arrays

Fikret Tokan and Filiz Güneş
Department of Electronics and Communication Engineering, Faculty of Electrics and Electronics
Yıldız Technical University, Yıldız 34349, Istanbul, Turkey

Abstract— The goal of this work is to describe a simple method of synthesizing a rectangular planar array antenna which has a flat top characteristic within the given $0° \leq \theta \leq 60°$ region in the $\phi = 0°$ principal plane to be used in volume scanning radars. In case that the radiation pattern distribution is given in the visible region, in literature, the analytical methods such as Fourier transformation [1], Woodward-Lawson [2, 3] or Dolph-Chebyshev [4] are extensively employed in the synthesis process. In our work, the overall far field pattern is built up with the individual participation of each ingredient linear array antenna. The requirements of the individual synthesis of the ingredient linear array is to collimate its main beam to the predetermined direction with a permissible beamwidth within the coverage region so that superposition of the far field ingredients can result in the overall pattern shaped with the flat top characteristic within the $0° \leq \theta \leq 60°$ region in the principal plane. In the individual synthesis process of a linear array antenna, the Dolph-Chebyshev analytical method is employed, which is a well-known robust method for a narrow main-beam and low sidelobe level (SLL) array antenna synthesis.

Thus, N linear array antennas are resulted with the low SLL radiation patterns collimated to the pre-determined directions such that when their far field radiation phasors are superpositioned, a rectangular planar array antenna is built up having a flat top main beam characteristic covered the specified region. If desired, the overall main beam characteristics can be made better by an optimization process applied to the individual excitation coefficients. In fact, we employed the genetic algorithm for this purpose. Furthermore, we applied this method to synthesize a planar half-wave dipole antenna array as given in Fig. 1, verified with the full-wave simulator of CST (Computer Simulation Technology).

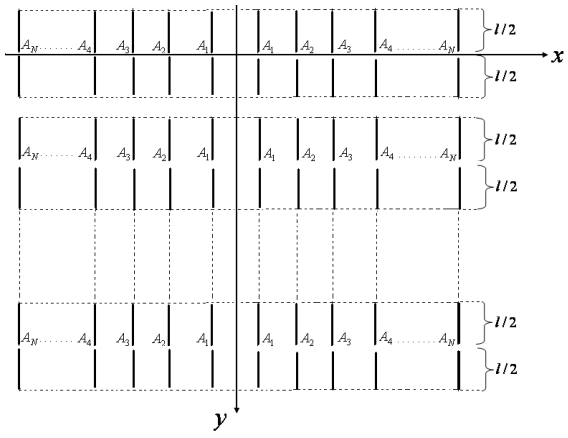

Figure 1: A rectangular planar half-wave dipole antenna array.

REFERENCES

1. Booker, H. G and P. C. Clemmow, "The concept of an angular spectrum of plane waves, and its relation to that of polar diagram and aperture distribution," *Proc. IEE*, Paper No. 992, Vol. 97, 11–17, Radio Section, London, 1952.
2. Woodward, P. M., "A method for calculating the field over a plane aperture required to produce a given polar diagram," *J. IEE*, Vol. 93, 1554–1558, 1946.
3. Woodward, P. M. and J. D. Lawson, "The theoretical precision with which an arbitrary radiation pattern may be obtained from a source of finite size," *J. IEE*, Vol. 95, 363–370, 1948.
4. Dolph, C. L., "A current distribution for broadside arrays which optimizes the relationship between beamwidth and sidelobe level," *Proc. IRE*, Vol. 34, 335–345, 1946.

Analysis of Microstrip Antennas by Knowledge-based Support Vector Machines

Nurhan Türker Tokan[1], **Filiz Güneş**[1], **Ali Kuş**[2], **and Fikret Tokan**[1]

[1]Electrical and Electronics Engineering Faculty
Department of Electronics and Communication Engineering
Yıldız Technical University, Istanbul 34349, Turkey
[2]Ericsson TURKEY, Büyükdere St., USO Center No. 61, Maslak 34398, Istanbul, Turkey

Abstract— Nowadays, two typical nonlinear learning machines are widely employed as the fast and flexible machines in the generalization of the highly nonlinear input-output discrete mapping relations in the microwave and antenna modeling: Artificial Neural-Network (ANN) and Support Vector Machine (SVM). Both of these nonlinear learning machines are as fast as the approximate models and can be as accurate as the detailed EM/physics models thus making learning machine-based CAD an efficient alternative. However, accuracy of these learning machines largely depends upon the accuracy of the training data which may be measured or simulated data. Accurate training data generation is expensive as it involves both CPU time (for detailed model computations) and human time (for repetitive calls for changes in the input parameter-domain), and can slow down the model development. There is a recent trend in the Electromagnetic (EM)-ANN area for investigating techniques that could potentially lower model development time by reduced use of accurate training data and lessened human involvement.

In this paper, knowledge-based support vector machines proposed by [1] is used for the analysis of microstrip antennas. Coarse data is obtained by using the analytical formulation of the microstrip antennas. Support vectors obtained by using coarse support vector regression machine (SVRM) is mapped to the fine model by an electromagnetic simulator and the fine data obtained is used in the training of SVRM. Thus, analysis model as fast as the coarse models and at the same time as accurate as the fine models is obtained for the microstrip antennas. The proposed knowledge-based support vector method is demonstrated by a typical worked example of microstrip antenna. Success of the method and performance of the resulted analysis model is presented and compared with ANN results.

REFERENCES

1. Güneş, F., N. T. Tokan, and F. Gürgen, "A knowledge-based support vector synthesis of the transmission lines for use in microwave integrated circuits," *Expert Systems with Applications*, Vol. 37, s.3302–3309, Nisan, 2010.

Design and Construction of UWB Antennas

J. Sosa-Pedroza, **E. Garduño-Nolasco**, **F. Martinez-Zúñiga**, **and M. Enciso**
Instituto Politécnico Nacional, SEPI-ESIME-Zacatenco, Edif. Z-4 3er Piso, CP 07738, México

Abstract— We present results of design of two Ultra Wide Band (UWB) quasi circular patch antenna one with CPW and the other with microstrip feeding. Both antennas are an evolution from a circular patch structure softening the edges to obtain improvements in the antenna parameters, agreeing with the theory proposed by John Kraus. After evolution there were improvements in reflection coefficient and number of resonant frequencies throughout the operating bandwidth. The operational frequency range is from 500 MHz to 15 GHz using a design frequency of 4.5 GHz. The antenna feeding impedance is proposed to be 50 ohms. There were constructed antennas with the best simulation response to test the practical performance of experiment.

The technique to increase the bandwidth of circular antenna was proposed by Kraus in 1988, smoothing the transition between feed line and the antenna; this technique is easily applied to patch antennas with microstrip or coplanar feeding; radiator patch and ground plane can provide an almost constant input impedance over wide bandwidths.

Recently some techniques have been developed to improve BW of circular planar antenna, as introducing a slot into the circular patch, adding new resonant frequencies. We propose in this paper a smooth transition between the circular planar antenna and its microstrip feeding, as was originally established by Kraus in his theoretical volcano smoke antenna.

Radiating elements patches of printed antennas have a variety of forms, as triangular, rectangular, square, elliptical, circular, among others. However, it has been found that circular structures have smaller dimensions related with the operation frequency. Moreover, the circular structure offers another important advantage: the only control variable for the structure design is the patch radius, that is the reason circular or disk antennas are very popular and widely used nowadays. We start with the design of a circular patch antenna working in a frequency of 4.5 GHz.

Antennas for Compact Communication Systems

Dau-Chyrh Chang[1], **Hsiao-Bin Liang**[2], **and Cheng-Wei Chen**[1]

[1]Oriental Institute of Technology, Taiwan
[2]Climax Technology Co., Ltd, Taiwan

Abstract— The most problems of nowadays compact communication systems are not only for the higher total radiation power (TRP), but also for the higher total isotropic sensitivity (TIS). The TIS of communication systems will be decreased by the electromagnetic interference (EMI) from other active parts of print circuit board (PCB). The smaller the size of compact communication system is, the serious problem of EMI will be happened at receiver. Due to the EMI problem, the sensitivity of communication system will be decreased. In this paper, various kinds of small antennas are designed and developed for the compact size of communication systems. The antenna design should consider the compact size of communication system. The simulation tool for designing the antenna inside the compact size of communication system is by using commercial available General Electromagnetic Simulation (GEMS). The improvement results of TRP and TIS for various kinds of communication system will be present at the full paper.

A Dual Band Fractal Circular Microstrip Patch Antenna for C-band Applications

Nitasha Bisht and Pradeep Kumar
Department of Electronics and Communication Engineering
Jaypee University of Information Technology, Solan, HP-173215, India

Abstract— This paper proposes the design of a circular patch antenna with fractals for C-band applications. The fractal antenna has been designed on the substrate with dielectric constant of 2.3 and thickness of 1.935 mm.The designed antenna has been fed with coaxial L probe feeding technique. The proposed circular patch antenna with fractals produces a dual band operation for in the C-band frequency range. The designed model is simulated using CST microwave studio software based upon finite difference time domain method. The simulated results for various parameters like return loss, radiation pattern etc have been presented. Such type of antennas is useful in satellite communication, radar, commercial and military application.

Rectangular Microstrip Patch Antenna with Photonic Band Gap Crystal for 60 GHz Communications

R. N. Tiwari[1], **P. Kumar**[2], **and Nitasha Bisht**[2]

[1]School of Engineering and Technology, Bahra University, India
[2]Department of Electronics and Communication Engineering
Jaypee University of Information Technology, India

Abstract— In this paper, the design of rectangular microstrip antenna with 2-D photonic band gap crystal as substrate (dielectric substrate with regular cylindrical periodic air-gap) for 60 GHz applications, has presented. The photonic band gap structure is used to enhance the radiation efficiency and the bandwidth of the antenna. The periodic structures designed to open up frequency bands within which the propagation of electromagnetic waves is forbidden irrespective of the propagation direction. The design is optimized using the Finite Difference Time Domain (FDTD) based CST microwave studio simulator. The designed periodic air-gap rectangular microstrip patch antenna gives a bandwidth up to 20.53% for 60 GHz applications. Various parameters like directivity of the antenna, efficiency of the antenna etc. are also shown.

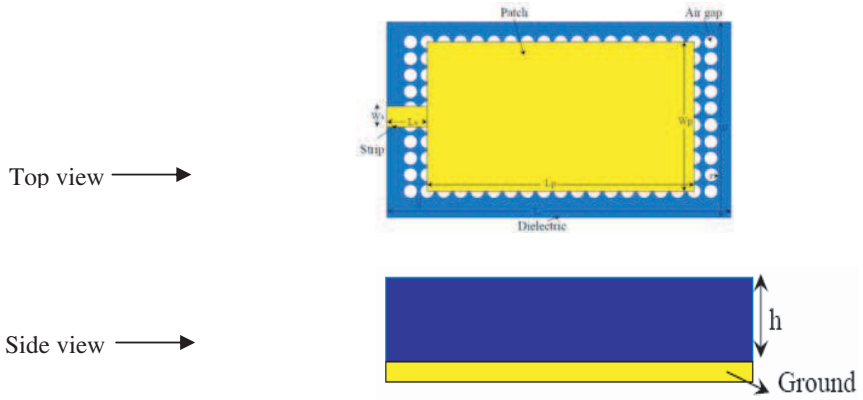

Figure 1: Geometrical configuration of rectangular microstrip antenna with photonic band gap structure.

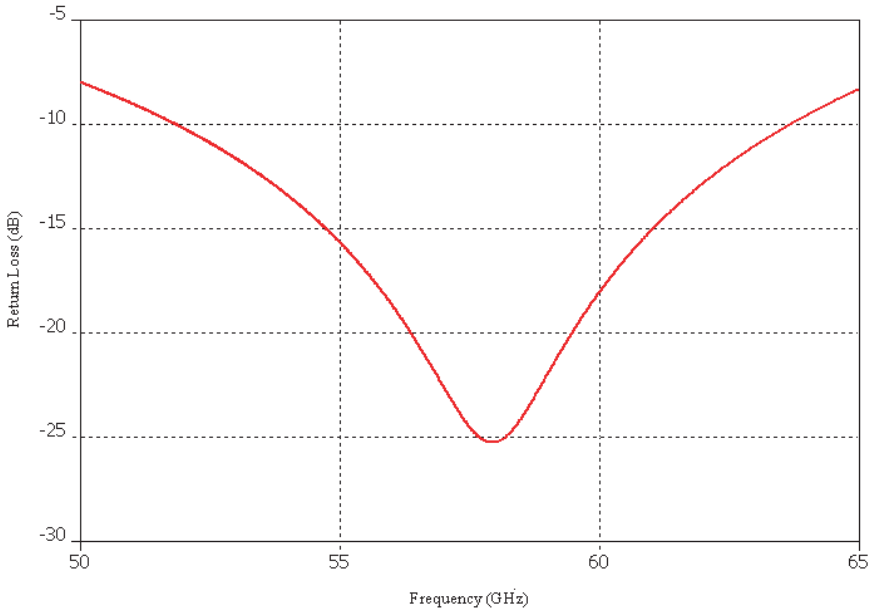

Figure 2: Return loss of the antenna.

MFIE for Numerical Analysis of Metal Aperture Antennas with the Waveguide Feeding Line

Hongxia Ye and Ya-Qiu Jin
Key Laboratory of Wave Scattering and Remote Sensing Information (MoE)
Fudan University, Shanghai 200433, China

Abstract— A new Magnetic Field Integral Equation (MFIE), based on the Huygens' surface equivalent principle, is presented to investigate the wave propagation and radiation from the rectangular metal aperture antenna fed by a geometry-matched waveguide transmission line. The affection of the feeding line on the antenna characteristics is included by introducing the vector mode functions of the waveguide theory for expansion of the equivalent electric and magnetic currents on the waveguide aperture. Then the Method of Moment (MoM) with the RWG base function and the Galerkin testing method, is used as a numerical tool to solve the MFIE to determine the unknown current on the equivalent surface. In order to describe the vector mode functions precisely, the dynamic dense-meshing scheme is used on the antenna aperture. Numerical simulation is performed for the rectangular metal aperture antenna (WR-90). The mode coefficients (Fig. 1) are shown for the physical analysis of the modes excitation on the waveguide terminal aperture. The reflection coefficients and the normalized admittance (Fig. 2) of the waveguide aperture are validated by comparison with the results from literatures. The radiation patterns and power analysis for different operating frequency are also presented. Numerical simulation indicates that when the operating frequency increases, the diffraction at the aperture terminal becomes stronger, and excites more high-order modes field, which generates stronger electromagnetic radiation to the exterior region.

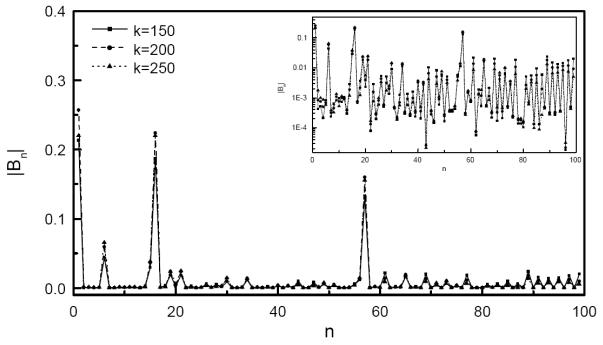

Figure 1: Reflection coefficient for each mode.

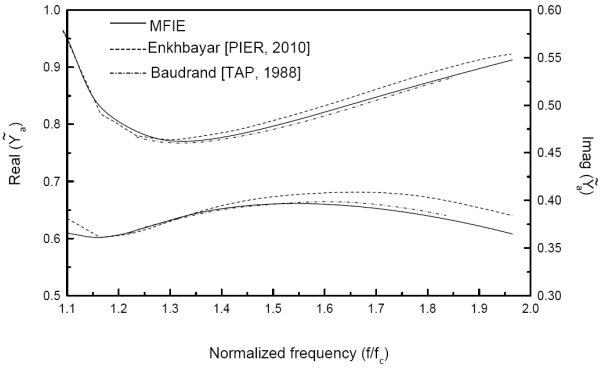

Figure 2: Normalized admittance vs. frequency.

ACKNOWLEDGMENT

This work was supported by the National Natural Science Foundation of China No. 61001007.

Novel Shape of UWB Microstrip Patch Antenna with Enhanced Gain Using EBG Structure

Mohammed M. Mohanna[1], **Deena A. Salem**[2], **Esmat A. F. Abdallah**[2], **and Hadia M. S. El-Henawy**[3]

[1]Ministry of Electricity & Energy, Egyptian Electricity Holding Company, Egyp
[2]Microstrip Department, Electronics Research Institute, Egypt
[3]Electronics and Communications Department, Ain Shams University, Egypt

Abstract— Interest in designing UWB antennas that operate over wide frequency range and that can be used for multiple channels or systems, has excelled as it enables high data transmission rate, low power consumption and simple hardware configuration in communication systems for different applications. Besides, the compact size and the non-dispersive properties are strongly needed for these applications.

Planar monopole antennas that consist of a rectangular patch loaded with slot(s) on the patch and the ground plane were presented in literature and proved to be very good candidates for such applications [1, 2]. However, they have some disadvantages such as low directivity and low gain, that is attributed to the surface waves, which affects the radiation efficiency. To eliminate these surface waves EBG substrates were introduced [3].

In this paper, a novel shape of microstrip UWB planar monopole with enhanced gain using EBG structure is presented. The structure is composed of a rectangular patch fed by a microstrip line constructed on a $22 \times 22\,\mathrm{mm}^2$ FR4 dielectric substrate of dielectric constant 4.65, and thickness 1.5 mm. The patch is mitered at the corners of the first radiating slot (45). Two slots were inserted in the partial ground plane lateral to the microstrip feed line. Mushroom-like circular EBG structures encircle the radiating patch, separated from the partial ground.

The new design achieves ultra wide bandwidth, with an omni directional radiation pattern, with enhanced gain, which may be attributed to the elimination of the surface waves in the antenna substrate. The operational bandwidth of this antenna extends from 3.5 to 13.5 GHz, with minimum return loss of −50 dB, with average peak directivity, gain and radiation efficiency of 7.5 dB, 6.5 dB, 82%, respectively. At the upper end of the spectrum, the gain increases to reach 11 dB.

An additional advantage of using EBG structures, which resonate at higher frequencies 22 to 29 GHz, is that the design applications may be extended to other areas such as vehicular applications.

The designed antenna was simulated using ready-made EM simulator, starting from initial design variables, parametric analyses was applied to obtain optimum dimensions. The obtained antenna was fabricated and measured. Both simulated and measured results were compared and very good agreement was achieved.

REFERENCES

1. Choi, S. H., J. K. Park, S. K. Kim, and J. Y. Park, "A new ultra-wideband antenna for UWB applications," *Microwave and Optical Technology Letters*, Vol. 40, No. 5, Mar. 5, 2004.
2. Zaker, R., C. Ghobadi, and J. Nourinia, "Novel modified UWB planar monopole antenna with variable frequency band-notch function," *IEEE Antenna and Wireless Propagation Letters*, Vol. 7, 2008.
3. Qu, D., L. Shafai, and A. Foroozesh, "Improving microstrip patch antenna performance using EBG substrates," *IEE Proc. Microwave, Antennas Propag.*, Vol. 153, No. 6, Dec. 2006.

Circularly Polarized Elliptical Slot Antenna with Enhanced Gain Using EBG Structure

Mohammed M. Mohanna[1], **Deena A. Salem**[2], **Esmat A. F. Abdallah**[2], **and Hadia M. S. El-Henawy**[3]

[1]Ministry of Electricity & Energy, Egyptian Electricity Holding Company, Egypt
[2]Microstrip Department, Electronics Research Institute, Egypt
[3]Electronics and Communications Department, Ain Shams University, Egypt

Abstract— Recently, circularly polarized antennas are receiving much attention; because of their advantages in both commercial and military applications e.g., satellite, terrestrial communications, RFID, etc.

Earlier, two novel designs of planar elliptical slot antennas were presented [1], which were printed on a dielectric substrate and fed by either microstrip line or coplanar waveguide with U-shaped tuning stub. The elliptical/circular slots have exhibited an ultra wideband (UWB) behavior. Besides, they showed nearly a unidirectional radiation pattern over a majority fraction of the bandwidth. Later, a printed elliptical slot antenna fed by different tapered microstrip line with U-shaped tuning stub and a circular ring-shaped tuning stub are proposed in [2] for UWB. The tapering improves the matching between the microstrip feed line and the tuning stub. All the above designs are adequate for UWB applications; however, some disadvantages exist, such as low directivity and low gain. Besides, the existence of surface waves, which affects directly the radiation efficiency.

In this paper, a circularly polarized elliptical patch antenna with enhanced gain using EBG structure is introduced. A new tapering profile that improves the matching and hence enhances the bandwidth is utilized. The tapering profile is based on the Willis-Sinha profile.

The design is composed of an elliptical slot antenna on the upper side of a $42 \times 42\,\text{mm}^2$ FR4 dielectric substrate of dielectric constant 4.65, and thickness 1.5 mm. On the lower side of the substrate, a Willis-Sinha tapered line feeds a modified U-shaped tuning stub. The later resembles a monopole antenna with a dipole-like omni directional patterns and a wide bandwidth. To enhance gain and bandwidth of the aforementioned antenna, mushroom like rectangular EBG structures were added to the lower side of the substrate to surround the U-shaped tuning stub.

This new design exhibits an ultra wide band performance that extends from 3.3 to 15 GHz with minimum return loss of −26 dB, with average peak directivity, gain and radiation efficiency of 8 dB, 7.5 dB, 88%, respectively. At the upper end of the spectrum, the gain increases to reach 11 dB.

The designed antenna was simulated using ready-made EM simulator, parametric analyses was applied to obtain optimum dimensions. The obtained antenna was fabricated and measured. Both simulated and measured results were compared and very good agreement was achieved.

REFERENCES

1. Li, P., J. Liang, and X. Chen, "Study of printed elliptical/circular slot antennas for ultra wideband applications," *IEEE Trans. on Antennas and Propagation*, Vol. 54, No. 6, June 2006.
2. Abuhalima, S., E. Abdallah, and D. Mohamed, "Ultra wideband elliptical microstrip antenna using different taper lines for feeding," *11th WSEAS International Conference on Communications*, 144–149, Agios Nikolaos, Crete Island, Greece, July 26–28, 2007.

Session 3A5
Electromagnetic Modeling, Inversion and Applications

The Visible Controlling of the Electromagnetic Stirring in the Steel Caster

Jianhua Li[1], **Ganquan Xie**[1], **Lee Xie**[1], **Feng Xie**[1], **Jing Li**[1], **Chien-Jang Wu**[2], **and Xianwu Zhou**[3]

[1]GL Geophysical Laboratory, USA
[2]Institute of Electro-Optical Science and Technology, National Taiwan Normal University, Taiwan
[3]University of Sciences and Technology, Beijing, China

Abstract— Up to now, the electromagnetic stirrings have been installed and operative in the steel caster in the steel factories in the China, India, Japan etc.. However, all of the electromagnetic stirring are blind operation. For improving he effect of the EM stirring and quality of the steel, we propose new GL EM, Heat, Flow, and crystal stress coupled modeling and inversion and EMAS quantum radar for the visible controlling of the electromagnetic stirring in the steel caster.

A New GL Anisotropic and Isotropic Invisible Cloak without Exceeding Light Speed Violation

Ganquan Xie, **Jianhua Li**, **Lee Xie**, **and Feng Xie**
GL Geophysical Laboratory, USA

Abstract— In this paper, we propose a new GL EM anisotropic and isotropic invisible cloak class without exceeding light speed. The GL cloak material in this paper is different from our paper ArXiv 1050.3999. The radial dielectric and permeanbility of GL EM cloak in this paper are large than one. The refractive index of the GL cloak material, $n(r)$, is large than one or equal to one. A unconventional GL radial EM cloak modeling and inversion are proposed here. By searching in a distinctive class of the rational function of $(h), h = r - R_1$, the GL EM cloak modeling and inversion create GL EM invisible cloak class without exceeding light speed. The GL EM cloaks can be practicable by using conventional optical materials. he properties of our GL EM cloak and their proofs are presented in this paper. The novel EM wave propagation and front branching in the GL cloak by GL EM modeling are presented in this paper. The EM wave front propagation in GL cloak is behind of the front in free space. In the GL cloak, the wave front is curved as a crescent like and propagates slower than the light in free space. Its two crescent front peaks intersect at a front branching point. At the front branching point, the front is split to two fronts. The novel front branching and crescent like wave propagation are displayed in figures in this paper. A more exciting breakthrough progress is that we discovered GL isotropic invisible cloak without exceeding light speed. The isotropic relative dielectric and permeability parameter are proposed as (4)–(5) and (7) in our full paper. All copyright and patent of the GL EM cloaks and GL modeling and inversion methods are reserved by authors in GL Geophysical Laboratory.

Applying Margolus-Levitin Theorem to Quantum Computers Emerges that Photons with Different Energy May Travel with Different Speeds

Antonio Puccini
Department of Neurophysiology, Order of Malta, Naples, Italy

Abstract— Margolus and Levitin's theorem (MLT) analyses the maximum speed of dynamical evolution that a computer can reach counting the maximum number of distinct states that an isolated physical system can pass through in a given period of time. For a classical computer, this would correspond to the maximum number of operations per second. The minimum time needed for a quantum system to pass from an orthogonal state to another has also previously been characterized in terms of the standard deviation of the energy Δ_E.

According to MLT the highest speed with which a physical system can move from a state to another is directly proportional to its energy: $T \geq h/4\Delta_E$. It does not depend on the nature of the system but only on the quantity of energy available for the computation. Let us suppose we could use new generation Quantum Computers, that is computers not working with electrons but with photons (Ps) of different energy, that is they travel with electromagnetic waves (EMWs) of different frequencies. What would happen? It seems we can expect a novelty, an innovative result. Why? Since we know from MLT that in every physical system the speed the system operates is directly proportional to the energy available, it comes that a future computer, operating with Ps of EM bands more energetic, should work with a higher speed than an identical computer operating with Ps less energetic. It will be obtained that the computers operating with Ps more energetic (that is of higher frequency) would have to compute with a higher velocity than those structurally identical but operating with Ps less energetic.

Roles of Assisting Scatterers on Solving Inverse Scattering Problem

Jianhua Shen[1], **Yu Zhong**[2], **Xudong Chen**[2], **and Lixin Ran**[1]

[1]Department of Information and Electronic Engineering, Zhejiang University, Hangzhou 310027, China
[2]Department of Electrical and Computer Engineering, National University of Singapore, 117576, Singapore

Abstract— This paper deals with the inverse scattering problem with the subspace-based optimization method (SOM), in which an assisting scatterer is placed around the object that is to be reconstructed. For simplicity, a conductor cylinder is adopted as the assisting scatterer. Due to the multiple scattering effects, the conductor cylinder is an important factor on the inverse scattering problem. Numerical simulations show that under a proper design of the simulation configuration, the conductor cylinder can induce some beneficial effect on improving the resolution of the reconstruction results.

Figure 1 shows configuration for the simulations. In free space background, a conductor cylinder with a radius of 0.5λ is located at the original O, where λ is the wavelength. The test domain is a square with a size of $2\lambda \times 2\lambda$, which is centered at the point $(2\lambda, 0)$. The objective scatterers inside the test domain adopts the 'Austria' profile and the relative permittivity of scatterers is $\varepsilon_r = 2$. The scatterers are composed of two discs with a radius of 0.2λ which centered at $(-1.7\lambda, 0.6\lambda)$ and $(2.3\lambda, 0.6\lambda)$ and one ring with an exterior radius of 0.6λ and an inner radius of 0.3λ which centered at $(2\lambda, -0.2\lambda)$. In the antenna region, 16 transmitters and 32 receivers are evenly distributed along a circle with a radius of 5λ. The angle of the antenna region is 135°.

Figure 2(a) shows the result of the simulation with the conductor cylinder and Figure 2(b) shows the result without the cylinder. The resolution gets improved using the conductor cylinder.

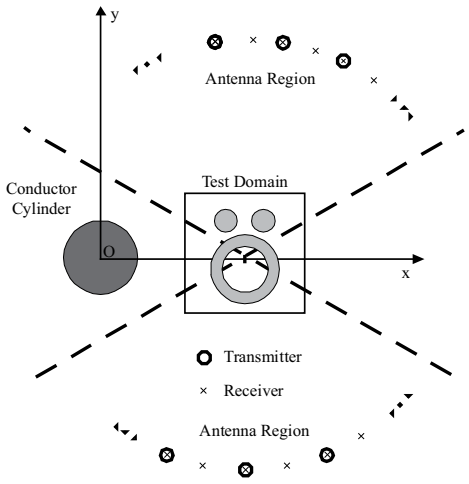

Figure 1: Configuration for the simulations.

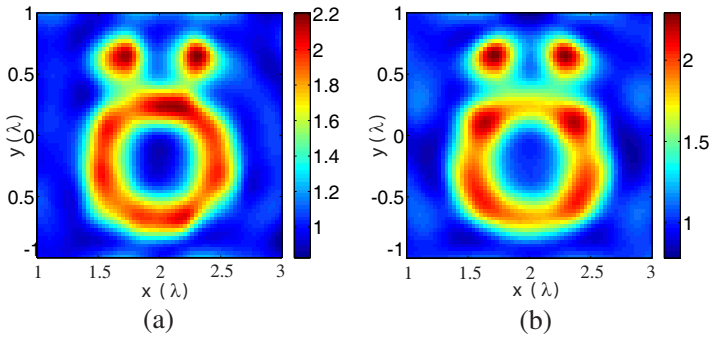

Figure 2: Results of the simulations.

Increasing the Efficiency of Forward-backward Time-stepping Reconstruction Method

H. Zhou and H. J. Zhang
State Key Laboratory of Petroleum Resource and Prospecting
Key Laboratory of Geophysical Exploration of China National Petroleum Corporation
Department of Geophysics, China University of Petroleum, Changping, Beijing 102249, China

Abstract— Ground-penetrating radar (GPR) has been applied to various fields and solved many detection problems. As one kind of interpretation methods, the techniques to reveal quantitative properties of subsurface from GPR data have been investigated by many researches. Among these methods, there are inverse scattering reconstruction techniques in the time- and frequency-domain.

We have discussed a forward-backward time-stepping (FBTS) method to reconstruct electrical property profiles of objects using the time-domain electromagnetic data. The gradients of the cost functional with respect to unknown parameters (permittivity and conductivity) are expressed explicitly by introducing an adjoint vector field $\mathbf{w}_m(\mathbf{p};\mathbf{r},t)$,

$$g_\varepsilon = 2\int_0^{cT}\sum_{m=1}^{M}\sum_{i=1}^{3} w_m^i(\mathbf{p};\mathbf{r},t)\,\frac{\partial v_m^i(\mathbf{p};\mathbf{r},t)}{\partial(ct)}\,d(ct) \tag{1}$$

$$g_\sigma = 2\int_0^{cT}\sum_{m=1}^{M}\sum_{i=1}^{3} w_m^i(\mathbf{p};\mathbf{r},t)\,v_m^i(\mathbf{p};\mathbf{r},t)\,d(ct) \tag{2}$$

where, c is speed of light in vacuum. The gradients are calculated by crosscorrelating $\mathbf{w}_m(\mathbf{p};\mathbf{r},t)$ with the wave field $\mathbf{v}_m(\mathbf{p};\mathbf{r},t)$ of the guessed model $\mathbf{p}$ of the mth transmitter. $\mathbf{v}_m(\mathbf{p};\mathbf{r},t)$ is calculated forward in time, however, $\mathbf{w}_m(\mathbf{p};\mathbf{r},t)$ excited by wave field residuals at the receivers' positions is calculated reverse in time. In order to calculate the gradients, $\mathbf{v}_m(\mathbf{p};\mathbf{r},t)$ of the whole reconstruction space at all time must be saved to the hard disk. During the calculation of the gradients, the saved data are read from hard disk and crosscorrelated with $\mathbf{w}_m(\mathbf{p};\mathbf{r},t)$ just calculated. As it is well known that the storage and read of data from hard disk is very time consuming, particularly for three-dimensional reconstruction problems because the amount of $\mathbf{v}_m(\mathbf{p};\mathbf{r},t)$ is very large. It is the bottleneck of this reconstruction method for large scale practical applications.

In this paper, the storage and read of $\mathbf{v}_m(\mathbf{p};\mathbf{r},t)$ is avoided by using random boundaries surrounding the whole model. In the random boundaries the permittivity distributes randomly, $\mathbf{w}_m(\mathbf{p};\mathbf{r},t)$ in this regions is scattered, and the scattered field is not coherent with $\mathbf{v}_m(\mathbf{p};\mathbf{r},t)$, the gradient is not evidently affected by the field from the random boundary regions. $\mathbf{w}_m(\mathbf{p};\mathbf{r},t)$ propagating in the guessed model with random boundaries is calculated from the largest time T to 0 by using the finite-difference time-domain (FDTD) method, and the electric field at 0 and the magnetic field at $\Delta t/2$ are saved to the hard disk. Δt is time step. During the calculation of $\mathbf{v}_m(\mathbf{p};\mathbf{r},t)$ by the FDTD method forward in time with absorbing boundaries, $\mathbf{w}_m(\mathbf{p};\mathbf{r},t)$ is also calculated from the saved data at 0 and $\Delta t/2$ forward in time by FDTD method with the random boundaries, and the gradient is then calculated using $\mathbf{v}_m(\mathbf{p};\mathbf{r},t)$ and $\mathbf{w}_m(\mathbf{p};\mathbf{r},t)$ at the same time sampling position. $\mathbf{w}_m(\mathbf{p};\mathbf{r},t)$ at any time can be recovered by using FDTD method.

A 2-D reconstruction example is conducted by the conventional method with storage and read of $\mathbf{v}_m(\mathbf{p};\mathbf{r},t)$, and the suggested method. The reconstructed results by using these methods are almost the same, however, the calculation time of the suggested method is about 78% of the conventional reconstruction method. The percentage is smaller if the reconstruction size and the number of transmitters are larger.

Since the data storage and read are extremely reduced, the time domain reconstruction method is very suitable for GPU (Graphic Processing Unit) parallel computation. By using the random boundary method and GPU parallel computation, the efficiency of the FBTS reconstruction method can be greatly increased.

Note on the Tangential Scattered Magnetic Field on a Perfectly Conducting Surface

Guyan Ni
College of Science, National University of Defense Technology, China

Abstract— Consider a plane wave $(\mathbf{E}^i, \mathbf{H}^i)$ incident on a perfectly conducting object. The incident wave produces surface currents density $\mathbf{J}_S$ on the conductor surface S, which generators a scattered electric field $\mathbf{E}^s$ and a scattered magnetic field $\mathbf{H}^s$. The scattered magnetic field outside the current-carrying surface is often expressed in terms of a Green's function as

$$\mathbf{H}^s(\mathbf{r}) = \frac{1}{4\pi}\int_S \nabla\left(\frac{\exp(-jkR)}{R}\right) \times \mathbf{J}_S(\mathbf{r}')dS' \tag{1}$$

where $j = \sqrt{-1}$, $R = |\mathbf{r} - \mathbf{r}'|$. However, when $\mathbf{r}$ is on the surface, then (1) is divergent. Hence, the tangential component of the scattered field $\hat{n} \times \mathbf{H}^s(\mathbf{r})$ on the surface is always expressed as

$$\lim_{\epsilon \to 0+} \frac{1}{4\pi}\int_S \hat{n} \times \left(\nabla\left(\frac{\exp(-jkR)}{R}\right) \times \mathbf{J}_S(\mathbf{r}')\right) dS', \tag{2}$$

where $R = |\mathbf{r} + \epsilon\hat{n} - \mathbf{r}'|$. A general viewpoint is that the integral (2) is convergent if the surface S is smooth, and it is widely used in the magnetic-field integral equation (MFIE).

However, in this paper, we consider the tangential component of the scattered field at a first-order smooth point P of a conductor. At the point, we show that the integral (2) is divergent if the surface current density at the point is nonzero. That is $\hat{n} \times \mathbf{H}^s$ is infinite. Hence, by the boundary condition, the surface current density at the point should be zero.

ACKNOWLEDGMENT

This work was supported by China Postdoctoral Special Science Foundation (No. 200902662), the National Natural Science Foundation of China (No. 10871231), and Pre-research Foundation of Weapon and Equipment (No. 9140A31020609KG0170).

Stability Analysis of Neutral Systems and Its Application to a Partial Element Equivalent Circuit (PEEC) Model

Guorui Cong, **Guyan Ni**, **and Jianshu Luo**
Department of Science, College of Science
National University of Defense Technology, Changsha, Hunan 410073, China

Abstract— It is well known that time domain integral equation techniques may suffer from stability problems. A main source of these issues is the delay of the coupled elements. The partial element equivalent circuit (PEEC) method has shown to be efficient in mixed electromagnetic (EM) and circuit analysis. The real circuit model, such as a partial element equivalent circuit, can be represented as delay differential equations (DDE) of neutral type. The stability analysis of this kind of systems is of much importance due to the fragility of DDE solvers. This paper is concerned with stability of linear neutral systems and its application to a PEEC model of neutral type.

Derivation of One-minute Rain Rate from Five-minute Equivalent for the Calculation of Rain Attenuation in South Africa

P. Owolawi
Department of Electrical Engineering, Mangosuthu University of Technology
Umlazi, Kwazulu-Natal, South Africa

Abstract— In accordance to International Telecommunication Union (ITU-R P. 618-6 and P. 530-8), estimation of rain attenuation need to be carried out at lower integration time i.e., $\geq$ 1 minute. Due to inherent advantages in shorter integration intervals, this has encouraged researchers to develop methods to solve the problem of conversion from higher integration times to their lower integration time equivalent.

The established conversion methods are grouped into three broad classes which are physical, analytical and empirical models. Majority of the contributors tend to use the empirical method extensively to convert from higher integration time to lower equivalent because of its simplicity and experimental dependent.

This paper presents conversion of rain rate from 5-minte to equivalent 1-minute integration time. A proposed hybrid method is based on optimized existing conversion methods. The approach is considered because of mixed geographical/climatic conditions of the southern Africa. The results of the method are compared with exiting models which are geographically dependent.

The hybrid method presented in this paper takes advantages of existing rain rate conversion methods with their inherent properties and adapts them for the region of interest by using a control site with at least one measured one-minute rain rate data to optimize the selected models. The rationale of the model can be abridged as follows: assume that a cumulative distribution (CDF) of a region with measured one-minute rain rate with their coefficients can be mirrored in another site by simply adjusting the values of the coefficients to find the cumulative identity with the existing CDF. Here the regional precipitation properties will still be maintained and the variability of the site will be taken care of. Since several rain rate conversion models already exist, it is easy to tap into their properties and identify them with the region of interest using appropriate optimization methods. It is anticipated that a combined rain rate conversion method will give better performance than an individual model because of the dynamics of rain rate distribution especially in Africa where multiple regimes of rain can occur within one rain rate event.

The resulting one-minute cumulative distribution of rain rate is fitted with polynomial, power, linear and logarithmic fits. The results show that the equiprobable approach gives better results than the conversion factor approach. In addition, the second order polynomial fit performs relatively better than its other counterparts. The evidence of good performance by the second order polynomial fit makes it a good candidate for conversion of rain rate from five-minute to equivalent one-minute in South Africa and her Islands. The coefficients of hybrid models are categories using Koppen method and finally second order polynomial fit is adopted for the region with their respective coefficients.

GL EM Modeling for Electromagnetic Remote Sensing Science and Technology in Multi-level Multi-scale Characteristics of in Geographic Information Systems

Lei Zhang[1, 2] and Ganquan Xie[3]

[1]Wuxi Research Center, Technical Physics of the Chinese Academy of Sciences, China
[2]Shanghai Institute of Technical Physics, Chinese Academy of Sciences, China
[3]GL Geophysical Laboratory, USA

Abstract— Urban heat island effect and multi-level multi-scale characteristics of in geographic information systems, the electromagnetic remote sensing science and technology has been extensive attention [1]. city living ecosystems despite the interference of artificial heat and other factors, but still shows a certain periodicity and regularity. this fully learn urban heat island research methodology proposed eco-city living concept of organic life forms, all kinds of material and energy exchange of the open complex ecological unit for heat illness summarized and analyzed. habitat comfort from the perspective of the heat and green living environment in the city and its co-exist in the physical production process, using infrared to detect heat sources and small-scale to highlight the space of three-dimensional and multi-tiered, multi-object and object nonlinear characteristics. heat from the urban living environment, assessed in terms of improving the thermal environment of the distribution of green and ecological control mechanism, studies have shown that urban living ecosystem construction and thermal environment has a direct impact on the geographical distribution relationships and is operational to control the use of green is strong technical means. therefore, the relevant innovative research methods and their effects will be described in qualitative and quantitative in simulation and the measured depth research.

In this paper, we will present GL EM modeling [2] simulation for urban heat island effect and multi-level multi-scale characteristics of in geographic information systems.

REFERENCES

1. Zhang, L., "Simulation on C/A codes and analysis of GPS/pseudolite signals acquisition," *Science In China, E. Technological Sciences*, Vol. 52, No. 5, 1459–1462, May 2009.
2. Xie, G., F. Xie, L. Xie, and J. Li, "New GL method and its advantages for resolving historical difficulties," *Progress In Electromagnetics Research*, Vol. 63, 141–152, 2006.

Sumudu Based Transient Magnetic Field Solutions for Maxwell's Equations

Fethi Bin Muhammad Belgacem
Department of Mathematics, Faculty of Basic Education, PAAET, Shaamyia, Kuwait

Abstract— When Sumudu transformed Maxwell's Equations yield transient electric and magnetic field solutions. Previously, the Sumudu Reciprocity property was used to extract electric field solutions for transversal electromagnetic planar waves, (TEMP), in a lossy medium. Here we present a parallel treatment for the magnetic field, using Sumudu newly established properties.

Sumudu Based Magetic Field Solutions for Maxwell's Equations:

This brief exposition is a continuation to the efforts expanded in [4] and [6], initially motivated by the desire of finding an alternative insight and solution method for Maxwell's equations presented in [1–3]. Various forms of solutions for the electromagnetic couple solutions and profiles have been found, using various techniques, subject to distinct assumptions on the medium coefficients and fields intial directions. Once more, we reconsidrer the problem of transient propagation in unbounded lossy media. The Dynamics of a planar, transverse electromagnetic (TEMP) wave propagating in the direction z in lossy media with constant permittivity ϵ, permeability μ, and conductivity $\sigma > 0$, are best described by Maxwell's equations,

$$\begin{cases} \text{(i) } \nabla \times \mathbf{E} = -\mu \dfrac{\partial \mathbf{H}}{\partial t}, \\ \text{(ii) } \nabla \times \mathbf{H} = -\mu \dfrac{\partial \mathbf{E}}{\partial t} + \sigma \mathbf{E}. \end{cases} \tag{1}$$

Based on transient excitation functions, the Laplace transform has been the traditional tool used for solving Maxwell's equations describing the TEMP problem (1). Alternatively, in [4] (see also [6]), the Sumudu transform was used to extract transient solutions for the Electric field.

Theorem 1. The transient electric field, $E(z,t)$, in the TEMP Equation (1) suject to a lossy medium conditions, is given by,

$$E(z,t) = e^{-\frac{b}{a}z} f(t - z/a) - a \int_{z/a}^{\infty} f(t-\tau) e^{-b\lambda} \frac{\partial}{\partial z} J_0 \left(\frac{b}{a} \sqrt{z^2 - (a\tau)^2} \right) e^{-t/u} d\tau,$$
$$\text{where, } a = 1/\sqrt{\mu\epsilon}, \ \ b = \sigma/2\epsilon, \tag{2}$$

where J_0 is the Bessel function of order 0, (see [7]), and for $t \geq 0$, $= f(t) = \lim_{z \to 0} E(z,t) = E(0,t)$.

Again, here we use the novel Sumudu technique but to establish similarly expressed solut ions for the magnetic field.

We recall that provided the function, $f(t)$ satisfies,

$$|f(t)| < \begin{cases} Me^{-t/\tau_1} & \text{for} \quad t \leq 0, \\ Me^{-t/\tau_2} & \text{for} \quad t \geq 0, \end{cases} \tag{3}$$

the Sumudu, $S[f(t)]$, of $f(t)$ is given by (see [6]),

$$S[f(t)](u) = G(u) = \int_0^{\infty} f(ut) e^{-t} dt, \quad -\tau_1 \leq u \leq \tau_2. \tag{4}$$

The Sumudu Transform of the Electric field, $F(z,u) = S[E(z,t)]$, was obtain,

$$F(z,u) = F(z,u) = F(u) e^{-\gamma z} = F(u) e^{-\frac{b}{a}z} e^{-\frac{1}{au}z} - auF(u) S[\Phi(z,v)], \tag{5}$$

with,

$$\Phi(z,v) = \begin{cases} e^{-bv} \dfrac{\partial}{\partial z} J_0 \left(\dfrac{b}{a} \sqrt{z^2 - (av)^2} \right), & \text{for} \quad v \geq z/a, \\ 0, & \text{for} \quad 0 < v < z/a. \end{cases} \tag{6}$$

The following Sumudu shift and convolution properties were used (see [6] for details),

$$S[f(t-t_0)] = F(u)e^{-t_0/u}, \;\; \&, \;\; S[f(t) * g(t)] = uF_1(u) * F_2(u). \tag{7}$$

We intend to show that the magnetic field can have a parallel expression. Rewriting Equation (1),

$$\begin{cases} \text{(i)} \;\; \dfrac{\partial E_x}{\partial z} + \mu \dfrac{\partial H_y}{\partial t} = 0, \\ \text{(ii)} \;\; \dfrac{\partial H_y}{\partial z} + \epsilon \dfrac{\partial E_x}{\partial t} + \sigma E_x = 0, \end{cases} \tag{8}$$

differentiating (i) with respect to the variable t, and (ii) with respect to the variable z, we get,

$$\begin{cases} \text{(i)} \;\; \dfrac{\partial^2 E_x}{\partial t \partial z} + \mu \dfrac{\partial^2 H}{\partial t^2} = 0, \\ \text{(ii)} \;\; \dfrac{\partial^2 H}{\partial z^2} + \epsilon \dfrac{\partial^2 E_x}{\partial z \partial t} + \sigma \dfrac{\partial E_x}{\partial z} = 0 \end{cases} \tag{9}$$

using the previous two equations and eliminating terms (assuming E is exact), we get,

$$\frac{\partial^2 H}{\partial z^2} = \mu\epsilon \frac{\partial^2 H}{\partial t^2} + \mu\sigma \frac{\partial H}{\partial t}. \tag{10}$$

Setting, $G(z,u) = S[H(z,t)]$, we use the Sumudu transformations of function derivatives, (see [5] for details),

$$S[f^{(n)}(t)] = \frac{G(u)}{u^n} - \frac{f(0)}{u^n} - \cdots - \frac{f^{n-1}(0)}{u}. \tag{11}$$

Using Equation (11) for $n = 1$ & $n = 2$, and Sumudu transforming Equation (10) we get,

$$\frac{\partial^2 G(z,u)}{\partial z^2} = \mu\epsilon \left[\frac{G(z,0)}{u^2} - \frac{H(z,0)}{u^2} - \frac{H'(z,0)}{u} \right] + \mu\sigma \left[\frac{G(z,u)}{u} - \frac{H(z,0)}{u} \right]. \tag{12}$$

Rearranging terms helps us obtain a differential equation in $G(z,u)$, where is simply a parameter,

$$\frac{\partial^2 G(z,u)}{\partial z^2} - \left(\frac{\mu\epsilon}{u^2} + \frac{\mu\sigma}{u} \right) G(z,u) = \left(\frac{\mu\epsilon}{u^2} + \frac{\mu\sigma}{u} \right) H(z,0) - \frac{\mu\epsilon}{u} H'(z,0) \tag{13}$$

Assuming the following initial conditions,

$$H(z, t \to 0) = h_0(z), \;\; \&, \;\; \partial H(z, t \to 0)/\partial t = h_0'(z), \tag{14}$$

and setting,

$$\rho = \frac{\mu\sigma}{u}, \; \lambda = \frac{\mu\epsilon}{u^2}, \;\; \&, \;\; \gamma^2 = \frac{\mu\epsilon}{u^2} + \frac{\mu\sigma}{u} = \lambda + \rho, \tag{15}$$

we obtain the relation,

$$\frac{d^2 G(z,u)}{dz^2} - \gamma^2 G(z,u) = \gamma^2 h_0(z) - \lambda h_0'(z) = V(z,u). \tag{16}$$

The homogeneous solution of (15), $G_h(z,u)$, (achieved if $V(z,u) = 0$, i.e., $h_0'(z)/h_0(z) = 1 + \rho/\lambda = 1 + u\sigma/\epsilon$) is given by,

$$G(z,u) = A(u)e^{\gamma z} + B(u)e^{-\gamma z}. \tag{17}$$

and its particular solution, $G_p(z,u)$ of which is given by,

$$G_p(z,u) = \frac{e^{\gamma z}}{2\gamma} \int e^{-\gamma z} V(z,u) dz + \frac{e^{-\gamma z}}{2\gamma} \int e^{\gamma z} V(z,u) dz. \tag{18}$$

We can always relate the boundary conditions of $H(z,t)$ to those of $E(z,t)$ using (1) and derivatives and tassumptions as ake advantage of assumptions in [4], however we assume direct values for the magnetic field boundary conditions. In a lossy medium with conductivity $\sigma > 0$, we assume,

$$\lim_{z \to 0} H(z,t) = H(0,t) = h(t), \;\; t \geq 0, \tag{19}$$

In this case, we get,

$$\begin{cases} A(u) = 0, \text{ and,} \\ B(u) = G(0,u) = S[h(t)] = G(u). \end{cases} \tag{20}$$

Consequently, using $V(z,u)$ instead of $W(z,u)$, in Equation (39) of [6], and changing the argument of J_0 accordingly, we have the following result.

Theorem 2. The transient Magnetic field, $H(z,t)$, solving the TEMP Equation (1) in lossy medium conditions, has a similar expression to Equation (2), with $h(t)$ substituting for $f(t)$.

TEMP like problems field couple solutions can be considered in the Sumudu Transform frame work. In view of its advantageous attributes and many quantities preserving properties, the Sumudu turns out to be an ideal tool for many science and engineering applications.

REFERENCES

1. Kong, J. A., *Maxwell Equations*, EMW Publishing, Cambridge, MA, 2002.
2. Harmuth, H. F. and M. G. M. Hussain, *Propagation of Electromagnetic Signals*, World Sci., Singapore, 1994.
3. Hussain, M. G. M., "Mathematical model for the electromagnetic conductivity of lossy materials," *Journal of Electomagnetic Wave and Appliations*, Vol. 19, No. 2, 271–279, 2005.
4. Hussain, M. G. M and F. B. M, Belgacem, "Transient solutions of maxwell's equations based on sumudu trans.," *Progress In Electromagnetics Research*, Vol. 74, 273–289, 2007.
5. Belgacem, F. B. M., "Introducing and analyzing deeper sumudu properties," *NSJ*, Vol. 13, No. 1, 23–41, 2006.
6. Belgacem, F. B. M., "Sumudu applications to maxwells equations," *PIERS Online*, Vol. 5, No. 4, 355–360, 2009.
7. Belgacem, F. B. M., "Sumudu transform applications to bessel equations and functions," accepted in AMS Special Issue, 2010.

Applications of the Natural Transform to Maxwell's Equations

R. Silambarasn[1] and F. B. M. Belgacem[2]

[1]M. S. Software Engg., V.I.T. University, Vellore, India
[2]Department of Mathematics, Faculty of Basic Education, PAAET, Shaamyia, Kuwait

Abstract— The theme of this paper is to solve the Maxwell's (partial differential) equations governing the planar transverse electromagnetic wave (TEMP) propagate in z direction in lossy medium with constant permittivity ϵ, permeability μ and conductivity σ.

$$\frac{\partial E_x}{\partial z} + \mu \frac{\partial H_y}{\partial t} = 0 \tag{1}$$

$$\frac{\partial H_y}{\partial z} + \epsilon \frac{\partial E_x}{\partial t} + \sigma E_x = 0 \tag{2}$$

for the Electric Field $E(z,t)$ and Magnetic field $H(z,t)$ using the initial and boundary conditions

$$E_x(\infty, t) = \text{finite} \tag{3}$$

$$E_x(z,0) = H_y(z,0) = 0 \tag{4}$$

$$\frac{\partial E_x(z,0)}{\partial z} = \frac{\partial H_y(z,0)}{\partial z} = 0 \tag{5}$$

$$\left[\frac{\partial E_x(z,t)}{\partial t}\right]_{t=0} = \left[\frac{\partial H_y(z,t)}{\partial t}\right]_{t=0} = 0 \tag{6}$$

$$E(0,t) = f(t); \quad t \geq 0 \quad \text{and} \quad 0; t < 0 \tag{7}$$

We apply the Natural integral transform of the function $f(t)$ for the t defined in positive real axis $(0, \infty)$, given by

$$\mathbb{N}^+[f(t)] = R(s,u) = \int_0^\infty e^{-st} f(ut)dt; \quad s > 0,\ u > 0 \tag{8}$$

to solve the Equations (1) and (2). We show the relationship of Natural transform to the Laplace and Sumudu transforms.The result here we obtained are using the properties of Natural transform such as, Natural transform of Convolution of two functions

$$\mathbb{N}^+[(f * g)] = uF(s,u)G(s,u) \tag{9}$$

and the Complex inverse Natural transform (Bromwich contour integral) defined by

$$\mathbb{N}^{-1}[R(s,u)] = f(t) = \lim_{T\to\infty} \frac{1}{2\pi i} \int_{\gamma - iT}^{\gamma + iT} e^{\frac{st}{u}} R(s,u)ds \tag{10}$$

The Electric $E(z,t)$ and Magnetic field $H(z,t)$ solutions here we obtained are in compact Convolution integral form.

Session 3A6
Electromagnetic Composite and Smart Materials for Microwave Applications 1

Account for a Distribution in Inclusion Shapes in the Effective Medium Approach

Konstantin N. Rozanov[1], **Marina Y. Koledintseva**[2], **and James L. Drewniak**[2]

[1]Institute for Theoretical and Applied Electromagnetic, Russian Academy of Sciences
13 Izhorskaya ul., Moscow 125415, Russia
[2]Center for Electromagnetic Compatibility, Missouri University of Science and Technology
4000 Enterprise Dr., HyPoint, Rolla Missouri 65401, USA

Abstract— Account for a distribution in inclusion shapes is known to be essential for predicting effective material parameters, the permittivity and permeability, of composite materials, especially if the frequency-dependent behavior of the material parameters is under treatment [1]. A number of approaches have been suggested in the literature [2–4] to account for such distributions. However, these theories propose no approach for determining of parameters of the distribution from measured data. Recently, a theory has been developed [5] accounting for the distribution and involving an approach to characterizing its parameters from the measured microwave frequency dependence of the permittivity and permeability. The theory [5] is suitable for composites filled with conductive particles, the shape of which is close to sphere. In the presentation, an approach to accounting for the shape distribution is developed for composites filled with elongated inclusions, such as flakes and needles. The study is aimed at modeling of electromagnetic behavior of the composites and at obtaining data on the intrinsic permeability of inclusions. The cases are discussed when the account for the distribution of inclusions in shapes is essential. Examples are given of the analysis of measured data on the microwave permittivity and permeability of various composites.

REFERENCES

1. Rozanov, K. N., A. V. Osipov, D. A. Petrov, S. N. Starostenko, and E. P. Yelsukov, "The effect of shape distribution of inclusions on the frequency dependence of permeability in composites," *J. Magn. Magn. Mater.*, Vol. 321, 738–741, Apr. 2009.
2. Gao, L. and J. Z. Gu, "Effective dielectric constant of a two-component material with shape distribution," *J. Phys. D — Appl. Phys.*, Vol. 35, 267–271, Feb. 2002.
3. Goncharenko, A. V., "Generalizations of the bruggeman equation and a concept of shape-distributed particle composites," *Phys. Rev. E*, Vol. 68, No. 041108, Oct. 2003.
4. Koledintseva, M. Y., S. K. R. Chandra, R. E. DuBroff, and R. W. Schwartz, "Modeling of dielectric mixtures containing conducting inclusions with statistically distributed aspect ratio," *Progress In Electromagnetics Research*, Vol. 66, 213–228, 2006.
5. Rozanov, K. N., M. Y. Koledintseva, and J. L. Drewniak, "A new mixing rule for predicting of frequency-dependent material parameters of composites," *Proc. 2010 URSI Int. Symp. on Electromagn. Theory*, 646–649, Berlin, Germany, Aug. 16–19, 2010.

The Tunable Microwave Dielectric Spectrum of Carbon Nanotube Membrane

L. Liu, Z. H. Yang, and L. B. Kong

Temasek Laboratories, National University of Singapore
5A Engineering Drive 2, Singapore 117411, Singapore

Abstract— Carbon nanotube (CNT) composites have attracted great attentions, because of their outstanding electrical, dielectrical, mechanical and thermal properties, which may find numerous exciting potential applications. CNTs have shown better elastic modulus and strengths than strongest steel and better electrical properties than copper wires. Such properties make CNTs ideal fillers for polymer composites with various applications, such as electrostatic discharge (ESD) and electromagnetic compatibility (EMC), as well as absorption of electromagnetic wave inside anechoic chamber. Compared with carbon fibers (CF) and carbon black (CB), CNTs can be filler of composites with high permittivity and frequency dispersion at extremely low concentrations [1].

Inspired by the nonlinear voltage-current relation in individual CNT components, we have disclosed novel tunable permittivity from bulk CNT-polymer composites [2]. It was found that the composites with CNTs of above 6 wt% exhibited tunable dielectric permittivity under external bias voltages, with real part decreasing and imaginary part increasing with increasing voltage [2]. However, the tunable permittivity was only measured at low frequency. Most wireless communication devices and radar systems have working frequencies from a few hundred MHz to a few GHz. Hence, it is of great interest to investigate tunable dielectric properties up to GHz.

In this study, multiwall carbon nanotube (MWCNT) membranes with thickness greater than 10 μm were prepared with spin-coating. Dielectric permittivity of the circular membranes was measured from 0.1 to 7 GHz using a single-port coaxial line method. The frequency and bias voltage dependent dielectric properties were interpreted based on percolation theory. MWCNT membranes could potentially be used to develop smart components and structures working at microwave frequencies.

REFERENCES

1. Liu, L., S. Matitsine, Y. Gan, L. Chen, L. Kong, and K. Rozanov, "Frequency dependence of effective permittivity of carbon nanotube composites," *J. Appl. Phys.*, Vol. 101, No. 9, 094106, 2007.
2. Liu, L., L. Kong, and S. Matitsine, "Tunable effective permittivity of carbon nanotube composites," *Appl. Phys. Lett.*, Vol. 93, No. 11, 113106, 2008.

Microwave Spin Wave Modes in Ferromagnetic Nanocrystalline Flake and Laminated Composites

Peiheng Zhou, Tao Liu, and Longjiang Deng
State Key Laboratory of Electronic Thin Films and Integrated Devices
University of Electronic Science and Technology of China, China

Abstract— Ferromagnetic nanocrystalline flakes and composites are potential candidates for use in high frequency magnetic devices due to their shape optimization for microwave permeability improvement and nanostructure-induced multi-resonance for bandwidth broadening. Previous work was done to explore the spin wave resonance origin and magnetic bounds relation application of these two features, but provided limited information on the excited spin wave modes and the effect of composite's morphology [1–3]. In this work, ferromagnetic nanocrystalline flakes and composites composed of laminated flakes and paraffine are studied. We utilize the standard Landau-Lifshitz-Gilbert equation and the modified Maxwell-Garnett formula to investigate the spin wave resonance frequencies and the effect of the orientation of flakes on the microwave spectrum of their composite. It is found that the spin wave modes are dependent on nanostructure size and surface effect. Lamination and damping effect can effectively tailor the microwave performance of flakes composites. Corresponding magnetic bounds relation is also introduced.

REFERENCES

1. Mercier, D., J.-C. S. Lévy, G. Viau, F. Fiévet-Vincent, F. Fiévet, P. Toneguzzo, and O. Acher, "Magnetic resonance in spherical Co-Ni and Fe-Co-Ni particles," *Phys. Rev. B*, Vol. 62, No. 1, 532, July 2000.
2. Zhou, P. H. and L. J. Deng, "Bounds on the dynamic magnetic properties of multiresonant nanostructure composites in exchange resonance model," *J. Appl. Phys.*, Vol. 105, 07A509, 2009.
3. Wen, F. S., H. B. Yi, L. Qiao, and F. S. Li, "Analyses on double resonance behavior in microwave magnetic permeability of multiwalled carbon nanotube composites containing Ni catalyst," *Appl. Phys. Lett.*, Vol. 92, 042507, 2008.

Micromagnetism Simulations on the Microwave Permeability of Bamboo-like Cobalt Nanowires

Mangui Han, **Li Cai**, **Jianliang Xie**, **Difei Liang**, **and Longjiang Deng**
State Key Laboratory of Electronic Thin Films and Integrated Devices
University of Electronic Science and Technology of China, Chengdu 610054, China

Abstract— Recently, there is an increasing interest in studying the dynamic magnetic properties of nanowires (NW). Among them, the dynamic permeability spectrum of NW arrays is of great importance in both fundamental and application fields. One attribute that makes this property desirable is that the eddy current loss interfering with permeability spectrum is greatly suppressed for nanowires. Another reason is that the resonance frequency of the uniform gyromagnetic mode for NW arrays can be tuned by varying the aspect ratio and material, applying dc fields, and changing the porosity of membranes in which NWs are embedded [1–4]. Here, employing the micromagnetism simulation technique, we report the dynamic permeability of a bamboo-like Co nanowire with a diameter of 40 nm, which is composed of two sections of Co nanowires separated by a non-magnetic section (10 nm). One section of nanowire has a constant length of 200 nm, while the other section of Co nanowire with a variable length from 40 nm to 200 nm, which is designed to investigate the effect of geometry of bamboo-like structure on the dynamic permeability of Co nanowires. Our results show that more than 4 permeability dispersion peaks have been found within the frequency range of 20 GHz–50 GHz. Besides, when the adjacent peaks are overlapped, the permeability dispersion peaks can be broadened. However, only two well separated permeability dispersion peaks can be found in a Co nanowire with a homogenous structure. Our simulation results show that bamboo-like nanowires can be used to tune the dynamic permeability properties. Finally, it should be noted that such a bamboo-like nanowire can be fabricated experimentally.

ACKNOWLEDGMENT

This work is financially supported by the National Basic Research Program of China (973) (No. 2010CB334702), China National Funds for Distinguished Young Scientists (No. 51025208), the Fundamental Research Funds for the Central Universities (No. ZYGX2009J036) and the Basic Research Funds of National Defense Department (No. 9140A10030409DZ0228).

REFERENCES

1. Gao, B., L Qiao, J. B. Wang, Q. F. Liu, F. S. Li, J. Feng, and D. S. Xue, *J. Phys. D: Appl. Phys.*, Vol. 41, 235005, 2008.
2. Ledieu, M., F. Schoenstein, J. H. Le Gallou, J. H. O. Valls, S. Queste, F. Duverger, and O. Acher, *J. Appl. Phys.*, Vol. 93, 7202, 2003.
3. Encinas-Oropesa, A., M. Demand, L. Piraux, I. Huynen, and U. Ebels, *Phys. Rev. B*, Vol. 63, 104415, 2001.
4. Encinas-Oropesa, A., M. Demand, L. Piraux, U. Ebels, and I. Huynen, *J. Appl. Phys.*, Vol. 89, 6704, 2001.

Miniaturized Patch Antennas with Ferrite/Dielectric/Ferrite Magnetodielectric Sandwich Substrate

Guo-Min Yang[1], **Ogheneyunume Obi**[2], **Ming Liu**[2], **and Nian X. Sun**[2]

[1]Key Laboratory of Wave Scattering and Remote Sensing Information
Department of Communication Science and Engineering
Fudan University, Shanghai 200433, China
[2]Department of Electrical and Computer Engineering
Northeastern University, Boston, MA 02115, USA

Abstract— With the continuous growth of wireless communication technologies, design and manufacturing of miniaturized microwave components are among most critical issues in communication systems. In the RF front-end, patch antennas with small size and high performance are highly desirable. Planar device size can be minimized by using a substrate with high relative permittivity. However, antennas with high-permittivity substrates result in decreased bandwidth and the excitation of surface waves, leading to lower radiation efficiency and larger element coupling in arrays. It also becomes difficult to achieve impedance matching on high-permittivity substrates, due to large reactance of the coaxial probes used to feed the antenna.

Achieving relative permeability larger than 1 ($\mu_r > 1$) in antenna substrates can lead to antenna miniaturization, enhanced bandwidth, tunable center frequency, polarization diversity, and beam steering. It is important for antenna substrates to be comprised of self-biased magnetic materials, in which no external bias field is applied. Magnetic thin films provide a unique opportunity for achieving self-biased magnetic patch antenna substrates with μ_r greater than 1and operating frequencies > 1 GHz. The strong demagnetization field for magnetic thin films, $H_{demag} = 4\pi M_s$, allows for a self-biased magnetization with high ferromagnetic resonance (FMR) frequencies up to several GHz.

In our previous work, new designs of electronically tunable patch antennas with magnetic metallic magnetic films were investigated [1]. Fielding addition, a new self-biased ferrite film of NiCo-ferrite was investigated and adopted in our recent research of antenna miniaturization [2]. In this paper, we report on patch antennas miniaturized by using Ferrite/Dielectric/Ferrite sandwich structures on the alumina substrate, thus essentially creating a magneto-dielectric substrate for practical applications. The magnetic patch antennas were fabricated by loading the antenna with a magneto-dielectric adjacent to the patch. These magnetic antennas show an enhanced bandwidth of up to 76% over the non-magnetic counterparts at 2 GHz, and a significantly enhanced gain by 2.4 dB over the non-magnetic antenna.

REFERENCES

1. Yang, G. M., X. Xing, A. Daigle, M. Liu, O. Obi, J. W. Wang, K. Naishadham, and N. X. Sun, "Electronically tunable miniaturized antennas on magnetoelectric substrates with enhanced performance," *IEEE Trans. Magn.*, Vol. 44, No. 11, 3091–3094, Nov. 2008.
2. Yang, G. M., X. Xing, A. Daigle, O. Obi, M. Liu, J. Lou, S. Stoute, K. Naishadham, and N. X. Sun, "Planar annular ring antennas with multilayer self-biased NiCo-Ferrite films loading," *IEEE Trans. Antennas Propag.*, Vol. 58, 648–655, Mar. 2010.

Tunable High Frequency Permeability of Metamaterials

Shunlin Zhong, **Mangui Han**, **Jianliang Xie**, **Difei Liang**, **and Longjiang Deng**
State Key Laboratory of Electronic Thin Films and Integrated Devices
University of Electronic Science and Technology of China, China

Abstract— The permeability of magnetic materials is critical for many high frequency magnetic devices. However, permeability values of traditional materials are very strongly dependent on their composition and microstructures [1–4], which are unchangeable once the materials have been fabricated and been made into devices. Sometimes, tunable permeability dispersion behaviors are demanded for applications where "smart" materials are required [5, 6]. In this paper, we proposed one type metamaterial structure with tunable permeability by electric voltage. In this structure, a capacity-variable diode was imbedded into a split ring resonator (SRR). Our results show that the effective capacitance of such a SRR element can be varied by the biased voltage of diode. Thereby, the resonance frequency and effective permeability of a SRR element can be tuned. Based on these results, a smart microwave magnetic metamaterial has been proposed. Employing HFSS software, the variations of resonance frequency and permeability of the SRR element has been simulated and calculated by changing the biased voltage. It is found that with the decreasing of capacitance due to the increasing biased voltage, the resonance frequencies are shifted toward lower values, and so do the resonance frequencies of permeability dispersion.

ACKNOWLEDGMENT

This work is financially supported by the National Basic Research Program of China (973) (No. 2010CB334702), China National Funds for Distinguished Young Scientists (No. 51025208), the Fundamental Research Funds for the Central Universities (No. ZYGX2009J036) and the Basic Research Funds of National Defense Department (No. 9140A10030409DZ0228).

REFERENCES

1. Lubitz, P. and F. J. Rachford, *J. Appl. Phys.*, Vol. 91, 7613, 2002.
2. Chen, W. B., M. G. Han, and L. J. Deng, *Acta Phys. Sin.*, Vol. 60, 712, 2010.
3. Li, Z. W., L. Chen, and C. K. Ong, *J. Appl. Phys.*, Vol. 94, 5918, 2003.
4. Tsutaoka, T., *J. Appl. Phys.*, Vol. 93, 2789, 2003.
5. Boardman, A. D., et al., *Laser & Photonics Review*, Vol. 5, 287, 2011.
6. Ekmekci, E., et al., *Optics Express*, Vol. 17, 16046, 2009.

A Comparative Study of Electromagnetic Interference Shielding Effectiveness of Carbon Nanotube Composites

Ping Li[1], **Xijiang Yin**[1], **Yueyan Shan**[2], **Junhong Deng**[3], **and Jin Lin**[1]

[1]Advanced Materials Technology Centre, Singapore Polytechnic, Singapore
[2]National Metrology Centre, A*Star, Singapore
[3]TUV SUD PSB, Singapore

Abstract— In this electronic era, electromagnetic interference (EMI) is known to cause the malfunction of electronic equipment, communication interference, leakage of sensitive business information and adverse health effects. Therefore, there is a strong demand for the application of EMI shielding technologies to safeguard public safety, security, health and environment. The use of conductive coatings and adhesives is one of convenient and effective approaches. They can be applied with utmost flexibility and large area to both the interior and exterior of electric and electronic enclosures to shield against EMI pollution. In this study, EMI shielding effectiveness of multi-walled carbon nanotube-filled composites were investigated in the frequency range of 30 M to 5 GHz. It was observed that the shielding effectiveness of composites was related to dimension and loading of carbon nanotube as well as the applied frequency range. At the same filler loading, small diameter carbon nanotube-filled composites exhibited higher shielding effectiveness compared to those filled with large diameter carbon nanotubes. The carbon nanotubes were more effective in high frequency range (> 2 GHz) than low frequency range (< 1 GHz). The results showed that the shielding effectiveness of the composite containing 8 wt% carbon nanotubes could achieve more than 26–28 dB, implying that such a composite have good potential for EMI shielding application. The EMI shielding effectiveness of different carbon nanotube-filled composites were comparatively studied.

ACKNOWLEDGMENT

This research is supported by Innovation Fund granted by Singapore Ministry of Education (MOE-2010-IF-1-018).

Development of Promising Magneto-dielectric Materials for Low Frequency Applications

L. B. Kong, Z. W. Li, Z. H. Yang, and L. Liu
Temasek Laboratories, National University of Singapore, 5A Engineering Drive 1, 117411, Singapore

Abstract— Antennas of HF (2–30 MHz) and VHF (30–90 MHz and 100–300 MHz) bands usually have rather large physical sizes. Miniaturization of HF and VHF antennas has been a challenge to designers. It is desired to reduce the physical dimensions of antennas, while their electrical dimensions are still maintained. Physically, magneto-dielectric materials, with matching permeability and permittivity can be used to shrink the physical dimension of antennas. During last several years, great achievements have been made in developing magneto-dielectric materials based on ferrite ceramics. For example, by doping with CuO and Bi_2O_3, $MgFe_2O_4$ ceramics can be modified to have almost equal values of permeability and permittivity, as well as sufficiently low magnetic and dielectric loss tangents, over 2–30 MHz. Similar technique has been applied to $Li_{0.5}Fe_{2.5}O_4$ ceramics, which have higher permeability and permittivity. Ni-Zn ferrites have promising magneto-dielectric properties with low loss frequencies of up to 100 MHz. By employing nanotechnology, Ni-Zn-Co ferrite nanosized ceramics have been developed, whose low loss frequencies have been pushed up to 500 MHz. There has also been report on fabrication of miniaturized T-DMB antenna, with low loss magneto-dielectric Ni-Mn-Co ferrite ceramics, for mobile handset applications. This review will summarize the recent progress in fabrication, characterization and application of such magneto-dielectric materials for antenna miniaturization.

Enhanced Microwave Absorption Properties of the Planar Metamaterials Structure and Absorber Slice Composites

Liang Qiao, **Tao Wang**, **Rui Han**, **Zhaoqi Zhang**, **and Fashen Li**
Institute of Applied Magnetism
Key Laboratory for Magnetism and Magnetic Materials of Ministry of Education
Lanzhou University, Lanzhou 730000, China

Abstract— In recent years, with the fast advancement of wireless communication, the absorbers of electromagnetic wave are becoming increasingly important in both civil and military applications. In generally, both small matching thickness and low reflectivity are the most important parameters for EM-absorbers [1]. Utilization of the Planar Metamaterials structures is becoming attractive in the electromagnetic and antenna community [2–5]. But few people pay attention to apply this novel structure on the surface of EM-absorber to improve impedance matching and enhance the microwave absorbing properties. In the present study, we have investigated the EM-absorber with the Planar Metamaterials structure. The EM-absorber is made of carbonyl-iron particles dispersed in epoxy resin matrix, while the Planar Metamaterials structure consists of nanocrystalline FeCuNbSiB rings which is packed in a square array. This new method for betterment of the absorption can trap microwave inside and decrease the matching thickness and reflectivity. In comparison, the microwave properties of different thickness of EM-absorber with and without the Planar Metamaterials structure are also presented. The optimal EM Reflection loss $RL = -32\,\mathrm{dB}$ is obtained at 3.8 GHz for the Planar Metamaterials structure on the surface of EM-absorber with thickness 3.44 mm (thick slice). Meanwhile, the EM-absorber without the Planar Metamaterials structure show that the Reflection loss is just $-25\,\mathrm{dB}$. Through simulation and analyzing the relationship, we find that the mechanism mainly due to the strong mutual coupling between the Planar Metamaterials structure and EM-absorber.

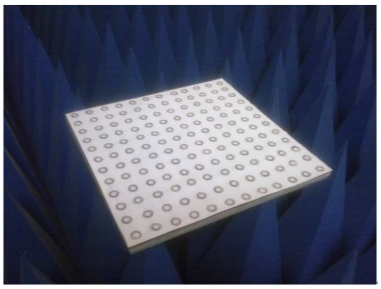

Figure 1: Array of printed rings on the absorber slice by ground plane.

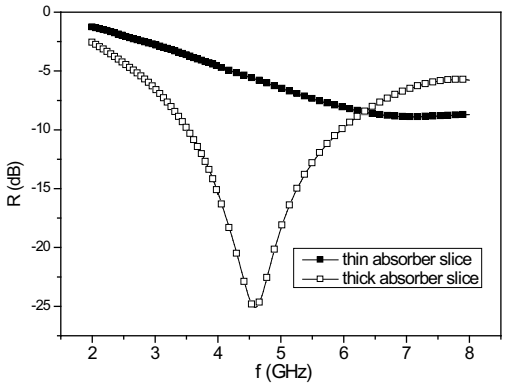

Figure 2: The frequency dependence of the Reflection loss of the thick and thin absorber slice. The relationship between reflection loss and matching thickness can be understood based on quarter-wave principle. With the increase of the thickness of slice, the corresponding matching frequency and reflection loss decrease.

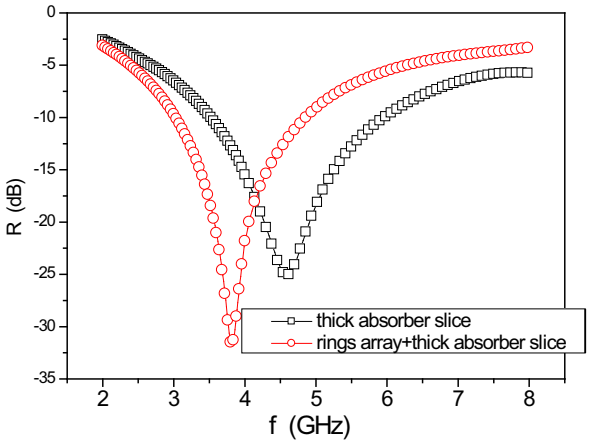

Figure 3: The Reflection loss of the thick absorber slice with and without rings array. With the rings array, the strong mutual coupling between the rings and the absorber slice decrease the corresponding matching frequency and reflection loss.

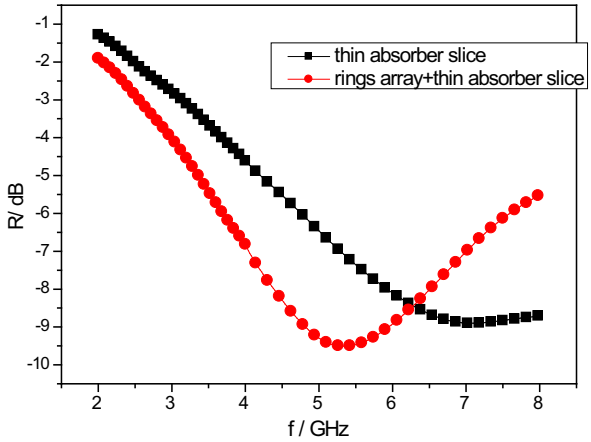

Figure 4: The Reflection loss of the thin absorber slice with and without rings array. It further corroborates the strong mutual coupling between the rings and the absorber slice.

REFERENCES

1. Rozanov, K. N., "Ultimate thickness to bandwidth ratio of radar absorbers," *IEEE Trans. Antennas Propag.*, Vol. 48, 1230, 2000.
2. Rahmat-Samii, Y. and H. Mosallaei, "Electromagnetic band-gap structures: Classification, characterization and applications," *Proc. Inst. Elect. Eng.-ICAP Symp.*, 560–564, Apr. 2001.
3. Sievenpiper, D., L. Zhang, R. F. J. Broas, N. G. Alexopolus, and E. Yablonovitch, "High-impedance electromagnetic surfaces with a forbidden frequency band," *IEEE Trans. Microwave Theory Tech.*, Vol. 47, 2059–2074, Nov. 1999.
4. Sievenpiper, D., J. Schaffner, B. Loo, G. Tangonan, R. Harold, J. Pikulski, and R. Garcia, "Electronic beam steering using a varactor-tuned impedance surface," *Proc. IEEE AP-S Dig.*, Vol. 1, 174–177, Jul. 2001.
5. Barlevy, A. S. and Y. Rahmat-Samii, "Characterization of electromagnetic band-gaps composed of multiple periodic tripods with interconnecting vias: Concept, analysis, and design," *IEEE Trans. Antennas Propagat.*, Vol. 49, 343–353, Mar. 2001.

Session 3A7
Poster Session 4

Optical Single Sideband Modulation Using Feedback Technique Based on SBS Effect in Fiber

P. H. Hsieh[1], **W. S. Tsai**[1], **Z. S. Lin**[1], **and H. H. Lu**[2]

[1]Department of Electrical Engineering, Ming Chi University of Technology
84 Gungjuan Rd., Taishan, Taipei 24301, Taiwan
[2]Department of Electro-Optical Engineering, National Taipei University of Technology
1, Sec. 3, Chung-Hsiao E. Rd., Taipei 10608, Taiwan

Abstract— We propose an optical single sideband (OSSB) modulation scheme using stimulated Brillouin scattering (SBS) to achieve OSSB modulation in fiber. Driving with 10.87 GHz RF signal into Mach-Zehnder modulator (MZM), due to the SBS effect, lower sideband of modulated signal is amplified and upper sideband is attenuated as well. By properly adjusting the phase shifter for phase difference between the two paths of electrical signal, output signal is OSSB format. After 25 km and 50 km SMF transmission, we can observe good system performances including sideband power ratio (SBPR) >12 dB and 10 dB, phase noise < -71 dBc/Hz and < -65 dBc/Hz measured by an optical spectrum analyzer (OSA) and an electrical spectrum analyzer (ESA), respectively.

Optical Single Sideband Modulation of 9-GHz RoF System Based on FWM Effects of SOA

P. H. Hsie[1], **W. S. Tsai**[1], **C. C Weng**[1], **and H. H. Lu**[2]

[1]Department of Electrical Engineering, Ming Chi University of Technology
84 Gungjuan Rd., Taishan, Taipei 24301, Taiwan
[2]Department of Electro-Optical Engineering, National Taipei University of Technology
1, Sec.3, Chung-Hsiao E. Rd., Taipei 10608, Taiwan, R.O.C.

Abstract— We propose an optical single sideband (OSSB) modulation scheme using self-phase modulation (SPM), cross-phase modulation (XPM) and four-wave mixing (FWM) effects of semiconductor optical amplifier (SOA) to achieve wavelength conversion. Drive with the 9 GHz RF signal into electro-absorption modulator laser (EML) and IM modulator. By properly adjust the phase shifter for phase difference between the two paths of electrical signal. FWM signal is OSSB format for a 25 km SMF transmission. We use an optical spectrum analyzer (OSA) to observe optical spectrum. Optical amplifier plays an important role in a long haul fiber transmission system, the use of SOA as an optical amplifier is very attractive since it can potentially be used to help upgrade fiber penetration, easily integrated and small compact. In this letter, we propose an OSSB modulation scheme using SPM, XPM and FWM effects of SOA to achieve wavelength conversion. The translation wavelength possessing OSSB modulation format can prevent fiber dispersion induced RF signal fading. Using the phase modulation effects in SOA to generate OSSB format is relatively simple to implement. It only needs SOA and electrical phase shifter to construct the OSSB system instead of a complex circuit or device to exploit the Hilbert transform of the conventional OSSB systems. Using this method to construct the OSSB system can substitute a complex circuit or device to exploit the Hilbert transform of the conventional OSSB system. In the future work, we can enhance the wavelength conversion efficiency and transmit digital signal in our proposed OSSB system.

Dynamic Characterization of EDFA Based on ASE Selective-feedback and Gain-clamping Techniques

Jhe-Min Lin, **Wen-Jeng Ho**, **and Chih-Yung Li**
Institute of Electro-Optical Engineering, National Taipei University of Technology
1, Sec. 3, Chung-Hsiao E. Rd., Taipei 106, Taiwan

Abstract— We proposed a wide dynamic range and low noise figure (NF) gain-clamped erbium-doped fiber amplifier (EDFA) with a stable performance by using the feedback loop technique which consisted of a fiber Bragg grating (FBG), an optical coupler, an optical circulator (OC) and a variable optical attenuator (VOA). Because the optical amplifiers for DWDM applications need not only had more channels bandwidth and gain flatness, but also consider the gain variation as adding or dropping the channels to the system. Thus the gain stability and gain flatness for EDFA are important characteristics in DWDM system.

In this work, we investigated firstly the gain and NF of gain-clamped EDFA as a function of the optical input signal power at different values of attenuation in the optical feedback loop. The flat and wide-band gain curves and NF of the proposed scheme are obtained at the attenuation values from 0 to 5 dB. Experimental results show that the gain of 16.2 dB with variation ±0.26 dB and the maximum NF of 6.6 dB (5.2–6.6 dB) were obtained for input signal power from −35 to −5 dBm. Therefore, a wide dynamic range of input signal of 30 dB is achieved. Then we applied a saturation-tone signal (on/off) to simulated a 16-channel DWDM signal (add/drop) to investigate the gain variation of probe signal through gain-clamped EDFA as channel signals adding or dropping to system. We obtained the gain variation of smaller than of 0.13 dB from the wavelength range of 1530 to 1560 nm.

In summary, a wide dynamic range and low noise figure C-Band gain clamped erbium-doped fiber amplifier based on ASE selective feedback and gain clamping was proposed and demonstrated. The proposed scheme is a simple and effective approach to provide a good gain clamping as well as a gain flattening and ultra stable dynamic performance.

ACKNOWLEDGMENT

The authors would like to thank the financial support from the National Science Council under Grant NSC 99-2622-E-027-030-CC3.

Generation and Transmission Characterization of Sub-picoseconds 1550 nm Optical RZ-pulse

Jheng-Jie Liu, **Wen-Jeng Ho**, **Jhe-Min Lin**, **Yi-Chia Hsieh**, **Hsuan-Ming Tang**, **and Yu-Feng Yang**
Institute of Electro-Optical Engineering, National Taipei University of Technology
1, Sec. 3, Chung-Hsiao E. Rd., Taipei 106, Taiwan

Abstract— In this paper, we experimentally demonstrated the 1550 nm optical RZ-pulse by using a RF-drive gain-switching distribution feedback (DFB) semiconductor laser, a fiber ring self-injection locking and NRZ-modulating techniques to generate a sub-picoseconds pulse train. To achieve high speed and high capacity operation, the high-bit-rate optical time division multiplexing/wavelength division multiplexing (OTDM/WDM) systems are very important for this target. Because multiplexed the optical pulses with a sufficiently narrow width would be greatly increased the transmission capacity. Therefore, some transmission performance's requirements in the optical time domain for the pulse signal are not only in high peak power but also in the smallest timing jitter. In general, RZ-pulse signal was preferred than NRZ one. On the other hand, the signal with a high side mode suppression ratio (SMSR) was also needful as used a gain-switching technique to generate an optical pulse due to reducing the timing jitter. Firstly, the gain-switching used in this work is carried out by combining a DC bias current of 10 mA and a RF signal of 15 dBm at 2.5 GHz for driving a DFB laser. The generated optical pulse from DFB laser is coupled into a 2×2 coupler through a polarization controller. The output of coupler was then amplified by an EDFA and filtered by a tunable optical filter to eliminate ASE noise. The filtered signal after through an optical attenuator (VOA), which controlled the injection ratio to DFB laser, was injected to a DFB diode, we called this approach was a fiber ring self-injection locking. The obtained short pulse of 60 ps was next modulated by a MZ-modulator with a 2.5 Gbit/s, $2^7 - 1$, NRZ format to generate RZ-pulses. The optical RZ-pulses generated from the proposed experimental setup were characterized by using an Optical Spectrum Analyzer (ADVENTEST Q8384) with a resolution of 0.02 nm and a 40 GHz Digital Communication Analyzer (Agilent 86100C). Finally, the bit error rate measurement was performed over the transmisstance distance of 50 km fiber link. At BER = 10^{-9}, the receiver power of -19.5 dBm and power penalty of 3.4 dB were obtained.

ACKNOWLEDGMENT

The authors would like to thank the financial support from the National Science Council under Grant NSC 99-2622-E-027-030-CC3.

Synthesis and Up-conversion Luminescence of $NaYF_4$:Yb^{3+}, Er^{3+}/PVP Nanotube

Peng Zou, **Xia Hong**, **and Yichun Liu**
Centre for Advanced Optoelectronic Functional Materials Research
Key Laboratory of UV Light-Emitting Materials and Technology
Ministry of Education, Northeast Normal University, Changchun 130024, China

Abstract— Drug releases and tracing technologies have attracted significant attention in drug delivery systems [1, 2]. Among the candidates of release materials, the nanotubular polyvinylpyrrolidone (PVP) that encapsulated drugs inside the polymer and provided a prolonged supply has been applied wildly in the bio-pharmaceutical due to its prominent structure and properties, such as non-toxicity, biocompatibility, solubility, hydrotropy and the property of complexation [3–5]. The limited properties of polymers, however, restrict their applications in drug tracing. It is well known that the rare-earth doped $NaYF_4$ up-conversion (UC) luminescence materials can lead to less photo damage to living organisms, weak background fluorescence, and deep detection range. It makes them ideal fluorescent labels for biological applications [6, 7]. If PVP nanotubes combine with rare-earth doped $NaYF_4$ nanoparticles, the wider potential applications including drug release and UC luminescence tracing in real time will be offered.

In the present work, the $NaYF_4$:Yb^{3+}, Er^{3+}/PVP nanotubes were synthesized successfully via electrospinning method. The average diameters of nanotubes were 280, 430 and 550 nm when the electrospinning voltages were 13, 10 and 7 kV, respectively. Comparing with the up-conversion (UC) luminescence properties of pure $NaYF_4$:Yb^{3+}, Er^{3+} nanoparticles (20 nm) under 980-nm excitation, the blue and green emissions of the composite nanotubes corresponding to $^2H_{9/2}-^4I_{15/2}$ and $^4S_{3/2}-^4I_{15/2}$ are stronger. In addition, the intensity ratios of $^4S_{3/2}-^4I_{15/2}$ to $^2H_{9/2}-^4I_{15/2}$ were changed with the electrospinning voltages. The energy transfer and non-radiative relaxation process of $NaYF_4$:$Yb^{3+}Er^{3+}$/PVP nanotubes are discussed. The multifunctional nanotubes are expected to display an important role for both fundamental studies and technological applications.

REFERENCES

1. Cheong, A. I. and X. Huang, *Science*, Vol. 24, 1308–1311, 2006.
2. Suh, b. J. and M. Dawson, *Adv. Drug Deliv. Rev.*, Vol. 57, 63–78, 2005.
3. Lau, A. I. F. and S. K. Saksena, *Prostaglandins*, Vol. 9, 893–900, 1975.
4. Charoo, B. N. A. and Z. Rahman, *Curr. Drug Deliv.*, Vol. 7, 125–136, 2010.
5. Lu, C. X. and C. Wang, *Small*, Vol. 5, 2349–2370, 2009.
6. Xiong, A. L. and Z. Chen, *Anal. Chem.*, Vol. 81, 8687–8694, 2009.
7. Wang, B. M. and C. Mi, *ACS Nano*, Vol. 3, 1580–1586, 2009.

Output Power Increment in an Yb-doped Fiber Amplifier by Inserting an Additional Unpumped Yb Doped Fiber

Hoon Jeong, **Hyoyeong Park**, **Seungtaek Kim**, **Sungbok Kang**, **and Jongseok Kim**
Manufacturing System R&D Department, Korea Institute of Industrial Technology, South Korea

Abstract— Master oscillator power amplifier (MOPA) technology has been widely used in high power or ultrashort-pulse fiber laser systems because the shape of laser pulse can be easily adjusted. Usually the first amplification stage of a 1064 nm fiber laser uses the core-pumped Yb-doped fiber amplifier (YDFA), but the gain or output power will be limited due to the strong amplifier spontaneous emission (ASE) in 1030 nm band. This paper presents the improved output power in an YDFA by inserting an additional un-pumped Yb doped fiber which absorbs the lost backward ASE emitted from the pump end. We achieved more than 10% increment of the output power in a low-power signal and the increment of the output power was decreased as the signal power increased. Moreover, inserting an additional unpumped Yb doped fiber restricted the unwanted 1030 nm lasing and increased the noise figure effectively in a low-power signal. We confirmed, therefore, that the inserting an additional unpumped Yb doped fiber in an YDFA is effectively increased the output power and noise figure by utilizing the lost backward ASE.

Efficient Generation of Broadband High-count Channels with Full Duty Cycle Amplitude Sampled Fiber Bragg Gratings

Xiaojun Zhu, **Chinhua Wang**, **Jing Ge**, **and Shixin Liu**
Key Lab of Modern Optical Technologies of Jiangsu Province
Institute of Modern Optical Technologies, Soochow University, Suzhou 215006, China

Abstract— Fiber gratings have found important applications in optical communication and fiber-sensing systems. Among the many applications, the increasing demand on the number of wavelength channels has attracted considerable interests in the design and implementation of multichannnel devices based on sampled fiber Bragg gratings (SFBGs) [1]. Two types of sampled fiber Bragg gratings are most frequently employed in practice, i.e., amplitude sampled fiber Bragg grating (ASFBG) and phase-only sampled fiber Bragg grating (PSFBG). The main drawback of the conventional ASFBG is the trade-off between the spectral range and the channel energy efficiency according to Fourier transform in which the spectral range in frequency domain is inversely proportional to the duty cycle in each sampling period. The more the output channel, the smaller the duty cycle, which directly results in the very low energy efficiency when an ASFBG is employed in a conventional way since a large portion of the fiber is absent of the grating. An interleaved structure was proposed to improve the fiber utilizing efficiency by inserting two or three sets of wavelength shifted ASFBGs to the grating-absent portion [2]. Although the channel density can be increased by the interleaving structure, it does not improve the energy efficiency since duty cycle of each set of ASFBG does not change. The most attractive feature of phase-only sampled FBGs (PSFBGs) is the high energy efficiency [3]. It has been estimated that for phase-only SFBGs, the peak refractive index modulation Δn must be increased by a factor of $\sqrt{N}$ only as opposed to N in the conventional ASFBGs in order to increase the number of wavelength channels N within a given bandwidth. The enhancement of the energy efficiency is, however, at the expense of increasing significantly the fabrication complexity. Recently, it has been shown that the multi-channel generation can be implemented by exploiting Talbot effect in sampled and chirped FBGs, in which the channel density (or free spectral range, FSR) can be effectively multiplied by changing the chirp coefficient with no need to change the sampling period as the case in conventional SFBGs [4]. It is shown that the similar energy efficiency to the case for phase-only SFBGs can be obtained using the amplitude sampled and chirped FBGs based on spectral Talbot effect, i.e., reducing the wavelength channel spacing (FSR) by a factor N requires Δn to be increased by approximately $\sqrt{N}$ in order to maintain the same peak reflectivity (per channel), which is a significant progress in energy efficiency improving in the type of ASFBGs. However, when we examine the structure of an ASFBG used under condition of Talbot effect, it is found that the duty cycle of each sampling period must also be kept small (< 0.2–0.3) in order to obtain clean multi-channel outputs (the uniformity of the amplitude and eliminate the spectral aberrations) [5, 6], which also results in low energy efficiency and the practical application is thus very limited. It is also noted that the energy enhancement in each channel in Talbot-based ASFBGs cannot be obtained by increasing the grating length due to the energy saturation caused by the grating chirp. The Talbot effect in PSFBGs for multi-channel generation has also been proposed [7] to enhance the energy efficiency with a limited fiber length. It is shown that, under the Talbot condition, the PSFBGs using less phase transitions is capable of generating superior high-count DWDM channels with high energy efficiency. Nonetheless, the manufacturing difficulty of PSFBGs still remians.

In this paper, we propose a novel ASFBG structure that has a full duty cycle ($= 1$) for efficient generation of broadband high-count channels operated under spectral Talbot effect. This structure integrates advantages of amplitude sampled FBGs (easy and straightforward making), phase-only sampled FBGs (high energy efficiency and short fiber length) and Talbot effect (inherit high efficiency in high-count channel output and arbitrily FSR tuning). It is shown that the energy efficiency of the structure is almost comparable to that of the PSFBGs with the same fiber length (no Talbot). The direct use of a simple Gaussian beam profile or combination of Gaussian profile yields high uniformity, high isolation and high-count channel outputs.

REFERENCES

1. Eggleton, B., P. A. Krug, L. Poladian, and F. Oullette, "Long periodic superstructure Bragg gratings in optical fibres," *Electron. Lett.*, Vol. 30, 1620–1622, 1994.

2. Castro, J. M., J. E. Castillo, R. Kostuk, C. M. Greiner, D. Iazikov, T. W. Mossberg, and D. F. Geraghty, "Interleaved sampled Bragg gratings with concatenated spectrum," *IEEE Photon. Technol. Lett.*, Vol. 18, 1615–1617, 2006.
3. Li, H., M. Li, and J. Hayashi, "Ultrahigh-channel-count phase-only sampled fiber Bragg grating covering the S, C, and L bands," *Opt. Lett.*, Vol. 34, 1938, 2009.
4. Wang, C. H., J. Azaña, and L. R. Chen, "Spectral Talbot-like phenomena in one-dimensional photonic bandgap structures," *Opt. Lett.*, Vol. 29, 1590–1592, 2004.
5. Azaña, J., C. H. Wang, and L. R. Chen, "Spectral self-imaging phenomena in sampled Bragg gratings," *J. Opt. Soc. Am. B*, Vol. 22, 1829–1841, 2005.
6. Chen, L. R. and J. Azaña, "Spectral Talbot phenomena in sampled arbitrarily chirped Bragg gratings," *Opt. Com.*, Vol. 250, 302–308, 2005.
7. Lu, Y., X. Zhu, C. Wang, and G. Zhang, "Broadband high-channel-count phase-only sampled fiber Bragg gratings based on spectral Talbot effect," *Opt. Express*, Vol. 16, 15584–15594, 2008.

Influence of Grating Period of Uniform Fiber Bragg Grating on Slow Light Delay

Shanglin Hou[1], **Yunbo Shang**[1], **Yanjun Liu**[1], **Jingli Lei**[1], **and Yongzhao Xu**[2]

[1]School of Science, Lanzhou University of Technology, Lanzhou, Gansu 730050, China
[2]Institute of Electronic Engineering, Dong Guan University of Technology
Dongguan, Guangdong 523808, China

Abstract— Fiber Bragg grating has developed dramatically and performed an important role in fiber communications and optical fiber sensing in recent 30 years. Recently, the introduction of slow light with a wide range of novel properties results in unique spectral characteristics of fiber Bragg gratings, especially slow light delay of fiber Bragg grating is studied emphatically. K. B. Rochford and S. D. Dyer reported reconstruction of minimum-phase group delay from fiber Bragg grating transmittance or reflectance measurements. The results indicate that phase reconstruction is compared to exact solutions using the reflectance from a uniform grating. An intermediate windowing process improves the recovery accuracy. J. T. Mok, ect. observed 0.68 ns pulses delayed by 4.7 pulse widths in a 30 cm silica FBG without pulse broadening. Improved slow-light delay performance of a broadband SBS system using fiber Bragg grating was reported. Tunable delay slow-light in an active fiber Bragg grating was also studied. These studies provide a very simple approach to control the light group delay. However, this approach requires very high power signal, which limits its practical implications.

The influence of grating period of uniform fiber Bragg grating on delay is discussed by using numerical simulation method based on the coupled mode theory and slow light delay characteristics is studied by parameters optimization. The calculated result shows that grating period has a remarkable impact on the delay this grating, between the reflection spectra and delay $_{\max}$ curve are blue-shifted, peak top become flattened and the bandwidth change broaden, the maximum value of the delay is 17.3013 μs occurs at the Bragg wavelength with $\Lambda = 0.5317\,\mu$m, especially slow light delay is an exponentially decaying of rapidly shocks. This provides basis references for designing slow light components based on fiber Bragg gratings.

Influence of SBS Gain Coefficient on Time Delay and Pulse Broadening in Fibers

Shanglin Hou[1], **Zhongyi Wang**[1], **Yunbo Shang**[1], **Yanjun Liu**[1], **Jingli Lei**[1], **and Yongzhao Xu**[2]

[1]School of Science, Lanzhou University of Technology, Lanzhou, Gansu 730050, China
[2]Institute of Electronic Engineering, Dong Guan University of Technology
Dongguan, Guangdong 523808, China

Abstract— The fiber-based stimulated Brillouin scattering coupled equations were solved by the method of implicit finite difference with prediction-correction. The influence of the Brillouin gain coefficient on time delay and pulse broadening was investigated within the gain range of $0 \sim 16$. The result indicates that the time delay and the pulse broadening factor increase with increasing gain in the small signal regime and decrease in the gain saturation regime. However, the Stokes pulse will reach gain saturation at a larger gain for smaller gain coefficient and its maximum time delay is accordingly larger.

Dual-concentric-core Photonic Crystal Fibers with Multi Outer Core Rings

I-Hung Tsai[1], **Der-Li Ye**[1], **and Jui-Ming Hsu**[1, 2]

[1]Department of Electro-Optical Engineering, National United University
Miaoli, Taiwan 360, Taiwan R.O.C.
[2]Optoelectronics Research Center, National United University
Miaoli, Taiwan 360, Taiwan R.O.C.

Abstract— To elastically design a dual-concentric-core photonic crystal fiber (DCC-PCF) for dispersion compensation, we use multi-layers of cladding holes as outer core rings. For a DCC-PCF structure, the outer core ring with smaller-diameter air holes separates the cladding region into inner and outer cladding. The mode-couple between inner and outer modes then results in a negative dispersion of the fiber. Figures 1(a) and 1(b) indicate the cross-sectional view of the 1-ring DCC-PCF (previous structure) and 3-ring DCC-PCF (proposed structure), respectively. In previous structure with single outer core ring, the designer is difficult to give well consideration to wavelength-adjusting and maximum dispersion coefficient simultaneously. In this study, we design the sizes of air holes at each layers of outer core ring deliberately. By using multi-layers of outer core ring, the maximum value of dispersion coefficient can be hold while the adjustment of the compensated wavelength is unrestricted. The design-elasticity enlarges the negative chromatic dispersion significantly. Figure 2 shows the dependence of the chromatic dispersion coefficient on wavelength for the structure of 1-ring (previous) and 3-ring (proposed) DCC-PCF. As shown in the figure, the 1-ring DCC-PCF has a minimum chromatic dispersion of about $D \approx -7700$ ps/km-nm whereas the 3-ring DCC-PCF has a minimum chromatic dispersion of about $D \approx -10500$ ps/km-nm at around a wavelength of 1.55 μm. Thus, the negative chromatic dispersion of the proposed structure is approximately 1.36 times larger than the former.

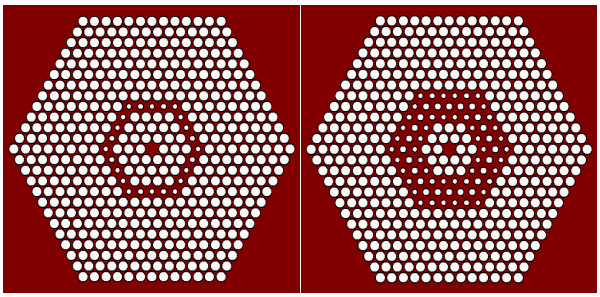

Figure 1: Cross-sectional view of (a) 1-ring DCC-PCF and (b) 3-ring DCC-PCF.

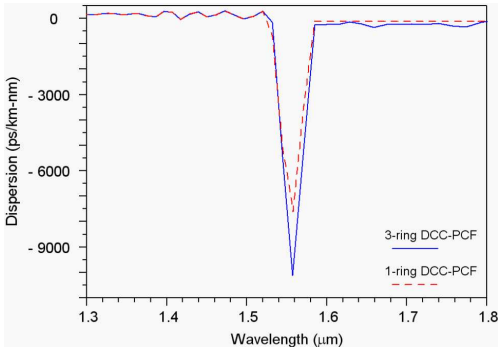

Figure 2: Dependence of the chromatic dispersion on wavelength for 1-ring and 3-ring DCC-PCF.

Polarization-maintaining Photonic Crystal Fiber with Ultra-high Modal Birefringence

Jui-Ming Hsu[1, 2] **and Der-Li Ye**[1]

[1]Department of Electro-Optical Engineering, National United University
Miaoli 360, Taiwan, R.O.C.
[2]Optoelectronics Research Center, National United University
Miaoli 360, Taiwan, R.O.C.

Abstract— To achieve a Polarization-maintaining photonic crystal fiber (PM-PCF) with ultra-high modal birefringence, three types of photonic crystal fiber (PCF) geometric structure (Figure 1) are simulated and compared with each other. Figure 1(a) shows the cross-sectional view of PM-PCF with eight large-holes (type I). Four pairs of large-holes with a diameter larger than that of the cladding-holes are situated at both sides of the core. The cross-sectional view shown as Figure 1(b) is a PM-PCF with ten large-holes (type II). The pitch and the diameters of cladding-holes and large-holes of type II are identical with type I while the five large-holes at each side touch side-by-side with each other inseparably. Figure 1(c) indicates the cross-sectional view of PM-PCF (type III) with two air-slabs, which is called as Air-Walls in this paper. The pitch and the diameter of cladding-holes of type III are the same as types I and II, the thickness of Air-Walls is identical with the diameter of large-holes of types I and II. Figure 2 compares the modal birefringence of these three types of PM-PCF. As shown in Figure 2, the birefringence value of type III is largest in the three types of structure, but the fabrication of the Air-Wall is quite difficult. We can choose type II as a compromising approach because its modal birefringence just less than type III slightly; nevertheless, its fabrication process is considerably simpler than that of type III. Finally, to shift the wavelength of peak-birefringence (refer to Figure 2) to habitual wavelength of optical-fiber communications, we shrink the geometric structure of type II properly. For the eventual proposed PM-PCF, the birefringence value at $\lambda = 1544.6\,\text{nm}$ is up to 26.98×10^{-3}.

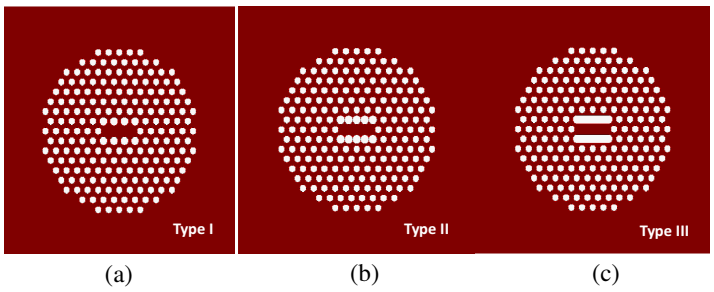

Figure 1: Cross-sectional view of PM-PCF with (a) 8 Large-holes, (b) 10 Large-holes and (c) Air-Wall structures.

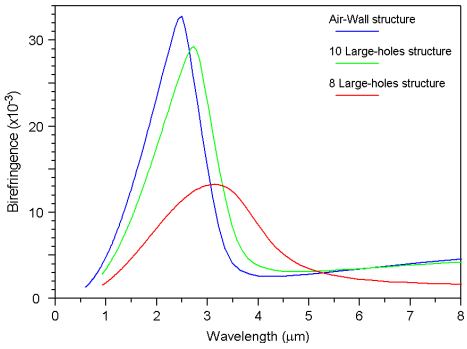

Figure 2: Dependence of birefringence on wavelength for PM-PCFs shown in Figure 1.

Dual-core Fiber for Temperature/Pressure Sensing

Daru Chen[1, 2], **Ming-Leung Vincent Tse**[1], **and H. Y. Tam**[1]

[1]Photonics Research Centre, Department of Electrical Engineering
The Hong Kong Polytechnic University, Hung Hom, Kowloon, Hong Kong SAR, China
[2]Institute of Information Optics, Zhejiang Normal University, Jinhua 321004, China

Abstract— A novel dual-core fiber (DCF) is proposed for temperature/pressure sensing. The DCF-based temperature/pressure sensor is simply formed by splicing a segment of DCF to two segments of single mode fibers (SMFs) by matching the fiber core of SMFs to one fiber core of the DCF on one side and to another fiber core of the DCF on the other side. When a broadband light is injected into the DCF-based temperature/pressure sensor, an output spectrum with a sine-function-like profile is observed because of the mode coupling between the two fiber cores of the DCF. The mode coupling between two fiber cores of the DCF is sensitive to the temperature/pressure-induced index change (due to the thermooptic effect or the photoelastic effect), which ensures the detection of the temperature/pressure applied to the DCF. Simulations show that there is a linear relationship between the temperature/pressure and the wavelength shift of the output spectrum of the DCF-based temperature/pressure sensor. In this paper, two DCFs are designed for the temperature sensor and the pressure sensor, respectively. For the DCF used for temperature sensing, two fiber cores are employed in the cross-section of the DCF. The DCF-based temperature sensor can be used for high temperature sensing with a measurement range limited by the melting point of the silica. For the DCF used for pressure sensing, two fiber cores and two air holes are employed in the cross-section of the DCF. Two large air holes are used to enhance the pressure-induced index change for the DCF which essentially provides a built-in transducing mechanism to enhance the sensitivity for the DCF-based pressure sensor. For both the temperature and the pressure sensing application, DCFs with different parameters are investigated in our paper.

Toughened Epoxy Filled with Ferromagnetic Particles as High Temperature Resistant Microwave Absorbing Coating

Zhenjiang Song, **Jianliang Xie**, **Jianing Peng**, **Peiheng Zhou**, **and Longjiang Deng**
State Key Laboratory of Electronic Thin Films and Integrated Devices
University of Electronic Science and Technology of China, Jianshe Road, Chengdu 610054, China

Abstract— In this work, microwave absorbing coatings consisted of toughened epoxy with polyurethane filled with ferromagnetic particles were prepared. The epoxy groups and isocyanate groups were investigated by Fourier Transform Infrared (FTIR). Mechanical properties of the coatings are effectively improved comparing to the one employing unmodified epoxy in room temperature. After heat treat at 150°C for approximate 100 hours, the coatings still have special impact strength45–50 kg · cmaccording to Chinese National Standards GB 1732-1993 and flexibility (2–3 mm) according to Chinese National Standards GB 6742-2007. Complex permittivity $\varepsilon(f)$ and permeability $\mu(f)$ of the ferromagnetic particles were measured using network analyzer in the frequency range from 2 to 18 GHz, to explain the reflection loss of the coatings were also measured in microwave chamber. The ferromagnetic particles and its random dispersion in the coatings were observed by field emission scanning electron microscope (FESEM).

On Plasmon Resonance Spectra of Various Metal Nanoparticles

Xiang'e Han, Paerhatijiang Tuersun, and Jin Li
School of Science, Xidian University, Xi'an 710071, China

Abstract— Metal nanoparticles show special optical properties, which are dependent on the size, shape, composition and dielectric constant of ambient medium. In this paper, the plasmon resonance spectra of silver nanoparticles with various shapes (sphere, triangle et al.) are simulated using classical Mie theory and several numerical methods (Finite Difference method, Discrete Dipole Approximation et al.). The numerical results of various methods are compared with the experimental ones by Mock et al., Department of Physics, University of California. The scopes of application of various numerical methods are introduced, and the error between theoretical results and experimental ones are analyzed. In the end, the effect of dielectric function models of metals on the plasmon resonance of nanoparticles is briefly studied.

Influence of Localized Surface Plasmon on Radiation Pattern of Nano-optical Antenna

S. F. Jiang, H. Gao, F. M. Kong, and K. Li
School of Information Science and Engineering, Shandong University, Jinan 250100, China

Abstract— Two nano-optical antenna (NOA) models comprised of a pair of gold nanorods (PNRs) and a pair of gold nanoellipsoids (PNEs) are introduced in this paper [Figs. (a) and (b)]. Their far-field directivities at 600 nm are carefully studied by FDTD method. To save the computer memory and insure the accuracy of calculation at the same time, local mesh refinement technology is used in this paper.

In our simulation, far-field directivity $D(\varphi,\theta)$ of NOA is calculated as follows: $D(\varphi,\theta) = 4\pi P(\varphi,\theta)/\iint P(\varphi,\theta)d\Omega$. The radiation patterns of NOA with different particle lengths (L) are checked in details.

Through our calculation, we find far-field directivity of NOA is analogous to that of dipole antenna, but the side lobes occur more easily and earlier for NOA as the length of NOA increases. Compared the results of PNRs [Fig. (c)] with PNEs [Fig. (d)], larger side-lobes and less directivity can be found in PNEs than PNRs, due to the stronger localized surface plasmon (LSP) in the PNE. Since the LSP can strongly influence the induced current distribution on NOA, we infer that it can also influence the radiation pattern of NOA. To verify that, we then use perfect electric conductor (PEC) nano-particles, which do not support LSP, to substitute gold ones with the same geometric parameters. These results are plotted in Figs. (e) and (f). Comparing these two groups of results, we find that the radiation patterns of PEC nano-particles still stay dipolar and no side-lobe occurs. This illustrates that LSP does have the influence on the radiation pattern of NOA. To further explore this influence, we change the strength of LSP by shortening the gap distance (G) between two nano-particles. Figs. (g) and (h) are the results of the condition where G equals to 8 nm. Comparing Figs. (c) and (g), smaller side lobe and more directivity can be found when G is shortened. The reason is that less higher-order modes of PNRs can be excited since total antenna length is shortened in this way, though LSP is enhanced. But for PNEs, the LSP is strong enough so that much more higher-order modes are excited and the induced current distribution in nano-particles is changed evidently, which acutely influences the radiation patterns. So we can find larger side-lobes and less directivity in Fig. (h). These results fully accord with our former inference. So the radiation patterns of our optical nano-antenna can be influenced by LSP excited at the tip of the gold nano-particles.

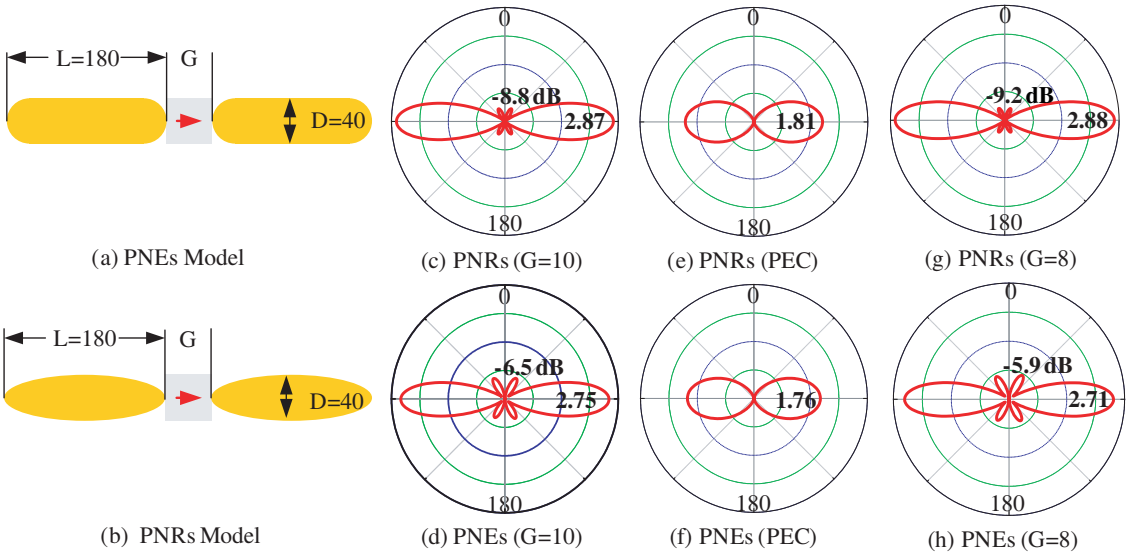

This paper illustrates that the appropriate angular directivity of gold nano-optical antenna can be achieved by choosing nano-particles with proper realist parameters and controlling LSP excited at the particle tips. Our results also hold a great promise for improving the performance of the nano-optical antenna for various applications.

Supercontinuum Generation in Different Zero-dispersion Photonic Crystal Fibers

Yanrong Song[1,2], **Jianyin Zhu**[1,2], **Xiao Zhang**[1,2], **Huihui Li**[1,2], **Lixiao Wei**[1,2], **and Pingxue Li**[3]

[1]Institute of Information Photonics Technology, Beijing University of Technology, Beijing 100124, China
[2]College of Applied Sciences, Beijing University of Technology, Beijing 100124, China
[3]Institute of Laser Engineering, Beijing University of Technology, Beijing 100124, China

Abstract— Supercontinuum (SC) could be used in optical frequency comb, sensor light sources and biological test, so it is very important to get a wide spectrum. Normally it was generated by injecting ultralshort pulses into micro-structure fibers, such as photonic crystal fibers (PCFs) or taped fibers. In 1996, the first photonic crystal fiber was made successfully by J. C. Knight, T. A. Birk [1]. In 2000, Ranka's team first reported the SC generation in PCF with anomalous dispersion at 800 nm [2]. From then, there are many research work on it. The SC generation in PCFs [3, 4] is influenced by dispersion, which included Grouped Velocity Dispersion (GVD), Third Order Dispersion (TOD), and by nonlinear effects, which include Self Phase Modulation (SPM), Self Steeping (SS), and Stimulated Raman Scattering (SRS) [5, 6]. In these effects, the influence of the GVD is very important, so we discussed this effect by experiment. In this paper, we used three different zero-dispersion PCFs to generate the SC by using an ultra-fast Ti : Sipphire laser with 130 fs pulse width with different conditions.

Figure 1 is the setup of the experiment. We used a Mira-900 Ti : Sipphire pulsed laser pumped by a Verdi-V6, the output pulses (800 nm, 130 fs, 80 MHz) are guided into the PC fibers by using an objective lens. A Faraday rotator is used to prevent the CW light from going back to the pump laser.

The Supercontinuum spectrums generated in three different zero-dispersion photonic crystal fibers with 130 fs ultrafast laser pulses. The photonic crystal fibers of zero-dispersion point at 800 nm, 1060 nm and 2 µm were engaged. From the experiment, we could see that the shorter the wavelength of the input pulses is, the wider the SC generated is. At the same time, the SC was discussed with different pump energies and different wavelength. The higher the pump source, the wider the SC is.

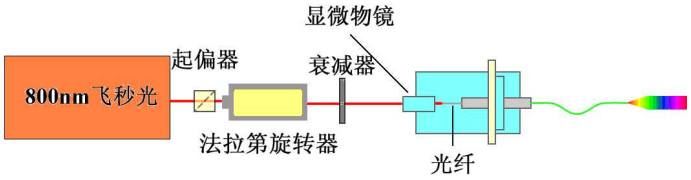

Figure 1: Setup of the experiment.

REFERENCES

1. Knight, J. C., T. A. Birk, et al., "All-silica single-mode optical fiber with photonic crystal cladding," *Opt. Lett.*, Vol. 21, 1547, 1996.
2. Randa, J. K., R. S. Windeler, and P. S. J. Rusell, "Visible continuum generation in air-silica microstructure optical fibers with anomalous dispersion at 800 nm," *Opt. Lett.*, Vol. 25, 25, 2000.
3. Russell, P., "Photonic crystal fibers," *Science*, Vol. 358, 299, 2003.
4. Wadsworth, W. J., A. Ortigosa-Blanch, J. C. Knight, T. A. Birks, T. P. Martin Man, and P. St. J. Russell, "Supercontinuum generation in photonic crystal fibers and optical fiber tapers: A novel light source," *J. Opt. Soc. Am. B*, 19, 2002.
5. Agrawal, G. P., *Nonlinear Fiber Optics*, 3rd Edition, Academic Press, New York, 2001.
6. Spillane, S. M., G. S. Pati, K. Salit, M. Hall, P. Kumar, R. G. Beausoleil, and M. S. Shahriar, "Observation of nonlinear optical interactions of ultralow levels of light in a tapered optical nanofiber embedded in a hot rubidium vapor," *Phys. Rev. Lett.*, Vol. 100, 233602, 2008.

Measurement of Weak Magnetic Fields

L. Kadlcik, J. Mikulka, and E. Gescheidtova
Department of Theoretical and Experimental Electrical Engineering
Brno University of Technology, Kolejni 4, Brno 612 00, Czech Republic

Abstract— In the envisaged paper the principle will be described of measuring magnetic fields with very low levels of induction, of the order of 1 μT. A method will be given for establishing the presence of small amounts of ferromagnetic material that can also be used to examine the homogeneity of weak magnetic fields.

The most important part of the designed device is a detection element that evaluates changes in the magnetic properties of the surroundings during its motion above the source of magnetic field, and interacts with the ferromagnetic material present. An integral part of the device is a demodulator that processes the signal being detected, from which only the part carrying useful information is selected. Useful information is deformed by convolution distortion and the signal must therefore be reconstructed in a suitable way. The reconstruction is associated with a decoder that facilitates the acquisition of additional information in cases when the reconstruction results are not quite unambiguous.

For the convolution distortion to be maximally suppressed it is necessary to choose a detector with the narrowest possible pulse response; the response width is directly proportional to the size of the area being detected. There are two basic types of detector; one type works on the basis of Faraday's induction law, the other type detects the presence of magnetic field on the basis of changes in the detection coil inductance. A detailed analysis of the functions of detectors working on different principles has shown that our requirements are best met by a simple ferromagnetic probe with a small core diameter. The detection part is designed in the form of a pen combined with an oscillator with a resonance frequency of 300 kHz. The basic oscillator element is a transistor in common base connection. The collector current is set to a value at which the transistor can supply sufficient energy into the resonance circuit and, at the same time, minimize noise. The demodulator is implemented by two PLL phase detectors, which are followed by a third-order low-pass filter with a cut-off frequency of 1 kHz. The circuit ends in a high-pass filter with a cut-off frequency of 0.34 Hz which eliminates the dc component of the signal.

The implemented meter will be used to establish the homogeneity of weak magnetic fields in biomedical applications.

The Contribution of Power Electronics Used in Hybrid Electric Vehicles to Energy Savings in Modern Society

Zdenek Cerovsky and Pavel Mindl
Czech Technical University, Czech Republic

Abstract— Paper deals with environmental influence of vehicles with internal combustion engines. New electric and hybrid electric car technology is much friendlier to the nature. Power electronics, free of electromagnetic interference problems, contributes to modern trends in powertrain development of electric and hybrid electric cars. The electromagnetic converter regimes are difficult. Special attention is paid to electromagnetic conditions and electric power splitting in the vehicle powertrain in this paper. Special features of hybrid vehicle for natural Animal Park are described.

Expansion of automobile traffic brought new problems with gas emissions and fuel consumption. Power sector, Transport and Industry produce nearly 70% of CO_2. Electric or Hybrid Electric vehicles can diminish gas emission markedly. The usage of electronics converters is inevitable. Electric vehicles have the highest potential to cut down CO_2 emissions. The main problem is the operating range of the vehicle which is limited by battery capacity and its weight. The electric hybrid vehicles have higher operating range. The reasonable combination of both energy sources gives the good solution for known operational duties. Operational duties simulation can be used as method for finding the best solution.

The experimental working stand has been set up. There are three main innovative features of this hybrid drive. The first are electronic converters with special working regimes, the second is the use of the super-capacitor (SC) as energy storage and the third is the use of the electric power splitter (EPS) constructed as a double rotor synchronous permanent magnet generator.

Physical model of the hybrid electric vehicle powertrain with the electric power splitter is depicted in Fig. 1.

The induction motor (IM1) simulates the internal combustion engine (ICE) which drives electric power splitter SGPM constructed as synchronous generator with two rotors. Both rotors rotate separately.

The induction machine IM2 simulates the car wheels. Traction induction motor TM is added and supplied from electronic converters EC3 and EC4. The EC3 rectifier has a special working regime. It rectifies the changing three phase voltage from the power splitter which is strongly changing but it is important to hold the outgoing DC voltage on a level which changes in low but given margins. Digital control scheme shown in Fig. 2 must be used to control the pulse with rectifier EC3 for solving this task.

The EC4 inverter has to change the little changing DC voltage into three phase system with changing frequency and voltage in rather high values. The role of both electronic converters is

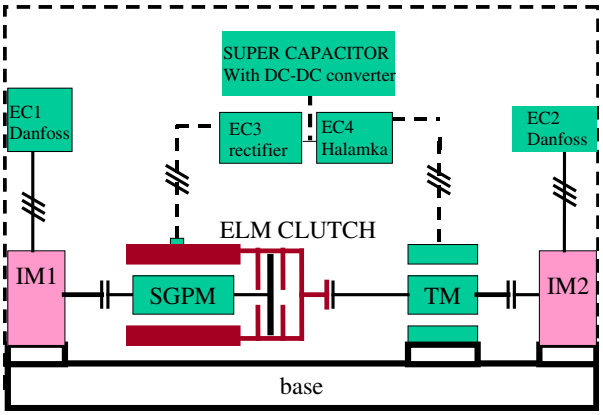

Figure 1: Physical scheme of the experimental laboratory model of the electric power splitting drive.

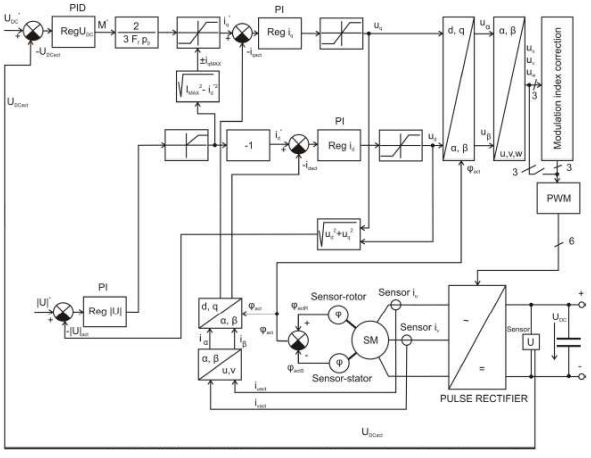

Figure 2: Block diagram for DC voltage control of pulse with rectifier.

crucial. The IM1 output power is divided into two parts. The first part flows via EC3, EC4 to TM. The second part is carried directly by means of electromagnetic torque in the air gap of generator SGPM to the TM shaft. The scheme is completed with a super capacitor used in lab but also electric battery can be used.

In full paper the simulation of a special vehicle having the duty to move in defined territory without using the combustion engine will be described together with elm problems of EC3 and EC4 converters. Given parameters are: terrain and driving cycle, total mass of the vehicle and energy stored in the battery. The power of internal combustion engine (ICE) is controlled by a special program taking into account good efficiency of the engine. In "noise protected" region it is stopped totally. Results of the simulation will be shown in many different graphs.

Ultrasonic-assisted Condensation of Chitosan with Salicylaldehyde and the Adsorption of Cr(VI) Ions in Magnetic Field

Lihong Duan[1], **Siyuan Guo**[2], **and Qiongjuan Zheng**[1]

[1]Institute of Polymer Science, College of Chemistry and Chemical Engineering
Sun Yat-sen University, Guangzhou 510275, China
[2]Light Industry & Chemical Engineering Research Institute, Food College
South China University of Technology, Guangzhou 510640, China

Abstract— The condensation reaction of chitosan (CTS) with salicylaldehyde (SD) was under taken both by ultrasonic-assisted and by traditional methods, and was compared on the two methods. The IR spectra of condensed chitosan from the two methods showed that their molecular structures were identical. The reaction conditions such as the kind of solvents, power density and irradiation time of ultrasonic, the pH condition and the reactant ratio were optimized using an orthogonal design. It was found that a shorter reaction time and a higher product yield could be got for the ultrasonic-assisted synthesis than that of traditional method. A condensation degree of 89.63% could be achieved under the optimization conditions: using 180 kW ultrasonic, taking 95% ethanol as solvent, at pH 4.0, with the SD/CTS ratio of 6 : 1, ultrasonic irradiating for 60 min. The adsorption of Cr(VI) ions onto chitosan and its condensation with salicylaldehyde was investigated in magnetic field . Batch adsorption experiments were carried out as a function of magnetic power and reacted time. The results showed that, magnetic field strengthen the adsorption capacity, especial for Schiff bases.

Table 1: The result of orthogonal design L_9 (3^4).

	Factors				Condensation degree (%)
	Acidity (pH)	Solvent	Irradiation time (min)	Ratio of SD/CTS	
1	3	water	60	4 : 1	68.01
2	3	95% ethanol	90	5 : 1	76.31
3	3	ethanol	120	6 : 1	67.41
4	4	water	90	6 : 1	84.82
5	4	95% ethanol	120	4 : 1	77.82
6	4	ethanol	60	5 : 1	80.04
7	5	water	120	5 : 1	83.32
8	5	95% ethanol	60	6 : 1	88.25
9	5	ethanol	90	4 : 1	69.35
K_1	211.73	236.15	236.30	215.18	
K_2	242.68	242.38	230.58	239.67	
K_3	240.92	216.80	228.55	240.48	
k_1	70.58	78.72	78.77	71.73	
k_2	80.89	80.79	76.86	79.89	
k_3	80.31	72.27	76.18	80.16	
R	10.31	8.52	2.59	8.43	

Microscopic Image Processing in Studying Diverticular Disease

J. Mikulka
Department of Theoretical and Experimental Electrical Engineering, Brno University of Technology
Kolejni 2906/4, Brno 612 00, Czech Republic

Abstract— This article deals with initial research of designing microscopic image processing methods in studying diverticular disease. In previous medical research a functional and structural changes were found in tissues of persons affected by diverticular disease. The acquired images were processed manually. The goal of image processing methods research for automatic or semiautomatic processing followed by manual supervising is to simplify and speed-up the image processing and evaluation of objects parameters.

In addition to speed-up the processing the goal is to increase the accuracy of evaluating the tissues properties. First step to increase the accuracy was to obtain more images representing several regions of the same tissue to averaging the results of densities in each image. Second step to increase the accuracy was to change the approach in area measurement of monitored regions because traditional manual methods are influenced by error (up to 50 %).

The article describes design of particular methods for processing of three kinds of images. The first set of images represents smooth muscle layer in which the goal is to evaluate number (density) of cell nuclei in area of the whole image. The second set of images represents myenteric plexus layer. The goal in this kind of images is to evaluating the ganglionic areas followed by determination of neurons or glial cells density. The third set of images represents interstitial cells of cajal (ICC). The goal of this kind of images processing is to evaluating number (density) of cells in observed area. The ICC's are monitored in smooth muscle layer and in myenteric plexus layer. In the first mentioned layer is evaluated the density of cells in whole image, in the second layer is evaluated density only inside the ganglionic area.

The aim of research is to design and implement image processing plug-ins which will be used as tools for speed-up the processing of huge sets of images and providing more information compared to manual processing.

Accuracy of Volumetry Depending on Smoothing Level

J. Mikulka, E. Gescheidtová, and K. Bartušek
Department of Theoretical and Experimental Electrical Engineering, Brno University of Technology
Kolejni 4, 612 00 Brno, Czech Republic

Abstract— Image processing in biomedical applications is strongly developing issue. There were described many methods and approaches for image preprocessing, segmentation and visualizing. In many cases it is useful to evaluate volume of examined objects and monitor its development in time. Typical example of examined object are tumors in human organs and monitoring their development depending on time and efficiency of treatment.

To imaging mentioned soft tissues is usually used tomography by magnetic resonance. Ideally, several tissue slices in three orthogonal planes (sagittal, coronal, transverse) are acquired. With slices in three planes is following reconstruction of shape of examined tissues most accurate. In case of acquired slices only in one plane the high spatial information lost occurs by image acquisition. Then it is necessary the shape of tissue appropriately reconstruct. At first the images are segmented and with use of particular segments the three dimensional model is composed. The reconstructed model has step-surface. There are several methods for smoothing the shape.

In this article, the methodology for shape smoothing are discussed. The results of volumetry with use of several smoothing levels are compared. Impact of shape smoothing to quality of reconstruction is discussed.

Synthesis of Arc Ladder Filters with Transmission Zeros for Using in the Feed Back of the Phase Lock Loop

Martin Friedl, **Lubomír Fröhlich**, **and Jiří Sedláček**
Brno, FEEC BUT, UTEE, Kolejní 2906/4, Brno 612 00, Czech Republic

Abstract— In the field of a measurement of the fast one shot processes there is necessary to use special frequency filters. This frequency filter is usually connected in the feed back circuit of the phase lock loop (PLL), where performs a fine tuning of the frequency. Therefore the synthesis and optimization of the ARC ladder filters with transmission zeros based on frequency dependent negative resistors (FDNR) was elaborated. Frequency filters designed using approximation functions with transfer zeros (like Inverse Tchebyschev or Cauer functions) exhibit in comparison to approximation functions with monotonic magnitude response in stop band essential higher steepness of magnitude response in area of transitive band of filter. Active RC filters synthesized using modern active elements grown from passive RLC filter prototypes with very small sensitivity on passive elements can be in comparison to their RLC prototypes realized relative easily. These filters designed using active FDNR blocks as LP (low pass) filters or using SI (Simulated inductors) active blocks in case of HP (high pass) filters can be designed with minimum active and passive elements. During resulting optimization filter design process must be an influence of real lossy active blocks (FNDR, SI) on resulting filter response respected. In contribution here are presented some possibilities of filter optimization from this point of view. There are also discussed and in some examples prescribed ways of filter synthesis with account of influence of lossy active blocks on resulting filter magnitude response in case of Inverse Tchebyschev and Cauer filter of LP and HP filters higher (from 3rd to 7th) filter orders.

REFERENCES

1. Bruton,L. T., *RC-Active Circuits Theory and Design*, Englewood Cliffs, Prentice-Hall, Inc., New Jersey, 1980, ISBN 0-13-753467-1.
2. Daryanani, G., *Principles of Active Network Synthesis and Design*, 495, Library of Congess Cataloging in Publication Data, Canada, 1976, ISBN 0-471-19545-6.
3. Pactitis, S., *Active Filters: Theory and Design*, CRC Press, USA, 274 str., 2008, ISBN 978-1-4200-5476-7.
4. Sedláček, J. and K. Hájek, *Kmitočtové Filtry*, 535, Technick Literatura, 1. vydání, Praha, BEN, 2002, ISBN 80-7300-023-7.

A 3D Magnetic Measurement for S/N < 0.01

Z. Roubal and T. Kříž
Department of Theoretical and Experimental Electrical Engineering, Brno University of Technology
Kolejní 2906/4, Brno 612 00, Czech Republic

Abstract— For measuring the magnetic impedance tomography (MIT) the 3D magnetic field meter was developed. Because the MIT is usually used in electromagnetically noisy area, it is necessary to use measurement techniques that are sufficiently insensitive to electromagnetic disturbances. The main spurious signals are mains frequency and signal from the switching power supplies. In our 3D sensor the Hall probes were used for magnetic field measurement. The signal from each of sensor is amplified in lock-in amplifiers, which suppresses unwanted spurious signals and selects only the desired signal; output is further filtered by low pass filter of order 10. The Gauss approximation of LP filter was used for minimal overshoot in impulse response. In the measurement device we correct phase shift of the reference signal automatically for maximum amplitude of the output signal. Before each measurement the influence of Earth's magnetic field is compensated. Map of the magnetic field obtained by the 3D sensor is used for reconstruction of the material properties of the measured sample.

ACKNOWLEDGMENT

The work described in the paper was financially supported by the research project GA102/09/0314, research plan MSM 0021630513 and project of the BUT Grant Agency FEKT-S-10-13.

REFERENCES

1. Dorrington, A. A. and R. Kunnemeyer, "A simple microcontroller based digital lock-in amplifier for the detection of low level optical signals," *IEEE Trans. Plasma Scien.*, Vol. 28, No. 1, 486–488, 2002.
2. Azzolini, C., A. Magnanini, M. Tonelli, G. Chiorboli, and C. Morandi, "Integrated lock-in amplifier for contactless interface to magnetically stimulated mechanical resonators," *3rd International Conference on Design and Technology of Integrated Systems in Nanoscale Era, 2008, DTIS 2008*, 1–6, 25–27, Mar. 2008.
3. De Marcellis, A., G. Ferri, and E. Palange, "A novel analog autocalibrating phase-voltage converter for signal phase-shifting detection," *IEEE Sensors Journal*, Vol. 11, No. 2, 259–266, Feb. 2011
4. Roubal, Z. and M. Steinbauer, "Design of electrometric amplifier for aspiration condenser measurement," *PIERS Proceedings*, 1430–1434, Xi'an, China, Mar. 22–26, 2010.
5. Friedl, M. and J. Sedlacek, "Optimization of ARC component filter sensitivity," *PIERS Proceedings*, 526–530, Xi'an, China, Mar. 22–26, 2010.
6. Kříž, T. and J. Dědková, "A new algorithm for electrical impedance tomography inverse problem," *PIERS Proceedings*, 127–131, Beijing, China, Mar. 23–27, 2009.
7. Hájek, K. and J. Sedláček, Kmitočtové filtry, Vydavatelství, BEN, Praha, 2002.

The Study of Transport of Substances in the Plant Stems

Michaela Burdková and Tomáš Kříž
Department of Theoretical and Experimental Electrical Engineering
Brno University of Technology, Kolejni 4, Brno 612 00, Czech Republic

Abstract— Monitoring of tissue structures of Euphorbia plants in non-destructive manner is possible using nuclear magnetic resonance-based tracking of angular momentum and the responses of nuclei placed in a magnetic field with defined induction and interaction with highfrequency electromagnetic waves. Characteristics of the response is dependent on the method of application of series of radiofrequency pulses. After the finish of phenomenon the resulting signal is detected by the receiving coil of tomograph. Measured plant is sensed by magnetic resonance imaging in several cuts oriented perpendicular to the axis of the stem of the plant. The cuts are designed in the same distances between them from the bottom of the root to the top edge of the plant. There is only part of the plant in the working area of the tomograph during the measurement.

The measurements are chosen using sensing techniques called spin echo and inversion recovery method. The acquired images are weighted by relaxation times T1 for spin echo method respectively by T2 for inversion recovery method. Pictures weighted by relaxation times are evaluated in the program Marevisi manually to determine vascular structure of plants. Longer relaxation times correspond to places where there is a greater presence of water. Contrasts in the image correspond to the chemical bonds in nutritive substances, viscosity agents and mobility of molecules.

The goal of project is a reconstructed image of the morphology of plants with an identifiable vascular tissues in stem cuts of plants, carried out using the method of spin echo and inversion recovery method with optimally chosen parameters. The images obtained in that manner enables the study of transport of substances in the stems of plants.

The Frequency Source for Precision Synchronous Triggering

Z. Roubal and R. Kadlec
Department of Theoretical and Experimental Electrical Engineering, Brno University of Technology
Kolejní 2906/4, Brno 612 00, Czech Republic

Abstract— In special applications which require very precise triggering we need high-quality crystal oscillator running on frequencies of the order of hundreds of megahertz. Butler oscillator as emitter follower is optimal for such high frequency range; moreover, this oscillator has not spurious oscillation. This paper deals with the optimization in terms of gain reserve at the oscillation frequency, maximizing short-term stability and minimizing power load on the crystal unit. For nonlinear analysis of the oscillator we have used the method of harmonic balance. From this method we obtain the dependence of power load on the crystal unit on damping resistance, which influence the oscillation frequency. In the next step is recalculated phase noise of crystal oscillator to short-term stability. In this work was used special synchronization of crystal oscillators.

ACKNOWLEDGMENT

The work described in the paper was financially supported by the research project GA102/09/0314, research plan MSM 0021630513, research plan MSM 0021630516 and project of the BUT Grant Agency FEKT-S-10-13.

REFERENCES

1. Odyniec, M., *RF and Microwave Oscillator Design*, Artech House, Boston, 2002.
2. Zelenka, J., *Piezoelektrické Rezonátory a Jejich Použití*, Academia, 1983.
3. Matthys, R. J., *Crystal Oscillators Circuit*, Krieger Publishing Company, 1991.
4. Benjaminson, A., "Designing crystal oscillators for improved phase-noise performance," *39th Annual Symposium on Frequency Control*, 140–144, 1985.
5. McClelland, T., C. Stone, and M. Bloch, "100 MHz crystal oscillator with extremely low phase noise," *Frequency and Time Forum, 1999 and the IEEE International Frequency Control Symposium, Proceedings of the 1999 Joint Meeting of the European*, Vol. 1, 331–334, 1999.
6. Frerking, M., *Crystal Oscillator Design and Temperature Compensation*, Van Nostrand Reinhold, 1978.
7. Čajka, J. and J. Kvasil, *Teorie Lineárních Obvodu*, SNTL, Praha, 1979.
8. Vrba, K. and F. Kouřil, *Teorie Nelineárních a Parametrických Obvodu*, SNTL, Praha, 1981.

Evaluation of Characteristics of HV Electrometric Amplifier with Low Input Current

Z. Roubal and R. Kadlec
Department of Theoretical and Experimental Electrical Engineering, Brno University of Technology
Kolejní 2906/4, Brno 612 00, Czech Republic

Abstract— In the special application, for example in chemistry, it is necessary to measure voltage of the order hundred volts from high-impedance source. Standard electrometric operational amplifier cannot be used, because their input range is limited to maximally ten volts and increasing the input range by voltage divider is of topic, when the required input resistance is, e.g., $10^{14}\Omega$. Ordinary resistive divider in the input of operational amplifier has typical maximum input resistance $10^{12}\Omega$. Special circuit arrangement can be used, where supply voltage of amplifier is dynamically shifted with input voltage. This configuration saves high input resistance of used electrometric amplifier and extends the input voltage range to desired value — in our configuration the extended range is $\pm 300\,\mathrm{V}$. In our design of HV electrometric amplifier we use high-voltage differential amplifier, which regulate the high-voltage source, supplying the electrometric operational amplifier. General feedback loop has to be frequency compensated and this compensation has been designed using Pspice simulator. In this article the experimentally verification of designed HV electrometric amplifier will be discussed.

ACKNOWLEDGMENT

The work described in the paper was financially supported by the research project GA102/09/0314, research plan MSM 0021630513 and project of the BUT Grant Agency FEKT-S-10-13.

REFERENCES

1. Levinzon, F. A., "Ultra-low-noise high-input impedance amplifier for low-frequency measurement applications," *IEEE Transactions on Circuits and Systems I: Regular Papers*, Vol. 55, No. 7, 1815–1822, August 2008
2. Roubal, Z. and M. Steinbauer, "Design of electrometric amplifier for aspiration condenser measurement," *PIERS Proceedings*, 1430–1434, Xi'an, China, March 22–26, 2010.
3. Friedl, M. and J. Sedlacek, "Optimization of ARC component filter sensitivity," *PIERS Proceedings*, 526–530, Xi'an, China,, March 22–26 2010.
4. *Low Level Measurements Handbook: Precision DC Current, Voltage, and Resistance Measurements*, 6th Edition, Keithley Instruments, Inc., Cleveland, Ohio, 2004.

Special High Voltage Function Generator

P. Marcon, **P. Fiala**, **M. Steinbauer**, **and M. Cap**
Department of Theoretical and Experimental Electrical Engineering
Brno University of Technology, Kolejni 2906/4, Brno 612 00, Czech Republic

Abstract— Goal of this project was to design, realize and test a special high voltage function generator. This generator was designed for special use. Purpose of the generator is to generate a variable electrical field. In course of design of the generator the properties of the output electrode voltage was the key element.

The high voltage function generator is designed as a switched flyback high voltage source. Voltage of the output electrode of the realized generator is possible to regulate in range 0 kV to 20 kV. Shape of the output voltage is possible to choose as sine, square or ramp. Frequency capabilities of this voltage source start on 0 Hz and reach 300 Hz. Frequencies close to 300 Hz are affected by the parasitic capacitance. For special use, the high output impedance was required. Generator use PWM modulated signal from control unit for regulating primary coil current of the high voltage transformer.

In this article is discuss the construction of the low voltage part of this device. Namely, power supply, control unit and the High voltage block. Results of the tests and all the voltage curves are shown in results. Design of this special high voltage function generator allow as to provide new special scientific tests.

REFERENCES

1. Brown, B. H., R. H. Smallwood, D. C. Barber, P. V. Lawford, and D. R. Hose, *Medical Physics and Biomedical Engineering: Medical Science Series*, Institute of Physics Publishing, 1999.
2. Kalousek, V., F. Stanek, and J. Schieblova, *Technika Vysokých Napětí*, Skripta VUT FEKT v Brne, Brno, 1989, ISBN 80-214-0015-3.
3. Gasparov-Grekhov, A. V. and V. L. Granenstein, *Applications of High-Power Microwaves*, Artech House, Boston, London, 1994.
4. Krejcirik, A., *Napajeci Zdroje II — Integrovane Obvody ve Spinanych Zdrojich*, BEN, technicka literatura, Praha, 1997, ISBN 80-86056-03-1.
5. Krejcirik, A., *Napajeci Zdroje I — Zakladni Zapojeni Analogovych a Spinanych Napajecich Zdroju*, BEN, technicka literatura, Praha, 1997, ISBN 80-86056-02-3.
6. Krejcirik, A., *Napajeci Zdroje III — Pasivni Soucastky v Napajecich Zdrojich a Preregulatory*, BEN, technicka literatura, Praha, 2002, ISBN 80-86056-56-2.
7. Faktor, Z., *Transformatory a Civky*, BEN, technicka literatura, Praha, 1999, ISBN 80-86056-49-2.

Filter for Processing of NMR Signal

Martin Friedl, **Jiří Sedláček**, **Lubomír Fröhlich**, **and Radek Kubásek**
Brno, FEEC BUT, UTEE, Kolejní 2906/4, Brno 612 00, Czech Republic

Abstract— One of the fields of science, where is going forward continual development, is the area of nuclear magnetic resonance (NMR). Bulk of the NMR issues concerns on signal processing in analog and digital form in NMR signal. In this paper is focused our attention on design of active analog filter with frequency dependent negative resistor (FDNR). There is designed active ARC filter based on ladder structure of the LCR filter, then the filter DCR is made through the use of Brutton transformation and finally the DCR filter is converted to the filter with FDNR elements. The designed and realized filter is used as a low pass filter, which aims to filter out the noise of NMR signal. The filter is placed behind the mixer, which converts the useful NMR signal to baseband. The designed and realized filter performs role of the anti-aliasing filter before the A/D converter.

REFERENCES

1. Bruton, L. T., *RC-Active Circuits Theory and Design*, Englewood Cliffs, Prentice-Hall, Inc., New Jersey, 1980, ISBN 0-13-753467-1.
2. Daryanani, G., *Principles of Active Network Synthesis and Design*, 495, Library of Congess Cataloging in Publication Data, Canada, 1976, ISBN 0-471-19545-6.
3. Pactitis, S., *Active Filters: Theory and Design*, 274 str., CRC Press, USA, 2008, ISBN 978-1-4200-5476-7.
4. Sedláček, J. and K. Hájek, *Kmitočtové Filtry*, BEN, technická literatura, 1. vydání Praha, 535, 2002, ISBN 80-7300-023-7.

Universal Arc Filters for Arc Oscillators with Automatic Sequential Filtration

Lubomír Frölich, **Jiří Sedláček**, **and Martin Friedl**
Brno, FEEC BUT, UTEE, Kolejní 2906/4, Brno 612 00, Czech Republic

Abstract— There are situations, when it is not possible to use standard types of filters, mainly because of demands on using of digital tuning of complex filter and concurrently usage of higher amount of transfer functions, which can be low pass — LP, high-pass — HP, band-pass —BP, bandreject — BR, but also low or high-pass notch — LPN / HPN and all-pass — AP. For this purpose, we mostly use 2nd order ARC filters, which contain three or more operational amplifiers (OA). Concerning these blocks, tuning or control of this filter is usually the easiest.

Except very familiar known filters as Akerberg-Mossberg, Kervin-Huelsman-Newcomb or Towa-Thoma, there is a further amount of circuit connections of universal ARC filters, which enable to realize the transfer function of biquad. The article mainly deals with some other circuits, which are not so familiar, but can be also successfully used as universal filters. These filters realizing required circuit functions with the possibility of tuning of basic parameters of the circuit have been used in special circuits with ARC oscillators for very low distortion with maximum suppression of third harmonics.

REFERENCES

1. Sedláček, J. and K. Hájek, *Kmitočtové Filtry*, 535, Technická Literatura, 1. vydání Praha, BEN, 2002, ISBN 80-7300-023-7.
2. Galiamichev, I. P., A. A. Lanne, V. Z. Lundin, and V. A. Petrakov, "The synthesis of active RC network," 296, Izdatel'stvo Sviaz', Moscow, 1975 (In Russian).
3. Hájek, K., "Přeladitelný nízkofrekvenční generátor s velmi nízkým zkreslením," OA 277259, 1992.
4. Sedláček, J. and K. Hájek, "ARC oscillators with ultra low distortion," *Proc. of Int. Symp. on Nonlin. Theory and Appl., NOLTA'98*, Crans-Montana, Vol. 3, 1201–1204, September 1998.

Visualization of Plant Fibres via Diffusion Tensor Imaging

E. Gescheidtová[1], **P. Marcon**[1], **and K. Bartusek**[1, 2]

[1]Department of Theoretical and Experimental Electrical Engineering
Brno University of Technology, Kolejni 2906/4, Brno 612 00, Czech Republic
[2]Institute of Scientific Instruments, Academy of Sciences of the Czech Republic
Kralovopolska 147, Brno 612 64, Czech Republic

Abstract— The paper deals with MR imaging of plant fibres (filaments) with the aid of Diffusion Weighted Imaging (DWI) and Diffusion Tensor Imaging (DTI). The methods help us to better understand the process of plant nutrition and come to know the inside structure of plants without damaging them. The NMR method known as the Pulse Field Gradient Spin Echo (PFGSE) was applied to the measurement of diffusion in plant samples.

The experiments were carried out on an MR tomograph system with a strong basic magnetic field with induction $B_0 = 4.7\,\mathrm{T}$ and a working space diameter of 120 mm (i.e., 200 MHz for 1H nuclei). Actively shielded gradient coils yield a maximum gradient field magnitude of 180 mT/m.

Onion and leek samples were used for the experiments. The Diffusion Weighted Image (DWI) was calculated from the values obtained by the PFGSE method. Each image voxel has an image intensity that reflects a single best measurement of the rate of water diffusion at that location.

The measurements were conducted under different conditions: without applying the gradients and applying the gradients in the direction of axes x, y, and z. However, these experiments did not fulfil our expectations, the structure of filaments nourishing the plants could not be distinguished clearly enough from the DWI images obtained. For this reason we added to the data measured also data obtained by the application of gradients in xy, yz, and xz orientations and calculated the diffusion tensor. The tensor was represented with the help of small ellipsoids; each voxel is formed by an ellipsoid. Processing the data in the Matlab environment and calculating the 3D DTI yielded a 5D matrix of variables. The calculation is more demanding and time-consuming but we obtained images with an evident structure of plant filaments.

REFERENCES

1. Johansen-Berg, H. and T. E. J. Behrens, *Diffusion MRI: From Quantitative Measurement to in vivo Neuroanatomy*, Elsevier, China, 2009.
2. Basser, P. J., J. Mattiello,, and D. Lebihan, "MR diffusion tensor spectroscopy and imaging," *Biophysical Journal*, Vol. 66, 259–267, January 1994.
3. Bartusek, K. and E. Gescheidtova, "MRI method of diffusion measurement in heterogeneous materials," *Measurement Science and Technology*, Vol. 19, 2008.
4. Marcon, P. and K. Bartusek, "Errors in diffusion coefficients measurement," *PIERS Proceedings*, 1035–1039, July 5–8, Cambridge, USA, 2010.
5. Bartusek, K. and E. Gescheidtova, "Testing the quality of magnetic gradient fields for studying self-diffusion processes in biological specimens by magnetic resonance methods," *Measurement Science and Technology*, Vol. 17, 2256–2262, 2006.
6. Barmpoutis, A., B. C. Vemuri, and J. R. Forder, "Tensor splines for interpolation and approximation of DT-MRI with applicationto segmentation of isolated rat hippocampi," *IEEE TMI: Transactions on Medical Imaging*, Vol. 26, No. 11, 1537–1546, 2007.

Dielectric Properties of Water Solutions with Small Content of Glucose in the Millimeter Wave Band and the Determination of Glucose in Blood

B. M. Garin, V. V. Meriakri, E. E. Chigrai, M. P. Parkhomenko, and M. G. Akat'eva
Kotel'nikov Institute of Radio Engineering and Electronics RAS, Fryazino Branch
Fryazino, Moscow Region 141190, Russia

Abstract— The dielectric properties of water and 0.9% NaCl in water with small content of sugar and glucose, as well as of human blood and skin, were measured in the millimeter-wave range.

The measurement methods were chosen so that one could use them for the nondestructive control of glucose content (i.e., measurement only reflection of an electromagnetic wave, without penetrating into the medium). To determine real ε' and imaginary ε'' parts of permittivity, one usually measures the power reflection coefficient and the phase of the reflected wave with the help of sophisticated and expensive network vector analyzers. We developed a sufficiently simple method and scheme, which consists in measuring the minimum of the power reflection coefficient $R(f) = R_{\min}(f_{\min})$ and the frequency $f_{\min}$ corresponding to this minimum from the following structure: a specially chosen plane-parallel matching plate made of a low-loss dielectric — a medium under measurement with high losses (water, solution, blood, skin).

This method was realized in the frequency range 28–120 GHz.

Dielectric properties of glucose solutions in water and in a 0.9% NaCl solution (physiological solution) have been measured for glucose concentrations W ranging from 5 to 0.25%. For practice it is very important to have high sensitivity to glucose concentration in water and physiological solution (blood imitator). Sensitivities of 2.2 dB per 0.5% wt. of glucose concentration in water and 0.9 dB per 0.2% wt. in physiological solution have been obtained. Extrapolation of these results to smaller values of glucose concentration W shows that the sensitivity may be increased to 0.04% wt.

Dielectric properties of blood for human temperature are measured *in vivo* (without preservatives) for the first time with a sufficiently high accuracy (the measurement accuracy of ε' and ε'' is ± 0.2) at frequencies of 42 and 66 GHz.

Our method allows a real-time determination of glucose content in blood by a single drop of blood. We established a clear correlation between glucose content W and the measured value of $R_{\min}$ as W increases after an oral glucose tolerance test (OGTT) on an empty stomach.

The dielectric properties and the reflectivity of skin on various parts of a human body have been measured on a number of test persons in the frequency range from 30 to 77 GHz. It has been established that fingertips, on the one hand, and forearms and earlobes, on the other, have substantially different values of $R_{\min}$ and $f_{\min}$. Moreover, they have individual values for different test persons. The values of ε' and ε'' have been measured near the elbow joint in the frequency range from 30 to 80 GHz. Above 40 GHz, these data have been obtained for the first time, whereas, at frequencies of 30–40 GHz, the values of ε'' obtained in our experiments are higher than those available in the literature. It was established a correlation between glucose content W after OGTT and the properties of skin.

The results of the measurements described can be used to implement real-time, including non-invasive, measurements of small glucose (sugar) content in water, physiological solution, and blood.

This method also has been applied to the determination of alcohol content in water, vine and beer.

A Novel Compact Frequency Selective Surface with a Stable Performance Based on Substrate Integrated Waveguide Technology

Hang Zhou[1], **Shaobo Qu**[1, 2], **Jieqiu Zhang**[1], **Jiafu Wang**[1], **Baoqin Lin**[1], **Hua Ma**[1], **Zhuo Xu**[2], **Peng Bai**[3], **and Weidong Peng**[3]

[1]College of Science, Air Force Engineering University, Xi'an, Shaanxi 710051, China
[2]Electronic Materials Research Laboratory, Key Laboratory of the Ministry of Education
Xi'an Jiaotong University, Xi'an, Shaanxi 710049, China
[3]Synthetic Electronic Information System Research Department
Air Force Engineering University, Xi'an, Shaanxi 710051, China

Abstract— A novel compact frequency selective surface (FSS) with a stable performance is presented. A narrow band-pass FSS operating at around 16.6 GHz is designed. The unit cell consists of a double-sided metalized substrate with a circular hole in the center as well as 24 metal stubs surrounding the circular hole. In this way, incident EM waves enter the circular cavity formed by the 24 metal stubs and excite a cavity resonance, leading to a narrow pass-band. An approximate analytical formula is introduced to calculate the cavity resonant frequency. The cavity resonance provides a very good wide-angle and polarization-independent stability. Further more, there is no other frequency resonance up to 28 GHz except the designed frequency. Finally, we get a FSS which has advantages of high selectivity, stable performance and compact volume.

Electric, Magnetic Resonances and the Ultrabroad Band Optical Response of Double Fishnet Metamaterials

Yong-Liang Zhang, Xian-Zi Dong, Zhen-Sheng Zhao, and Xuan-Ming Duan
Organic Nanophotonic Laboratory, Technical Institute of Physics and Chemistry
Chinese Academy of Science, Beijing 100190, China

Abstract— Electromagnetic metamaterials (MM) are artificially engineering composite materials with nanoscale inclusions and unconventional electromagnetic (EM) functionality that can't find in naturally occurring materials. MMs with desired homogenized constitutive parameters, i.e., permittivity ε, permeability μ and refraction index n have demonstrated potential benefits in various applications including super-resolution imaging, electromagnetic cloak, novel waveguids and antennas, bio-sensors, integrated photonic circuits, and many more.

Among the various designs of MM, the double fishnet structures [1], which is the combination of pair of metal slabs and continuous wires, have demonstrate superior performance in the frequency region ranging from infrared regime to the visible. It has been shown that the localized surface plasmons (LSPRs) play an important role for the specific EM response [2]. For two dimensional arrays of air hole in a single metal film, there is a resonance in the spectrum with nearly unity transmission due to the excitation of LSPRs. When a further layers is added, the LSPRs will couple with each other when the layers spacing is compared with the decaying length of LSPRs. The magnetic resonance of the double fishnet MM is result from the anti-symmetric mode of the LSPRs.

In this paper, we consider a modification of the well known fishnet structure. We proposed and numerically investigate a design of MM with 2D elliptical air holes milled in the silver film. We found the EM response is strongly influenced by the orientation of the ellipse in the layers. A ultrabroad band frequency region with negative permittivity and permeability is found when the angle between the major axis of the ellipses is 90 degree. We also study the frequency dependent of the resonances with the angle, spacing and the aspect ratio of the ellipses. We interpret the characteristics of the EM behavior with the mode coupling between the LSPRs supported by 2D array of elliptical air holes milled in a single silver film. It's interesting that there are two distinct resonances driven by the electric and magnetic field, respectively. Our findings may be useful to understanding the underlying physics of the fishnet MIM and the potential photonics and plasmonics applications.

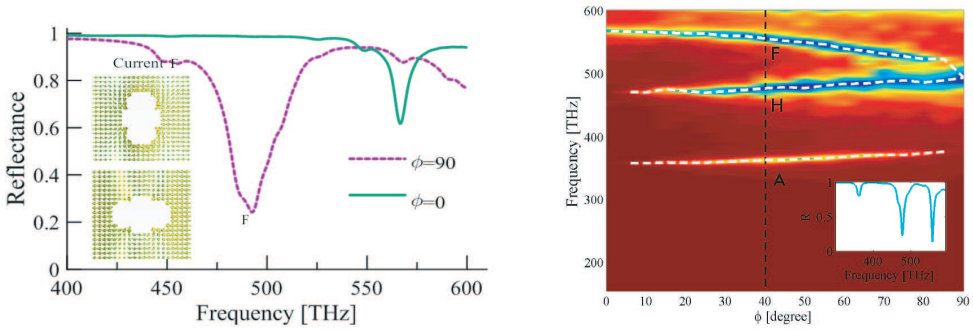

Figure 1.

REFERENCES

1. Penciu, R. S., M. Kafesaki, T. Koschny, E. N. Economou, and C. M. Soukoulis, *Phys. Rev. B*, Vol. 75, 235114, 2007.
2. Parsons, J., E. Hendry, J. R. Sambles, and W. L. Barnes, *Phys. Rev. B*, Vol. 80, 245117, 2009.

Wave Transformers Based on Transformation Optics Theory

Xin-Hua Wang[1], **Shao-Bo Qu**[1, 2], **Zhuo Xu**[2], **Hua Ma**[1], **Jia-Fu Wang**[1], **Lei Lu**[1], **Hang Zhou**[1], **Fei Yu**[1], **and Yuqing Li**[1]

[1]College of Science, Air Force Engineering University, Xi'an 710051, China
[2]Electronic Materials Research Laboratory, Key Laboratory of Ministry of Education
Xi'an Jiao-Tong University, Xi'an 710049, China

Abstract— Transformation optics theory offers a revolutionary way of designing new functional devices. In this paper, the Laplace equations plus Dirichlet boundary conditions are used to obtain the material parameter tensors of the transformation medium. Wave shape transformer, wave splitter and wave synthesizer were designed using this method. Full wave simulations based on the finite element method verified this method. These new functional devices are more favorable than the traditional ones because of their low loss and high transmission efficiency.

Hybrid Electromagnetic Cloaks Mediated by Surface Plasmons: Nonperfect but Practical

Shaobo Qu[1, 2], **Jiafu Wang**[1], **Baiyu Yang**[1], **Hua Ma**[1, 2], **Zhuo Xu**[2], **and Song Xia**[2]

[1]College of Science, Air Force Engineering University
Xi'an, Shaanxi 710051, China
[2]Electronic Materials Research Laboratory
Xi'an Jiaotong University, Xi'an, Shaanxi 710049, China

Abstract— We demonstrated, for the first time ever, a practical hybrid electromagnetic cloak that works effectively under both TE and TM polarizations. To realize such a cloak, a TE cloak and a TM cloak were firstly designed to work at the same frequency. By combining the two cloaks, a hybrid cloak was realized. Different from the transformation-based cloaks, the proposed cloaks are based on the highly surface-confined property of surface plasmons. The cloaking performance of such cloaks is nonperfect. However, such cloaks can be made very thin and moreover are much easier to be realized in practice. Both simulations and experiments verified our design.

Tunable Dual-band Filter Based on Photonic Crystals Doped by Unmagnetized Plasma

Xiang-Kun Kong[1, 2], **Shao-Bin Liu**[1], **Ping Wang**[1], **Xin Li**[1], **and Li Liu**[1]

[1]College of Electronic and Information Engineering, Nanjing University of Aeronautics and Astronautics Nanjing 210016, China

[2]Department of Physics, Zhenjiang Watercraft College, Zhenjiang 212003, China

Abstract— A novel tunable dual-band filter from one-dimensional photonic crystals doped by unmagnetized plasma is analyzed. Two defective PCs composed by ZnSe and Na_3AlF_6 with one defect layer made by unmagnetized plasma stacked in symmetric geometry are considered. By the transfer matrix method and Bloch's theorem, it is found that the frequency of the defect modes can be modulated by plasma frequency and defect thickness. Without changing the structure of the photonic crystal, the defect modes can be modulated in a larger frequency range. These results may provide theoretical instructions for designing new optoelectronic devices.

Response of Plasma Flow Field to Nuclear Electromagnetic Pulse in Near Space

Bo-Rui Bian, **Shao-Bin Liu**, **Xiang-Kun Kong**, **and Chun-Zao Li**
College of Electronic and Information Engineering
Nanjing University of Aeronautics and Astronautics, Nanjing 210016, China

Abstract— With the development of national missile defense system, we must rely on new ways to penetrate the existing strategic balance to maintain. Near space vehicle is one of the most promising means of a highly efficient of penetration. Near space vehicle can effectively circumvent the Kinetic Energy Interceptor, but low-yield nuclear detonation may be faced with a typical combat scenario. Nuclear explosions in near space on the impact of near space vehicle are particularly important. In this paper, finite-difference time-domain (FDTD) method has been discussed for complete simulation of nuclear electromagnetic pulse (NEMP) originating from an atmospheric nuclear detonation in near space. The Compton current formula and the simplified model of solving the Maxwell's equations are described. In addition, the typical results that the plasma flow field of near space vehicle is generated by the ionization between high-speed flight and the thin air in near space are presented. The coupling between nuclear electromagnetic pulse (NEMP) in nuclear exploding source region and the plasma flow field of near space vehicle is studied. To achieve this purpose, the radiated field in nuclear exploding source region is calculated using a late-model iterative equation including the electron plasma extra conductivity effect. Because of the free electron plasma extra conductivity, the corresponding conduction current is offset by the Compton current, resulting in significant decline in the peak transverse electric field. The presented results may be used in electromagnetic compatibility analysis of near space vehicle.

Guided Modes in a Slab Waveguide with Air Core Layer and Left-handed Materials Claddings

Lu Fa Shen[1], **Jia-Cheng Qiu**[1], **and Zi-Hua Wang**[2]

[1]Science College, Huzhou Teachers College, Zhejiang, China
[2]Key Laboratory of Specialty Fiber Optics and Optical Access Networks
Shanghai University, Shanghai, China

Abstract— A symmetric three-layer slab waveguide with air as core and anisotropic left-handed materials as claddings is investigated. Some dispersion equations are derived and corresponding dispersion curves are plotted, respectively. From these curves, with the increase of the waveguide thickness, their operating frequencies become widely such as surface TE_0 mode, surface TE_1 mode and oscillating TM_1 mode. However, for the surface TM_0 mode, its dispersion curves move down and operating frequencies get narrow, and for oscillating TE_1 mode, its dispersion curves move to left and cutoff frequencies become less. Since all experimental realization of left-handed materials have narrow bands, thus, these new features may give us a direction to increase band width.

Electromagnetic Radar Absorber Designed by Patching or Incorporating Lossy FSSs

Hui Bin Zhang, **Pei Heng Zhou**, **Liang Chen**, **Di Fei Liang**, **Jian Liang Xie**, **and Long Jiang Deng**
State Key Laboratory of Electronic Thin films and Integrated Devices
University of Electronic Science and Technology of China, Chengdu, China

Abstract— To broaden the operating frequency band of RA (Radar Absorber), multilayer structure is usually employed instead of single layer, but the thickness of RA increases at the same time [1, 2]. In this paper, another kind of RA, radar absorbing coating collaborated with lossy frequency selective surfaces (FSSs) is studied to achieve both wide absorption band and thin thickness. A design method based on the equivalent circuit model is introduced to indicate the theoretical design principles and determine the performance of proposed RA. Electromagnetic RAs working in a range of 2–18 GHz are obtained in the form of ferromagnetic coating patching or incorporating with lossy FSSs. Lossy FSSs are introduced by spraying and etching polymer composite film filled with carbon black. Absorption obtained by experiments, the proposed design method analysis and CST simulations are compared. It is shown that the operating frequency band of RAs can be shifted down by FSSs patching and broadened by FSSs incorporating while the increase in the thickness is negligible. According to the design method, the optimum absorption of the RAs is affected both by the substrate features (the electromagnetic parameters and the thickness) and the FSS elements (the shape, the impedance and the position). Finally, several types of lossy FSS-based layered electromagnetic RAs following the design method are fabricated and tested, including a 1-mm-thick RA with a center frequency shifted down from 6 GHz to 2.5 GHz by FSSs patching and a 2-mm-thick RA with a −10 dB operating bandwidth broadened from 3–6 GHz to 2–7.5 GHz by FSSs incorporating.

REFERENCES

1. Rozanov, K. N., "Ultimate thickness to band width ratio of radar absorbers," *IEEE Trans. Antennas Propag.*, Vol. 48, No. 8, 1230–1234, 2000.
2. Wallace, J. L., "Broadband magnetic microwave absorbers: Fundamental limitation," *IEEE Trans. Magn.*, Vol. 29, No. 6, 4209–4214, Nov. 1993.

New-type Low Power and Anti-interference Transmission Module

Hsien-Wei Tseng[1], **Yih-Gunag Jan**[2], **Ming-Hsueh Chuang**[3], **Wei Chien**[4], **Chih-Yuan Lo**[2], **Liang-Yu Yen**[2], **and Pei-Jun Chen**[1]

[1]Computer and Communication Engineering, De Lin Institute of Technology, Taiwan, R.O.C.
[2]Electrical Engineering, Tamkang University, Taiwan, R.O.C.
[3]Electronic Engineering, National Taiwan University of Science and Technology, Taiwan, R.O.C.
[4]Electronic Engineering Department, De Lin Institute of Technology, Taiwan, R.O.C.

Abstract— Today, the wireless radio technology has been applied extensively in our life. In the future trend the main stream is to develop a low power wireless transceiver circuit. On the other hand, the short distance transmission technology has been applied in many fields such as industrial production, medical treatment and surveillance, scientific research and consumer electronics, etc. With the short distance wireless transmission technology, it will solve the problem of possible obstacles due to the constraints of environment restriction and unfavorable working conditions in the wire-line equipments installations. Furthermore it also possesses the advantages of low cost and product portability. Especially this technology is applied more extensively in portable products. With the progress of science and technology, the component counts in the chip increases rapidly; and consequently we will stress in this paper of how to design low power consumption circuits. Based on the reasons as described above, the purpose of this paper is to design and to implement the hardware realization of a wireless transmission module to have low power consumption product and meanwhile to solve the interference problem. In this project we will propose a new type of transmission method to attain the tasks of low power consumption and low level of synchronous interference problems. This new-type technical has lower bit error rate and easier receives the signal. In this project, it will use simple electronic components to build a transmission platform in performing the transmitting and receiving functions. After completing the measurement tests of this transmission platform it will proceed to the hardware implementation of this prototype by using FPGA (Field Programmable Gate Array) to complete this module of "A New Type of Low Power and Anti-Interference Transmission Module" to attain the tasks of having low power and long battery life product, to reduce the volume and size of the transmission module, and to solve the synchronization interference problem. Also the fundamental consideration in performing this project is to determine how to adhere to the issues of environment protection and energy saving, consequently this paper is not only has its extension capability but also will ignite all researches toward high level of technology developments.

Session 3P1a
Plasmonic Nanophotonics 2

Optical Log-periodic Dipole Array (LPDA) Antenna for Broadband Field Enhancement and Directional Emission

Chia-Hung Lin[1], **Ruey-Lin Chern**[2], **and Hoang-Yan Lin**[1]

[1]Department of Electrical Engineering, Graduate Institute of Photonics and Optoelectronics
National Taiwan University, Taipei 106, Taiwan
[2]Institute of Applied Mechanics, National Taiwan University, Taipei 106, Taiwan

Abstract— Optical antennas, an analogue to their radio-frequency (RF) counterparts made of metal nanoparticles, have emerged as a topic receiving intensive study in recent years. The plasmonic resonance nature and the long-range transmission functionalities similar to the RF antennas make them a promising candidate for many applications, ranging from polarizors to biosensors and photodetetors.

Here, inspired by the RF technology design concept, we demonstrate by numerical simulation that a nano-optical log-periodic dipole array (LPDA) antenna can be used to deliver highly-directional beam as well as field enhancement over a wide bandwidth. The LPDA antenna is first designed for a perfect electric conductor (PEC) according to the conventional RF technology design rules. Then the Drude-type fit to the experimental data of real metals, such as silver (Ag), is used to adjust the length of each dipole element in the scaling down process to reflect the plasmonic resonance nature. The near field enhancement and far field characters such as radiation pattern and directivity are studied by full-wave numerical simulation. When coupled to a series of point emitters with progressive phase difference taken into account, the LPDA antenna shows an endfire beam pattern over a wide wavelength range, defined as a front-to-back (F/B) ratio larger than 3 dB. A comparison between the LPDA antenna and an optical Yagi-Uda antenna shows that the LPDA antenna has a slightly smaller directivity but a much wider end-fire beam bandwidth. The far field pattern also reveals the beam width is larger in the H-plane than in the E-plane for the LPDA antenna, which is consistent with the knowledge of the RF counterparts.

ACKNOWLEDGMENT

This work was supported in part by National Science Council of the Republic of China under Contracts No. NSC 99-2221-E-002-121-MY3 and NSC 99-2221-E-002-140.

Plasmonic Zener Tunneling in Metal-dielectric Waveguide Arrays

Ruei-Cheng Shiu and Yung-Chiang Lan
Institute of Electro-Optical Science and Engineering
National Cheng Kung University, Taiwan, R.O.C.

Abstract— Plasmonic Bloch oscillations, an analog of electron Bloch oscillations in lattice, are periodic oscillations of optical beams that propagate in metal-dielectric waveguide arrays (MDWAs), which is caused by the alternating total internal reflection and Bragg reflection between the two boundaries of the waveguide arrays. When the electric field imposed on the lattice is increased, electron Zener tunneling will occur at the Brillouin zone boundary. However, plasmonic Zener tunneling has been never observed in MDWAs. Neither has the possibility that the optical beam tunneling into the next band will experience another Bloch oscillation been investigated.

In this study, plasmonic Zener tunneling and the succeeding plasmonic Bloch oscillation in MDWAs are explored by performing both FDTD simulations and theoretical analyses. The MDWAs consists of alternative silver layers and dielectric layers. The relative permittivities of the dielectric layers have a constant gradient across the waveguide arrays.

The plasmonic Zener tunneling is observed at the position of total reflection (Bloch wavevector $kx = 0$), which is caused by that the gap between the first and second equal-kz (longitudinal wavevector) bands is minimum at $kx = 0$, originated from the effectively (transverse) negative refraction index of the MDWAs. The relation between tunneling rate and permittivity gradient is elucidated. The FDTD-simulated contours of magnetic field intensity correlate well with the predicted ray trajectory using Hamiltonian optics. Furthermore, the tunneling beam is also observed to undergo Bloch oscillation in the FDTD simulation. This Bloch oscillation leads to beam's curling due to change of the direction of the energy flow. Depending on the incident frequency, the curling beam will move backward, move forward, or even remain unmoved.

Manipulating Radiation Patterns by Exciting Local Surface Plasmon Resonances in Plasmonic Nanostructures

Wei-Chih Liu
Department of Physics, National Taiwan Normal University, Taiwan

Abstract— Plasmonics has been employed to realize the nanoscale photonic devices, to confine and manipulate electromagnetic fields in subwavelength scale. For a nanostructure whose size is much smaller than the illuminating wavelength, its optical properties can usually be described by the dipole radiation model. Nevertheless, metallic nanoparticles with specific geometric arragement exhibit local and high-order surface plasmon resonances, which have even better field localization and enhancement in the vicinity of metallic nanoparticles. They also have higher sensitivities to the variation of the surrounding medium. Those advantages make the local surface plasmon mode a better candidate to local field enhancement and optical sensing.

Local plasmon resonance and coupling of coated metallic nanoparticles was studied numerically by finite-difference time-domain (FDTD) simulations. For the simplest configuration, a metallic nanoparticle coated with dielectric material was used to excite high-order plasmon by controlling the refractive index, radius of the coated medium, and incident wave frequency. Array of metallic nanoparticles with coated dielectric environment is also capable to excite local plasmon resonance between nanoparticles and to manipulate its radiation patterns. The coated dielectric shell plays the rolte to control local environment and local surface plasmon resonance and radiation patterns are sensitive to the local environment. Other approach to excite local surface plasmon resonances is to change the shape of nanoparticle to break symmetry. For example, a vertical-cut nanoparticle minimized dipole mode at resonance condition. Here the resonance conditions and sensitivity of local plasmonic modes were investigated by FDTD simulations systematically. The spectra properties of local plasmon modes and coupling of metallic nanoparticles have important applications for chemical or bio-sensor and nanophotonic devices.

Cascade Enhancement of Optical Transmission through Composite Subwavelength Apertures in Terms of Hybridization Theory

Kuan-Ren Chen[1, 2, 3], **Anatoliy V. Goncharenko**[1], **and Jian-Shiung Hong**[2, 3]

[1]Department of Physics, National Cheng Kung University
1 University Road, Tainan 70101, Taiwan, R.O.C.
[2]Institute of Electro-optical Science and Engineering
National Cheng Kung University, 1 University Road, Tainan 70101, Taiwan, R.O.C.
[3]Advanced Optoelectronic Technology Center
National Cheng Kung University, 1 University Road, Tainan 70101, Taiwan, R.O.C.

Abstract— The enhanced transmission of light through a subwavelength aperture in a metal film is an interesting and important research topic in plasmonic nano-photonics. It is believed to be a complex phenomenon involving several mechanisms. One (nonresonant) mechanism originates from the field enhancement by the charge accumulated near the edges of the aperture. The other mechanism is due to resonant excitation of surface plasmons (SPs) of various kind: in-plane SPs (long-range surface plasmon-polaritons and short-range "creeping waves") and vertical resonances (standing waves directed normally to the film plane). As was shown recently, the plasmons of metallic nanostructures can behave like electrons in quantum systems, namely they can mix and hybridize in analogy with the electron wave functions. This "plasmon hybridization" can control the optical properties of metal nanostructures, in particular, it can give rise to enhanced optical transmission. Using Finite-Difference-Time-Domain simulations, we study the enhanced transmission of light through a thin film perforated with composite subwavelength apertures with a goal to optimize the light transmission controlling aperture parameters. Our strategy is based on the effect of cascade enhancement of light transmission in terms of hybridization theory. We have found that, under certain conditions, the transmission through the composite aperture can be greatly enhanced as compared with that of its constituents resulting in the effect like the cascade enhancement. The hybridization of the SPs seems to play a significant role in the cascade enhancement of optical transmission.

Plasmon Waveguide Consisting of Silver-shell Nanorods in Hexagonal Lattice for Long-range Propagation

Yuan-Fong Chau[1] and You Zhe Ho[2]

[1]Department of Electronic Engineering, Ching Yun University, Jung-Li 320, Taiwan, R.O.C.
[2]National Taiwan University, Taiwan, R.O.C.

Abstract— A two-dimesional plasmon waveguide in the form of rows of silver-shell nanorods in hexagonal lattice is proposed and compared to the solid-silver case. Transport of energy due to surface plasmon coupling is investigated with finite element method for visible range wavelengths. The proposed waveguide is divided into several sections with each region consisting of ten nanorods. Results show that the waveguide flow energy exhibits long-range propagation ($> 8\,\mu$m, See Figure 1) by using series connection of each section, which plays the major roles in coupling between them.

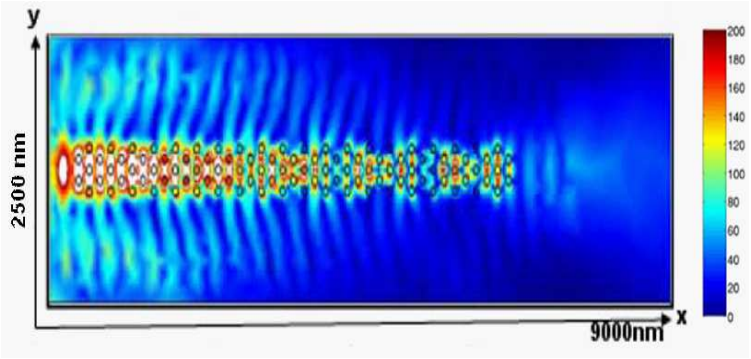

Figure 1: Magnetic field component Hy of the propagating beam in the waveguide ($> 8\,\mu$m).

ACKNOWLEDGMENT

The authors acknowledge the financial support from the National Science Council of the Republic of China (Taiwan) under Contract No. NSC 99-2112-M-231-001-MY3 and NSC-99-2120-M-002-12.

REFERENCES

1. Chau, Y.-F., H.-H. Yeh, and D. P. Tsai, "Near-field optical properties and surface plasmon effects generated by a dielectric hole in a silver-shell nanocylinder pair," *Appl. Opt.*, Vol. 47, 5557–5561, 2008.
2. Saj, W., "FDTD simulations of 2D plasmon waveguide on silver nanorods in hexagonal lattice," *Opt. Express*, Vol. 13, 4818–4827, 2005.

Controlling the Fluorescence of Single Molecules with Optical Antennas

S. Goetzinger[1], **K.-G. Lee**[1], **X. Chen**[1], **H. Eghlidi**[1], **A. Renn**[1], **and V. Sandoghdar**[2]

[1]Laboratory of Physical Chemistry, ETH Zurich, Zurich 8093, Switzerland
[2]Max Planck Institute for the Science of Light, Erlangen 91508, Germany

Abstract— It is well known that the properties of an emitter depend not only on the emitter itself but also on its environment. In this presentation we will discuss how optical antennas can be used to enhance light-emitter interaction and how the emission properties of a single emitter can be dramatically altered. Two types of antennas are presented. With a metallic nanoantenna consisting of a single gold nanoparticle attached to the end of a dielectric tip, we experimentally achieved enhancements up to 30 times for the fluorescence of a single molecule. By accounting for the tip shaft and the sample interface in finite-difference time-domain calculations, we explain why the measured fluorescence enhancements are higher in the presence of an interface than the values predicted for a homogeneous environment. Key parameters such as gold nanoparticle size, tip-molecule distance, and refractive index of the substrate are considered for the optimal outcome. Such a nanoantenna can be used as a scanning near-field probe to image single molecules with a resolution better than 20 nm [1].

In another experiment we embedded a single organic molecule in a planar dielectric antenna which directs the emission towards the collection optics. We realized a single-photon source with near-unity collection efficiency and a record count rate of 50×10^6 photons per second [2]. With our current design we collect 96% of the photons emitted by a single molecule. Our approach is wavelength insensitive and compatible with cryogenic experiments. We will discuss various details of the design, fabrication and characterization of our dielectric planar antenna and its various applications to other types of single emitters such as semiconductor quantum dots, diamond color centers, or ions in the solid-state.

REFERENCES

1. Eghlidi, H., et al., *Nano Letters*, Vol. 9, 4007, 2009.
2. Lee, K.-G., X. W. Chen, H. Eghlidi, P. Kukura, R. Lettow, A. Renn, V. Sandoghdar, and S. Götzinger, "A planar dielectric antenna for directional single-photon emission and near-unity collection efficiency," *Nature Photonics*, Vol. 5, 166–169, January 30, 2011, DOI: 10.1038/NPHOTON.2010.312.

Session 3P1b
Optics and Photonics 1

Biosensors Based on Waveguided Metallic Photonic Crystals

Xinping Zhang[1], **Xuemei Ma**[2], **Fei Dou**[1], **Pengxiang Zhao**[2], **and Hongmei Liu**[1]

[1]Institute of Information Photonics Technology, College of Applied Sciences
Beijing University of Technology, Beijing 100124, China
[2]College of Life Science and Bio-Engineering
Beijing University of Technology, Beijing 100124, China

Abstract— Metallic photonic crystals (MPCs) [1] based on the coupling between the particle plasmon resonance (PPR) or localized surface plasmon resonance (LSPR) and the photonic resonance modes are the promising candidates for the development of sensors [2, 3] and optoelectronic devices [4–6]. A biosensor based on the waveguided MPCs is reported in this work for the sensitive testing of biomolecular interactions, which provides practical approaches for the label-free detection of specific bioreactions and for drug screening. The enhancement of the sensitivity or the amplification of the sensor signal by the coupling between the waveguide resonance mode and the PPR breaks through the "bottleneck" of the intrinsic response sensitivity defined by the spectral shift of the PPR. The detection of the HIV virus is demonstrated through sensing the specific reaction between the HIV1 capsid protein (p24) antigen and the monoclonal anti-p24 antibody to show the successful realization and application of this kind of biosensors. Strong narrow-band spectroscopic response that is defined as the sensor signal has been obtained at an antigen concentration of 500 ng/ml or 0.5 ppm with potentially large space for improvement. The most important advantages of this sensor over the conventional biochemical methods lie in that no labeling on the biomolecules is required and that the dynamics of the bioreactions can be recorded with a high time resolution. Furthermore, this sensor device is featured with the simple fabrication technique of the MPCs using solution-processible gold nanoparticles [7, 8] and the simple spectroscopic measurements involved in the practical operation as compared with the conventional couterpart based on surface plasmon resonance.

REFERENCES

1. Christ, A., S. G. Tikhodeev, N. A. Gippius, J. Kuhl, H. Giessen, *Phys. ReV. Lett.*, Vol. 91, 1839011–1839014, 2003.
2. Kabashin, A. V., P. Evans, S. Pastkovsky, W. Hendren, G. A. Wurtz, R. Atkinson, R. Pollard, V. A. Podolskiy, and A. V. Zayats, *Nature Materials*, Vol. 8, 867–871, 2009.
3. Anker, J. N., W. P. Hall, O. Lyandres, N. C. Shah, J. Zhao, and R. P. Van Duyne, *Nature Materials*, Vol. 7, 442–453, 2008.
4. Zhang, X. P., B. Q. Sun, J. M. Hodgkiss, and R. H. Friend, *Adv. Mater.*, Vol. 20, 4455–4459, 2008.
5. Zhang, X. P., H. M. Liu, J. R. Tian, J. Y. Song, and L. Wang, *Nano Lett.*, Vol. 8, 2653, 2008.
6. Yu, N., J. Fan, Q. J. Wang, C. Pflügl, L. Diehl, T. Edamura, M. Yamanishi, H. Kan, and F. Capasso, *Nature Photonics*, Vol. 2, 564–570, 2008.
7. Zhang, X. P., B. Q. Sun, R. H. Friend, H. C. Guo, D. Nau, and H. Giessen, *Nano Lett.*, Vol. 6, 651–655, 2006.
8. Zhang, X. P., H. M. Liu, and S. F. Feng, *Nanotechnology*, Vol. 20, 425303, 2009.

Spontaneous Emission in 2D Arbitrary Inhomogeneous Environment

Peng-Fei Qiao[1], **Wei E. I. Sha**[1], **Yongpin P. Chen**[1], **Wallace C. H. Choy**[1], **and Weng Cho Chew**[1, 2]

[1]Department of Electrical and Electronic Engineering
The University of Hong Kong, Pokfulam Road, Hong Kong, China
[2]Department of Electrical and Computer Engineering
University of Illinois, Urbana-Champaign, USA

Abstract— Control of spontaneously emitted light lies at the heart of quantum optics. It is essential for diverse applications ranging from lasers, light-emitting diodes, solar cells, and quantum information. According to the quantum electrodynamics theory, the spontaneous emission (SE) of an atom can be a weak-coupling radiation process due to the vacuum fluctuations of electromagnetic field. A suitable modification of inhomogeneous environment is required so that the vacuum fluctuations controlling the SE can be manipulated. Inhibiting unwanted SE and boosting desired ones will promote the novel optoelectronic designs tailored to industrial standard. The local density of states (LDOS) counts the number of electromagnetic modes where photons can be emitted at the specific location of the emitter, and can be interpreted as the density of vacuum fluctuations. The inhibition or enhancement of SE boils down to how the LDOS of photons is controlled.

In this work, the SE of the excited atoms in 2D arbitrary inhomogeneous environment has been systematically studied. The LDOS determines the radiation dynamics of a point source (for 3D) or a line source (for 2D). In particular, it also determines the SE rate, and the LDOS is represented by the electric dyadic Green's function. The numerical solution of the electric Green's tensor has been accurately obtained by the finite-difference frequency-domain method with the proper approximations of the monopole and dipole sources. The SE of the atoms in the photonic crystal and plasmonic metal plates has been comprehensively and comparatively investigated. For both systems, the SE strongly depends on their respective dispersion relations and could be modified or tuned by the finite-structure or finite-size effects. This work is important for the SE engineering and optimized design of optoelectronic devices.

Optical Properties of Graphene and BN Sandwiched Graphene Based on the First-principle Theory and Kramers-Kronig Relation

Xiao Lin[1, 2], **Yang Xu**[2], **and Hongsheng Chen**[1, 2]

[1]The Electromagnetics Academy at Zhejiang University
Zhejiang University, Hangzhou 310027, China
[2]Department of Information and Electronic Engineering
Zhejiang University, Hangzhou 310027, China

Abstract— We present a detailed and systematical study of the optical properties of monolayer graphene and BN sandwiched graphene without charge doping in the photon energy range of 0 eV to 9 eV based on the first principle theory and Kramers-Kronig relation, including the conductance, permittivity, refractive index, transmittance, reflectance and absorbance. We find the universality of the real part of optical conductance of monolayer graphene does not survive above 1.0 eV and the imaginary part of conductance of monolayer graphene has the same order of magnitude as the real part, which is non-ignorable in the whole frequency range. As a comparison, the properties of monolayer graphene and BN sandwiched graphene with charge charge doping are also investigated.

Development of Terahertz Wave Radiation Control Device

Keita Okada, Mitsuhiro Shinomiya, Tosihiko Kiwa, and Keiji Tsukada
Department of Electrical & Electronic Engineering, Division of Industrial Innovation Sciences
Graduate School of Natural Science & Technology, Okayama University
3-1-1 Tsushimanaka, Kita-ku, Okayama 700-8530, Japan

Abstract— Recently, the development of the terahertz (THz) wave imaging technology and the device has progressed rapidly. Especially, the imaging systems with THz pulses excited by femtosecond lasers are attracted because of its broad band spectra of the THz source. The THz imaging generally requires mechanical beam scanning to obtain the 2D or 3D images. Therefore, this type of systems requires relatively large mechanical movable components in order to steer the THz beam or move the objects. In this study, we have proposed and developed a THz wave radiation control device which can electrically switch the direction of the THz wave radiation.

The proposed device consisted with the 8×8 arrayed THz emitters. The each device was prepared by depositing the Metal/SiO_2/Si thin films on a sapphire substrate. The femtosecond laser is irradiated from the sapphire substrate side to this device and THz wave emitted to free space. The bias voltage could be independently applied to each metal film, and thus the amplitude of THz wave from each emitter could be controlled by the bias voltage.

When the laser was irradiated with a given incident angle to the device, the phase shift of THz was occurred along the projection line of the laser to the device surface because the arrival timing of the laser pulse shift. The fact indicates that each emitter can generate the THz wave with a different phase. Thus the direction of the THz wave can be controlled by turning of the specific emitters as the result of phased-array effect. Actually, prior to the experiment, we simulate the emission pattern from the device using the small-dipoles model, and confirmed that the direction of the THz wave depends on the pattern of the turned-on emitters. The test device was also fabricated by a standard semiconductor fabrication process and we successfully demonstrated the independent control of the amplitude of each emitter.

Subgridding Scheme for FDTD in Cylindrical Coordinates

Adam Mock
School of Engineering and Technology, Central Michigan University, USA

Abstract— This presentation will discuss subgridding approaches applicable to the finite-difference time-domain (FDTD) method in cylindrical coordinates. In cylindrical coordinates, the cell size along the azimuthal (ϕ) direction increases as the radius increases according to $\Delta s = i\Delta r\Delta\phi$, where i is the radial index, Δr is the radial discretization length and $\Delta\phi$ is the azimuthal angular discretization. Even for uniform Δr and $\Delta\phi$, the actual FDTD cell size along $\phi(\Delta s)$ increases as i increases. This results in high resolution for small i and low resolution for large i. This inherent non-uniformity in cell size for cylindrical coordinates FDTD motivates the development of techniques for controlling the cell size, so that the overall geometry is resolved more uniformly which will lead to better accuracy with the same amount of computational effort.

The proposed method will be applied to the analysis of microstructured optical fibers (MOFs). MOFs differ from standard optical fibers by the inclusion of micrometer scale geometric features in the cross section that run the entire length of the fiber [1]. Figure 1(a) illustrates the magnetic field associated with a MOF made up of a triangular hole array with 7 holes missing from the center. More details on the numerical procedures can be found in our previous work [2]. The field is confined to the central defect region due to both a larger effective index there as well as Bragg reflection from the periodic dielectric constant surrounding the defect region. Figure 1(b) illustrates the FDTD gridding scheme implemented in cylindrical coordinates investigated in this work. Both a course grid and a fine grid are displayed along with the interface between the two. In the example shown in Figure 1(b), the spatial resolution is improved at a given i by reducing the azimuthal angular discretization $\Delta\phi$ by two. The spatially staggered arrangement associated with the Yee approach makes interfacing course and fine grids challenging. This presentation will report on interpolation strategies used to estimate field values at points needed to update field components on the course grid/fine grid boundary. Results for error in the frequency and propagation loss as a function of βa (where a is the distance between holes in the triangular lattice) when compared to an FDTD calculation run in which the entire geometry is discretized using the fine grid are shown in Figures 1(c) and (d). Linear, cubic, trigonometric and cubic spline interpolations were investigated. Figure 1(c) shows that the subgridding introduces less than 1% error into the calculated propagating mode frequencies for a given β value and that cubic, trigonometric and cubic spline interpolations are all better than linear interpolation. Figure 1(d) shows that except for one data point corresponding to trigonometric interpolation at $\beta a = 3.8$ the subgridding introduces less than 30% error into the calculated propagation loss as a function of β. For the propagation loss, it appears that the linear interpolation method exhibits the lowest error when compared to a purely fine grid calculation. Interpretation of these results will be elaborated in the presentation.

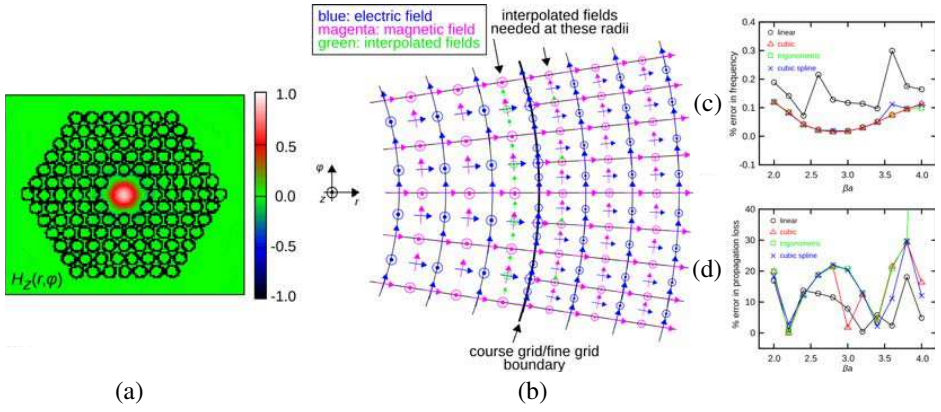

Figure 1: (a) Field distribution in microstructured optical fiber. (b) Course grid/fine grid boundary. Error in (c) frequency and (d) propagation loss associated with different interpolation schemes applied to obtain unknown fields illustrated in green in (b).

REFERENCES

1. Russell, P. S. J., "Photonic-crystal fibers," *IEEE Journal of Lightwave Technology*, Vol. 24, No. 12, 4729–4749, 2006.
2. Mock, A. and P. Trader, "Photonic crystal fiber analysis using cylindrical FDTD with Bloch boundary conditions," *PIERS Online*, Vol. 6, No. 8, 783–787, 2010.

Nonlinear Electromagnetics in Negative Index Metamaterials

A. K. Popov
University of Wisconsin-Stevens Point, USA

Abstract— Nanostuctured negative-index metamaterials (NIMs) form a novel class of artificial electromagnetic materials that promises revolutionary breakthroughs in photonics. Such metamaterials are expected to play a key role in the development of novel photonic microdevices and all-optical data processing chips. Significant progress has been achieved recently in the design of bulk, multilayered, negative-index, plasmonic slabs. The problem, however, is that these structures introduce strong losses inherent to metals that are difficult to avoid. Unlike ordinary materials, the energy flow and wave vector (phase velocity) are counter-directed in NIMs. Negative-index properties and, therefore, backwardness of electromagnetic waves are usually achievable only within a certain wavelength band. Metamaterials remain ordinary, positive index, outside such interval. This opens the opportunities of unique schemes of nonlinear-optical coupling between the ordinary and backward electromagnetic waves, which meet the requirements of the phase matching. It is because all wave vectors remain parallel, whereas some of the energy flows inside the metamaterial appear counter-directed. Such unusual nonlinear propagation processes exhibit extraordinary properties not achievable in ordinary nonlinear optical materials and not described in the literature [1–6]. This paper is to propose several such coupling schemes and to present analysis of the operational properties for one of them in the context of their applications to compensating strong losses inherent to plasmonic metamaterials and to design novel photonic devices for to optical sensing and data processing. Each of the schemes provides different distribution of the coupled fields (hot zones) across the originally strongly absorbing metamaterial slab. The outlined possibilities to implement originally strongly absorbing microscopic samples of plasmonic metal-dielectric composites for the remote all-optically tailoring of their transparency and reflectivity as well as the options for creating of unique ultracompact photonic sensing devices is demonstrated through numerical simulations. Different schemes of coherent energy transfer from strong control field to the negative-index signals described here present alternative approaches to compensating losses in NIMs based on the population inversion (such as recent breakthrough reported in [7]).

ACKNOWLEDGMENT

Stimulating discussions with V. M. Shalaev and S. A. Myslivets and support of this work by the National Science Foundation under Grant No. ECCS-1028353 are greatly acknowledged.

REFERENCES

1. Shadrivov, I. V., A. A. Zharov, and Y. S. Kivshar, *J. Opt. Soc. Am. B*, Vol. 23, 529–534, 2006.
2. Scalora, M., G. D'Aguanno, M. Bloemer, M. Centini, N. Mattiucci, D. de Ceglia, and Yu. S. Kivshar, *Opt. Express*, Vol. 14, 4746–4756, 2006.
3. Popov, A. K. and V. M. Shalaev, *Opt. Lett.*, Vol. 31, 2169–2171, 2006.
4. Elyutin, S. O., A. I. Maimistov, and I. R. Gabitov, *JETP*, Vol. 111, 157–169, 2010.
5. Popov, A. K., *Eur. Phys. J. D*, Vol. 58, 263–274, 2010.
6. Popov, A. K. and T. F. George, *Computational Studies of New Materials II: From Ultrafast Processes and Nanostructures to Optoelectronics, Energy Storage and Nanomedicine*, Chapter 13, Edited by T. F. George, D. Jelski, R. R. Letfullin, and G. Zhang, World Scientific, Singapore, 2010.
7. Xiao, S., V. P. Drachev, A. V. Kildishev, X. Ni, U. K. Chettiar, H.-K. Yuan, and V. M. Shalaev, *Nature*, Vol. 466, 735–738, 2010.

Session 3P2
Metamaterials for Achieving Extraordinary Properties and Performances

Manipulating Electromagnetic Wave Polarization through Reconfigurable Metamaterial Structure

Yijun Feng, Bo Zhu, Jinglong Fan, Junming Zhao, and Tian Jiang
School of Electronic Science and Engineering, Nanjing University, Nanjing 210093, China

Abstract— Metamaterials, as an artificial material, open the access to controlling material constitutive parameters in terms of values, distributions, anisotropy and chirality through material structure designing. Owing to their unique features, metamaterials have been applied to manipulate electromagnetic (EM) characteristics including polarizations, such as polarization manipulation through anisotropic metamaterials [1, 2] and chiral metamaterials [3, 4] in microwave regimes. For polarization manipulation and modulation, it is still required to have flexible control (preferable of electrical control) of polarization in transmission or reflection of the EM waves.

In this paper, we will demonstrate new ways to freely manipulate EM polarization through tunable or reconfigurable metamaterials. We will firstly demonstrate a controllable electromagnetic wave reflector/absorber for different polarizations with metamaterial involving electromagnetic resonant structures coupled with diodes. Through biasing at different voltages to turn on and off the diodes, we are able to reconfigure the structure between nearly total reflection and total absorption of a particularly polarized incident wave. By arranging orthogonally orientated resonant cells, the metamaterial can react to different polarized waves by selectively biasing the corresponding diodes. Then, we will demonstrate a polarization modulation scheme at the microwave band based on the EM reflection of the controllable metamaterial reflector/absorber. By illuminating the metamaterial with a specific linearly polarized EM wave and tuning the bias voltage on diodes, the reflected EM wave can be linearly polarized with the polarization angle continuously controlled from 0° to 90° at the resonant frequency, or the reflection can be right-handed or left-handed elliptically polarized with the major axis angle controlled between 0° and 90°, when operated off the resonant frequency. We will present the design, EM simulation, fabrication and experimental validation of the proposed ideas which allows us to electrically manipulate and modulate the EM wave polarization flexibly.

ACKNOWLEDGMENT

Supported by the National Nature Science Foundation of China (60990322, 60990320, 60801001), and the Ph.D. Programs Foundation of Ministry of Education of China (20100091110036).

REFERENCES

1. Hao, J., et al., *Phys. Rev. Lett.*, Vol. 99, 063908, 2007.
2. Chin, J. Y., M. Lu, and T. J. Cui, *Appl. Phys. Lett.*, Vol. 93, 251903, 2008.
3. Ye, Y. and S. He, *Appl. Phys. Lett.*, Vol. 96, 203501, 2010.
4. Li, T. Q., et al., *App. Phys. Lett.*, Vol. 92, 131111, 2008.

The Quantum Property of Coupled Metamaterial

Shuming Wang, Shiyao Mu, Cong Zhu, Ping Xu, Tao Li, Hui Liu, and Shining Zhu
National Laboratory of Solid State Microstructures, Department of Physics
Nanjing University, Nanjing, 210093, China

Abstract— In recent years, there has been increasing interest in studying the quantum characteristics in plasmonic metamaterials. By using the Hamiltonian combined with second quantization, we have investigated the basic excitation of the coupled metamaterials and presented a quantum description of them. The interaction between the excitation of the coupled metamaterial and the exciton in the quantum dot material has been further considered with the aid of the interaction Hamiltonian. To prove our theoretical treatment, we have done a two-photon interference experiment that indicates the quantized exciting in coupled metamaterial. In such a damping system, a set of Langevin equations has been used to deal with the quantum motion of the system. And the stimulated emission has been found, which can be used to form a nano-laser. The quantum description of coupled metamaterial and the interaction system could work as the fundamental method in paving the way for studies on quantum effects in coupled metamaterials.

Dirac "Photon" in Metamaterials

Kazuaki Sakoda
Quantum Dot Research Center, National Institute for Materials Science
1-1 Namiki, Tsukuba 305-0044, Japan

Abstract— Photon-dispersion engineering with structured materials like photonic crystals [1] and metamaterials [2] has become a powerful tool in the optical science and communication technology. In some applications, the linear photon dispersion relation at high frequencies in the Brillouin-zone center is required, which previously was difficult to achieve with conventional structures. Combined with the time-reversal symmetry of the wave equation, the linear dispersion implies the Dirac "photon", which is the counterpart of the Dirac "fermion" in graphene. Recently this problem was solved by using left-handed materials and its theoretical foundation was provided by the transmission line theory [2]. In this presentation, I will reformulate this problem from a view point of the structural electromagnetic resonance and its spatial symmetry based on the tight-binding picture (Fig. 1) [3], and give the conditions for the linear dispersion. I will further extend the tight-binding calculation to the case of degenerate resonance modes with different polarizations and propose the method of *controlled symmetry reduction*, which easily realizes the linear dispersion in optical frequencies [4].

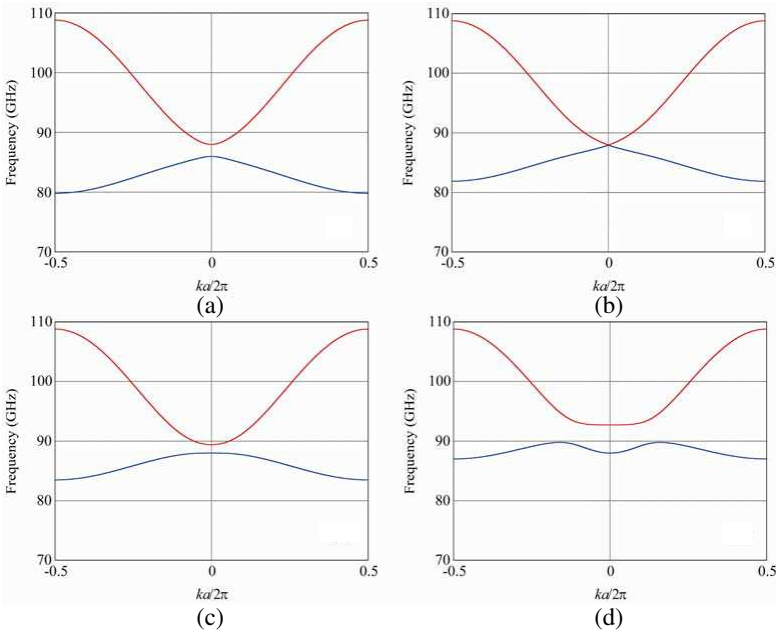

Figure 1: Dispersion curves of one-dimensional metamaterials calculated by the tight-binding approximation. According to the amount of the frequency separation between the two resonance modes of the metamaterial unit structure ((a) the largest separation to (d) the smallest separation), dispersion curves are first quadratic (a), then linear (b), and finally quadratic (c) (d) again in the vicinity of the Brillouin-zone center [3].

REFERENCES

1. Sakoda, K., *Optical Properties of Photonic Crystals*, 2nd Edition, Springer Verlag, Berlin, 2004.
2. Caloz, C. and T. Itoh, *Electromagnetic Metamaterials — Transmission Line Theory and Microwave Applications*, Wiley, Hoboken, 2006.
3. Sakoda, K. and H.-F. Zhou, *Opt. Express*, Vol. 18, 27371, 2010.
4. Sakoda, K. and H.-F. Zhou, *J. Appl. Phys.*, submitted.

Switching of Forward and Backward Wave Propagation in a Two-dimensional Nonlinear Transmission-line Metamaterial

Zhengbin Wang[1, 2], **Yijun Feng**[1], **Junming Zhao**[1], **Zhenzhong Yu**[1], **and Tian Jiang**[1]

[1]School of Electronic Science and Engineering, Nanjing University, Nanjing 210093, China
[2]College of Science, Nanjing University of Posts and Telecommunications, Nanjing 210003, China

Abstract— Inductance and capacitance loaded transmission-line (TL) structures have been employed to investigate the electromagnetic (EM) wave propagation in left-handed (LH) metamaterials owing to their many advantages, such as broadband, low loss and easy to realize experimentally [1]. Recently left-handed nonlinear transmission lines (LH NLTLs), which incorporate loaded nonlinear capacitance or inductance elements with the ordinary LH TL structures, have proved to be a simple and easy-to-realize system to investigate the EM wave propagation in nonlinear LH media [2, 3]. However, all these researches are in one-dimensional, which limit the study of wave propagation phenomena. Here, we will present the investigation of the wave propagation in a two-dimensional (2D) LH NLTL metamaterial.

We will first establish the theory that describes the generation and propagation of the fundamental wave and its high harmonics in a 2D nonlinear and self-induced tunable metamaterial. Then, we will show the detailed design of the 2D LH NLTL metamaterial and its nonlinear and tunable performance. The special dispersion characteristic of the LH NLTL enables the fundamental frequency (FF) wave and its second or third harmonics operating in opaque, LH or right-handed (RH) states. Furthermore, we find the nonlinear metamaterial is intensity dependent and may switch between the LH medium and the RH medium (as shown in Fig. 1). We believe that this analogous study will bring more information and provide a realizable method to explore the nonlinear metamaterials.

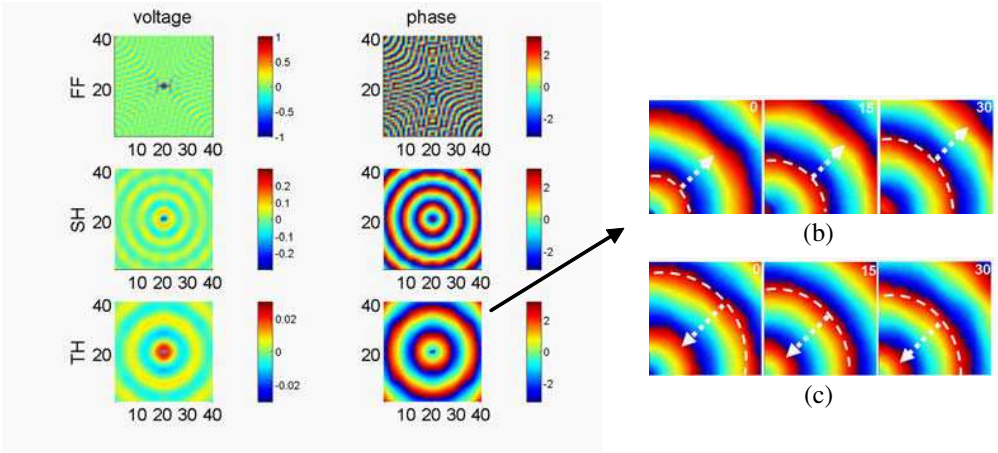

Figure 1: A point source operated at 0.35 GHz propagates inside the 2D LH NLTL metamaterial (40×40 cells). (a) Voltage and phase distributions of the FF, 2nd, and 3rd harmonic field with the 1 V source. The insets show the dynamic phase maps of the 3rd harmonic wave demonstrating (b) the forward wave with 1 V source, or (c) the backward wave with 5 V source.

ACKNOWLEDGMENT

Supported by the National Nature Science Foundation of China (60990322, 60990320, 60801001), and the Ph.D. Programs Foundation of Ministry of Education of China (20100091110036).

REFERENCES

1. Lai, A., C. Caloz, and T. Itoh, *IEEE Microwave Magazine*, Vol. 5, 34, 2004.
2. Shahvarpour, A., S. Gupta, and C. Caloz, *J. Appl. Phys.*, Vol. 104, 124510, 2008.
3. Kozyrev, A. B. and D. W. Van Der Weide, *Appl. Phys. Lett.*, Vol. 96, 104106, 2010.

Making a Solid Metallic Film Perfectly Transparent

Zhengyong Song, **Qiong He**, **and Lei Zhou**
Surface Physics Laboratory (State Key Laboratory) and Department of Physics
Fudan University, Shanghai 200433, China

Abstract— It is highly desirable to make a metal transparent for light, owing to many application requests for transparent metals in optoelectronics devices such as solar cells. Extraordinary optical transmission (EOT) is one of the mechanisms to make an opaque metal transparent, but such a mechanism typically requires the metallic film to be perforated with subwavelength openings such as holes [1] or slits [2]. In addition, to achieve a high transmission, strict periodicity is required for the opening array perforated on the metal film, which adds substantial fabrication difficulties.

In this work [3], we proposed an alternative approach to make an *undamaged* metal film *perfectly* transparent. By attaching two subwavelength metamaterial layers consisting of metal-dielectric stripes to the opaque metallic layer, we found that the entire system becomes *perfectly transparent* when the geometrical and material parameters satisfy certain conditions (Fig. 1). The present transparency is governed by a particular resonant tunneling effect, which can be explained by an effective medium theory (see the pink line in Fig. 1). Since our mechanism neither requires a strict periodic arrangement of the metal-dielectric stripes nor any openings on the opaque metallic plate, the proposed structure is relatively easy to fabricate in practice compared to the EOT-based structures. We employed full-wave simulations and experiments to verify the idea in visible (simulation) and microwave (experiment) frequency regimes.

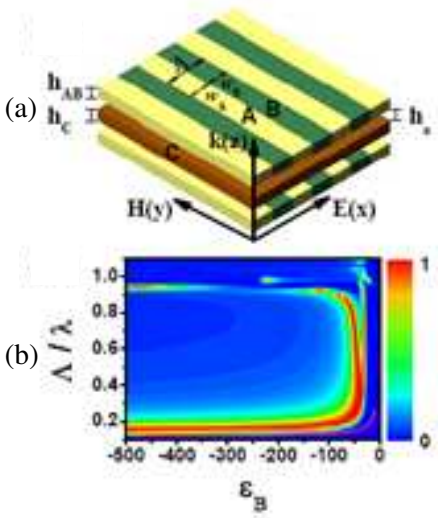

Figure 1: (a) Schematic illustration of the structure. (b) Transmission as functions of ε_B and Λ/λ.

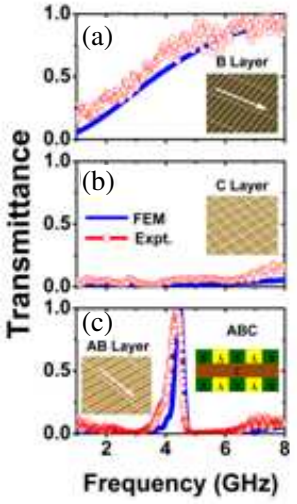

Figure 2: (a) Measured (open circles) and simulated (solid lines) transmission spectra of B layer, (b) C layer, (c) and ABC structure. The designed samples are shown in the insets.

REFERENCES

1. Ebbesen, T. W., et al., *Nature*, Vol. 391, 667, London, 1998.
2. Porto, J. A., et al., *Physical Review Letters*, Vol. 83, 2845, 1999.
3. Song, Z. Y., et al, unpublished.

Optical Properties of Metallic Helix Array

Hongqiang Li[1], **Chao Wu**[1], **Zeyong Wei**[1], **Xing Yu**[1], **Fang Li**[1], **and C. T. Chan**[2]

[1]Physics Department, Tongji University, Shanghai 200092, China
[2]Department of Physics, Hong Kong University of Science and Technology
Clear Water Bay, Kowloon, Hong Kong, China

Abstract— Helix array, as one typical member in the family of chiral metamaterials, possesses a lot of exotic optical properties that have not been recognized before. In this talk, a semi-analytical photonic band theory of helix array and related fine features, such as longitudinal mode, fixed points at irreducible Brillouin zone boundary et al, are presented. The calculations and experimental verification on the negative refraction via a chiral route, the axial and transverse propagation in helix array, as well as asymmetric transmission and dichroism are also discussed.

REFERENCES

1. Pendry, J. B., "A chiral route to negative refraction," *Science*, Vol. 306, No. 5700, 1353–1355, 2004.
2. Gansel, J. K., et al., "Gold helix photonic metamaterial," *Science*, Vol. 325, No. 5947, 1513–1515, 2009.
3. Wu, C., H. Li, Z. Wei, X. Yu, and C. T. Chan, "Theory and experimental realization of negative refraction in a metallic helix array," *Phys. Rev. Lett.*, Vol. 105, No. 24, 105, 247401, 2010.

A Reflectionless Ultra-thin Microwave Wave-plate Based on Metamaterial

Wujiong Sun, **Qiong He**, **Jiaming Ha**, **and Lei Zhou**
Department of Physics, Fudan University, Shanghai 200433, China

Abstract— It is highly desirable to efficiently control the polarization of electromagnetic (EM) wave, due to many application requests. Conventional methods to manipulate the polarization of light (based on Faraday, Kerr, birefringence effects, etc.) typically require a system much thicker than wavelength, which are inconvenient for low-frequency applications. Although an optical grating can be very thin, it suffers the energy loss problem since the system is not perfectly transparent.

Metamaterials, artificial materials composed by resonant microstructures to exhibit arbitrary values of effective ε and μ, open a new way to manipulate the polarization. It was recently shown that a specifically designed metamaterial reflector can efficiently manipulate EM wave polarizations [1]. The device is much thinner than wavelength and does not suffer the energy loss issue since it is perfectly reflecting for EM waves [1]. However, the reflection geometry makes it inconvenient for practical applications due to the interference between incident and reflected waves. While some newly proposed metamaterial devices [2] can avoid the interference problem, they are typically *not* perfectly transparent for EM waves so that the energy-loss issues remain unsolved.

Here we design an ultra-thin metamaterial wave-plate (see Fig. 1) to manipulate EM wave polarizations in transmission geometry. The proposed device is much thinner than wavelength, *perfectly transparent* for EM waves at the working frequency, and can manipulate the EM wave polarizations efficiently. The key idea of the design is to adjust the perfect transmissions for two incident polarizations, which are governed by different mechanisms, to occur at the same frequency. Microwave experiments are performed on realistic samples to demonstrate the polarization manipulation effects, with obtained results agreeing well with numerical simulations (see Fig. 2) [3].

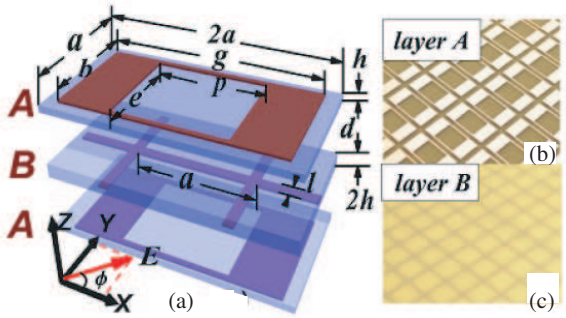

Figure 1: Geometry of the device and sample pictures.

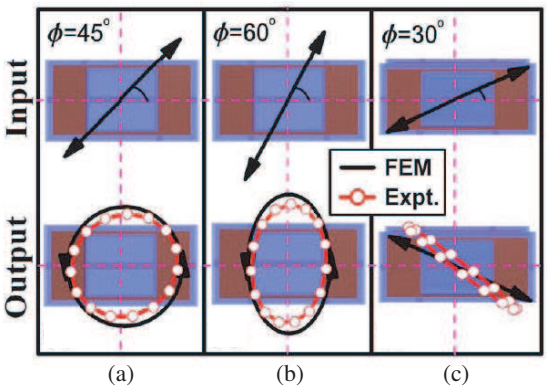

Figure 2: Polarization manipulation effects by our designed device.

REFERENCES

1. Hao, J., Y. Yuan, L. Ran, T. Jiang, J. A. Kong, C. T. Chan, and L. Zhou, *Phys. Rev. Lett.*, Vol. 99, 063908, 2007.
2. Chin, J. Y., M. Z. Lu, and T. J. Cui, *Appl. Phys. Lett.*, Vol. 93, 251903, 2008.
3. Ye, Y. and S. He, *Appl. Phys. Lett.*, Vol. 96, 203501, 2010.
4. Sun, W., Q. He, J. Hao, and L. Zhou, *Opt. Lett.*, Vol. 36, 927, 2011.

Super Imaging with a Plasmonic Metamaterial: Role of Aperture Shape

Shiyi Xiao, **Qiong He**, **Xueqing Huang**, **and Lei Zhou**
Department of Physics, Fudan University, Shanghai 200433, China

Abstract— Conventional imaging devices are subject to the half-wavelength diffraction limit, so that many efforts were recently devoted to proposing new optical imaging systems that can beat the diffraction limit. In 2004, Pendry et al. demonstrated that metallic plates with slits or square holes support spoof surface plasmon polaritons (SPPs) [1]. Inspired by these peculiar SPP properties, holy metallic plates (HMPs) with different aperture-shape were recently suggested to realize subwavelength imaging [2, 3]. There are, however, still several issues remaining unsolved. For example, the role played by the aperture shape is not elucidated and it is not clear what happens if another shape is chosen.

In this paper [4], we analytically studied the imaging properties of a series of HMPs with apertures in either square or fractal shapes (see Figs. 1(a) and (b)), and found two *analytical* conditions for such structures to work as super lenses:

$$\lambda_c \gg d \quad \text{and} \quad S_0 \ll 1 \tag{1}$$

where λ_c is the working wavelength, d is the lattice constant of the aperture array and S_0 is the coupling strength between the external radiations and the fundamental waveguide mode inside the aperture.

As an illustration, we employed finite-difference-time-domain (FDTD) simulations to study the images formed by four square-aperture HMPs with different values of a/d, and depicted the calculated patterns in Fig. 1(c). We also employed FDTD simulations to numerically compute the overlapping strength S_0 for the fractal aperture. Calculations show that, in contrast to the square aperture where S_0 is solely determined by a/d, here for fractal shape S_0 can be tuned by an additional parameter — the width w of each slit. We find that S_0 of the fractal aperture can be made much smaller than that of the square aperture (both have $a/d = 0.9$) by simply decreasing w. This explains why the plasmonic HMP lens with fractal-aperture [3] is more superior than the square-aperture lens [2].

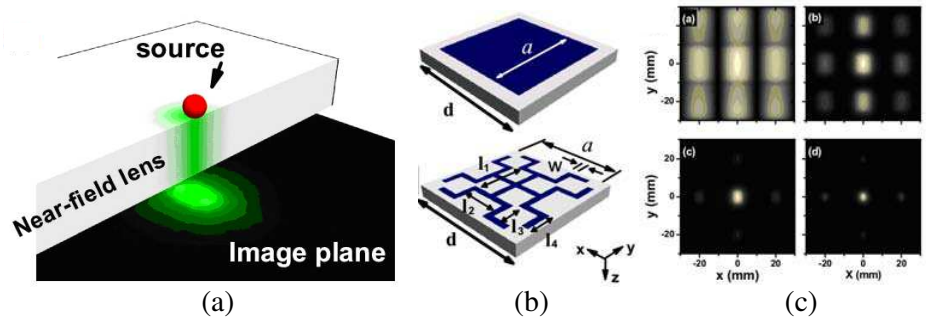

Figure 1: (a) Geometry of the near-field super imaging. (b) Square holes and fractal-like slit patterns. (c) E-field patterns on the image planes of four square-aperture HMPs with different values of a/d: (a) $a/d = 0.9$, (b) $a/d = 0.5$, (c) $a/d = 0.3$ and (d) $a/d = 0.1$.

REFERENCES

1. Garcia-Vidal, F. J., L. Martin-Moreno, and J. B. Pendry, *J. Opt. A: Pure Appl. Opt.*, Vol. 7, S97, 2005.
2. Jung, J., F. J. García-Vidal, L. Martín-Moreno, and J. B. Pendry, *Phys. Rev. B*, Vol. 79, 153407, 2009.
3. Huang, X., et al., *Opt. Express*, Vol. 18, 10377, 2010.
4. Xiao, S., et al., *Metamaterials*, 2011, in press.

Extraordinary Imaging Properties of Hyperbolic Plasmonic Metamaterial Based Lenses

Changbao Ma and Zhaowei Liu
Department of Electrical and Computer Engineering, University of California, San Diego
La Jolla, CA 92093-0407, USA

Abstract— Optical lenses are pervasive in various areas of sciences and technologies. It is well known that the resolving power of a lens and thus optical systems is limited by the diffraction of light. Recently, various superlenses have been emerging to achieve deep subwavelength scale resolution owning to the extraordinary material properties provided by the artificial metamaterials. Despite their success in achieving super resolving power, such superlenses behave distinctively compared to their conventional counterpart. For instance, they cannot focus a plane wave, i.e., no Fourier transform function, which represents a significant defect from both theoretical and practical points of view. To solve that issue, we have recently proposed two types of phase compensated metamaterial lenses: the metamaterial immersion lens (MIL) and the metalens. While having super resolving power, both the MIL and the metalens can focus a plane wave. Such Fourier transform ability is a fundamental function of a lens and the basis of Fourier optics and optical data processing.

We further show that the hyperbolic metalenses, one type of super resolution metalenses made by hyperbolically dispersive plasmonic metamaterials, perform as either converging lenses or diverging lenses depending on which direction one looks at them. Similar to a recent "Janus device" demonstrating multiple optical functions along multiple directions based on the principles of transformation optics, a hyperbolic metalens is a "Janus lens" having two different focusing behaviors (two faces) in opposite directions. This distinctive focusing behavior leads to extraordinary imaging properties that do not exist in common lenses. We derive the imaging equations of the hyperbolic metalenses and their exotic imaging properties are numerically verified. These new imaging properties, along with their super resolving power, significantly expand the horizon of imaging optics and optical system design.

New Circular Fractal Sensors for Near-infrared Wavelengths

R. Malureanu[1], **A. Sandru**[2], **A. Novitsky**[1], **and A. Lavrinenko**[1]

[1]Department of Photonics Engineering, Danish Technical University, Denmark
[2]Department of Electronic Technology and Fiability, Politehnica University of Bucharest, Romania

Abstract— In the last years, the use of metals in optics has been seen in a new light due to advances in theory and modelling of metal-dielectric structures. Due to their unusual behavior, the term "metamaterials" was coined to describe these class of structures.

One of the new possibilities in applying the metamaterials concepts is by using fractal structures [1, 2]. Such structures combine the advantages of the photonic crystals with the ones of frequency selective surfaces [1] thus allowing e.g., obtaining high selective reection using small components. Typically, fractal metamaterials have been reported in microwaves or THz. In this paper, we present the optical properties of the new type of red/near IR fractal resonator, designed aiming at fabrication possibilities.

Due to fabrication issues, we designed a fractal structure having circles as its base elements. By appropriate choosing of the disks' dimensions, a sharp resonance in the second and third generations of the fractals is seen at 810 nm (see Figure 1(a)). Such resonance can be used for sensing applications. The theoretical selectivity this structure reaches is of 780 nm/RIU making it one of the most sensitive structures up to now.

The fractal metamaterial shows high independency of reflection/tranmsission properties with the incidence angle (see Figure 1(b)), thus alleviating the engineering problems that might arise from its use in the real-life applications.

In this paper, we have presented a new type of fractal resonator feasible for reproducible fabrication, which shows enhanced transmission at 810 nm wavelength. When used as a sensor, the theoretical sensitivity is of 780 nm/RIU, one of the biggest ever presented in this range.

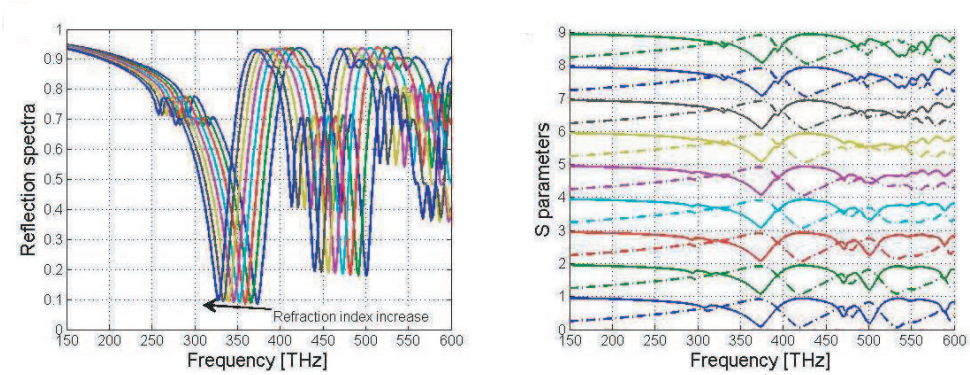

Figure 1: (a) The variation of the reflection spectra with respect to the refraction index of the surrounding media. The refraction index varies from 1 to 1.14 in steps of 0.02; (b) Transmission (dashed) and reflection (solid) spectra when varying the incidence angle from 0 to 80 degrees. The graphs were displaced for better viewing.

ACKNOWLEDGMENT

R. M., A. L. acknowledge partial financial support from FTP NIMbus project. A. N. acknowledge partial financial support from THzCOW project.

REFERENCES

1. Zhou, L., C. T. Chan, and P. Sheng, "Theoretical studies on the transmission and reflection properties of metallic planar fractals," *J. Phys. D: Appl. Phys.*, Vol. 37, 368, 2004.
2. Malureanu, R., A. Lavrinenko, D. Cooke, P. U. Jepsen, S. Xiao, and L. Zhou, "Transmission and reflection properties of terahertz fractal metamaterials," *Conference on Lasers and Electro-Optics and Quantum Electronics and Laser Science Conference*, CTuF7, San Jose, USA, May 16–21, 2010.

Numerical Analyses of the Realization of the D'B' Boundary Condition for Planar Surfaces

Ari Sihvola and Ismo V. Lindell
Department of Radio Science and Engineering, School of Science and Technology
Aalto University, Box 13000, FIC00076 AALTO, Espoo, FINLAND

Abstract— In electromagnetics, special attention has recently been paid to new boundary conditions. Among interesting novel sets of such electromagnetic boundaries are the so-called DB and D'B' boundaries [1]. At a DB boundary, the normal components of the electric and magnetic flux densities vanish [2, 3], whereas the condition at a planar D'B' boundary is that the normal derivatives of the normal components of these flux densities are zero.

While there are procedures to create a material realization for the DB boundary using various types of anisotropic and even bi-anisotropic medium structures [4], the realization of a D'B' boundary has turned out to be very difficult to achieve. However, in March 2011 the idea was put forward that making use of a DB boundary, using a strongly anisotropic layer with so-called waveguiding medium the DB effect is tranformed to a D'B' boundary condition [5]. In particular, the axial components (components along the normal to the planes in the structure) of both the permittivity and permeability dyadics have to grow towards infinity. A quarter-wave thickness of such a planar layer transforms the DB condition into D'B' for the whole spectrum of plane waves, regardless of their transversal wavenumbers.

In this presentation, this theoretical idea to synthesize the D'B' boundary is studied numerically. In particular, the non-ideality aspects of real materials are given attention, in other words the question how well a structure can approximate the D'B' behavior even if it is made of real materials that do not have extreme anisotropic parameter ratios.

REFERENCES

1. Lindell, I. V., H. Wallén, and A. H. Sihvola, "General electromagnetic boundary conditions involving normal field components," *IEEE Antennas and Wireless Propagation Letters*, Vol. 8, No. 16, 877–880, 2009.
2. Rumsey, V. H., "Some new forms of Huygens' principle," *IRE Transactions on Antennas and Propagation*, Vol. 7, No. 5, S103–S116, December 1959.
3. Lindell, I. V. and A. H. Sihvola, "Zero-Axial-Parameter (ZAP) medium sheet," *Progress In Electromagnetics Research*, Vol. 89, 213–224, 2009.
4. Lindell, I. V. and A. H. Sihvola, "Electromagnetic boundary and its realization with anisotropic metamaterial," *Physical Review E (Statistical, Nonlinear, and Soft Matter Physics)*, Vol. 79, No. 2, 026604, 2009.
5. Lindell, I. V., A. Sihvola, L. Bergamin, and A. Favaro, "Realization of the D'B' boundary condition," *IEEE Antennas and Wireless Propagation Letters*, 2011, submitted for publication; Also ArXiV:1103.3931v1, March 2011.

Absorption and Giant Magnification with a Thin Metamaterial Structure

Sailing He[1, 2], **Yi Jin**[1], **Sanshui Xiao**[3], **and Niels Asger Mortensen**[3]

[1]Centre for Optical and Electromagnetic Research
State Key Laboratory of Modern Optical Instrumentations
Zhejiang University, Hangzhou 310058, China
[2]Division of Electromagnetic Engineering, School of Electrical Engineering
Royal Institute of Technology, S-100 44 Stockholm, Sweden
[3]DTU Fotonik, Department of Photonics Engineering
Technical University of Denmark, DK-2800 Kongens Lyngby, Denmark

Abstract— Some of our recent results in metamaterial-based absorbers will be reviewed, including an arbitrarily thin metamaterial structure for perfect absorption and giant magnification. In our common understanding, for strong absorption or amplification in a slab structure, the desire of reducing the slab thickness seems contradictory to the condition of small loss or gain. In this paper, this common understanding is challenged. A special material of zero permittivity ε or permeability μ provides us some special properties [1–3]. Here we will show that special materials with zero real(ε) and real(μ) (hereinafter referred to as ZRMs) can find amazing applications in absorption and magnification. A slab is sandwiched between two semi-infinite layers, and the top layer, the slab, and the bottom layer are denoted as layers 0, 1 and 2, respectively. The permittivity and permeability of layer n are denoted by ε_n and μ_n, respectively. With the assumption of a time harmonic factor $\exp(-i\omega t)$, positive imag(ε) and imag(μ) represent loss, and negative ones represent gain. The magnetic field is along the z axis. It is shown (see Fig. 1) that an arbitrarily thin metamaterial layer can perfectly absorb or giantly amplify an incident plane wave at a critical angle when the real parts of the permittivity and permeability of the metamaterial are zero while the absolute imaginary parts can be arbitrarily small.

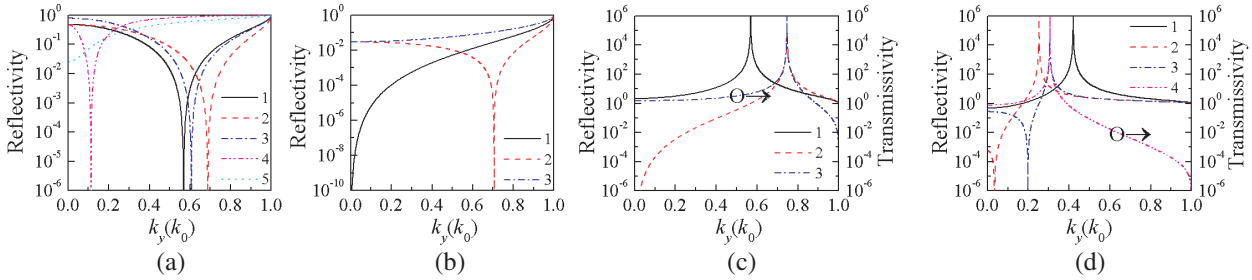

Figure 1: Reflectivity and transmissivity of a slab. In (a), $d_1 = 0.1\lambda_0$ for curves 1–4 and $d_1 = \lambda_0$ for curve 5, and ($\varepsilon_1/\varepsilon_0$, μ_1/μ_0) has small values of i(0.3, 0.3), i(0.5, 0.3), i(0.3, 0.1), i(0.01, 0.3), and i(0.1, 0.3) for curves 1–5, respectively. In (b), $d_1 = 0.1\lambda_0$, and ($\varepsilon_1/\varepsilon_0$, μ_1/μ_0) has large values of i(20, 20), i(20, 10), and i(10, 20) for curves 1–3, respectively. In (a) and (b), the slab is of a PEC substrate. In (c), $d_1 = 0.1\lambda_0$, ($\varepsilon_1/\varepsilon_0$, μ_1/μ_0) = $(-0.3i, -0.3i)$, and layer 2 is a PEC for curve 1 and of free space for curves 2 and 3. In (d), $d_1 = 0.1\lambda_0$ for curve 1 and $d_1 = 0.5\lambda_0$ for curves 2–4, ($\varepsilon_1/\varepsilon_0$, μ_1/μ_0) = $(-0.1i, 0.3i)$, and layer 2 is a PEC for curves 1 and 2 and of free space for curves 3 and 4.

REFERENCES

1. Enoch, S., et al., *Phys. Rev. Lett.*, Vol. 89, 213902, 2002.
2. Alekseyev, L. V., et al., *Appl. Phys. Lett.*, Vol. 97, 131107, 2010.
3. Silveirinha, M. G. and N. Engheta, *Phys. Rev. Lett.*, Vol. 97, 157403, 2006.

Maxwell's Fisheye Lens for Subwavelength Focusing

Yungui Ma
Centre for Optical Electromagnetic Research, Department of Optical Engineering
Zhejiang University, Hanzhou 310058, China

Abstract— One of the most active trends in materials science, physics and engineering is the development of metamaterials, initially inspired by one paper by Sir John Pendry [1]. In this paper, Pendry showed that a piece of negatively refracting material could act as a perfect lens. Ordinary lenses cannot resolve structures much smaller than the wavelength, but perfect lenses make infinitely sharp images, at least in theory. Imaging is of vital importance to the way electronic chips are produced, photolithography, where the structures of transistors are photographed onto the chip. The resolution limit of ordinary lenses forces chipmakers to use light with increasingly shorter wavelength, which is increasingly difficult. Therefore, practical ways of getting around the resolution limit could revolutionize one of the key technologies of the silicon age. However, for fundamental reasons [2], negatively refracting materials are inherently absorptive, and absorption turns out not only to lower the intensity, but to ruin the super resolution of the theoretically perfect lens. Only "poor man's lenses" of an imaging range shorter than 100 nm, much shorter than the wavelength of light, have been demonstrated [3], but such lenses are not of any practical use.

Here we demonstrate imaging with subwavelength resolution over superwavelength distances in passive materials with positive refraction, an idea [4] that challenges the accepted wisdom of subwavelength imaging. Instead of light, we use microwaves that are electromagnetic waves like light, but with cm wavelengths and GHz frequencies, which allows us to investigate the electromagnetic fields of the imaging waves with a degree of detail currently inconceivable in optics. Our microwave experiments establish that subwavelength imaging is possible with positive refraction, encouraging applications where imaging matters most: for light. Additional advantage of our approach based on non-negative index materials, is no loss and thus broadband. The lens fabricated consists of concentric cylindrical rings of copper-printed circuit-board etched in a special pattern. Figure 1(a) shows the photography of fabricated device. The imaging effect was given in Figure 1(b) where sharp peak was observed at the image point, indicating strong subwavelength resolving ability of current fisheye lens.

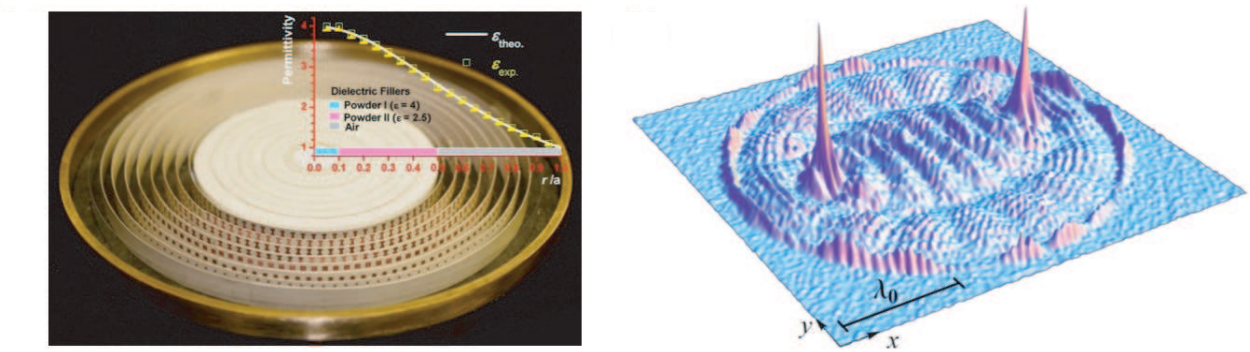

(a) (b)

Figure 1: (a) Copper structures on circuit boards create the index profile of the fish-eye lens. (b) Experimentally obtain field amplitude with source (left) and image point (point).

REFERENCES

1. Pendry, J., *Phys. Rev. Lett.*, Vol. 85, 3966, 2000.
2. Stockman, M. I., *Phys. Rev. Lett.*, Vol. 98, 177404, 2007.
3. Fang, N., et al., *Science*, Vol. 308, 534, 2005.
4. Leonhardt, U., *New J. Phys.*, Vol. 11, 093040, 2009.

Session 3P3
Atmospheric Scattering, Radiative Transfer and Remote Sensing

A Combined Atmospheric Radiative Transfer Model (CART) and Its Applications

Heli Wei, **Xiuhong Chen**, **Ruizhong Rao**, **and Yingjian Wang**
Key Laboratory of Atmospheric Composition and Optical Radiation
Anhui Institute of Optics and Fine Mechanics
Chinese Academy of Sciences, P. O. Box 1125, Hefei, Anhui 230031, China

Abstract— It is critical to accurately calculate the absorption and scattering of radiation by the atmospheric molecules, aerosol and clouds, which is also essential to the implementation of various remote sensing techniques. This paper reports on a fast atmospheric radiative transfer model called Combined Atmospheric Radiative Transfer model (CART) and its applications. The CART has been developed to rapidly calculate atmospheric transmittance and background radiance in the wavelnumber range from 1 to 25000 cm^{-1} or for wavelengths longer than 0.4 micrometers. The spectral resolution of CART is 1 cm^{-1}, this spectral resolution is adequate for many tasks.

The algorithm of the absorption by atmospheric molecules is based on a fitting to the line-by-line calculation; An aerosol extinction model is presented based on Mie theory and real measured aerosol optical parameters (such as size distribution and altitude distribution), as well as the assumed aerosol category; A computationally efficient method is developed to compute the multiple-scattering radiances based on fitting radiances pre-calculated from the discrete ordinate radiative transfer (DISORT) at several wavenumbers. The radiance calculations in the CART consider contributions from the atmospheric self-emission, solar radiance single-scattered and multiple scattered into the path. Molecular continuum absorption, molecular scattering, and aerosol absorption and scattering are also included. The CART can be used to compute spectral transmittance, thermal radiance, scattering radiance, direct solar irradiance, by atmospheric molecules, aerosol and clouds.

CART may be applied to in the fields such as remote sensing of atmosphere, clouds, and surface albedo. Case studies in the applications of CART are shown: simulations of atmospheric transmittance, upwelling and downwelling infrared brightness temperatures, upwelling visible/infrared spectral radiances. Furthermore, we will use the CART for the retrieval of atmosphere, clouds and other information in the atmosphere.

Speeding up the Polarized Radiative Transfer Model

Minzheng Duan
LAGEO, Institute of Atmospheric Physics, Chinese Academy of Sciences, Beijing 100029, China

Abstract— Polarization becomes more and more important in current and future remote sensing of aerosol and cloud, as it could provide more information than that of intensity-only measurements. While forward simulation of polarization of light during its transfer in the earth-atmosphere system is still a burden for non-look-up-table retrieval, and a fast, stable and accurate forward model is of the first prerequisite in developing novel inverse algorithm. To speed up the polarized simulations, a new approximation of the Stokes Vector through scalar radiative transfer is introduced into our previous developed model SOSVRT, which is a polarized radiative transfer model based on successive order of scattering. This approximation method is tested and validated with clear sky, aerosol heavy-loading atmosphere, low cloud and high thin cloud, the results show that the efficiency of the new version of SOSVRT is greatly enhanced without losing accuracy, especially for optically thick scattering media such as atmosphere with heavy aerosol and/or cloud, the computation time reduce by tens of times.

Application of a PPDF-based Atmospheric Light-scattering Correction to Carbon Dioxide Retrievals from GOSAT Observations

Andrey Bril, **Sergey Oshchepkov**, **and Tatsuya Yokota**
National Institute for Environmental Studies, Japan

Abstract— Current knowledge about sources and sinks distributions of atmospheric carbon dioxide (generally accepted as a dominant greenhouse gas) is still insufficient for reliable climate predictions. Utility of satellite CO_2 observations can be limited by the atmospheric light-scattering which remains a major source of the gas retrieval errors. Recent studies [1, 2] have proposed light-scattering corrections based on analyses of photon path length statistics. The measured signal is expressed in terms of a photon path length probability density function (PPDF) with further parameterization of the PPDF. In this study, we present a methodology, numerical simulations and initial results of PPDF-based carbon dioxide retrievals from the observation data of Greenhouse Gases Observing Satellite (GOSAT). Thermal and near infrared Fourier-transform-spectrometer named TANSO-FTS onboard GOSAT (on orbit since January 23, 2009) measures reflected sunlight in three narrow bands within near-infrared region (0.76, 1.6, and 2.0 μm) which are used for columnar CO_2 and PPDF parameters retrieval. We focus on the observations with strong optical path modifications due to atmospheric light scattering, in particular, on sun-glint observations in presence of aerosols and sub-visual cirrus clouds and on near-nadir observations during existing dust aerosols in high altitudes over deserts regions. Two mode of the PPDF-based approach is discussed: 1) selection of the observations with negligibly small optical path modification which allows CO_2 retrievals under the assumption of a non-scattering atmosphere; it is based on PPDF retrievals in oxygen A-band. 2) Simultaneous CO_2 and PPDF retrievals in all three GOSAT near-infrared bands.

REFERENCES

1. Bril, A., et al., *Appl. Optics*, Vol. 46, 2460, 2007.
2. Oshchepkov, S., et al., *JGR*, Vol. 114, D19207, 2009.

A Fast Radiative Transfer Model for Simulating Hyperspectral and Narrow Band Cloudy Sky Infrared Radiances

Chenxi Wang and Ping Yang
Department of Atmospheric Sciences, Texas A&M University, College Station, TX 77843, USA

Abstract— This study explores the development of a computationally efficient high spectral resolution cloudy-sky radiative transfer model (HISCRTM) for simulating upwelling radiances at the top of the atmosphere (TOA). Specifically, a database of clear-sky transmittances is computed by using the rigorous line-by-line radiative transfer model (LBLRTM) for up to seven molecular species. The ice cloud reflection, transmission, emissivity and effective temperature functions are pre-computed by using the discrete ordinates radiative transfer model (DISORT). With a spectral resolution of $1\,\mathrm{cm}^{-1}$ and a wide spectral range covering the infrared region from $300\,\mathrm{cm}^{-1}$ to $5{,}000\,\mathrm{cm}^{-1}$, the HISCRTM has an inherent advantage of being straightforward for applications to hyperspectral IR sensors such as the Atmospheric InfraRed Sounder (AIRS) and the Infrared Atmospheric Sounding Interferometer (IASI) for both forward simulations and operational retrievals Furthermore, this model facilitates efficient computation of clear-sky subdatabase suitable for narrow band satellite sensors, such as the Moderate Resolution Imaging Spectroradiometer (MODIS) and the Cloud-Aerosol Lidar and Infrared Pathfinder Satellite Observations (CALIPSO) Imaging Infrared Radiometer (IIR). In the future, similar simulations are applicable to the Geostationary Operational Environmental Satellite (GOES-R) Advanced Baseline Imager (ABI) the Visible Infrared Imaging Radiometer Suite (VIIRS) and the Crosstrack Infrared Scanner (CrIS).

Light Extinction by a Sphere in Absorbing Medium: Near-field versus Far-field Approaches

Qiang Fu and Wenbo Sun
Department of Atmospheric Sciences, University of Washington, Seattle, WA, USA

Abstract— Although light scattering by a spherical particle in a non-absorbing medium is well understood based on Mie theory, how to obtain the scattering and absorption by a particle in an absorbing medium has been a subject of debate. Fu and Sun (2001) derived analytic equations for the single-scattering properties of a spherical particle embedded in an absorbing medium using the near field at the surface of the particle, which avoids difficulty in obtaining the extinction based on the optical theorem where the far field is used. Mishchenko (2007) revisited the far-field approach and derived the extinction cross-section of a sphere in absorbing medium. In this study, we will compare the result from Fu and Sun (2001) and that from Mishchenko (2007), and reconcile differences between them.

Raindrop Size Distribution Model for the Prediction of Rain Attenuation in Durban

P. Owolawi
Department of Electrical Engineering, Mangosuthu University of Technology
Umlazi, Kwazulu-Natal, South Africa

Abstract— The development of complex radio access networks has resulted in increasing spectrum occupancy and demand for higher bandwidths; hence it is imperative to employ the advantages of higher frequencies, which are capable of supporting these demands. The obvious candidates are microwave and millimeter bands. The advantages offered by microwave and millimeter waves have attracted immense interest from academia and the communications industry. The main characteristics of both waves include short wavelength (hence small components), large bandwidth, and frequency re-use. The interaction of the waves with atmospheric constituents, especially with hydrometeors, result in serious impairment of the signal at these frequencies: these impairments include attenuation, scattering and depolarization.

In satellite and terrestrial links, signals transmitted at these frequencies interact with raindrops because it covers a substantial path of the links. An electromagnetic wave propagating through a region containing raindrops suffers two attenuating effects: one is absorption through which part of its energy is absorbed by the raindrops and transformed into heat; and the other is scattering where part of energy is scattered in all directions. The comprehensive study of these two attenuating mechanisms is based on understanding the characteristics of raindrops.

Earlier modeling technique of raindrop size distribution seems to have begun with fits to the average drop distributions measured at single rain rate. Most of these fits were applied directly to the drop size distribution data as demonstrated by Marshall and Palmer where direct graphical fitting approach was used.

In order to improve the modeling approach and results, there is need to employ a systematic method such as the method of moment and maximum likelihood to estimate modeling parameters. The present work deals with statistical modeling of raindrop size distribution data collected in the coastal region of South Africa. The maximum likelihood estimator method is employed with lognormal distribution to estimate the dropsize distribution. The raindrop size is classified into two regimes based on the available data. The goodness-of-fit method (Kolmogrov-Smirnov test (K-test) is employed to optimize the selected model for different rain rate regime. The results are compared with the existing models such as the work done by Ajayi, Marshall and Palmer, Timothy and Atlas. The proposed South Africa model seems appropriate for the region.

Comparison of Aerosol Radiative Forcing Observed by AERONET and MODIS at Xianghe Station — Comparison of the Aerosol Product and Its Radiative Forcing between AERONET and MODIS

Yan Wang[1], **Fengsheng Zhao**[2], **and Zhengqiang Li**[1]

[1]Institute of Remote Sensing Application, Chinese Academy of Sciences, Beijing 100101, China
[2]Beijing Normal University, Beijing 100875, China

Abstract— This paper presents aerosol optical depth (AOD) data and aerosol radiative forcing obtained from AErosol RObotic NETwork (AERONET) and Moderate resolution Imaging Spectroradiometer (MODIS) from September 2004 to September 2005 at Xianghe, China. The results show that aerosol optical depth derived from MODIS has good agreement with AERONET observation at Xianghe station through this period. In average, MODIS AOD showed a small systematical overestimation than that of AERONET. The higher MODIS AOD also results overestimation of aerosol radiative forcing than AERONET one, e.g., 12–17 Wm^{-2} on the ground, 2–3 Wm^{-2} on the top of atmosphere, and 9–12 Wm^{-2} in the atmosphere respectively.

2-D Pattern Synthesis for Cylindrical Arrays

C. Liu, Z. Ding, and X. Liu
Department of Communication Engineering, Hefei University of Technology, Hefei, Anhui 230009, China

Abstract— There has been significant attention paid to the area of conformal array pattern synthesis in recent years. One of the most differences between conformal array and traditional array is that the beam pattern can not be obtained by the product of array factor and element pattern. Many algorithms have proposed of the conformal array pattern synthesis, but most of them have a large amount of computation, especially used in 2-D pattern synthesis. In this paper, a low complexity algorithm of 2-D pattern synthesis for cylindrical arrays is introduced. Since the cylindrical array consists of a series of identical circular arrays, the whole array can be seen as a linear array whose elements are these identical circular arrays. Then array beam pattern can still be obtained by the product rule. Therefore, the 2-D beam pattern can be obtained by the product of the linear and circular arrays' beam pattern and the synthesis process is decomposed into two individual 1-D pattern syntheses of subarrays to approach the desired sidelobe level. The linear array controls the beam pattern of azimuth while the circular array controls the beam pattern of elevation. Computational complexity has been significantly decreased due to the Dimension reduction. In the adaptive beamformer, when the inferences are more than array sensor, the sidelobe level in the area of interferences will be depressed. According to this feature, we add lots of virtual interferences in the azimuth or elevation area and control the beam pattern by adjusting the intensity of the interferences. Numerical examples illustrate the effectiveness of the proposed method and the beam pattern of azimuth and elevation has little effect on each other.

Particle Optical Properties of Ice Crystals and Dust Aerosols

Ping Yang[1], **George Kattawar**[2], **and R. Lee Panetta**[1]

[1]Department of Atmospheric Science, Texas A&M University, USA
[2]Department of Physics and Astronomy, Texas A&M University, USA

Abstract— In this talk, we will review the recent progress in the study of the single-scattering properties (i.e., the extinction coefficient, single-scattering albedo, and phase matrix) of nonspherical ice crystals within cirrus clouds and nonspherical aerosols (dust particles, in particular). We have been using the finite-difference time domain (FDTD) method, the discrete dipole approximation (DDA), and an improved geometric optics (IGOM) method to compute the single-scattering properties of nonspherical particles. We have incorporated the so-called edge effect associated with the surface wave into IGOM extinction and absorption efficiencies. The simulation results in the solar and thermal infrared spectral regimes will be presented. Furthermore, the impact of particle nonsphericity on remote sensing and radiative transfer simulations involving ice cloud and aerosol properties will also be discussed.

Evaluation of Radiative Heating Rate in Tropical Tropopause Layer

Lei Lin, **Qiang Fu**, **and Jing Su**
Lanzhou University, China

Abstract— The tropical tropopause layer (TTL) which is from $\sim$ 14.5 to 18.5 km is a transition layer between the stratosphere and troposphere in the tropics. Almost all air in the stratosphere comes from the TTL. Since the radiative relaxation time in the TTL is long, a small errors in the radiative heating rate calculation would lead to a large errors in the model-simulated temperatures in the TTL. In addition the simulated radiative heating rate in the TTL is often used to derive the vertical velocity. Since the radiative heating rate in the TTL can be as small as 0.1 K/decade, a very accurate radiative heating rate calculation including all radiative active species is required. In this study, we will quantify the radiative heating rates in the TTL using the line-by-line calculations in both thermal infrared and solar spectra as reference calculations. We will then evaluate the TTL radiative heating rates from various efficient radiation models including Fu-Liou radiation model which used the correlated k-distribution method to treat the gaseous absorption.

Session 3P4
Antenna and Array Design and Simulation Techniques 3

A Multi-band Mobile Phone Antenna with CPW-FED for Applications of LTE700, GSM900/1800, DCS, PCS, UMTS, BLUETOOTH, and WIMAX

Chia-Yen Wei[1], **Tian-Fu Hung**[1], **Andy Yang**[2], **Jim Wu**[2], **Thomas Yuan**[2], **Sheau-Shong Bor**[3], **and Hai-Tao Sun**[3]

[1]Ph.D. Program in Electrical and Communications Engineering
Feng-Chia University, Taichung, Taiwan, R.O.C.
[2]Lorom Industrial Co., Ltd., Taipei, Taiwan, R.O.C.
[3]Department of Electrical Engineering, Feng-Chia University, Taichung, Taiwan, R.O.C.

Abstract— Multi-band compact antenna is proposed to apply in the wireless communications including long term evolution (LTE700), Global System for Mobile Communication (GSM), Digital Communication System (DCS), Personal Communication Service (PCS), Integration of Mobile and Fixed Network (3G), Bluetooth, and WiMAX. It adopts multi-branch-line technique and is fed by a 50 Ohm CPW line.

Simulated and Measured data in the proposed antenna were consistent and the better antenna performance made sure it can be used in the mobile phone for the multi-band applications. Additionally, the antenna performances such as impedance bandwidth, antenna gain, and radiation patterns corresponding to antenna parameters, were studied and analyzed.

An Aperture-couple Stack Antenna with Minkoski-island-based Patch for Circular Polarization and Wide-band Applications

Sheau-Shong Bor[1], **Tian-Fu Hung**[2], **Chia-Yen Wei**[2], **Ji-Chyun Liu**[3], **and Hai-Tao Sun**[1]

[1]Department of Electrical Engineering, Feng-Chia University, Taichung, Taiwan, R.O.C.
[2]Ph.D. Program in Electrical and Communications Engineering
Feng-Chia University, Taichung, Taiwan, R.O.C.
[3]Department of Electrical Engineering, Ching Yun University, Chung-Li, Tao-Yuan, Taiwan, R.O.C.

Abstract— A stack antenna with Minkoski-island-based patch for circular polarization and wide band applications has presented in this paper. The proposed antenna structure is stacked by two FR4 substrates. The bottom substrate is fed by single-feed line coupled with aperture. The Minkoski-island-based patch is etched on the top substrate, which excite the wide band response with dual-mode and circular polarization with orthogonal mode. The stack antenna presents the axial ratio (AR) with 3-dB bandwidth 30 MHz (1.2%) in 2.44 GHz and the wide band response with 10-dB bandwidth 290 MHz (12%). The radiation patterns show the directional patterns which are obtained for 2.34 GHz and 2.5 GHz band respectively with peak power gains 0.11 dBi and 0.2 dBi. It can be applied to the WLAN band.

UHF SATCOM Broadband CP Antenna: Moxon Type Bent-dipoles over a Ground Plane

Edip Niver[1] **and İbrahim Tekin**[2]

[1]Electrical Engineering, New Jersey Institute of Technology, Newark, NJ, USA
[2]Electronics Engineering, Sabancı University, İstanbul, Turkey

Abstract— In this paper, we investigate and compare two different antenna types for UHF SATCOM applications; proposed Moxon type (bent dipole) and conventional egg beater (loop) antennas in terms of antenna performance and physical size. Bent dipole and egg beater antennas are simulated using HFSS software tool. Prototype antenna for Moxon type is also fabricated and measured for its return loss using Agilent network analyzer and compared to that of an egg beater antenna. Antenna gains are also simulated. Simulation results show that Moxon type antenna has more impedance bandwidth than egg beater antenna with smaller dimensions and hence can be used for broadband SATCOM applications.

Introduction: For UHF SATCOM mobile applications, antennas are required to have high-performance including a broadband operation, circular polarization as well as a large angular coverage from horizon to zenith. For airborne systems at these frequencies, wavelength could be on the order of meters and conventional antennas may be "too big" for deployment. Compact size antennas with desired antenna performance become very crucial part of these airborne systems. In this paper, a novel antenna "Moxon type" bent dipole is proposed for circular polarization and its performance is compared to a conventional egg beater antenna whose dimensions are larger than the proposed antenna. For UHF satcom applications, broadband antennas can be employed such as sleeve dipoles [1]. However, for mobile applications, the antenna size is critical and obtaining a circular polarization with sleeve dipoles will result in complicated antenna structures. Egg beater antennas are another choice for obtaining circular polarization with loop antennas at UHF frequencies [2]. Egg beater antennas may not be easily deployable on mobile platforms due to their dimensions.

Moxon Type Bent Dipole Antenna for Circular Polarization: The two bent dipole antennas are located perpendicular to each other as shown in Figure 1. The bent dipole antennas are made of four L shaped metallic rectangular conductors which have square cross-sectional areas. A sketch of one of the bent dipole antennas is shown in Figure 2. The length of the one arm of the dipole is $L + W$, the arm is bent toward a ground plane from L distance away from the center of the dipole. The end point of the bent dipole antenna is H away from the ground plane as in Figure 2. The bent dipole is fed from the center of the antenna with a differential input. The RHCP is obtained simply by placing two dipole bent antennas perpendicular to each other, one in x-z plane, the other in y-z plane as in Figure 1.

The electromagnetic simulations are performed using HFSS (for antenna) and ADS (matching circuit) software.

Simulation results show that the bent dipole antenna has good return loss properties within the frequencies of 240–310 MHz UHF satcom band, and its physical size is much smaller compared to an conventional egg beater antenna. Measurement results in terms of return loss and antenna gain will be presented at the conference.

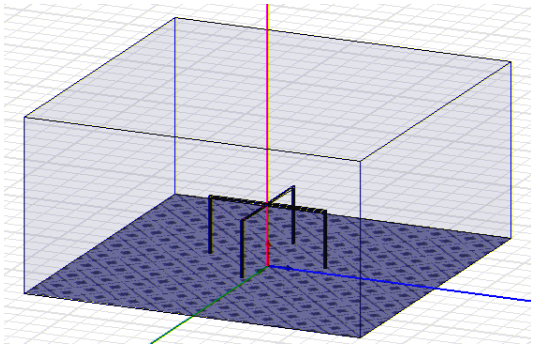

Figure 1: Two perpendicular bent dipole antennas for circular polarization radiation.

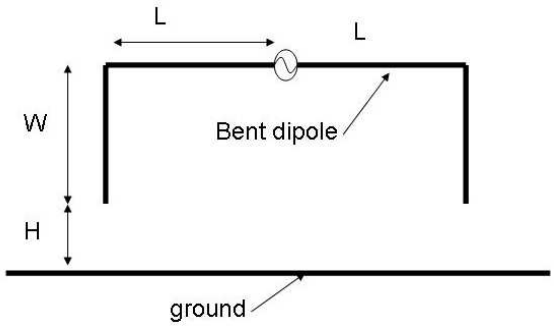

Figure 2: Bent dipole antenna over a ground plane.

REFERENCES

1. Stutzman, W. L. and G. A. Thiele, *Antenna Theory and Design*, 2nd Edition, Wiley, New York, 1998.
2. Denisonn, M. and J. Fielding, (Editors), *RSGB Radio Communication Handbook*, 9th Edition, UK, 2007.

Wideband Slotted Planar Antenna with Defected Ground Structure

Ayman A. R. Saad[1], **Elsayed E. M. Khaled**[2], **and Deena A. Salem**[3]

[1]Kosseir Radio, Telecom Egypt, Kosseir, Egypt
[2]Electrical Engineering Department, Assiut University, Assiut, Egypt
[3]Microstrip Department, Electronics Research Institute, Giza, Egypt

Abstract— Wireless communication systems are evolving towards miniaturization and multi functionality, which made designing multi-band antennas with wide impedance bandwidths while maintaining high radiation efficiency is crucial to construct a wireless communication system. Moreover, designing miniatured antennas are essential to meet wireless industry requirements for mobile communications devices. The scope of this research includes miniaturization process that compromises between the size and performance of the antenna. Design and implementation of novel multi-band low profile antennas that satisfy the industrial requirements are presented.

Incorporating up to seven slots in the conventional microstrip rectangular antenna acquires the multi-band performance of the antenna that maintains the required multi functionality and maintains the antenna's thin profile characteristic [1]. The geometrical configuration of the slots can be chosen according to a certain application to yield the required operational frequencies with wide bandwidths. The frequency range 2–8 GHz which is appropriate for many applications such as WLAN, Mobile WiMAX, and WCDMA is considered.

The effect of the structure of the ground plane on the antenna performance is also studied by mounting the proposed antenna structure on two different types of ground planes, the first is a conventional perfect electrical conductor (PEC) ground plane and the other is a defected ground structure (DGS), which is created by etching square lattices in the ground plane. There are two major advantages associated with using DGS ground planes. First, such structures enable wider bandwidths with enhanced gain and higher radiation efficiency. Second, these structures forbid the propagation of electromagnetic waves in a certain frequency band. Therefore, they can be used to block surface waves that usually corrupt antenna performance at a certain frequency band [2].

Comparing the results obtained using the full ground plane and that using the DGS shows that the latter's effects on the performance of the proposed antenna is better than the PEC effects. It demonstrates the ability of the DGS to enhance the radiation parameters of the designed antenna in the required frequency bands. The equivalent circuit model of the DGS unit cell underneath the microstrip line with the parameter extraction method is presented to study the effects of DGS structure on the antenna performance. Simulated results are obtained using IE3D simulator software which is based on method of moment (MoM).

The antenna is fabricated and the measured data show very good agreement with the simulated results. The results demonstrate wider bandwidth and high gain than that of conventional PEC ground plane. The antenna is capable of achieving multi-wideband operations with return loss (RL) less than 10 dB in the frequency range of 2–8. Moreover almost a 26% size reduction is achieved which make the antenna suitable for mobile and portable applications.

REFERENCES

1. Khaled, E. E. M. and A. A. R. Saad, "Multi-wideband compact microstrip patch antenna based on slot matching," *Progress in Electromagnetics Research C*, Vol. 4, 169–177, 2008.
2. Yang, F. and Y. Rahmat-Samii, "Microstrip antennas integrated with electromagnetic band-gap (EBG) structures: A low mutual coupling design for array applications," *IEEE Trans. Antennas Propag.*, Vol. 51, 2939–2949, 2003.

Adaptive Beamforming Technique for Virtual Antenna Using Modified Interpolated Spatial Smoothing Algorithm

Wenxing Li[1], **Yipeng Li**[1], **Lili Guo**[1], **Wenhua Yu**[2], **and Raj Mittra**[2]

[1]Harbin Engineering University, Harbin 150001, China
[2]The Pennsylvania State University, University Park, PA 16802, USA

Abstract— In this paper we present an effective algorithm to inhibit the coherent interference with the virtual antenna based on the traditional interpolated spatial smoothing algorithm. Using the interference subspace projection concept, we establish an interference space utilizing the virtual array interfere steering vectors and then project the transformation matrix to it. The theoretical analysis has demonstrated that the interference components in the virtual covariance matrix can be enhanced. Then by employing the minimum variance distortionless response (MVDR) beam forming method, it can improve the robustness of adaptive beamforming with virtual antenna array, and significantly enlarge the inhibition gains on the coherent interference and output signal to interference and noise ratio (SINR).

An Integrated UWB and Bluetooth Antenna with Dual Band-notched Characteristic

K. C. Law, S. W. Cheung, and T. I. Yuk
Department of Electrical and Electronic Engineering, The University of Hong Kong, Hong Kong, China

Abstract— This paper presents an integrated Ultrawideband (UWB) and Bluetooth microstrip monopole antenna with a dual band notched characteristics. The antenna consists of an elliptical ring as the radiator to cover the frequency bands for both the Bluetooth (2.4–2.5 GHz) and UWB (3.1–10.6 GHz) applications. A triangular resonator and a meander-defected-ground structure (DGS) are used to produce two notches at the centre frequencies of 2.856 GHz and 5.5 GHz, respectively.

The designed antenna has a compact area of $31.5 \times 39.75\,\text{mm}^2$ and is fabricated on Roger PCB, RO4350B, with a relative permittivity of 3.48, thickness of 0.762 mm and loss tangent of 0.0037. It has an operating frequency band from 2.32 GHz to over 12 GHz, with a notched frequency band from 2.66–3.08 GHz and another notched band from 5.11–6.21 GHz, to reject the unwanted signals in the frequency bands for the Bluetooth and Wireless Local Area Network, respectively.

To create a notch in the Bluetooth band, a triangular resonator is placed at the centre of the elliptical-ring radiator. The centre frequency and bandwidth of the notch can be easily controlled by adjusting the dimensions of the triangular resonator. To create another notched band to reject the unwanted radio signals in the IEEE802.11a/n (5.15–5.825 GHz), a meander-DGS is employed. With the high attenuation characteristic of DGS, the peak gain can be suppressed by more than 12 dB at the frequency of around 5.5 GHz, which is deeper than the notches designed for other integrated UWB and Bluetooth antennas.

Coaxial Line Fed HMSIW *H*-plane Horn Antenna

S. A. Razavi and M. H. Neshati
Department of Electrical Engineering, Ferdowsi University of Mashhad, Iran

Abstract— Recently the substrate integrated waveguide (SIW) technology has widely used in implementation of microwave devices and antennas. Horn antenna is one of the antennas implemented by this technology. Based on the authors' knowledge, there are few works on SIW horn antennas and no work is done on half mode substrate integrated waveguide (HSIW) horn antennas.

When only the mode TE_{10} is propagating in SIW waveguide, the maximum value of E-field is located at the vertical center plane along the propagating direction and the center plane can be considered as an equivalent magnetic wall. As a result, the HMSIW can be simply achieved by dividing the SIW into two equal parts. But in horn antennas, in addition to TE_{10} mode the higher order modes are slightly exist (the effect of higher order modes is more intensive if the length of the horn is chosen improperly) so the above approximation (consideration of center plane as an equivalent magnetic wall) is not yet valid and the antenna's performance will be considerably degraded if it is divided into two parts from the center line.

In this paper, we proposed a scheme in order to provide a HMSIW horn antenna in witch the field distribution is approximately half of the corresponding one in SIW horn antenna. The proposed antenna is fed by coaxial line unlike the previous works on HMSIW components witch are fed by microstrip line. Based on the authors' knowledge, all the previous HMSIW antennas are fed by microstrip line. But, this kind of feeding suffers from parasitic radiation (witch may degrade the radiation pattern of the horn antenna in E-plane) and high conductor loss in high frequencies so we used coaxial line as the feed in order to avoid these imperfections. The proposed antenna is simulated with HFSS software and its radiation properties are compared with the SIW horn antenna. Results illustrate that the radiation characteristics of our antenna (the proposed HMSIW horn antenna) and the SIW horn antenna are in good agreement while the size of the proposed antenna is about 40% of SIW horn antenna.

Side-lobe Searching Algorithm for Measured Antenna Far-field Patterns

Le Kuai[1] **and Zhenxin Cao**[2]

[1]Department of Electronic Engineering, Chengxian College, Southeast University, Nanjing 210088, China
[2]State Key Laboratory of Millimeter Waves, School of Information Science and Engineering
Southeast University, Nanjing 210096, China

Abstract— In this paper, we first talk about the features of measured far-field antenna patterns, and then some kind of representative data of measured antenna patterns is shown. Due to the effects of many factors like test environment and instability of measurement system, the patterns we usually get are not very smooth. There are many ripples which is called "spur" on the pattern. So if we use generic method to process these tested data, we may probably get wrong results. For example, sometimes a spur may be wrongly regarded as a side-lobe. According to the features of far-field antenna patterns and the problems we have mentioned above, a new processing and analytical algorithm for far-field antenna patterns is proposed. In this algorithm, we firstly find out all peak values. Each peak value belongs to a lobe or a spur. Then we put forward a special integral method for calculating peak areas and a new decision rule. We analyze and process far-field antenna patterns according to the result of the integral and the decision rule which we have put forward. Finally, we validate the correctness of the algorithm by analyzing some kind of typical antenna patterns, and also analyze the time complexity and space complexity of the algorithm. It shows that this algorithm can be applied to not only searching for side-lobes in measured far-field antenna patterns which have spurs, but also calculating other parameters of antenna patterns, such as maximum, beam width, etc.. So, it is a high-reliability, wide-applicability and high-operation-speed algorithm.

A Broad-beam Cavity Backed Slot-coupled MSA Array Using Parasitic Patches

T. Puklibmoung, P. Krachodnok, and R. Wongsan
School of Telecommunication Engineering, Institute of Engineering
Suranaree University of Technology, Nakhon Ratchasima, Thailand

Abstract— This paper presents a broad-beam cavity backed slot-coupled microstrip antenna (MSA) array using parasitic patches. This structure is excited by a linear electric probe that is located at the center of inner surface of the rectangular cavity. To achieve broad-beam antenna, phase of each array element in the microstrip array antenna is specific designed to emulate the curvature of the parabolic backscatter function by adjusting the distance between parasitic patches. The proposed antenna is suitable to apply for wireless local area network (WLAN) communication and low earth orbit (LEO) satellite communication systems. The numerical results are given by computer simulation technology (CST) software. From the numerical results, the frequency response of return loss (S_{11}) and radiation patterns can be investigated. The simulation results show a maximum gain of the operation frequency 10 GHz is 5.7 dBi and half power beam width (HPBW) of radiation pattern is about 120°.

Patch Antennas for TTC Applications of Mini-satellites

Nai-Zhi Wang, Xi-Bo Wang, Jianzhou Li, and Jia-Dong Xu
School of Electronic and information, Northwestern Ploytechnical University, Xi'an 710129, China

Abstract— In recent years, with the development of miniaturization technologies such as very large scale integration (VLSI), and digital signal processing (DSP), small satellites are becoming more and more attractive. And it is known that during both the period of attitude adjustment after the separation and working time of a satellite, TTC (Telemetry, Tracking, and Command) are very important functions necessary for the proper operation of a satellite. In this paper, firstly a design process of a dual band patch antenna, which can operate at 2 GHz and 2.2 GHz for TTC applications on small satellites is presented, followed by the approach of the placement optimization of TTC patch antennas onboard for mini-satellite. In order to obtain one better strategy, the construction of the antenna is discussed and two schemes of antennas placement are introduced. Though the results secured by electromagnetic computation, it is indicated that situating three patch antennas respectively on three adjacent walls and the forth one on the cut-off bottom corner can provide a satisfactory omni-directional radiation pattern. To reduce the complexity, a new method to conform patch antenna on the mini-satellite is proposed by bending the antenna along one edge of the cube in a top corner. By comparison and analysis, it is concluded that one bended patch antenna can perform as well as four ordinary ones do so that it can effectively cut off the weight and volume of the spacecraft, and facilitate the feeding intricacy. All the S-parameter and radiation pattern results used for analysis were calculated with the CEM software CST Microwave Studio, which is based on the finite integral technique (FIT).

Optimal Calculation of the Directivity of Arrays with Azimuthal Element Pattern Symmetry

E. H. Van Lil, J.-W. De Bleser, and A. R. Van De Capelle
Div. ESAT-TELEMIC, K. U. Leuven, Kasteelpark Arenberg 10, Bus 2444, B-3001 Heverlee, Belgium

Abstract— A simple analytical formula for the directivity of an array of arbitrary line sources is derived. It turns out to be a generalization of the well known expression for the directivity of an array of isotropic elements [1, 2].

Derivation and Application of the Formulas: This formula results in expressions with spherical Bessel functions (limited to order 2 for the trivial case of the Hertzian dipole), but allowing arbitrary excitations.

It should be noted that this method can be applied to any element power pattern that can be expanded in terms of the sines and cosines of the angle with the line sources, either theoretically or by experimental fitting.

Efficient Computer Implementation: For regular (i.e., equidistant) arrays an efficient computational algorithm is proposed. For practical applications (corporate feeding of the array) the excitation coefficients vary barely with frequency and hence the power correlation coefficients of the excitation coefficients can be computed in advance. This is done by computing those correlation coefficients in one vector, destroying the excitation coefficients. Until the $(E(N/2)-1)$th (E is the integer just lower than or equal to $N/2$, where N is the number of array elements) calculation the new element is added in the vector after the end of the vector containing the excitation coefficient. The total number of memory elements is thus $N + E(N/2) - 1 = E((3N-2)/2)$. After the $(E(N/2)-1)$th coefficient, the next element can be placed directly in the excitation element vector, because those excitation coefficients are no longer required. At this stage the original excitation coefficients start to be destroyed in the computation. After buffering the first elements can be copied in place. A simple example for different arrays is given in Figure 1. We will also show that this approach can be used efficiently for indoor (broadband) propagation computations.

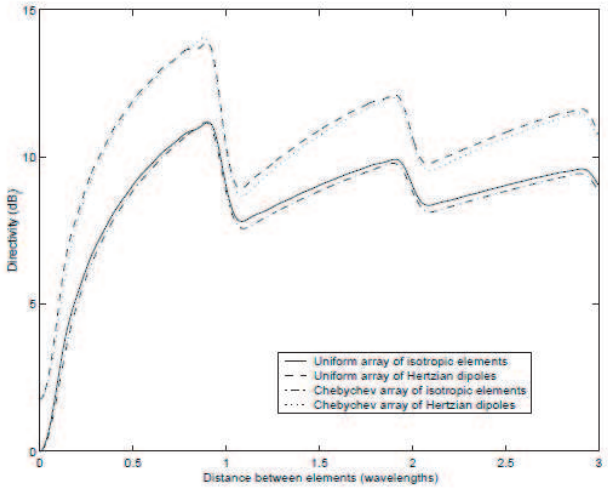

Figure 1: Example of gain computations for 20 element arrays (uniform, −20 dB Chebychev, both with isotropic elements and Hertzian dipoles).

REFERENCES

1. Stutzmann, W. and G. Thiele, *Antenna Theory and Design*, John Wiley & Sons, New York, 1981.
2. Ma, M. T., *Theory and Application of Antenna Arrays*, Artech House, 1974.

A Novel UWB Filter with Dual-notch-bands Characteristic Using Radial-multimode Loaded Stub Resonator

C. Y. Liu, **T. Jiang**, **Y. S. Li**, **and J. Zhang**
College of Information and Communications Engineering
Harbin Engineering University, Harbin, Heilongjiang 150001, China

Abstract— Since the Federal Communications Commission (FCC) released the frequency band from 3.1 to 10.6 GHz for commercial communication applications in February 2002, the ultra-wideband (UWB) radio system has been receiving great attention from both academy and industry. However, since the UWB system can cover a very wide frequency band, there is interference with the existing narrowband WLAN radio signals. So, an important issue for UWB systems is how to avoid interference with relatively strong narrowband signals within the allocated UWB spectrum. To solve this problem, this paper presents a novel approach for designing compact ultra-wideband (UWB) band-pass filter with a good dual-notched band characteristic. By using a radial-multimode loaded stub resonator, one notch-band can be got. Another notch-band can be generated by the half-wavelength parasitic micro-strip Resonator. The main advantage of the proposed filter is the frequency of the notched band can be tuned easily in a wide frequency range. The first notch-band can be changed form 4 GHz to 6 GHz. The second notch-band can be changed form 7 GHz to 9 GHz. Electric filed distribution and equivalent model is also given depending on the odd/even excitation resonance condition. The characteristics of the filter are analyzed. To verify the proposed methods, filter is designed and fabricated. Measured results show the proposed UWB properties from 3 to 10.8 GHz. The UWB filter's dual-notch-bands whose center frequencies are 4.5 GHz and 7.7 GHz and have 10 dB fractional bandwidths of about 2.2% and 1.3%, respectively. These filters can be integrated in UWB radio systems and efficiently enhance the interference immunity from undesired signals such as wireless local area network (WLAN) and WiMAX.

Session 3P5
Computational Electromagnetic, Hybrid Methods

Fast Numerical Simulation of Responses of Array Multicomponent Induction Logging Tool in Horizontally Stratified Inhomogeneous TI Formation by NMM

Hongnian Wang[1], **Ping Hu**[1], **and Honggen Tao**[2]

[1]College of Physics, Jinlin University, Changchun 130012, China
[2]Wireline Logging Company, Daqing Drilling Engineering Company, Daqing 163412, China

Abstract— A new multi-component array induction logging tool (MCAIL) consists of a triaxial transmitter coils and several triaxial receiver coils with different offset distances so it can provides the information about the distribution of both horizontal and vertical resistivities of anisotropy formation. However, due to the EM field by its two coplanar transmitters not being axially symmetrical, the responses of MCAIL are often solved by 3D numerical modeling and its workload is usually very large.

In this paper, we will improve numerical matching mode method (NMM) and establish a fast numerical simulation of responses of MCAIL in a horizontally stratified inhomogeneous TI formation. First, using the singularity of derivative of formation conductivity function with respective to radial distance at cylindrical interfaces, we introduce two new singular differential operators to the partial differential equation about electrical field, thus obtain the new partial differential equation with singular terms about EM field to compensate the influence of the accumulation surface charges at the interfaces on it. Then, applying NMM to compute two stiff matrixes of the equation and their corresponding eigenvalues and eigenvectors, we can obtain the semianlytic expression of EM field in cylindrically layered TI medium. Furthermore, using reflection matrix, generalized reflection matrix and transmission matrix at all horizontal interfaces, we give the semianlytic expression of magnetic tensor Green's function by magnetic current source in horizontal-layer inhomogeneous TI medium to compute the MCAIL response. Finally, numerical results validate the algorithm and further investigate the response characteristic of MCAIL.

Optimizing Performance of Parallel FDTD With NUMA Policy and MCA Parameters Turning

Geng Chen[1], **Ke-Jian Chen**[2], **Lei Zhao**[1, 3], **and Wenhua Yu**[1]

[1]Center for Computational Science and Engineering, School of Mathematical Sciences
Xuzhou Normal University, China
[2]School of Computer Science and Technology, Xuzhou Normal University, China
[3]State Key Laboratory of Millimeter Waves, Southeast University, China

Abstract— Symmetric Multi-Processing (SMP) nodes with multi-core Chip-Multiprocessors (CMP) have been widely used in High-Performance Cluster (HPC). For a HPC system, the Message Passing Interface (MPI) library have a multi-layer hierarchical communication structure, and the Non-Uniform Memory Access (NUMA) architectures have been reintroduced. Therefore, the mapping from MPI processes to cores is very important, which may impact the overall performance of the HPC systems. In this paper, the NUMA policy and MCA parameters turning are used to optimize the parallel Finite-Difference Time-Domain (FDTD) software performance accelerated by HPC system which includes 18 nodes (36 CPUs with 144 cores, Intel Xeon X5550 2.7 GHz processor). Firstly, we investigate the effect of processor affinity on parallel FDTD performance by binding each rank to the node, CPU, and core. Comparing the simulation results, we find that the processor affinity has significant impacts on the performance and binding each rank to CPU is almost two times faster than binding each rank to core. Then, NUMA policy was build in the parallel FDTD code to reduce memory access time by providing each node with its own local memory. Numerical results show that the performance of parallel FDTD with Numactl is about 1.5 times faster than without Numactl.

HSS Preconditioning for the Time-harmonic Maxwell Equation in Mixed Form

Di Zhao
Computational Analysis and Modeling Program, Louisiana Tech University, USA

Abstract— We will discuss the time-harmonic Maxwell equations in this paper:

$$\begin{aligned} \nabla \times \nabla \times E - k^2 E &= f \quad \text{in } \Omega, \\ n \times E &= 0 \quad \text{in } \partial\Omega. \end{aligned}$$

Decomposing the field E as

$$E = u + \nabla\varphi,$$

and substituting into the time-harmonic Maxwell equation, we obtain:

$$\begin{aligned} \nabla \times \nabla \times u + \nabla \times \nabla \times (\nabla\varphi) - k^2(u + \nabla\varphi) &= f, \\ n \times u + n \times (\nabla\varphi) &= 0. \end{aligned}$$

Setting

$$p = k^2\varphi$$

and by vector calculus identity of curl of the gradient

$$\nabla \times (\nabla\varphi) = 0,$$

we obtain:

$$\begin{aligned} \nabla \times \nabla \times u - k^2 u - \nabla p &= f, \\ \nabla \cdot u &= 0, \end{aligned}$$

which is equal to its matrix form:

$$\begin{bmatrix} \nabla \times \nabla \times -k^2 & -\nabla \\ \nabla\cdot & 0 \end{bmatrix} \begin{bmatrix} u \\ p \end{bmatrix} = \begin{bmatrix} f \\ 0 \end{bmatrix}.$$

We will discretize the time-harmonic Maxwell equations by discontinuous Galerkin's method, and solve the linear system by GMRES. We will apply the preconditioner symmetric/skew-symmetric separation (HSS) to accelerate the solution speed of the linear system by GMRES.

Finite Volume Algorithm to Simulate Responses of Multi-component Induction Tools in 3D Inhomogeneous Anisotropic Formation Using Coupled Scalar-Vector Potentials

Ye Zhang, **Hongnian Wang**, **and Shouwen Yang**
School of Physics, Jinlin University, Changchun 130012, China

Abstract— In order to correctly interpret multi-component induction logging (MCIL) data in complex anisotropic formations, we use a novel finite volume algorithm to research and realize the 3D simulation of MCIL's responses. To avoid appearance of LINs (low induction numbers) problem caused by either low frequency or high resistivity during modeling and enhance convergence velocity of numerical solution, we first reformulate Maxwell's equation into Helmholtz equations in terms of coupled scalar-vector potentials with Coulomb gauge by applying Helmholtz decomposition of electric field. Then we use a new Yee's non-uniform staggered girds, finite volume averaging and interpolation technique to discrete the Helmholtz equations. After that, we obtain a large, sparse and complex linear system of equations with a block diagonally dominant structure. A combination of BICGSATB with an incomplete LU-decomposition precondition is efficiently applied to iteratively solve the system. Besides, the numerical results show that the numerical results by the algorithm are well consistent with that by NMM and analytic methods in some simple models, and their average relative errors are less than 3%.

Finally we systematically investigate natures of 3D responses of MCIL in complex anisotropic formation through computation and comparison of the responses of the tool in different bed thickness, anisotropic coefficients, invasion radius and so on.

Fast RCS Computation over a Frequency Band Using High-order MoM and AWE Technique

Jun Yan, **Jun Hu**, **Kai Zheng**, **Ming Jiang**, **and Zaiping Nie**
School of Electronic Engineering, University of Electronic Science and Technology of China
Chengdu, Sichuan 611731, China

Abstract— The high-order method of moments (HO-MoM) combined with the asymptotic waveform evaluation (AWE) technique is applied to obtain the radar cross section (RCS) of an arbitrarily shaped three-dimensional (3-D) perfect electric conductor (PEC) body over a frequency band. The frequency relevant systematic equation about the unknown current on the PEC body is formulated using the electric field integral equation (EFIE) and HO-MoM at the central frequency. By using AWE technique, the unknown equivalent surface current is firstly expanded in a Taylor's series at the central frequency, and then the Taylor series coefficients are matched via the Padé approximation to a rational function. The surface current is available at any frequency within the desired frequency band through the obtained rational function. Due to the invoking of HO-MoM, the unknowns are reduced remarkably, and a same geometric mesh grid is used during the whole frequency band. Compared with traditional HO-MoM, the HO-MoM with AWE technique avoids to fill the impedance matrix and solves the unknown surface current at each sampling frequency, so it is extremely efficient for large scale electromagnetic problems at wide frequency band. Numerical results will be presented to show the efficiency and capability of the present method.

Fast Parameterized Inversion of Multicomponent Induction Logging Data in Horizontally Layered TI Formation

Shouwen Yang and Hongnian Wang
School of Physics, Jilin University, Changchun 130012, China

Abstract— We advance a fast parameterized inversion algorithm to simultaneously reconstruct the horizontal and vertical conductivities, the interface depth each bed from the multicomponent induction logging (MCIL) data in horizontal layered TI formations. Applying transmission line method (TLM) gives the analytic solution of tensor Green's function in the frequency-wavenumber domain. The perturbation equations are derived about the changes in responses of MCIL caused by perturbation in model parameters. The computations of the Sommerfeld integrals are solved by the cubic spline interpolation and the recursive formulae of Bessel function. As a result, it is set up the fast computation of the MCIL responses and their Frchet derivative with respective to all model vectors. Finally, we iteratively reconstruct all the model parameters to realized the best fit of the input logging data with the modeling data by the normalization of Fréchet derivative and singular-value-decomposition (SVD). Theoretical inversion results validate the inversion method and its anti-noise ability.

Solving Multi-scale Electromagnetic Problems by Integral Equation Based Domain Decomposition Method with Adaptive Interior-outer Iterative Technique

Ming Jiang, **Jun Hu**, **Hanru Shao**, **Jun Yan**, **and Zaiping Nie**
School of Electronic Engineering, University of Electronic Science and Technology of China
Chengdu, Si Chuan 611731, China

Abstract— As popular integral equation method (IEM), Method of Moment (MoM) is a widely used numerical method for electromagnetic (EM) problems, but MoM system is ill-conditioned for many realistic structures with different scales, tiny fine details. It leads to slow convergence and low accuracy issues, so it is not appropriate for many multi-scale EM problems like antenna on electrically large platform, signal integrity in high speed integrated circuit. To attain efficient and accurate solutions, a novel integral equation method based on domain decomposition method (IE-DDM) is proposed recently by Jin-fa Lee. Non-overlapped DDM framework is used to realize fast and accurate solution of different sub-regions. This method can improve the spectral properties of the MoM matrix in complicated multiple scale EM issues as an efficient and effective pre-conditioner. For the complex structures which the geometry possesses large platforms and tiny fine details together, we can deal with them respectively and use non-uniform meshes in different regions. Another merit of the presented method is that it can be coupled with fast matrix-vector products flexibly in each sub-region such as MLFMM, AIM, FFT or ACA. In this paper, an adaptive interior-outer iterative technique is developed in order to achieve better convergence. Finally, some typical numerical examples will be presented to validate the efficiency and robustness of the IE-DDM method with adaptive interior-outer iterative technique.

Forward the ADI-PSTD Algorithm to 2.5-Dimensional Full Wave Problems

Hong-Xing Zheng
Tianjin University of Technology and Education, China

Abstract— The finite-difference time-domain (FDTD) method is a very useful tool in modeling transient electromagnetic field [1]. However, numerous examples demonstrated that a sampling density of 10C20 cells per minimum wavelength is required to obtain acceptable results. Improving the accuracy and efficiency of the FDTD method has been an active research topic. Among such efforts, pseudospectral time domain (PSTD) method is a remarkable improvement in efficiency over the FDTD method [2]. In recent years, two different PSTD approaches, the Fourier PSTD method and the Chebyshev PSTD method, have been developed for unbounded media. The Chebyshev PSTD method together with a suitable well-posed perfectly matched layer (PML) can deal with complex objects with a great flexibility. To increase computational efficiency, the alternating-direction-implicit (ADI) technique [3] is developed for the simulation of electromagnetic wave propagation and scattering in conductive and inhomogeneous media. In many applications, such as geophysical subsurface sensing and microwave waveguides, the medium is invariant with one coordinate variable. The three-dimensional full wave problem can be solved by a time-domain algorithm for a series of two-dimensional problems. Such problems are thus called 2.5-dimensional problems. In this approach, the ADI-PSTD algorithm has been developed to solve the 2.5-dimensional problem. The Fourier PSTD scheme, together with the PML absorbing boundary condition, has been modeled microwave waveguides. To treat curved geometries more effectively, the multidomain Chebyshev PSTD technique is applied to the ground penetrating radar problems. When the ADI technique is used, the computer resources have been reduced further. Numerical results show an excellent agreement with analytical solutions, and show the advantages over the global-domain Fourier ADI-PSTD method in terms of geometric flexibility. The accuracy of these schemes have also been demonstrated when they are applied to wide-band waveguide problems.

ACKNOWLEDGMENT

This work is supported by the National Natural Science Foundation of China under Grant 60871026.

REFERENCES

1. Yee, K. S., "Numerical solution of initial boundary value problems involving Maxwell's equations in isotropic media," *IEEE Trans. Antennas Propagat.*, Vol. 14, 302–307, May 1966.
2. Liu, Q. H., "The PSTD algorithm: A time-domain method requiring only two cells per wavelength," *Microwave Opt. Technol. Lett.*, Vol. 15, 158–165, 1997.
3. Namiki, T., "3-D ADI-FDTD method-unconditionally stable time-domain algorithm for solving full vector Maxwell's equations," *IEEE Trans. Microwave Theory Tech.*, Vol. 48, 1743–1748, Oct. 2000.

Performance of Incident Hard and Soft Sources in the ADI-PSTD Method

Hong-Xing Zheng and Jing-Jing Li
Tianjin University of Technology and Education, China

Abstract— The pseudospectral time-domain (PSTD) method uses the differentiation theorem for Fourier transforms to numerically implement the spatial derivatives in Maxwell's equations [1]. According to the Nyquist sampling theorem, the spatial-differencing process in the PSTD converges with "infinite order" accuracy for grid-sampling densities more than two points per wavelength. Thus, the PSTD method is a promising scheme for reducing numerical dispersion artifacts. However, a source specifies the field at a single grid point with a temporal driving function; it represents a spatial delta function. Such source causes difficulties for the fast Fourier transforms inherent in the PSTD algorithm, then introduces aliasing errors referred to as Gibbs phenomena [2]. Therefore, a spatially compact wave source specified with a temporal driving function is typically preferred in most practical modeling problems. In this approach, the implementation of two classes of spatially compact wave sources has been discussed. The sources were coupled energy into the PSTD lattice. One is transparent current source; and the other is hard field source. To increase the computational efficiency, an alternating-direction-implicit (ADI) technique [3] is also used. Using 1-D ADI-PSTD simulations, the compact sources spanning only two spatial grid cells completely eliminates the problem of Gibbs phenomena. Numerical investigations have revealed that the error introduced by one of the two adjacent sources exactly cancels the error introduced by the other. In 2-D ADI-PSTD simulations, the compact "twin-source" scheme has been extended to demonstrate error-free excitation of waveguide modes. Fundamental mode excitation in a dielectric slab waveguide via an infinite electric line source in a two-dimensional grid has been implemented. These source conditions in two practical ADI-PSTD modeling examples demonstrate successfully.

ACKNOWLEDGMENT

This work is supported by the National Natural Science Foundation of China under Grant 60871026.

REFERENCES

1. Liu, Q. H., "The PSTD algorithm: A time-domain method requiring only two cells per wavelength," *Microwave Opt. Technol. Lett.*, Vol. 15, 158–165, June 1997.
2. Taflove, A. and S. Hagness, *Computational Electrodynamics: The Finite-Difference Time-Domain Method*, 2nd Edition, Artech House, Boston, MA, 2000.
3. Zheng, H.-X. and K. W. Leung, "An efficient method to reduce the numerical dispersion in the ADI-FDTD," *IEEE Trans. Microwave Theory Tech.*, Vol. 53, 2295–2301, July 2005.

Three Dimensional ADI-FDTD/PSTD Simulations for Plasma Applications

Hong-Xing Zheng
Tianjin University of Technology and Education, China

Abstract— Plasma is a highly frequency-dispersive medium. Recently, extensive applications have been found such as ionosphere wave propagation and microwave excited plasma source for semiconductor processing. The frequency dispersion of plasma can significantly change the electromagnetic response. To analize the frequency dispersion properly, the finite-difference time-domain (FDTD) method has been applied to the plasma [1]. When simulating an open-region problem, the perfectly matched layer (PML) has been used [2]. The PML has been demonstrated to be the most efficient to date, which can give zero reflection at the truncating boundary for almost all frequency, and all incident angles. Although the FDTD method is with widespread applications, to ensure the accuracy of the computed spatial derivatives of electromagnetic fields, the FDTD method requires a fine spatial discretization of more than 10 cells per minimum wavelength, which limits the scale of problem solvable. As one of the improvements, the pseudospectral time-domain (PSTD) algorithm has been recently developed for nondispersive media [3], and proves to provide high accuracy and efficiency for large-scale problems. This new algorithm was then extended to general dispersive media and for ground-penetrating radar applications in dispersive media. In this approach, the 3-D FDTD and PSTD algorithms, with PML absorbing boundary condition, are used for simulation of the nonmagnetized plasma as a special case of general inhomogeneous, dispersive, conductive media. To increase the computational efficiency, the alternating- direction-implicit (ADI) technique [4] is also used. Several examples, such as laser-pulse propagation in plasma hollow channels, surface-wave propagation along a plasma column of finite length, and energy deposition of electron cyclotron resonance plasma source, demonstrate the capability and effectiveness of these algorithms. The numerical results show that the ADI-PSTD algorithm is more efficient and accurate than the ADI-FDTD algorithm, and is suitable for large-scale problems.

ACKNOWLEDGMENT

This work is supported by the National Natural Science Foundation of China under Grant 60871026.

REFERENCES

1. Luebbers, R. J., F. P. Hunsberger, and K. Kunz, "A frequency-dependent finite-difference time-domain formulation for transient propagation in plasma," *IEEE Trans. Antennas Propagat.*, Vol. 39, 29–39, Jan. 1991.
2. Berenger, J. R., "A perfectly matched layer for the absorption of electromagnetic waves," *J. Comp. Phys.*, Vol. 114, 185–200, 1994.
3. Liu, Q. H. and G.-X. Fan, "A frequency-dependent PSTD algorithm for general dispersive media," *IEEE Microwave Guided Wave Lett.*, Vol. 9, 51–53, Sept. 1999.
4. Zheng, H.CX. and K. W. Leung, "An efficient method to reduce the numerical dispersion in the ADI-FDTD," *IEEE Trans. Microwave Theory Tech.*, Vol. 53, 2295–2301, Jul. 2005.

Efficient Computation of Sommerfeld Integral by Cubic Spline Interpolation to Determine Spatial Domain Dyadic Green's Function in Horizontally Layered TI Medium

Jianmei Zhou and Hongnian Wang
School of Physics, Jinlin University, Changchun 130012, China

Abstract— It is very important to fast compute the spatial domain dyadic Green's function in horizontal layered TI formations for use of integral equation to solve 3D EM field. The Green's function is usually expressed by the Sommerfeld integral with complex kernel functions. Their integrands always contain singular points so their numerical integrations often show rapid oscillations and slow convergent characteristics and their computations are very time-consuming.

Based on the complexity of the kernel function in horizontal layered TI formations in magnetotelluric exploration, we advance a simple and novel approach called as cubic spline interpolation method (CSIM) to quickly solve the Sommerfeld integral. First, we divide the integral range into a series of small segments with gradual increase of the lengths and compute the values of the kernel functions at all nodes. Then we use cubic spline functions to interpolate the kernel function and obtain the semianlytic expression of the function. We can further transform the integral into a series of simple Bessel integral with kernel of polynomial functions at each segment. Furthermore, using Bessel function recursion formula and the asymptotic expansion of Lommel formula to analytically solve all the integrals and sum them, we cal efficiently obtain numerical results of spatial domain dyadic Green's function. The numerical results show that the new algorithm largely increases efficiency of computation of the Green's function and faster than other digital filter techniques.

Contribution to the Electromagnetic Modeling and Simulation of Planar Junctions Using Boundary Element Method

Malika Ourabia
University of Sciences and Technologies Houari Boumediene, Algeria

Abstract— A combination of a planar junction analysis as resonator by use of the boundary element method and a planar waveguide model from an accurate hybrid mode investigation has been proposed. The multimode parameters are calculated with a good accuracy from a simple identification in the system of equations given by the boundary method. In addition to a considerable gain of computing time with this method, it is easy to handle complicated structures.

In our investigation a boundary element method using Green's function and a planar waveguide model are used. We introduce the edge line concept as a developed alternative to the usual waveguide model approach. This concept is based on the observation of the current leakage at each side of strip-line. This approach not only gives a boundary condition applicable to planar circuit model but also permits to consider the frequency dependent of fringing effect to be achieved. Then we develop equivalent circuit and some numerical consideration. We simulated the effects of edge line by two edge line coupled to the principal line.

For multimode analysis, it is desirable to separate the voltages and currents of different modes propagating in the outgoing transmission lines. This separation can be carried out by dividing the externals ports of the network into sub-ports of smaller widths. The number of sub-ports at each external port should be at least equal to the number of modes propagating in the transmission line so that the model parameters can be obtained by Fourier series expansion. The admittance matrix of network, relating voltages and currents at the sub-port, may be evaluated using the Green's function approach and segmentation method for simple shapes, and numerical methods for arbitrary shapes. In the Green's function approach, the planar shape is considered to be obtained from segments whose Green's functions are available. The resulting admittance matrix is obtained from those of the segments by using segmentation method.

The present approach can be applied easily to the analysis of multiport junctions and cascade blocks for a filter. This filter is constituted by three cells; the final matrix of the filter has obtained by cascading their matrices respectively.

Session 3P6a
Electromagnetic Composite and Smart Materials for Microwave Applications 2

Microwave Properties of Composite Metamaterials with Glass-coated Amorphous Microwires

F. X. Qin[1], **H. X. Peng**[1], **L. V. Panina**[2], **M. Ipatov**[3], **and A. Zhukov**[3]

[1]Advanced Composite Center for Innovation and Science, Department of Aerospace Engineering
University of Bristol, University Walk, Bristol, BS8 1TR, UK
[2]School of computing, Communication and Electronics, University of Plymouth
Drake Circus, Plymouth, Devon, PL4 8AA, UK
[3]Dpto. de Fisica de Materiales, Fac. Quimicas, Universidad del Pais Vasco, Bilbao, 20018, Spain

Abstract— The development of composites containing ferromagnetic fillers has attracted much interest in the scientific and engineering community in recent years. Compared to conventional dielectrics, this kind of magnetodielectric composites can perform much better in a range of engineering applications, such as antenna substrates in terms of minimized radiation quality factor due to the effect of magnetic dispersion and loss making it very useful for the antenna miniaturization [1]. The contribution of the magnetic constituents finds further application in composite industry, whereby the ferromagnetic microwires are embedded into the composite matrix in a certain manner to generate a plasma- or resonance-like spectra of effective permittivity at GHz frequencies [2, 3]. One of the major challenges for such application is the adjustability of electromagnetic properties, which is much needed for re-configurable devices [4]. Ferromagnetic microwire composites have the potential to meet this purpose, in that the tunable collective response can be controlled by tailoring the local magnetic properties without changing the structural parameters in the presence of external stimuli such as magnetic field, stress and temperature [5, 6].

Experimentally, the composite metamaterials were prepared by embedding continuous Co-rich microwires, as building blocks, in a periodical manner into glass fibre reinforced epoxy and silicone rubber of 50 by 50 cm, respectively. The microwave properties of the resultant composites were conducted by free-space measurements at 0.9–17 GHz in the presence of field (for epoxy matrix) or stress (for rubber matrix). It has been shown that the tunable electromagnetic parameters (transmission, reflection and effective complex permittivity) of the composites are readily approachable with the application of a small magnetic field or stress. The obtained results reveal that both transmission and reflection decrease with external field due to the fact that the magnetoimpedance effect gives rise to increasing loss factor and raises the absorption. There is also a strong dispersion of effective permittivity ($\varepsilon = \varepsilon' - i\varepsilon''$) extracted from S-parameters. At zero external field, with increasing frequency, ε' increases from negative values to positive at somewhere near plasma frequency, which is justified by the significant increase of transmission. Both ε' and ε'' increase with the field alongside a transformation of dispersion mode from regular to anomalous at certain frequency range depending on the composite mesostructure. The stress tunable properties are also demonstrated in the rubber-based composites with more complex stress dependences of electromagnetic parameters. Thus, the relevant information of external field can be identified in the microwire composites through all these microwave characteristics, which can then be exploited technically for a spectrum of engineering applications such as structural health monitoring.

REFERENCES

1. Ikonen, P. M. T., et al., *IEEE Trans. Antennas Propag.*, Vol. 54, 3391, 2006.
2. Peng, H. X., et al., *J. Non-Cryst. Solids*, Vol. 355, 1380, 2009.
3. Makhnovskiy, D. P. and L. V. Panina, *Progress in Ferromagnetism Research*, edited by V. N. Murray, Nova Science Publishers Inc., Hauppauge, NY, 2005.
4. Ipatov, M., V. Zhukova, L. V. Panina, and A. P. Zhukov, "Ferromagnetic microwires composite metamaterials with tuneable microwave electromagnetic parameters," *PIERS Proceedings*, 1657–1661, Moscow, Russia, August 18–21, 2009.
5. Liu, L., S. Matitsine, C. B. Tang, and L. B. Kong, "Measurement of tunable permeability and permittivity of microwires composites at microwave frequency," *PIERS Proceedings*, 1662–1666, Moscow, Russia, August 18–21, 2009.
6. Phan, M.-H. and H.-X. Peng, *Prog. Mater. Sci.*, Vol. 53, 323–420, 2008.

A Study on the SRRs Function on Metamaterial Screen Absorber

Yang Qiu Xu, **Pei Heng Zhou**, **Hui Bin Zhang**, **Di Fei Liang**, **and Long Jiang Deng**
State Key Laboratory of Electronic Thinfilms and Integrated Devices
University of Electronic Science and Technology of China, Chengdu, China

Abstract— Compared with traditional absorbers, metamaterial screen absorber breaks the limit in the minimum thickness and obtain near unity absorption [1, 2]. Most reported designs in this kind of absorber are periodic metal resonant structures at the top of a dielectric substrate supported by ground metal plate. They are generally sensitive to the incident angle, polarization and azimuth of the incident wave, and impeded by the narrow absorption frequency band in practical application. This work introduces our attempts to optimize the metamaterial screen absorbers by the virtue of functional SRRs. Our structures are made of periodic copper SRRs at the top of a FR-4 substrate backed by a copper ground. Based on the coupling of adjacent SRRs, our first structure obtains good absorption in a wide range of incident angle even if the polarization and azimuth of the incident field changes, but the resonant frequency is dependent on the azimuth of the incident field. Expanding the absorber structure by adding functional SRRs, our second structure broadens the absorption frequency band in normal incidence, but the incident angle, polarization and azimuth of the incident field influence this wide-band function.

Though our structures are not totally insensitive to the polarization and azimuth of the incident field, we proposed potential ways to improve the metamaterial screen absorbers function and realize their application.

REFERENCES

1. Landy, N. I., S. Sajuyigbe, J. J. Mock, D. R. Smith, and W. J. Padilla, *Phys. Rev. Lett.*, Vol. 100, 207402, 2008.
2. Tao, H., C. M. Bingham, A. C. Strikwerda, D. Pilon, D. Shrekenhamer, N. I. Landy, K. Fan, X. Zhang. W. J. Padilla, and R. D. Averitt, *Phys. Rev. B*, Vol. 78, 241103(R), 2008.

Relationships between the RCSR Properties of a Coated Slab and Absorbing Characteristic of the Coated RAM

Hai-Yan Chen, **Long-Jiang Deng**, **Pei-Heng Zhou**, **Liang Chen**, **Jian-Liang Xie**, **and Zhi-Wei Zhu**
State Key Laboratory of Electronic Thin Film Integrated Device
University of Electronic Science and Technology of China, Chengdu 610054, China

Abstract— Relationships between the radar cross section reduction (RCSR) properties of a coated slab and the characteristic of the coated radar absorbing materials (RAM) are studied. The slab with radar cross section (RCS) patterns coated with RAM are calculated for either horizontal polarization (HH) or vertical polarization (VV) incident plane wave using a uniform geometrical theory of diffraction for loss surfaces. Comparing the reflection or absorption characteristic of the RAM to the properties of the bi-static RCS of the coated slab, approximate analysis results show that the two are dependent. Surface waves are considered wherever there is reactive surface impedance. The mono-static RCS of the coated slab can be mainly benefited from edge effectiveness for surface wave. The attenuation constants of surface wave in the coated RAM are analyzed. Examining the RCS patterns, we can observe that the effect of RCSR for the coated slab can achieve an optimum at 75° of incidence angle, which can be also interpreted from the characteristic of the coated RAM. The most difficult part in the RCSR design occurs at low frequency, which can be improved by optimizing the characteristic of the coated RAM.

Experimental Study of Microwave Permeability of FeCoBSi Thin Films Prepared on Thin Flexible Substrates

Haipeng Lu, **Jing Yang**, **and Longjiang Deng**
State Key Laboratory of Electronic Thin Films and Integrated Devices
University of Electronic Science and Technology of China, Chengdu 610054, China

Abstract— Nowadays, a lot of research has been carried out to develop ferromagnetic thin films for the use in high frequency devices such as high-frequency micro inductors or micro transformers. However, more and more new applications such as flexible EMI suppressors require flectional samples which under a suitable form [1]. This was the motivation for the experimental study of thin films deposited on thin flexible substrates. The paper deals with FeCoBSi films based on mylar substrates, aiming at the structure and microwave properties of the films. The influence of the different winding methods of the samples on microwave permeability is specialized studied. The objective is deriving correlations between the preparation process and dynamic parameters by analyzing the experimental data on thin ferromagnetic films.

$Fe_{66}Co_{17}B_{16}Si_1$ thin films were produced on flexible 11.5 μm thick mylar substrates by DC magnetron sputtering. The permeability has been measured from 500 MHz up to 18 GHz using a coaxial technique described elsewhere [2]. There are two winding methods for preparing the measuring samples which were suitable for the geometry of the coaxial line cavity. One method is to rolling the FeCoBSi thin film inside and the other method is to rolling the film outside (Fig. 1). Although there is no significant difference from the appearance point of view to the spiral samples, the different winding methods may typically lead to different measure results on microwave permeability (Fig. 2).

FeCoBSi film is a material with positive magnetostrictive coefficient. When we roll the film to a spiral sample by the method that ferromagnetic film outside, a strong tensile stress is caused. Then the internal magnetic moments of the ferromagnetic film tend to re-orientated along the direction of tensile stress as well as the circumferential direction. The angle between the microwave magnetic field and the easy magnetization axis of the ferromagnetic film decreases, and thus the microwave permeability also decreases.

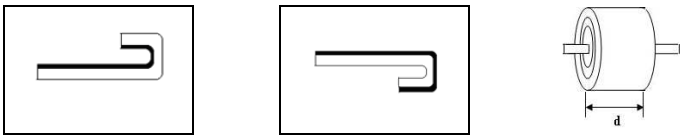

Figure 1: Two winding methods for preparing the roll samples for measuring. (a) Film rolling inside. (b) Film rolling outside. (c) Roll sample for measuring.

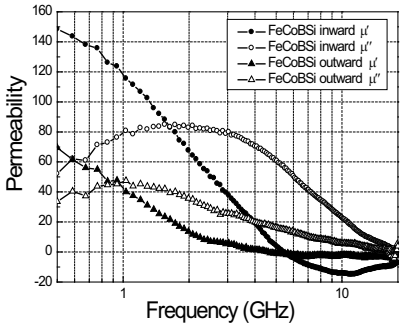

Figure 2: Permeability as a function of frequency for FeCoBSi thin films.

REFERENCES

1. Valls, O., D. Damiani, et al., *Digests of the Intermag Conference*, FD07, 2002.
2. Acher, O., J. L. Vermeulen, et al., *J. Magn. Magn. Mater.*, Vol. 136, 269, 1994.

A Simple Calibration Method for the Shorted Stripline Permeability Measurement

S. N. Starostenko and K. N. Rozanov
Institute for Theoretical and Applied Electromagnetics, Izhorskaya 13/19, Moscow 125412, Russia

Abstract— Permeability measurement of thin films is usually performed in a shorted strip-line cell, as the increase of experimental frequency band is erroneously associated with the increase of cell resonance frequency. The desire to increase the measurement frequency leads to shortening the cell length [1], but the shorter is the cell, the shorter and the less matched is the coaxial to strip coupling, therefore the lower is the field strength and the smaller is the volume of uniform field inside the cell. The larger is the field inhomogeneity, the smaller must be the sample dimensions. These limitations on sample size and field strength define the threshold of permeability detected with a particular network analyzer. The numerical procedures [2, 3] to account for field inhomogeneity are known [2, 3], but they are complicated and rarely employed in practice; the accurate measurement of low-permeability samples is still a problem.

The above problems arise from unaccounted for S-parameters of coaxial-to-stripe coupling that limits the measurement frequency well below the cell resonance. The standard three-load (open-short-matched) calibration technique [4] can not be applied to the coupling that is inside an all-in-one cell. Different calibration techniques that include the measurement of a reference sample with known constitutive parameters have been developed. [1,5] The more advanced procedure [6] accounts for sample shape and for resonance on its dimensions, but these procedures perform a partial calibration that neglects at least one of coupling parameters.

The accuracy of a shorted strip-line technique for permeability determination of at microwaves may be significantly enhanced by a full calibration procedure with a pair of complimentary reference samples. The first one is a permeable composite with known dependence of constitutive parameters on frequency. The second one is either a lossless dielectric with high permittivity, or a strip of impermeable metal. The dimensions of reference samples are selected so that the opposite reflectivity phases within the measured frequency band are obtained. The calibration procedure includes the measurement of complex reflection coefficients of an empty cell, and of the cell loaded with each of the reference samples. To decrease the threshold of detected permeability and to unmask and reveal the calibration errors the measurements are performed in a long cell where the resonance frequency is much lower than the upper frequency limit.

For samples with a low permeance factor the measurement error is 10 to 20 times lower compared to the prototype technique [6]. The effect of permittivity on measured permeability is accounted for. The technique is validated by permeability measurements of test samples and may be implemented to calibrate a variety of partially filled all-in-one transmission lines.

REFERENCES

1. Bekker, V., K. Seemann, and H. Leiste, *J. Magn. Magn. Mater.*, Vol. 270, 327, 2004.
2. Wu, Y. Q., Z. X. Tang, Y. H. Xu, B. G. Zhang, and X. He, *IEEE Trans Magn.*, Vol. 46, 886, Mar. 2010.
3. Liu, Y., L. Chen, C. Y. Tan, H. J. Liu, and C. K. Ong, *Rev. Sci. Insr.*, Vol. 76, 063911, 2005.
4. Mason, S. J., *Proc. IRE*, Vol. 41, 1144, 1953.
5. Ledieu, M. and O. Acher, *IEEE Trans. Magn.*, to be published.
6. Starostenko, S. N., K. N.Rozanov, and A. V. Osipov, *J. Appl. Phys.*, Vol. 103, 07E914, 2008.

GMI Output Stability of Glass-coated Co-based Microwires for Sensor Application

Jing-Shun Liu[1], **Xiao-Dong Wang**[1], **Fa-Xiang Qin**[2], **and Fu-Yang Cao**[1], **Da-Wei Xing**[1], **Hua-Xin Peng**[2], **Xiang Xue**[1], **and Jian-Fei Sun**[1]

[1]School of Materials Science and Engineering, Harbin Institute of Technology, Harbin 150001, China
[2]Advanced Composite Center for Innovation and Science (ACCIS), University of Bristol
University Walk, Bristol BS8 1TR, United Kingdom

Abstract— We report a study here on the technique of Cu electro-plated wire-connecting for stabilizing the GMI output of $Co_{68.15}Fe_{4.35}B_{15}Si_{12.5}$ glass-coated amorphous microwires at the magnetic field ranging from 0 Oe to 4.2 Oe. The GMI output stability was characterized by a precision impedance analyzer and in a magnetically shielded space (MSS). The results show that this method could reduce the emission of RF electro-magnetic wave and driving signal attenuation, minimize the disturbance of stray capacity and parasitic capacity, and suppress high frequency destabilization and concussion at the relatively high frequency ($\geq$MHz), hence effectively improve the GMI output stability for high-resolution magnetic sensor application.

REFERENCES

1. Nguyen, L. T., D. McDonald, A. R. Danker, and P. Ng, "Optimization of copper wire bonding on Al-Cu metallization," *IEEE Trans. Compon. Pack. A*, Vol. 18, No. 2, 423–429, 1995.
2. Liu, J. S., J. F. Sun, D. W. Xing, X. Xue, S. L. Zhang, H. Wang, and X. D. Wang, "Experimental study on the effect of wire bonding by Cu electroplating on GMI stability of Co-based amorphous wires," *Phys. Status Solidi A*, Vol. 208, No. 3, 530–534, 2011.

Session 3P6b
Materials, Devices, Fabrications and Characterizations of Organic Electronics

Electromagnetic Spinning of Nanofibers Using Polymer Bubbles

Ji-Huan He
National Engineering Laboratory for Modern Silk, College of Textile and Engineering
Soochow University, 199 Ren-ai Road, Suzhou 215123, China

Abstract— The electrospinning process is of instability [1], which causes energy waste and makes the fibers in a chaotic form. Magnetic force was first introduced in the traditional electrospinning process, the induced Ampere force can dramatically reduce the radius of the whipping circle [2], see Fig. 1.

The bubble electrospinning is suitable for mass production of nanofibers [3–7], see Fig. 2. However, due to instability of the spinning process, charged jets move whirly, and the adjacent jets might combine into a single fiber, greatly affecting the quality of the obtained fibers.

In this presentation we will apply an excitation coil above the electrospun solution to minimize control the whipping circle of each charge jet.

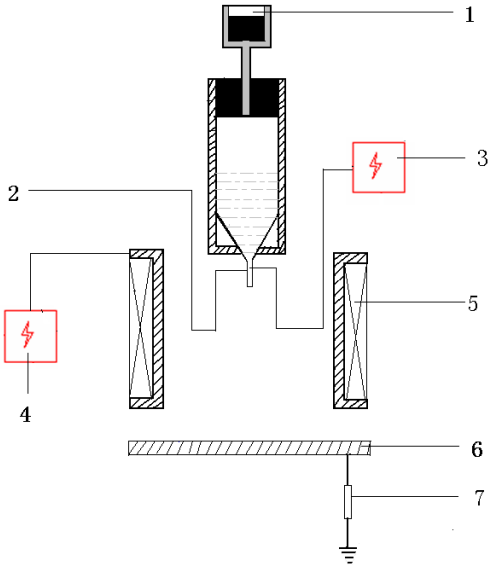

Figure 1: Magnetic-electrospinning setup (1 — pump, 2 — nozzle, 3, 4 — high voltage supply, 5 — excitation coil, 6 — grounded collecting plate, 7 — resistance).

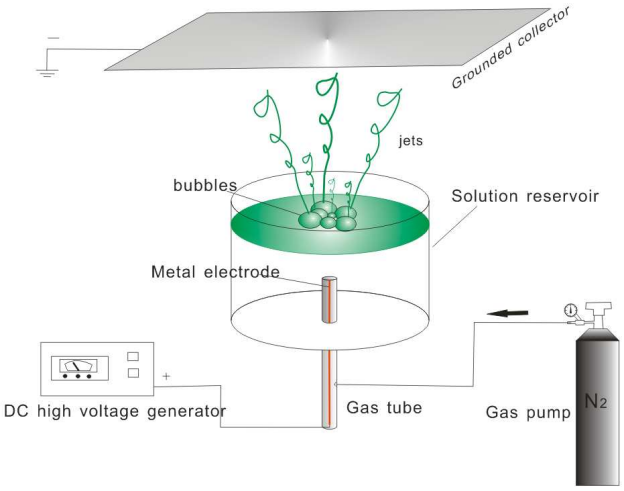

Figure 2: Experimental setup.

ACKNOWLEDGMENT

The resent work is supported by National Natural Science Foundation of China under Grant Nos. 10802021 and 10802021.

REFERENCES

1. He, J. H., Y. Q. Wan, and J. Y. Yu, "Allometric scaling and instability in electrospinning," *International Journal of Nonlinear Sciences and Numerical Simulation*, Vol. 5, No. 3, 243–252, 2004.
2. Wu, Y., J. Y. Yu, J. H. He, et al., "Controlling stability of the electrospun fiber by magnetic field," *Chaos Solitons & Fractals*, Vol. 32, No. 1, 5–7, 2007.
3. He, J. H., Y. Liu, L. Xu, et al., "BioMimic fabrication of electrospun nanofibers with high-throughput," *Chaos Solitons & Fractals*, Vol. 37, No. 3, 2008, 643–651.
4. Liu, Y., Z. F. Ren, and J. H. He, "Bubble electrospinning method for preparation of aligned nanofibre mat," *Materials Science and Technology*, Vol. 26, No. 11, 1309–1312, 2010.

5. Yang, R. R., J. H. He, L. Xu, et al., "Effect of solution concentration on diameter and morphology of PVA nanofibres in bubble electrospinning process," *Materials Science and Technology*, Vol. 26, No. 11, 1313–1316, 2010.
6. Ren, Z. F. and J. H. He, "Single polymeric bubble for the preparation of multiple micro/nano fibers," *Journal of Applied Polymer Science*, Vol. 119, No. 2, 1161–1165, 2011.
7. Yang, R. R., J. H. He, L. Xu, et al., "Bubble-electrospinning for fabricating nanofibers," *Polymer*, Vol. 50, No. 24, 5846–5850, 2009.

Very-high Color-rendering Index OLEDs

Jwo-Huei Jou
Department of Materials Science and Engineering, National Tsing Hua University
Hsin-Chu 30013, Taiwan, R.O.C.

Abstract— Very-high color-rendering index (CRI) lighting is very important for use in surgery operation, exhibition, and photography etc. The market value of very-high CRI lighting sources is the highest among all. We will demonstrate the design and fabrication of the first OLED with CRI as high as 98. There are at least two approaches to achieve the desired very-high CRI; i.e., mainly by depositing multiple light-emitting dyes with full spectrum complementary emission into separate emissive layers via the use solvent pre-mixed method to prepare the deposition sources. For example, one very-high CRI device has employed 5 fluorescent and phosphorescent emitters. With the use of a nano interlayer in between two white emissive layers to modulate the entering carriers, all the emission of the 5 emitters arise and form a full spectrum in the visible range, resulting to a 98 CRI at 1000 nits. Another approach achieving CRI greater than 95 with efficacy at least 2 or more times of incandescent bulb will be presented also.

Ambipolar Transporting Pyridine-containing Anthracene Derivatives for Highly Efficient OLEDs

Lian Duan and Yong Qiu
Department of Chemistry, Tsinghua University, Beijing 100084, China

Abstract— Organic light-emitting diodes (OLEDs) have attracted much research interest due to their potential application in flat-panel displays and lighting [1]. The charge balance in OLEDs is essential for achieving high device performance. Up to now, lots of high-mobility hole transporting materials (HTMs) have been designed and synthesized [2]. However, electron transporting materials (ETMs) with high mobility are relatively rare [3]. Therefore, developing high performance ETMs with high electron mobility and good stability are crucially important for further improving OLED performance. To improve the electron mobility of organic semiconductors, azaaromatics, like phenanthroline, quinoline, pyridine, triazole were incorporated into the π-conjugated systems [4, 5]. However, OLEDs using azaaromatics containing materials as ETM usually show short lifetimes [4, 5]. In this paper, we report pyridine-containing anthracene derivatives with high electron and hole mobilities of around $10^{-3}\,\mathrm{cm^2V^{-1}s^{-1}}$. Furthermore, cyclic voltammetry measurements find that both the cations and anions of the new materials are stable, which may improve the stability of OLEDs using these new materials as ETMs.

REFERENCES

1. Tang, C. W. and S. A. VanSlyke, *Appl. Phys. Lett.*, Vol. 51, 913–915, 1987.
2. Katsuma, K. and Y. Shirota, *Adv. Mater.*, Vol. 10, 223–226, 1998.
3. Uchida, M., T. Izumizawa, T. Nakano, et al., *Chem. Mater.*, Vol. 13, 2680–2683, 2001.
4. Jarikov, V. V., K. P. Klubek, C. T. Brown, et al., *J. Appl. Phys.*, Vol. 104, 074914, 2008.
5. Jarikov, V. V., *Appl. Phys. Lett.*, Vol. 92, 24410, 20083.

All Phosphorescent White Organic Light-emitting Devices with High Color Stability and Low Efficiency Roll-off

Mao-Kuo Wei[1], Yi-Chi Bai[1], Chih-Hung Hsiao[2], Yi-Hsin Lan[2], Jiun-Haw Lee[2], Pei-Yu Lee[3], Tien-Lung Chiu[3], Chung-Chieh Lee[4], Chih-Chiang Yang[4], Man-Kit Leung[4], Shun-Wei Liu[5], and Chin-Ti Chen[5]

[1]Institute of Opto-Electronic Engineering and Department of Materials Science and Engineering
National Dong Hwa University, Hualien, Taiwan
[2]Graduate Institute of Photonics and Optoelectronics and Department of Electrical Engineering
National Taiwan University, Taipei, Taiwan
[3]Department of Photonics Engineering, Yuan Ze University, Chung-Li, Taiwan
[4]Department of Chemistry and Institute of Polymer Science and Engineering, National Taiwan University
No. 1, Sec.4, Roosevelt Rd., Taipei 10617, Taiwan
[5]Institute of Chemistry, Academia Sinica, No. 128, Sec. 2, Academia Rd., Nankang, Taipei 11529, Taiwan

Abstract— In this paper, we have demonstrated device design of white organic light-emitting devices (OLEDs) with three phosphorescent emitters. Here, the red, green, and blue dopants were tris(2-phenylquinoline)iridium(III) [Ir(2-phq)3], fac-tris(phenylpyridine) iridium [Ir(ppy)3], and iridium(III)bis [4, 6-di-fluorophenyl-pyridinato-N,C2] picolinate (FIrpic), respectively. By engineering the doping profiles (thicknesses, concentration, and arrangement) of the emitter layer (EML), OLEDs with high color stability and low efficiency roll-off can be achieved simultaneously. In our devices, total EML thickness was kept thick (more than 25 nm) for achieving low efficiency roll-off. Carrier distribution and energy transfer paths should be kept same (or similar) under different current injections which were important criteria for stable color coordinates. We started the device design from bi-chromatic OLEDs with 9% FIrpic and 9% Ir(ppy)3 in the host N, N-dicarbazolyl-3, 5-benzene (mCP) for blue and green emission respectively. By inserting a thin undoped mCP layer between blue and green emitter for confining carriers and excitons, color stability can be achieved. An alternative was to use two hosts with hole- and electron-transporting characteristics with green and blue emitter doped inside, respectively, denoted as EML1 and EML2 for the same purpose. Although mCP exhibited bipolar transport characteristics, the hole mobility was about one order of magnitude higher than its electron mobility, which was used as the host of EML1. Here, we employed 2,2'-bis[5-phenyl-2-(1,3,4)oxadazolyl]biphenyl (OXD), which exhibited bipolar characteristics with much higher electron mobility than hole one, as the host of EML2. Finally, red dopant was selectively doped in the suitable position with low concentration (i.e., 0.5%) for not disturbing the carrier transport characteristics and boosting up device efficiency.

Session 3P7
Poster Session 5

Small Antenna Chamber Design and Measurement

Guan-Yu Chen[1], **Kuo-Liang Wu**[1], **Y. D. Chen**[2], **and Jwo-Shiun Sun**[1]

[1]Department of Electronic Engineering, National Taipei University of Technology, Taiwan
[2]Antenna and EMC Laboratory, HTC Corporation, Taiwan

Abstract— The mobile phone under test of far-field range testing has been the plan (Fig. 1) at the Cellular Telecommunications & Internet Association (CTIA) certification program test requirements for performing radiated power and receiver performance measurement. It is a 3D system for measuring low gain antennas and is well matched for PDA Phone or wireless antenna testing.

Figure 1: The 3D small OTA chamber design.

Phase Modulation for Spectral Switches of an Asymmetrical Slit

Pin Han
Institute of Precision Engineering, National Chung Hsing University
250, Kuo Kuang Road, Taichung 402, Taiwan, R.O.C.

Abstract— In this paper we provide a new scheme that utilizes both the aperture mechanism and phase control mechanism to manipulate the spectral switches of an asymmetrical slit. It can provide two advantages over previous schemes as: (1) The data transmitting angle employing the spectral switch can be selected arbitrarily; (2) Compared with the past strategy utilizing light source or mechanical methods, the modulation speed is very fast due to the usage of phase control mechanism by Pockel effect. Not only the theoretical analysis is presented, but also the numerical results are shown how the two goals are achieved.

On the Electrically Driven Motion

S. L. Vesely[1], **A. A. Vesely**[2], **and C. A. Dolci**[3]

[1]I.T.B. — C.N.R., Italy
[2]Via L. Anelli 13, Milano, Italy
[3]Liceo Einstein, Milano, Italy

Abstract— Electricity is closely intertwined with chemical sciences, not only because electrical/optical measuring systems are increasingly being used in chemistry, but also since batteries have been the first useful electrical power source. Since Lorentz and Drude, current is regarded as a convective motion of charged particles, both when interpreting the functioning of electronic measuring systems, as well as for analyzing redox transformations that generate power. The functioning of electronic circuits and devices can be modeled according to statistical mechanics. Furthermore, measurements taken during experiments, being associated with linear methods, and usually subdivided into logical steps, can also be modeled likewise. However, it is difficult to extend statistical mechanics so as to explain electrolytic currents, because chemical processes are an integral part of the model chosen to represent ionic currents. Arrhenius theory explains salts dissociations in aqueous solutions using the law of mass action. It interprets electrolysis in terms of neutralization reactions at the electrodes, and assumes that the conductance ratio is broadly proportional to the ionization degree of the solute. As it is known that power mostly involves irreversible conversions, a model valid for powerless chemical reactions has to break down when usable power starts to be actually generated. Thus, the question arises of how non-linearity becomes noticeable in particle transport models.

The electrolytic law already faces the question of the limit of validity of linear chemical theories. M. Faraday observed that the amount by weight of chemical decomposition of an acid, a base, or a salt is proportional to the time-integral of the current, as measured by a galvanometer. He proposed to define the *equivalent* of each material liberated at one electrode (or deposited at the cathode) by means of its electrochemical equivalent. The gas-kinetic approach is sufficient to identify the *equivalent* of the metal of a simple inorganic salt with the molarity of the substance deposited at the cathode. The conductance may result from the difference between anions and cations speeds, taking into account their mobility, provided that oxidation degree is constant. However, if the current could be simply ascribed to ionic transport, chemical reactions would admit a linear description, e.g., allowing a synoptic table of all substances arranged by such *equivalent*. On the contrary, organic chemistry provides plenty of complex substances that defeat such approach. Although gaseous bubbles gurgling at the electrodes of an electrolytic cell may evoke the idea of a simple particle motion driven by electricity, biochemists developed separative techniques where transported particles don't carry charges all the way from one electrode to the other; such techniques involve immobilizing the pH gradient between the electrodes so that sought compounds accumulate at their isoelectric points.

Modern physical explanations evolved by positing more capabilities into the particles. The reductionistic approach was improved by explaining even chemical reactions in terms of elementary mechanical processes. Thus, valence theory was traced back to the behavior of the so-called "optical" electrons in the outer atomic shells, and ions mobility was diversified by solvation processes and mutual interactions. As theories of electrically driven motion in solutions became more complex, the office of determining the masses of substances passed from electrolysis on to atomic mass spectrometry. The latter technology in turn evolved, and besides mass isotopy, led to the discovery of mass defect, nuclear shell deformation, excited isomers, and more. In our opinion, the particularizations of the model required on each step forward, rather than reflecting an enduring increase of our knowledge of the matter, may suggest that statistical mechanics modeling consistently fails to capture the characteristic traits of electrochemical conversions, even for low currents. For an alternative approach, rather than consider non-equilibrium dynamics of complex systems, we would avoid the transport model altogether, and associate chemical reaction rates to their electric signals directly. This way, as long as the signal detection stays approximately linear, changes in electrical response reflect changes in chemical composition. When an experimental setup allows lowering or raising a chemical reaction rate, the procedural steps used to control it could be considered an "explanation" of that chemical process.

Novel Nonlocal Gauge Functions in Electrodynamics and Their Effect on Quantum Mechanical Phases

Konstantinos Moulopoulos
Department of Physics, University of Cyprus, Nicosia 1678, Cyprus

Abstract— We report on previously overlooked generalized solutions of the standard gauge transformation equations of Electrodynamics: the generalized "gauge functions" go beyond the usual Dirac phase factor and exhibit a new form of nonlocal quantal behavior, with the well-known Relativistic Causality of classical fields affecting directly the phases of quantum mechanical wavefunctions. The full form of a general gauge function (that connects systems moving in different sets of scalar and vector potentials — but experiencing the same classical fields at the observation point), apart from Dirac phases (spatial or temporal integrals of potentials), is shown to also contain terms of classical fields that act nonlocally (in spacetime) on the local solutions of the time-dependent Schrödinger equation. As a result, the phases of wavefunctions in the Schrödinger picture are affected nonlocally by spatially and temporally remote magnetic and electric fields, in specific ways that are fully explored. These nonlocal contributions on wavefunction phases, apparently overlooked in path-integral approaches, give physical behaviors that go beyond the usual Aharonov-Bohm effects (magnetic or electric): (i) Application to cases of particles passing through nonvanishing magnetic or electric fields leads to cancellations of Aharonov-Bohm phases at the observation point; these cancellations are linked to behaviors at the semiclassical level (to the old Werner & Brill experimental observations — or to more recent reports of Batelaan & Tonomura) but are shown to be far more general (true not only for narrow wavepackets in semiclassical motion but also for completely delocalized (spread-out) quantum states). By using these cancellations, certain previously unnoticed sign-errors in the literature are corrected, and the deeper reason why certain time-dependent semiclassical arguments are consistent with static results in purely quantal Aharonov-Bohm configurations is naturally explained. (ii) Application to time-dependent situations provides a remedy for incorrect results propagating in the literature (concerning an uncritical use of Dirac phase factors — especially in cases of time-dependent vector potentials and space-dependent scalar potentials) and leads to phases that contain an Aharonov-Bohm part and a field-nonlocal part: the interplay between the two parts is shown to recover Relativistic Causality in earlier "paradoxes" (such as the so-called van Kampen thought-experiment) and to complete Peshkin's qualitative discussion of the electric Aharonov-Bohm effect in a causal manner. A more general consideration indicates that the temporal nonlocalities reported here demonstrate in part a causal propagation of phases of quantum mechanical wavefunctions in the Schrödinger picture. Therefore, the new formulation offers a direct way to address questions regarding time-dependent single- vs double-slit experiments and the associated causal issues (issues that have recently attracted attention, with respect to the inability of current theories to address them).

Investigation of Illusion Optics Devices Implemented by Transmission-line Metamaterials with Full Tensors

Guo Chang Liu, **Chao Li**, **and Guang You Fang**
Institute of Electronics, Chinese Academy of Sciences, Beijing 100190, China

Abstract— With the proposition of transformation optics, there emerged a lot of novel electromagnetic devices such as the invisibility cloaks, field concentrators, illusion optics devices and so on, which provide a unconventional functions for arbitrarily control the behaviors of electromagnetic waves. The practical implementation of such devices must take use of metamaterials (MTMs) for that the devices needs anisotropic and non-uniform medium parameters. As a candidate of MTMs with wideband and low loss properties, periodic transmission line (TL) networks were widely used to mimic MTMs with unique characteristics. However, the effective medium parameters possessed by TL MTMs before are all diagonal in the Cartesian basis, which limit the development of MTMs with more complex paramters. Recently, a group in the University of Michigan proposed a new structure of TL MTMs with arbitrary full tensors, in other words it can achieve any 2D anisotropic and non-uniform materials. In this paper, this kind of tensor TL metamaterials was introduced to the field of illusion optics invisibility system. Two circuit simulations are presented, one is a square invisibility cloak that cloaks objects at a distance outside the cloaking shell and the other is an illusion optics system which optically transforms one object to another. The results are then compared with the results of full-wave simulation based on finite-element method. The dependence of the performance on the variation of the frequencies and the amount of loss were also analyzed. It's found that TL MTMs with full tensors can be well applied to mimic transformation optics devices with complex medium parameters distributions.

About the Zero Point Energy, Zero Point Mass, Zero Point Temperature and Zero Point Motion in the Subatomic World and Photonics

Antonio Puccini
Department of Neurophysiology of Order of Malta, Naples, Italy

Abstract— The Heisenberg Uncertainty Principle states that no particle can be completely motionless (since it is not possible to know two *complementary parameters* of a particle at the same time), it will at least oscillate around a plane: in this case we will talk about *Zero Point Motion*. From Quantum Mechanics we learn that a real particle will never have a null energy, but it will always have a minimum possible energy called *Zero Point Energy*. We also learn from Quantum Mechanics that Absolute Zero temperature can never be reached. At this temperature, in fact, the motion would cease and we would be able to know simultaneously the two *complementary parameters* we mentioned before: the position and the momentum of the same particle. In a number of cases, in fact, extremely low temperature have been reached, but never touching $-273,15^{\circ}$ Celsius. Thus we will talk about *Zero Point Temperature*.

Relativity's Theory, on its turn, tells us that mass and energy are equivalent. Einstein, in fact, realized that scientists were wrong keeping about the mass and E as two phenomena which though linked, were basically different. On the contrary, he understood that they had exactly equal behaviours: both expanded and contracted according to an identical factor. Under every significant aspect, Einstein concluded mass and E were entities *indistinguishable and interchangeable*, and formulated his famous formula: $E = mc^2$. So any particle having energy should carry a mass, though tiny, corresponding to the energy of the examined particle divided the square of the speed of light.

Comment on "Permanence of Light Velocity" by Applying the New Theory on Electromagnetic Wave

Yelin Xu[1] and Qiang Xu[2]

[1]Institute of Biophysics, Chinese Academy of Sciences, Beijing 100101, China
[2]Institute of Theoretical Physics of Haikou, Haikou 570206, China

Abstract— The author's latest paper on electromagnetic wave indicated that, electromagnetic wave has the function of continuously adjusting it self's velocity automatically, namely CAVA. Here, we will continue to discuss CAVA. After the theoretical analyses based on experimental results, this paper reaches the conclusion that CAVA has advantage as well as disadvantage. The advantage is that, under the condition that the light source is stationary, the velocity of electromagnetic wave keeps invariable because of CAVA, and this improves the quality of radio communication; the disadvantage is that real light velocity is variable while the light source is moving, but CAVA is not able to distinguish its true features and adjusts it to C stereotyped, and this brings us the false appearance of the permanence of light velocity. This paper indicates that, when the light source is stationary, light velocity is invariable; when the light source is moving, light velocity is variable.

By analyzing a lens in cosmic space, the author finds that, for a beam of light with arbitrary speed in vacuity, its velocity will turn to C once it passes the lens.

When the light source is on a fixed star, suppose we see on the earth the velocity of the star moving away from us in uniform rectilinear motion is u. When the light source is relatively stationary and the earth is moving away from the light source, if the observer is on the star, he will find the velocity of the light moving on the star and the light moving in the vacuum universe all to be C, and the velocity of the light travelling on the earth to be $C + u$ (because of the speed-increasing effect of CAVA); and if the observer is on the earth, he will see that the velocity of the light moving towards the earth is $C - u$ (because of the speed-decreasing effect of CAVA), and the velocities of the light travelling on the earth and away from the earth aerosphere are all C. As for the situation that the earth is relatively stationary and the light source is moving away from the earth, the result is as the above.

When the light source is on the earth, first suppose that the light emitter train is relatively stationary and the receiver train is moving away from the emitter at the velocity of u. If the observer is on the emitter train, he will find the velocities of the light moving on this train and the light moving on the earth all to be C, and the velocity of the light moving on the receiver train to be $C + u$; and if the observer is on the receiver train, he will see that the velocities of the light moving towards the receiver train and away from the receiver train in the air are all $C - u$, and the velocity of the light moving on the receiver train is C. As for the situation that the light emitter train is moving away from the receiver train at the velocity of u and the receiver train is relatively stationary, if the observer is on the emitter train, he will find the velocity of the light moving on the emitter train to be C, and the velocities of the light travelling on the earth in the air and the light on the receiver train all to be $C + u$; and if the observer is on the receiver train, he will see that the velocities of the light rushing towards the receiver train in the air, the light moving on the receiver train and the light running away from the receiver train in the air are all C.

Physics text books indicate that light velocity is permanent; whereas French scientist G. Sagnac's experiment, the existence of Doppler Effect, and the red shift measurement result of the star spectrum in the universe all strongly proved that light velocity is alterable.

To sum up, the rule of light velocity should be: when the light source is stationary, light velocity is permanent; when the light source is moving, light velocity is alterable.

A Note on Variational Theory for Piezoelectricity with Voids

Ji-Huan He
National Engineering Laboratory for Modern Silk, College of Textile and Engineering
Soochow University, 199 Ren-ai Road, Suzhou 215123, China

Abstract— A classical (not Gurtin-type) variational theory for piezoelectric materials with voids is established by the semi-inverse method.

Main Result: By the semi-inverse method, we establish a variational principle with 10 kinds of independent variables:

$$J(u_i, \sigma_{ij}, \varepsilon_{ij}, \varphi, e_i, h_i, g, E_i, D_i, \Phi) = \iiint_{\Omega} L \mathrm{d}\Omega. \tag{1}$$

where the Lagrangian is expressed in the form

$$L = u_i(\sigma_{ij,j} + \rho\bar{f}_i) + \varphi(h_{i,i} + g + \rho l) + \varepsilon_{ij}\sigma_{ij} - \frac{1}{2}\varepsilon_{ij}E_{ijkl}\varepsilon_{kl} - \varepsilon_{ij}M_{ijk}e_k + \varepsilon_{ij}\beta_{kij}E_k$$
$$+D_i(E_i+\Phi_{,i})+\rho_e\Phi-\frac{1}{2}E_i a_{ij}E_j-E_i p_{ij}e_j+e_i h_i-\frac{1}{2}e_i A_{ij}e_j+\lambda(g-\varsigma\varphi-\eta_{ij}\sigma_{ij}-a_i h_i-c_i D_i)^2 \tag{2}$$

where λ is a penalty parameter, i.e., $\lambda \gg 0$.

Making the above functional stationary, we can obtain the needed governing equations.

REFERENCES

1. He, J. H., "Generalized hellinger-reissner principle," *ASME Journal of Applied Mechanics*, Vol. 67, No. 2, 326–331, 2000.
2. Nunziato, J. W. and S. C. Cowin, "A nonlinear theory of elastic materials with voids," *Arch. Rational Mech. Anal.*, Vol. 72, 175–201, 1979.

Microwave Permeability of Planar Anisotropy $Ce_2Fe_{17}N_{3-\delta}$ Powders and Its Composite

Wenliang Zuo, **Jianqiang Wei**, **Tao Wang**, **and Fashen Li**
Institute of Applied Magnetics
Key Laboratory of Magnetism and Magnetic Materials of the Ministry of Education
Lanzhou University, Lanzhou 730000, China

Abstract— $Ce_2Fe_{17}N_{3-\delta}$ powders were prepared by arc-melting, milling and nitrogenation method The microstructure and static magnetic properties were analyzed by x-ray diffraction (XRD) and vibrating sample magnetometer (VSM), respectively The *c*-planar alignment of $Ce_2Fe_{17}N_{3-\delta}$ composite was evaluated with the XRD date of an aligned composite sample. The effective complex permeability of $Ce_2Fe_{17}N_{3-\delta}$ powders/resin epoxy composite with various volume concentrations were measured in the frequency range of 0.1–15 GHz. The intrinsic static permeability of $Ce_2Fe_{17}N_{3-\delta}$ powder was calculated by Bruggerman (BG) effective medium theory. The natural resonance frequency of $Ce_2Fe_{17}N_{3-\delta}$ was obtained using Landua-Lifshitz-Gilbert (LLG) equation. The Snoek's product of the effective susceptibility static permeability and the resonance frequency is much larger than the value of conventional Snoek's limit. As a novel microwave soft magnetic material, the planar anisotropy $Ce_2Fe_{17}N_{3-\delta}$ powder composite have excellent microwave soft magnetic properties.

Investigation on Peak Frequency of the Microwave Absorption for Planar $Ce_2Fe_{17}N_{3-\delta}$/resin Composite

J. Q. Wei, **W. L. Zuo**, **T. Wang**, **and F. S. Li**
Key Laboratory of Magnetism and Magnetic Materials of Ministry of Education
Institute of Applied Magnetics, Lanzhou University, Lanzhou 730000, China

Abstract— Microwave reflection characteristics of planar $Ce_2Fe_{17}N_{3-\delta}$/epoxy resin composite with various volume concentration were investigated in 0.1–18 GHz. The frequency response of permeability and permittivity for the samples was measured by the coaxial line method using a vector network analyzer (Agilent E8363B). The reflection loss was determined by simulation and by measuring the S_{11} parameters after rear face of samples was terminated. The minimum reflection loss was found moving towards the lower frequency region with increasing the sample thickness. Quantitatively analysis reveals that the peak frequencies of the dips (minimum reflection loss) obey the quarter-wavelength ($\lambda/4$) formula. It implies that the quarter-wavelength formula can be successfully applied to understand and predict the peak frequency of the microwave absorption for ferromagnetic metal-based composites.

A Design of Size-reduced Low Pass Filter Using Artificial Dielectric Substrate Structure

Jakyung Koo[1], **Jaehoon Lee**[1], **Jun Lee**[1], **Jongsik Lim**[1], **Yongchae Jeong**[2], **Sang-Min Han**[1], **and Dal Ahn**[1]

[1]Soonchunhyang University, Korea
[2]Chonbuk National University, Korea

Abstract— A design of size-reduced microwave low pass filter using artificial dielectric substrate (ADS) structure is described in this paper. The ADS structure in Fig. 1, which has been proposed by Caloz group in 2007, consists of the upper layer on which microstrip lines and circuit patterns are printed, and the lower layer which has a lot of metalized via-holes. The effective permittivity and permeability of the ADS structure increase due to the lots of metalized via-holes, so they contribute to the size-reduction of high frequency circuits. In this work, a low pass filter (LPF), as an example, which is one of widely used high frequency circuits for wireless systems is designed and measured for the verification of the proposed idea of size-reduction using the ADS structure. A stub-type 2 GHz LPF is designed on the normal microstrip substrate (Fig. 2) and compared to the size-reduced LPF patterned on the ADS structure (Fig. 3). When the thicknesses of the upper and lower substrates are 5mils and 31mils, respectively, and their dielectric constant is 2.2, the core size of the normal LPF (the dotted area in Fig. 2) on the 36mil-thick substrate is 653.71 mm^2(= 32.25 mm × 20.27 mm). However the dotted box for the pure LPF area (Fig. 3) of the miniaturized design using the ADS structure is only 330.7 mm^2(= 21.93 mm × 15.08 mm), which is only 50.6% of the normal design. The measured S-parameters shown in Fig. 4 present typical performances as a LPF with the worst S_{21} and S_{11} are −0.85 dB and −11.4 dB without a critical degradation in the characteristics as a LPF.

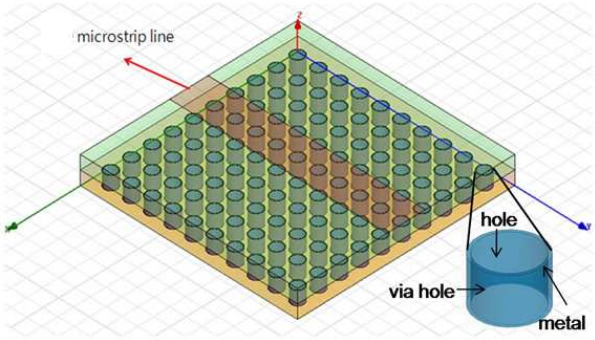

Figure 1.

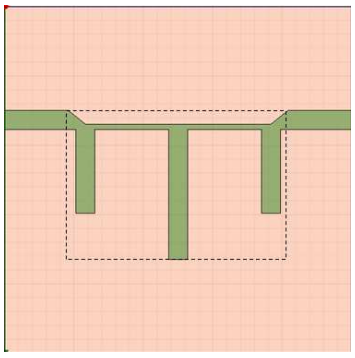

Figure 2.

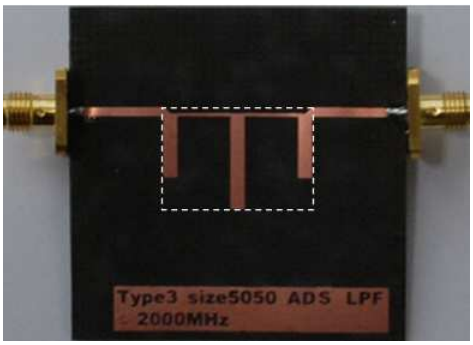

Figure 3.

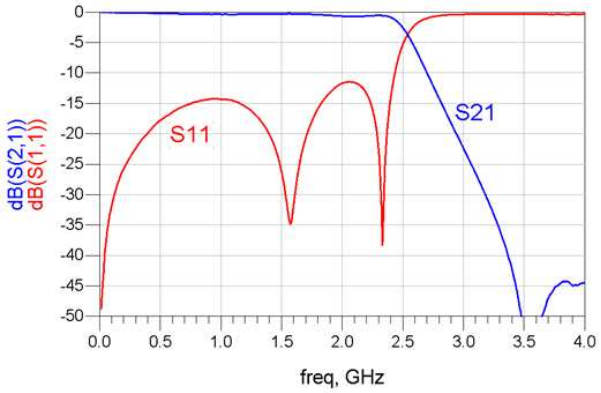

Figure 4.

ACKNOWLEDGMENT

This work was supported by the National Research Foundation of Korea Grant funded by the Korean Government (MEST) (KRF-2009-220-D00074 and 2010-0009211).

Performance Comparison of Radar Target Classification for Monostatic and Bistatic RCS

Sung-Jun Lee, **In-Sik Choi**, **and Seung-Jae Lee**
Department of Electronic Engineering, Hannam University, Daejeon, Korea

Abstract— The transmitter and receiver positions are of great importance in bistatic rdar. The radar cross section (RCS) of a target varies with these positions, and the target classification performance is considerably influenced by RCS. In this paper, the target classification performance using the monostatic and bistatic RCS of four different wire targets was analyzed. The optimum receiver position was found by comparing the calculated classification probabilities while changing the position of the receiver of the bistatic radar. The simulations results show that optimally positioned bistatic radar yields better results than does the monostatic radar. Figure 1 shows the comparison of the classification performance between monostatic RCS and bistatic RCS configurations using the STFT. These result indicates that the optimum bistatic radar has better performance than the monostatic radar for the targets used.

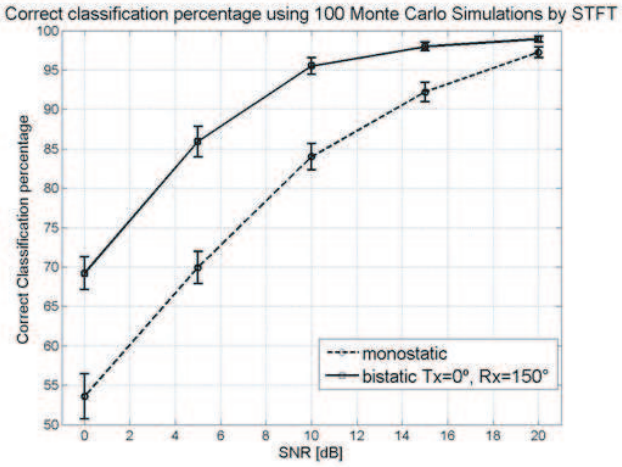

Figure 1: Comparison of correct classification performance between monostatic and bistatic RCS.

ACKNOWLEDGMENT

This work was supported by the Basic Science Research Program through the National Research Foundation of Korea (NRF) funded by the Ministry of Education, Science & Technology (No. 2011-0003209). This work was also partially supported by the Security Engineering Research Center, granted by the Korea Ministry of Knowledge Economy. Corresponding author: In-Sik Choi (recog@hnu.kr).

Wavelength Tunable Micro-Fabry-Perot Interferometers Based on Thermal-optic Effect

Yu-Hsin Hsieh[1], **Nan-Kuang Chen**[1, 2], **and Junjie Zhang**[3]

[1]Department of Electro-Optical Engineering, National United University, Miaoli 360, Taiwan, R.O.C.
[2]Optoelectronics Research Center, National United University, Miaoli 360, Taiwan, R.O.C.
[3]Shanghai Institute of Optics and Fine Mechanics, Chinese Academy of Science, Shanghai 201800, China

Abstract— We demonstrate wavelength-tunable reflection-type micro-Fabry-Perot resonators with extinction ratio of above 34 dB by attaching a high-index thin tellurite glass film ($< 15\,\mu$m) at the cleaved fiber (SMF-28) end. The wavelength tuning of this device is based on photothermal effect. The heat generation is always an important issue in high power fiber laser protection and the heat monitoring is thus necessary. In this micro-Fabry-Perot resonators, the wavelength tuning is achieved by using a pulsed Nd:YAG laser and halogen bulb, respectively. The pulsed 1064 nm Nd:YAG laser is operated under an average power of 6.8 W, a pulsed width of around 5 µs, a repetition rate of 0.5 kHz, pulse energy of 13.6 mJ, and a peak power of 2.72 kW. The Nd:YAG laser light is focused by a 10× objective and the Fabry-Perot resonators is located 3 mm away form the focal point and the resonant wavelength move toward longer wavelengths when the cw 980 nm pump power gradually increases. The resonant peaks go back to the origin in a few minutes, similar to the order of thermal relaxation time of tellurite glass. No optical pulses can be measured using a high speed photodiode and an autocorrelator. So, the wavelength tuning effect mainly comes from the local pulsed laser heating on tellurite molecules. A 2.6 nm (1567.6 ∼ 1570.2 nm) can be achieved under a pump power of 129 mW. This Fabry-Perot resonators with a high extinction ratio is simple, compact, cost-effective, all-optical tunable and is highly promising for pulsed high power fiber laser protection and sensor applications.

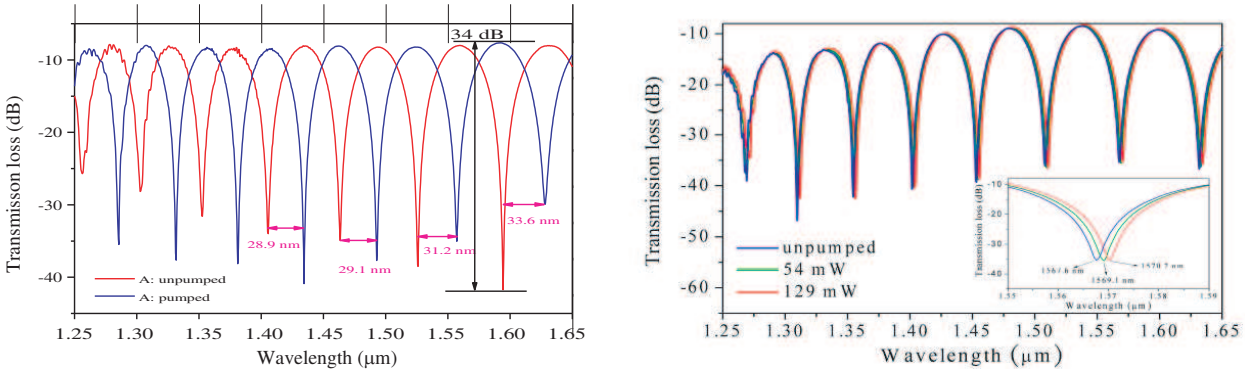

Figure 1: (a) Spectral responses of sample A under the Nd : YAG laser power of 6.8 W and (b) wavelength shift under variant cw 980 nm pump power conditions. The inset shows the local wavelength shift at the 1.55 µm region.

Research on Encode Methods of Train-ground Wireless Credible Transmission System

Guochun Wan and Mei Song Tong
Department of Electronic Science and Technology, Tongji University, Shanghai 201804, China

Abstract— An efficient and reliable train-ground wireless communication system is the key to insure the safety of the train. Therefore, it must achieve reliable and real-time transmission in interference and fading channel environment. In order to meet the request of the control and command system of the train, special measures are used against the decline of bit error rate (BER) to improve the reliability of data transmission in the channel encoder design of train-ground communication system.

Various ways to be suitable for wireless communication between a running train and ground are discussed in this paper, mainly GPRS (General Packet Radio Service) and GSM-R (Global System for Mobile communications for Railways), including their brief introductions, performances and characteristics. It provides directions to selections to select a best way of credible train-ground wireless communication system.

While the communication based train control (CBTC), due to its advantages in high precision in train positioning (which does not depend on the track circuit) and realizing the bidirectional, successive, large capability in the wireless communication between trains and ground facilities, is becoming the development trend in the current track traffic signal control system.

We introduced the concept of random and algebra construction, definition of FEC (Forward Error Control) codes parameter. A new method to construct channel codes based on Mixed Richardson-Urbanke (RU) was introduced. Then, a hybrid/sq code construction method has been researched. Compared with the existing channel codes based on RU sets, our design has two main advantages: Firstly, it can be easily encoded with linear complexity by using cyclic register. Secondly, the structure allow for small storage requirements, as well as for encoding and decoding via fast and simple circuits. The hybrid RU codes perform well with the iterative decoding based on belief propagation on an AWGN (Additive White Gaussian Noise) channel.

Parametric Transformation and Parametric Resonance of Confined Acoustic Phonons and Confined Optical Phonons by an External Electromagnetic Wave in Doping Superlattices

N. Q. Bau[1], **N. V. Nghia**[2], **and L. T. Hung**[3]

[1]Department of Physics, Viet Nam National University Hanoi, 334 Nguyen Trai, Hanoi, Vietnam
[2]Department of Physics, Water Resources University, 175 Tay Son, Hanoi, Vietnam
[3]University of Education, Viet Nam National University Hanoi, 144 Xuan Thuy, Hanoi, Vietnam

Abstract— The parametric transformation and parametric resonance of confined acoustic phonons and confined optical phonons by an external electromagnetic wave in doping superlattices are theoretically studied by using a set of quantum kinetic equations for phonons. The analytic expression of the parametric transformation coefficient K_1 and the threshold amplitude $E_{\text{threshold}}$ of the field in doping superlattices are obtained. Unlike the case of unconfined phonons, the formula of K_1 and $E_{\text{threshold}}$ contains a quantum number m characterizing confined phonons. Their dependence on the temperature T of the system, the the wave vector $\vec{q}_\perp$ and the frequency Ω of the electromagnetic wave is studied. Numerical computations have been performed for n-$GaAs/p$-$GaAs$ doping superlattices. The results have been compared with the case of unconfined phonons which show that confined phonons cause some unusual effects.

All-optical Controllable Double State Switch Based on DIT by Using QD

K. Abbasian, **N. Pasyar**, **and A. Rostami**
School of Engineering Emerging-Technologies, University of Tabriz, Tabriz 51666, Iran

Abstract— In this article, we have simulated an all-optical double state controllable switch based on dipole induced transparency using photonic crystal (PC) cavity doped by a 4-level QD [1]. This switch operation is based on the dipole induced transparency phenomenon, where the optical signal has been coupled through the input fiber to the photonic crystal cavity and the optical control fields has been applied normally to the PC surface. We have realized this switch by solving Schrodinger and Poisson equations for inserted 4-level QD in photonic crystal rods, self consistently. Also, by using the proposed structure and applying the control field in the Purcell condition, the absorbing photonic crystal cavity has been converted to transparent one and switching operation has been obtained. In this paper, we have discussed frequency operation of the switch and shown that a high quality all-optical switching operation can be obtained.

REFERENCES

1. Eftekhari, K., K. Abbasian, and A. Rostami, "Proposal for all-optical controllable switch using dipole-induced transparency (DIT)," *Optics Communications*, Vol. 283, 1817–1825, 2010.

Terahertz Wave Generation Using Nonlinear Optical Approaches

Yalin Lu[1] and K. Reinhardt[2]

[1]Laser Optics Research Center, Physics Department, United States Air Force Academy
Colorado Springs, CO 80840, USA
[2]United States Air Force Office of Scientific Research, AFOSR/NE
875 North Randolph Street, Suite 326, Arlington, VA 22203, USA

Abstract— This paper reviews recent progresses in terahertz wave generation using nonlinear optical approaches using ferroelectric and semiconductor nonlinear crystals. The discussion starts from the principle, materials related, results from experimental demonstrations, and then to an overall comparison among various methods/materials. New designs able to effectively solve technical issues related to strong terahertz absorption of material will be paid with special attention. Their potential applications in materials science will be briefly introduced.

Meeting the Phase Requirement for High-performance EBG Resonator Antennas

Yuehe Ge
Electronic Engineering, College of Information Science and Engineering,
Huaqiao University, China

Abstract— In recent years, metamaterials have been developed for enhancing the performance of antennas or for obtaining characteristics that are not easily achieved in nature. Among them are the EBG structures with special properties that are required to form EBG resonator antennas. Such antennas have the advantages of simple structure, high directivity and low cost of production. EBG resonator antennas are mainly composed of a resonant cavity, which is bounded by two surfaces and excited by a normal antenna. One of the surfaces is either a metallic conductor or a fully reflecting artificial magnetic conductor (AMC). The other surface is usually formed by a strongly but partially reflecting EBG structure. 1-D, 2-D and 3- D EBG structures have been considered for this purpose.

In order to obtain high-performance EBG resonator antennas, both the reflection coefficient magnitude and the phase of the EBG structures are crucial. The reflection coefficient should be sufficiently large to achieve high gain. Its phase should satisfy the cavity resonance condition at the operating frequency. For these purposes, the performance (the reflection coefficient magnitude and the phase) of 1-D EBG structures can only be adjusted by changing the permittivity of each layer, whilst those requirements of 3-D EBG structures are easily to be met, though the structures are relatively complicated. In the 2-D case, it is essentially a specially designed frequency selective surface (FSS) or a partially reflective surface (PRS), which can strike the balance between the simple structure and the performance adjustment. In this paper, 2-D EBG structures are designed to meet the special requirements of both the reflection coefficient magnitude and the phase, for the use of wideband or dual-band EBG resonator antennas.

Based on the cavity resonance condition, a wider operating bandwidth can be achieved by designing the PRS so that its reflection phase increases with frequency, unlike in a standard PRS where the phase decreases with frequency. Two PRS examples, composed of a single dielectric layer with two specially designed dipole arrays or slot arrays printed on the two sides, respectively, are given to demonstrate the design principle of wideband EBG resonator antennas.

The challenge to design an EBG-resonator antenna to operate in two bands lies that the phase condition for cavity resonance has to be satisfied in both bands. Several methods have been presented in the past to design dual-band EBG resonator antennas. In this paper a new design approach is presented. The cavity resonance condition can be achieved by making the metamaterial inclusions on the surface of a single FR4 dielectric layer to resonate at a special frequency. Then, it is possible to meet the phase requirement for cavity resonance at *two* frequencies, one below the surface special frequency and one above the special frequency. Hence dual-band cavity resonance and dual-band antenna operation can be achieved using a single-layer surface.

Characterization of Planar Multiport Junction

Malika Ourabia
University of Sciences and Technologies Houari Boumediene, Algeria

Abstract— A new and efficient method is presented for the analysis of arbitrarily shaped discontinuities. The discontinuities is characterized using a hybrid spectral/numerical technique.

The structure presents an arbitrary number of ports, each one with different orientation and dimensions.

This article presents a hybrid method based on multimode contour integral and mode matching techniques. The process is based on segmentation and dividing the structure into key building blocks.

We use the multimode contour integral method to analyze the blocks including irregular shape discontinuities.

Finally, the multimode scattering matrix of the whole structure can be found by cascading the blocks. Therefore, the new method is suitable for analysis of a wide range of waveguide problems.

Therefore, the present approach can be applied easily to the analysis of any multiport junctions and cascade blocks.

The accuracy of the method is validated comparing with results for several complex problems found in the literature. CPU times are also included to show the efficiency of the new method proposed.

High-resolution Miniature Fiber Pressure Sensor Using Abrupt-tapered Mach-Zehnder Interferometers

Wei-Chih Kuo[1], **Zhi-Zheng Feng**[1], **Shin-Wei Shen**[1], **Yu-Hsin Hsieh**[1], **and Nan-Kuang Chen**[1, 2]

[1]Department of Electro-Optical Engineering, National United University, Miaoli 360, Taiwan, R.O.C.
[2]Optoelectronic Research Center, National United University, Miaoli 360, Taiwan, R.O.C.

Abstract— We demonstrate tunable Mach-Zehnder interferometers with an extinction ratio of above 20.8 dB by introducing two points of abruptly tapering in a short length (< 1.2 cm) of highly Er/Yb co-doped fiber (EYDF). The EYDF is immersed in a point flame where the bilateral edges of flame can provide a higher heating temperature than that of the inner portion so that the abrupt tapers can be achieved when the two heated points are suddenly pulled away in opposite directions. The diameters of the waist and lengths of the two abrupt tapers are 57.8 and 1.4 mm, and 54.9 and 1.5 mm. The distance between the two centers of the abrupt tapers is 5.23 mm. The nonadiabatic tapers can help the excitations of cladding modes from core mode and the interference occurs when the phase difference between core and cladding modes are satisfied after a certain propagation length. A fiber with a higher numerical aperture is found to be beneficial to the high extinction ratio of loss peak. The interferometer is tested as a compressed sensor based on the maximum transmission loss wavelength shift.

The weight of counterpoise is gradually added and the corresponding spectral responses are measured and shown in Fig. 1(a), where some interference patterns were shown $0 \sim 0.07$ g and 0.005 g per measurement times. The maximum wavelength shift is 21.6 nm over 1596–1617.6 nm under an optical resolution (RES) of 1 nm. The interference pattern will move to the short wavelength. From Fig. 1(b). The weight 0.0, 2.0, 4.0, 6.0 g is gradually added, respectively. The maximum transmission loss wavelength shift can be achieved 148.8 nm from 1617.2 nm to 1468.4 nm.

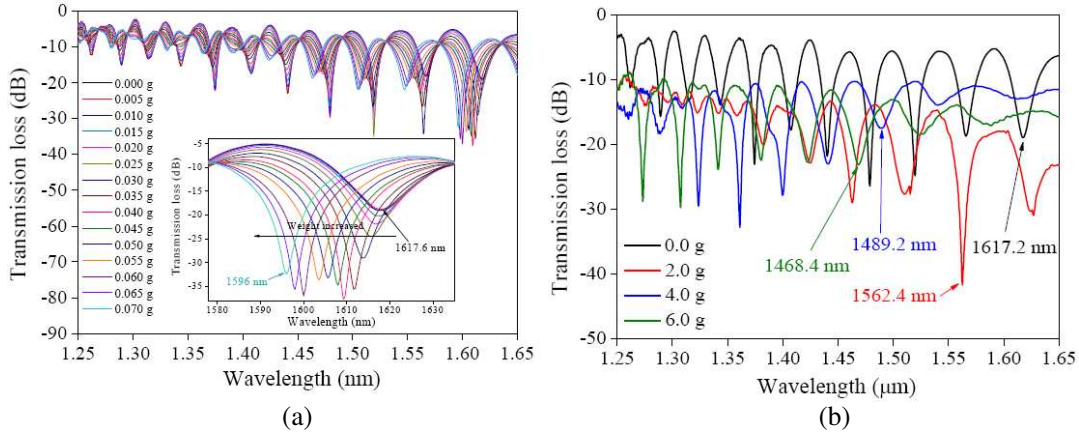

Figure 1: Spectral responses of abrupt tapered EYDF with 58, 54 μm, span 5.3 mm. (a) $0 \sim 0.07$ g, the maximum wavelength shift is 21.6 nm. over 1596–1617.6 nm. (b) $0 \sim 6$ g, the maximum wavelength shift is 148.8 nm. over 1617.2–1468.4 nm under an (RES) of 1 nm.

Characteristics for Crosstalk between Dual Microstrip Transmission Lines in PCB

Xin Wang[1], **Hui Huang**[1, 2], **and Qi Liu**[1]

[1]School of Electrical Engineering, Beijing Jiaotong University, Beijing 100044, China
[2]State Key Laboratory of Millimeter Waves, Nanjing 210096, China

Abstract— A detailed study of crosstalk between dual microstrip transmission lines in PCB is presented. The crosstalk response to signal frequency, the distance between microstrip transmission lines, the length of microstrip transmission line and the thickness of substrate are analyzed respectively. The calculation of S-parameter is obtained based on the finite element method. The simulation result indicates that crosstalk strength varies with the length of microstrip line, the distance between dual microstrip transmission lines and the substrate thickness.

Surface Modes at Interface between Lossy Gyroelectric and Isotropic Media

Xin Wang[1], **Hui Huang**[1, 2], **and Bo Yi**[1]

[1]School of Electrical Engineering, Beijing Jiaotong University, Beijing 100044, China
[2]State Key Laboratory of Millimeter Waves, Nanjing 210096, China

Abstract— A detailed analysis of surface wave at the interface between gyroelectric and isotropic medium is presented. Two cases including lossless and lossy gyroelectric medium are considered. The conditions for the existence of surface modes in each case are analyzed, showing that the existence is determined by the components of wave vector k_y^2, k_{xi} and k_{xi2}. Take gyroelectric medium for an example, the existence interval of surface wave is obtained. Comparison of surface wave in lossy medium and lossless medium is presented.

Advanced Nanostructured Glassceramics for Photonics

N. V. Nikonorov[1], **V. A. Aseev**[1], **A. I. Ignatiev**[1], **E. V. Kolobkova**[2], **and A. I. Sidorov**[1]

[1]Saint-Petersburg University of Information Technologies, Mechanics, and Optics, Russia
[2]Saint-Petersburg State Technological Institute, Russia

Abstract— Five types of nanostucturied glassceramics have been developed for photonic applications. These glassceramics exhibit good laser, photorefractive, non-linear, plasmonic, and ion-exchangeable characteristics in comparison with glassy and crystalline analogs. Some examples of optical elements and devices based on the glassceramics (lasers, amplifiers, limiters, sensors, holographic filters) have been demonstrated. The first material presents a laser lead-fluoride nanoglassceramics doped with Er, Yb and Nd. It is shown that, rare earth ions play a role of nucleation centers and precipitate in crystalline phase, for example, $PbErOF_4$. Spectral, luminescent and laser properties of the nanoglassceramics have been demonstrated and compared with fluoride crystals. Possibility of utilization of the nanoglassceramics in fiber laser and amplifiers have been discussed.

The second material presents a forsterite nanoglassceramics doped with tetravalent chromium ions. It was experimentally shown that tetravalent chromium ions are embedded in the forsterite nanocrystalline phase. It was found that the quantum yield of the luminescence of the forsterite nanoglassceramics is close to that for the forsterite single crystal. The results have demonstrated the possibility of synthesizing transparent nanoglassceramics doped with Cr(4+) ions whose spectral and luminescence properties are highly competitive with those of forsterite single crystals. It was demonstrated that the transparent nanoglassceramics can be used for drawing optical fibers. This offers new possibilities for designing broadband optical fiber lasers and amplifiers based on the use of transition metal ions.

The third nanoglassceramics exhibits good non-linear properties and presents a glass host with precipitated nano-dimensional crystalline phase of complicated composition (CuCl/Br/I or AgCl/Br/I). It is shown that an optical response appears in the materials when the energy density was 0.1–1 nJ/cm^2 while the appearance time of the response was less than 35 ps. The cause of the appearance of the nonlinear-optical response is the photogeneration of unstable color centers. These results can be used when developing nonlinear-optical media to control optical signals in integrated-optics systems, as well as for radiation limiters.

The fourth material presents a glass doped with highly concentrated silver metallic nanoparticles (3–7 nm) or precipitated nanocrystals of NaF-AgBr (20–30 nm) covered by silver metallic thin film. Several technologies have been used for creation of such structures — laser radiation or electron beam treatment, ion exchange and thermal treatment. Such structures possess a plasmonic resonance. Some plasmonic devices can be realized on the materials-plasmonic waveguides and switches, luminescent sensor and biosensors.

The fifth material is a new polyfunctional photo-thermo-refractive (PTR) glassceramics doped with erbium and ytterbium has been developed for the first time. The material combines itself three opportunities: fabrication of lasers or amplifiers, recording of volume Bragg gratings (VBG) or holographic optical elements (HOE), fabrication of planar waveguides or fiber. The PTR glassceramics exhibits good spectral, luminescent, and lasing characteristics, as well as photorefractive and ion exchangeable properties. The VBGs have high mechanical, chemical, and thermal durability. Optical characteristics of the VBGs are stable over high temperature (up to 500°C) and under high power/energy laser beam. The diffractive efficiency of VBGs archives 95%. Different devices on the base of the polyfunctional PTR glassceramics have been developed for photonic applications.

Erbium and Ytterbium-erbium Doped Nano-glasseramics for Photonic Application

V. Aseev[1], **E. Kolobkova**[2], **N. Nikonorov**[1], **K. Moskaleva**[1], **and Y. Nekrasova**[1]

[1]Saint-Petersburg University of Information Technologies, Mechanics, and Optics, Russia
[2]Saint-Petersburg State Technological Institute, Russia

Abstract— Lead-fluoride nano-glassceramics doped with erbium and ytterbium-erbium have been developed and synthesized. The size of crystalline phase achieved up to 40 nm. Rare-earth ions play a role of nucleation centers. An X-ray diffraction analysis of the samples after the secondary heat treatment showed that the crystalline phase has a composition of $PbYOF_3$. Spectral and luminescence properties of nano-glassceramics in visible, near and middle IR spectral range have been investigated. Spectral and luminescence properties of virgin and thermal treated samples have been investigated in visible (0.4–0.8 mkm) and near (1.5 mkm) and middle (3 mkm) IR-ranges. It was shown that the emitting probabilities of different transitions changed during the treatment. The entry of rare-earth ions in crystal phase results in widening of emission spectra because of fluoride surrounding. For spectral range around 1,5 mkm we demonstrated the increase of emission spectra width for Er-doped glass-ceramics from 59 nm for the virgin glass up to 71 nm for the nano-glassceramic. The thermal treatment results in appearance of Stark structure in absorption and luminescence spectra and their deformation. Also it was shown that the energy transfer from ytterbium to erbium probabilities changed during the treatment. Erbium and ytterbium-erbium doped nano-glassceramics are promising candidates for different photonics applications, sensors, fiber and waveguide lasers.

Perturbation Method and Eigenmode Solution Anomalies with Modelling Lossy 3D Resonators

Stepan Lucyszyn[1], **Stergios Papantonis**[1], **and Makoto Kuwata-Gonokami**[2]

[1]Optical and Semiconductor Devices Group, Department of Electrical and Electronic Engineering
Imperial College London, Exhibition Road, London SW7 2AZ, United Kingdom
[2]Department of Physics, Graduate School of Science
The University of Tokyo, 7-3-1 Hongo, Bunkyo-ku, Tokyo 113-0033, Japan

Abstract— The detuning of resonators can be characterised using the perturbation method, when combined losses are not too high; this method has been around since at least 1946 [1]. This is also true for metal-pipe rectangular waveguide (MPRWG) cavity resonators, when the finite conductivity of the metal walls are not too low. However, the perturbation methods cannot be used for any arbitrary value of conductivity. For this reason, commercial software is often used for determining the Eigenmode frequencies and unloaded Q-factors for such resonators.

The High Frequency Structure Simulator (HFSS$^{\text{TM}}$) software, by ANSYS, is generally recognised as the industry-standard software for undertaking 3D full-wave electromagnetic field simulations. While claiming to be a high performance simulator for arbitrary 3D volumetric passive device modelling, it suffers from problems associated with metal-based structures (e.g., MPRWGs and their associated cavity resonators having electrically-thin walls [2] or operating at terahertz frequencies [3]).

This paper identifies, quantifies and characterizes the systematic errors in both HFSS$^{\text{TM}}$ and also CST Microwave Studio® (CST MWS), for calculating the Eigenmode frequencies and unloaded Q-factors of MPRWG cavity resonators having walls with arbitrary values of bulk DC conductivity σ_o (covering a span of more than 14 orders of magnitude).

Table 1: Extracted parameters for modelling square cavities using HFSS$^{\text{TM}}$ with FCB.

b [μm]	ψ_o [μm]	ς	σ_{xo} [S/m]	ω_I/ω_{xo}	$\omega_{xo}L$ [Ohms]	$X_{so}(\sigma_{xo},\omega_{xo})$ [Ohms]	$X_x(\sigma_{xo},\omega_{xo})$ [Ohms]	ϱ
30	$a/24$	0.439053	353	1.76276	39.5632	66.9558	8.2660	1.5704
100	$a/10$	0.548920	100	1.61936	103.3601	131.2505	28.3268	1.2573
300	$a/6$	0.813750	58	1.52768	182.6052	177.4363	75.1781	1.0411

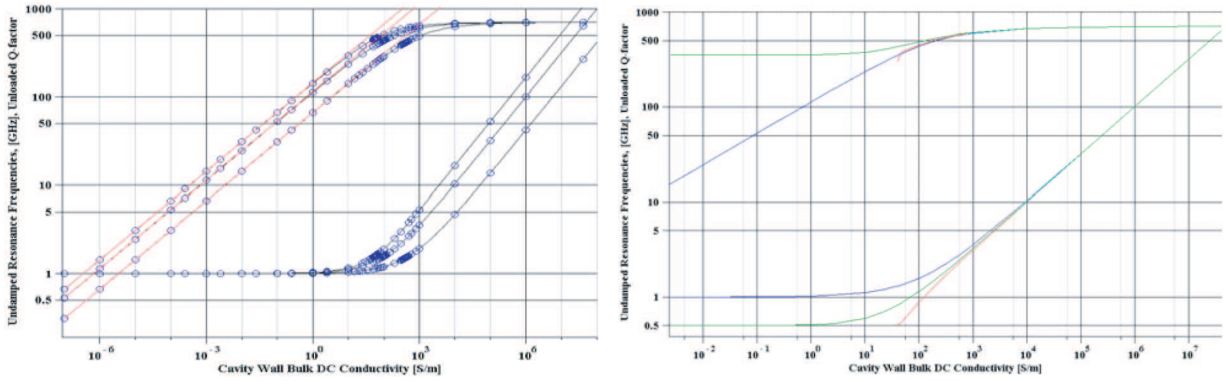

(a) (b)

Figure 1: Numerical simulation data from HFSS$^{\text{TM}}$: (a) three cavities using FCB walls (blue circles) and corresponding semi-analytical model results using the parameters in Table 1 (black curves), red lines show the corresponding ultra-low conductivity approximation model fit; (b) $300 \times 100 \times 300\,\mu\text{m}^3$ cavity using FCB (blue), LIB (green) and solid metal (red) walls.

As an example, with HFSS^{TM} using the finite conductivity boundary (FCB) to represent lossy square cavity walls, the calculated undamped angular resonance frequency ω_o can be accurately characterised by solved the following equation:

$$\left[X_{so}(\sigma_o,\omega_o)+\left(\omega_o L-\frac{1}{\omega_o C}\right)\right]+[\varsigma\cdot X_{so}(\sigma_o,\omega_o)-\varrho\cdot X_x(\sigma_o,\omega_o)]\equiv 0 \tag{1}$$

where surface impedance, $Z(\sigma_o,\omega_o)=\sqrt{\frac{j\omega_o\mu_o\mu_r}{\sigma_o}}\equiv R_{so}(\sigma_o,\omega_o)+jX_{so}(\sigma_o,\omega_o)$ and $R_{so}(\sigma_o,\omega_o)=X_{so}(\sigma_o,\omega_o)$, with the simple classical skin-effect dispersion model for normal metals at room temperature (the displacement current term is ignored in this particular model). Once ω_o is calculated, the unloaded Q-factor Qu_o can be determined from the following expression:

$$Qu_o=\left[1+\frac{\omega_o L}{R_{so}(\sigma_o,\omega_o)}\right]-\left[\frac{X_x(\sigma_o,\omega_o)}{R_{so}(\sigma_o,\omega_o)}\right] \tag{2}$$

The terms in red brackets represent systematic error in HFSS^{TM} for the FCB approach. Three air-filled square cavity resonators having internal dimensions ($a\times b\times d$) of $300\times 30\times 300\,\mu m^3$, $300\times 100\times 300\,\mu m^3$ and $300\times 300\times 300\,\mu m^3$ were investigated. Using the extracted parameters given in Table 1, the corresponding model results for the HFSS^{TM} data can be seen in Fig. 1(a), with the left-side curves corresponding to the undamped resonance frequencies and the right-side curves corresponding to the unloaded Q-factors. It will be seen that there is a perfect match between the HFSS^{TM} data and the semi-analytical model presented here, which includes the characterization of systematic error terms.

The full paper will also show the results for the Layered Impedance Boundary (LIB) and solid metal wall (with solve-inside) approaches, used with HFSS^{TM}, shown in Fig. 1(b), and also the perturbation method approach used with CST MWS.

REFERENCES

1. Slater, J. C, "Microwave electronics," *Reviews of Modern Physics*, Vol. 18, No. 4, 441–512, Oct. 1946.
2. Choi, J. Y. and S. Lucyszyn, "HFSS^{TM} modelling anomalies with electrically thin-walled metal-pipe rectangular waveguide simulations," *10th IEEE High Frequency Postgraduate Student Colloquium (10th HF-PgC) Digest*, 95–98, Leeds, Sep. 2005, ISBN: 0-7803-9500-X.
3. Zhou, Y. and S. Lucyszyn, "HFSS^{TM} modelling anomalies with THz metal-pipe rectangular waveguide structures at room temperature," *PIERS Online*, Vol. 5, No. 3, 201–211, 2009.

Analytical Solution of Single-scattering Approximation on Radiative Transfer for Nonhomogeneous Media

Feng Zhang[1, 2], **Leiming Ma**[1], **Hua Zhang**[3], **and Zhongping Shen**[4]

[1]Shanghai Typhoon Institute, China Meteorological Administration, Shanghai 200030, China
[2]Chinese Academy of Meteorological Sciences, Beijing 100081, China
[3]National Climate Center, China Meteorological Administration, Beijing 100081, China
[4]Shanghai Climate Center, Shanghai 200030, China

Abstract— In the radiative transfer computations, the single scattering approximation is of great value. It not only reflects the basic features of radiation fields, but also is the basis of some numerical method (e.g., successive order of scattering method). In this paper, we will formulate the analytical solution of single-scattering approximation for nonhomogeneous media according to asymptotic integral theory. The analytical solution keeps the continuity of the inherent optical properties (IOPs) and is inspired to how to take continuity of IOPs into the computation radiative transfer calculations. Move over, we get reflected and transmitted intensities and bidirectional reflectance for nonhomogeneous media.

We apply the analytical solution to discuss the peculiar discountinutiy in the intensity of light, the unphysical discontinuities in the radiaitation, homogeneous media and nonhomogeneous media. Our analytical solution avoids the unphysical discountinuty in the radiation filed, and single-scattering approximation for homogeneous media can be recovered in it. In addition, the accuracy of the analytical solution, which is examined by isotropic scattering in an inhomogeneous semi-infinite media, is reliable.

Waveguides with Nanostructured Claddings for Scattering Suppression in Plasmonic Optics

E. A. Bezus[1, 2], **L. L. Doskolovich**[1, 2], **and N. L. Kazanskiy**[1, 2]

[1]Image Processing Systems Institute of the Russian Academy of Sciences, Samara 443001, Russia
[2]Technical Cybernetics Department, Samara State Aerospace University, Samara 443001, Russia

Abstract— Electromagnetic modes supported by the interfaces between metal and dielectric media (surface plasmon polaritons, SPP) have recently attracted a lot of interest due to their potential applications in optical sensors, lithography and photovoltaics. Optical information processing at the nanoscale has been a key direction, where the use of SPP is especially promising [1]. While various types of plasmonic elements (waveguides, reflectors, beam-splitters and lenses) have been proposed, the efficiency of the most of them is dramatically affected by the parasitic scattering. Scattering losses typical for SPP diffraction on a dielectric block located directly on the propagation surface amount 30–50%.

Known approaches for scattering elimination are based on the usage of anisotropic metamaterials [2]. However, the design and fabrication of such metamaterials and their integration into the plasmonic elements constitutes a separate scientific and technological problem. In the present work, a simpler approach based on micro- or nanostructuring of the plasmonic waveguide is proposed. In particular, we demonstrate using rigorous electromagnetic simulations that creation of a groove (Fig. 1(a)) or embedding a dielectric block (Fig. 1(b)) into the dielectric cladding of the plasmonic waveguide can provide efficient control of the propagation constant of the plasmonic mode (and thus perform an efficient SPP phase modulation) while maintaining the transverse field profile almost constant (and hence significantly reducing the scattering losses). In Fig. 1(c), an example of SPP scattering suppression is shown. Blue curve corresponds to scattering losses associated with SPP transmission through a dielectric block located directly on the propagation surface, green curve corresponds to structure shown in Fig. 1(b) (a gap with thickness of several tens of nanometers is introduced between the metal and the block). Structure parameters: $\lambda_0 = 800\,\text{nm}$, $\varepsilon_d = 1.96$, $\varepsilon_b = 4$, ε_m corresponds to gold. Length $l_{\max}$ provides 2π phase delay. It is evident from Fig. 1(c) that maximal scattering is reduced from 33% to 1.4%.

Proposed technique for scattering suppression can be used for designing plasmonic elements such as lenses, plasmonic crystals, Bragg reflectors.

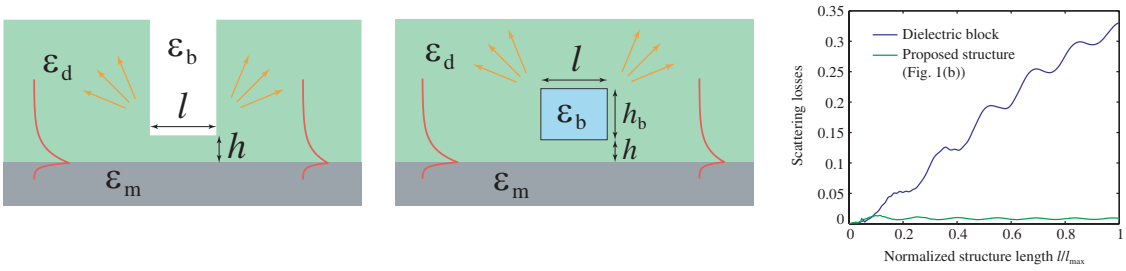

(a) (b) (c)

Figure 1: (a), (b) Proposed structure geometries, (c) example of scattering suppression.

ACKNOWLEDGMENT

This work was financially supported by RFBR grants Nos. 11-07-00145, 11-07-00153, 10-07-00553 and 10-02-01391 and RF Presidential grants No. NSh-7414.2010.9 and MD-1041.2011.2.

REFERENCES

1. Gramotnev, D. K. and S. I. Bozhevolnyi, "Plasmonics beyond the diffraction limit," *Nature Photonics*, Vol. 4, 83–91, 2010.
2. Elser, J. and V. A. Podolskiy, "Scattering-free plasmonic optics with anisotropic metamaterials," *Phys. Rev. Lett.*, Vol. 100, 066402, 4 pages, 2008.

Transmission Line Matrix Method for Two-dimensional Modeling of Terahertz Gaussian Beam Propagation

Daniel M. Hailu, **Shahed Shahir**, **Arash Rohani**, **and Safieddin Safavi-Naeini**
CIARS (Center for Intelligent Antenna and Radio Systems), Electrical and Computer Engineering Dept.
University of Waterloo, 200 University Avenue West, Waterloo, ON., N2L 3G1, Canada

Abstract— We present a two-dimensional Transmission Line Matrix (2D TLM) to simulate wave propagation and scattering inside and around an inhomogeneous cylinder for terahertz (THz) imaging. As a particular application, the proposed method is used to construct the dielectric profile or image of cylindrical sample. We compare and validate the 2D TLM with FDTD using TM-mode propagation through infinitely long lossless and lossy polyethylene cylinders.

ACKNOWLEDGMENT

This work was supported in part by the Natural Sciences and Engineering Research Council of (NSERC), and RIM.

Remote Sensing Monitoring for Surface Water in Mining Area in Northwest China

Baodong Ma[1] **and Lixin Wu**[1, 2]

[1]Institute for Geoinformatics & Digital Mine Research, Northeastern University, Shenyang, China
[2]State Key Laboratory of Earth Surface Processes and Resource Ecology
Beijing Normal University, Beijing, China

Abstract— Northwest China is rich in coal resources will become the main base of energy supply in the future. Because natural conditions cause extremely poor water resources, the eco-environment is very fragile. However, the drainage in a coal mine under exploitation may cause negative influence on the development of the water resources. Study on environmental impact of coal development on the water resources can provide early warning to the eco-environment aggravation caused by coal development in Northwest China.

This paper took Shendong mining area as an example. It locates in northwest China, and has annual yield of more than 100 million tons raw coal. Near the mining area, Shenhu Lake (Hongjiannao lake), the biggest desert freshwater lake in China, is the main surface water body, and plays an important role in protecting environment. A time sequence of the lake area variation from 2000 to 2009 was constructed by using 16-day MODIS NDVI (Normalized Difference Vegetation Index) data. According to reflectance properties of feature and definition of NDVI, NDVI value is different for water body and other features. So water body can be identified by NDVI threshold. In addition, because of the change of solar incidence and water depth, different NDVI threshold in different time of the whole year was chosen respectively. As a result, 170 area images of Shenhu Lake were produced. To facilitate the analysis, the data could be composed using the mean area images for the whole year.

The results show that the water area of Shenhu Lake shrank sharply from 49.6 km^2 in 2000 to 34.9 km^2 in 2009. Based on data and remote sensing information, water consumption was calculated to estimate water budget of the lake. The study shows that the lake area variation was controlled by precipitation before 2005. After 2006, annual drainage in the mining area increased to 50 million m^3 and the lake area decreased due to less groundwater recharge resulting from lowering of the water table. In other word, increased drainage year by year in mining area caused groundwater depression cone, and then groundwater around the mining area moved to the depression cone. Ultimately, recharge from groundwater for the lake decreased and the lake area shrank.

Analysis of the Design and Optimization of a Yagi Antenna with High Gain in Meteorological Communication

Jue Li[1], **Bin Fang**[1], **Shi-Sheng Jin**[1], **and Wei-Wei Cheng**[2]

[1]Guizhou Meteorological Information Center, Guiyang, Guizhou 550002, China
[2]Institute of Microelectronics and Optoelectronics
Zhejiang University, Hangzhou, Zhejiang 310027, China

Abstract— This paper designs a 3-element Yagi beam aerial in free space for a frequency of 150 MHz using EZNEC, which has the maximum possible gain at the frequency, and is with front/back ratio of at least 10 dB, and input impedance to be purely resistive. Besides, it determines the optimum length of each element and the optimum spacing between elements (S), which requires readjustment of the element lengths.

Design and Analysis of a New Oscillator Circuit for Communication Based on Wien Bridge Structure

Qing Zhang[1], **Sheng-Yun Luo**[2], **and Wei-Wei Cheng**[3]

[1]Computer and Information Engineering College
Guizhou University for Nationalities, Guiyang, Guizhou 550002, China
[2]College of Science, Guizhou University for Nationalities, Guiyang, Guizhou 550002, China
[3]Institute of Microelectronics and Optoelectronics, Zhejiang University, Hangzhou, Zhejiang 310027, China

Abstract— This paper makes a detail analysis of the several important parameters of oscillator, which focus on the gain, distortion, stability of the gain, 180° phase shift, RC circuit for the oscillator design, and design a Wien bridge oscillator circuit based on the analysis, with the oscillating frequency 100 kHz by varying component values with 2.8% distortion.

The Research of the Turbo Coding Technology in the High-speed Underwater Communication with OFDM Mode

Wei Lan[1], **Bin Fang**[1], **Shi-Sheng Jin**[1], **and Wei-Wei Cheng**[2]

[1]Guizhou Meteorological Information Center, Guiyang, Guizhou 550002, China
[2]Institute of Microelectronics and Optoelectronics
Zhejiang University, Hangzhou, Zhejiang 310027, China

Abstract— This article describes the high-speed underwater acoustic communication of the key technologies of the OFDM underwater acoustic communication system, make an analysis of the advantages and disadvantages of the key technology of TURBO codes design based on high-speed underwater acoustic OFDM communication coding scheme, and it conducts the simulation and analysis, and finally, the reliability of the TURBO code in high-speed underwater acoustic OFDM communication is analyzed.

Session 4A2a
Metamaterials, Surface Plasmonics and Their Applications

Electromagnetic Coupling and Resonance Modes Separation of Metallic Split Ring Resonator Pair at Microwave Frequencies

Min Liu, **Ping Chen**, **and Rui-Xin Wu**
School of Electronic Sciences and Engineering, Nanjing University, Nanjing 210093, China

Abstract— In the past decade, metamaterials consisting of periodic metallic resonator structures have attracted extensive interest due to their novel functionalities, such as negative refraction, invisibility, artificial magnetism, optical transform and so on. In most early works, the elements of periodic metamaterials were deemed to be uncoupled to each other. Therefore, the effective properties of bulk metamaterials were usually modeled as an averaged response of all elements in periodic structures. Nevertheless, recently, it has been shown that the interactions between the elements in periodic metamaterials can induce some novel phenomena, which are absent in the conventional uncoupled metamaterials. For example, Liu et al. have demonstrated at terahertz frequencies that the electromagnetic (EM) couplings in the stack of several identical metallic split-ring resonators (SRRs) can generate multiple discrete resonance modes.

In present work, the propagation of microwave through the metmaterials made of metallic split-ring resonator pairs (SRRPs) was theoretically and experimentally studied. The EM responses of SRR and SRRP structures have been investigated with the equivalent circuit model. It was found that the SRRP structure can generate two discrete resonance modes, which is different with the EM response of SRR. The gap of two resonance modes was found to depend on the twist angle between the SRRs in the pair and their relationship has been explored. Furthermore, the samples of periodic metamaterials made of SRR and SRRPs have been fabricated and their transmission spectrums have been measured by an Agilent E8363A vector network analyzer at $8 \sim 13.5$ GHz. The experimental results agree well with the theoretical and simulation results.

Frequency Selectivity of One-dimensional Subwavelength Gratings in the Mid-Infrared

Nan Zhang, **Pei Heng Zhou**, **Li Xia Zhuo**, **Xiao Long Weng**, **and Jian Liang Xie**
State Key Laboratory of Electronic Thin Films and Integrated Devices
University of Electronic Science and Technology of China, Chengdu, China

Abstract— In recent years, the study of subwavelength gratings were mostly focused on working mechanisms and applications in the visible and near-infrared spectral range [1]. Few works concern the mid-infrared. In fact, in the field of infrared detection, those gratings are considered to play important roles as filter window to reduce the signal processing and improve the signal process speed [2]. Gratings use in the mid-infrared is important in this purpose.

In this work, frequency selectivity of one-dimensional aluminum subwavelength slit gratings was investigated. The transmission property was simulated by FDTD method to study the effect of structural elements, in other words, periodslit ratio and metal thickness. Corresponding gratings with a thickness about 250 nm were fabricated on the n-type silicon wafer by magnetron sputtering and microelectronic process. Both the simulation and FTIR (Fourier Transmission Infrared spectroscopy) measurement results indicated coherently apparent frequency selectivity of the transmission spectrum in the mid-infrared. From the point of Woods Anomaly theory, the transmission characteristics of this kind of gratings were analyzed, comparing with a typical two-dimensional grating, says the rectangular hole arrays, has also been done.

REFERENCES

1. Ghaemi, H. F., T. Thio, D. E. Grupp, T. W. Ebbesen, and H. J. Lezec, *Phys. Rev. B*, Vol. 58, 6779, 1998.
2. Tsai, M.-W., T.-H. Chuang, H.-Y. Chang, and S.-C. Lee, *Appl. Phys. Lett.*, Vol. 89, 093102, 2006.

Subwavelength Imaging with SPP Waveguides

Weibin Zhang[1, 2] **and Hongsheng Chen**[1, 2]

[1]The Electromagnetics Academy at Zhejiang University
Zhejiang University, Hangzhou 310027, China
[2]Department of Information and Electronic Engineering
Zhejiang University, Hangzhou 310027, China

Abstract— Subwavelength imaging has been researched for quite a long time and several methods have been proposed. Such as superlens and hyperlens which are studied most have been realized in different ways with different frequency. In this letter, we proposed another method to realize subwavelength imaging. This method is based on some very small SPP waveguides which help us to transmit the evanescent waves before they decay. In this way the diffraction limit can be overcame and a spatial resolution of about 1/6 of the vacuum wavelength can be obtained. We demonstrate both simulation and experimental studies of the method in this letter.

Resonance Relation for Coated Spheres with Radial Anisotropy

H.-Z. Liu[1, 2], **K. Mouthaan**[1], **M. S. Leong**[1], **and S. Zouhdi**[2]

[1]National University of Singapore, Singapore
[2]Laboratoire de Génie Electrique de Paris, LGEP-Supélec, France

Abstract— For a sphere with positive permittivity, weak dipolar scattering prevails when the object is electrically small. However, for a small sphere with negative permittivity, giant scattering termed plasmonic resonance takes place due to the excitation of surface plasmon polaritons (SPPs). With the core-shell structure, Alu and Engheta [1] speculated that SPPs can be supported when as least one layer possesses negative permittivity. Earlier work by Ni et al. [2] demonstrated that anisotropic core-shell spheres with either metal shell or metal core are capable of supporting SPPs. Coated anisotropic spherical particles are of particular interest to this work due to their emerging applications in optical devices and plasmonic nanoantennas.

In this work, we generalize the resonance condition developed by Alu and Engheta by taking the effect of dielectric anisotropy into account. We examine ranges of permissible constitutive parameters in conjunction with radial ratio. It is observed that increasing dielectric anisotropy in the core can lead to a wider admissible range of constitutive parameters for supporting SPPs. A reverse trend is observed for having dielectric anisotropy in the shell. Furthermore, it is shown that as the order of SPPs increases, the admissible region shrinks.

In practice, negative permittivity is sensitive to frequency variations as described by the Drude model. Therefore, the derived resonance relation is useful for the design of composite coated structures containing both metal and anisotropic materials at frequencies of interest.

REFERENCES

1. Alu, A. and N. Engheta, *J. Appl. Phys.*, 2005.
2. Ni, et al., *Appl. Phys. A*, 2011.

A Metal-dielectric Multilayer Film Applied to Enhance the Transmission of Two Counter-propagating Lights

Yaoju Zhang, **Xiaowei Ji**, **Youyi Zhuang**, **and Chongwei Zheng**
College of Physics and Electronic Information, Wenzhou University, Wenzhou, Zhejiang 325035, China

Abstract— In last two decades, single-molecule fluorescence microscopy has been widely used to study the physical and chemical behaviour of individual molecules and has become an increasingly important tool for molecular biology [1]. Total internal reflection fluorescence microscopy (TIRFM) among several techniques of determining single molecule orientations by fluorescence measurements is a widely used imaging technique that is useful in probing the structure and dynamics of the basal surfaces of cells due to its excellent surface selectivity and ability to suppress background fluorescence [2]. In TIRFM, only fluorophores located within about 100 nm of the surface are excited by the evanescent field, while those located further away from the surface are not efficiently excited by the exponentially decaying evanescent wave. A single-layer metal film is often coated on surface of the coverslip in TIRFM [3–7] to efficiently excite fluorescence molecules. However, the coated single-layer metal film decreases largely the transmission of emission fluorescence which propagation direction is contrary to the propagation direction of the excitation light so that the intensity of detected image cannot be substantiality strengthened. In this paper, a metal-dielectric (Ag-Si_3N_4) multilayer nanometer film is structured. The transmission of two counterpropagation lights from the composite film is analyzed by using the characteristic matrix method in the film optics. Compared with the single-layer metal thin film, this composite film can increase not only the transmission of the excitation light but also the transmission of the emission light. If such a composite film is used to practical TIRFM, the intensity of single-molecule fluorescence image can be markedly intensified.

REFERENCES

1. Kulzer, F. and M. Orrit, "Single-molecule optics," *Annual Review of Physical Chemistry*, Vol. 55, 585–611, 2004.
2. Axelrod, D., "Total internal reflection fluorescence microscopy in cell biology," *Traffic*, Vol. 2, No. 11, 764–774, 2001.
3. Yoshita, M., K. Koyama, M. Baba, and H. Akiyama, "Fourier imaging study of efficient near-field optical coupling in solid immersion fluorescence microscopy," *J. Appl. Phys.*, Vol. 92, No. 2, 862–865, 2002.
4. Borejdo, J., Z. Gryzyncski, N. Calander, P. Muthu, and I. Gryzyncski, "Application of surface plasmon coupled emission to study of muscle," *Biophys. J.*, Vol. 91, No. 7, 2626–2635, 2006.
5. Tang, W. T., E. Chung, Y.-H. Kim, P. T. C. So, and C. J. R. Sheppard, "Investigation of the point spread function of surface plasmon-coupled emission microscopy," *Opt. Express*, Vol. 15, No. 8, 4634–4646, 2007.
6. Moal, E. L., E. Fort, S. Lvque-Fort, F. P. Cordelires, M.-P. Fontaine-Aupart, and C. Ricolleau, "Enhanced fluorescence cell imaging with metal-coated slides," *Biophys. J.*, Vol. 92, No. 6, 2150–2161, 2007.
7. Aguet, F., S. Geissbhler1, I. Mrki, T. Lasser, and M. Unser, "Super-resolution orientation estimation and localization of fluorescent dipoles using 3-D steerable filters," *Opt. Express*, Vol. 17, No. 8, 6829–6848, 2009.

Long Wavelength Spectroscopic Characterization of Embedded Bismuth Ferrite Nanorod Arrays

Yalin Lu[1], **J. F. Sell**[1], **M. D. Johnson**[1], **K. Reinhardt**[2], **and R. J. Knize**[1]

[1]Laser Optics Research Center, Physics Department, United States Air Force Academy
Colorado Springs, CO 80840, USA
[2]United States Air Force Office of Scientific Research, AFOSR/NE
875 North Randolph Street, Suite 326, Arlington, VA 22203, USA

Abstract— Embedding a magneto-responsive nanorod array into a dielectric substance, in either random or ordered ways, is interesting to many potential applications, due to the addition of structural modulation into the multi-physical parametric system. One potential interest is its spectroscopic response over infrared to terahertz broad wavelength range. In this abstract, we fabricated a bismuth ferrite nanorod array embedded in alumina, and measured it spectroscopic response from visible to terahertz frequencies. Its nonlinear properties was also investigated.

Session 4A2b
THz, T-ray, T-waves

Femtosecond Laser-induced THz Emission as a Probe for Opto-electronic Properties of Thin Films

Patrick Hoyer[1], **Stefan Nolte**[2], **Gabor Matthäus**[2], **and Kevin Füchsel**[2]

[1]Fraunhofer-Gesellschaft, Hansastr. 27c, München 80686, Germany
[2]Friedrich Schiller University of Jena, Institute of Applied Physics, Jena D-07745, Germany

Abstract— Today, several methods are discussed to evaluate the quality of thin film and crystalline solar cells [1–4]. In this paper we present a non destructive method with the potential to evaluate the electronic properties of semiconductor multilayer systems using femtosecond laser-induced THz emission.

Black silicon is proposed as a new material for solar energy conversion [5, 6] and is furthermore known to show an enhanced THz emission in comparison to polished Si [7]. Here, we present THz measurements of semiconductor-insulator-semiconductor (SIS) solar cells on black silicon with different interface modifications and photovoltaic behavior. The cells where fabricated by deposit a thin tunnel layer of silica and a thin film of indium tin oxide (ITO) on the silicon substrate, whereas the insulator properties where modified. In general, short light pulses absorbed by a semiconductor induce an electric dipole. If the rise and decay of this dipole shows a dynamic behavior in the picosecond time range, an emission of broadband THz radiation can be observed [8]. The THz generation itself is influenced by several parameters like doping, electric field strength, electron mobility, carrier lifetime or absorption length. Depending on the electronic properties of the substrate, the deposited films as well as the interface properties the space charge layer is influenced. Drastic modifications in the electronic structure of the substrate occur, when a junction is formed during the fabrication process. As a consequence, the field of the space charge layer changes. However, the space charge layer is responsible for the separation of electrons and holes and thus influences the generation of THz radiation.

Figure 1 shows the general effect. The light-induced emission of the THz radiation of SIS solar cells on black silicon with different interface modifications; sample 1) without photovoltaic behavior sample 2) with photovoltaic behavior.

In the paper, the fundamental mechanism and possible applications are discussed.

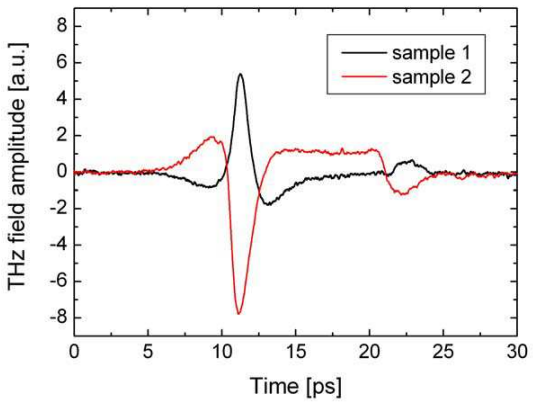

Figure 1: Effect of interface modification: sample 1: Without photovoltaic behavior; sample 2: with photovoltaic behavior.

REFERENCES

1. Glatthaar, M., et al., "Spatially resolved determination of the dark saturation current of silicon solar cells from electroluminescence images," *Journal of Applied Physics*, Vol. 105, 113110/1–6, 2009.
2. Hinken, D., et al., "Determination of the effective diffusion length of silicon solar cells from photoluminescence," *Journal of Applied Physics*, Vol. 105, 104516/1–6, 2009.

3. Würfel, P., et al., "Diffusion length of silicon solar cells from luminescence images," *Journal of Applied Physics*, Vol. 101, 113110/1–10, 2007.
4. Sinton, R. A., A. Cuevas, and M. Stuckings, "Quasi-steady-state photoconductance, a new method for solar cell material and device characterization," *Proc of the 25th IEEE Photovoltaic Specialists Conference*, 457–460, 1996.
5. Koynov, S., et al., "Black nonreflecting silicon surfaces for solar cells," *Applied Physics Letters*, Vol. 88, 203107, 2006.
6. Fuechsel, K., U. Schulz, N. Kaiser, T. Käsebier, E.-B. Kley, and A. Tünnermann, "Nanostructured SIS solar cells," *Proc. SPIE*, 772502, 2010.
7. Hoyer, P., et al., "Terahertz emission from black silicon," *Applied Physics Letters*, Vol. 93, 91106, 2008.
8. Zhang, X.-C., et al., "Generation of femtosecond electromagnetic pulses from semiconductor surfaces," *Applied Physics Letters*, Vol. 56, 1011–1013, 1990.

Extraction of Non-thermal THz Emission from a High Electron Mobility Transistor

Y. Zhou, **Y. D. Huang**, **W. Xue**, **X. X. Li**, **S. T. Lou**, **X. Y. Zhang**, **D. M. Wu**, **H. Qin**, **and B. S. Zhang**

Key Laboratory of Nanodevice and Application, Suzhou Institute of Nano-Tech and Nano-Bionics Chinese Academy of Sciences, 398 Ruoshui Road, Suzhou Industrial Park, Jiangsu 215123, China

Abstract— In this paper, we propose and demonstrate a quantitative technique to extract the non-thermal terahertz (THz) emission from a high-electron-mobility transistor (HEMT). The THz emission is extracted from a strong background thermal radiation which lies in the terahertz spectrum too. Based on the technique, we obtained both efficiencies for terahertz emission and thermal emission. We found that the onset voltage of THz emission is below $V_{ds} \approx 1\,\mathrm{V}$ and the efficiency is maximized at $V_{ds} \approx 2\,\mathrm{V}$. Both THz emission and thermal emission saturate above $V_{ds} > 9\,\mathrm{V}$.

Terahertz Spectroscopy of Biochar

E. M. Pogson[1], **E. Constable**[1], **J. Horvat**[1], **R. A. Lewis**[1], **and S. D. Joseph**[2]

[1]University of Wollongong, Wollongong, NSW 2522, Australia
[2]University of NSW, NSW 2052, Australia

Abstract— Investigation into the material properties of various biochars is reported for a maximum range 0.1–1.5 Terahertz (THz). Previous results for three biochars [1] displayed distinct variances in their absorption coefficient and refractive index for Saligna, BMC5 and Sawdust. This is of import due to the lack of screening methods to distinguish various biochars and may also help in understanding their workings. Biochar is a carbon-rich solid material produced by heating biomass in an oxygen-limited environment and is intended to be added to soils as a means to sequester carbon and maintain or improve soil functions [2]. Biochar has the potential to reduce soil degradation; food insecurity, nitrogen and phosphorus rich runoff from fields, and climate change. Biochar is a complex system and any features may be significant and will be studied. Biochar can be used as an effective fertiliser for various crops without negative harmful sideeffects common with chemical fertilisers [3]. The effect of biochar on crop productivity is variable depending on the various bio-physical interactions that occur with the soil when different biochars are applied. A quantitative way of providing information on different biochars and their components is thus being sought. Hopefully THz will in future provide this information. Current developments include results for several new samples, including spectra of their key material compositions, to understand why these prominent features might occur. This has been achieved using two systems; Two Colour Terahertz (THz), and Terahertz Time Domain Spectroscopy (THz-TDS). The wavelength range of these two systems overlaps meaning that both have been used for greater coverage. Chemically treated Saligna biochar has the same absorption coefficient as untreated Saligna biochar. Other effects such as temperature may also have a significant role on variation in material properties. Various biochars will be compared. Fig. 1 shows the absorption coefficient for Saligna treated and untreated and another biochar, Eucalyptus, displaying differing properties such as a larger absorption coefficient. This is distinguished using THz-TDS.

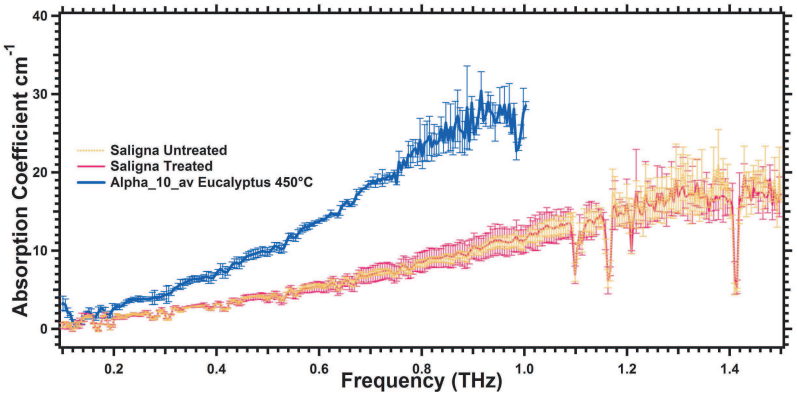

Figure 1: The frequency dependant absorption coefficient of Saligna Treated, Saligna Untreated and Eucalyptus Biochars. Data has been cut-off before it becomes unreliable due to very large absorption of the signal.

REFERENCES

1. Pogson, E. M., J. Horvat, R. A. Lewis, and S. D. Joseph, "Detection of biochar components for soil fertility using THz-TDS," *35th International Conference on Infrared Millimeter and Terahertz Waves*, 1–2, 2010.
2. Joseph, S. D., M. Camps-Arbestain, Y. Lin, P. Munroe, C. H. Chia, J. Hook, L. Van Zwieten, S. Kimber, A. Cowie, B. P. Singh, J. Lehmann, N. Foidl, R. J. Smernik, and J. E. Amonette, "An investigation into the reactions of biochar in soil," *Australian Journal of Soil Research*, Vol. 48, 501–515, 2010.
3. Renner, R., "Rethinking biochar," *Environmental Science and Technology*, Vol. 41, No. 17, 5932–5933, 2007.

Characterisation of Fiber Metamaterial Resonances Using Terahertz Time Domain Spectroscopy

E. M. Pogson[1], R. A. Lewis[1], A. Wang[2], P. G. Hunt[2], M. C. J. Large[2], A Bendavid[3], A. Tuniz[2], B. T. Kuhlmey[2], and S. C. Fleming[2]

[1]Institute for Superconducting and Electronic Materials
University of Wollongong, Wollongong, NSW 2522, Australia
[2]Institute of Photonics and Optical Science (IPOS), School of Physics
University of Sydney, Sydney, New South Wales 2006, Australia
[3]Science and Engineering, Commonwealth Scientific and Industrial Research Organization
P. O. Box 218, Lindfield, Sydney, NSW 2070, Australia

Abstract— Metamaterials are artificial materials, composed of sub-wavelength "atoms" that can collectively exhibit effective electromagnetic responses not found in nature [1]. There are various ways of making metamaterials. The samples used here are metamaterials made using a novel method of fiber drawing. This is accomplished by a dielectric square preform being drawn then sputtered on three sides with 250 nm of silver to produce extended slotted resonators and finally spooled into an array. These metamaterials will exhibit a resonance which can be controlled in production by controlling the orientation of the coated fiber. The metamaterials' electronic properties are dependent upon whether the resonators are symmetric or asymmetric with respect to the propagating wave [2]. Resonances occur when the electric field is perpendicular to the fiber. Thus the magnetic field is parallel to the fibers and there is a magnetic flux through the resonator loop. This is seen in Fig. 1(a) where there is a sharp resonance.

When the metamaterial is rotated 90° the fibers are horizontal and there is no resonance. This is shown in Fig. 1(b). The experimental transmittance has been determined using Terahertz Time Domain Spectroscopy (THz-TDS). The set up and procedure is detailed in [3]. The expected theoretical results agree well with the experimental data with a resonance seen at 0.34 THz as seen in Fig. 1(a). These metamaterials also possess a negative magnetic permeability and this is confirmed using numerical parameter retrieval techniques. This may enable the development of woven negative index materials [1].

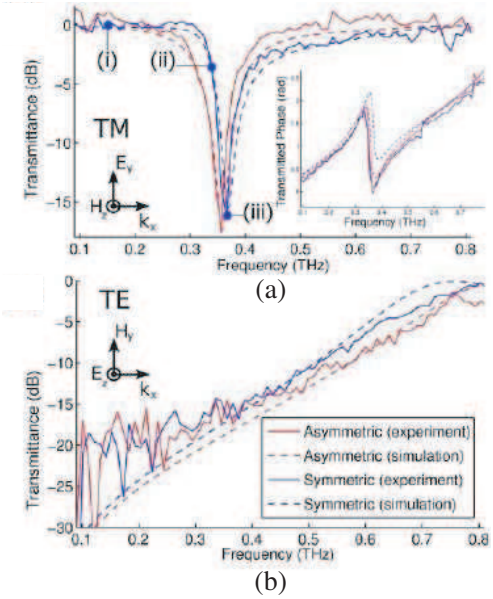

Figure 1: The experimental (full lines) and simulated (dotted lines) transmittance of a fiber metamaterial when fibers are placed: (a) perpendicular to the electric field (with phase inset) and (b) parallel to the electric field.

REFERENCES

1. Wang, A., A. Tuniz, P. G. Hunt, E. M. Pogson, R. A. Lewis, A. Bendavid, S. C. Fleming, B. T. Kuhlmey, and M. C. J. Large, "Fiber metamaterials with negative magnetic permeability in the terahertz," *Optical Materials Express*, Vol. 1, 2011, in press.
2. Li, Z., K. Aydin, and E. Ozbay, "Determination of the effective constitutive parameters of bianisotropic metamaterials from reflection and transmission coefficients," *Phys. Rev. E*, Vol. 79, 26610, 2009.
3. Pogson, E. M., R. A. Lewis, M. Koeberle, and R. Jacoby, "Terahertz time-domain spectroscopy of nematic liquid crystals," *SPIE*, Vol. 7728, 77281Y, 2010.

Terahertz Photocurrent in Point Contact Devices

J. D. Sun, **D. M. Wu**, **B. S. Zhang**, **and H. Qin**
Key Laboratory of Nanodevice and Application, Suzhou Institute of Nano-Tech and Nano-Bionics
Chinese Academy of Sciences, 398 Ruoshui Road, Industrial Park, Suzhou City, Jiangsu 215123, China

Abstract— Quantum point contacts (QPCs) are nanoscale constrictions for electron wave packets. QPCs are usually realized in a high-mobility two-dimensional electron gas (2DEG) by applying negative bias to split Schottky gates. We explored the photocurrent in point contact (PC) devices induced by terahertz (THz) electromagnetic wave in the frequency range from 850 GHz to 930 GHz. Directional photocurrent were observed by varying the conductance of the point contacts. Furthermore, photocurrent from two point contacts in series was measured and exhibited fairly independent THz responses. A model based on homodyne mixing of THz electric field was examined. The results suggest that voltage-controlled nonlinear point contact devices could be suitable for high sensitive THz detection above 1 THz.

Session 4A3
SAR Systems and Signal Processing

Integrated UAVSAR Simulator and Processor Software (iSARX)

T. S. Lim, **C. S. Lim**, **and V. C. Koo**
Faculty of Engineering & Technology, Multimedia University
Jalan Ayer, Keroh Lama, Bukit Beruang, Melaka 75450, Malaysia

Abstract— Synthetic aperture radar (SAR) has been recognized as an essential component of future surveillance systems. One of the major challenges associated with SAR is image formation process. The generation of a two-dimensional image out of the SAR raw data is a computational intensive task. SAR sensors produce gigabytes of raw data that have to be processed into SAR image, thus the selection of the right SAR image algorithm for a particular system is very important to ensure time and cost efficiency without compromising the accuracy of the image. This is a time-consuming task without a reconfigurable and comprehensive software package. Thus, a new UAVSAR integrated simulator and processor software, called iSARX, is developed to aid the system designers in optimizing all the system parameters and performance. The iSARX is developed using Matlab platform, which is capable to perform mission planning, terrain modeling, autofocus and image processing algorithms evaluations as well as for understanding SAR processes. Various plots are available for image quality analysis in iSARX software package. The design of iSARX is based on modular simulation and processing platform, which consists of various independent modules that share a pool of data files. Each module may be developed and executed separately, depending on individual applications. The data format of iSARX is a simplified version of the CEOS (Committee of Earth Observations Satellites) standard on SAR data set. The SAR data records will use the same data format for all SAR product types in iSARX. By having common formats, users from various working groups would be able to analyze and merge data from multiple resources. In the iSARX performance evaluation, simulated and actual SAR raw data were used for further analysis and comparison of the three selected image formation algorithms.

Satellite SAR System and Image Simulations by a GPU-based Algorithm

Cheng-Yen Chiang[1], **Kun-Shan Chen**[1], **Yang-Lang Chang**[2], **and Tim Lee**[1]

[1]Center for Space and Remote Sensing Research
Department of Computer and Information Engineering, National Central University, Jhongli, Taiwan
[2]National Taipei University of Science and Technology, Taipei, Taiwan

Abstract— A simulation tool is vital for spaceborne SAR system mission, platform, and payload. Besides, SAR image understanding and interpretation is essential for remote sensing applications of earth. SAR image databases are the important role in development of aid target recognition and identification system. This paper presents a GPU-based simulation of satellite SAR images. The simulation includes the computation of RCS of targets, orbital parameters estimation, SAR echo signal generation, and image focusing. Generally, CPU is optimized to minimize latency experienced by one thread or several threads. It is designed to be good at everything, whether it is parallel processing or not. As for GPU, work load is assumed to be highly parallel — many data to be processed by same algorithm. Based on that assumption, each processing unit is designed to handle many threads. Processing units work as a group to maximize throughput of all threads. Latency can be hidden by skipping stalled threads, if there are few compared to number of eligible threads. Grouping means shared control logics and cache. By this fact and to release the heavy computational burden, a GPU based algorithm is dedicatedly developed so that a very high verisimilitude including the sensor and target geo-location relative to the Earth, movement of sensor, SAR system parameters and geometric characteristics of the target, etc, may be achievable. Numerous test runs show that substantial computational cost is reduced while maintaining very high accuracy for all simulation chains.

The Design and Development of Unmanned Aerial Vehicle Synthetic Aperture Radar

Yee Kit Chan and V. C. Koo
Faculty of Engineering & Technology, Multimedia University
Jalan Ayer Keroh Lama, Bukit Beruang, Melaka 75450, Malaysia

Abstract— An Unmanned Aerial Vehicle (UAV) airborne synthetic aperture radar (SAR) is being developed at Multimedia University, Malaysia with collaboration from Agency of Remote Sensing Malaysia (ARSM). The SAR system is a C-band, single polarization, linear FM pulse radar system. The system will be used for monitoring and management of earth resources such as paddy fields, oil palm plantation and soil surface. This paper describes the design and development of the UAVSAR. In particular, the design and construction of the microwave system, microstrip antenna, control and timing unit, and chirp generator are described.

A SIMO Step-frequency Radar Technology for Imaging and Reconstruction of a 3D Complex Target

Wei Li and Ya-Qiu Jin
Key Laboratory of Wave Scattering and Remote Sensing Information (MoE)
Fudan University, Shanghai 200433, China

Abstract— A single input and multiple output (SIMO) Step-Frequency (SF) radar technology is presented. Numerical simulations of polarized scattering from a 3D complex-shaped electric-large target and the target profile reconstruction from 3D imaging are implemented.

The SIMO-SF radar utilizes the linear SF radar array with a single-transmitting and multiple-receiving antennas working in downward-looking spotlight mode and moving in transverse to form a 2D synthetic array. It works in the $1 \sim 3$ GHz band. The central radar of the array is used as both the transmitter and receiver, and the others are the receivers only. Suppose the radar number be N, the data acquisition time of the SIMO can be N times smaller than the SISO (single input and single output) model.

Our numerical BART method (bidirectional analytic ray tracing) and conventional FEKO software are first employed to calculate polarized scattering from the electric-large complex shaped target. An improved 3D RMA (range migration algorithm) is then utilized to making the radar imaging. In order to implement SIMO radar, the approximated signal spectrum is derived in the implicit phase term of the Taylor series. Finally, reconstruction of the 3D PEC target, i.e. a tank-like one, is demonstrated.

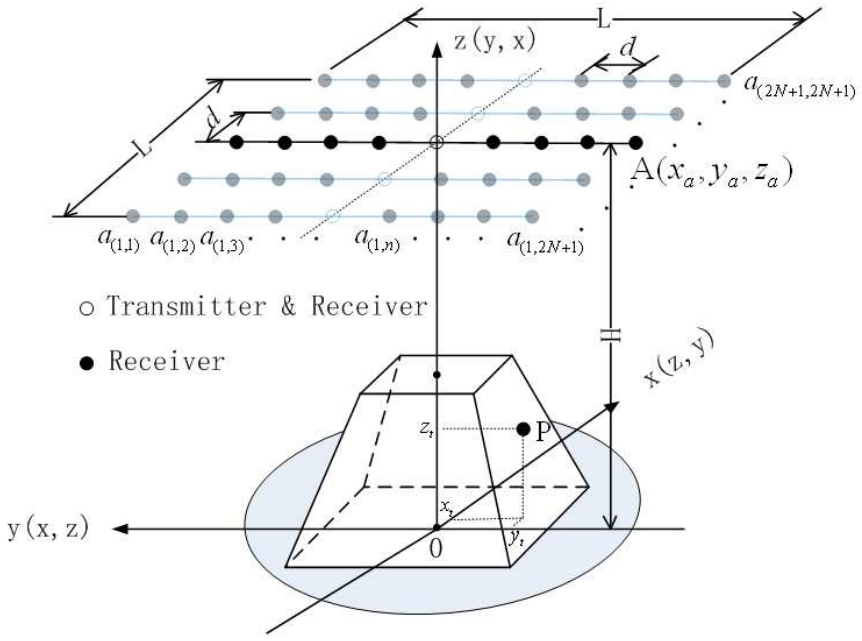

Figure 1: The 3D imaging and reconstruction of a complex-shaped electric-large target using SIMO-SF radar.

Circularly Polarized Array Antennas for Synthetic Aperture Radar

Yohandri[1, 2], **J. T. Sri Sumantyo**[1], **and H. Kuze**[1]

[1]Josaphat Microwave Remote Sensing Laboratory, Center for Environmental Remote Sensing
Chiba University, 1-33 Yayoi-cho, Inage-ku, Chiba 263-8522, Japan
[2]Physics Department, State University of Padang, Kampus UNP
Jln. Prof. Hamka Air Tawar, Padang, Sumatera Barat 25131, Indonesia

Abstract— The circularly polarized synthetics aperture radar (CP-SAR) sensor is a new sensor intended for earth observation applications, with the advantage of sensitive measurements on earth object characteristics, providing the greater amounts of information than conventional linear-polarization systems. In this research, the CP-SAR sensor is designed to transmit and receive the microwave in circular polarization. To realize the circular polarization, this CP-SAR system is composed by Left Handed Circular Polarization (LHCP) and Right Handed Circular Polarization (RHCP) sub array antenna, where the transmission (Tx) is working in RHCP or LHCP, and reception (Rx) is working in both RHCP and LCHP. The array antennas are developed using simple corner-truncated square-patch elements with a novel feeding method. In addition, we use a circular sector power divider with odd-number feeding, which is an improved version of the feeding method proposed in another similar research. The fabricated antenna based on the simulation using method of moment (MoM) gives a good circular polarization with an impedance bandwidth and 3-dB axial ratio bandwidth is 6.1% and 1.0%, respectively for LHCP, while 6.2% and 1.0%, respectively for RHCP. The full antenna, in turn, will be installed on an Unmanned Aerial Vehicle (UAV) JX-1 in Center for Environmental Remote Sensing, Chiba University. In the near future, CP-SAR is expected to improve the characteristics of conventional SAR system, especially to extract some new physical information on the earth surface.

Design and Development of a Ground Based Frequency Modulated Continuous Wave Imaging Radar System

Y. K. Chan, **C. Y. Ang**, **and V. C. Koo**
Faculty of Engineering & Technology, Multimedia University
Jalan Ayer Keroh Lama, Bukit Beruang, Melaka 75450, Malaysia

Abstract— This paper describes the design and development of a ground based Frequency Modulated Continuous Wave (FMCW) radar system in Multimedia Univeristy (MMU), Malaysia. In this project, a ground-based fully polarometric, C-band, high bandwidth linear FM-CW imaging radar system is to be designed and constructed. The system should have the capability to measure the complex scattering return of distributed targets using FMCW system and obtained fully polarimetric signals which can be used to provide more accurate identification and classification of the geophysical media.

A GPS/SINU Design for Motion Sensing and Compensation Using Extended Kalman Filter for Airborne UAVSAR

C. H. Lim, **C. S. Lim**, **W. Q. Tan**, **T. S. Lim**, **and V. C. Koo**
Faculty of Engineering and Technology, Multimedia University
Jalan Ayer Keroh Lama, Melaka 75450, Malaysia

Abstract— For many years, Synthetic Aperture Radar (SAR) has been a fascinating and efficient tool for microwave imaging of Earth's surface. Recent trend in SAR sensor development focuses on light weight, low cost systems such as Unmanned Aerial Vehicle (UAV)-based SARs. The Multimedia University, in collaboration with Malaysian Remote Sensing Agency (ARSM) has developed a new C-band (5.3 GHz) UAVSAR for remote sensing applications.

Two preliminary flight tests had been carried out in 2010. An onboard high performance single board computer is used to perform raw data storing, processing and motion compensation. A simplified SAR processing algorithm, based on the classical range-doppler algorithm, is developed to enable image preview in real-time. One of the biggest challenges of this UAVSAR system is the degradation of image quality due to motion errors. Because of the size and the weight of the UAV, it is very difficult to maneuver steadily in cloudy and windy conditions. The flight path may have significant trajectory deviations from the ideal path and the variations of the UAV's forward velocity and attitude (yaw, pitch, and roll) further complicate the problem. In order to improve the image quality, a modified motion compensation algorithm is integrated into the existing SAR processing software. The algorithm makes use of an onboard GPS and an INU for motion error estimations.

This paper gives an overview of the challenges faced in a typical UAVSAR processing, and proposed an integrated solution for SAR processing with motion compensation capabilities.

Motion Compensation for UAVSAR Raw Data

C. H. Lim, T. S. Lim, and V. C. Koo
Faculty of Engineering and Technology, Multimedia University
Jalan Ayer Keroh Lama, Melaka 75450, Malaysia

Abstract— For many years, Synthetic Aperture Radar (SAR) has been a fascinating and efficient tool for microwave imaging of Earth's surface. It's all weather capabilities, day and night with high resolution ground surface imaging has make it one of main research focus for remote sensing. SAR sensors can be either placed on an UAV-airborne or mounted on spacecrafts for ground detections.

SAR raw data processing remains as one of the challenging task for high resolution imaging [1, 2]. Standard SAR signal processing techniques assumes a straight line path for the SAR sensor [3]. Such assumption provides an efficient approximation for spaceborne SAR sensor. In the case of airborne SAR sensor, however, such approximation may leads to massive degradation on the final image. The degradation is due to the SAR sensor's motion error, which includes significant trajectory deviations from the ideal path and the variations of airborne forward velocity and attitude (yaw, pitch, and roll) [4]. In order to minimize the effect of motion error, SAR motion compensation must be performed. The idea of motion compensation is to acquire the undistorted image in the presence of motion error. The compensation is achievable by either including the motion compensation (MOCO) algorithms [5, 6] in the SAR signal processing chain, or by motion error extraction from SAR raw data for compensation [3, 7]. The first method requires additional information provided by global positioning system (GPS) and inertia navigation system (INU) mounted together with the airborne, while the second method extracts the motion errors by analyzing the raw data.

In this paper, the authors proposed a modified motion compensation (MOMOCO) algorithm for UAVSAR project funded by Malaysian Remote Sensing Agency (ARSM). A lightweight UAV airborne with [what]-band SAR system has been developed under this project. The MOMOCO algorithm is designed to compensate the SAR raw data acquired from the UAVSAR system during the flight missions. The algorithm makes use of the GPS and INU for motion error estimations. The objective is to acquire an undistorted image from the processing of SAR raw data with motion error for UAVSAR project.

REFERENCES

1. Soumekh, M., *Synthetic Aperture Radar Signal Processing with MATLAB Algorithm*, John Wiley & Sons, Inc, New York, 1999.
2. Cumming, I. G. and F. H. Wong, *Digital Processing of Synthetic Aperture Radar Data: Algorithms and Implementation*, Artech House, 2005.
3. Franceschetti, G. and R. Lanari, *Synthetic Aperture Radar Processing*, CRC, New York, 1999.
4. Xing, M., X. Jiang, and R. Wu, "Motion compensation for UAV SAR based on raw radar data," *IEEE Transactions on Geoscience and Remote Sensing*, Vol. 47, No. 8, 2870–2883, August 2009.
5. Fornaro, G., "Trajectory deviation in airborne SAR: Analysis and compensation," *IEEE Transaction on Aerospace Electronic System*, Vol. 35, No. 3, 997–1009, July 1999.
6. Fornaro, G., G. Franceschetti, and S. Perna, "On center-beam approximation in SAR motion compensation," *IEEE Geoscience and Remote Sensing*, Vol. 3, No. 2, 276–280, April 2006.
7. Li, Y., M. Xing, and Z. Bao, "A new method of motion error extraction from radar raw data for SAR motion compensation," *International Conference on Radar, CIE'06*, October 2006.

Session 4A4
Microstrip and Printed Antennas

A New Dual Band E-shaped Slot Antenna Design for Wireless Applications

Jawad K. Ali
Department of Electrical and Electronic Engineering, University of Technology, Baghdad, Iraq

Abstract— An E-shaped printed slot antenna is presented as a candidate to cover dualband operation over the entire wireless local area network (WLAN) frequency bands of 2.4–2.5 GHz and 4.9–5.8 GHz. The E-shaped slot structure has been etched in the ground plane, and the 50 microstrip line feed is etched on the reverse side of the substrate. An additional trapezoidal slot has been etched attached to the slot structure on the feeding side to facilitate matching. The antenna structure has been modeled and its performance has been evaluated using a method of moment based electromagnetic simulator, IE3D from Zeland Software Inc. Simulation results show that, the proposed antenna offers good return loss response (for S_{11} less than -10 dB) at the two bands with reasonable radiation performance. A comprehensive numerical study has been conducted to demonstrate the effects of various slot parameters on the resulting antenna performance. It has been found that the ratio of the two resonating frequencies f_{o2}/f_{o1} can be varied in the range of 3–6, without changing the antenna external dimension. This provides the antenna designer with a flexible tool to use the proposed slot antenna in other multiband communication applications.

UTD-PO Solution for the Calculation of the *E*-plane Radiation Pattern of Rectangular Horn Antennas with V-shaped Corrugations

José-Víctor Rodríguez, **Fernando Quesada-Pereira**,
Mayte Martínez-Inglés, **María Martínez-Quinto**, **Juan Pascual-García**,
José-María Molina-García-Pardo, **and Leandro Juan-Llácer**
Universidad Politécnica de Cartagena, Cartagena, Murcia, Spain

Abstract— A new method based on a hybrid uniform theory of diffraction-physical optics (UTD-PO) formulation for the obtaining of the *E*-plane radiation pattern of *E*-plane corrugated rectangular horn antennas with V-shaped corrugations is presented. The method has been validated through comparison with numerical data obtained through the application of an electric field integral equation (EFIE) solved by the method of moments (MoM) and, in this sense, it should be noted that the proposed solution is mathematically less complex and computationally more efficient than such technique. The scheme of the *E*-plane of the corrugated rectangular horn antenna considered in this work can be observed in Fig. 1.

A comparison between the *E*-plane radiation pattern of such a horn antenna — considering 40 V-shaped corrugations — obtained with both the proposed UTD-PO solution and the EFIE technique can be observed in Fig. 2, where the radiation pattern of a conventional rectangular horn (without corrugations) has also been depicted. As can be seen from the figure, a good agreement can be found between the two methods. It can be pointed out that the UTD-PO calculations depicted in Fig. 2 required just 5.5 seconds to compute whereas the EFIE technique results took 101 seconds in the same computer, which means quite a longer time. As can also be observed, the reduction in side-lobe level due to the presence of corrugations is considerable and, besides, both the width of the main beam and its saddle are reduced compared to the conventional horn pattern.

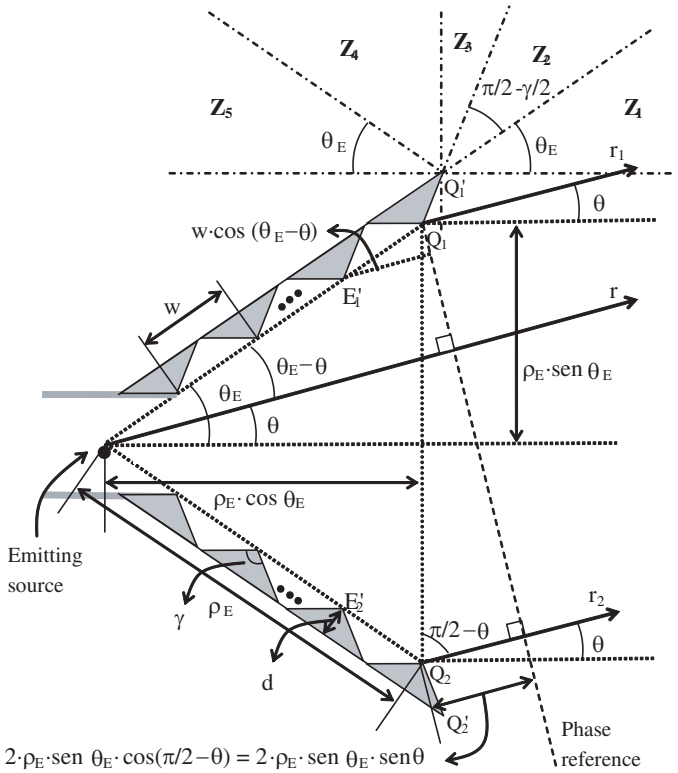

Figure 1: Scheme of the *E*-plane of a corrugated rectangular horn antenna.

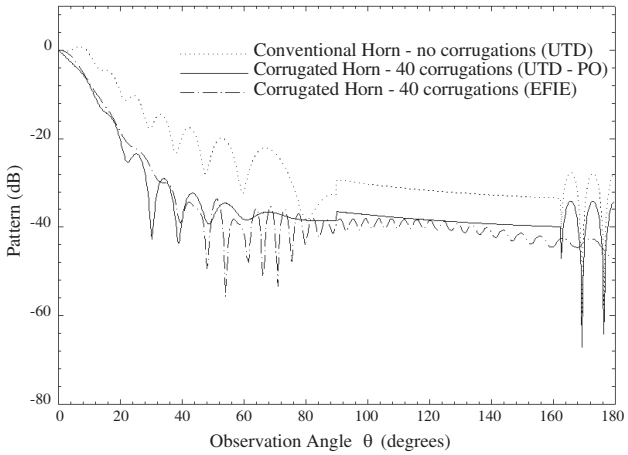

Figure 2: Comparison between radiation patterns of a corrugated horn antenna with 40 V-shaped corrugations — obtained with the proposed UTD-PO method and the EFIE technique — and that of a conventional horn (without corrugations). $\rho_E = 13.5\lambda$, $\theta_E = 17.5°$, $\gamma = 35°$, and $d = 0.35\lambda$.

ACKNOWLEDGMENT

This work was supported by the Ministerio de Educación y Ciencia, Spain (TEC2010-20841-C04-03) and the Fundación Séneca of Murcia, Spain, (08818/PI/08).

Experimental Study of a Single-feed Planar Antenna for DTV Reception

Herman Hideyuki Uchida[1], **Hiroyasu Matsui**[2], **and Toshio Wakabayashi**[3]

[1]Tokai University, 4-1-1 Kitakaname, Hiratsuka, Kanagawa, Japan
[2]DX Antenna Co., Ltd., 2-15, Hamasaki-Dori, Hyogo, Kobe, Hyogo, Japan
[3]Tokai University, 2-3-23, Takanawa, Minato, Tokyo, Japan

Abstract— The fading phenomenon due to standing waves is one of the factors of quality deterioration in mobile communication technologies. Authors have proposed a single-feed planar antenna that has the receiving function of a PMA (Planar Monopole Antenna) that receives the standing wave of the electric field and that of a PSA (Planar Slot Antenna) that receives the standing wave of the magnetic field, and suppresses changes in received signal level due to the fading phenomenon resulting from standing waves. However, it has a narrow bandwidth, therefore, broadbanding of the antenna was required. In this study, a single-feed planar antenna which bandwidth is broadened for receiving the terrestrial broadcasting in UHF (Ultra High Frequency) band is proposed in order to improve the deteriorated receiving characteristics due to the fading phenomenon resulting from standing waves. It has two antenna components; a B-PMA (Broadband Planar Monopole Antenna) which is an electric antenna and a B-PSA (Broadband Planar Slot Antenna) which is a magnetic antenna, and is composed of the two components by single-feed structure. Since it has a single-feed point, it can improve receiving characteristic without using a switching circuit, a combiner, and a phase shifter. The return loss characteristics of the proposed antenna and its components are analyzed by the FDTD (Finite Difference Time Domain) method, and compared with the measurement results. The analytical and experimental results clearly declare that the bandwidth of the proposed antenna is broadened to receive the Japanese terrestrial DTV (Digital Television). Moreover, the analytical and experimental results correspond well.

Combined Fractal Geometries for the Design of Wide Band Microstrip Antennas with Circular Polarization

Homayoon Oraizi and Shahram Hedayati
Department of Electrical Engineering, Iran University of Science and Technology
Narmak, Tehran 16846-13114, Iran

Abstract— In this paper, we propose the combination of several fractal geometries for microstrip patch antenna for the achievement of their miniaturization and multi banding characteristics. By placing air gaps under the microstrip patches (actually making suspended microstrips) the bandwidths of antennas are drastically improved. By cutting appropriate rectangular and triangular slits as perturbations on the edges of fractal geometries, circular polarizations may be realized in the radiation patterns.

Design of Internal Dual Band Printed Monopole Antenna Based on Peano-type Fractal Geometry for WLAN USB Dongle

Ali J. Salim and Jawad K. Ali
Department of Electrical and Electronic Engineering, University of Technology, Baghdad, Iraq

Abstract— With the development of national missile defense system, we must rely on new ways to penetrate the existing strategic balance to maintain. Near space vehicle is one of the most promising means of a highly efficient of penetration. Near space vehicle can effectively circumvent the Kinetic Energy Interceptor, but low-yield nuclear detonation may be faced with a typical combat scenario. Nuclear explosions in near space on the impact of near space vehicle are particularly important. In this paper, finite-difference time-domain (FDTD) method has been discussed for complete simulation of nuclear electromagnetic pulse (NEMP) originating from an atmospheric nuclear detonation in near space. The Compton current formula and the simplified model of solving the Maxwell's equations are described. In addition, the typical results that the plasma flow field of near space vehicle is generated by the ionization between high-speed flight and the thin air in near space are presented. The coupling between nuclear electromagnetic pulse (NEMP) in nuclear exploding source region and the plasma flow field of near space vehicle is studied. To achieve this purpose, the radiated field in nuclear exploding source region is calculated using a late-model iterative equation including the electron plasma extra conductivity effect. Because of the free electron plasma extra conductivity, the corresponding conduction current is offset by the Compton current, resulting in significant decline in the peak transverse electric field. The presented results may be used in electromagnetic compatibility analysis of near space vehicle.

A New Miniaturized E-shaped Printed Monopole Antenna for UWB Applications

Jawad K. Ali and Ahmad S. Hussain
Department of Electrical and Electronic Engineering, University of Technology, Baghdad, Iraq

Abstract— In this paper, a compact UWB printed monopole antenna design is proposed. The monopole antenna has the form of an E-shaped structure printed on a substrate with relative dielectric constant of 3.38, and thickness of 1.52 mm. The matching through the UWB response is satisfied using a reduced ground plane. The proposed antenna is fed by a 50 Ω unsymmetrical microstrip line. The ground plane is printed beneath the microstrip line. Modeling and performance evaluation of the proposed antenna have been carried out using the commercially available electromagnetic simulator, IE3D from Zeland Software Inc. A parametric study is performed to show the effects of the different antenna parameters on the overall antenna performance. The performance of the antenna is mainly affected by geometrical and electrical parameters, such as the width and length of the branches of the E-shape structure, feed gap as well as the ground plane. Simulation results show that the proposed antenna possesses an operating bandwidth, for return loss ≤ -10 dB, extending from approximately 2.93 GHz to about 13 GHz which covers the entire UWB band of 3.1 GHz to 10.6 GHz. A comparative study, with other antennas reported in the literature, shows that the proposed antenna offers many attractive features making it a suitable candidate for use in UWB applications.

Reconfigurable 8 — Shape PIFA Antenna Using PIN Diode

Trong Duc Nguyen[1], **Yvan Duroc**[2], **Vu Van Yem**[3], **and Tan Phu Vuong**[1]

[1]Laboratory LAHC, Institute Microelectronic Electromagnetic and Photonic, Grenoble INP — Minatec
3 Parvis Louis Neél, BP 257, 38016 Grenoble Cedex 1, France
[2]Laboratory LCIS, Grenoble INP, 50 Barthélémy de Laffemas, BP 54, 26902 Valence Cedex 9, France
[3]School of Electronics and Telecommunications, Hanoi University of Science and Technology
1 Dai Co Viet Road, Hanoi, Vietnam

Abstract— Nowadays the development of mobile communication and the miniaturization of radio frequency transceivers are experiencing an exponential growth, hence increasing the need of compact antennas. As a result, new antenna prototypes have been developed to provide a large bandwidth as well as a small size. The PIFA antenna is one of the most interesting models. The PIFA has several advantages such as the ease of fabrication, a low implementation cost, a compatibility and conformity of ground plane with complex geometries. The PIFA is widely used in mobile devices and offers compact size and multi-band operation. The reduction of the PIFA antennas size may be achieved by several techniques. Some designers have used capacitive elements, LC resonator while others rely on the mechanical alteration of the structure such as used meander or reactive loading. Furthermore, a reconfigurable antenna can reuse its entire volume at different operating bands so the physical size of the antenna can be reduced. For multi-band operation, different techniques for creating multi-band PIFA antennas have been introduced such as varying the shape of the radiating patch, adding some slots on the patch or adding parasitic elements to create an additional resonant frequency, even using more radiating elements shared with the same feed and ground. In this paper, we propose a new reconfigurable PIFA antenna that can be tuned in two frequency bands from 2 GHz to 3 GHz and from 4 GHz to 7 GHz by changing the geometry of the radiating patch. Starting at an initial 8-shape patch antenna (Figure 1) by connecting or disconnecting one or more PIN diode we can obtain ten different structures corresponding to ten different geometries such as I-shape patch, E-shape patch, S-shape patch etc (Table 1). With each patch obtained from ten different geometries, we collect the corresponding antenna with the operating frequency band from 2 GHz to 7 GHz. We also develop an automatic embedded Genetic Algorithm (GA) in Computer Simulation Technology tool for multiple antenna parameters optimization. The novel RPIFA antenna is designed optimized and implemented using the developed GA model. The simulation and measurement results of antenna parameters are compared to show the performance of the developed antenna.

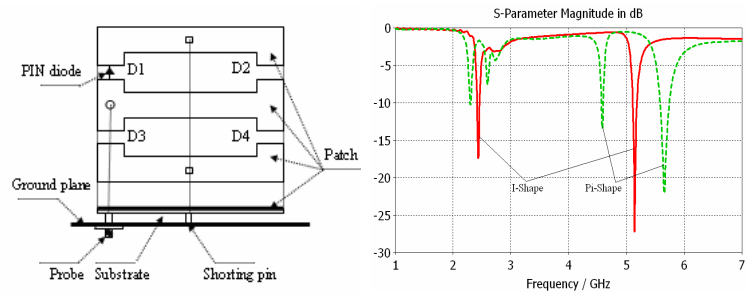

Figure 1: The architecture of 8-shape PIFA antenna and S_{11} parameter of some configurations of PIFA antenna are obtained.

Diode1 (D1)	D2	D3	D4	Form of patch
0	0	0	0	I
0	0	0	1	U
0	0	1	0	П
0	0	1	1	O
0	1	0	1	W
1	0	0	1	S
1	0	1	0	E
1	0	1	1	6
1	1	0	1	9
1	1	1	1	8
D_i=0: OFF, D_i=1:ON, i=1-4				

Table 1: Status of PIN diodes and form of antenna's patch.

Miniaturized Surface Wave Dipole Antenna for Millimeter Wave Application

Zachariah C. Alex and G. Shrikanth Reddy
School of Electronics Engineering, Vellore Institute of Technology University
Vellore, Tamil Nadu 632014, India

Abstract— A study on Surface wave Antenna for millimeter wave application is carrier out. In the proposed work a simple dipole is chosen and its length is reduced and optimized for millimeter wave, i.e., 60 to 80 GHz applications. This miniaturized dipole is backed by periodic patches which is responsible for guiding surface wave along the partial ground slab, giving in phase reflection and a monopole like characteristic with a null at broad side direction. Through the proposed structure the achieve band width is of 20 GHz (−10 db), i.e., 60 to 70 GHz, with a maximum gain of 8 dbi at 64 GHz and an average gain of 6.8 dbi for whole band width. The analysis of other antenna parameter like co polarization, cross polarization and current distribution is also done. The analysis is based on commercially available Electromagnetic simulator CST 2010 based on Finite integral transform and the mesh cells were chosen around 50 lakhs for high accuracy purpose.

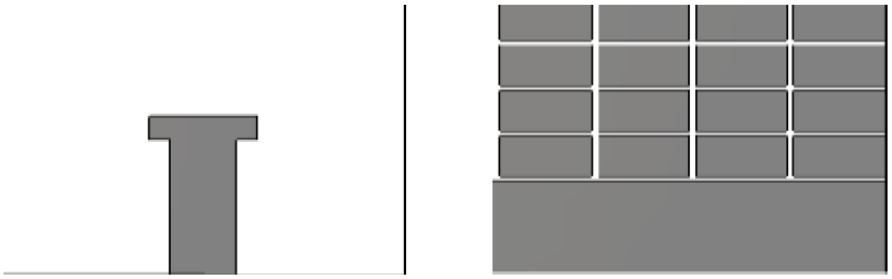

Figure 1: (a) Miniaturized dipole with microstrip feed. (b) partial ground structure with periodic patches.

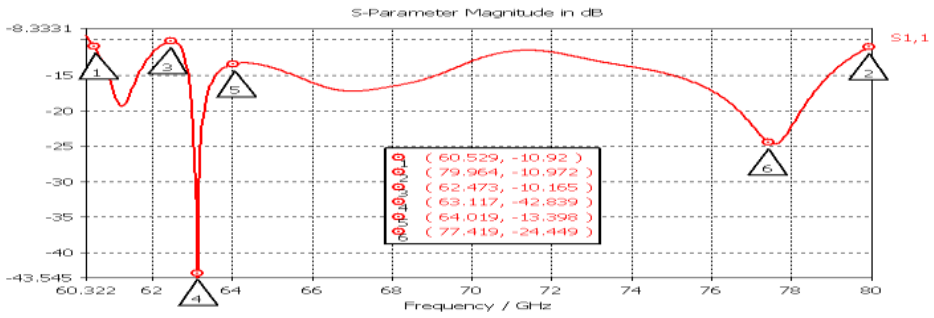

Figure 2: Return loss graph of the proposed structure.

Extended Dipole Antenna with AMC Spiral Ground and Via Holes for Millimeter Wave Application

G. Shrikanth Reddy and Zachariah C. Alex
School of Electronic Engineering, Vellore Institute of Technology University
Vellore, Tamil Nadu 632014, India

Abstract— In the proposed paper Umbrella shaped Dipole antenna is chosen and its radius is optimized for Millimeter wave band, i.e., 60 GHz. The Extended dipole is given Microstrip feed and it is backed by Artificial Magnetic Conductor (AMC) ground added with closed cap via holes. In the proposed work the dimensions of Spiral ground and vias are optimized and their combine effects were used to suppress surface wave effect, which were responsible for decrement in the antenna characteristics.

Spiral Grounds with via holes a LC circuit phenomena can be obtained, which is their by utilized to obstruct the flow of surface wave. Here the Extended Dipole is drawn on Perfect Electric Ground, Spiral Ground, Spiral Ground with Via holes and their results in terms of return loss, Antenna gain and Efficiency, Co and Cross polarization level etc, were analyzed, and it was found that Antenna with Spiral ground and Via holes give better results as compare to others. The obtained band width with proposed Antenna is 6 GHz, i.e., 57 to 63 GHz, with gain of 7 dbi.

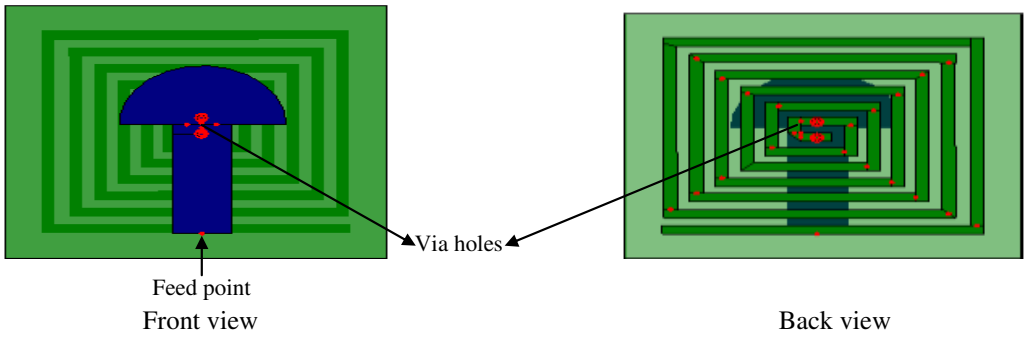

Figure 1: Extended Umbrella shaped Dipole backed by AMC Spiral ground with Via holes.

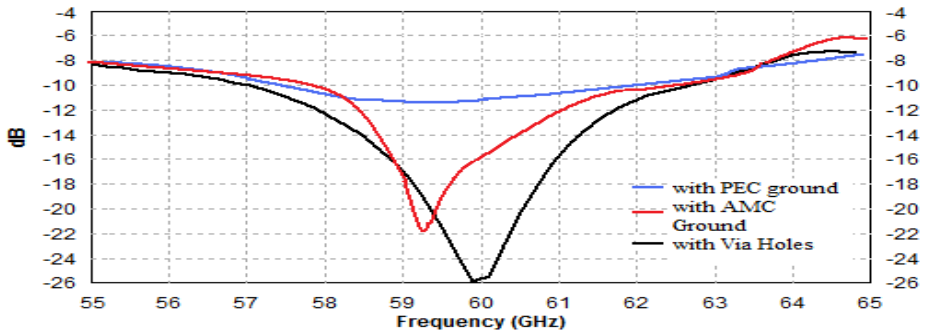

Figure 2: Compared Return Loss Graph for Proposed structure.

Gain and Bandwidth Enhancement of a Microstrip Antenna Using Partial Substrate Removal in Multiple-layer Dielectric Substrate

Neeraj Rao and Dinesh Kumar V.
PDPM Indian Institute of Information Technology, Design & Manufacturing Jabalpur, India

Abstract— Many ways of enhancing gain and bandwidth of a microstrip patch antenna have been suggested in literature. But these methods improve either gain or bandwidth, but not both. In this paper, a novel antenna design for simultaneous improvement of patch antenna gain and bandwidth has been proposed using partial substrate removal in a multiple-layer dielectric (Fig. 1).

A microstrip patch antenna is widely used in compact and portable communication devices due to its small size, thin profile configurations, conformity and low cost. In spite of these remarkable advantages, the patch suffers some serious drawbacks like low bandwidth (due to small size). Bandwidth can be increased but at the cost of size of the patch, making it large and bulky. To overcome this problem, a *multiple-layer dielectric substrate has been used to improve bandwidth*, in this paper. There are different types of losses in antenna, one of which is *surface wave loss* due to of the permittivity of the material and thickness of the substrate. Due to excitation of surface waves, patch antenna also suffers from reduced gain and efficiency as well as unacceptably high levels of cross-polarization and mutual coupling within an array environment at high frequencies. In this paper, *parts of the substrate surrounding the patch have been strategically removed to suppress surface wave losses, and thereby increase gain.*

It is known that for a particular resonant frequency, the bandwidth increases with increase in size of patch antenna for a high dielectric. The patch antenna of low dielectric has a moderate bandwidth but large size. Bandwidth decreases with increase in the dielectric value of the substrate. The two substrates have been combined so as to include the quality of both high and low dielectric, i.e., high bandwidth and low patch size respectively [1]. A microstrip patch antenna implemented on silicon ($\varepsilon_r = 11.9$) has moderate bandwidth with a small sized patch and that implemented on glass ($\varepsilon_r = 4.6$) has a high bandwidth. In this paper, a multiple-layer substrate is made by sandwiching one layer of glass ($\varepsilon_r = 4.6$) in between two layers of silicon ($\varepsilon_r = 11.9$) so as to reduce the antenna size as much as possible. Here, silicon ($\varepsilon_r = 11.9$) has been used directly below the patch so as to maximize the size reduction. As a result, the size is increased slightly, but the bandwidth is increased greatly. The method to improve the gain is to reduce the loss of the microstrip antenna. The gain of the antenna can be increased by reducing the loss due to surface wave propagation. One method to do so is by replacing the substrate of patch with low dielectric values or with air ($\varepsilon_r = 1$). Periodic structures of electromagnetic band-gap (EBG) can be used to block the surface waves from propagating in a certain band gap. A common method to generate EBG structures is to drill holes in substrate to synthesize a lower dielectric constant substrate [2]. However, in this paper, a rather simpler version of EBG structure approach has been used by partially removing the substrate surrounding the patch instead of drilling periodic holes. Removing the substrate partially stops the propagation of surface wave in the substrate, which reduces the power coupled in backward direction and enhances the forward coupled power [3]. As a result the gain increases.

The proposed antenna has been implemented using CST Studio Suite^{TM} 2010 and tested for removal of substrate in various configurations like — along radiating and non-radiating edges, making trenches of different widths all-around the patch, below the patch and on all its sides. These configurations have been analyzed for removal of substrate on the top first layer (Silicon). Analysis of resulting reflection loss, gain and bandwidth shows that using the proposed antenna design, best gain-bandwidth trade-off is achieved by removal of top silicon substrate layer ***along non-radiating edges giving 290 MHz bandwidth and gain 3.893 dB (reflection loss:*** -11.557 ***dB) at operating frequency of 5.988 MHz***. Maximum bandwidth of 319.4 MHz is achieved at gain of 3.656 dB at operating frequency 6.244 GHz, while maximum gain of 3.893 dB (reflection loss -11.214) at bandwidth 290 MHz is obtained at 5.988 GHz. This is a remarkable improvement over bandwidth of 70.512 MHz and gain 2.986 dB at 5.4 GHz obtained by using only multiple-layer dielectric substrate without any partial removal. This is also a noteworthy improvement over gain of 3.440 dB and bandwidth 88.2 MHz at 6.16 GHz obtained using partial substrate removal on single-layer dielectric substrate (silicon) as shown in Fig. 2. Hence, the proposed antenna design based on partial substrate removal on top silicon layer along non-radiating edges in a multiple-layer dielectric substrate can be considered highly suitable for applications

requiring simultaneously high bandwidth and gain. Investigation of partial substrate removal in various configurations on two and more layers (in various different combinations) is also in progress.

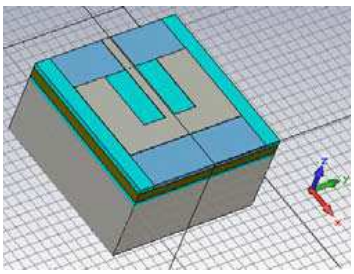

Figure 1: Proposed antenna design using partial substrate removal along non-radiating edges in multiple-layer substrate.

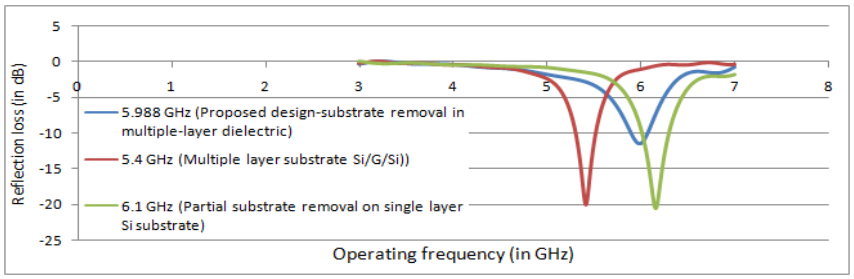

Figure 2: Reflection loss (in dB) for different configurations of dielectric substrate showing improvement in bandwidth.

REFERENCES

1. Kim, J.-H., H. C. Kim, and K. Chun, "Performance enhancements of a microstrip antenna with multiple layer substrates," *International Symposium on Signals, Systems and Electronics 2007 (ISSSE '07)*, 319–322, Digital Object Identifier: 10.1109/ISSSE.2007.429447, 2007.
2. Zhou, Y., F. Yu, T. Shen, P. J. Ge, J. Gen, and J. Len, "Investigation of patch antennas based on embedded multiple PBG structure," *IEEE Photonics Technology Letters*, Vol. 20, No. 20, October 15, 2008.
3. Yeap, S. B. and Z. N. Chen, "Microstrip patch antennas with enhanced gain by partial substrate removal," *IEEE Transactions on Antennas and Propagation*, Vol. 58, No. 9, September 2010.

Session 4A5
Optics, Fiber Optics, Laser

Non-spatial Filtering for Laser Beams with Volume Bragg Grating in Photo-Thermo-Refractive Glass

Xiang Zhang[1], **Jiansheng Feng**[1], **Shang Wu**[2], **Baoxing Xiong**[2], **and Keming Jiang**[2]

[1]Wuhan National Laboratory for Optoelectronics, School of Optoelectronic Science and Engineering
Huazhong University of Science and Technology, Wuhan 430074, China
[2]Key Lab of Modern Optical Technologies of Jiangsu Province, Institute of Modern Optical Technologies
Soochow University, Suzhou, Jiangsu 215006, China

Abstract— Traditional filter consisting of lenses and a pinhole on the focus of the lenses has limitations for high power lasers. The angular filtering with the selectivity of volume Bragg grating (VBGs) is the other method for improving the near field distribution of laser beams. The design and evaluation methods of angular filters are investigated in this paper. According to the coupled wave theory, the variation of the peak diffraction efficiency and full width at first zero (FWFZ) with respect to different grating parameters, such as thickness, grating period, refractive index modulation or tile angle of grating vector, is analyzed. The product of thickness and refractive index modulation makes the periodic variation of peak diffraction efficiency, which varies with the incident wavelength. While the grating period is less than a specific value (0.4 μm in this paper), the peak diffraction efficiency reduced sharply. The FWFZ increases linearly with the addition of grating period, but reduces with the addition of thickness. The FWFZ reaches the minimum when the tilt angle of grating vector is 90 deg.

The required angular filters for different laser wavelength, such as 532 nm, 632.8 nm or 1064 nm, are also investigated. If well designed, a high diffraction efficiency of 99% and required angular selectivity of ≤ 1 mrad for the above wavelengths are obtained. With an error tolerance analysis, it shows that the thickness and refractive index modulation on VBGs play a principal influence in the preparation of angular filters compared with grating period and tilt angle grating vector.

A demonstration experiment is performed with the VBG with thickness of 2.5 mm, period of 0.96 μm and tilt angle of 0.03 deg. The cutoff frequency of 1 mm^{-1}, diffraction efficiency of $\sim 97\%$ is obtained, and the results coincide well with the simulation.

Simulation of Chirped Volume Bragg Grating with a Partition-integration Method

Jiansheng Feng[1], **Xiao Yuan**[1, 2], **Xiang Zhang**[1], **Shang Wu**[2], **Kuaisheng Zou**[2], **and Guiju Zhang**[2]

[1]Wuhan National Laboratory for Optoelectronics, School of Optoelectronic Science and Engineering Huazhong University of Science and Technology, Wuhan, Hubei 430074, China
[2]Institute of Modern Optical Technologies and Key Lab of Modern Optical Technologies of Jiangsu Province, Soochow University, Suzhou, Jiangsu 215006, China

Abstract— Ultrashort laser pulses obtained by pulse compression are widely used in the various fields of science, spectroscopy, communication techniques and material processing. Pulse compression and stretching could be obtained with dispersive elements, such as surface gratings, prism pairs etc. The chirped volume Bragg gratings (CVBGs) maybe another effective method due to its simple configuration, easy alignment and high damage threshold. To analyze the characteristics with CVBGs, a partition-integration method is proposed and used to study the group dispersion, bandwidth and contrast of the compressed pulse. In this theory, the CVBG is divided into short segments, in which each segment the gratings are assumed to be uniform and no spatial chirp which could be characterized with a matrix based on Kegolnik' theory. With this approach, the frequency response and dispersion property are simulated and show an interesting relationship with the thickness and refractive index modulation of grating. As the increase of thickness and refractive index modulation, the peak diffraction efficiency approaches 100% monotonically, but the ripples on the linear group delay uprise. It is a tradeoff between the high diffraction efficiency and rare dispersion ripple.

Ultrashort pulse compression and stretching with CVBGs are also investigated in this paper. By inserting or removing the chirp, the well designed CVBGs could even compress a linear chirped pulse into the Fourier-transform-limited (FTL) pulse or stretch a FTL pulse into a pulse with arbitrary duration. The ratio of compression and stretching only depend on the thickness once the material of CVBGs is chosen. The simulation show that the range of compression could be from hundreds of picoseconds to tens of femtoseconds.

Polarization Properties of Transmitting Volume Bragg Gratings in Photo-thermo-refractive Glass

Shang Wu[1], **Xiao Yuan**[1], **Xiang Zhang**[1, 2], **Jiansheng Feng**[2], **Kuaisheng Zou**[1], **and Guiju Zhang**[1]

[1]Key Lab of Modern Optical Technologies, Institute of Modern Optical Technologies
Soochow University, Suzhou, Jiangsu 215006, China
[2]Wuhan National Laboratory for Optoelectronics, School of Optoelectronic Science and Engineering
Huazhong University of Science and Technology, Wuhan 430074, China

Abstract— The diffraction characteristics of transmitting volume Bragg gratings are important for applications in angular filtering and efficient laser beam propagation. In this paper, a series of experiments are performed to investigate the polarization properties of transmitting volume Bragg gratings (TBGs) recorded in photo-thermo-refractive glass. It is shown that the polarization states of source beam are not affected through TBGs. Both linear and elliptical polarizations are investigated. The peak diffraction efficiency and angular selectivity of these phase volume gratings are shown independent on the polarization states of source beam, which obeys the predictions of Kogelnik's coupled wave analysis that accounts for plane wave monochromatic illumination.

A series experiments are designed to study the polarization properties of TBGs with the degrees of polarization of source beam decreasing. Under a certain degree of polarization, the polarization states of source beam are changed after diffracted by TBGs, the diffraction efficiency and angular selectivity of TBGs are no longer independent on the incident beam polarization consequently. Rigorous coupled-wave analysis is applied to interpret the experimental results.

Coupled wave analysis is the most widely applied theory while modeling the diffraction properties of TBGs, yet there are no systematic experimental researches reported to verify Kogelnik's hypothesis concerning polarized incident beams before. The study about polarization properties of TBGs can be used for reference in the field of spatial filtering, for certain polarization state beams are needed in the operation of some high power laser systems.

Optical Fiber System for Wavelength Calibration in Next Generation Giant Astronomical Telescopes

Jinping He[1] and Dong Xiao[2]

[1]National Astronomical Observatories, Nanjing Institute of Astronomical Optics & Technology
Chinese Academy of Sciences, Nanjing 210042, China
[2]Key Laboratory of Astronomical Optics & Technology
Nanjing Institute of Astronomical Optics & Technology, Chinese Academy of Sciences
Nanjing, 210042, China

Abstract— In the next decade, several giant astronomical telescopes whose apertures range from 30 m to 40 m would be in operation. Each telescope would equip with high resolution spectrograph. In order to hunt earth-like extrasolar planet, the precision for radial velocity measurement has to achieve cm/s precision. Emerging as a suitable calibration source, laser frequency comb technique could satisfy these harsh requirements of the measurement. To incorporate the laser frequency comb with the high resolution spectrograph, a optical fiber system would deliver the calibration light from the laser frequency comb to the high resolution spectrograph. As the laser frequency comb would have a octave span of wavelength coverage, a broadband optic coupling system with minimum transmission loss would be critical for the connection between the laser frequency comb and optical fiber system. For the optical fiber system, mode scrambling techniques also need to be investigated since the technique would improve the ability of the instrument to obtain the radial velocity information. Since the focal ratio degradation exist in the fiber system, the design of the optical coupling system between the fiber system and the high resolution spectrograph would try to relief such degradation. Above all, environment factor, such as temperature, air pressure and humidity, also need to be taken into serious consideration, while the radial velocity measurement approach cm/s precision.

High Time Resolution Fiber Laser Source with the Tunable Pulse Duration

Shiwei Wang, **Maoqing Liu**, **and Jianqiu Xu**
Key Laboratory for Laser plasmas and Physics Department, Shanghai Jiaotong University, China

Abstract— We report a novel high time resolution fiber laser source with the tunable pulse duration and its application to exactly measurement. Just as a spatial lens can expand or focus a beam in space, so can a time-lens broaden or compress a pulse in time. In the pulse generation setup, placing a time-lens in a loop, we maximize the efficiency of bandwidth generation by using one time-lens driven at low power to emulate a stack of many lenses. Besides, the electro-optic chirping compression method with the electro-optic phase modulator featuring lens modulation is applicable to the negative group delay dispersion as well as positive group delay dispersion. Furthermore, the system is compact, all fiber, and allowed large tuning of the repetition rate and continuous tuning of the pulse width and center wavelength. The stable pulse can be obtained from the above system. With a detector, the system can successfully send out a series of pulse and collect directly the reflect laser beam from the moving surface, therefore, the pulse can be used to measure the distance and the velocity. Moreover, the deviation can be limited to the order of ps. In our experiment, pulse is generated from a continuous wave laser without mode locking and centered at 1053 nm. The optic switch is biased and switched by two marker signals (square pulses) from the AWG and the control signal's synchronization accuracy can be controlled at 20 ps. In other words, we can get a higher resolution measurement with this way.

Anomalous Transmission Properties of epsilon-near-zero Metamaterials

Jie Luo, **Huanyang Chen**, **Yun Lai**, **Ping Xu**, **and Lei Gao**
Jiangsu Key Laboratory of Thin Films, Department of Physics
Soochow University, Suzhou 215006, China

Abstract— We investigate in detail the anomalous transmission properties of epsilon-near-zero metamaterials. When coated defects are embedded in the ENZ metamaterials, the behaviors of total transmission and total reflection can be realized. The finding is that thin coatings of the defects can dramatically change the transmission behaviors. The permittivity differences of dielectric shells for total reflections and transmissions in the INZ or ENZ metamaterial could be very small, implying potential applications, such as ultrasensitive sensors and switches.

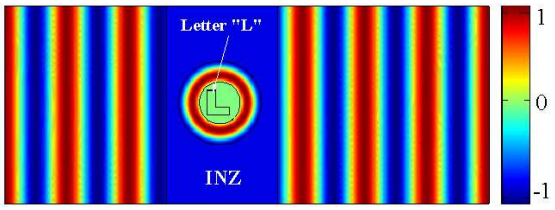

Figure 1: The magnetic field distribution of the INZ metamaterial waveguide with a coated PMC defect, and a letter "L" made of air is put inside the PMC.

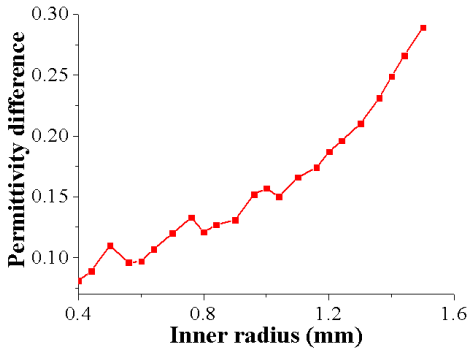

Figure 2: The relationship between the inner radius of the PMC core and the permittivity difference.

REFERENCES

1. Hao, J., W. Yan, and M. Qiu, "Super-reflection and cloaking based on zero index metamaterial," *Appl. Phys. Lett.*, Vol. 96, 101109, 2010.
2. Nguyen, V. C., L. Chen, and K. Halterman, "Total transmission and total reflection by zero index metamaterials with defects," *Phys. Rev. Lett.*, Vol. 105, 233908, 2010.
3. Xu, Y. and H. Chen, "Total reflection and transmission by epsilon-near-zero metamaterials with defects," *Appl. Phys. Lett.*, Vol. 98, 113501, 2011.
4. Luo, J., P. Xu, L. Gao, Y. Lai, and H. Chen, "Manipulate the transmissions using index-near-zero or epsilon-near-zero metamaterials with coated defects," Submitted.

Polymer Laser Based on Actively Waveguide Grating Structures

Tianrui Zhai and Xinping Zhang
Institute of Information Photonics Technology and College of Applied Sciences
Beijing University of Technology, Beijing 100124, China

Abstract— The actively waveguide grating structures (AWGS) are demonstrated as distributed feedback (DFB) configurations for polymer lasers. The thin film of a typical light-emitting polymer poly [(9,9-dioctylfluorenyl-2,7-diyl)-alt-co-(1,4-benzo-{2,1',3} -thiadiazole)] acts both as the gain medium and as the waveguide. The polymer film can be made by spinning the polymeric semiconductor poly onto a silica substrate, and then the grating can be fabricated on top of the polymer film through interference lithography. A number of advantages of the AWGS over the conventional DFB configurations are illustrated by theoretical analysis and experimental verifications. Theoretical analysis indicate that the advantages of the AWGS for the polymer lasers lies the following aspects: (1) High-quality thin film of the active materials is produced without being modulated by the grating structures, which ensures high-quality transverse mode and narrow linewidth of the laser emission. (2) The AWGS configuration facilitates stronger confinement and much better oscillating modes than those based on the active layer on top of a Bragg grating or on the Bragg grating written into the active materials. More importantly, this AWGS is insensitive to the defects or inhomogeneity in the grating structures; (3) The AWGS configuration enables the most efficient utilization of the active volume. (4) Both the thickness of the active waveguide and the period of the grating structures can be controlled precisely and independently. This enables more quantitative evaluation and understanding of the laser actions. Experimental results show that the pump threshold of our proposed polymer laser based on AWGS is 115 $\mu J/cm^2$ and the laser emission is centered at 563.8 nm with a linewidth smaller than 0.5 nm. Furthermore, this kind of AWGS configuration offers a promising route to achieve electrically pumped polymer lasers.

Extrahigh Color Rendering Color Temperature Tunable White Light LED Cluster with Warm-white Red Green Blue LEDs

G. X. He[1], **J. Xu**[1], **and H. F. Yan**[2]

[1]Department of Applied Physics, Dong Hua University, 1882 Yan'an Road (W), Shanghai 200051, China
[2]Shanghai Yaming Lighting Co., Ltd., 1001 Jiaxin Road, Jiading District, Shanghai 201801, China

Abstract— The realization of correlated color temerature (CCT) tunable white sources with a combination of high color rendering index (CRI) and the special CRI of R9 for strong red is an important challenge in the field of solid-state lighting. The CCT tunable WW/R/G/B LED cluster with extrahigh color rendering has been found by simulation analysis, which consists of three WW LEDs (excited wavelengh $\lambda_o = 450.5\,\text{nm}$, CCT $= 3183\,\text{K}$, $\Phi = 62.1\,\text{lm}$, $P_{in} = 1.15\,\text{W}$, and $\eta = 53.9\,\text{lm/W}$ at $I_F = 350\,\text{mA}$), one red LED ($\lambda_o = 634.1\,\text{nm}$, $\Phi = 34.4\,\text{lm}$, and $P_{in} = 0.83\,\text{W}$ at $I_F = 350\,\text{mA}$), one green LED ($\lambda_o = 513.9\,\text{nm}$, $\Phi = 41.0\,\text{lm}$, and $P_{in} = 1.24\,\text{W}$ at $I_F = 350\,\text{mA}$), and one blue LED ($\lambda_o = 456.2\,\text{nm}$, $\Phi = 10.2\,\text{lm}$, and $P_{in} = 1.18\,\text{W}$ at $I_F = 350\,\text{mA}$). The predicted and measured results of WW/R/G/B LED cluster at an ambient temperature (T_a) of 45°C are shown in Table 1.

Table 1: The predicted and measured results of the WW/R/G/B LED cluster at $T_a = 45°\text{C}$.

Predicted results	CCT (K)	2703	2952	3431	3922	4490	4976	5715	6547
	$\text{dC} \times 10^{-3}$	+1.2	+1.6	−0.9	−2.6	−4.9	−5.2	−3.0	−3.3
	CRI	93	93	94	95	96	96	96	95
	R9	94	88	90	93	98	98	94	91
	R (9–12)	85	82	84	84	86	85	86	85
	Φ (lm)	173.7	173.5	172.2	169.2	166.4	163.3	159.2	155.0
	η (lm/W)	57.9	57.9	56.2	54.4	52.4	50.9	48.9	47.1
Measured results	CCT (K)	2719	3028	3458	3983	4537	5008	5723	6497
	$\text{dC} \times 10^{-3}$	−1.1	−2.6	−3.6	−4.5	−4.7	−5.4	−4.6	−4.9
	CRI	93	93	94	94	95	94	94	94
	R9	90	94	92	95	96	95	96	93
	R (9–12)	84	85	83	84	85	85	84	83
	Φ (lm)	170.5	166.3	174.8	169.5	163.0	162.7	156.0	151.9
	η (lm/W)	56.8	55.8	56.9	56.4	51.9	50.9	48.5	46.8

Spectral Optimization of Warm-white LED with Red LED Instead of Red Phosphor under Conditions of CRI $\geqslant$ 90 and R9 $\geqslant$ 90

G. X. He[1], **J. Xu**[1], **and H. F. Yan**[2]

[1]Department of Applied Physics, Dong Hua University, 1882 Yan'an Road (W), Shanghai 200051, China
[2]Shanghai Yaming Lighting Co., Ltd., 1001 Jiaxin Road, Jiading District, Shanghai 201801, China

Abstract— We proposed a model for spectra of white-light LED consisting of red LED and phosphor-coated white LED (p-W LED) with blue LED die, green phosphor and orange phosphor. The optimal spectra of the p-W LED and the red LED, as well as the warm-white LED (WWLED) with CCT = 2700 K have been found by nonlinear program for maximizing the luminous efficacy of radiation (LER) while both color rendering index (CRI) and special CRI R9 for strong red above 90. Optimal peak wavelengths of red LED, blue LED die, silicate green and orange phosphors are 626 nm, 454 nm, 535 nm and 584 nm, respectively. Their optimal relative radiation fluxs are 30.8%, 9.7%, 33.4% and 26.1%, respectively. The CCT and chromaticity coordinates (u, v) of the p-W LED are 4599 K and (0.1854, 0.3593), respectively. The simulation results show that the optimal WWLED could realize white-light with CRI = 92, R9 = 90, R(9-12) = 88 as well as LER = 343.6 lm/W at CCT of 2700 K. The p-W LED (CCT = 4579 K, Φ = 96.5 lm, P_{in} = 1.10 W, and LE = 87.7 lm/W at I_F = 350 mA) with a InGaN blue LED die (451.6 nm), 56% silicate green (535 nm) and 44% orange (584 nm) phosphors, and the AlGaInP red LED (627.2 nm, Φ = 44.2 lm, and P_{in} = 0.74 W at I_F = 350 mA) are fabricated and measured at an ambient temperature (Ta) of 45°C. The experimental results show that the real WWLED can realize the warm-white-light with CCT = 2653 K, CRI = 90.4, R9 = 93.7 and R(9-12) = 88.3, LER = 340.7 lm/W as well as LE (luminous efficacy) = 80.2 lm/W. Furthermore, the WWLED can realized CCT tunable warm-white light with CRIs of 86 $\sim$ 93, R9s of 86 $\sim$ 95 and LEs of 78.2 $\sim$ 80.3 lm/W at CCTs of 2392 K to 3014 K by adjusting drive current of red LED. The luminous efficacy of the WWLED with extrahigh color rendering properties will rise to about 114 lm/W if the p-W LED with LE of 125 lm/W is used.

Design of an All-optical Controllable Switch Using Dipole Induced Transparency (DIT)

K. Abbasian[1], **K. Eftekhari**[2], **and A. Rostami**[1]

[1]School of Engineering-Emerging Technologies, University of Tabriz, Tabriz 51666, Iran
[2]Technical & Engineering University of Bonab, Province of East Azarbaijan, Iran

Abstract— In this paper, we have proposed an all-optical controllable switch with ultrahigh speed by using dipole induced transparency effect applied on 5-level nanocrystal doped in photonic crystal (PC) cavity. By applying the third control field the PC cavity, comprising 5-level nanocrystal , has been converted to transparent one and switching operation has been occurred. Then by applying the second or first control field, the transparent PC cavity has been changed to opaque one again. However, applying both of the second and the first control field simultaneously can change the opaque PC cavity to transparent medium again. Analytical relation of this all optical switch has been presented and investigated in different situations parameters on switching characteristics.

Session 4A6
High Power Electromagnetics (HPE) & Electromagnetic Pulse (EMP)

System-level Susceptibility Analysis for Intentional EMI Based on Bayesian Networks

Congguang Mao, **Hui Zhou**, **Zhitong Cui**, **Aibin Zhai**, **and Beiyun Sun**
Northwest Institute of Nuclear Technology, Xi'an 710024, China

Abstract— It has been validated that the high-power electromagnetic environments can cause the electronic or electrical systems permanent damages or functional upsets. So the protection or hardening of the critical infrastructures has attracted more attentions of the governments and scientists [1]. The system-level assessment and investigation is very necessary to find the susceptible elements and diagnosis the fault modes and effects induced by the environmental electromagnetic interferences. A special IEC standard for the assessment has been published in July 2009 [2]. And according to the assessment activities and concepts [3], the Bayesian Networks (BN) is introduced to resolve the complex systematic problem, and the modeling method is presented [4]. In this paper the system susceptibility analysis processes will be discussed in details. Different from the fault tree analysis (FTA), a traditional reliability tool, the items of the electromagnetic environments are directly included in the BN structural functions. The definite engineering meaning of this new coefficient, together with the other common parameters such as probabilistic and critical impedance, is illuminated. Thus the modeling and analysis make up of a relatively whole procedure of the assessment, and can provide the guideline to the system-level tests and protection designs for the intentional EMI.

REFERENCES

1. Radasky, W. A., C. E. Baum, and M. W. Wik, "Introduction to the special issue on high-power electromagnetics (HPEM) and intentional electromagnetic interference (IEMI)," *IEEE Trans. on Electromagn. Compat.*, Vol. 46, 314–321, August 2004.
2. IEC/TS 61000-5-9, "System-level susceptibility assessments for HEMP and HPEM," July 2009.
3. Mao, C. and H. Zhou, "Bayesian networks modeling in system-level susceptibility assessments for intentional EMI," *Proceedings of the Ninth International Electromagnetic Compatibility Symposium*, Wroclaw, Poland, September 2010.
4. Mao, C., H. Zhou, J. Fu, B. Sun, and H. Yu, "Introduction to the system-level susceptibility assessments for HEMP and HPEM," *PIERS Proceedings*, 1746–1750, Beijing, China, March 23–27, 2009.

Time Domain Analysis of Nonlinear Load Terminated in Shielded Cable

Yinghui Zhou, **Lihua Shi**, **and Liyuan Su**
EMC Lab, PLA University of Science and Technology, China

Abstract— The nonlinear loads is often used to protect devices connected in cables. Most of theory analysis to the nonlinear loads is modeled by the Pspice software. In this paper, the authors creat a model to analyze the induced current and induced voltage in the terminated nonlinear load.

Firstly, the digital filtering technique is combined with the FDTD method and the induced voltage and induced current in the shielded layer are obtained under the external electromagnetic field.

Then, transfer impedance of the shielded cable will be measured and the induced voltage and induced current in the core line can be calculated.

Again, according to the relative international standard, the nonlinear device testing system is built and its response characters can be measured.

Finally, introducing the nonlinear device response character (U-R relation) to the proposed time domain calculation model, the induced voltage and induced current in the nonlinear load will be obtained under the external injected electromagnetic field.

By the proposed calculation and measurement system, the induced voltage and induced current can be acquired respectively. Then, combining the measured data, the protection effect of the nonlinear load to device terminated in shielded cable against the external electromagnetic field can be analyzed validly.

Research on High Voltage Electrostatic Discharge to EED and Fuze

Tuan Zhao, **Lixia Wang**, **Qingmei Feng**, **Hongzhi Yao**, **and Xiangfei Ji**
State key Laboratory of Applied Physics-Chemistry
Shaanxi Applied Physics-Chemistry Research Institute, Xi'an 710061,China

Abstract— EEDs (the electric explosive devices) are not only absolutely necessary igniting and blasting components in special power sources, but also the most dangerous and susceptive subsystems in weapon systems. The safety and reliability of whole weapon's system are directly decided by the safety and the reliability of EED. The research on anti-electrostatic technology of EED is in the demand of development of science and technology of military affairs, and is the important part of improving safety and the reliability of weapon system.

According to the requirement of MIL-STD-331B, the testing equipment of 300 kV electrostatic discharge of aerial supply to fuze's system including EED, with maximal voltage of 300 kV, capacitance of 1000pF and maximal resistance of 1 Ω, was successfully manufactured. The configuration of this equipment is shown in Fig. 1. The waveform of test result on 100 Ω calibrated resistance is shown in Fig. 2.

Using the high voltage electrostatic discharge system, the fuze (contained EED) and EED in the case of pin-pin and pin-case was tested to evaluate the safety and the reliability. The research results will be shown in the full version of this article.

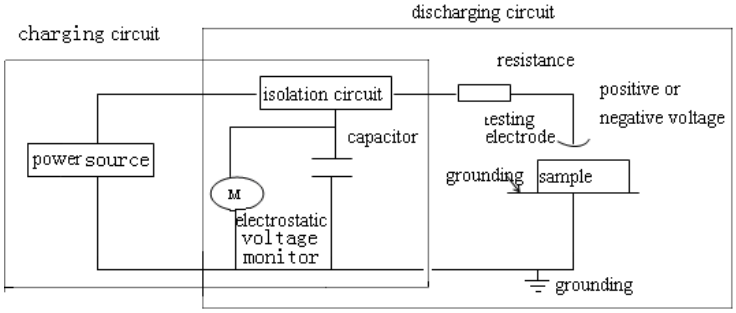

Figure 1: The configuration of high voltage electrostatic discharge test system on EED and fuze.

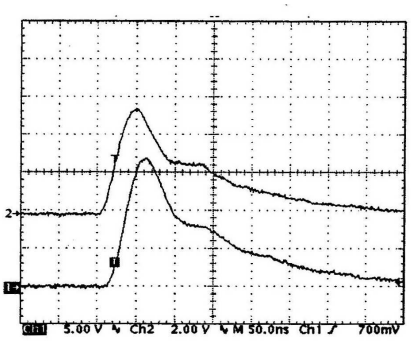

Figure 2: Current and voltage waveforms of calibrated resistance with capacitor charged valtage of 300 kV, channel 1 is current waveform; channel 2 is voltage waveform.

Analytic Solution of Electromagnetic Pulse (EMP) Coupling to Multiconductor Transmission Lines

Yan-Zhao Xie, Hui Xiang, and Dong-Yang Sun
Northwest Institute of Nuclear Technology, P. O. Box 69-10, Xi'an, China

Abstract— This paper aims to extend the DARIT theory to the field of EMI coupling to MTL. Figure 1 shows the concise principle of iterative procedures. The diagram of Iteration 1 is shown in Figure 1(a). At this iteration, there are no coupling effects due to the neighboring line since the initial states of the lines are zeros. The only exciting source is from the illuminating EM wave.

$$\frac{dv_j^{(1)}(x,s)}{dx} + z'_{jj}(s)i_j^{(1)}(x,s) = V'_j(x,s),$$
$$\frac{di_j^{(1)}(x,s)}{dx} + y'_{jj}(s)v_j^{(1)}(x,s) = I'_j(x,s).$$

$V'_J(x,s)$ and $I'_j(x,s)$ are the source terms which detailed expressions depending upon the coupling model used. Note that they are the general source terms at each iteration due to the incoming EM wave.

The diagram of Iteration 2 is shown in Figure 1(b). The formulation in this step could be expressed by

$$\frac{dv_k^{(2)}(x)}{dx} + z'_{kk}i_k^{(2)}(x) = -\sum_{\substack{j=1\\ j\neq k}}^{N} z'_{kj}i_j^{(1)}(x) + V'_k(x),$$
$$\frac{di_k^{(2)}(x)}{dx} + y'_{kk}v_k^{(2)}(x) = -\sum_{\substack{j=1\\ j\neq k}}^{N} y'_{kj}v_j^{(1)}(x) + I'_k(x).$$

The summation terms in the right side of the above equations are the neighboring effects due to the coupling of the adjacent lines. Since this iteration, the exciting sources include two terms as shown, the updated terms due to the adjacent lines and the general terms due to the incoming EMI.

Similarly, we can derive the formulation after Iteration 2. The corresponding diagram is shown in Figure 1(c). Generally, the satisfactory solution could be obtained after only 3 iterations since most practical MTLs belong to weak coupling cases, otherwise the crosstalk signal would be too much serious.

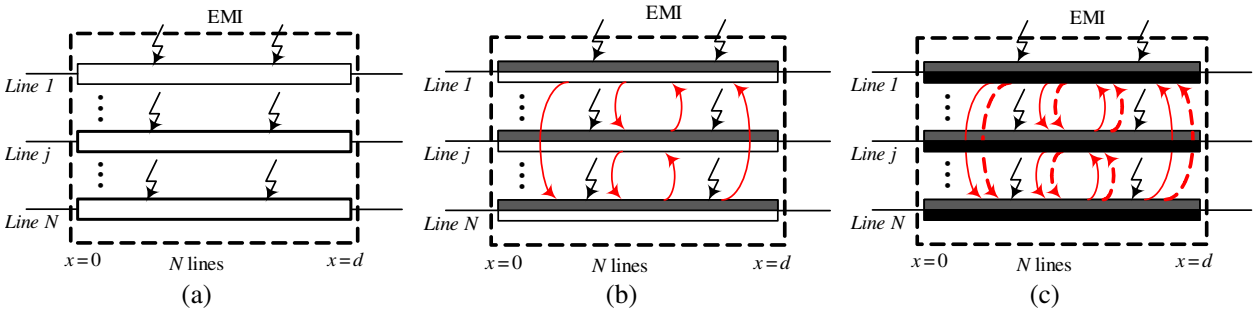

Figure 1: The diagrams of 1, 2, and more iterations of proposed method for EMI coupling. (a) 1-iteration, (b) 2-iteration, (c) 3-, and more iterations.

A Method for Assessing EED against HPEM

Hong-Zhi Yao[1, 2], **Qing-Mei Feng**[1, 2], **Tuan Zhao**[1, 2], **and Xiang-Fei Ji**[1, 2]

[1]Science and Technology on Applied Physical Chemistry Laboratory, Xi'an 710061, China
[2]Shaanxi Applied Physics-Chemistry Research Institute, Xi'an 710061, China

Abstract— The methods used for assessing HERO(hazards of electromagnetic radiation to ordnance) and the measurement method for the induced energy or current about EED which located in special electromagnetic radiation environment were discussed in this paper. The infrared fiber optical temperature sensor is suitable for the measurement of induced current caused by high power electromagnetic radiation on electro-explosive device (EED) since the transmission link of the sensor is infrared optical fiber which is immune to electromagnetic radiation. To overcome the limited measurement rate, radiative temperature measurement techniques seem most promising. This paper investigates the application of an infrared mercury-cadmium-telluride (MCT) based on radiation thermometer within a high-power electromagnetic (HPEM) environment in order to measure induced EED energy and to determine EED's safety. According to the test requirement, the temperature range of the senor should be between 50° to 2000°. The response time of the MCT detector should be less than 1ms. The InSb detector is even faster because of its smaller edge length of 100 mm compared to 250 mm for the MCT detector. However, the MCT is the preferable detector because its maximum spectral response is shifted to higher wavelengths. This makes the detector more sensitive for lower temperature. The experimental results using the infrared sensor suggest that the measurement of bridge-wire temperature caused by induced current is satisfactory, which would be a reliable and improved method for evaluating the susceptibility of EED to HPEM.

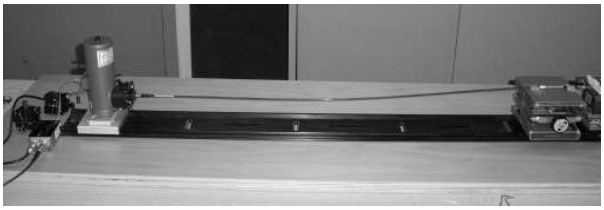

Figure 1: Photo of test system.

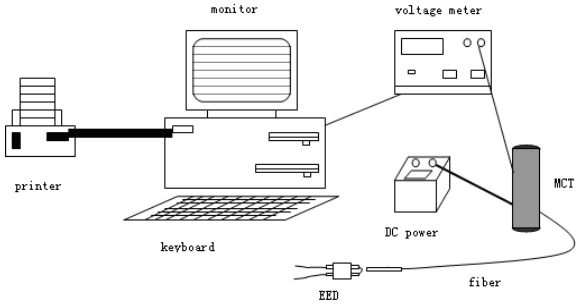

Figure 2: Configuration of test system.

Measurement of the Shielding Effectiveness of Connector by Improved Triaxial Method

Qi Zhang, **Li-Hua Shi**, **Ying Hui Zhou**, **Cheng Gao**, **and Yong Chao Guo**
Engineering Institute of Engineering Corps, PLA, University of Science & Technology
Nanjing, Jiangsu 210007, China

Abstract— Protection of electronic system from high intensity radio frequency(HIRF) interferences receives more and more attention in avionic systems. Shielding effectiveness (SE) is an important parameter that describes the electromagnetic protection ability of cable shields. In the design of electronic system in flights, it is required to compare the shielding property of different kinds of cable connectors. A triaxial test fixture for measuring SE of cable connectors is designed according to IEC 62153-4-7. Compared to the most commonly used test fixtures, this fixture is designed to eliminate the influence of cable shields and bonding condition at cable ends on SE of the connector under test. Therefore the material property and the manufacturing quality of the connector itself can be evaluated. Two kinds of connectors made of aluminum alloy and metal composite, respectively, are tested and compare by using the established triaxial test fixture. Test results show that the SE curve of the two connector are very close to each other (the red and light blue ones, in Fig. 1) if the cable influence is not eliminated, and the quality of connectors can not be identified clearly. By using the newly designed test fixture, the difference of the connector can be found (the blue and black ones, in Fig. 1). It is proved that the test fixture designed in this paper can be used as a good approach for selection of cable connectors.

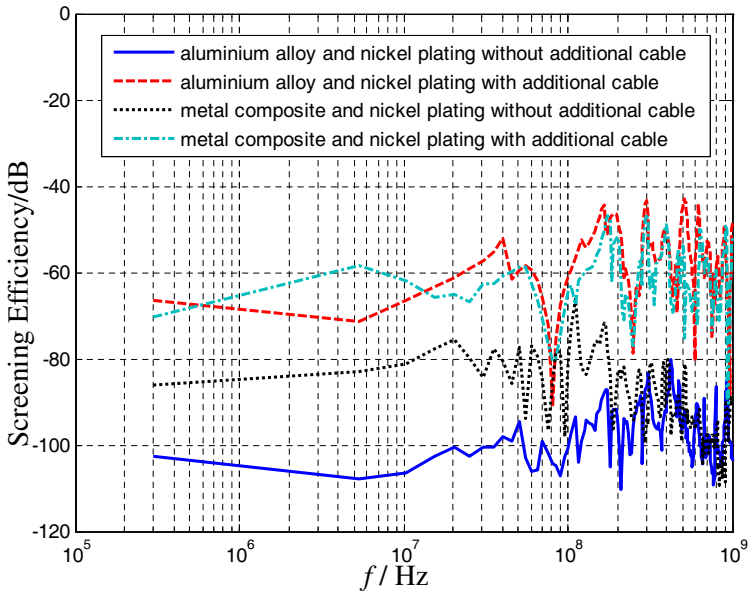

Figure 1: Measurement SE of two connectors.

A Small-sized Fast Rise Time HEMP Simulator

Yanxin Li, **Qiwu Wang**, **Lihua Shi**, **Cheng Gao**, **Feng Lu**, **and Bihua Zhou**
Nanjing Engineering Institute, No. 1 Haifuxiang, Nanjing, Jiangsu 210007, China

Abstract— Nowadays, HEMP simulator is widely studied. In reference [1], a portable pulse electric field shielding effectiveness measurement device, which can be used in fieldwork, is designed. But the pulse electric field simulator of the device can not meet the requirement of the MIL-STD-461E or IEC61000-2-9 specification. Because the rise time of the device is 4nslower than 2.5 ns of the specification. In this paper, a small-sized fast rise time HEMP simulator is designed. The structure of the small-sized fast rise time HEMP simulator is made of four components, including automatic high voltage source, pulse generator, antenna and match load, showed in Fig1. The automatic high voltage source produces high direct current voltage for the pulse generator automatically, and can control the discharge procedure. The structure of the pulse generator is showed in Fig. 2. The circuit diagram of the simulator is showed in Fig. 3. Through replacing the traditional gas by refined rapeseed oil in the discharge switch, a moving electrode reduces the inductance of the discharge circuit. Therefore, the rise time of the pulse is more fast, up to 2 ns. A microcomputer(MPU) controls the charge procedure and monitors the charge voltage. If the voltage reaches the presented level, the MPU instructs the electromagnet to move, and then the upper electrode is pushed to the nether electrode, so the high voltage pulse capacitor discharge. Because no gas control circuit is need, the structure of the simulator is simpled.

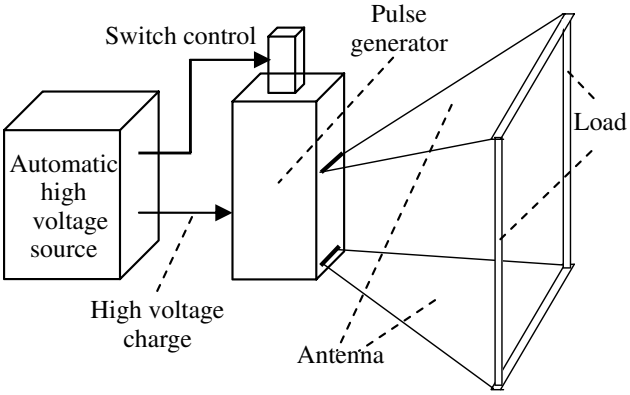

Figure 1: The structure of the small-sized fast rise time HEMP simulator.

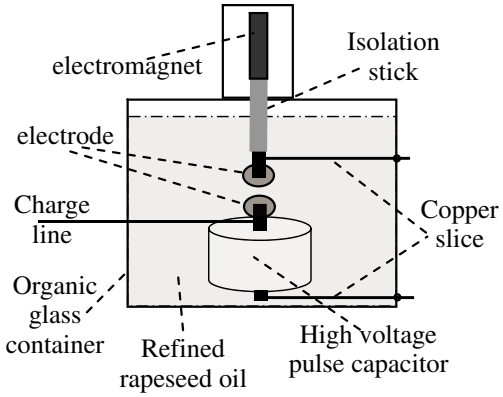

Figure 2: The structure of the pulse generator.

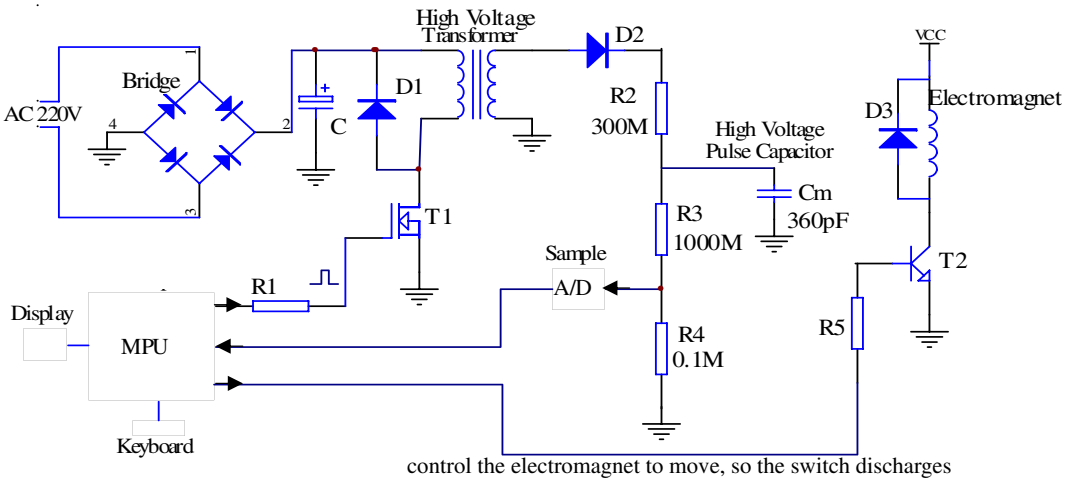

Figure 3: The circuit diagram of the simulator.

REFERENCES

1. Lu, F., B. Chen, H. Wan, and B. Zhou, "Portable electric field shielding effectiveness measurement device," *High Voltage Technology*, Vol. 32, No. 8, 49–51, 87, 2006.

Coupling Energy Analysis and Calculation of HEMP on EED

Xiangfei Ji, **Qingmei Feng**, **Tuan Zhao**, **and Hongzhi Yao**
Science and Technology on Applied Physical Chemistry Laboratory
Shaanxi Applied Physics-Chemistry Research Institute, Xi'an, Shannxi 710061, China

Abstract— In order to analyze the impact of HEMP on EED, the energy distribution of HEMP at different frequency bands and the coupling energy of HEMP on EED should be studied firstly. In this paper, the effective aperture of the antenna and electromagnetic hazards analysis were used to calculate the coupling energy of HEMP on EED.

The configuration of opening foot lines style of EED is equivalent to the dipole antenna model to some extent. In terms of the length of EED feet, the resonant frequency and the antenna bandwidth could be determined. High-altitude electromagnetic pulse (HEMP) is generally expressed as a double exponential function,

$$E(t) = E_0 k(e^{-\alpha t} - e^{-\beta t}),$$

where E_0 is the peak electric field strength, k is the correction factor, α, β are the parameter of the pulse trailing edge and the pulse leading edge, respectively. $E(f)$ is obtained by Fourier transform, Spectral density $S(f) = \frac{2|E(f)|^2}{Z_0}$. According to the antenna bandwidth, W — the coupling energy of HEMP on EED can be obtained by integrating spectral density HEMP over the frequency band of interest,

$$W = \int_{f1}^{f2} S(f) A_e df.$$

The calculated results (theoretical value) were compared to the experimental results (test value), as shown in Table 1.

Table 1: Comparison of the test value and the theoretical value.

EED foot length (cm)	Bell waveform			MIL-STD-461E waveform		
	Electric field strength (V/m)	coupling energy (J)		Electric field strength (V/m)	coupling energy (J)	
		Test value	Theoretical value		Test value	Theoretical value
90	4×10^4	$10^{-6} \sim 10^{-5}$	1.3×10^{-5}	4×10^4	$10^{-6} \sim 10^{-5}$	1.9×10^{-5}
	4.7×10^4		9.6×10^{-6}	4.7×10^4		2.6×10^{-5}
200	4×10^4	10^{-4}	3.1×10^{-4}	4×10^4	10^{-4}	5.1×10^{-4}
	4.7×10^4		4.3×10^{-4}	4.7×10^4		7.3×10^{-4}

We can see from the table, the test results and theoretical calculation results are basically at the same magnitude, indicating that the theoretical analysis model is reasonable. This method can be used to estimate the effects of different nuclear electromagnetic pulse field strength on EED.

A Multi-step Electromagnetic Topology Method to Compute the Coupling of External Electromagnetic Fields and Inner Wires of a Cavity through Apertures

Guyan Ni, **Ying Li**, **and Jianshu Luo**
Department of Mathematics and System Science, College of Science
National University of Defense Technology, Changsha, Hunan 410073, China

Abstract— In this paper, we introduce a multi-step electromagnetic topology (EMT) method to analyze interactions of external EM fields and inner wires of a cavity through apertures. The method involves three basic steps. The first step obtains an interaction sequence diagram to analyze the interaction processes for the electromagnetic coupling. The second step obtains different models to compute parameters of each junction in the diagram. For instance, based on the equivalence principle, we will use a semi-analytical approach based on the Modal Green Function and the method of moment (MoM) to compute an equivalent source for the aperture and employe Baum-Liu-Tesche (BLT) equations and Agrawal's or Taylor's formulations to calculate the coupling of field-to-wire. The last step calculates all junctions' parameters. We use above models to compute each junction's parameters from one junction to the next according the interaction sequence diagram. By multi-step iteration the coupling computation is finished. Compared with the traditional EMT theory, the new method has a remarkable change that is not need to compute a scattering supermatrix. Numeric results confirm the validity of the method.

ACKNOWLEDGMENT

This work was supported by China Postdoctoral Special Science Foundation (No. 200902662), the National Natural Science Foundation of China (No. 10871231), and Pre-research Foundation of Weapon and Equipment (No. 9140A31020609KG0170).

Session 4P2a
Defected Ground Structure (DGS) and Its Applications

A Miniaturized Low Pass Filter Using Common Defected Ground Structures

Jun Lee[1], **Jaehoon Lee**[1], **Jongsik Lim**[1], **Yongchae Jeong**[2], **Sang-Min Han**[1], **and Dal Ahn**[1]

[1]Soonchunhyang University, Republic of Korea
[2]Chonbuk National University, Republic of Korea

Abstract— A new design method for a miniaturized low pass filter (LPF) for microwave frequency region using a common defected ground structure (CDGS) is described in this paper. As has been widely known already, defected ground structures (DGS) are etched patterns on the ground plane around transmission lines such as microstrip and coplanar waveguide. The representative geometry of DGS is dumb-bell shape, as shown in Fig. 1, which cause the additional inductive and capacitive components equivalently. Thus the characteristic impedance and slow wave factor of the microstrip line increase, so it is useful in design new type of circuits and reducing the circuit size. If two microstrip lines exist back-to-back to each other's ground plane, the DGS pattern may exist commonly on the shared ground plane (Fig. 2) and give two microstrip lines the well known advantages commonly. Therefore, the advantages of previous DGS LPF (Fig. 3) such as compact size may be doubled by folding the microstrip line section and consisting of the common DGS (CDGS) as shown in Fig. 4. As the result, the half-sized LPF is obtained using CDGS. In order to show the validity of the proposed design, an example of LPF using CDGS and double-sided microstrip lines is designed using the dielectric substrate with 2.2 of dielectric constant and 31 mils of thickness. The size of the designed LPF using CDGS is only 52.6% (Fig. 5) compared to that designed by the previous LPF with the conventional DGS. It is shown that the performances of the proposed LPF are well preserved after the size-reduction with the S_{11} and S_{21} are $-25\,\mathrm{dB_{min}}$ and $-0.1\,\mathrm{dB_{max}}$, respectively.

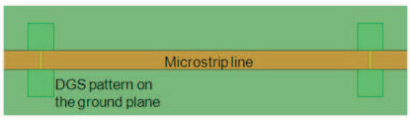

Figure 1.

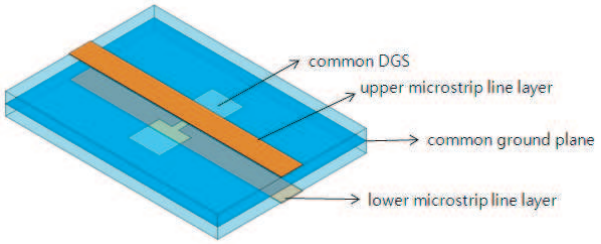

Figure 2.

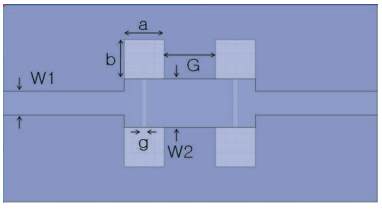

Figure 3.

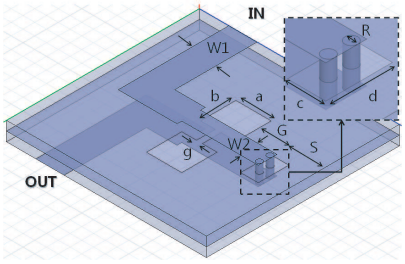

Figure 4.

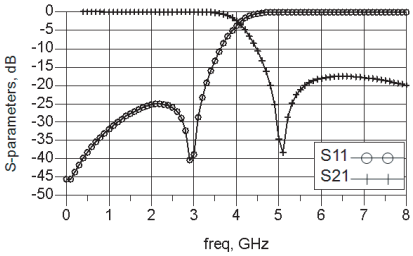

Figure 5.

ACKNOWLEDGMENT

This work was supported by the National Research Foundation of Korea Grant funded by the Korean Government (MEST) (KRF-2009-220-D00074 and 2010-0009211).

New Design of a Rectenna System Using Defected Ground Structures

Taemin Choi, **Seok-Jae Lee**, **Heejong Lee**, **Sangtai Yu**,
Jongsik Lim, **Dal Ahn**, **and Sang-Min Han**
Soonchunhyang University, Asan, Chungnam 336-745, Republic of Korea

Abstract— A rectenna is a rectifying antenna system which converts microwave energy to DC electricity. From previous studies, it has been researched for efficient RF collections and efficiency increments. However, currently it is required to be designed with low-complexity and miniaturization. In this paper, a new design of a rectenna system using defected ground structures (DGSs) is proposed with a small form-factor integrable to other circuits. The proposed system replaces bulk microwave filters on the circuit side of a PCB to DGSs on the back-side to decrease the system size. Fig. 1 shows the configuration of the proposed rectenna system with DGSs at 2.4 GHz. The configuration consists of a receiving antenna, microstrip lines, a schottky diode (HSMS-2580, Agilent Technologies), a resistive load, and DGSs. Two filters are replaced with the DGS1 between an antenna and a diode and the DGS2 for a DC feed between a diode and a resistor. While the DGS1 is designed by dual-DGSs to reject re-radiation of occurred harmonic signals of 4.8, 7.2 GHz, the DGS2 requires the only DC path. By tuning the resistive load, the optimum efficiency can be achieved. The performances of the DGSs are presented in Fig. 2. The DGS1 can reject the harmonic frequency components for 60.35 dB, 34.91 dB at 4.8 GHz, 7.2 GHz, respectively. The DGS2 can pass DC signal at less than 2.4 GHz. The proposed rectenna system can achieve the simple architecture integrable to smallest mobile devices without battery usages.

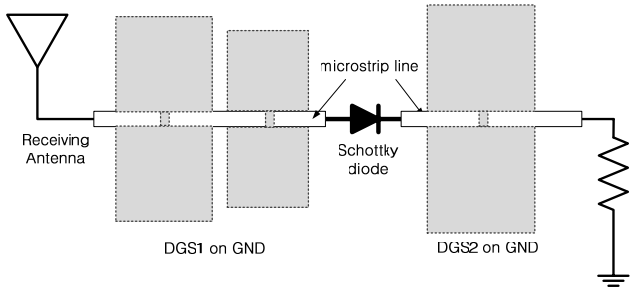

Figure 1: Proposed rectenna system using DGS.

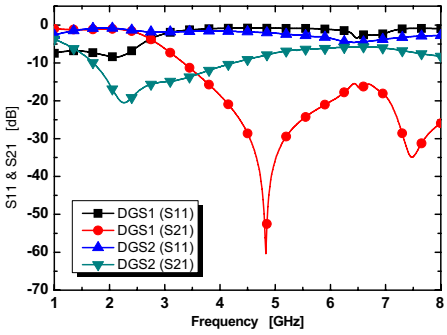

Figure 2: DGS transmision performances.

ACKNOWLEDGMENT

This research was supported by Basic Science Research Program (grant No. 2009-0065375) and Global Research Network Program (grant No. KRF-2009-220-D00074) through the National Research Foundation of Korea (NRF) funded by the Ministry of Education, Science and Technology.

Equivalent Circuit Model for Two Layer Dumbbell Type Defected Ground Structures

D. Baatarkhuu[1], Y. S. Choi[1], S. T. Yu[1], T. Tharoeun[1], H. Liu[2], and D. Ahn[1]

[1]Soonchunhyang University, Republic of Korea
[2]East China Jiaotong University, China

Abstract— A new equivalent circuit model for two layer dumbbell type defected ground structure (DGS) is presented in this paper. Many papers for defected ground structure are published through international journals and conferences during past ten years. But, most of cases are studied for microstrip structures. In this paper, we introduced two layer dumbbell type DGS and derived equivalent circuit model. Figure 1 shows the two layer dumbbell type defected ground structure.

From this structure, we expected the characteristics that has more equivalent capacitance of DGS. To verify the expectation, we simulated Fig. 1 structure using ANSYS HFSS Ver. 12.1 and extracted the equivalent circuit parameter using ANSYS Designer V. 6.0. Figure 2 shows the equivalent circuit structure from ANSYS Designer V. 6.0 and Figure 3 shows the comparison between EM simulation results and circuit simulation results. From Figure 3, we found they are very good agreements. From this results, we could expect multi-layer defected ground structure could be developed.

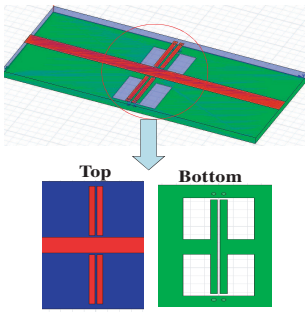

Figure 1.

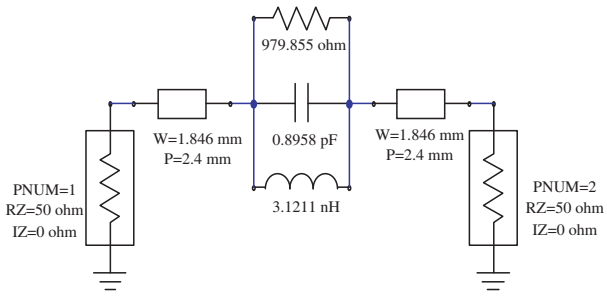

Figure 2.

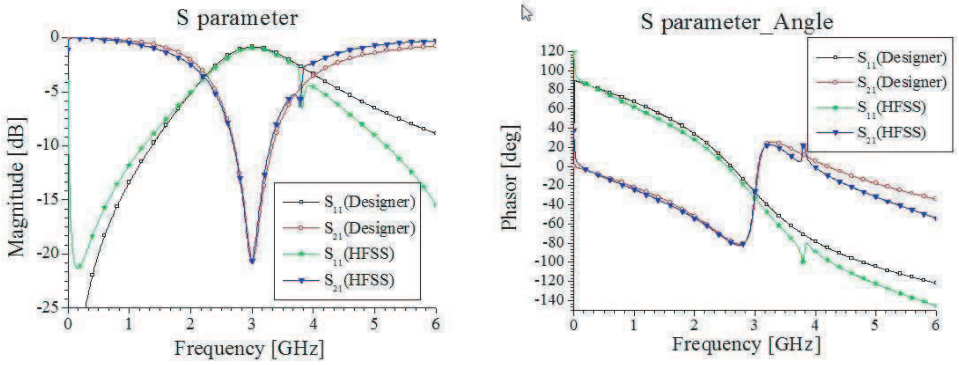

Figure 3.

ACKNOWLEDGMENT

This work was supported by the National Research Foundation of Korea Grant funded by the Korean Government (MEST) (KRF-2009-220-D00074).

Novel Bandpass Filter Using Defected Multi-mode Resonators (DMR)

Haiwen Liu[1], **Jing Wan**[1], **Liyun Shi**[1], **Xuihui Guan**[1], **and Dal Ahn**[2]

[1]College of Information Engineering, East China of Jiaotong University, Nanchang, China
[2]Dept. of Electrical Communication Engineering, Soonchunhyang University, Chungnam, R. O. Korea

Abstract— Modern wireless communication systems require various types of wide-band components to enable digital transmission via microwave bands. High-performed wideband bandpass filter (BPF) is one of the most popular components for wide-band applications. Several studies were reported by using a single stepped-impedance resonator (SIR) by strong input/output coupling. Half wavelength ($\lambda/2$) transmission line resonator with a pair of center loaded stubs is used to design dual-mode and triple-mode wideband filters. Those filters using stub-loaded structure has a good selectivity for the transmission zeros close to the passband. Also, a filter for size reduction is designed by replacing the UIR loading stub with $\lambda/4$ SIR.

Recently, microwave BPFs are popularly designed on the ground plane, such as defected ground structure (DGS), DGS stubs, defected SIRand so on. However, multi-mode characteristics of the defected structures are rarely mentioned for circuit synthesis. In this letter, a novel multi-mode resonator structure with defected open loop resonator and defected stub is introduced. According to slotline and defected SIR theory, multi-mode characteristics of the proposed defected multi-mode resonator (DMR) are improved for wideband application. A new wideband BPF using DMR is designed, analyzed and fabricated. Both simulated and measured results are given to prove validity of this design.

Based on slotline theory, a defected multi-mode resonator (DMR) with defected open loop resonator and defected stub is proposed in this letter. Also, design equations of the DMR resonant frequencies are investigated. Moreover, defected stepped-impedance resonator (SIR) is analyzed and applied to tune multi-mode characteristics of DMR for wideband bandpass filter(BPF) design. To verify the proposed method, an experimental filter is fabricated. The measured results exhibit good agreement with the simulations.

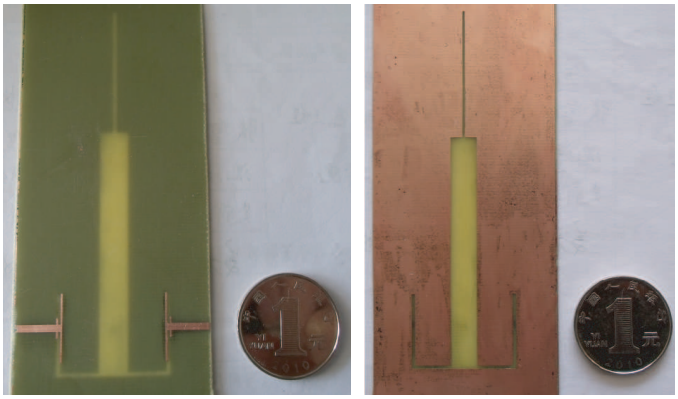

(a) Top view (b) Bottom view

Figure 1: Photographs of the proposed filter.

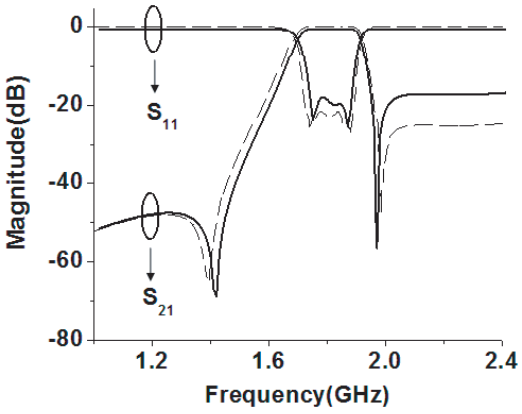

Figure 2: Simulated (dashed line) and measured.

Triple Mode Resonator Bandpass Filters with Source-load Coupling

K. C. Lee, H. T. Su, and M. K. Haldar
School of Engineering, Computing and Science, Swinburne University of Technology (Sarawak Campus)
Jalan Simpang Tiga, Kuching 93350, Sarawak, Malaysia

Abstract— This paper presents an analytical technique for the study of transmission zeros of a microstrip bandpass filter. A triple mode resonator proposed in our formal work consists of an open loop resonator with a stepped impedance resonator connecting to the mid point of the open loop resonator where a grounding via is located. By analysing the basic resonator structure, the open loop resonator with the grounding via in the symmetrical plane of the resonator will produce one transmission zero on the left side of the resonant frequency of the resonator as shown in Figure 1. This figure also shows the triple mode resonator without the grounding via structure has a transmission zero on the right side of its resonant frequency. The final bandpass filter has an improved selectivity, a good insertion loss and odd resonance suppression in its wideband.

In addition, this paper also discusses how the coupling of the feed structures improves the transmission zero which is located on the left side of bandpass passband to obtain a better selectivity for the bandpass passband. Another transmission zero can be introduced on the right side of the bandpass passband to improve the stopband of the filter. This is done by further adjusting the length and the coupling of the feed structures. The location of the transmission zero in the stopband can be easily estimated. This filter demonstrates high selectivity, compact size, and predictable transmission zeros.

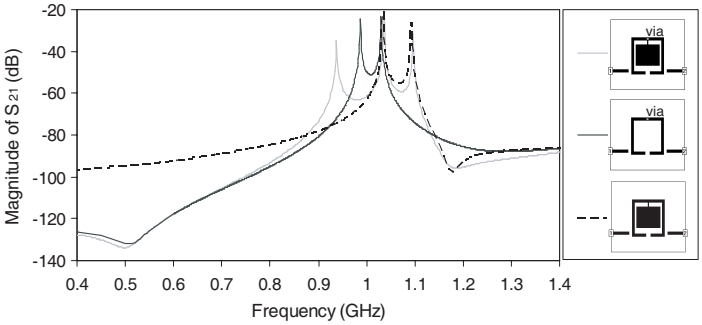

Figure 1: Simulated frequency responses of various weakly coupled resonators to observe the appearance of transmission zeros. (Top diagram) Triple-mode resonator, (Middle diagram) open-loop resonator with a grounding via in the middle of the structure, and (Bottom diagram) triple-mode resonator without the grounding via.

Reconfigurable Beam Steering Antenna for Smart Antenna

Yongjin Kim
Department of Electrical Information, Inha Technical College
253 Yonghyun-Dong, Nam-Gu, Inchon, Republic of Korea

Abstract— Smart antenna technologies such as a reconfigurable antenna radiation beam patterns and beamforming have recently received increasing interest for various mobile communications. Smart antenna systems are usually considered as a switched beam and adaptive-array system for mobile base station facilities to increase the capacity of the wireless network by steering antenna beam pattern to any direction of interest. Currently, the characteristics of the smart antenna are extended to personal mobile communication devices to satisfy the requirement of new service including MIMO application. In this paper, we propose a reconfigurable beam steering antenna for smart antenna system. The antenna structure is based on the combined model of dipole and loop antenna. By changing switches on/off configurations, the antenna structure can be changed and antenna radiation patterns are cancelled or compensated to the certain direction. The structure of the proposed antenna is shown in Fig. 1. The simulation results of radiation patterns are shown in Fig. 2. The proposed antenna operates in 1.5–1.6 GHz range ($S_{11} < -10$ dB) and the maximum gain is 4.34 dBi. Simulation results confirmed the beam steering characteristics by using four imaginational switches.

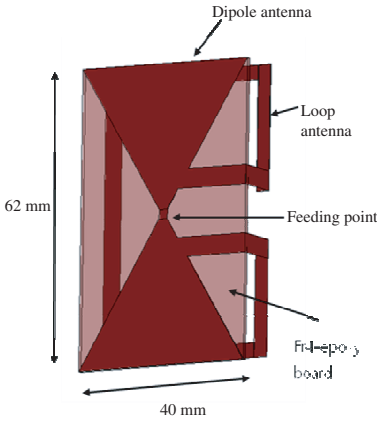

Figure 1: Proposed combined antenna.

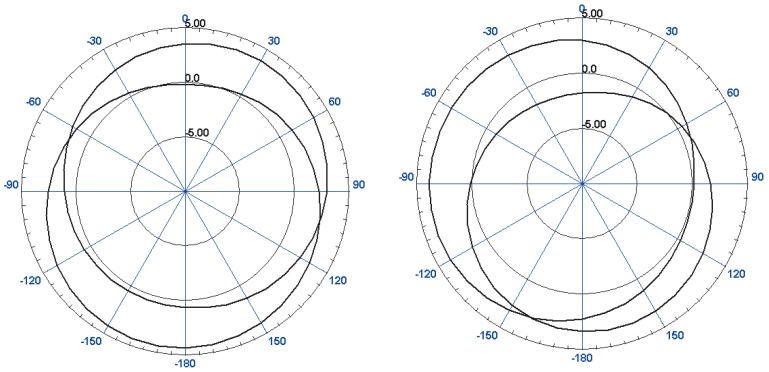

Figure 2: Simulated antenna radiation patterns.

ACKNOWLEDGMENT

This research was supported by Basic Science Research Program through the National Research Foundation of Korea (NRF) funded by the Ministry of Education, Science and Technology (2010-0003839).

Session 4P2b
Bioelectromagnetics, RF Biological Effect

Bioradar Recording and Processing of Information about Biological Object

L. N. Anishchenko[1], **A. S. Bugaev**[2], **and S. I. Ivashov**[1]

[1]Remote Sensing Laboratory, Bauman Moscow State Technical University, Russia
[2]Moscow Institute of Physics and Technology, Russia

Abstract— Bioradiolocation is a method for detection and diagnostic of biological objects, even behind optically opaque obstacles, by means of radar. It is based on the reflected signal modulation by movement of the body surface and internals. Objects in the human's body, subjected to periodic fluctuations are cardiac muscle and lungs. Patient's physical activity and medical state determines the values of these frequencies.

There are many areas where bioradiolocation could be applied among them are space medicine (monitoring of astronauts movements inside and outside of spacecraft, and remote monitoring of their health), sleep medicine, disaster medicine, antiterrorist operations etc. [1].

The main task of bioradiolocation is remote or non-contact measurement of movement, breathing and pulse parameters of biological objects behind an obstruction or in open space at some distance.

At Bauman Moscow State Technical University (BMSTU) method of bioradiolocation has been studied since 2002. At the beginning surface penetrating radar was used for bioradar. But experiments showed that bioradiolocation requires specific apparatuses and algorithms to be designed [2]. That is why in 2005 a new bioradar was created at Remote Sensing Laboratory, BMSTU. As opposite to previous radar it uses step frequency modulated signal, which allows to estimate distance to the object under exanimation. The radar has following technical characteristics:

Number of frequencies	16
Sampling frequency	62.5 Hz
Operating frequency band	3.6–4.0 GHz
Recording signals band	0.03–5 Hz
Dynamic range of the recording signals	60 dB

With the bioradar several types of the experiments were carried out.

1) Comparative experiments for bio-radiolocation and optical measurements of chest movements during breathing. A quick-shot camera and radar were applied simultaneously. Data from quick-shot camera and bio-radar has the highest correlation for abdominal area movements.
2) Comparative experiments for contact and non-contact methods. During this type of experiments breathing and pulse parameters were simultaneously measured by contact method using rheocardiomonitor and non-contact method of bioradiolocation. 27 male and 25 female adult examinees participated in the experiments, for each of whom radar and rheocardiomonitor signals were recorded three times (duration of one record is 1 min). Values of breathing and pulse frequencies for contact and non-contact methods were compared, which is shown that they have agreement about 95%.
3) Sleeping monitoring. This experiment is included into the program MARS-500, which started in June 2010 at Institute of Medical and Biological Problems, Moscow. It contains simulating different aspects of an interplanetary manned flight. The main part is a series of experiments on long-term isolation of the crew in conditions of the specially built ground-based experiment facility. Bioradar will be used for remote measurements of movement activity, breathing and heart rate parameters of the crew while sleeping. It will detect any changes in these parameters, which may indicate sleep disorders (common problem for long-term isolation and space flights).
4) Human adaptive capabilities estimation for physical and mental stress [3].
5) Estimation of the laboratory animal movement activity. During experiment the animal was placed into a box with dielectric walls. Transmitting and receiving antennas of the radar were pointed to the box. Corner reflector was used to reduce influence of the distance

between the animal and antennas block on power density of the received signal. Specific frequency spectrums for different animal condition were obtained. The spectrums differ one from another greatly by magnitude and form. That is why it is possible to distinguish different types of animals' movements.

At present a new bioradar is under creation. It will operate at higher frequency band of 14–15 GHz. This would increase resolution capability of the radar and thus improve the quality of received information.

ACKNOWLEDGMENT

This work was supported by grants of the President of Russian Federation MK-118.2011.9, Ministry of Education and Science of the Russian Federation and RFBR.

REFERENCES

1. Staderini, E. M., "UWB radars in medicine," *IEEE Aerospace and Electronic Systems Magazine*, 13–18, January 2002.
2. Ivashov, S. I., V. V. Razevig, A. P. Sheyko, and I. A. Vasilyev, "Detection of human breathing and heartbeat by remote radar," *Progress In Electromagnetics Research Symposium*, 663–666, Pisa, Italy, March 28–31, 2004.
3. Anishchenko, L. N. and V. B. Parashin, "Estimation of adaptive capabilities of a human organism by means of bioradiolocation," *Proc. of 5th Russian-Bavarian Conference on Biomedical Engineering*, 147–148, Munich, Germany, 2009.

Recent Challenges of Bioelectromagnetism

Ondřej Kučera[1, 2], **Jiří Pokorný**[2], **Michal Cifra**[2], **and Daniel Havelka**[1]

[1]Faculty of Electrical Engineering, Czech Technical University in Prague, Prague, Czech Republic
[2]Institute of Photonics and Electronics, Academy of Sciences of the Czech Republic
18251 Prague 8, Chaberská 57, Czech Republic

Abstract— Biological electromagnetism remains open question for almost one century. Despite partial experimental evidence, this topic is considered highly controversial; however, recent findings attracts more reliable attention. This paper summarizes challenges ahead of us solving which may significantly contribute to our understanding of electromagnetic activity of living cells or which may bring desired *experimentum crucis*. It is argued that the attention should be paid to mesoscopic structures and interfaces in living cells. The influence of polar supramolecular structures, the role of the water, and metabolic activity are discussed and suggested implications are reviewed. Measurement limitations, arising from the nature of the object and phenomena under test, are pointed out and the nanotechnological approach is advocated.

Biological Effect of Extremely Low Frequency Electromagnetic Field (ELF-EMF) on Osteoblasts

Li-Jun Sun, **Xiao-Yun Lu**, **and Jian-Bao Zhang**
Key Laboratory of Biomedical Information Engineering of Ministry of Education
School of Life Science and Technology, Xi'an Jiaotong University, Xi'an 710049, China

Abstract— Since Bassett et al. (1977) first applied extremely low frequency electromagnetic field to the treatment of non-union tibial fractures and obtained the encouraging results, the biological effect of ELFEMF has been paid much more attention. Until now numerous reports have confirmed that ELFEMF stimulation could increase bone formation by enhancing the recruitment, proliferation, and differentiation of osteoblasts and inhibiting the apoptosis of osteoclasts, but the mechanism involved is very complex and still obscure. Some reports showed that the production of PGE2, NO were detected immediately after onset of ELFEMF. Meanwhile intracellular calcium was considered to play an important role in mediating the anabolic effects of ELFEMF on osteoblasts. Our previous studies revealed that the responses of osteoblasts on EMF were mainly depending on its waveform, and the biological effect of different EMF might achieved through various cell signaling pathway including calcium/Calmodulin pathway, P2 receptor and PLC pathway. Both suramin and neomycin, the inhibitors of calcium, could reduce the positive effective of EMF on the proliferation of osteoblasts. In this study, we would like to review the possible mechanism underline the effect of ELFEMF on osteoblasts.

REFERENCES

1. Zhang, X. J., J. B. Zhang, X. M. Qu, and J. Wen, "Effects of different extremely low-frequency electromagnetic fields on osteoblasts," *Electromagnetic Biology and Medicine*, Vol. 26, 167–177, 2007.
2. Chang, W. H., L. T. Chen, et al., "Effect of pulse-burst electromagnetic field stimulation on osteoblast cell activities," *Bioelectromagnetics*, Vol. 25, 457–465, 2004.
3. De Mattei, M., N. Gagliano, et al., "Changes in polyamines, c-myc and c-fos gene expression in osteoblast-like cells exposed to pulsed electromagnetic fields," *Bioelectromagnetics*, Vol. 26, 207–214, 2005.
4. Khatib, L., D. E. Golan, and M. Cho, "Physiologic electrical stimulation provokes intracellular calcium increase mediated by phospholipase C activation in human osteoblasts," *FASEB J.*, Vol. 18, 1903–1905, 2004.

A Conjunct Analysis for Breast Cancer Detection by Volume Rendering of Low Dosage Three Dimensional Mammogram

R. Dharanija and T. Rajalakshmi
Electronics & Instrumentation Engineering Department, Panimalar Engineering College
Anna University, India

Abstract— Breast cancer is the fifth most common cause of cancer death after lung cancer, stomach cancer, liver cancer, and colon cancer. Breast cancer is the most common cause of cancer in women and the second most common cause of cancer death in women. The earlier the breast cancer is detected the more the chances of treatment and even cure. If detected early, the five-year survival rate exceeds 95%.

A majority of breast cancers are diagnosed as a result of an abnormality seen on a mammogram. A mammogram is actually a 2-D x-ray image of the breast. The radiologist, who specializes in reading x-ray images, can identify differences between a normal breast and one that may show signs of cancer. Mammography is a test that allows the doctor to look at images of the inside of the breasts.

However, it is possible for a 2D mammogram to look normal even though a breast cancer is actually present. This is more common in patients of younger age where the breast tissues are denser and thus spotting an abnormality becomes difficult. Also, it is possible for a 2D mammogram to look abnormal when there is actually no cancer and in this case additional testing is required. To overcome limitations of these kinds in breast cancer detection, the patient had to undergo additional testing procedures. One such additional procedure is the recently developed 3-D (Tomosynthesis) technology which allows us to see cancers that might be hidden and using a three-dimensional image along with a 2-D mammogram provided a clearer picture.

Despite the fact that 3D mammography eliminates overlapping of tissue that is seen in conventional 2-D mammograms, it was noted that using 3-D mammography technique as an adjunct with 2-D mammograms doubled the radiation dose the patient received, increasing cancer risk.

This paper gives an idea of how 2D image can be obtained from the 3D mammogram data without the need to take 2-D slices additionally and hence avoiding issues related to over dose of radiation. Volume rendering technique is proposed which displays a 2D projection of a 3D discretely sampled data set.

The Effect of MRET Polymer Compound on SAR Values of RF Phones

Igor V. Smirnov
Global Quantech, Inc., Encinitas, CA 92024, USA

Abstract—

Aim: This research is related to the proposed hypothesis regarding the ability of defined polar polymer compound (MRET polymer, US Patent 6369399 B1) applied to RF phones to increase the dielectric permittivity of waterbased solutions and to reduce the SAR (Specific Absorption Rate) values inside the "phantom head" filled with the jelly simulating muscle and brain tissues. Due to the highly organized state of fractal structure of MRET polymer compound and the phenomenon of piezoelectricity this polymer is the stationary source of low-frequency magnetic field with composite space structure and very weak amplitude (about 1 Oersted) when exposed to the external high frequency EMR generated by RF phone. The low-frequency magnetic field generated by MRET polymer can affect the hydrogen lattice of the molecular structure of water and subsequently modify the electrodynamic properties of water. The increase of dielectric permittivity of water finally leads to the reduction of the absorption rate of electromagnetic field by living tissue [3].

Method: The fact of the reduction of SAR values is confirmed by the research conducted in June–July of 2006 at RF Exposure Laboratory, Escondido, California. The SAR values were calculated based on the measurements of E-field. The series of measurements in 242 points were accomplished for RF phones without MRET polymer material and with MRET polymer material applied to RF phones for the Uni-Phantom head filled with head tissue simulating liquid. The brain and muscle mixtures consist of a viscous gel using hydroxethylcellullose (HEC) gelling agent and saline solution. Preservation with a bactericide is added and visual inspection is made to make sure air bubbles are not trapped during the mixing process. The mixture is calibrated to obtain proper dielectric constant (permittivity) and conductivity of the desired simulated tissue. The APREL Laboratories ALSAS system with a dosimetric E-field probe E-020 was used for the measurements. The dipole was mounted so that the dipole feed point was positioned below the center marking of the flat phantom and dipole was oriented parallel to the body axis (the long side of the phantom). The standard measuring distance was in the range of 10 mm from the dipole center to the solution surface. The coarse grid with a grid spacing of 10 mm was aligned with dipole. The 5x5x8 fine cube was chosen for the cube integration. The dipole input power (forward power) was 250 mW ± 3%. The results are normalized to 1 W input power. The laboratory environment conditions were as follows during the calibration sequence:

Ambient Temperature of the laboratory: 22°C ± 1.0°C.
Temperature of the Tissue: 20°C ± 1.0°C.
Relative Humidity: 41%.

The investigation was conducted on cellular phones: Sanyo Model PM-8200(S) S/N 2D29555E, Kyocera Wireless Model 2325 S/N 457E8CE6, and LG Model VX6000 S/N 12KS030845; TX frequency range: 824.70–848.31 MHz and 1851.25–1908.75 MHz; Maximum RF output: 23 dBm conducted; Signal modulation: CDMA; Antenna type (length): Standard with each model; Volume of MRET polymer compound applied to each RF phone: 180 mg.

Results: The measurements in this investigation are taken to simulate the RF exposure effects under worst-case conditions. Precise laboratory measures were taken to assure repeatability of the tests. The tested RF phone complies with the requirements in respect to all parameters subject to the test.

The Standard Uncertainty for the Area Scan and Zoom Scan Peak SAR values is 18.6%. The level of Uncertainty for the mean values of SAR for 1 gram of tissue is **6.6%** and for 10 gram of tissue is **2.8%** [2]. The application of MRET polymer to RF phones does not significantly affect the air measurements of RF phone signals and subsequently does not lead to any significant distortion of transmitted RF signals. The incorporation of 180 mg of MRET polymer material in the RF phones showed also that "Hot Spots" remained in the same location as without the MRET polymer and their amplitudes decreased in **90%** of data points. In **70%** of data points was observed the significant decrease of SAR values in the range of **10%** to **60%**. The incorporation of MRET polymeric material in the RF phones leads to the reduction of the majority of SAR

values: **19** SAR values out of **20** meaningful SAR values in this experiment were reduced in the range of **0.3%**–**29.0%**, and only **1** SAR value increased by **0.6%**. The reduction of SAR values calculated on the basis of E-field probe measurements inside the "phantom head" confirms that the subtle low frequency oscillations generated by MRET polymer material actually increase the value of dielectric permittivity of the simulating brain tissue jelly resulting in the reduction of SAR values in the "phantom head".

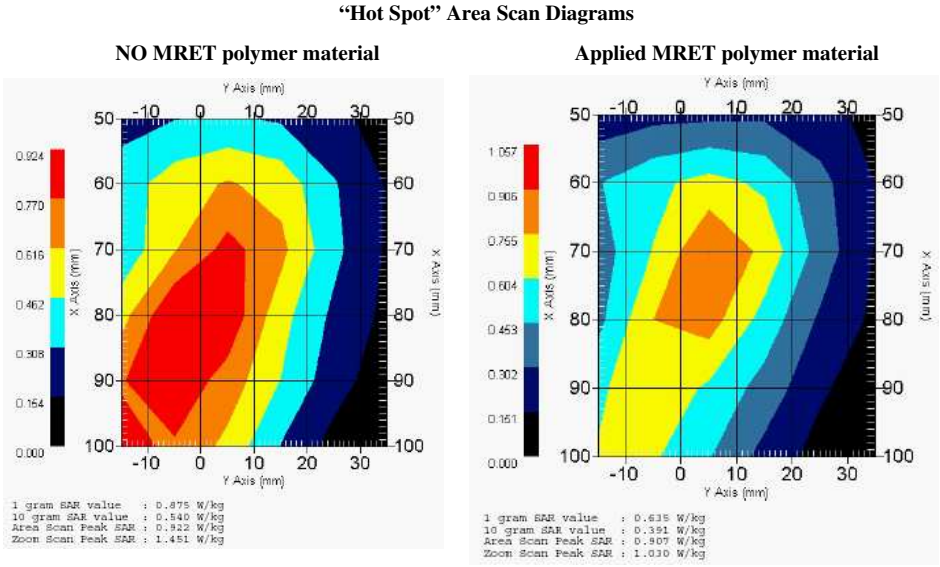

Figure 1: Phone Model: LG VX6000; Frequency: 1900.00 MHz; Max. Transmitted Power: 0.256 W; Phantom data: APREL-SAM Left Ear; Probe Sensitivity: 1.20 1.20 1.20 $\mu V/(V/m)^2$.

REFERENCES

1. IEEE Standard 1528-2003, "IEEE recommended Practice for determining the Peak-Spatial Average Specific Absorption Rate (SAR) in the Human Head from Wireless Communication Devices: Measurement Techniques," October 2003.
2. Moulton, J. M., "R&D testing SAR evaluation," Test Report No. R&D 20060601, RF Exposure Lab, Escondido, California, June–July 2006.
3. Smirnov, I. V., "Polymer material providing compatibility between technologically originated EMR and biological systems," *Explore Magazine*, Vol. 15, No. 4, 2006.

Simulation of a Detailed Human Throat Model in a Circular Antenna System for Electromagnetic Hyperthermia Application

Omer Isık, Erdal Korkmaz, and Ashrf Aoad
Department of Electrical and Electronics Engineering, Fatih University, Istanbul, Turkey

Abstract— Electromagnetic Hyperthermia is a cancer treatment method in which the human tissues are exposed to electromagnetic (EM) radiation aimed to absorb EM energy in targeted tissues causing local temperature elevation. There are many publications showing that high temperatures (42°C–45°C) in cancerous cells ruin the cells protein build, changes the cell construction and even kills them. Since the cancerous cells dispositions are weaker than healthy ones, the healthy cells near the cancerous cells are damaged lesser. In addition there is no toxicity in the method it is appropriate to apply in conjunction with other treatment methods. For hyperthermia application there are two essential problems to cope, firstly generation heat in targeted region while keeping surrounding tissues temperature in safe limits and secondly monitoring and controlling the temperature at the targeted regions. The remedy for the first problem is to focus the fields in targeted tissues such that the fields there constructively add while in surrounding tissues not. To that end the antennas used in the system should have narrow radiation beam, small in size to be able to use more antennas, and frequency characteristics for enough penetration into the tissues. In this paper we present the simulation of a detailed human throat model exposed to EM radiation in a circular antenna system to increase the temperature locally around 42°C. The antennas used in the system have the required characteristics for hyperthermia application and its adequateness is discussed. In addition a parameter optimization of the system has been demonstrated to increase the effectiveness of the system.

Session 4P3
Microwave Remote Sensing and Polarimetry, SAR

Scattering from Periodic Cone Structure Array

M. Jin[1], **M. Bai**[1], **W. Y. Chen**[2], **J. K. He**[2], **and J. G. Miao**[1]

[1]Microwave Engineering Lab, Beihang University, Beijing 100191, China
[2]Shanghai Aerospace Electronic Technology Institute, Shanghai 201109, China

Abstract— Calibration targets used for satellite board microwave radiometer (MWR) are commonly in shape of cone structure array. Those targets are made of metallic cones, which are coated with high emissivity material. These metal cones are built to heat the coating material uniformly, thus the targets can provide a standard brightness temperature for the MWR. According to Kirchhoff's law of thermal radiation, at thermal equilibrium, the emissivity and reflectivity of an object satisfies the equation, $e = 1 - r$. As a result, the numerical evaluation of emissivity is usually conducted by scattering computation, and the experimental evaluation is commonly implemented by scattering measurement. Another reason for choosing the scattering measurement routine lies in that the brightness radiation from the calibration targets is relatively tiny, and implying an environment with efficiently a low noise level can be technically difficult and extremely expensive. However, even in the routine of scattering measurement, due to the low reflectivity of an actual calibration target, the scattering pattern is still hard to be measured accurately.

The numerical simulation of scattering from those calibration targets offers significant information for the design, parameter optimization, and experimental emissivity evaluation. Imposing periodic boundaries, and implying an infinite 2D array of coated cones, one can get an efficient manner of emissivity evaluation. On the other hand, bi-static measurements for scattering from a full size calibration target need more detailed information about scattering pattern from simulations. In the former works, scattering from a finite size array of coated cones were studied, with normally incident plan-waves and Gaussian beams. Those results provided meaningful information for the scattering-measurement routine. However, simulations using incident beams with an incline incident direction may offer more.

In this paper, the finite difference time domain (FDTD) method with Yee-cells is used, to calculate the scattering from a full size calibration target irritated by a beam, which is generally the case of the bi-static measurement of a calibration target. The near-field and far-field scattering patterns are obtained and compared with each other. Cases of different incident directions are considered. And a parallel calculation is implemented to overcome the calculation burden, based on the message passing interface (MPI). Those results are to offer information of scattering pattern for the experimental emissivity evaluation.

Cylindrical Slot Antennas for Monitoring the Quality of Milled Rice

K. Y. You[1], **J. Salleh**[1], **Z. Abbas**[2], **and L. L. You**[3]

[1]Radio Communication Engineering Department, University Teknologi Malaysia
UTM Skudai 81310, Malaysia
[2]Department of Physics, University Putra Malaysia, UPM Serdang 43400, Malaysia
[3]Department of Human Biology, School of Medicine and Health Sciences
International Medical University, Kuala Lumpur 57000, Malaysia

Abstract— This paper presents a cylindrical slot antenna sensor to determine the quality of rice based on the percentage of moisture content and percentage of broken rice. The reflection coefficient of rice were measured using both single and parallel slot sensors of infinite ground plane in the frequency range from DC to 6 GHz using a Vector Network Analyzer (VNA). Ten varieties of rice with moisture content between 8% and 16% were tested in this work. Calibration equations were established to relate the measured reflection coefficient to moisture content which in turn allow prediction of the percentages of broken rice. From the measurement results, the parallel two slot sensor showed the high sensitivity of reflection coefficient to the moisture content in the rice sample, as well as the percentage of cracked rice in the samples.

Leaf Area Index Inversion Based on Ground Passive Microwave Measurement Experiment

Jianli Shuang[1], **Shanjun Liu**[1], **Lixin Wu**[1, 2], **Qi Li**[1], **and Jianying Zhuo**[1]

[1]Institute for Geo-informatics & Digital Mine Research, Northeastern University, Shenyang 110819, China
[2]Academe of Disaster Reduction and Emergency Management, Beijing Normal University
Beijing 100875, China

Abstract— The passive microwave sensor can provide significant information compared with optical and infrared sensors due to its penetrating property. It plays an important role in the detection of growth vigour of corps. However, past passive microwave detection experiments concentrated mainly on the observation of corps in one growth season, consecutive detection is less. Moreover, the effect of row direction on microwave brightness temperature was less considered.

In this paper, the passive microwave detection experiments were conducted to invert Leaf Area Index (LAI) of corn in Huailai county of Hebei province of China from August to September in 2010. Two passive microwave radiometers, frequency respectively at 6.7 GHz and 18.7 GHz were used to measure the brightness temperature variation of corn both horizontal and vertical polarizations in different growth stage .The measurement angle varied from 0° to 60° at interval of 5° and the measurement direction varied respectively in parallel, vertical to the row and cross 45° with the row. The detection period included eight stages of corn growth. In addition, LAI-3000 was used to obtain the corn's LAI of every growth stage.

After the experiment the relationship between MPDI and LAI was analyzed. The result showed that a well exponential relationship exists between MPDI and LAI for both microwave frequencies. With the increase of measurement angle, the exponential relationship is more obvious. When observation is parallel to the row, two MPDIs at 6.6 and 18.7 GHz have a good linear relationship, but when observation is vertical to the row or cross 45° with the row the linear relationship becomes weak.

The experimental result shows that passive microwave remote sensing can detect the growth vigour of corps, and the observing angle and direction are very important for detection.

Three Dimensional Visualization of Pol-InSAR Image

Guangyi Zhou[1], **Tao Xiong**[1, 2], **and Jian Yang**[1]

[1]Department of Electronic Engineering, Tsinghua University, Beijing 100084, China
[2]Nokia Research Center, Beijing 100176, China

Abstract— Synthetic Aperture Radar (SAR) is a kind of imaging radar with all weather, all time working capabilities. Visual interpretation plays an important role in remote sensing applications, in particular for the surveillance of natural disasters, such as earthquake, debris flow and so on. With resolution improvement, it becomes easier to perform the visual interpretation on the SAR images. Naturally, the original SAR data should be visualized as an image suitable for the human observation ahead of visual interpretation.

The visualization of the single channel SAR image is to transform the original SAR data to a gray image with 256 gray levels. In this paper, we propose a transformation for the single channel SAR data based on the data statistics. Polarimetric SAR (Pol-SAR) measures the target's reflectivity in four polarization channel combinations (HH, HV, VH and VV). This capability makes it possible to visualize the Pol-SAR data as a color image.

SAR interferometry is an important technique [1] which can be used to obtain the elevation information from the interferometric phase. Combining the visualization result of the SAR image above, we can realize the three dimensional (3-D) visualization of the interferometric SAR (InSAR) data. Polarimetric interferometric SAR (Pol-InSAR) [2] measures for each resolution element in the scene from two slightly different look angles and provides both polarimetric and interferometric information simultaneously. The Pol-InSAR data can be used to realize 3-D visualization with color information. Pol-InSAR system is just like human eyes, which have the capability to observe 3-D color scene.

For the InSAR or Pol-InSAR data of the mountainous regions, the elevation information can be obtained through phase unwrapping technique. The visualization results for the mountainous regions are shown in Fig. 1 and Fig. 2. For the Pol-InSAR data of the flat terrain, especially the areas of the countryside or town, the height of the trees and buildings can be retrieved using the ESPRIT algorithm [3]. The visualization result is shown in Fig. 3.

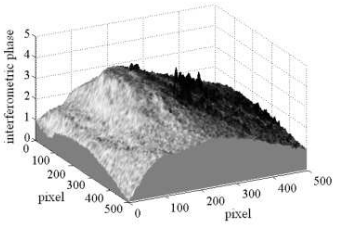

Figure 1.

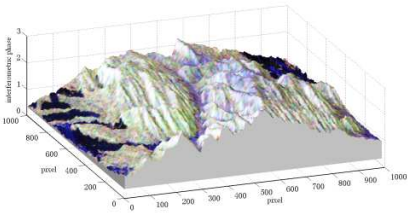

Figure 2.

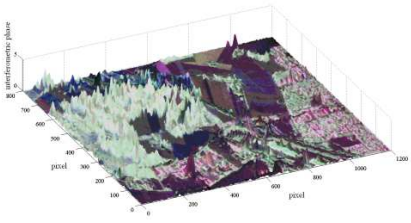

Figure 3.

REFERENCES

1. Graham, L. C., "Synthetic interferometric radar for topographic mapping," *Proc. IEEE*, Vol. 62, 763–768, June 1974.
2. Cloude, S. R. and K. P. Papathanassiou, "Polarimetric SAR interferometry," *IEEE Trans. on Geoscience and Remote Sensing*, Vol. 36, 1551–1565, 1998.
3. Yamada, H., Y. Yamaguchi, E. Rodriquez, et al., "Polarimetric SAR interferometry for forest canopy analysis by using the super-resolution method," *Geoscience and Remote Sensing Symposium*, Vol. 3, 1101–1103, 2001.

Classification of Forest Vegetation Species Based on Reconstruction of Tomography

Peifeng Ma[1, 2], **Hong Zhang**[1], **and Chao Wang**[1]

[1]Key Laboratory of Digital Earth, Center for Earth Observation and Digital Earth, CAS, Beijing, China
[2]Graduate University of Chinese Academy of Sciences, Beijing, China

Abstract— In this paper, we propose a method of extracting the information of tomography in penetrable volume scattering circumstances and apply it to classification of forest vegetation species. The classification process is mainly implemented by distinguishing different scattering tomography of different tree species. Firstly we assume three principal scattering profile structures in volume scattering: a) strong canopy response; b) strong center of trees response; c) strong ground-trunk dihedral response. The extinction in RVoG model they respectively correspond to decreases gradually. Based on the three profile, three functions are constructed shown in Figure 1: a) exponential function (the maximum of scattering amplitude is at the top of the tree); b) Gaussian function (the maximum of scattering amplitude is at the center of the tree); c) inverted exponential function (the maximum of scattering amplitude is at the bottom of the tree), which are used to represent the three volume scattering modes. In addition, three basic geometry of tree are introduced, including triangle, rhombus and inverted triangle. Then the profile structure can be simulated by analyzing the basic geometry of trees and polarization mode. Assuming a prior knowledge of tree height and ground phase we can estimate the four complex coherence of four polarization channel in PolInSAR and a 2×2 matrix of complex coherence can be developed. Supposing the contribution of the three geometry to the final coherence is α, β and γ, we can generate the equation relationship between total coherence and each coherence of three geometry. By solving the equation set the three contribution values can be calculated, which indicates the tomography can be estimated for different species and polarization channels and we can identify the tree species using these parameters. Finally this method is validated using simulated data and real data.

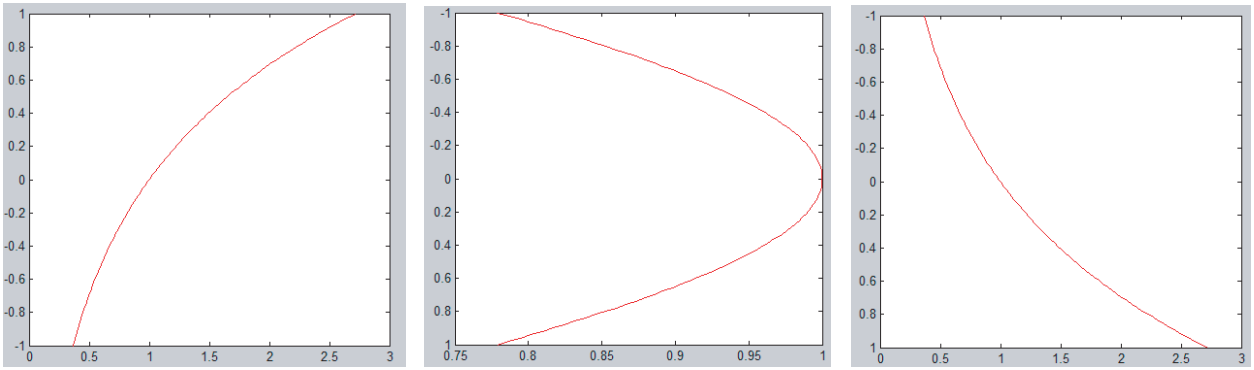

(a) (b) (c)

Figure 1: Three functions with respect to three scattering profile structure.

REFERENCES

1. Papathanassiou, K. P. and S. R. Cloud, "Single baseline polarimetric SAR interferometry," *IEEE Trans. Geosci. Remote Sensing*, Vol. 39, 2352–2363, 2001.
2. Cloud, S. R., "Polarization coherence tomography," *Radio Science*, Vol. 41, 27, 2006.
3. Ferrazzoli, P. and L. Guerriero, "Experimental and model investigation on radar classification capability," *IEEE Trans. Geosci. Remote Sensing*, Vol. 37, No. 2, 960–968, 1999.

H-α Decomposition and Alternative Parameters for Dual Polarization SAR Data

Zili Shan[1, 2], **Chao Wang**[1], **Hong Zhang**[1], **and Jiehong Chen**[1, 2]

[1]Center for Earth Observation and Digital Earth, Chinese Academy of Science, Beijing 100094, China
[2]Graduate University of Chinese Academy of Science, Beijing, China

Abstract— Target decomposition theories lay particular emphasis on separating the target scattering mechanism into a weighted sum of several basic scattering mechanisms depending on the target polarization information. Cloude and Pottier have proposed an entropy based decomposition method for full polarization data, supposing the polarization scattering characteristics can be represented by the space of the entropy H and the averaged scattering angel α. Their method is based on the eigenvalue decomposition of Hermitian matrices. The H-α decomposition has such good properties as rotation invariant, unrelated to specified probability density distribution and to cover the total scattering mechanism space. There are two basic polarization data modes namely full polarization and dual polarization. For example, the data of Envisat, PALSAR or TerraSAR are usually provided as dual polarization. Therefore, this paper investigates the H-α decomposition under the HH-VV mode to exploit the dual polarization data more efficiently. Experiment results indicate that different classes of scattering mechanisms can still be separated in the H-α space of the HH-VV polarization mode although some ambiguities of classes are observed. Moreover, since the angle α has an obscure physical meaning alternatives such as E and β are proposed respectively for both the H and α parameters in this paper. The parameter E, derived from the rotation invariant of the Hermitian matrix, has the same maximum and minimum property as the entropy H. And β has an explicit physical meaning as the proportion of non-surfacing scattering power in the total power. Another advantage of E and β is that they can be derived without the time costing eigenvalue decomposition. Further experiment results show that the alternative parameters possess similar representing ability of scattering mechanism as H and α under the dual polarization mode.

Forest Model for Height Estimation Using POLinSAR Data

Jiehong Chen[1, 2], **Hong Zhang**[1], **Chao Wang**[1], **and Yixian Tang**[1]

[1]Key Laboratory of Digital Earth, Center for Earth Observation and Digital Earth, CAS, Beijing 100094, China

[2]Graduate University of Chinese Academy of Sciences, Beijing 100049, China

Abstract— Forest canopy height is an important parameter that is strongly correlated with timber volume, biomass, carbon stocks and ecological values such as habitat quality, and is key to the terrestial carbon cycle and biomass models and in forest inventory.

Forest canopy height can be retrieved by POLinSAR. POLinSAR proposed in 1998 combines two independent radar techniques, polarimetry aperture radar and SAR interferometry. Polarimetry aperture radar is sensitive to the shape, the dielectric constants and orientation of the scatterers, while SAR interferometry is sensitive to the spatial distribution and height of the scatterers. POLinSAR is superior to any of the two independent techniques in extracting vertical structure of forest.

It is usually using POLinSAR data to estimate forest height by bulding the relations between observables and geophysical parameters through modeling the forest canopy and its interaction with electromagnetic waves. The Random Volume over Ground (RVoG) model is such a extensively used model. The two layers RVoG is constituted by a homogeneous random oriented volume of particles characterized by a constant extinction, representing the forest-vegetation layer, over an impenetrable ground surface.

Therefore, the structure function of RVoG model assumes the ground has a delta interaction with incident electromagnetic wave, then the ground coherence is assumed to be 1. But the ground coherence isn't always unit in fact. In this paper we will modify the ground response from mathematic and geophysical aspect to investigate two complementary models. In the first model, the delta response in the structure fucntion is replaced by a gaussion response; in the second model the underlying surface coherence is assumed smaller than 1. In both complementary models ground coherence is no longer unit, and we will use simulated data produced by PolSARpro software and airborne quad-pol data to compare inversion results with those estimated from RVoG model.

REFERENCES

1. Treuhaft, R. N., S. N. Madsen, M. Moghaddam, and J. J. van Zyl, "Vegetation characterics and underlying topography from interferometric radar," *Radio Science*, Vol. 31, 1449–1485, Nov.–Dec. 1996.
2. Treuhaft, R. N. and P. R. Siqueira, "The vertical structure of vegetated land surfaces from interferometric and polarimetric radar," *Radio Science*, Vol. 35, 141–177, 2000.
3. Cloude, S. R. and K. P. Papathanassiou, "Three-stage inversion process for polarimetric SAR interferometry," *IEE Proceedings Radar Sonar & Navigation*, Vol. 15, 125–134, 2003.
4. Garestier, F. and T. Le Toan, "Forest modeling for height inversion using single-baseline InSAR/Pol-InSAR data," *IEEE Transactions on Geoscience and Remote Sensing*, Vol. 48, No. 3, Mar. 2010.
5. Ballester-Berman, J. D. and J. M. Lopez-Sanchez, "Coherence loci for a homogeneous volume over a double-bounce ground return," *IEEE Geoscience and Remote Sensing Letters*, Vol. 4, No. 2, 317–321, 2007.

Improved Sigma Filter for Speckle Filtering of PolinSAR Imagery

Hong Zhang[1], **Wuping Lu**[1], **Chao Wang**[1], **Jiehong Chen**[1, 2], **and Bo Zhang**[1]

[1]Key Laboratory of Digital Earth, Center for Earth Observation and Digital Earth, CAS, Beijing 100094, China
[2]Graduate University of Chinese Academy of Sciences, Beijing, China

Abstract— The authors propose an improved sigma filter for the speckle filtering of polarimetric interferometry data. Polarimetric interferometry is a new research area that has great potential for vegetation characterization and tree height estimation. As in other SAR applications, speckle is a problem. The Lee sigma filter was developed in 1983 based on the simple concept of two-sigma probability, and it was reasonably effective in speckle filtering. However the speckle model used in Lee sigma filter is the negative exponential model, which is only suitable for uniform regions. For the texture and very uneven regional areas, the effectiveness of this filter is to be questioned. In this paper, we extend and improve the Lee sigma filter by introducing generalized Gamma model, which can be applied to a variety of areas. In addition, we incorporate the the phase processing to improve the interferometric coherence. The proposed algorithm is applied to spaceborne and airborne SAR data to demonstrate its overall speckle filtering characteristics as compared with other algorithms.

REFERENCES

1. Lee, J. S., et al., "Polarimetric SAR speckle filtering and its implication for classification," *IEEE Transactions on Geoscience and Remote Sensing*, 1999.
2. Vasile, G., et al., "Intensity-driven adaptive-neighborhood technique for polarimetric and interferometirc SAR parameters estimation," *IEEE Transactions on Geoscience and Remote Sensing*, 2006.
3. Lee, J. S., et al., "Speckle filtering of dual-polarization and polarimetric SAR data based on improved sigma filter," 2008.
4. Lee, J. S., et al., "Improved sigma filter for speckle filtering of SAR imagery," *IEEE Transactions on Geoscience and Remote Sensing*, 2009.
5. Anastassopoulos, V., et al., "High resolution radar clutter statistics," *IEEE Trans. AES*, Vol. 35, No. 1, 43–59, 1999.
6. Cloude, S. R. and K. P. Papathanassiou, "Polarimetric SAR interferometry," *IEEE Transactions on Geosciense and Remote Sensing*, 1998.

An Analysis Method on Scattering Characteristics of Finite Periodic Array

Zhiping Li[1], **Xuan Li**[2], **Jungang Miao**[1,2], **Dawei Liu**[1], **and Wenle Liang**[1]

[1]Electromagnetics Laboratory, Beihang University, Beijing, China
[2]Science and Technology on Space Microwave Laboratory, Xi'an, China

Abstract— The structure with periodic array structure is a common structure in electromagnetic fields. For example, the array antennas, the frequency selective surface, the absorbing materials, etc. Especially, the calibration load used in the microwave radiometer calibration system is often made of this periodic array, which is constructed by a metal base coated absorbing materials or made from certain absorbing materials directly such as ferrite, crystalline silicon. In general, the absorbing materials are the magnetic materials, whose electromagnetic parameters are difficult to be obtained. However, the electromagnetic parameters are the key elements in analyzing the scattering characteristics of the target. A novel and simple analysis method on the scattering characteristics of the finite periodic array is proposed in this paper, taking advantage of this periodic array structure, and regardless of the unit material.

In this paper, the effect of the array arrangement and the unit structure on the scattering distribution of the finite periodic array is derived, and the array lobe factor theory is obtained. Under the premise that the interaction among the scattering from the units is neglected, the total scattering field is approximately equal to lobe factor of unit by lobe factor of array. Then, the verification for the array lobe factor theory is performed based on Finite Difference Time Domain (FDTD) method combined by perfect material layer (PML), and the results show that the angle error is less than 1 degree when the scattering lobe factor theory is adopted to estimate the scattering distribution of the finite periodic array, thus the scattering lobe factor theory may be adopted to estimate the lobe position conveniently.

The Simulation and Measurement of Scattering Property and Emissivity of the Microwave Radiometer Calibrator

Wenle Liang[1], **Xuan Li**[2], **Jungang Miao**[1, 2], **and Dawei Liu**[1]

[1]Electromagnetics Laboratory, Beihang University, Beijing 100191, China
[2]Science and Technology on Space Microwave Laboratory, Xi'an 710100, China

Abstract— With the development of quantification of microwave remote sensing technology, particularly the rapid development of marine, meteorological and earth resources monitoring technologies, the remote sensing data with higher quality are required. Since the accuracy of calibration directly affects the receiving data in higher quality, calibration of microwave radiometer is important.

The accuracy of measurement of calibrator emissivity is necessary for calibration of microwave radiometer. In this paper the method of bistatic measurement system was chosen to measure the emissivity of calibrator. Compared to monostatic measurement system, bistatic measurement system is more complicated with higher requirements. The optimization of the measuring parameters including bistatic angle range, distance, illuminating range of the antenna beam and the aperture of receiving antenna are presented in this study.

Ferrite material coated periodic array is taken as a unit of calibrator, and finite periodic array is utilized as the calibrator. The scattering property is measured and the emissivity of the calibrator is evaluated using bistatic measurement. The measurement is used to analyze scattering field of the calibrator as well as obtain the emissivity by integrating the differential scattering coefficient of the backscattered field.

In the process of the optimization, parameters are changed one by one with other conditions unchanged to view the results and be compared with the theoretical value. We research the relationship between the parameters and emissivity, so as to optimize system working parameters and then get the best design scheme.

Experimental Investigations of Conductor Detection Using Radio-frequency Transmitter-receiver Pairs

S. E. Irvine
Defence Research and Development Canada, Suffield, Medicine Hat, AB, T1A 8K6, Canada

Abstract— Sensing of linear conductors is critical to avoid utilities both in free-space (cable avoidance for aircraft) and underground (excavation). The latter of these two is arguably more important since burying utilities has become more favourable then placing them overhead. Sensing buried utilities is not only important in order to reduce the number of accidents associated with excavating, but also to be able to map the continuously expanding hidden infrastructure beneath cities and densely populated areas. As evidence of this, review articles have been written which describe the various technologies developed for utility detection [1, 2] and their importance.

Here I present results of experimental investigations of conductor detection using a simple arrangement consisting of a single transmitter-receiver pair. The signal at the receiver coil and its variation with distance from a wire is tabulated and represents the response function of the apparatus. The measured response function is compared with a simple analytical model and excellent agreement is achieved. Since the transmitter and receiver are dipoles in nature, the shape of the response function depends highly on their orientation with respect to each other and the wire. Additional measurements are obtained for a variety of orientations and are also compared with the simple model. Again, excellent agreement is achieved for alternate orientations.

The geometry and analytical model are first discussed. This is followed by a presentation of the experimental arrangement and results for one set of dipole orientations. Additional dipoles orientations are shown and all results are compared with the model. I also measure the signal variation with height above the conductor (which is a wire) for two sets of dipole orientations. Discussion of the particular characteristics of the response functions and considerations for optimal performance follows. Such data will help to understand the functioning of fielded devices. These results are also important for experimental verification of model calculations for a basic Tx/Rx arrangement. Finally, this data is expected to stimulate ongoing research into more complex geometries.

REFERENCES

1. Metje, N., P. R. Atkins, M. J. Brennan, D. N. Chapman, H. M. Lim, J. Machell, J. M. Muggleton, S. Pennock, J. Ratcliffe, M. Redfern, C. D. F. Rogers, A. J. Saul, Q. Shan, S. Swingler, and A. M. Thomas, "Mapping the underworld — State-of-the-art review," *Tunn. Undergr. Sp. Tech.*, Vol. 22, 568–586, 2007.
2. Kolera B. T. and L. E. Bernold, "Intelligent utility locating tool for excavators," *J. Constr. Eng. M. ASCE*, Vol. 132, 919–927, 2006.

Session 4P4a
Computational Electromagnetics, EM Method and Simulation 2

Fast Parametric Models for Microwave Components Using Vector Fitting, Neural Networks and Space-mapping Techniques

Zhiyu Guo[1], **Qi-Jun Zhang**[1], **and Jianjun Gao**[2]

[1]Department of Electronics, Carleton University
1125 Colonel by Drive, Ottawa, Ontario, K1S 5B6, Canada
[2]School of Information Science and Technology, East China Normal University
500 DongChuan Road, Shanghai 200241, China

Abstract— This paper presents a new method to create a fast parametric equivalent circuit model for microwave components using vector fitting combined with neural network & space-mapping techniques. A major important contribution of this paper is to compensate the difference brought by converting negative resistors which are generated by transforming poles and residues of approximating rational functions to equivalent circuit element values into positive resistors using neural network & space-mapping techniques. First, the admittance data of patch antenna is derived through EM simulator HFSS, and with the help of rational functions, we utilize vector fitting algorithm to identify the poles and residues in the rational functions to fit the original admittance data of patch antenna. Then through poles and residues, SPICE compatible equivalent circuit is determined directly. In the meantime, by judging the poles real or complex conjugate pair we could choose the topology of equivalent circuit and calculate the RLC values. Next, we make full use of neural network & space-mapping techniques to complete the method. For one thing, neural network could model a large frequency and geometry dimensional range of patch antenna. For another thing, space-mapping technique gives an excellent solution about how to deal with the presences of negative resistors. Finally, the results between EM simulator data and final outputs of neural network are given to demonstrate the method very effectively and accurately. Compared with EM simulator one advantage of this method is much faster. Compared with vector fitting algorithm another advantage is that such a method could make geometry parameters of microwave components variables and the resulting model could be applied to do optimization.

Electromagnetic Simulation of a Bulk Current Injection Test Setup for Automotive Applications

F. Grassi and S. A. Pignari
Department of Electrical Engineering, Politecnico di Milano
P.za Leonardo da Vinci, 32, I-20133-Milano, Italy

Abstract— Electromagnetic Compatibility (EMC) test procedures based on the Bulk Current Injection (BCI) technique are widely diffused in the automotive sector for immunity assessment of equipments interconnected by wiring harnesses. The procedure is cost-effective and not time-consuming. Additionally, it allows for onboard testing as well as for pre-compliance verifications at the early design-stage. However a difficulty is expressed for the shortage of reasonably accurate methods to predict the noise levels actually injected into the terminal units. This is particularly true in the practical case of multi-wire bundles, since the fixture for probe-calibration foreseen by the Standards (i.e., the so-called *jig*) is designed to reproduce the external characteristics of a bunch of wires (as an ideal single-ended interconnection, [1]), but it inherently is unable to account for its transmission characteristics, involving different propagation modes. Particularly, differential lines used for data communication [e.g., bus lines used to implement the controller area network (CAN) technology] represent simple but relevant examples of cable harnesses for which standard calibration procedures do not provide accurate indication on the actual noise levels entering the terminal units. As a consequence, consistent correlation between immunity levels obtained by the BCI technique and by other testing methods foreseen by automotive Standards is also not straightforward. For instance, in [2] the higher severity of the BCI test with respect to the transverse electromagnetic (TEM) cell method was shown by measurements.

In this work, the dominant phenomena involved in the injection of RF current onto differential lines are investigated by resorting to electromagnetic (EM) simulation of a typical BCI test setup. Particularly, hybrid EM modeling, [3], is adopted for the simulation of the BCI probe, and experimental measurements are used for model assessment. The probe is clamped onto a pair of wires (both parallel and twisted wire-pairs are considered in this analysis) running above ground and terminated in suitable lumped-parameter circuit networks, representative of the terminal units. Common mode (CM) and differential mode (DM) components of the noise levels induced at the terminations of the line are numerically predicted, and correlated to specific characteristics of the line and of the terminal networks. Particular attention is focused on the role that the degree of unbalance of the terminal units plays on DM-noise levels. This aspect is investigated by a specific set of simulations, and is interpreted in terms of CM-to-DM conversion due to unbalance of the terminal units.

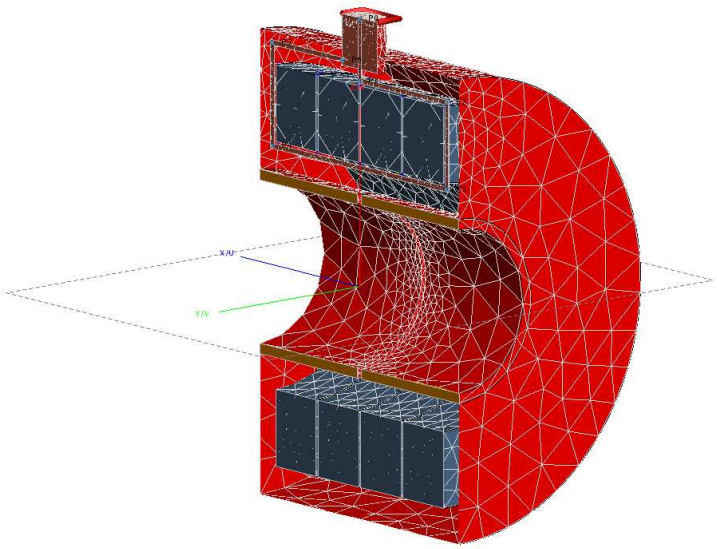

Figure 1: EM model of the injection device (BCI probe).

REFERENCES

1. Grassi, F. and S. A. Pignari, "Characterization of the bulk current injection calibration-jig for probe-model extraction," *Proc. 2010 IEEE Int. Symp. on Electromagn. Compat.*, 344–347, Fort Lauderdale, FL, USA, Jul. 2010.
2. Rostamzadeh, C. and S. A. Pignari, "Test procedure for CAN bus susceptibility evaluation based on the use of radio frequency detectors," *Proc. XIXth General Assembly of International Union of Radio Science (U.R.S.I.)*, Commission AE, Paper AE.2, Chicago, IL, USA, Aug. 2008.
3. FEKO Suite 6©EM Software and Systems, S.A. (Pty) Ltd., Stellenbosch, South Africa, ww.feko.info.

The Numerical Solution of Aperture Penetrating Integral Equations Based on Wavelet Galerkin Method

Jianshu Luo and Zhenzheng Ouyang
College of Science, National University of Defense Technology, Changsha 410073, China

Abstract— There are many literatures studied computation of aperture penetrating fields. In frequency domain,most of the methods be based on dipole moment method and power method. Dipole moment methods are generally for low frequencies, whereas power methods are for high frequencies. These methods are not suitable for middle frequencies.

In this paper, it is result in aperture penetrating integral equations based on geometrical boundary conditions of cavity with an aperture. Then, it is analyzed singularity of penetrating field integral equations. Under wavelet Galerkin method framework, we designed a numerical solution method to solve aperture penetrating integral equations. And, we analyzed stable and convergency of the numerical solution method. Furthermore, the error analysis and computation complex of the numerical method are presented. At last, numerical examples are presented to demonstrate computational efficiency of the proposed algorithm.

Analysis and Simulation for RF Interconnect

Jian-Fei Xu and Na Yan
ASIC & System State Key Laboratory, Fudan University, China

Abstract— As the development of the speed and scale of ULSI, the date rate between different core becomes higher and higher. Traditional date communication way in the chip or among the system meets some limits which are hard to overcome. Researchers are looking for new means to achieve high date rate and low energy. RF interconnect is an important way to reach the goal. A RF interconnect system include RF transmitter, microwave transmission line or antenna, RF receiver. The baseband signal is modulated by a high frequency signal such as 50 GHz; then the signal is transmitted through transmission line or antenna; at the other end, the signal is amplified and demodulated. In this way, the attenuation in the channel can be reduced and the transmission distance can be longer. In this way, RF interconnect can be used in both on-chip and chip-chip communication. In this work, the concept and characteristics of RF interconnect are recalled and different new interconnect methods are discussed. Then a design of RF interconnect system is discussed and simulated by system model in ADS environment. In this design, a FDMA (frequency division multiple access) transceiver system is used. Three carrier frequencies are 25 GHz, 45 GHz and 65 GHz. Baseband signal is modulated and transmitted through a common microwave transmission line. The date rate of each RF band is 2 Gb/s, so the total date rate is 6 Gb/s. The performances of each part of the system are illustrated in the simulation. This simulation also shows us which part should be paid more attention to when we design a RF interconnect system.

Session 4P4b
Mobile Antennas, UWB Antenna and Array

Miniaturised Slot Loop Antennas on Dielectric and Magnetic Substrates

Fang He and Z Wu
School of Electrical and Electronic Engineering, The University of Manchester
Manchester M13 9PL, UK

Abstract— Digital cellular handsets and other portable devices are widely used in everyday life. Therefore, it is a challenge to miniaturise antennas into very limited space inside mobile terminals. The traditional narrow band antenna miniaturisation loads the antenna with different materials, especially very high permittivity dielectric materials (permittivity is from 9 to 100). However, degradation of antenna performance and difficulty of impedance matching are the two main drawbacks to this material loading miniaturisation method. A newly-developed method is to load composite magneto-dielectric materials instead of pure dielectric ones. Applying magnetic material can improve bandwidth and efficiency performance while suppressing field confinement. Furthermore, because the characteristic impedance of magneto-dielectric material is close to the surrounding medium, it is much easier for impedance matching in a wider bandwidth.

Recently, an organic magnetic material was introduced and manufactured in China. This material has stable magnetic performance and high relative permittivity and permeability. It is suitable for designing compact and broadband microstrip antennas. The research done by Chinese scholars shows that the new organic magnetic material can reduce the antenna size from approximately 32% to 40% while improving impedance bandwidth from 3.2 to 6 times compared with normal dielectric materials.

A novel technology applied to antenna miniaturisation is folded patch antenna, which has been reported in the literature. The antenna patches or strips are folded in multi-layers to form a 3D antenna model. Therefore, the antenna length is increased efficiently to keep the antenna geometry more compact than the conventional planar design. The research results showed that the folded patch antenna can achieve nearly 40% miniaturisation. Moreover, decreasing the separation distance between the folded patches can lower the resonation frequencies. Instead, folded slot loop antennas fabricated on dielectric or organic magnetic substrate are reported in this paper with a consideration of their applications for WLAN and UWB applications. The effect of organic magnetic material will be discussed and compared with normal FR4 material. The measured S-parameters and far-field patterns will also be presented.

Studies of Planar Antennas with Different Radiator Shapes for Ultra-wideband Body-centric Wireless Communications

Y. Y. Sun, S. W. Cheung, and T. I. Yuk
Department of Electrical and Electronic Engineering,
The University of Hong Kong, Pokfulam Road, Hong Kong, China

Abstract— In the design of antennas for body-centric wireless communications systems using the ultrawide band (UWB), the main factors to be considered are the physical size, link loss along the body surface, radiation characteristic in the proximity of the human body, front-to-back ratio and simplicity, etc.. Many UWB antennas with different shapes have been studied and proposed, but none of them give a thorough study on UWB antennas with different shapes of radiators for body-centric wireless communications systems. This paper studies the performances of planar UWB antennas using a radiator of different shapes such as triangle, rectangle, pentagon, hexagon, annual ring, circle and ellipse (horizontal and vertical) for body-centric wireless communications. The planar antennas studied consist of a radiator and a microstrip-feed line on one side of the substrate and a ground plane on the other side.

Optimization of each antenna is carried out using computer simulation tool. The return loss, peak gain and radiation pattern of the antenna on-body, are compared to the results of the antenna in free space. Results of studies show that, with an elliptical radiator, the antenna has a relatively better performance in terms of bandwidth, gain and radiation pattern, among the antennas studied. The antenna can achieves a very wide impedance bandwidth, with Voltage-Standing-Wave Ratio (VSWR) ≤ 2, from about 2.9 GHz to more than 18 GHz, an average peak gain of nearly 3 dBi and a quite stable omnidirectional radiation pattern across the UWB band.

The results also show that the antenna with an elliptical radiator has a more reliable performance in body-area-network (BAN) applications, thus the antenna is a good candidate for UWB BAN body-centric wireless communications.

Bandwidth Improvements Using Ground Slots for Compact UWB Microstrip-fed Antennas

L. Liu, **S. W. Cheung**, **and T. I. Yuk**
Department of Electrical and Electronic Engineering, The University of Hong Kong, Hong Kong, China

Abstract— The paper studies the method of using a ground slot for bandwidth improvement of compact ultra-wide band (UWB) antennas with microstrip line feed. Impedance matching through the UWB is a challenging problem for the design of antennas. In this paper, the method of cutting a small slot on the upper edge of the ground plane under the feed line for impedance matching is explored. Different shapes of slots such as rectangle, triangle, hexagon, circle, trapezoid, and ellipse, etc., placed under the feed line of the patch antennas are studied for impedance matching through the UWB.

The effects of the slots on the performances of the antennas, in terms of impedance bandwidth, radiation patterns, gain, and efficiency, are studied. Results show that a ground slot with proper dimensions placed under the feed line can improve impedance matching and hence increase the bandwidth without affecting the radiation pattern. Moreover, the ground slot can also substantially reduce the antenna size. Thus cutting a slot on the ground is a simple and effective way to increase the bandwidth for UWB applications.

Results of studies also show that, by using a slot on the ground plane under the feed line, a patch antenna with a compact size of 35 mm × 23 mm can achieve a bandwidth of about 3–16 GHz for VSWR < 2. Moreover, it has a stable omnidirectional radiation pattern across the whole bandwidth, an average gain of 3 dBi and an average efficiency of 70%. The method proves to be very useful for the design of UWB antennas.

Compact Directional UWB Antenna with Improved Performance

Fuguo Zhu[1], **Steven Gao**[1], **Anthony T. S. Ho**[2], **Tim Brown**[3], **and Jiadong Xu**[4]

[1]Surrey Space Centre, University of Surrey, Guildford, GU2 7XH, UK
[2]Department of Computing, University of Surrey, Guildford, GU2 7XH, UK
[3]Center for Communications System Research, Guildford, GU2 7XH, UK
[4]School of Electronics and Information, Northwestern Polytechnical University, Xi'an 710072, China

Abstract— A compact planar directional ultra-wideband (UWB) antenna with high front-to-back ratio is proposed in this paper. The antenna is fabricated on a printed circuit board (PCB), having a circular patch on one side and a slot ground plane excited by a fork-shaped feeding stub on the other side. Directional radiation is achieved by using a reflector below the antenna. Three types of directional UWB antennas are analyzed and compared. Compared to other reported antennas, the proposed antenna has advantages of low profile and also higher gain in lower frequency band of UWB. The distance between the antenna and the reflector is 12 mm ($0.16\lambda_0$, λ_0 is the free space wavelength at the lowest frequency). Measured results agree very well with the simulated results. The measured results confirm that the proposed antenna features a 10-dB return loss bandwidth from 4.1 to 8.8 GHz, a broadside gain from 6.81–9.36 dBi, over 17 dB front-to-back ratio, and stable radiation patterns over the whole frequency band.

Band-notch Patch Ultra-wide Band Antenna

Ayman A. R. Saad[1], **Deena A. Salem**[2], **and Elsayed E. M. Khaled**[3]

[1]Kosseir Radio, Telecom Egypt, Kosseir, Egypt
[2]Microstrip Department, Electronics Research Institute, Giza, Egypt
[3]Electrical Engineering Department, Assiut University, Assiut, Egypt

Abstract— High data rate transmission with high efficiency, minimum distortion in the received signal emphasis the use of ultra wideband (UWB) wireless communication systems (3.1–10.6 GHz) which requires UWB antenna designs. Many of such antennas configurations have been proposed and developed [1]. Communications with UWB frequency operation can be obtained using planar antenna. However, these antennas need a band rejection filter to avoid interference with existing standard wireless networks such as WLAN in USA (5.15–5.35 GHz, 5.725–5.825 GHz) and HIPERLAN/2 in Europe (5.15–5.35 GHz, 5.47–5.725 GHz). To avoid adding new circuits to the communication system, band-notching technique can be applied directly to various UWB planar antennas by loading the radiator of the antenna with a slot that resonates at the center frequency of the stop band [2]. In this paper, a new UWB planar antenna is proposed, that employs a single slotted patch electromagnetic band gap (spEBG) element, placed at the opposite side of the substrate beneath the radiating patch, to obtain and control the rejected frequency bands at 5.5 GHz for UWB applications. The design process involves two phases; the first phase is to design a new shape of UWB planar antenna. Then, the second phase is to incorporate the designed antenna with the spEBG element which can achieve the required frequency band-notched characteristic for UWB applications.

The designed antenna is etched on FR4 substrate of dimensions of $L_{\mathrm{Sub}} \times W_{\mathrm{Sub}} = 20 \times 56\,\mathrm{mm}^2$ with a thickness $h = 1.6\,\mathrm{mm}$ and relative permittivity $\varepsilon_r = 4.2$, loss tangent $\tan\delta = 0.01$, with a reduced ground plane with length $L_g = 10\mathrm{mm}$. The patch has dimensions of $L_p = 6\,\mathrm{mm}$ and $W_p = 8\,\mathrm{mm}$. The antenna is fed by a 50-Ω microstrip line that consists of a strip of width $W_f = 3\,\mathrm{mm}$, and length $L_f = 7\,\mathrm{mm}$ printed on the surface of the substrate. The feed gap (g) is 2 mm. We proposed a new method to obtain the required band-notched characteristic by employing a single slotted patch as a band-reject beneath the original radiating patch. The additional patch comprises a U-shaped slot. The slot parameters are selected to optimize the band-rejected performance with a center frequency of 5.5 GHz. The slot has a uniform width 1 mm, two vertical lengths of $l_1 = l_2 = 5\,\mathrm{mm}$ and a horizontal length $l_3 = 7\,\mathrm{mm}$. A strip of width 0.5 mm is considered around the slots. The electromagnetic software Zeland IE3D is used to analyze the antenna. The antenna is fabricated and the measured data of return loss highly agreed with the simulated results. It is apparent that the proposed antenna can operate efficiently over the frequency band from 3.7 to 11.4 GHz with a sharp band rejection from 5.29 to 5.96 GHz. The proposed antenna has good gain flatness and high efficiency over the frequency band of operation excluding the rejected band.

REFERENCES

1. Danideh, A., R. Sadeghi Fakhr, and H. R. Hassani, "Wideband co-planar microstrip patch antenna," *Progress In Electromagnetics Research Letters*, Vol. 4, 81–89, 2008.
2. Liu, H.-W., C.-H. Ku, T.-S. Wang, and C.-F. Yang, "Compact monopole antenna with band-notched characteristic for UWB applications," *IEEE Antenna and Wireless Propagation*, Vol. 9, 397–400, 2010.

Novel Design of Proximity-fed Ultra-wide Band Annular Slot Antenna

Ayman A. R. Saad[1], **Elsayed E. M. Khaled**[2], **and Deena A. Salem**[3]

[1]Kosseir Radio, Telecom Egypt, Kosseir, Egypt
[2]Electrical Engineering Department, Assiut University, Assiut, Egypt
[3]Microstrip Department, Electronics Research Institute, Giza, Egypt

Abstract— Since the Federal Communications Commission (FCC) in USA released the unlicensed commercial use of ultra-wide band (UWB) radio system (3.1–10.6 GHz) in 2002, various types of planar UWB antennas with band-notch property has been proposed and developed for wireless communication systems, with maintaining the existing narrow band services [1, 2]. Most of the available literatures focused on designing planar band-notched UWB antennas with microstrip line-feed technique [3]. In this work, a different feeding technique is adopted, which is proximity-feed. Besides, new techniques are applied to acquire the band-notch property.

A circular patch is placed non-concentrically in a ground plane aperture (GPA), with a microstrip line on the other side of the substrate. This configuration yielded a UWB performance. The band-notch property is obtained by using three different techniques. In the first technique, a single complementary split ring resonator (CSRR) is etched off the circular patch. In the second technique, a complementary spiral loop resonator (CSLR) is etched off the circular patch. Whereas, in the third technique, a U-shaped slot is etched off the microstrip line. The main idea is to adjust the resonant frequency of the etched slots with the rejection band required, to provide the band notch property over the desired frequency range. The challenge is to tune the resonant frequencies by adjustment of the dimensions of the etched slots.

The proposed antenna is fabricated on a $30 \times 30\,\text{mm}^2$ FR4 substrate of 1.5 mm thickness with a dielectric constant of 4.7, loss tangent $\tan\delta = 0.02$. A circular slot has a radius $R = 12.0\,\text{mm}$ etched in the ground plane. A $50\,\Omega$ microstrip line with width of $w_f = 3.0\,\text{mm}$ and length of $l_f = 11.5\,\text{mm}$ is used. A circular patch of radius $r = 6.0\,\text{mm}$, is placed non-concentrically, in the circular slot. The electromagnetic software, Zeland IE3D is used to analyze the antenna. The performance of the antenna is analyzed using parametric study to investigate the tuning effects of the resonator parameters on the impedance matching. The prototype antenna is fabricated and the measured data of the return loss versus frequency show very good agreement with the simulated results. It is apparent that the designed antenna satisfies a 10 dB return loss requirement in the frequency band from 2.86 to 8.48 GHz, with band-notch at 5.5 GHz band, which corresponds to the WLAN services. The proposed antenna has a simple shape and provides almost omnidirectional patterns, relatively flat gain and high radiation efficiency over the entire UWB frequency band excluding the rejected band.

REFERENCES

1. Schantz, H. G. and G. P. Wolenec, "Ultra-wideband antenna having frequency selectivity," U.S. Patent Publication No. 2003/0090436 A1, 2003.
2. Choi, J., S. Hong, and U. Kim, "The design of an UWB antenna with notch characteristic," *PIERS Online*, Vol. 3, No. 7, 987–990, 2007.
3. Zhang, Y., W. Hong, C. Yu, Z.-Q. Kuai, Y.-D. Don, and J. Y. Zhou, "Planar ultrawideband antennas with multiple notched bands based on etched slots on the patch and/or split ring resonators on the feed line," *IEEE Transactions on Antennas and Propagation*, Vol. 56, No. 9, 3063–3068, Sep. 2008.

Optimization of Radiation Patterns of Array Antennas

V. Rajya Lakshmi[1] and G. S. N. Raju[2]

[1]Department of Electronics and Communication Engineering
Anil Neerukonda Institute of Technology and Sciences, Visakhapatnam, India
[2]Department of Electronics and Communications Engineering
AU College of Engineering (A), Andhra University, Visakhapatnam, India

Abstract— The array antennas exhibit flexibility in the design of radiation patterns. Conventionally, they are designed by controlling amplitude levels, phase levels, space distribution and elements. In practice, for pre-designed radiating elements in the array, one of the above parameters is considered for the design keeping the others fixed. However, in the present work the method of thinning is used to reduce sidelobes without disturbing null-to-null beamwidth. When the elements of the array are uniformly excited, the first sidelobe level is found to be −13.5 dB. It is of interest here to reduce them considerably from the conventional level. The methodology involves the application of genetic algorithm to blind the required radiating elements in such a way the resultant pattern is optimized.

It is well known that the aperiodic arrays produce low sidelobe amplitude patterns by suitably positioning equally weighted elements. It is possible to increase the density of the elements in some locations and decrease the same in other locations. But in the present method, the density of radiating elements along the array axis becomes random. Thinning an array means either blinding some elements or removal of elements in a uniformly spaced or periodic array to create suitable element density across the aperture.

It is found from the results, the sidelobes are reduced to the extent of above −30 dB. The pattern is found to be marginally altered with the number of iterations taken. The computations are carried out for the generation of radiation patterns for different arrays containing the number of elements 20, 50, 100. It has been possible to conclude that the sidelobes are reduced without enhancing the beamwidth using the present approach.

Session 4P5
Optics and Photonics 2

Longitudinally Polarized Light

Haifeng Wang and Boris Luk'yanchuk
A*STAR, Data Storage Institute
DSI Building, 5 Engineering Drive 1, NUS, Singapore 117608, Singapore

Abstract— Light wave is described as a transversal wave by Maxwell equations, i.e., its polarization is always perpendicular to its propagation direction. However, tightly focused radial polarized light has strong longitudinal components, which take about 45% of the total energy in the central lobe when the numerical aperture of the lens is 0.95 [1], and this ratio can increase to 81% after applying a binary optical element shown in Fig. 1(a), where the energy density of radial component is only about 8% of the longitudinal component, i.e., this beam is substantially a longitudinally polarized beam, as is shown in Fig. 1(b). This longitudinally polarized laser beam propagates about 4 wavelengths without divergence, with a beam size of about 0.43λ, as is shown in Fig. 1(c).

Longitudinally polarized light has many attractive applications, for example, in particle acceleration [2], fluorescent imaging [3], second-harmonic generation [4], Raman spectroscopy [5], and scattering scanning near-field optical microscopy [6], it can also suppress cracks and generate smoother interface in material processing [7, 8]. This talk will address solutions to generating longitudinally polarized light, its applications in various fields and its prospects.

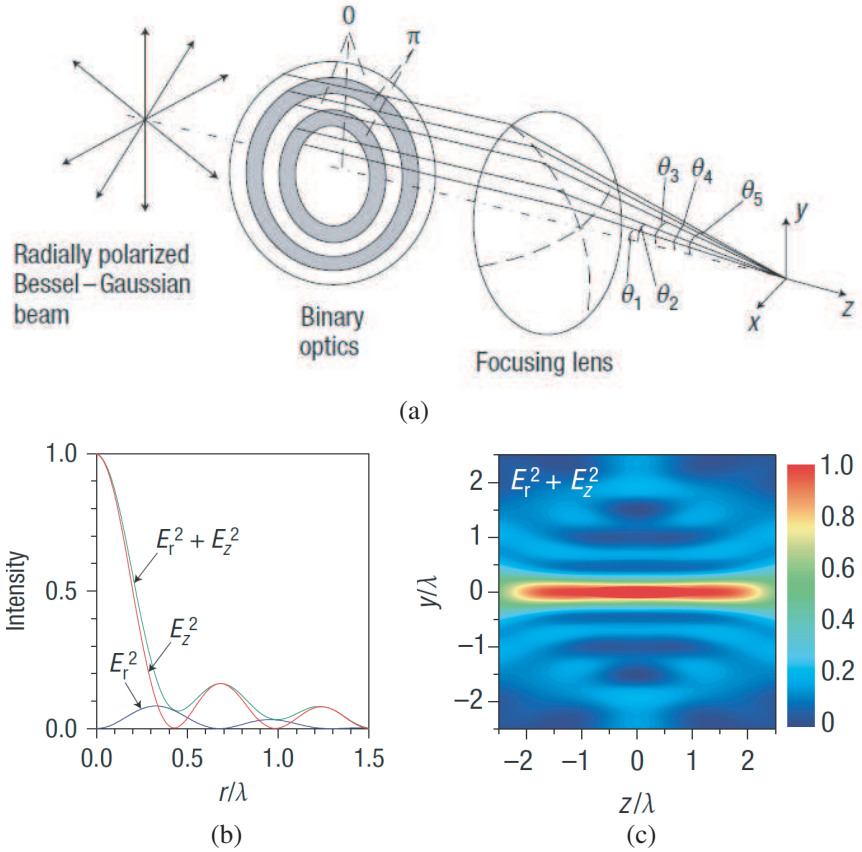

Figure 1: Longitudinally polarized light generation: (a) schematic setup, (b) electric density profile of longitudinal component, radial component and the total, (c) total electric density image on the y-z plane.

REFERENCES

1. Wang, H., L. Shi, B. Luk'yanchuk, C. Sheppard, and C. T. Chong, "Creation of a needle of longitudinally polarized light in vacuum using binary optics," *Nature Photonics*, Vol. 2, 501–505, 2008.

2. Fontana, J. R. and R. H. Pantell, "A high-energy, laser accelerator for electrons using the inverse Cherenkov effect," *J. Appl. Phys.*, Vol. 54, 4285–4288, 1983.
3. Novotny, L., M. R. Beversluis, K. S. Youngworth, and T. G. Brown, "Longitudinal field modes probed by single molecules," *Phys. Rev. Lett.*, Vol. 86, 5251–5254, 2001.
4. Biss, D. P. and T. G. Brown, "Polarization-vortex-driven second-harmonic generation," *Opt. Lett.*, Vol. 28, 923–925, 2003.
5. Lin, J., F. Lu, H. Wang, W. Zheng, C. J. R. Sheppard, and Z. Huang, "Improved contrast radially polarized coherent anti-Stokes Raman scattering microscopy using annular aperture detection," *Appl. Phys. Lett.*, Vol. 95, 133703, 2009.
6. Xiao, M., "Theoretical treatment for scattering scanning near-field optical microscopy," *J. Opt. Soc. Am. A*, Vol. 14, 2977–2984, 1997.
7. Hnatovsky, C., V. Shvedov, W. Krolikowski, and A. Rode, "Revealing local field structure of focused ultra-short pulses," *Phys. Rev. Lett.*, Vol. 106, 123901, 2011.
8. Iwase, H., S. Kokubo, S. Juodkazis, and H. Misawa, "Suppression of ripples on ablated Ni surface via a polarization grating," *Opt. Express*, Vol. 17, 4388–4396, 2009.

Cerenkov-type Second Harmonic Generation and Its Application to Three-dimensional Nonlinear Microscopy

Yan Sheng[1], **Wieslaw Krolikowski**[1], **Ady Arie**[2], **and Kaloian Koynov**[3]

[1]Laser Physics Center, Research School of Physics and Engineering
Australian National University, Canberra, ACT 0200, Australia
[2]School of Electrical Engineering, Tel-Aviv University, Tel-Aviv 69978, Israel
[3]Max Planck Institute for Polymer Research, Ackermannweg 10, Mainz 55128, Germany

Abstract— We present experimental studies on the Čerenkov-type second harmonic generation (SHG) in two-dimensional nonlinear photonic structures (NPS). We demonstrate the observation of conical second harmonic generated when illuminating the NPS by a weakly focused fundamental Gaussian beam. We show that the Čerenkov second harmonic generated in the domain wall regions is much stronger than that produced in the homogenous domains. Based on this effect, we create a simple nonlinear microscope which allows direct, three dimensional non-destructive imaging of the inverse domain pattern in NPS with a sub-micrometer resolution.

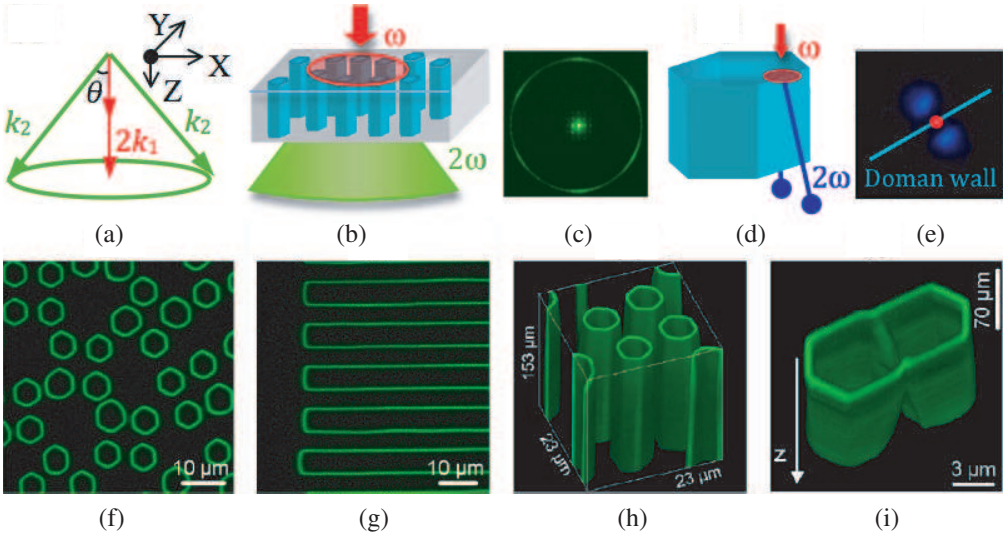

Figure 1: (a) Phase-matching condition for the Čerenkov-type SHG. (b) Schematic of the conical Čerenkov SH emission in NPS. (c) Experimentally recorded Čerenkov SHG (large green circle). (d) Schematic of the Čerenkov SH emission from a single domain wall. (e) Experimentally recorded pair of Čerenkov SH signals (two blue spots) after tightly focusing of a laser beam at a single domain. (f) and (g) Domain structures imaged by the Čerenkov-type SHG. (h) and (i) 3D visualization of the domain structures as well as the merging process of two initially separated domains.

REFERENCES

1. Saltiel, S. M., Y. Sheng, N. Voloch-Bloch, D. N. Neshev, W. Krolikowski, A. Arie, K. Koynov, and Yu. S. Kivshar, *IEEE. J. Quantum Electron.*, Vol. 45, 1465, 2009.
2. Sheng, Y., S. M. Saltiel, W. Krolikowski, A. Arie, K. Koynov, and Yu. S. Kivshar, *Opt. Lett.*, Vol. 35, 1317, 2010.
3. Wang, W., Y. Sheng, Y. Kong, A. Arie, and W. Krolikowski, *Opt. Lett.*, Vol. 35, 3790, 2010.

Bending (Accelerating) Airy Beams

I. M. Besieris[1] and A. M. Shaarawi[2]

[1]The Bradley Department of Electrical and Computer Engineering
VPI&SU, Blacksburg, Virginia 24061, USA
[2]The Physics Department, The American University in Cairo
P. O. Box 2511, Cairo 11511, Egypt

Abstract— A finite-energy *bending* Airy beam solution to the paraxial equation in free space was first formulated analytically by Siviloglou and Christodoulides and subsequently demonstrated experimentally by Siviloglou, Broky, Dogariu and Christodoulides. This work was motivated by the infinite-energy (nonspreading) *accelerating* Airy solution to the Schrödinger equation introduced by Berry and Balazs in the context of quantum mechanics. An Airy beam is slowly diffracting; it can retain its intensity properties over several diffraction lengths while bending laterally along a parabolic path despite the fact that its centroid is constant. Another feature, which has been demonstrated both analytically and experimentally, is that an Airy beam propagating in free space can perform ballistic dynamics akin to those of projectiles moving under the action of gravity. These exotic properties suggest various physical applications, such as Airy beam-mediated particle cleaning and vacuum electron acceleration. Ultra intense Airy beams have been used to create curved plasma channels. Airy beams have been studied in connection with unbiased photorefractive media. Accelerating spatiotemporal Airy wavepackets can defy effectively both dispersion and diffraction.

Both bending Airy beams and accelerating Airy wavepackets are characterized by self-healing properties; they tend to reform in spite of the severity of imposed perturbations. The robustness of such beams in scattering and turbulent environments has been studied numerically and experimentally in the optical regime.

The specific purpose in this presentation is to examine bending Airy beam solutions in the presence of canonical deterministic inhomogeneities. Toward this goal, use will be made of an isospectral technique. Two-dimensional and three-dimensional solutions will be discussed in detail.

Cylindrical Vector Beams are Eigenstates of Total Angular Momentum

Shuang-Yan Yang[1], **Ting-Ting Wang**[1], **and Chun-Fang Li**[1, 2]

[1]Department of Physics, Shanghai University, Shanghai 200444, China
[2]State Key Laboratory of Transient Optics and Photonics
Xi'an Institute of Optics and Precision Mechanics, Chinese Academy of Sciences, Xi'an 710119, China

Abstract— It is well known [1] that the Laguerre-Gaussian beams carry orbital angular momentum by phase factors $e^{il\phi}$ and spin angular momentum by polarization ellipticity σ. This is because they are paraxial beams that are uniformly polarized. Such a simple result does not hold for general non-paraxial case [1994]. In this paper, we will show that cylindrical vector beams are eigen states of total angular momentum $\hat{J}_z$ in both paraxial and non-paraxial cases. Following Ref. [3], we find that a cylindrical vector beam that has a scalar angular spectrum of $f(k_\rho)e^{il\phi}$ is an eigen state of $\hat{J}_z$. The eigen value is $l\hbar$ that is independent of the polarization ellipticity.

REFERENCES

1. Allen, L., M. W. Beijersbergen, R. J. C. Spreeuw, and J. P. Woerdman, *Phys. Rev. A*, Vol. 45, 8185, 1992.
2. Barnett, S. M. and L. Allen, *Opt. Commun.*, Vol. 110, 670, 1994.
3. Li, C.-F., *Phys. Rev. A*, Vol. 78, 063831, 2008.

Characterization of Vector Diffraction-free Light Beams

Ting-Ting Wang[1], **Shuang-Yan Yang**[1], **and Chun-Fang Li**[1, 2]

[1]Department of Physics, Shanghai University, Shanghai 200444, China
[2]State Key Laboratory of Transient Optics and Photonics
Xi'an Institute of Optics and Precision Mechanics of the Chinese Academy of Sciences
Xi'an 710119, China

Abstract— It is shown that the vectorial character of diffraction-free light beams can be represented by a previously introduced [1] unit vector **I**. To each specified **I**, there always corresponds a complete set of orthonormal vectorial diffraction-free modes, which acts as a basis for expanding an arbitrary vectorial light beam. When **I** is perpendicular to the propagation direction, one arrives at the scalar diffraction-free beam [2, 3] in the paraxial approximation. When **I** is parallel to the propagation direction, one arrives at the cylindrical-vector diffraction-free beam [4]. The effect of **I** on the longitudinal component is discussed, which indicates that contrary to the usual viewpoint [5], one can not tell whether a light beam is paraxial or not by only examining whether its longitudinal component is negligible or not.

REFERENCES

1. Li, C.-F., *Phys. Rev. A*, Vol. 78, 063831, 2008.
2. Durnin, J., *J. Opt. Soc. Am. A*, Vol. 4, 651, 1987.
3. Durnin, J., J. J. Miceli, Jr., and J. H. Eberly, *Phys. Rev. Lett.*, Vol. 58, 1499, 1987.
4. Bouchal, Z. and M. Olivík, *J. Mod. Opt.*, Vol. 42, 1555, 1995.
5. Martínez-Herrero, R., P. M. Mejías, and G. Piquero, *Characterization of Partially Polarized Light Fields, Springer Series in Optical Sciences*, Vol. 147, 1, 2009.

The Enhancement of the Light Scattering/Absorption from the Correlation Effect between Molecules

Wei-Xing Xu
NewTech Monitoring Inc., 1872 Birchview Dr, Oshawa, Ontario, L1K 3B9, Canada

Abstract— In this paper we first proposed the concepts of the correlated spectra/non-correlated spectra and discussed the correlation effect between molecules on the light scattering/absorption of the molecule. Furthermore, we also explored the potential application of this correlation effect in photo chemistry and related fields.

Self-field Theory, General Relativity and Quantum Theory

A. H. J. Fleming
Biophotonics Research Institute, Melbourne, Australia

Abstract— There are theoretical similarities between general relativity (GR) and quantum field theory (QFT). Among the most fundamental are that both are based on 2nd order wave equations and their associated potential theories and gauge considerations. In comparison SFT is based on the 1st order Maxwellian with its field variables that have a much reduced emphasis on gauge. Both GR and QFT are based around single particle analysis rather than the mutual effects that couple particles together studied in SFT. Finally both GR and quantum theory employ a metric that in the view of SFT serves to accommodate the over constraint of the basic equations. In both cases this is linked to a theoretical requirement for a zero-mass photon. Thus both quantum theory and GR depend upon a zero mass photon and hence from the point of view of SFT both quantum theory and GR are theoretical approximations. For quantum theory zero mass springs from the earliest observations of beta decay and again when a negligible rest mass of the photon could hardly be compared with the seemingly endless radiation from within the nucleus of the bombs dropped on Hiroshima and Nagasaki in 1945. The cosmological principle that had its genesis in the Vatican's unscientific and dogmatic dealings with Galileo was a way to avoid having any universal center of gravity thus making the same mistake again. Nevertheless it is only an approximation in the light of SFT where it is seen that non-homogeneity and anisotropy are both present in the gravitational structure itself where space is divided into different gravitational regions. This structure depends on the composite nature and non-zero mass of the photon. The space within the Universe cannot be thought of as the surface of an expanding balloon other than as a theoretical approximation that holds for GR. It is known that at smaller than cosmological domains the cosmological principle does not hold for instance for any possible surviving location of the Big Bang. We may think of a biological tissue such as liver where the dielectric constant is averaged over the microstructure such as biological cells. While such an approximation is useful for numerical estimation it cannot be assumed to hold in any fine detail across smaller domains; this holds for both a homogenous isotropic model of liver and of the Cosmos.

REFERENCES

1. Fleming, A. H. J., "Electromagnetic self-field theory and its application to the hydrogen atom," *Physics Essays*, Vol. 18, No. 3, 265–285, 2005.
2. Fleming, A. H. J., "Self-field theory, analytic spectroscopy of the ordinary photon," *Proc. 2nd Electromagnetics Health and Environment Intl. Conf.*, 18–23, Wroclaw, Poland, 2007.
3. Fleming, A. H. J., "Analytic estimate for the mass of the photon," *PIERS Proceedings*, 1604–1607, Moscow, Russia, 2009.
4. Fleming, A. H. J., Self-field theory — A possible gravitational structure for galaxies, *PIERS Proceedings*, 823–827, Cambridge, USA, July 5–8, 2010.
5. Fleming, A. H. J., *Self-field Theory — A New Mathematical Description of Physics*, Pan Stanford Publishing, 2011.

Two-dimensional Tunable Plasma Photonic Crystal Filters

Limei Qi[1], **Fengqin Lu**[2], **and Liang Shang**[1]

[1]College of Physics and Engineering, Qufu Normal University
No. 57, West Jingxuan Road, Qufu 273165, China
[2]Group of Physics, Senior High School of Fengcheng, No. 1, Yingmou Road, Laiwu 271100, China

Abstract— Since the pioneering work of Yablonovich and John in 1987, the past decades have witnessed an extended development of photonic crystals, also known as photonic band gap (PBG) materials. One of their important properties is to control the flow and distribution of the electromagnetic waves, which opens many technical applications in lossless PC waveguides, low-threshold PC lasers, high-Q cavity, and so on. Early researches meanly concentrated on the conventional photonic crystals consisting of dielectrics and metal metals materials. In 2004, one-dimensional plasma photonic crystal composed of alternating thin plasma and dielectric material was proposed by Hojo et al, it was found that PBG of the plasma photonic crystal can be tuned by plasma density as well as plasma width. Then, plasma photonic crystals were attracted much attention for their controllable PBG by plasma density, collision frequency as well as external magnetic field. However, most works focused on plasma photonic crystals with periodic structures, and few works paid attention to plasma photonic crystals with defects structures. In this paper, two-dimensional unmagnetized plasma photonic crystals with line defects are studied based on plane wave method and finite-difference time-domain method. Transmission characteristics of the two-dimensional plasma photonic crystal waveguides are analyzed, it is found that defect modes of the waveguides can be controlled by plasma density. This feature of plasma photonic crystal waveguides would have potential application in designing tunable photonic crystal waveguides.

ACKNOWLEDGMENT

This work was supported by the National Natural Science Foundation of China (No. 11047193), and the promotive research fund for excellent young and middle-aged scientists of Shandong Province (No. BS2010CL025).

The Dependence of the Acoustomagnetoelectric Current on the Parameters of a Cylindrical Quantum Wire with an Infinite Potential in the Presence of an External Magnetic Field

N. Q. Bau[1], **N. V. Nhan**[2], **and N. V. Nghia**[3]

[1]Department of Physics, College of Natural Sciences, Hanoi National University, Hanoi, Vietnam
[2]Department of Physics, Academy of Defence Force, Air Force, Hanoi, Vietnam
[3]Department of Physics, Water Resources University, Hanoi, Vietnam

Abstract— The acoustomagnetoelectric effect in a cylindrical quantum wire with an infinite potential in the presence of an external magnetic field is investigated by using Boltzmann kinetic equation for an acoustic wave whose wavelength $\lambda = 2\pi/q$ is smaller than the mean free path l of the electrons and hypersound in the region $ql \gg 1$, (where q is the acoustic wave number). The analytic expression for the acoustomagnetoelectric current I^{ac} is calculated in the case: relaxation time of momentum τ is constant approximation and degenerates electrons gas. The nonlinear dependence of the expression for the acoustomagnetoelectric current I^{ac} on the acoustic wave numbers q and on the parameters of the cylindrical quantum wire are obtained. Numerical computations are performed for AlGaAs/GaAs cylindrical quantum wire with an infinite potential. The results are compared with the normal bulk semiconductors and the superlattices to show the values of the acoustomagnetoelectric current I^{ac} in the cylindrical quantum wire are different than they are in the normal bulk semiconductors and the superlattices.

The Parametric Resonance of Confined Acoustic Phonons and Confined Optical Phonons by an External Electromagnetic Wave in Cylindrical Quantum Wires with an Infinite Potential

N. Q. Bau[1], L. T. Hung[2], and L. T. T. Phuong[3]

[1]Department of Physics, Viet Nam National University Hanoi, 334 Nguyen Trai, Hanoi, Vietnam
[2]University of Education, Viet Nam National University Hanoi, 144 Xuan Thuy, Hanoi, Vietnam
[3]College of Education, Hue University, 34 Le Loi, Hue City, Vietnam

Abstract— The parametric resonance of confined acoustic phonons and confined optical phonons by an external electromagnetic wave in cylindrical quantum wires with an infinite potential is studied by using a set of quantum kinetic equations for confined phonons. The analytical expression of the threshold amplitude $E_{\text{threshold}}$ of the field in a cylindrical quantum wires with an infinite potential is obtained. The formula of $E_{\text{threshold}}$ contains two quantum numbers (m, k) characterizing confined phonons. The dependence of the threshold amplitude $E_{\text{threshold}}$ on the temperature T of the system, the the wave vector $\vec{q}_z$, the frequency Ω of an external electromagnetic waves and the radius of the wires R is studied. Numerical computations and graphs are performed for GaAs-GaAsAl cylindrical quantum wires. The results are compared with the case of unconfined phonons.

Physical Processes of the Nonlinear Optical Response of Glasses with Semiconductor and Metallic Nanoparticles

Alexander A. Kim and N. V. Nikonorov
National Research University Information Technology, Mechanics and Optics, Russia

Abstract— Previously studied materials show the following results. In the optical composite media based on the glass matrix with nanoparticles of metal halide under the influence of laser radiation can be observed the effect of optical confinement in a broad spectral range, due to photogeneration of color centers. The formation of such unstable centers, whose life can vary widely from 10^{-12} to 10^{-5} s, depending on the metal halide can occur in a wide range of excitation energy from 10^{-10} to 10^{-3} J/cm^2.

Also, the presence of impurities in wide-gap semiconductors generates additional levels and accordingly creates a saturating nonlinear-optical limitation. The relaxation time of such processes is usually an order of magnitude compared with the excitation pulse. Saturation of interband absorption, photogeneration of color centers leads to a change in the refractive index and other effects.

The phenomenon of enlightenment in such materials with nanoparticles of metal chalcogenides studied in sufficient detail. This effect was observed in suspensions of nanoparticles of silver halide under the influence of picosecond pulses in the visible spectrum.

I have studied experimentally the nonlinear optical effects in glasses with nanocrystals of CuCl. This material showed a wide dynamic range of the effect of the nonlinear optical limitation from 10^{-10} to 10^{-4} J/cm^2 in silicate glasses, and from 10^{-6} to 10^{-3} J/cm^2 in potassium-aluminum-borate glasses. In my work, paid special attention to this distinction, which is explained by the different reaction of the surrounding glass matrix. So I studied potassium-aluminum-borate glasses with nanocrystals CuBr. Despite the similarity of the structures with CuCl, the parameters of the nonlinear optical response are quite different, since the threshold of nonlinear response starts at 10^{-4} J/cm^2.

Porous silica glasses with nanoparticles of AgI also have a permanent restriction in the range of 10^{-11} to 10^{-7} J/cm^2.

Based on experimental data of other authors and our own experimental research developed a theoretical model of the physical processes that occur simultaneously in composite media based on chalcogenide glass, copper and silver. The constructed mathematical model allows us to predict the nonlinear optical properties of such media and manage your response by controlling the size and composition of nanoparticles. This work will play a key role in the creation of new composite media with nonlinear optical effects.

Session 4P6
Microwave and Millimeter Wave Circuits and Devices, CAD

Applying Capacitive Terminal of Microwave Transmission Line as Sensitive Sound Transducer

Jian Qian, **Shaomin He**, **Xidong Fu**, **Zhicai Xu**, **and Ping Chen**
Key Laboratory of Modern Acoustics, Ministry of Education, Nanjing Univeristy, China

Abstract— This is to introduce a novel sound transducer called microwave microphone, including its principle, parameter optimization, experiment verification and application prospect.

The left figure shows a transmission line ended by a capacitive load. When a CW microwave signal propagates along the line and reaches the terminal, it will be reflected. The reflecting coefficient can be easily expressed as $\Gamma = \frac{1-j\omega CZ_0}{1+j\omega CZ_0}$. Where, Z_0 is the characteristic impedance of the line, C, the capacitance, and ω, the angular frequency. The phase angle of Γ is given by $\phi = -2\tan^{-1}(\omega CZ_0)$. If one of the capacitance electrode is made of a thin metal film, which will vibrate along with the incident sound wave, the capacitance C will change instantly, and hence the ϕ will change correspondingly. It means that the reflecting wave is phase-modulated by the sound wave. The changing rate is reasonably expressed by $\frac{d\phi}{dC} = \frac{-2\omega Z_0}{1+(\omega Z_0 C)^2}$. Simplifying the capacitor as two plat plates and neglecting the fringe effect. The capacity should be $C = \varepsilon_r\varepsilon_0 S/t$. Where, S is the area of the electrode and t, the gap between them. Then we have $\frac{d\phi}{dt} = \frac{d\phi}{dC}\frac{dC}{dt} = \frac{2\omega Z_0 C}{1+(\omega Z_0 C)^2}\frac{1}{t}$. Now we conclude that in order to get the maximum changing rate of the ϕ relative to t, the smaller t the better, and the capacitance C should satisfy the relation $\omega CZ_0 = 1$. Namely, $C = \frac{1}{\omega Z_0}$, and $\frac{d\phi}{dt} = \frac{1}{t}$. This changing rate is much bigger contrast to reflecting in space, where, $\frac{d\phi}{dt} = \frac{4\pi}{\lambda}$. For example, under 10 GHz, if set $t = 0.01$ mm, the difference between them would reach 47.6 dB. In terms of carrier cancellation technique, an experiment system has been set, which verified that its sensitivity is far beyond the commonly used electret microphones. Due to the demodulation system is more complex and expensive than that of electret microphones, this kind of microphone might not be competitive in common use. However, in view of this transducer itself absolutely does not contain any nonlinear elements, if it is wrapped with rubber shell and filled with low-loss liquid dielectrics, it may easily construct a pressure-difference-balanced hydrophone and works under deep water and has important application prospect.

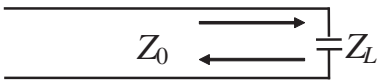

Figure 1.

ACKNOWLEDGMENT

This project is supported by Key Laboratory of Modern Acoustics, Ministry of Education, Nanjing University.

Full-wave Analysis of Two Parallel Slotlines on a Common Substrate

Vaclav Kotlan[1], **Jan Machac**[1], **Francisco Mesa**[2], **and Raul Rodriguez-Berral**[2]

[1]Faculty of Electrical Engineering, Czech Technical University in Prague
Technicka 2, 166 27 Praha 6, Czech Republic
[2]Department of Applied Physics 1, University of Seville
ETSI Informatica, Av. Reina Mercedes s/n, Seville 41012, Spain

Abstract— Present-day planar microwave circuits are based on planar transmission lines. These lines are open, i.e., they can radiate part of the energy out of the line. The most frequently used lines are: microstrip line, coplanar waveguide, coplanar strips, and slotline. Until now, most interest has been devoted to the microstrip line and the coplanar waveguide, and much less attention has has been paid to the slotline.

As planar lines are open, and can radiate, a mutual coupling between two lines located in parallel on a substrate can be fatal to circuit behavior. The spurious crosstalk caused by this coupling can ruin the proper circuit function. This paper provides a useful study of the high-frequency crosstalk effects that can appear between two slotlines located in parallel on the same substrate. The analysis consists of a full-wave integral equation formulation solved in the spectral domain using the method of moments (Galerkin's method). The total wave propagating along the two lines is calculated by using proper basis functions for the field across the slots. This wave consists of a set of bound modes as well as the continuous spectrum (which comprises both leaky modes and the residual wave excited on the structure). In our semi-analytical model, only one slotline has a source (active line) whereas the second line is without any direct feeding (passive line). A current source in the active line is connected across the slot. The numerical results thus obtained show how an electric field is induced in the passive slotline due to coupling, and how the field in the active line differs from the field along a single slotline without any other closely located line. Results for the most important working regimes are discussed. The first important working regime is at the frequency band when only bound mode exists. The second regime is at the frequencies where bound and leaky modes appear simultaneously, and the last regime is at high frequencies, where only leaky waves propagate. Certainly, transmission lines must be designed to operate in the first working regime of only bound-mode propagation.

In summary, the paper presents a detailed parametric study of the two coupled slotlines. The wave propagating on the active slotline together with the wave propagating along the passive slotline are compared with the wave that propagates along a single slotline. In addition, the analysis of the crosstalk in the two parallel slotlines on the common substrate is verified experimentally. The measured field distributions fit the calculated field distributions quite well.

ACKNOWLEDGMENT

The experiment performed in this work was supported by the Grant Agency of the Czech Republic under projects 102/09/0314, and numerical simulation was supported by project 102/08/H018. The theoretical work was supported by project of the Czech Technical University in Prague SGS10/271/OHK3/3T/13, and by the Spanish Ministerio de Educacin y Ciencia and European Union FEDER funds, project TEC2007-65376.

Advances in the Theory of A, B, C Numbers and Its Application to Waveguide Propagation

Mariana Nikolova Georgieva-Grosse[1] and Georgi Nikolov Georgiev[2]

[1]Consulting in Physics and Computer Sciences, Meterstrasse 4, D-70839 Gerlingen, Germany
[2]Faculty of Mathematics and Informatics
University of Veliko Tirnovo "St. St. Cyril and Methodius", BG-5000 Veliko Tirnovo, Bulgaria

Abstract— A, B and C numbers are called positive real ones, defined by means of the expressions: $A = A_- - A_+$, $B = B_- - B_+$, $C = C_- - C_+$ in which $A_\pm = \sigma_{1\pm}/\sigma_{2\pm}$ or $A_\pm = \sigma_{2\pm}/\sigma_{1\pm}$, $B_\pm = \sigma_{1\pm}\bar{r}_0$ or $B_\pm = \sigma_{2\pm}\bar{r}_0$ and $C_\pm = (\sigma_{1\pm}/\sigma_{2\pm})\,\bar{r}_0$ or $C_\pm = (\sigma_{2\pm}/\sigma_{1\pm})\,\bar{r}_0$, depending on whether $\sigma_{2\pm} \equiv |\alpha|$ or $\sigma_{1\pm} \equiv |\alpha|$ where $\sigma_{1\pm}$ and $\sigma_{2\pm}$ $(1 > \sigma_{1-} \geq \sigma_{1+} \geq \sigma_{2-} \geq \sigma_{2+} \geq 0)$ are the real roots of the biquadratic equation $\sigma_\pm^4 - \left(1 - \bar{\beta}_{2\pm}^2\right)\sigma_\pm^2 + 4\bar{\beta}_{2\pm}^2 k_\pm^2 = 0$, $(1 - \bar{\beta}_{2\pm} \geq 4\bar{\beta}_{2\pm}\,|k_\pm|)$ [1–3]. Here $\bar{\beta}_{2\pm} = \zeta_{k_\pm,n}^{(c)}/\left(2\bar{r}_0\right)$ $(\bar{\beta}_{2\pm} = \chi_{k_\pm,n}^{(c)}(\rho)\,/\,(2\bar{r}_0))$, $\zeta_{k_\pm,n}^{(c)}$ $(\chi_{k_\pm,n}^{(c)}(\rho))$ are the positive purely imaginary zeros of the function $\Phi(a,c;x)$ $(F(a,c;x,\rho) = \Phi(a,c;x)\,\Psi(a,c;\rho x) - \Phi(a,c;\rho x)\,\Psi(a,c;x))$, $\Phi(a,c;x)$ and $\Psi(a,c;x)$ are the Kummer and Tricomi confluent hypergeometric functions [4], $a = c/2 - jk$ is complex, $c = 3$, $x = jz$ is positive purely imaginary, z, ρ, $\bar{r}_0$ are real, positive, $0 < \rho < 1$, $\bar{r}_0 > \zeta_{0,n}^{(c)}/2$ $(\bar{r}_0 > \chi_{0,n}^{(c)}(\rho)\,/2)$, k, α are real, $-\infty < k < +\infty$, $-1 < \alpha < 1$, $n = 1, 2, 3, \ldots$ [1–3]. Applying an iterative technique for the case, connected with $\Phi(a,c;x)$ in which $\bar{r}_0$ and $|\alpha|$ satisfy the relation: $\zeta_{0,n}^{(c)}/2 < \bar{r}_0\sqrt{1-\alpha^2} < L(c,n)\,/\,|\alpha|$ ($L(c,n)$ — certain positive real numbers, e.g., $L(3,1)$ =6.59365 41068 [2, 5]) and assuming $\bar{r}_0 \leq 10$, it has been established that the domain of existence of each of the numbers has a lower limit [2].

Extending the approach mentioned in this study the influence of $\bar{r}_0$ and $|\alpha|$ on the quantities A, B and C is examined for $\bar{r}_0 > 10$. It is found out that if $\bar{r}_0 \geq 2L(c,n)$, the domains in question possess upper limits which are traced. It is shown that the same are linked with the envelope lines in the phase diagrams of the circular waveguide, entirely filled with azimuthally magnetized ferrite, propagating normal TE_{0n} modes which mark off the boundary of the area of phase shifter operation of configuration from the side of higher frequencies, if α is interpreted as the off-diagonal tensor element of the anisotropic medium, $\bar{r}_0 = \beta_0 r_0\sqrt{\varepsilon_r}$ is the normalized in an appropriate way guide radius r_0, $\bar{\beta}_{2\pm} = \zeta_{k_\pm,n}^{(c)}/\left(2\bar{r}_0\right)$ specifies the eigenvalue spectrum of the fields, $k = \alpha\bar{\beta}/\left(2\bar{\beta}_2\right)$ where $\bar{\beta} = \beta/\left(\beta_{\,0}\sqrt{\varepsilon_r}\right)$, $\bar{\beta}_2 = \beta_2/\left(\beta_0\sqrt{\varepsilon_r}\right)$ (β and $\beta_2 = \left[\omega^2\varepsilon_0\mu_0\varepsilon_r\left(1-\alpha^2\right)\right]^{1/2}$ are the phase constant and radial wavenumber), $\beta_0 = \omega\sqrt{\varepsilon_0\mu_0}$ is the free space phase constant, ε_r is the relative permittivity of the ferrite, $\sigma_{1\pm}$ and $\sigma_{2\pm}$ denote $\bar{\beta}_\pm$ $(|\alpha_\pm|)$ and $|\alpha_\pm|$ $(\bar{\beta}_\pm)$, resp., ($\zeta_{k_\pm,n}^{(c)}$ — roots of structure's characteristic equation, written by complex Kummer function), n — number of the mode [1–3, 5]. (The subscripts "+" and "−" relate to $k_+ > 0$ and $k_- < 0$, resp. to positive ($\alpha_+ > 0$) and negative ($\alpha_- < 0$) magnetization.) The new and the old (pertinent to the cut-off regime of the configuration [1–3]) limits are ones to which the formulae for computation of the differential phase shift produced by the structure, suggested earlier [6], are valid.

REFERENCES

1. Georgieva-Grosse, M. N. and G. N. Georgiev, "The A, B, C numbers and their application in the theory of waveguides," *PIERS Proceedings*, 1043–1047, Moscow, Russia, August 18–21, 2009.
2. Georgieva-Grosse, M. N. and G. N. Georgiev, "On the A, B, C numbers and their application in the theory of circular waveguide with azimuthally magnetized ferrite," *PIERS Online*, Vol. 6, No. 4, 370–374, 2010.
3. Georgieva-Grosse, M. N. and G. N. Georgiev, "Comparative study on the computational modeling and application of the classes of A, B, C numbers," *Proc. Thirteenth Int. Conf. Electromagn. Adv. Applicat. ICEAA'11*, Turin, Italy, September 12–17, 2011, (Invited Paper in the Special Session "Future challenges in mathematical and computational electromagnetics and its applications II" organized by M. N. Georgieva-Grosse and G. N. Georgiev), (in press).
4. Tricomi, F. G., *Funzioni Ipergeometriche Confluenti*, Edizioni Cremonese, Rome, Italy, 1954.
5. Georgiev, G. N. and M. N. Georgieva-Grosse, "A new property of the complex Kummer function and its application to waveguide propagation," *IEEE Antennas Wireless Propagat. Lett.*, Vol. 2, 306–309, December 2003.

6. Georgiev, G. N. and M. N. Georgieva-Grosse, "Formulae for differential phase shift computation in an azimuthally magnetized circular ferrite waveguide," *Proc. Millenn. Conf. Antennas Propagat. AP-2000*, article ID 1002, 4 pages, CDROM, Davos, Switzerland, April 9–14, 2000.

An Extra Reduced Size Dual-mode Bandpass Filter for Wireless Communication Systems

Jawad K. Ali and Nasr N. Hussain
Department of Electrical and Electronic Engineering, University of Technology, Baghdad, Iraq

Abstract— A new miniaturized dual-mode microstrip bandpass filter is presented as a candidate for use in wireless communication applications. The filter structure has been fractally generated based on the 4th iteration Minkowski-variant pre-fractal geometry, using the conventional dual-mode square ring resonator as the initiator in the fractal generation process. The proposed microstrip bandpass filter design has been modeled, and its performance has been analyzed using a full-wave EM simulator, Sonnet Software, Inc., at the 2.4 GHz ISM band. It has been found that the presented filter design offers a size reduction of about 88% as compared with the conventional dual-mode microstrip square ring resonator under the same design specifications. This size reduction is considered better than that reported in the literature. In addition; simulation results show that the filter has acceptable return loss and transmission responses besides the miniaturized size gained. The proposed filter design methodology can be generalized as a flexible design tool for compact microstrip bandpass filters for a wide variety of wireless communication systems. The filter is supposed to be suitable for microwave applications as a low cost mass-producible, high performance and compact component.

New Defected Microstrip Structure Bandstop Filter

J.-K. Xiao[1] and W.-J. Zhu[2]

[1]School of Electronical & Mechanical Engineering, Xidian University, Xi'an 710071, China
[2]School of Computer and Information, Hohai University, Changzhou 213022, China

Abstract— Currently, the defected ground structure (DGS) has been widely employed to improve filter performance and reduce filter size. DGS is proved efficiency for harmonic suppression and has stopband performance in microwave circuits design, and especially the periodical DGSs, which extend the stopband greatly. DGS increases the effective capacitance and inductance of microstrip line, and as a result, it restrains the spurious responses by rejecting harmonic in microwave circuits, and the performances of filters or other microwave components are effectively improved. However, DGS introduces wave leakage through the ground plane.

Compared with DGS circuit, the defected microstrip structure (DMS) unit is made by etching two vertical narrow slots in the microstrip line, so, the enclosure problems needn't be considered because there is no leakage through the ground plane. DMS is more easily integrated with other microwave circuits, and has an effectively reduced circuit size compared with DGS, and simultaneously, DMS exhibits the properties of slow-wave, rejecting microwaves in certain frequencies and has an increasing electric length of certain circuits which are similar to the well known DGS but without any manipulation of the ground plane.

In the present work, the stop-band performance of DMS is studied, and new single band, dual-band and tri-band bandstop filters with DMS are proposed. The dual-band and tri-band bandstop filters are fabricated, and the experiment demonstrates the new design. The new DMS bandstop filters have advantages of good frequency selectivity, low loss and simple circuit topology, and simultaneously,has a miniature circuit size of no more than 30 mm × 1.2 mm.

Dual-band Bandpass Filter Using SIR Structure

J.-K. Xiao[1] and W.-J. Zhu[2]

[1]School of Electronical & Mechanical Engineering, Xidian University, Xi'an 710071, China
[2]School of Computer and Information, Hohai University, Changzhou 213022, China

Abstract— In many communication related applications, it is important to keep RF filter structures to a minimum size and weight, and filter performances to a low passband insertion losses, high frequency selectivity, and flat group delay within the passband, et al.. Currently, with the rapid development of modern wireless communications, bandpass filters with dual and multi-band operation become more and more important in communication systems and have been paid much attention for the multifunctional and miniaturization requirement of portable equipment. The traditional microstrip parallel-coupled half-wavelength resonator bandpass filters have narrow stopband between the fundamental response and the first spurious response, so the stepped-impedance resonator (SIR) was presented in the past years to not only restrain the spurious responses, but also shorten the resonator size. SIR also can be used to design tri-band even multi-band filters for tuning the higher order resonant modes conveniently. However, the deficiency of this kind of resonator is its resonant frequencies are dependent, and transmission zeros are difficult to implement.

This report presents bandpass filters with dual-band by using single SIR, and the 2-path coupling is not required. The designed filters have advantages of compact structures, dual-band operation and low passband insertion losses, et al., and have prospect to apply in wireless communication systems.

An Investigation of Unloaded Quality Factor of $\lambda/2$ and $\lambda/4$ Resonators

Somboon Theerawisitpong[1], **Toshitatsu Suzuki**[2], **and Yozo Utsumi**[2]

[1]Department of Technical Education, Faculty of Technical Education
Rajamangala University of Technology Thanyaburi
39 Moo 1, Rangsit-Nakorn Nayok Road, Klong Hok, Thanyaburi, Pathumtani 12110, Thailand
[2]Department of Electrical and Electronic Engineering, Nippon Institute of Technology
4-1 Gakuendai, Miyashiro-machi, Minami Saitama-gun, Saitama-ken 345-8501, Japan

Abstract— In the research field of microwave circuits design, it is well known that microstrip filters can be realized with either half-wavelength ($\lambda/2$) or quarter-wavelength ($\lambda/4$) resonators [1–5]. Besides, it is also found that most of conventional filters are designed based on $\lambda/2$ resonator meanwhile miniaturized filters are designed based on $\lambda/4$ resonator. Because of $\lambda/4$ resonator is shorter than $\lambda/2$ resonator by two times, thus those miniaturized filters can be realized with $\lambda/4$ resonator but unloaded quality factor (Q_0) of filters may be decreased. In our study, the assumption of decreased Q_0 of $\lambda/4$ resonator has been proved with investigation of Q_0 of $\lambda/2$ and $\lambda/4$ resonators. It is found that Q_0 of $\lambda/4$ is decreased and is less than that of $\lambda/2$ resonator, due to current density loss at the short-end of $\lambda/4$ resonator. In particular, the circumstance of current density loss at the short-end of $\lambda/4$ resonator has been obviously demonstrated by simulation of current density distribution on resonator surface, which is also compared with that of current density loss on $\lambda/2$ resonator. Furthermore, Q_0 of $\lambda/2$ and $\lambda/4$ resonators is also measured by vector network analyzer. In our experiment, $\lambda/2$ and $\lambda/4$ resonators have been fabricated on a 1.2 mm-thick laminate having $\varepsilon_r = 2.6$ and $\tan\delta = 0.0015$. It is found that the measured Q_0 of $\lambda/4$ resonator is less than that of $\lambda/2$ resonator, which is near to calculated Q_0 obtained by simulation. In summary, it can be concluded that Q_0 of $\lambda/4$ is less than that of $\lambda/2$ resonator, due to current density loss at the short-end of $\lambda/4$ resonator, which has been confirmed as proposed in this paper with simulated and experimental results. Consequently, we can summarize that filters having high Q_0 can be realized by using $\lambda/2$ resonator and decreased Q_0 is yielded by using $\lambda/4$ resonator.

REFERENCES

1. Jayatilaka, H. C., D. M. Klymyshyn, M. Börner, and J. Mohr, "Compact thick metal diplexer with multi-coupled folded half wavelength resonators," *Progress In Electromagnetics Research C*, Vol. 18, 1–8, 2011.
2. Deng, P.-H. and P.-T. Chiu, "New bandpass filters using half-wavelength and branch-line resonators," *Progress In Electromagnetics Research C*, Vol. 16, 241–249, 2010.
3. Chen, Y.-W., Y.-J. Liu, and M.-H. Ho, "The quasi-elliptic bandpass filter using quarter-wavelength stepped impedance resonators," *PIERS Online*, Vol. 2, No. 6, 605–608, 2006.
4. Wu, H.-W., Y.-K. Su, M.-H. Weng, and R.-Y. Yang, *Microw. Opt. Tech. Lett.*, Vol. 50, No. 10, 2694–2696, 2008.
5. Theerawisitpong, S., T. Suzuki, N. Morita, and Y. Utsumi, *ISAP-2009*, 899–920, 2009.

Design of an Extra-low-loss Broadband Y-branch Waveguide Splitter Based on a Tapered MMI Structure

Pengfei Wang[1, 2], **Gilberto Brambilla**[1], **Yuliya Semenova**[2], **Qiang Wu**[2], **and Gerald Farrell**[2]

[1]Optoelectronics Research Centre, University of Southampton, Southampton, SO17 1BJ, UK
[2]Photonics Research Center, School of Electronic and Communications Engineering
Dublin Institute of Technology, Kevin Street, Dublin 8, Ireland

Abstract— An optimal design method for an extra low loss broadband buried Y branch is presented over a broadband wavelength range from 1500 $\sim$ 1600 nm. A tapered multimode waveguide section, which was used earlier to reduce the excess loss, is designed optimally when the light distribution at the end of the multimode waveguide section is matched to the profile of the symmetric supermode for the structure of the two branching waveguides. An optimization method that combines the genetic algorithm and a gradient-based search method is used to obtain the optimal geometrical parameters for the multimode waveguide section as well as the widths for the input and branching waveguides. With these optimized parameters, even there is an offset between the input standard singlemode fibre and waveguide in packaging, the wavelength dependence of the output ratio between the two branches is small (less than 0.03 dB).

Scanning Near-field Millimeter Wave Microscope Combining Dielectric Tapered Probes and Metal Tips

B. Zhu[1], **S. Vanloocke**[2], **V. Matvejev**[1], **J. Stiens**[1], **D. De Zutter**[2], **and R. Vounckx**[1]

[1]Laboratory for Micro-and Photon Electronics, Department of Electronics and Informatics
Vrije Universiteit Brussel, Pleinlaan 2, 1050 Elsene, Brussels, Belgium
[2]Department of Information Technology (INTEC), UGent, Sint-Pietersnieuwstraat 41, Gent 9000, Belgium

Abstract— The microwave regime in the frequency spectrum has been extensively utilized for communication, imaging, nondestructive testing, and security purposes. Millimeter-(30–300 GHz) and Terahertz-(300–3000 GHz) waves provide unique opportunities for the development of novel applications in the active near-field imaging and spectroscopy of microscopic objects. Conventional optical imaging systems in the mm- and THz range ($0.1 < \lambda < 10$ mm) cannot resolve microscopic details as the resolution in the far-field is limited by the wavelength (Rayleigh criterion). The amplitude and phase of the near-field (evanescent wave) contain high resolution spatial information which is highly dependent on the local structure. Hence, recently, near-field microscopes with higher resolution have been frequently reported. For imaging, object investigation and nondestructive testing using millimeter and THz technologies, electromagnetic beams are required to be collimated and focused to attain higher resolution. Typically, imaging systems use biconvex lenses and parabolic mirrors. In this paper, we built a free-space scattering-type scanning near-field millimeter wave microscope using two tapered dielectric tips and a sample in between. Nylon, Teflon and PVC tapered tips are compared in this system. Experiments reveal that intensity contrasts for different taper materials are due to the loss tangent of the different kind of dielectric tapered waveguides. The image resolution depends on the distance of the tip and the sample, the material of the tip, and the sharpness of the tip, even more the dielectric property of the sample. All the experiments agree with the simulations. In order to improve the contrast and resolution of the near-field images, we additionally positioned a metal probe tip between the dielectric taper and the object under test. First experiment results on this signal improvement concept will be reported for a 2 µm tungsten probe, yielding an increased field enhancement.

A New Method for the Characterizing and Modeling of Arbitrarily Shaped Multiport Junctions

Malika Ourabia
University of Sciences and Technologies Houari Boumediene, Algiers, Algeria

Abstract— An approach for modeling and numerical simulation of passive planar structures using the edge line concept is developed. With this method, we develop an efficient modeling technique for microstrip discontinuities. The technique obtains closed form expressions for the equivalent circuits which are used to model these discontinuities. Then it would be easy to handle and to characterize complicated structures like T and Y junctions, truncated junctions, arbitrarily shaped junctions, cascading junctions and more generally planar multiport junctions. Another advantage of this method is that the edge line concept for arbitrary shape junctions operates with real parameters circuits. The validity of the method was further confirmed by comparing our results for various discontinuities (bend, filters) with those from HFSS as well as from other published sources.

New Method to Calculate the Low Frequency Noise Hooge Parameter: Applications to SiGe HFET

Luis Manuel Rodríguez, **Mauro A. Enciso-Aguilar**, **and Martha C. Galaz Larios**
Escuela Superior de Ingeniería Mecánica y Eléctrica, Instituto Politécnico Nacional, México D. F.

Abstract— A new extraction method for the Hooge parameter based on high frequency and low frequency measurements is presented for the first time. We emphasis on the role played by the resistive and electrostatic parasitics on the accuracy of the Hooge parameter. We illustrate this new approach by calculating the Hooge parameter for a $Si/Si_{0.6}Ge_{0.4}$ n-HFET and we compare these values with those calculated by classical method.

Author Index